ENDOTHELIAL DYNAMICS IN HEALTH AND DISEASE

EDITED BY: Jaap Diederik Van Buul, Stephan Huveneers, Mariona Graupera and Elizabeth Anne Vincent Jones

PUBLISHED IN: Frontiers in Physiology and Frontiers in Cell and Developmental Biology

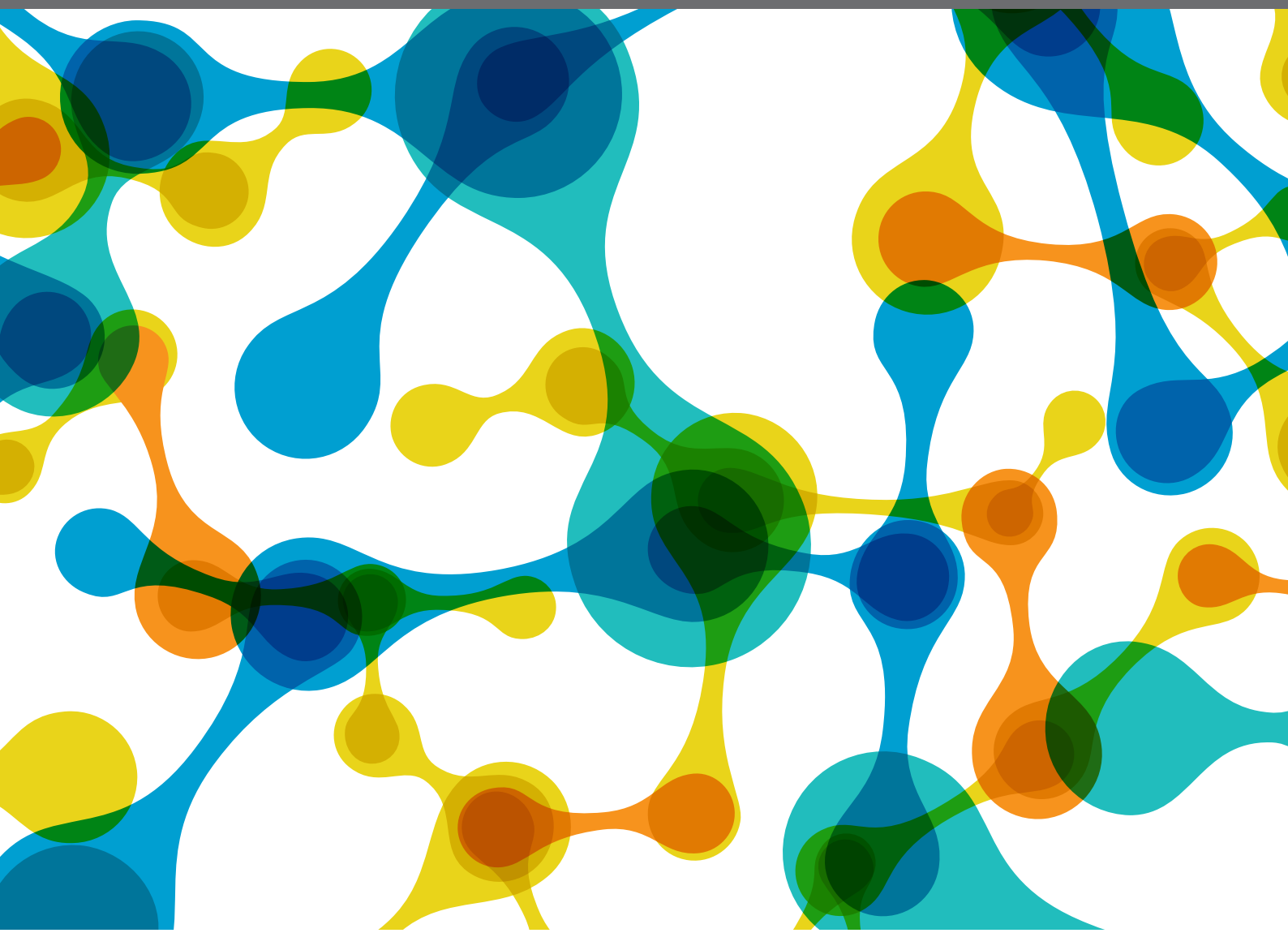

frontiers Research Topics

frontiers

ISSN 1664-8714
ISBN 978-2-88966-352-1
DOI 10.3389/978-2-88966-352-1

About Frontiers

Frontiers is more than just an open-access publisher of scholarly articles: it is a pioneering approach to the world of academia, radically improving the way scholarly research is managed. The grand vision of Frontiers is a world where all people have an equal opportunity to seek, share and generate knowledge. Frontiers provides immediate and permanent online open access to all its publications, but this alone is not enough to realize our grand goals.

Frontiers Journal Series

The Frontiers Journal Series is a multi-tier and interdisciplinary set of open-access, online journals, promising a paradigm shift from the current review, selection and dissemination processes in academic publishing. All Frontiers journals are driven by researchers for researchers; therefore, they constitute a service to the scholarly community. At the same time, the Frontiers Journal Series operates on a revolutionary invention, the tiered publishing system, initially addressing specific communities of scholars, and gradually climbing up to broader public understanding, thus serving the interests of the lay society, too.

Dedication to Quality

Each Frontiers article is a landmark of the highest quality, thanks to genuinely collaborative interactions between authors and review editors, who include some of the world's best academicians. Research must be certified by peers before entering a stream of knowledge that may eventually reach the public - and shape society; therefore, Frontiers only applies the most rigorous and unbiased reviews.
Frontiers revolutionizes research publishing by freely delivering the most outstanding research, evaluated with no bias from both the academic and social point of view. By applying the most advanced information technologies, Frontiers is catapulting scholarly publishing into a new generation.

What are Frontiers Research Topics?

Frontiers Research Topics are very popular trademarks of the Frontiers Journals Series: they are collections of at least ten articles, all centered on a particular subject. With their unique mix of varied contributions from Original Research to Review Articles, Frontiers Research Topics unify the most influential researchers, the latest key findings and historical advances in a hot research area! Find out more on how to host your own Frontiers Research Topic or contribute to one as an author by contacting the Frontiers Editorial Office: researchtopics@frontiersin.org

ENDOTHELIAL DYNAMICS IN HEALTH AND DISEASE

Topic Editors:
Jaap Diederik Van Buul, University of Amsterdam, Netherlands
Stephan Huveneers, Amsterdam University Medical Center (UMC), Netherlands
Mariona Graupera, Institut d'Investigacio Biomedica de Bellvitge (IDIBELL), Spain
Elizabeth Anne Vincent Jones, Faculty of Medicine, KU Leuven, Belgium

Citation: Van Buul, J. D., Huveneers, S., Graupera, M., Jones, E. A. V., eds. (2021). Endothelial Dynamics in Health and Disease. Lausanne: Frontiers Media SA.
doi: 10.3389/978-2-88966-352-1

Table of Contents

frontiers in Physiology

EDITORIAL
published: 19 November 2020
doi: 10.3389/fphys.2020.611117

Editorial: Endothelial Dynamics in Health and Disease

Elizabeth A. V. Jones[1,2], *Mariona Graupera*[3,4], *Jaap D. van Buul*[5] *and Stephan Huveneers*[6*]

[1] Centre for Molecular and Vascular Biology, KU Leuven, Leuven, Belgium, [2] Department of Cardiology, Cardiovascular Research Institute Maastricht, Maastricht University, Maastricht, Netherlands, [3] Vascular Biology and Signalling Group, ProCURE, Oncobell Program, Institut d'Investigació Biomèdica de Bellvitge (IDIBELL), L'Hospitalet de Llobregat, Barcelona, Spain, [4] CIBERONC, Instituto de Salud Carlos III, Madrid, Spain, [5] Sanquin Research and Landsteiner Laboratory, Leeuwenhoek Centre for Advanced Microscopy, Swammerdam Institute for Life Sciences, University of Amsterdam, Amsterdam, Netherlands, [6] Department of Medical Biochemistry, Amsterdam Cardiovascular Sciences, Amsterdam University Medical Center, Location AMC, University of Amsterdam, Amsterdam, Netherlands

Keywords: endothelial cell, angiogenesis, VE-cadherin, cytoskeleton, mechanotransduction, VEGF signaling, lymphatic vessels, blood vessels

Editorial on the Research Topic

Endothelial Dynamics in Health and Disease

This special Research Topic of Frontiers in Physiology and Frontiers in Cell and Developmental Biology collates a series of review and research articles on the dynamic properties of endothelial cells, the key inner lining cells of blood and lymphatic vessels. Over the past decade, we have learnt that the vasculature is not a static tissue, but instead relies on the dynamic interactions of endothelial cells with each other, with the vascular microenvironment and with other cell types. For instance, new vessel formation occurs through collective migration and critically relies on rearrangements of interactions between endothelial cells. As such, endothelial cells are equipped with a variety of dynamic molecular systems that allow these cells to adapt to physiological and pathophysiological changes. Studying the systems that underlie endothelial dynamics brings fundamental insights into how vessels form and respond to their microenvironment. This knowledge is crucial to understand the development of cardiovascular disease, and it provides potential leads to guide the opening and closing of the vasculature for therapeutic applications in chronic inflammation and cancer.

Endothelial tissue integrity depends on adherens junctions that are based on the actin-anchored VE-cadherin receptor (**Figure 1**). The importance of the VE-cadherin complex has been widely studied in the context of endothelial barrier function (Orsenigo et al., 2012; Smith et al., 2020) (lymph)angiogenesis (Carmeliet et al., 1999; Bentley et al., 2014; Hägerling et al., 2018; Yang et al., 2019), inflammation (Wessel et al., 2014; van Steen et al., 2020), and flow sensing (Tzima et al., 2005; Lagendijk et al., 2017; Caolo et al., 2018). Duong and Vestweber now overview the complementary mechanisms that take place at endothelial cell-cell junctions beyond the VE-cadherin receptor in intact blood and lymphatic vessels. The importance of other adhesion receptors such as ESAM, Claudins and their anchoring to the dynamic actomyosin cytoskeleton is discussed as important contributors to endothelial integrity. In an original research paper by Werner et al., a new member of VE-cadherin-based endothelial junctions is identified: the actin-binding protein Coronin 1B. The authors investigated the molecular mechanism behind actomyosin relaxation and subsequent protrusive cytoskeletal activity evoked by Coronin 1B to seal the junctions.

Endothelial cell biology is controlled by VEGF signaling. Li et al. have investigated the importance of VEGF-A-mediated VEGFR2 activation and downstream VE-cadherin phosphorylation in experimental myocardial infarction models. Intriguingly, VEGFR2 Y949F knock-in mice are protected from cardiac edema, and these findings indicate that vascular leakage may be therapeutically targeted to improve heart tissue perfusion after infarction. The

OPEN ACCESS

Edited by:
Andreea Trache,
Texas A&M University, United States

Reviewed by:
Irena Levitan,
University of Illinois at Chicago, United States

****Correspondence:***
Stephan Huveneers
s.huveneers@amc.uva.nl

Specialty section:
This article was submitted to Vascular Physiology, a section of the journal Frontiers in Physiology

Received: *28 September 2020*
Accepted: *20 October 2020*
Published: *19 November 2020*

Citation:
Jones EAV, Graupera M, van Buul JD and Huveneers S (2020) Editorial: Endothelial Dynamics in Health and Disease. Front. Physiol. 11:611117. doi: 10.3389/fphys.2020.611117

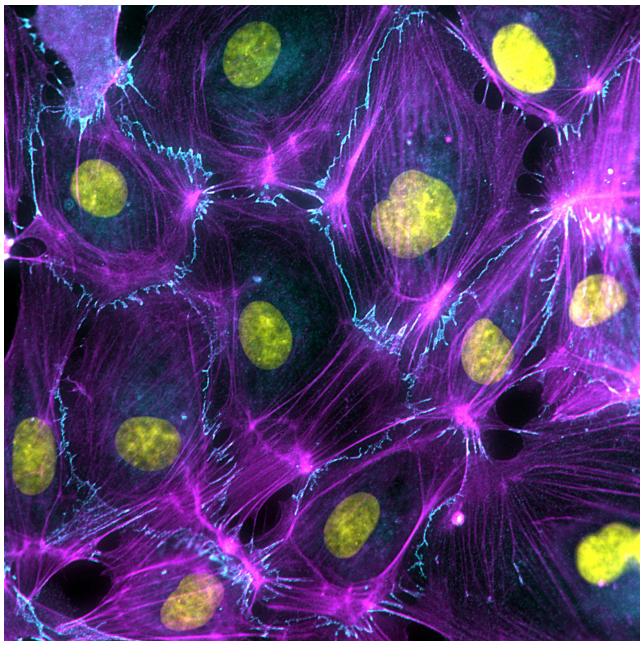

FIGURE 1 | Endothelial cell dynamics is driven by the activity and organization of the actin cytoskeleton (Magenta), which anchors to VE-cadherin-based cell-cell junctions (Cyan).

Neuropilins act as coreceptors for the VEGFRs and are well-known to support angiogenic signaling (Lampropoulou and Ruhrberg, 2014; Simons et al., 2016). Alghamdi et al. have investigated the angiogenic function of NRP2. The authors show that NRP2 promotes endothelial cell migration through regulating the trafficking of the fibronectin-binding integrin α5β1.

Integrins mediate the connection between the vascular extracellular matrix (ECM) and the contractile actomyosin cytoskeleton. Tight crosstalk occurs between endothelial adhesion structures during mechanotransduction: integrins translate forces from the ECM to actomyosin-based contractility, which in turn controls pulling forces on endothelial cell-cell contacts (Huveneers et al., 2015). Failure to respond to forces has direct consequences for vessel development and barrier function and underlies stiffness-related cardiovascular disease. Gordon et al. discuss the forces at play in vascular biology and provide a detailed overview of currently available advanced tools to study force-dependent events in blood and lymphatic endothelial cells cultured *in vitro* under physiological relevant conditions.

To be able to fully understand the impact of blood flow-derived forces on vascular development, one has to turn to *in vivo* experimental models. The review by Campinho et al. elaborates on the importance of various flow-derived mechanical cues on endothelial cell polarization, migration, cell shape changes, and proliferative functions at a single cell level. Endothelial responses to flow are outlined within the context of sprouting angiogenesis, intussusceptive angiogenesis, anastomosis, lumen formation, vessel stabilization, vessel size, and endothelial to haematopoietic transitions. An original research paper by Lv et al. addresses the correlations between flow-mediated dilation, polymorphisms in the gene encoding angiotensin-converting enzyme and endothelial secreted angiotensin II levels in pre-menopausal women.

It is increasingly clear that live imaging is necessary to understand the temporal endothelial activities in the developing vasculature and to this end zebrafish have become a powerful model system. Okuda and Hogan focus on new tools and insights in endothelial dynamics in vascular cell biology based on studies in zebrafish. A detailed toolbox of available genetic models to study endothelial properties during various stages of angiogenesis and their role in vascular development and disease are provided. Live imaging in zebrafish have also revealed exciting new concepts in our understanding of the origin of lymphatic vessels in tumors. In the review from Gutierrez-Miranda and Yaniv, the various endothelial and non-endothelial origins of lymphatics and their contribution to physiological development of the lymphatics and cancer lymphangiogenesis are discussed.

Genetic interference and fluorescence-based endothelial monitoring has led to impressive insights of endothelial cell dynamics during angiogenesis and vascular repair (Eilken and Adams, 2010; Simons et al., 2015; Angulo-Urarte et al., 2018). In the final review of this Research Topic Garcia-Gonzalez et al. compared the pro's and con's of the currently available state-of-the-art conditional genetic mouse models to investigate vascular dynamics at single cell and high molecular resolution. A historical perspective is provided as well as a comprehensive overview of the current sophisticated reporter tools to fluorescently label individual cells and perform lineage tracings in the vasculature (e.g., endothelial cells, pericytes, cardiomyocytes, or vascular smooth muscle cells) in combination with specific loss- or gain-of-function of molecular players.

Taken together, the field is poised to address many key outstanding questions in endothelial and vascular biology. Many previous studies have focused on the dynamics of endothelial cells during the initiation of sprouting in newly forming vasculature. But what happens at intermediate stages of vessel formation is less well-studied. Are comparable molecular systems responsible for vascular elongation and maintenance? Are there differences in endothelial dynamics between blood and lymphatic vessels? Which steps are decided on single cell level, and which require collective responses? We anticipate that current mechanistic insights and endothelial models allow the next generation of vascular researchers to address these caveats in the field of vascular biology and disease.

AUTHOR CONTRIBUTIONS

This manuscript was written by all authors. All authors have performed editorial reviewing tasks for this Research Topic.

FUNDING

EJ was funded by Fonds Wetenschappelijk Onderzoek (G0B5920N) and EU H2020 (848109); MG by CERCA Programme/Generalitat de Catalunya for institutional support and by the research grants SAF2017-89116R-P (FEDER/EU) from MCIU (Spain) co-funded by European Regional Developmental Fund (ERDF), a Way to Build Europe; JB by the Netherlands Organization of Scientific Research VICI (016.196.632); and SH by the Netherlands Organization of Scientific Research ZonMW VIDI (016.156.327).

REFERENCES

Angulo-Urarte, A., Casado, P., Castillo, S. D., Kobialka, P., Kotini, M. P., Figueiredo, A. M., et al. (2018). Endothelial cell rearrangements during vascular patterning require PI3-kinase-mediated inhibition of actomyosin contractility. *Nat. Commun.* 9:4826. doi: 10.1038/s41467-018-07172-3

Bentley, K., Franco, C. A., Philippides, A., Blanco, R., Dierkes, M., Gebala, V., et al. (2014). The role of differential VE-cadherin dynamics in cell rearrangement during angiogenesis. *Nat. Cell Biol.* 16, 309–321. doi: 10.1038/ncb2926

Caolo, V., Peacock, H. M., Kasaai, B., Swennen, G., Gordon, E., Claesson-Welsh, L., et al. (2018). Shear stress and VE-cadherin. *Arteriosc. Thromb. Vasc. Biol.* 38, 2174–2183. doi: 10.1161/ATVBAHA.118.310823

Carmeliet, P., Lampugnani, M. G., Moons, L., Breviario, F., Compernolle, V., Bono, F., et al. (1999). Targeted deficiency or cytosolic truncation of the VE-cadherin gene in mice impairs VEGF-mediated endothelial survival and angiogenesis. *Cell* 98, 147–157. doi: 10.1016/s0092-8674(00)81010-7

Eilken, H. M., and Adams, R. H. (2010). Dynamics of endothelial cell behavior in sprouting angiogenesis. *Curr. Opin. Cell Biol.* 22, 617–625. doi: 10.1016/j.ceb.2010.08.010

Hägerling, R., Hoppe, E., Dierkes, C., Stehling, M., Makinen, T., Butz, S., et al. (2018). Distinct roles of VE-cadherin for development and maintenance of specific lymph vessel beds. *EMBO J.* 37:e98271. doi: 10.15252/embj.201798271

Huveneers, S., Daemen, M. J., and Hordijk, P. L. (2015). Between Rho(k) and a hard place: the relation between vessel wall stiffness, endothelial contractility, and cardiovascular disease. *Circ. Res.* 116, 895–908. doi: 10.1161/CIRCRESAHA.116.305720

Lagendijk, A. K., Gomez, G. A., Baek, S., Hesselson, D., Hughes, W. E., Paterson, S., et al. (2017). Live imaging molecular changes in junctional tension upon VE-cadherin in zebrafish. *Nat. Commun.* 8:1402. doi: 10.1038/s41467-017-01325-6

Lampropoulou, A., and Ruhrberg, C. (2014). Neuropilin regulation of angiogenesis. *Biochem. Soc. Transac.* 42, 1623–1628. doi: 10.1042/BST20140244

Orsenigo, F., Giampietro, C., Ferrari, A., Corada, M., Galaup, A., Sigismund, S., et al. (2012). Phosphorylation of VE-cadherin is modulated by haemodynamic forces and contributes to the regulation of vascular permeability *in vivo*. *Nat. Commun.* 3:1208. doi: 10.1038/ncomms2199

Simons, M., Alitalo, K., Annex, B. H., Augustin, H. G., Beam, C., Berk, B. C., et al. (2015). State-of-the-art methods for evaluation of angiogenesis and tissue vascularization: a scientific statement from the American Heart Association. *Circ. Res.* 116, e99–e132. doi: 10.1161/RES.0000000000000054

Simons, M., Gordon, E., and Claesson-Welsh, L. (2016). Mechanisms and regulation of endothelial VEGF receptor signalling. *Nat. Rev. Mol Cell Biol.* 17, 611–625. doi: 10.1038/nrm.2016.87

Smith, R. O., Ninchoji, T., Gordon, E., André, H., Dejana, E., Vestweber, D., et al. (2020). Vascular permeability in retinopathy is regulated by VEGFR2 Y949 signaling to VE-cadherin. *eLife* 9:e54056. doi: 10.7554/eLife.54056

Tzima, E., Irani-Tehrani, M., Kiosses, W. B., Dejana, E., Schultz, D. A., Engelhardt, B., et al. (2005). A mechanosensory complex that mediates the endothelial cell response to fluid shear stress. *Nature* 437, 426–431. doi: 10.1038/nature03952

van Steen, A. C. I., van der Meer, W. J., Hoefer, I. E., and van Buul, J. D. (2020). Actin remodelling of the endothelium during transendothelial migration of leukocytes. *Atherosclerosis* (in press). doi: 10.1016/j.atherosclerosis.2020.06.004

Wessel, F., Winderlich, M., Holm, M., Frye, M., Rivera-Galdos, R., Vockel, M., et al. (2014). Leukocyte extravasation and vascular permeability are each controlled *in vivo* by different tyrosine residues of VE-cadherin. *Nat. Immunol.* 15, 223–230. doi: 10.1038/ni.2824

Yang, Y., Cha, B., Motawe, Z. Y., Srinivasan, R. S., and Scallan, J. P. (2019). VE-cadherin is required for lymphatic valve formation and maintenance. *Cell Rep.* 28, 2397.e4–2412.e4. doi: 10.1016/j.celrep.2019.07.072

Conflict of Interest: MG is a consultant for Medicxi (London, UK) and has a research agreement with Merck & Co. Inc (North Wales, PA, USA) and with Venthera (Palo Alto, CA, USA).

The remaining authors declare that the research was conducted in the absence of any commercial or financial relationships that could be construed as a potential conflict of interest.

frontiers in Physiology

MINI REVIEW
published: 21 May 2020
doi: 10.3389/fphys.2020.00519

Mechanisms Ensuring Endothelial Junction Integrity Beyond VE-Cadherin

*Cao Nguyen Duong and Dietmar Vestweber**

Department of Vascular Cell Biology, Max Planck Institute for Molecular Biomedicine, Münster, Germany

Endothelial junctions provide blood and lymph vessel integrity and are essential for the formation of a vascular system. They control the extravasation of solutes, leukocytes and metastatic cells from blood vessels and the uptake of fluid and leukocytes into the lymphatic vascular system. A multitude of adhesion molecules mediate and control the integrity and permeability of endothelial junctions. VE-cadherin is arguably the most important adhesion molecule for the formation of vascular structures, and the stability of their junctions. Interestingly, despite this prominence, its elimination from junctions in the adult organism has different consequences in the vasculature of different organs, both for blood and lymph vessels. In addition, even in tissues where the lack of VE-cadherin leads to strong plasma leaks from venules, the physical integrity of endothelial junctions is preserved. Obviously, other adhesion molecules can compensate for a loss of VE-cadherin and this review will discuss which other adhesive mechanisms contribute to the stability and regulation of endothelial junctions and cooperate with VE-cadherin in intact vessels. In addition to adhesion molecules, endothelial receptors will be discussed, which stimulate signaling processes that provide junction stability by modulating the actomyosin system, which reinforces tension of circumferential actin and dampens pulling forces of radial stress fibers. Finally, we will highlight most recent reports about the formation and control of the specialized button-like junctions of initial lymphatics, which represent the entry sites for fluid and cells into the lymphatic vascular system.

Keywords: VE-cadherin, adhesion molecules, endothelial junctions, vascular permeability, angiogenesis

OPEN ACCESS

Edited by:
Mariona Graupera, Bellvitge Biomedical Research Institute, Spain

Reviewed by:
Andrew Patrick Kowalczyk, Emory University, United States
Heinz-Georg Belting, University of Basel, Switzerland

***Correspondence:**
Dietmar Vestweber
vestweb@mpi-muenster.mpg.de

Specialty section:
This article was submitted to Vascular Physiology, a section of the journal Frontiers in Physiology

Received: *18 February 2020*
Accepted: *27 April 2020*
Published: *21 May 2020*

Citation:
Duong CN and Vestweber D (2020) Mechanisms Ensuring Endothelial Junction Integrity Beyond VE-Cadherin. Front. Physiol. 11:519. doi: 10.3389/fphys.2020.00519

INTRODUCTION

Intercellular junctions enable endothelial cells to form multicellular structures that develop into sprouts and primitive vascular tubes. Through remodeling into arteries, capillaries and veins, complex vascular structures evolve associated with perivascular cells (Adams and Alitalo, 2007). Endothelial cells then form the inner lining of a complex and diverse vasculature, where endothelial junctions guard and control vascular permeability and leukocyte trafficking (Vestweber et al., 2014). A multitude of cell adhesion molecules supports and controls endothelial junction integrity in the adult organism, thereby guarding traffic of molecules and cells across the vessel wall (Trani and Dejana, 2015).

These adhesion molecules form tight junctions and adherens junctions which are less clearly separated in endothelial cells than it is known for epithelia. The vasculature in different organs varies in many aspects due to organ specialization (Aird, 2007a,b; Augustin and Koh, 2017;

Potente and Mäkinen, 2017). In accordance to this, the molecular requirements for endothelial junction integrity diverges between tissues. It emerged recently that this is also the case for lymphatic vessels in different organs.

The purpose of this review is to highlight, which of the many adhesion molecules at endothelial cell contacts are indeed essential for the formation, the stability and the regulation of endothelial junctions. An overview about the adhesion molecules is given in **Figure 1** and **Table 1**. In addition, we want to discuss organ specific differences. The role of endothelial adhesion molecules in leukocyte transmigration through endothelial barriers will only be marginally addressed and we refer the reader for this topic to recent reviews (Nourshargh and Alon, 2014; Vestweber, 2015; Muller, 2016).

COMPOSITION OF ADHESION MOLECULES AT ENDOTHELIAL JUNCTIONS

Endothelial cell contacts are formed and regulated by junctional adhesion molecules that constitute closely associated tight and adherens junctions which mediate and control cell contact integrity and molecular permeability across the endothelial barrier. Adherens junctions are generally considered to provide stability of interendothelial cell contacts and control permeability for large molecular weight plasma components. VE-cadherin represents its major constituent, as antibodies against VE-cadherin or gene inactivation are sufficient to perturb endothelial monolayers *in vitro* and enhance vascular permeability for plasma proteins *in vivo* (Gotsch et al., 1997; Matsuyoshi et al., 1997; Gulino et al., 1998; Corada et al., 1999; Frye et al., 2015; Duong et al., 2020). VE-cadherin is essential for the development of the vascular system (Carmeliet et al., 1999; Gory-Faure et al., 1999) and is probably the adhesion molecule with highest endothelial specificity, with some expression on trophoblasts and fetal stem cells (Aird, 2007a), perineural cells (Colom et al., 2012) and the perineurium of peripheral nerves (Smith et al., 1998; Ouyang et al., 2019).

Nectins are much better studied in epithelial cells than in endothelial cells (Rikitake et al., 2015). Of the classical members, nectin-2 and nectin-3 support endothelial junction integrity *in vitro* (Martin et al., 2013; Son et al., 2016; Bekes et al., 2019), and the nectin related poliovirus receptor (PVR/CD155) is involved in leukocyte extravasation (Reymond et al., 2004).

In contrast to adherens junctions, tight junctions control permeability for ions and small molecules (<800 dalton) and therefore are not evenly distributed throughout the vasculature. They are most prominent in the blood-brain barrier (BBB) and the blood-retina barrier as well as in arterioles (Simionescu et al., 1976; Tietz and Engelhardt, 2015). Central components of tight junctions are claudins (Cldn), tetraspanning membrane proteins, of which Cldn5 is found in vessels in all organs (Morita et al., 1999). Expression of Cldn3, Cldn12, and Cldn1 in brain capillary endothelial cells is rather controversial (Ohtsuki et al., 2008; Tietz and Engelhardt, 2015; Vanlandewijck et al., 2018), and while Cldn3 is inducible during mouse brain angiogenesis (Liebner et al., 2008) it is clearly absent in adult brain endothelium (Castro Dias et al., 2019). Occludin is another bona fide tight junction component of endothelial and epithelial cells, however, its gene inactivation does not cause obvious defects in the vasculature (Saitou et al., 2000). The junctional adhesion molecules (JAMs) are 2 Immunoglobulin-domain proteins of which four are expressed on endothelial cells: JAM-A, JAM-B, and JAM-C and the related endothelial cell-selective adhesion molecule (ESAM). The JAMs are not specific for endothelial cells, with JAM-A and JAM-C being expressed on epithelia and leukocytes and JAM-B on Sertoli cells (Bradfield et al., 2007a). The JAMs are well studied for their role in epithelial barriers and leukocyte extravasation (Bradfield et al., 2007a). ESAM was originally identified as an adhesion molecule specifically expressed on endothelial cells and platelets (Hirata et al., 2001; Nasdala et al., 2002), which is generally not expressed on epithelia, with the exception of the mesothelium (Duong et al., 2020). In addition, ESAM is a marker for primitive hematopoietic progenitors (Ooi et al., 2009; Yokota et al., 2009).

Adhesion molecules at endothelial cell contacts, which are not assigned to junctional complexes are the platelet endothelial cell adhesion molecule (PECAM)-1, CD99 and CD99L2. PECAM-1 is found on endothelial cells, various leukocytes and platelets (Lertkiatmongkol et al., 2016) and on trophoblast cells during invasion of spiral arteries (Blankenship and Enders, 1997). It is very well established for its role in leukocyte diapedesis through the endothelial barrier (Muller, 2011) and plays a role in endothelial cell integrity (Privratsky et al., 2011) as well as in pathological angiogenesis (Cao et al., 2009), although gene inactivated mice do not show vascular defects (Duncan et al., 1999). CD99 and CD99L2 are not specific for the vascular system, they participate in leukocyte extravasation (Vestweber, 2015; Muller, 2016; Li et al., 2019), but are not relevant for endothelial junction integrity or angiogenesis.

JUNCTIONAL ADHESION MECHANISMS ESSENTIAL FOR THE DEVELOPMENT OF THE BLOOD VASCULAR SYSTEM

Of the many adhesion molecules at endothelial cell contacts, VE-cadherin is the only one, which is essential for the formation of the vasculature and therefore essential for embryonic development. Gene inactivation of VE-cadherin leads in mice to embryonic lethality at E9.5 due to severe vascular defects (Carmeliet et al., 1999; Gory-Faure et al., 1999). Whereas assembly of endothelial cells in vascular structures is still possible, the subsequent remodeling and maturation is defective, resulting in gross dilation of some vessels and disconnected endothelial cells. Defects were likely related to enhanced apoptosis and lack of survival of endothelial cells (Carmeliet et al., 1999).

For ESAM, a subtle role during segmental artery formation in zebrafish embryos was suggested affecting anastomosis of intersegmental vessels when VE-cadherin was absent (Sauteur et al., 2017). However, no vascular defects were found in single ESAM zebrafish mutants, and no defects

in angiogenesis were found in ESAM$^{-/-}$ mouse embryos (Ishida et al., 2003; Wegmann et al., 2006). Pathological angiogenesis in adult ESAM$^{-/-}$ mice such as tumor angiogenesis or neovascularization of implanted matrigel plugs was impaired (Ishida et al., 2003). While ESAM deficiency in mice causes death of half of all ESAM$^{-/-}$ fetuses, this is not due to defects of the vascular system, but caused by impaired definitive hematopoiesis in the fetal liver (Ueda et al., 2019), in line with ESAM being a marker of primitive hematopoietic progenitors (Ooi et al., 2009; Yokota et al., 2009).

PECAM-1 is not essential for embryonic development, yet contributes to angiogenesis in Matrigel plug assays and *in vitro* tube formation assays (Cao et al., 2009). Likewise, occludin and Desmoglein (DSG)-2 are expressed on a subset of endothelial progenitor cells (EPCs) in human cord blood, where they support the formation of tube structures *in vitro* (Ebert et al., 2016; Kanayasu-Toyoda et al., 2018). Also, Nectin-2 supports endothelial tube formation *in vitro* (Son et al., 2016).

MAINTENANCE OF PHYSICAL INTEGRITY OF ENDOTHELIAL JUNCTIONS IN BLOOD VESSELS OF THE ADULT ORGANISM

Analyzing the need of VE-cadherin for maintenance of vascular integrity in the adult organism, it was found that induced gene inactivation of VE-cadherin (Cdh-5^{iECKO}) caused vascular leaks for plasma proteins (Frye et al., 2015). However, this effect was limited to only some organs such as heart and lung, and was not observed for skin or brain. Similar organ specific effects were caused by antibodies against VE-cadherin (Corada et al., 1999; Duong et al., 2020). Although subcutaneous bleeding followed by death was caused within several days after intraperitoneally injecting anti VE-cadherin hybridoma cells (Matsuyoshi et al., 1997), similar effects were not seen in Cdh-5^{iECKO} mice, which survived for more than 20 days without VE-cadherin (Frye et al., 2015). Interestingly, neither adhesion blocking antibodies nor gene inactivation caused plasma leaks in dermis or brain (Corada et al., 1999; Frye et al., 2015; Duong et al., 2020). More surprisingly, a detailed analysis by electron microscopy revealed that neither blocking nor gene inactivation of VE-cadherin caused physical rupture of adherens junctions, even in organs where plasma leaks were detected, like in lung and heart (Frye et al., 2015; Duong et al., 2020). This demonstrated, that once endothelial junctions have completely formed in blood vessels of various adult organs, VE-cadherin is not essential anymore for maintenance of their physical integrity. While N-cadherin can replace VE-cadherin in its absence in junctions between cultured endothelial cells (Giampietro et al., 2012; Frye et al., 2015), a similar compensation of the loss of VE-cadherin by N-cadherin could be excluded *in vivo* in VE-cadherin deficient mice (Frye et al., 2015). In addition, other cadherins were excluded since β-catenin was not detectable at endothelial junctions of micro vessels devoid of VE-cadherin (Frye et al., 2015). This is quite remarkable, since it means that, once established, endothelial adherens junctions are stable *in vivo* in the absence of a classical cadherin. This also highlights a central difference between endothelial junctions *in vitro* and *in vivo*. In summary, these studies reveal that, first, only a subset of organs such as lung and heart depend on VE-cadherin to avoid plasma leaks and, second, endothelial junctions do not lose their physical integrity in the absence of VE-cadherin even in organs where plasma leaks occur (Frye et al., 2015). Third, this surprising stability is not due to a replacement of VE-cadherin by other classical cadherins (Frye et al., 2015).

Obviously, other adhesion mechanisms must exist, which support the stability of endothelial junctions. Comparing ESAM, JAM-A and PECAM-1, it was recently shown that gene inactivation of ESAM induced plasma leaks in the lung, but not in heart, skin or brain, whereas no such effects were seen in any of these organs in the absence of JAM-A or PECAM-1 (Duong et al., 2020). Importantly, blocking of VE-cadherin with antibodies in ESAM$^{-/-}$ mice led to almost immediate lethality due to physical rupture of endothelial junctions of the lung vasculature which caused massive thrombosis, whereas no such effects were found in WT mice or mice deficient for JAM-A or PECAM-1 (Duong et al., 2020). Similar effects were seen in this study for VE-cadherin/ESAM double gene deficient mice. Thus, ESAM is essential to prevent plasma leaks in the lung vasculature and is able to prevent physical rupture of endothelial junctions in the lung if VE-cadherin is absent.

ADHESION MOLECULES WHICH REGULATE THE BARRIER FUNCTION OF BLOOD ENDOTHELIUM

In addition to the important role of VE-cadherin for endothelial junction stability, VE-cadherin is also an important and essential target for the regulation of endothelial junction opening and closure. Tyrosine phosphorylation is a key event for the regulation of VE-cadherin function and presence at junctions (Vestweber et al., 2014). Regulation of the phosphorylation of Y685 and Y658 of VE-cadherin were reported to control bradykinin induced endothelial permeability (Orsenigo et al., 2012). Based on the analysis of knock in mice expressing point mutated forms of VE-cadherin instead of WT VE-cadherin it was shown that the induction of vascular permeability by histamine or VEGF depended on the increase of phosphorylation of Y685 of VE-cadherin (Wessel et al., 2014). Interestingly, this tyrosine was not relevant for leukocyte extravasation. Instead, the dephosphorylation of Y731 of VE-cadherin was required for the diapedesis of leukocytes through endothelium *in vivo* (Wessel et al., 2014). Again, this tyrosine was only relevant for leukocyte extravasation but not for the induction of vascular permeability. Thus VE-cadherin is an important target for the opening of endothelial junctions *in vivo*, yet is addressed in different ways for the regulation of permeability and leukocyte diapedesis.

Endothelial cell-selective adhesion molecule also modulates the induction of vascular permeability and leukocyte extravasation *in vivo*, however, in a different way than expected. In ESAM gene deficient mice the induction of vascular

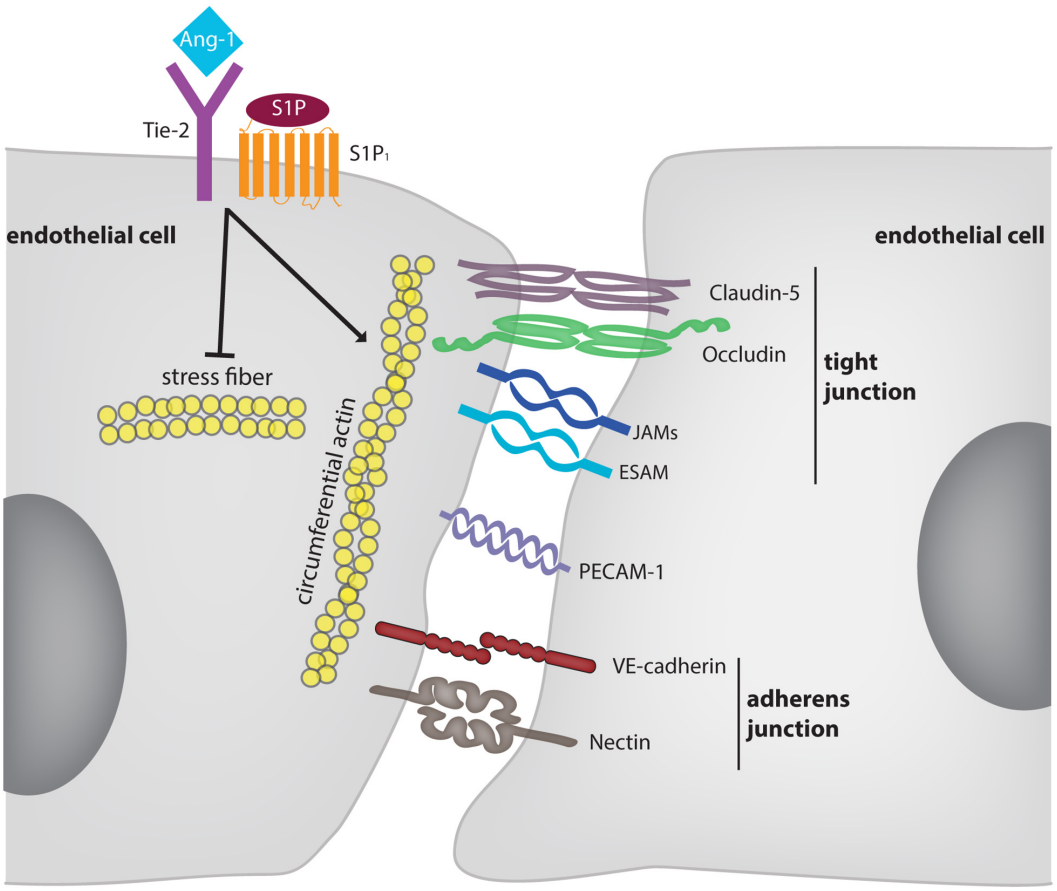

FIGURE 1 | Molecular mechanisms supporting and modulating endothelial junction integrity. The diagram depicts adhesion molecules which contribute to the barrier function of endothelium for solutes. For some of these molecules (e.g., nectins) evidence was only provided *in vitro*. Membrane proteins, such as CD99 and CD99L2 were omitted since they are selectively involved in leukocyte extravasation, but not in junction stability. The receptors Tie-2 and S1P1 are exemplary for mechanisms which stabilize endothelial junctions in an indirect way. These mechanisms are partly dependent and partly independent on VE-cadherin.

permeability by histamine and VEGF in the skin was reduced and the extravasation of leukocytes in cremaster and peritoneum was delayed (Wegmann et al., 2006). Thus, despite its supportive role of junction stability (at least in the microvasculature of the lung), ESAM assists in the opening of junctions under inflammatory conditions. This activity might be related to the support of RhoA activation in endothelial cells (Wegmann et al., 2006). Interestingly, JAM-C was also found to rather support junction destabilization, since interference with JAM-C reduced permeability induction by inflammatory mediators (Orlova et al., 2006). Mechanistically, this study showed that the loss of JAM-C enhanced Rap1 activity. A supportive role for JAM-C for permeability induction was also reported by others, in combination with effects of JAM-C on $\alpha_V\beta_3$ integrin localization and the activity of Rap1b, but not Rap1a (Li et al., 2009). With respect to leukocyte diapedesis through the endothelium, JAM-C also plays a special role. Blocking its activity with antibodies enhanced reverse transmigration of leukocytes through endothelial junctions (Bradfield et al., 2007b; Woodfin et al., 2011). Furthermore, it was found recently that local microvascular leakage promotes movement of interstitial chemokines into the bloodstream (against the direction of leakage), which supports abluminal-to-luminal transmigration of neutrophils (Owen-Woods et al., 2020).

Despite the lack of an essential role of PECAM-1 or JAM-A for endothelial junction stability in the absence of pathological challenge, a regulatory role under inflammatory settings has been established for PECAM-1. It supports maintenance of the endothelial barrier against inflammatory challenges *in vivo* (Ferrero et al., 1995; Graesser et al., 2002; Carrithers et al., 2005; Maas et al., 2005). In addition, the cytoplasmic domain of PECAM-1 supports the barrier integrity of cultured endothelial cells and recovery of junctions upon dissociation with thrombin (Liao et al., 2018). The role of JAM-A for the formation and stability of epithelial cells is very well established (Laukoetter et al., 2007), whereas its role for endothelial junctions is less well studied. In rabbits it was shown that antibodies against JAM-A caused corneal swelling and impaired junction reformation in cultured corneal endothelial cells in calcium depletion assays (Mandell et al., 2006) and LPS-induced pulmonary edema was enhanced in JAM-A$^{-/-}$ mice (Mitchell et al., 2015).

JAM-A, PECAM-1, CD99, and CD99L2 and the Nectin PVR (CD155) are all well established as supporters of leukocyte

TABLE 1 | Functions of adhesion molecules at endothelial cell contacts.

Adhesion molecule	Angiogenesis	Baseline junction integrity	Control of vascular permeability induction	Lymph-angiogenesis
PECAM-1	*In vitro* tube formation and *in vivo* matrigel plug assay (Cao et al., 2009)	No defect in endothelial junction integrity in KO mice (Duong et al., 2020)	Enhanced effects of inflammation inducing agents upon blocking or depletion (Ferrero et al., 1995; Graesser et al., 2002; Carrithers et al., 2005; Maas et al., 2005; Liao et al., 2018)	
JAM-A	Matrigel plug assays (Cooke et al., 2006); angiogenesis in corneal wound healing assays (Chatterjee et al., 2013)	No defect in endothelial junction integrity in KO mice (Duong et al., 2020)	Enhanced effects of inflammation inducing agents upon blocking or depletion (Mandell et al., 2006; Mitchell et al., 2015)	
JAM-C	Antibodies and soluble JAM-C interfere with neovascularization in the retina (Lamagna et al., 2005; Hou et al., 2012; Economopoulou et al., 2015)		Reduced effects of inflammation inducing agents upon blocking or depletion (Orlova et al., 2006; Li et al., 2009)	
ESAM	Support of VE-cadherin function in anastomosis in zebrafish embryo (Sauteur et al., 2017); no role in mouse embryonic angiogenesis (Wegmann et al., 2006; Ueda et al., 2019), but tumor angiogenesis and matrigel plug assay (Ishida et al., 2003)	Plasma leaks in lung, but not heart, skin and brain in KO mice (Duong et al., 2020); rupture of endothelial junctions in lung upon simultaneous block of ESAM and VE-cadherin (Duong et al., 2020)	Reduced effects of inflammation inducing agents upon gene inactivation (Wegmann et al., 2006)	
Cldn5		Increased leaks for small molecular weight tracers across BBB, yet no defect in tight junction ultrastructure (Nitta et al., 2003)		
DSG-2	*In vitro* tube formation from endothelial progenitors and *in vivo* matrigel plug assay (Ebert et al., 2016)			
Nectin-2	*In vitro* tube formation (Son et al., 2016)			
VE-cadherin	Embryonic lethality due to defects in vascular remodeling in gene inactivated mice (Carmeliet et al., 1999; Gory-Faure et al., 1999)	Organ specific plasma leaks upon blocking or gene inactivation (Corada et al., 1999; Frye et al., 2015; Duong et al., 2020); rupture of endothelial junctions in lung upon simultaneous block of ESAM and VE-cadherin (Duong et al., 2020)	Relevance of tyrosine phosphorylation for junction regulation (Orsenigo et al., 2012; Wessel et al., 2014)	Organ specific defects upon gene inactivation (Hägerling et al., 2018)

extravasation, which is discussed elsewhere (Nourshargh and Alon, 2014; Vestweber, 2015; Muller, 2016; Maas et al., 2018).

Claudins determine the selective permeability of tight junctions for ions or small molecular weight tracers. New born Cldn5-deficient mice showed increased passage of such tracers across the blood brain barrier, whereas the ultrastructure of tight junctions were unaffected (Nitta et al., 2003) and in a model of ischemic stroke, Cldn5 was targeted by matrix metalloproteinases (Yang et al., 2007).

Besides adhesion molecules, also the tyrosine kinase receptors Tie-2 and the sphingosine 1-phosphate receptor 1 ($S1P_1$) stabilize endothelial junctions and counteract inflammation induced vascular permeability (Thurston et al., 1999; Wang and Dudek, 2009). For both receptor systems it was shown *in vitro* that stimulation enhanced the presence of VE-cadherin at endothelial junctions or counteracted its endocytosis (Lee et al., 1999; Gavard et al., 2008). In addition, S1P had barrier enhancing effects *in vitro* even when VE-cadherin was blocked or removed (Xu et al., 2007) and endotoxin induced vascular permeability in the mouse lung could be counteracted by Tie-2 activation even in mice gene inactivated for VE-cadherin (Frye et al., 2015). Furthermore, interference with Tie-2 expression *in vivo* enhanced baseline vascular permeability in the lung, arguing that Tie-2 is also contributing to baseline vascular integrity (Frye et al., 2015). Tie-2 and $S1P_1$ stabilize endothelial junctions by modulating actomyosin fiber tension of radial stress fibers and circumferential actin via the regulation of Rac1, Cdc42, and Rho (Mammoto et al., 2007; Wang and Dudek, 2009; David et al., 2011; Frye et al., 2015; Braun et al., 2019). In addition, actin polymerization and dynamics regulate junction formation and stability (Cao and Schnittler, 2019).

Integrins can also indirectly affect endothelial junction integrity by mechanisms which still need more investigation.

Gene inactivation of the β_1-integrin chain impaired proper localization of VE-cadherin and thereby endothelial junction integrity *in vivo* (Yamamoto et al., 2015). In agreement with this, talin dependent integrin activation was reported to regulate VE-cadherin localization and endothelial barrier function (Pulous et al., 2019). The Abl kinase inhibitors imatinib and bosutinib were found to prevent LPS-induced alveolar protein extravasation in the lung and acted on junctions potentially via reducing the turnover of integrin supported focal adhesions (Aman et al., 2012; Botros et al., 2020).

DEVELOPMENT AND MAINTENANCE OF LYMPHATIC ENDOTHELIAL JUNCTIONS

The lymphatic vasculature takes up extravasated fluid and cells and transports them back to the blood circulation (Alitalo et al., 2005; Tammela and Alitalo, 2010; Koh and Petrova, 2018). Fluid entry occurs through blunt-ending initial lymphatics. Their junctions differ from those of lymphatic collectors by overlapping flaps at cell contacts, which allow fluid entry and are anchored on their sides by button like junctions (Baluk et al., 2007). While the button-like junctions contain VE-cadherin, ESAM, JAM-A, Cldn5 and occludin, the flap-like areas contain PECAM-1 (Baluk et al., 2007). Button junctions appear just before birth (Yao et al., 2012). The coxsackie- and adenovirus receptor (CAR), a protein related to the JAMs and ESAM, was described at junctions of human dermal lymph endothelial cells (Vigl et al., 2009) and its induced deletion at E12.5, but not at a later time point in development, caused dilation of subcutaneous lymphatic vessels and edema (Mirza et al., 2012).

VE-cadherin is indispensable for the development of certain lymph vessel beds (Hägerling et al., 2018). During embryonic development, deletion of VE-cadherin in lymphatic endothelial cells caused impaired lymphangiogenesis and embryonic lethality. Induced gene deletion postnatally or in the adult organism caused different effects in different organs. VE-cadherin deletion in adult mice did not impair dermal lymphatics and left button-like junctions intact. Although some adhesion molecules such as PECAM-1, JAM-A, and JAM-C were upregulated, N-cadherin expression was not affected and was not found in button like junctions. In contrast to dermal lymphatics, mesenteric lymph vessels were much more sensitive to the loss of VE-cadherin, which caused mesenteric lymph vessel disintegration, even in adults (Hägerling et al., 2018). This was accompanied by hyperproliferation of lymphatic endothelial cells in mesenteries. In addition, lymphatic valve formation was generally affected by deletion of VE-cadherin (Hägerling et al., 2018; Yang et al., 2019).

Button like lymph endothelial junctions are essential for fluid uptake. The formation of these special junctions requires the Tie-2 ligand Angiopoietin-2, and was accompanied by the phosphorylation of Y685 of VE-cadherin (Zheng et al., 2014). The induced deletion of neuropilin 1 and FLT1 was recently described as a genetic defect which prevents the formation of button like junctions by enhancing the availability of VEGF-A (Zhang et al., 2018). As a physiological inducer, the gut microbiota was discovered as an essential stimulator of VEGF-C which is needed for the formation of button like junctions in initials of the intestine (lacteals) (Suh et al., 2019).

CONCLUSION

As outlined above, VE-cadherin is certainly a major player for the formation and maintenance of endothelial junctions, in the blood as well as the lymphatic vasculature. Yet, fully established endothelial junctions can be maintained *in vivo* in the absence of VE-cadherin and even any other classical cadherin at least for weeks without physical rupture. Recent evidence established that it is ESAM which prevents rupture of vascular junctions in the lungs of these mice. Since ESAM is a tight junction-associated molecule, this raises the question how tight and adherens junctions cooperate with each other in providing vascular junction stability. In addition, we need a better understanding of the processes that regulate radial acto-myosine stress fibers and circumferential acto-myosine in cooperation with the anchoring of junctional adhesion molecules and their outside in signaling. Furthermore, crosstalk between integrin dependent focal adhesion turn over and junction stability is a newly emerging topic that is important for the understanding of endothelial junction dynamics and regulation of vascular permeability. Finally, the relevance of certain adhesion molecules and signaling mechanisms for the integrity of endothelial junctions clearly varies between different tissues, which will be an important aspect to study in the future.

AUTHOR CONTRIBUTIONS

DV and CD wrote and edited the manuscript.

FUNDING

This work was supported by grants from the Deutsche Forschungsgemeinschaft (SFB1348, B1; SFB 1009, A1; KFO 342, P2) to DV and the Max Planck Society and was performed within the DFG Excellence Cluster Cells in Motion.

REFERENCES

Adams, R. H., and Alitalo, K. (2007). Molecular regulation of angiogenesis and lymphangiogenesis. *Nat. Rev. Mol. Cell Biol.* 8, 464–478. doi: 10.1038/nrm2183

Aird, W. C. (2007a). Phenotypic Heterogeneity of the endothelium I. Structure, Function, and Mechanisms. *Circ. Res.* 100, 158–173. doi: 10.1161/01.res.0000255691.76142.4a

Aird, W. C. (2007b). Phenotypic Heterogeneity of the Endothelium II. Representative Vascular Beds. *Circ. Res.* 100, 174–190. doi: 10.1161/01.res.0000255690.03436.ae

Alitalo, K., Tammela, T., and Petrova, T. V. (2005). Lymphangiogenesis in development and human disease. *Nature* 438, 946–953. doi: 10.1038/nature04480

Aman, J., Van Bezu, J., Damanafshan, A., Huveneers, S., Eringa, E. C., Vogel, S. M., et al. (2012). Effective treatment of edema and endothelial barrier dysfunction

with imatinib. *Circulation* 126, 2728–2738. doi: 10.1161/CIRCULATIONAHA.112.134304

Augustin, H. G., and Koh, G. Y. (2017). Organotypic vasculature: from descriptive heterogeneity to functional pathophysiology. *Science* 357, 771–782. doi: 10.1126/science.aal2379

Baluk, P., Fuxe, J., Hashizume, H., Romano, T., Lashnits, E., Butz, S., et al. (2007). Functionally specialized junctions between endothelial cells of lymphatic vessels. *J. Exp. Med.* 204, 2349–2362. doi: 10.1084/jem.20062596

Bekes, I., Löb, S., Holzheu, I., Janni, W., Baumann, L., Wöckel, A., et al. (2019). Nectin-2 in ovarian cancer: How is it expressed and what might be its functional role? *Cancer Sci.* 110, 1872–1882. doi: 10.1111/cas.13992

Blankenship, T. N., and Enders, A. N. (1997). Expression of platelet-endothelial cell adhesion molecule-1 (PECAM) by macaque trophoblast cells during invasion of the spiral arteries. *Anat. Rec.* 247, 413–419. doi: 10.1002/(sici)1097-0185(199703)247:3<413::aid-ar13>3.0.co;2-s

Botros, L., Pronk, M. C. A., Juschten, J., Liddle, J., Morsing, S. K. S. H., Van Buul, J. D., et al. (2020). Bosutinib prevents vascular leakage by reducing focal adhesion turnover and reinforcing junctional integrity. *J. Cell Sci.* [Epub ahead of print].

Bradfield, P. F., Nourshargh, S., Aurrand-Lions, M., and Imhof, B. A. (2007a). JAM family and related proteins in leukocyte migration. *Arterioscler. Thromb. Vasc. Biol.* 27, 2104–2112. doi: 10.1161/atvbaha.107.147694

Bradfield, P. F., Scheiermann, C., Nourshargh, S., Ody, C., Luscinskas, F. W., Rainger, G. E., et al. (2007b). JAM-C regulates unidirectional monocyte transendothelial migration in inflammation. *Blood* 110, 2545–2555. doi: 10.1182/blood-2007-03-078733

Braun, L. J., Zinnhardt, M., Vockel, M., Drexler, H. C., Peters, K., and Vestweber, D. (2019). VE-PTP inhibition stabilizes endothelial junctions by activating FGD5. *EMBO Rep.* 20:e47046. doi: 10.15252/embr.201847046

Cao, G., Fehrenbach, M. L., Williams, J. T., Finklestein, J. M., Zhu, J. X., and Delisser, H. M. (2009). Angiogenesis in platelet endothelial cell adhesion molecule-1-null mice. *Am. J. Pathol.* 175, 903–915. doi: 10.2353/ajpath.2009.090206

Cao, J., and Schnittler, H. (2019). Putting VE-cadherin into JAIL for junction remodeling. *J. Cell Sci.* 132:jcs222893. doi: 10.1242/jcs.222893

Carmeliet, P., Lampugnani, M.-G., Moons, L., Breviario, F., Compernolle, V., Bono, F., et al. (1999). Targeted Deficiency or Cytosolic Truncation of the VE-cadherin Gene in Mice Impairs VEGF-Mediated Endothelial Survival and Angiogenesis. *Cell* 98, 147–157. doi: 10.1016/s0092-8674(00)81010-7

Carrithers, M., Tandon, S., Canosa, S., Michaud, M., Graesser, D., and Madri, J. A. (2005). Enhanced susceptibility to endotoxic shock and impaired STAT3 signaling in CD31-deficient mice. *Am. J. Pathol.* 166, 185–196. doi: 10.1016/s0002-9440(10)62243-2

Castro Dias, M., Coisne, C., Lazarevic, I., Baden, P., Hata, M., Iwamoto, N., et al. (2019). Claudin-3-deficient C57BL/6J mice display intact brain barriers. *Sci. Rep.* 9:203.

Chatterjee, S. Y., Wang, Y., Duncan, M. K., and Naik, U. P. (2013). Junctional adhesion molecule-A regulates vascular endothelial growth factor receptor-2 signaling-dependent mouse corneal wound healing. *PLoS One* 8:e63674. doi: 10.1371/journal.pone.0063674

Colom, B., Poitelon, Y., Huang, W., Woodfin, A., Averill, S., Del Carro, U., et al. (2012). Schwann cell-specific JAM-C-deficient mice reveal novel expression and functions for JAM-C in peripheral nerves. *FASEB J.* 26, 1064–1076. doi: 10.1096/fj.11-196220

Cooke, V. G., Naik, M. U., and Naik, U. P. (2006). Fibroblast growth factor-2 failed to induce angiogenesis in junctional adhesion molecule-A-deficient mice. *Arterioscler. Thromb. Vasc. Biol.* 26, 2005–2011. doi: 10.1161/01.atv.0000234923.79173.99

Corada, M., Mariotti, M., Thurston, G., Smith, K., Kunkel, R., Brockhaus, M., et al. (1999). Vascular endothelial-cadherin is an important determinant of microvascular integrity in vivo. *Proc. Natl. Acad. Sci. U.S.A.* 96, 9815–9820. doi: 10.1073/pnas.96.17.9815

David, S., Ghosh, C. C., Mukherjee, A., and Parikh, S. M. (2011). Angiopoietin-1 requires IQ domain GTPase-activating protein 1 to activate Rac1 and promote endothelial barrier defense. *Arterioscler. Thromb. Vasc. Biol.* 31, 2643–2652. doi: 10.1161/ATVBAHA.111.233189

Duncan, G. S., Andrew, D. P., Takimoto, H., Kaufman, S. A., Yoshida, H., Spellberg, J., et al. (1999). Genetic evidence for functional redundancy of platelet/endothelial cell adhesion molecule-1 (PECAM-1): CD31-deficient mice reveal PECAM-1-dependent and PECAM-1-independent functions. *J. Immunol.* 162, 3022–3030.

Duong, C. N., Nottebaum, A. F., Butz, S., Volkery, S., Zeuschner, D., Stehling, M., et al. (2020). Interference With ESAM (Endothelial Cell-Selective Adhesion Molecule) Plus Vascular Endothelial-Cadherin Causes Immediate Lethality and Lung-Specific Blood Coagulation. *Arterioscler. Thromb. Vasc. Biol.* 40, 378–393. doi: 10.1161/ATVBAHA.119.313545

Ebert, L. M., Tan, L. Y., Johan, M. Z., Min, K. K., Cockshell, M. P., Parham, K. A., et al. (2016). A non-canonical role for desmoglein-2 in endothelial cells: implications for neoangiogenesis. *Angiogenesis* 19, 463–486. doi: 10.1007/s10456-016-9520-y

Economopoulou, M., Avramovic, N., Klotzsche-Von Ameln, A., Korovina, I., Sprott, D., Samus, M., et al. (2015). Endothelial-specific deficiency of Junctional Adhesion Molecule-C promotes vessel normalisation in proliferative retinopathy. *Thromb. Haemost.* 114, 1241–1249. doi: 10.1160/TH15-01-0051

Ferrero, E., Ferrero, M. E., Pardi, R., and Zocchi, M. R. (1995). The platelet endothelial cell adhesion molecule-1 (PECAM1) contributes to endothelial barrier function. *FEBS Lett.* 374, 323–326. doi: 10.1016/0014-5793(95)01110-z

Frye, M., Dierkes, M., Küppers, V., Vockel, M., Tomm, J., Zeuschner, D., et al. (2015). Interfering with VE-PTP stabilizes endothelial junctions in vivo via Tie-2 in the absence of VE-cadherin. *J. Exp. Med.* 212, 2267–2287. doi: 10.1084/jem.20150718

Gavard, J., Patel, V., and Gutkind, J. S. (2008). Angiopoietin-1 prevents VEGF-induced endothelial permeability by sequestering Src through mDia. *Dev. Cell* 14, 25–36. doi: 10.1016/j.devcel.2007.10.019

Giampietro, C., Taddei, A., Corada, M., Sarra-Ferraris, G. M., Alcalay, M., Cavallaro, U., et al. (2012). Overlapping and divergent signaling pathways of N-cadherin and VE-cadherin in endothelial cells. *Blood* 119, 2159–2170. doi: 10.1182/blood-2011-09-381012

Gory-Faure, S., Prandini, M. H., Pointu, H., Roullot, V., Pignot-Paintrand, I., Vernet, M., et al. (1999). Role of vascular endothelial-cadherin in vascular morphogenesis. *Development* 126, 2093–2102.

Gotsch, U., Borges, E., Bosse, R., Böggemeyer, E., Simon, M., Mossmann, H., et al. (1997). VE-cadherin antibody accelerates neutrophil recruitment *in vivo*. *J. Cell Sci.* 110, 583–588.

Graesser, D., Solowiej, A., Bruckner, M., Osterweil, E., Juedes, A., Davis, S., et al. (2002). Altered vascular permeability and early onset of experimental autoimmune encephalomyelitis in PECAM-1-deficient mice. *J. Clin. Invest.* 109, 383–392. doi: 10.1172/jci0213595

Gulino, D., Delachanal, E., Concord, E., Genoux, Y., Morand, B., Valiron, M. O., et al. (1998). Alteration of endothelial cell monolayer integrity triggers resynthesis of vascular endothelium cadherin. *J. Biol. Chem.* 273, 29786–29793. doi: 10.1074/jbc.273.45.29786

Hägerling, R., Hoppe, E., Dierkes, C., Stehling, M., Makinen, T., Butz, S., et al. (2018). Distinct roles of VE-cadherin for development and maintenance of specific lymph vessel beds. *EMBO J.* 37:e98271. doi: 10.15252/embj.201798271

Hirata, K., Ishida, T., Penta, K., Rezaee, M., Yang, E., Wohlgemuth, J., et al. (2001). Cloning of an immunoglobulin family adhesion molecule selectively expressed by endothelial cells. *J. Biol. Chem.* 276, 16223–16231. doi: 10.1074/jbc.m100630200

Hou, X., Hu, D., Wang, Y. S., Tang, Z. S., Zhang, F., Chavakis, T., et al. (2012). Targeting of junctional adhesion molecule-C inhibits experimental choroidal neovascularization. *Invest. Ophthalmol. Vis. Sci.* 53, 1584–1591. doi: 10.1167/iovs.11-9005

Ishida, T., Kundu, R. K., Yang, E., Hirata, K., Ho, Y. D., and Quertermous, T. (2003). Targeted disruption of endothelial cell-selective adhesion molecule inhibits angiogenic processes *in vitro* and *in vivo*. *J. Biol. Chem.* 278, 34598–34604. doi: 10.1074/jbc.m304890200

Kanayasu-Toyoda, T., Ishii-Watabe, A., Kikuchi, Y., Kitagawa, H., Suzuki, H., Tamura, H., et al. (2018). Occludin as a functional marker of vascular endothelial cells on tube-forming activity. *J. Cell. Physiol.* 233, 1700–1711. doi: 10.1002/jcp.26082

Koh, G. Y., and Petrova, T. V. (2018). Orga-specific lymphatic vasculature: from development to pathophysiology. *J. Exp. Med.* 215, 35–49. doi: 10.1084/jem.20171868

Lamagna, C., Hodivala-Dilke, K. M., Imhof, B. A., and Aurrand-Lions, M. (2005). Antibody against junctional adhesion molecule-C inhibits angiogenesis and

tumor growth. *Cancer Res.* 65, 5703–5710. doi: 10.1158/0008-5472.can-04-4012

Laukoetter, M. G., Nava, P., Lee, W. Y., Severson, E. A., Capaldo, C. T., Babbin, B. A., et al. (2007). JAM-A regulates permeability and inflammation in the intestine *in vivo*. *J. Exp. Med.* 204, 3067–3076. doi: 10.1084/jem.20071416

Lee, M. J., Thangada, S., Claffey, K. P., Ancellin, N., Liu, C. H., Kluk, M., et al. (1999). Vascular endothelial cell adherens junction assembly and morphogenesis induced by sphingosine-1-phosphate. *Cell* 99, 301–312. doi: 10.1016/s0092-8674(00)81661-x

Lertkiatmongkol, P., Liao, D., Mei, H., Hu, Y., and Newman, P. J. (2016). Endothelial functions of platelet/endothelial cell adhesion molecule-1 (CD31). *Curr. Opin. Hematol.* 23, 253–259. doi: 10.1097/moh.0000000000000239

Li, X., Stankovic, M., Lee, B. P., Aurrand-Lions, M., Hahn, C. N., Lu, Y., et al. (2009). JAM-C induces endothelial cell permeability through its association and regulation of {beta}3 integrins. *Arterioscler. Thromb. Vasc. Biol.* 29, 1200–1206. doi: 10.1161/ATVBAHA.109.189217

Li, Y. T., Goswami, D., Follmer, M., Artz, A., Pacheco-Blanco, M., and Vestweber, D. (2019). Blood flow guides sequential support of neutrophil arrest and diapedesis by PILR-β1 and PILR-α. *eLife* 8:e47642. doi: 10.7554/eLife.47642

Liao, D., Mei, H., Hu, Y., Newman, D. K., and Newman, P. J. (2018). CRISPR-mediated deletion of the PECAM-1 cytoplasmic domain increases receptor lateral mobility and strengthens endothelial cell junctional integrity. *Life Sci.* 193, 186–193. doi: 10.1016/j.lfs.2017.11.002

Liebner, S., Corada, M., Bangsow, T., Babbage, J., Taddei, A., Czupalla, C. J., et al. (2008). Wnt/beta-catenin signaling controls development of the blood-brain barrier. *J. Cell Biol.* 183, 409–417. doi: 10.1083/jcb.200806024

Maas, M., Stapleton, M., Bergom, C., Mattson, D. L., Newman, D. K., and Newman, P. J. (2005). Endothelial cell PECAM-1 confers protection against endotoxic shock. *Am. J. Physiol. Heart Circ. Physiol.* 288, H159–H164.

Maas, S. L., Soehnlein, O., and Viola, J. R. (2018). Organ-Specific mechanisms of transendothelial neutrophil migration in the lung, liver, kidney, and aorta. *Front. Immunol.* 9:2739. doi: 10.3389/fimmu.2018.02739

Mammoto, T., Parikh, S. M., Mammoto, A., Gallagher, D., Chan, B., Mostoslavsky, G., et al. (2007). Angiopoietin-1 requires p190 RhoGAP to protect against vascular leakage *in vivo*. *J. Biol. Chem.* 282, 23910–23918. doi: 10.1074/jbc.m702169200

Mandell, K. J., Holley, G. P., Parkos, C. A., and Edelhauser, H. F. (2006). Antibody blockade of junctional adhesion molecule-A in rabbit corneal endothelial tight junctions produces corneal swelling. *Invest. Ophthalmol. Vis. Sci.* 47, 2408–2416.

Martin, T. A., Lane, J., Harrison, G. M., and Jiang, W. G. (2013). The expression of the nectin complex in human breast cancer and the role of nectin-3 in the control of tight junctions during metastasis. *PLoS One* 8:e82696. doi: 10.1371/journal.pone.0082696

Matsuyoshi, N., Toda, K., Horiguchi, Y., Tanaka, T., Nakagawa, S., Takeichi, M., et al. (1997). In vivo evidence of the critical role of cadherin-5 in murine vascular integrity. *Proc. Assoc. Am. Phys.* 109, 362–371.

Mirza, M., Pang, M. F., Zaini, M. A., Haiko, P., Tammela, T., Alitalo, K., et al. (2012). Essential role of the coxsackie- and adenovirus receptor (CAR) in development of the lymphatic system in mice. *PLoS One* 7:e37523. doi: 10.1371/journal.pone.0037523

Mitchell, L. A., Ward, C., Kwon, M., Mitchell, P. O., Quintero, D. A., Nusrat, A., et al. (2015). Junctional adhesion molecule A promotes epithelial tight junction assembly to augment lung barrier function. *Am. J. Pathol.* 185, 372–386. doi: 10.1016/j.ajpath.2014.10.010

Morita, K., Sasaki, H., Furuse, M., and Tsukita, S. (1999). Endothelial claudin: claudin-5/TMVCF constitutes tight junction strands in endothelial cells. *J. Cell Biol.* 147, 185–194.

Muller, W. A. (2011). Mechanisms of leukocyte transendothelial migration. *Annu. Rev. Pathol.* 6, 323–344. doi: 10.1146/annurev-pathol-011110-130224

Muller, W. A. (2016). Transendothelial migration: unifying principles from the endothelial perspective. *Immunol. Rev.* 273, 61–75. doi: 10.1111/imr.12443

Nasdala, I., Wolburg-Buchholz, K., Wolburg, H., Kuhn, A., Ebnet, K., Brachtendorf, G., et al. (2002). A transmembrane tight junction protein selectively expressed on endothelial cells and platelets. *J. Biol. Chem.* 277, 16294–16303. doi: 10.1074/jbc.m111999200

Nitta, T., Hata, M., Gotoh, S., Seo, Y., Sasaki, H., Hashimoto, N., et al. (2003). Size-selective loosening of the blood-brain barrier in claudin-5-deficient mice. *J. Cell Biol.* 161, 653–660. doi: 10.1083/jcb.200302070

Nourshargh, S., and Alon, R. (2014). Leukocyte migration into inflamed tissues. *Immunity* 41, 694–707. doi: 10.1016/j.immuni.2014.10.008

Ohtsuki, S., Yamaguchi, H., Katsukura, Y., Asashima, T., and Terasaki, T. (2008). mRNA expression levels of tight junction protein genes in mouse brain capillary endothelial cells highly purified by magnetic cell sorting. *J. Neurochem.* 104, 147–154.

Ooi, A. G., Karsunky, H., Majeti, R., Butz, S., Vestweber, D., Ishida, T., et al. (2009). The adhesion molecule esam1 is a novel hematopoietic stem cell marker. *Stem Cells* 27, 653–661. doi: 10.1634/stemcells.2008-0824

Orlova, V. V., Economopoulou, M., Lupu, F., Santoso, S., and Chavakis, T. (2006). Junctional adhesion molecule-C regulates vascular endothelial permeability by modulating VE-cadherin-mediated cell-cell contacts. *J. Exp. Med.* 203, 2703–2714.

Orsenigo, F., Giampietro, C., Ferrari, A., Corada, M., Galaup, A., Sigismund, S., et al. (2012). Phosphorylation of VE-cadherin is modulated by haemodynamic forces and contributes to the regulation of vascular permeability *in vivo*. *Nat. Commun.* 3:1208. doi: 10.1038/ncomms2199

Ouyang, X., Dong, C., and Ubogu, E. E. (2019). In situ molecular characterization of endoneurial microvessels that form the blood-nerve barrier in normal human adult peripheral nerves. *J. Peripher. Nerv. Syst.* 24, 195–206. doi: 10.1111/jns.12326

Owen-Woods, C., Joulia, R., Baraway, A., Rolas, L., Ma, B., Nottebaum, A. F., et al. (2020). Local microvascular leakage promotes trafficking of activated neutrophils to remote organs *in vivo*. *J. Clin. Invest.* 130, 2301–2318. doi: 10.1172/JCI133661

Potente, M., and Mäkinen, T. (2017). Vascular heterogeneity and specialization in development and disease. *Nat. Rev. Mol. Cell Biol.* 18, 477–494. doi: 10.1038/nrm.2017.36

Privratsky, J. R., Paddock, C. M., Florey, O., Newman, D. K., Muller, W. A., and Newman, P. J. (2011). Relative contribution of PECAM-1 adhesion and signaling to the maintenance of vascular integrity. *J. Cell Sci.* 124, 1477–1485. doi: 10.1242/jcs.082271

Pulous, F. E., Grimsley-Myers, C. M., Kansal, S., Kowalczyk, A. P., and Petrich, B. G. (2019). Talin-dependent integrin activation regulates VE-Cadherin localization and endothelial cell barrier function. *Circ. Res.* 124, 891–903. doi: 10.1161/CIRCRESAHA.118.314560

Reymond, N., Imbert, A. M., Devilard, E., Fabre, S., Chabannon, C., Xerri, L., et al. (2004). DNAM-1 and PVR regulate monocyte migration through endothelial junctions. *J. Exp. Med.* 199, 1331–1341.

Rikitake, Y., Mandai, K., and Takai, Y. (2015). Nectins and nectin-like molecules in development and disease. *J. Cell Sci.* 125, 3713–3722. doi: 10.1016/bs.ctdb.2014.11.019

Saitou, M., Furuse, M., Sasaki, H., Schulzke, J. D., Fromm, M., Takano, H., et al. (2000). Complex phenotype of mice lacking occludin, a component of tight junction strands. *Mol. Biol. Cell* 11, 4131–4142.

Sauteur, L., Affolter, M., and Belting, H. G. (2017). Distinct and redundant functions of Esama and VE-cadherin during vascular morphogenesis. *Development* 144, 1554–1565. doi: 10.1242/dev.140038

Simionescu, M., Simionescu, N., and Palade, G. E. (1976). Segmental differentiations of cell junctions in the vascular endothelium, Arteries and veins. *J. Cell Biol.* 68, 705–723.

Smith, M. E. F., Jones, T. A., and Hilton, D. (1998). Vascular endothelial cadherin is expressed by perineural cells of peripheral nerve. *Histopathology* 32, 411–413.

Son, Y., Lee, B., Choi, Y. J., Jeon, S. A., Kim, J. H., Lee, H. K., et al. (2016). Nectin-2 (CD112) is expressed on outgrowth endothelial cells and regulates cell proliferation and angiogenic function. *PLoS One* 11:e0163301. doi: 10.1371/journal.pone.0163301

Suh, S. H., Choe, K., Hong, S. P., Jeong, S. H., Mäkinen, T., Kim, K. S., et al. (2019). Gut microbiota regulates lacteal integrity by inducing VEGF-C in intestinal villus macrophages. *EMBO Rep.* 20:e46927. doi: 10.15252/embr.201846927

Tammela, T., and Alitalo, K. (2010). Lymphangiogenesis: molecular mechanisms and future promise. *Cell* 140, 460–476. doi: 10.1016/j.cell.2010.01.045

Thurston, G., Suri, C., Smith, K., Mcclain, J., Sato, T. N., Yancopoulos, G. D., et al. (1999). Leakage-resistant blood vessels in mice transgenically overexpressing angiopoietin-1. *Science* 286, 2511–2514.

Tietz, S., and Engelhardt, B. (2015). Brain barriers: Crosstalk between complex tight junctions and adherens junctions. *J. Cell Biol.* 209, 493–506. doi: 10.1083/jcb.201412147

Trani, M., and Dejana, E. (2015). New insights in the control of vascular permeability: vascular endothelial-cadherin and other players. *Curr. Opin. Hematol.* 22, 267–272. doi: 10.1097/MOH.0000000000000137

Ueda, T., Yokota, T., Okuzaki, D., Uno, Y., Mashimo, T., Kubota, Y., et al. (2019). Endothelial cell-selective adhesion molecule contributes to the development of definitive hematopoiesis in the fetal liver. *Stem Cell Rep.* 13, 992–1005. doi: 10.1016/j.stemcr.2019.11.002

Vanlandewijck, M., He, L., Mäe, M. A., Andrae, J., Ando, K., Del Gaudio, F., et al. (2018). A molecular atlas of cell types and zonation in the brain vasculature. *Nature* 554, 475–480. doi: 10.1038/nature25739

Vestweber, D. (2015). How leukocytes cross the vascular endothelium. *Nat. Rev. Immunol.* 15, 692–704. doi: 10.1038/nri3908

Vestweber, D., Wessel, F., and Nottebaum, A. F. (2014). Similarities and differences in the regulation of leukocyte extravasation and vascular permeability. *Semin. Immunopathol.* 36, 177–192. doi: 10.1007/s00281-014-0419-7

Vigl, B., Zgraggen, C., Rehman, N., Banziger-Tobler, N. E., Detmar, M., and Halin, C. (2009). Coxsackie- and adenovirus receptor (CAR) is expressed in lymphatic vessels in human skin and affects lymphatic endothelial cell function in vitro. *Exp. Cell Res.* 315, 336–347. doi: 10.1016/j.yexcr.2008.10.020

Wang, L., and Dudek, S. M. (2009). Reguation of vascular permeability by sphingosine 1-phosphate. *Microvasc. Res.* 77, 39–45. doi: 10.1016/j.mvr.2008.09.005

Wegmann, F., Petri, J., Khandoga, A. G., Moser, C., Khandoga, A., Volkery, S., et al. (2006). ESAM supports neutrophil extravasation, activation of Rho and VEGF-induced vascular permeability. *J. Exp. Med.* 203, 1671–1677.

Wessel, F., Winderlich, M., Holm, M., Frye, M., Rivera-Galdos, R., Vockel, M., et al. (2014). Leukocyte extravasation and vascular permeability are each controlled in vivo by a different tyrosine residue of VE-cadherin. *Nat. Immunol.* 15, 223–230. doi: 10.1038/ni.2824

Woodfin, A., Voisin, M. B., Beyrau, M., Colom, B., Caille, D., Diapouli, F. M., et al. (2011). The junctional adhesion molecule JAM-C regulates polarized transendothelial migration of neutrophils *in vivo*. *Nat. Immunol.* 12, 761–769. doi: 10.1038/ni.2062

Xu, M., Waters, C. L., Hu, C., Wysolmerski, R. B., Vincent, P. A., and Minnear, F. L. (2007). Sphingosine 1-phosphate rapidly increases endothelial barrier function independently of VE-cadherin but requires cell spreading and Rho kinase. *Am. J. Physiol. Cell. Physiol.* 293, C1309–C1318.

Yamamoto, H., Ehling, M., Kato, K., Kanai, K., Van Lessen, M., Frye, M., et al. (2015). Integrin β1 controls VE-cadherin localization and blood vessel stability. *Nat. Commun.* 6:6429. doi: 10.1038/ncomms7429

Yang, Y., Cha, B., Motawe, Z. Y., Srinivasan, R. S., and Scallan, J. P. (2019). VE-Cadherin is required for lymphatic valve formation and maintenance. *Cell Rep.* 28, 2397–2412. doi: 10.1016/j.celrep.2019.07.072

Yang, Y., Estrada, E. Y., Thompson, J. F., Liu, W., and Rosenberg, G. A. (2007). Matrix metalloproteinase-mediated disruption of tight junction proteins in cerebral vessels is reversed by synthetic matrix metalloproteinase inhibitor in focal ischemia in rat. *J. Cereb. Blood Flow Metab.* 27, 697–709.

Yao, L. C., Baluk, P., Srinivasan, R. S., Oliver, G., and Mcdonald, D. M. (2012). Plasticity of button-like junctions in the endothelium of airway lymphatics in development and inflammation. *Am. J. Pathol.* 180, 2561–2575. doi: 10.1016/j.ajpath.2012.02.019

Yokota, T., Oritani, K., Butz, S., Kokame, K., Kincade, P. W., Miyata, T., et al. (2009). The endothelial antigen ESAM marks primitive hematopoietic progenitors throughout life in mice. *Blood* 113, 2914–2923. doi: 10.1182/blood-2008-07-167106

Zhang, F., Zarkada, G., Han, J., Li, J., Dubrac, A., Ola, R., et al. (2018). Lacteal junction zippering protects against diet-induced obesity. *Science* 361, 599–603. doi: 10.1126/science.aap9331

Zheng, W., Nurmi, H., Appak, S., Sabine, A., Bovay, E., Korhonen, E. A., et al. (2014). Angiopoietin 2 regulates the transformation and integrity of lymphatic endothelial cell junctions. *Genes Dev.* 28, 1592–1603. doi: 10.1101/gad.237677.114

Conflict of Interest: The authors declare that the research was conducted in the absence of any commercial or financial relationships that could be construed as a potential conflict of interest.

frontiers in Cell and Developmental Biology

ORIGINAL RESEARCH
published: 26 May 2020
doi: 10.3389/fcell.2020.00395

NRP2 as an Emerging Angiogenic Player; Promoting Endothelial Cell Adhesion and Migration by Regulating Recycling of α5 Integrin

Abdullah A. A. Alghamdi[1†‡], Christopher J. Benwell[2†], Samuel J. Atkinson[1‡], Jordi Lambert[3‡], Robert T. Johnson[1‡] and Stephen D. Robinson[1,2]*

[1] School of Biological Sciences, University of East Anglia, Norwich Research Park, Norwich, United Kingdom, [2] Gut Microbes and Health, Quadram Institute Bioscience, Norwich Research Park, Norwich, United Kingdom, [3] Faculty of Medicine and Health Sciences, University of East Anglia, Norwich Research Park, Norwich, United Kingdom

Angiogenesis relies on the ability of endothelial cells (ECs) to migrate over the extracellular matrix via integrin receptors to respond to an angiogenic stimulus. Of the two neuropilin (NRP) orthologs to be identified, both have been reported to be expressed on normal blood and lymphatic ECs, and to play roles in the formation of blood and lymphatic vascular networks during angiogenesis. Whilst the role of NRP1 and its interactions with integrins during angiogenesis has been widely studied, the role of NRP2 in ECs is poorly understood. Here we demonstrate that NRP2 promotes Rac-1 mediated EC adhesion and migration over fibronectin (FN) matrices in a mechanistically distinct fashion to NRP1, showing no dependence on β3 integrin (ITGB3) expression, or VEGF stimulation. Furthermore, we highlight evidence of a regulatory crosstalk between NRP2 and α5 integrin (ITGA5) in ECs, with NRP2 depletion eliciting an upregulation of ITGA5 expression and disruptions in ITGA5 cellular organization. Finally, we propose a mechanism whereby NRP2 promotes ITGA5 recycling in ECs; NRP2 depleted ECs were found to exhibit reduced levels of total ITGA5 subunit recycling compared to wild-type (WT) ECs. Our findings expose NRP2 as a novel angiogenic player by promoting ITGA5-mediated EC adhesion and migration on FN.

Keywords: Neuropilins, endothelium, integrins, protein trafficking, cell migration

OPEN ACCESS

Edited by:
Stephan Huveneers, Amsterdam University Medical Center (UMC), Netherlands

Reviewed by:
Eloi Montanez, University of Barcelona, Spain
Jaap Diederik Van Buul, University of Amsterdam, Netherlands

***Correspondence:**
Stephen D. Robinson
stephen.robinson@quadram.ac.uk

† These authors have contributed equally to this work

‡ Present address:
Abdullah A. A. Alghamdi, Department of Biology, Faculty of Science, Albaha University, Albaha, Saudi Arabia
Samuel J. Atkinson, Cancer Research UK Beatson Institute, Glasgow, United Kingdom
Jordi Lambert, Division of Cardiovascular Medicine, University of Cambridge, Cambridge Biomedical Campus, Cambridge, United Kingdom
Robert T. Johnson, School of Pharmacy, University of East Anglia, Norwich Research Park, Norwich, United Kingdom

Specialty section:
This article was submitted to Cell Adhesion and Migration, a section of the journal Frontiers in Cell and Developmental Biology

Received: *07 February 2020*
Accepted: *29 April 2020*
Published: *26 May 2020*

Citation:
Alghamdi AAA, Benwell CJ, Atkinson SJ, Lambert J, Johnson RT and Robinson SD (2020) NRP2 as an Emerging Angiogenic Player; Promoting Endothelial Cell Adhesion and Migration by Regulating Recycling of α5 Integrin. Front. Cell Dev. Biol. 8:395. doi: 10.3389/fcell.2020.00395

INTRODUCTION

Neuropilins (NRPs) are single non-tyrosine kinase receptors belonging to a family of type I transmembrane glycoproteins (MW ∼130–140 kDa) (Soker et al., 1998). To date, two NRP orthologs have been identified in vertebrates, NRP1 and NRP2, both of which share a very similar domain structure and an overall 44% amino acid homology (Pellet-Many et al., 2008; Zachary, 2014). Their expression and function have been identified in many cell types, including nerve cells, endothelial cells (ECs), epithelial cells, immune cells, osteoblasts and tumor cells (Bielenberg et al., 2004; Zachary, 2014). In ECs, it is believed that NRPs play an essential role in sprouting angiogenesis and lymphogenesis through the selective binding to members of the vascular endothelial growth factor (VEGF) family. Following this complex formation, NRPs function as co-receptors with VEGFRs to enhance the VEGF-induced

activation of many intracellular pathways (Prahst et al., 2008). As such, the functions of NRP have been implicated in influencing cell adhesion, migration and permeability during angiogenesis, under both physiological and pathological conditions (Fukasawa et al., 2007; Valdembri et al., 2009; Ellison et al., 2015). Studies have, however, provided evidence to suggest that NRPs can mediate ligand signaling independently of VEGFRs, in addition to regulating VEGFRs independently of VEGF binding. Based on early transgenic mouse studies in this field, it was originally speculated that NRP1 is mainly expressed on arteries, arterioles and capillaries, whereas NRP2 is expressed on veins, venules and lymphatic vessels (Herzog et al., 2001; Yuan et al., 2002). However, subsequent studies have revealed that both NRPs are expressed in normal blood and lymphatic ECs, and both play essential roles in forming blood and lymphatic vasculature networks (Bouvree et al., 2012; Jurisic et al., 2012; Mucka et al., 2016). Despite this, investigations into elucidating the roles of endothelial NRPs during angiogenesis have, for the most part, focused on NRP1 (Zachary, 2014). With regard to NRP2, studies have instead focused on annotating a role in cancer cells, where its upregulation is consistent with cancer progression in a number of cell types [e.g., neuroblastomas (Fakhari et al., 2002), non-small cell lung carcinoma [NSCLC] (Kawakami et al., 2002), human prostate carcinoma, melanoma (Bielenberg et al., 2004), lung cancer (Tomizawa et al., 2001; Kawakami et al., 2002; Lantuejoul et al., 2003), myeloid leukemia (Vales et al., 2007), breast cancer (Bachelder et al., 2001) and pancreatic cancer (Fukahi et al., 2004)]. Interestingly, Favier et al. (2006) recapitulated this upregulation of NRP2 observed in cancer cells by overexpressing NRP2 in human microvascular ECs (hMVECs), and found that cell survival in these ECs was significantly increased following stimulation with either VEGF-A- or VEGF-C. Furthermore, NRP2 knockdown significantly inhibited both VEGF-A- and VEGFC-induced migration, suggesting that NRP2 as a potential pharmacological target. Crucially, this work highlighted the importance of understanding the cross-talk between NRP2 and other receptors (mainly VEGF, integrins and plexins) in ECs, which will aid in the design of novel drugs to better control the mechanisms underlying angiogenesis and lymphangiogenesis in autoimmune diseases and tumor development (Favier et al., 2006). We have previously described a link between NRP1 and the β3-integrin (ITGB3) subunit during VEGF-induced angiogenesis. We reported that complete loss of the Itgb3 gene enhanced EC permeability through the upregulation of VEGF-VEGFR2-ERK1/2 signaling (Robinson et al., 2004), and that NRP1 and ERK1/2 expression was elevated in ITGB3-NULL ECs. Subsequent targeting of NRP1 in ITGB3-NULL mice revealed a significant inhibition of VEGF-induced angiogenesis compared to WT mice, indicating that the elevation of angiogenesis in the absence of the Itgb3 gene is dependent on NRP1 expression (Robinson et al., 2009; Ellison et al., 2015). In this study we aimed to investigate whether NRP2 shares a similar interaction with ITGB3 or other integrins in ECs.

RESULTS

NRP2 Function Is Not Regulated by ITGB3 During VEGFR2-Mediated Signaling or Migration Over FN Matrices

We previously showed the involvement of NRP1 during VEGF-stimulated angiogenesis to be dependent upon ITGB3 in ECs (Ellison et al., 2015). Due to the structural homology between NRP1 and NRP2 (Zachary, 2014), we decided to first consider whether, like NRP1, NRP2's function shares a dependency on ITGB3 during VEGF-mediated angiogenic responses in ECs. To investigate this, we isolated mouse lung microvascular endothelial cells (mLMECs) from both wild-type (WT) and ITGB3-heterozygous (β3HET) mice and immortalized them with polyoma-middle-T antigen (PyMT) by retroviral transduction. As in previous studies, we decided to use β3HET cells for these analyses, rather than β3-integrin knockout (β3NULL) cells, because we have shown they are a good model for studying the role of αvβ3-integrin in cell migration, whilst evading changes arising from the complete loss of the integrin on both alleles (e.g., up-regulated VEGFR2 expression) (Ellison et al., 2015; Atkinson et al., 2018). DNA was extracted from multiple immortalized lines and analyzed by PCR to confirm their genetic status as either WT or β3HET cells (**Supplementary Figure S1A**). We subsequently confirmed the EC identity of each immortalized line by examining the expression of EC markers including VE-Cadherin (Sivarapatna et al., 2015; Ikuno et al., 2017), in addition to quantifying the expression of ITGB3 in β3HET ECs. Each clone was confirmed to express canonical EC markers, and all β3HET ECs were confirmed to express approximately 50% ITGB3 compared to their WT counterparts (**Supplementary Figures S1B–D**). We reported previously that in β3HET ECs, NRP1 expression is upregulated, and that NRP1 appeared only to play a role in post development angiogenesis when ITGB3 expression is reduced (Ellison et al., 2015). Western blot quantification of NRP2 expression between WT and β3HET protein lysates showed a similar elevation in NRP2 expression in β3HET ECs (**Figure 1A**), suggesting the existence of a regulatory nexus between NRP2 and ITGB3, which we felt warranted further exploration.

As NRP2 has been shown to regulate VEGF-induced signaling in both human lymphatic (Caunt et al., 2008), and lymphatic microvascular ECs, we examined whether NRP2 regulates proangiogenic signaling responses to VEGF and if the effects are dependent on ITGB3. Using NRP2 specific siRNA (**Supplementary Figure S1E**) versus a control siRNA transfected into our WT and β3HET ECs, we measured differences in VEGFR2 and ERK phosphorylation over a time course of 15 min. We observed only marginally attenuated VEGFR2 and ERK phosphorylation by Western blot analysis in response to NRP2 silencing and, importantly, saw no differences between WT and β3HET ECs (**Figure 1B**), suggesting that ITGB3 does not regulate NRP2 dependent VEGF induced signaling in our cells.

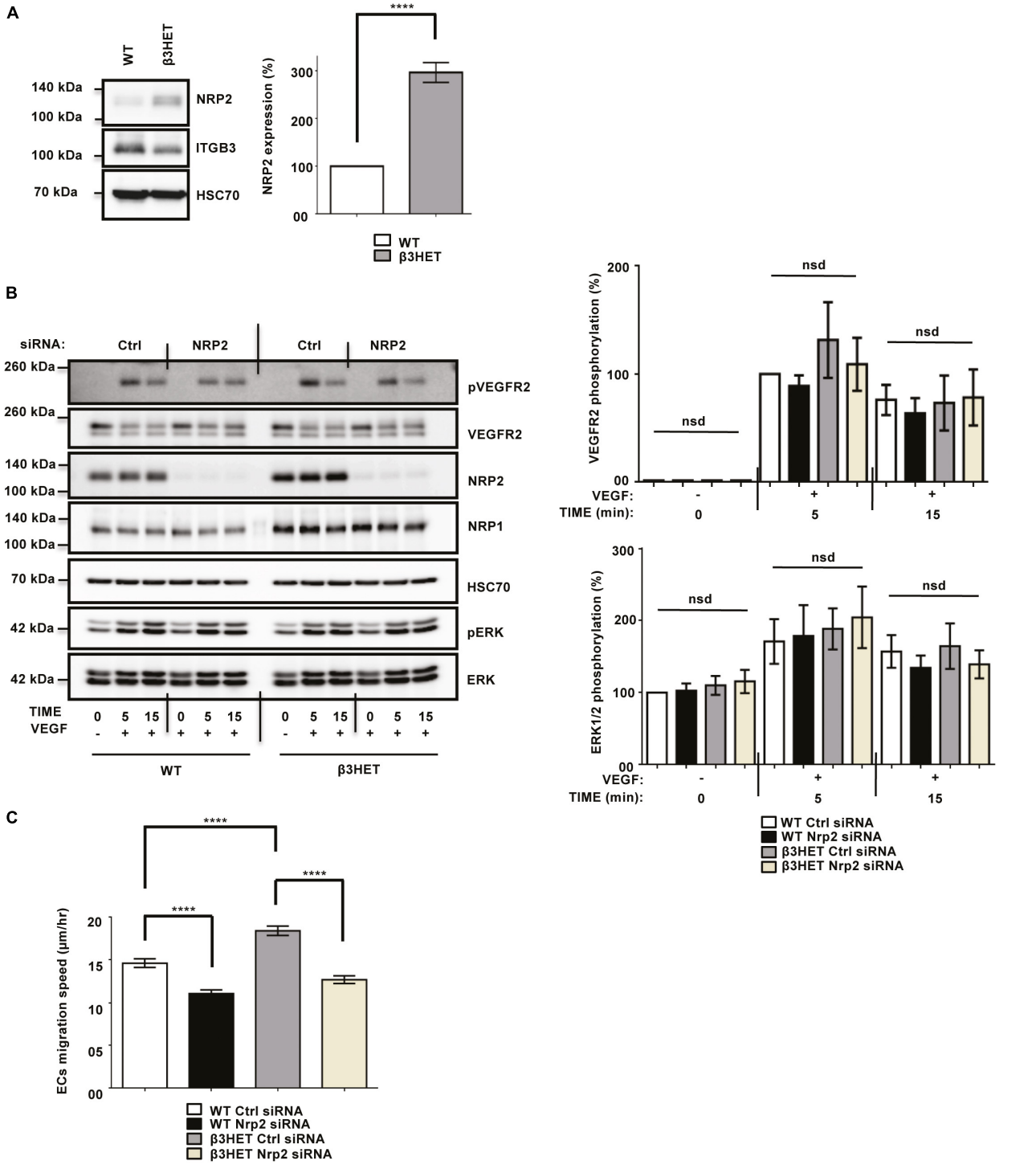

FIGURE 1 | NRP2 is not regulated by ITGB3 during VEGFR2-mediated signaling or during migration over FN. **(A)**: WT and β3HET ECs were plated onto FN and incubated for 48 h at 37°C and 5% CO_2. EC extracts were immunoblotted using antibodies to NRP2, ITGB3 and HSC70. $N = 3$ independent experiments, $^{****}P < 0.0001$. **(B,C)**: siRNA-transfected ECs were plated onto FN and incubated for 48 h at 37°C and 5% CO_2. ECs were subsequently starved in serum-free media and stimulated with VEGF (30 ng/ml) for the indicated timepoints. EC extracts were immunoblotted using antibodies to phospho-VEGFR2, VEGFR2, NRP2, NRP1, HSC70, phospho-ERK and ERK. $N = 6$ independent experiments, $P > 0.05$ (nsd). Left panel shows representative Western blot images, right panel shows densitometric analysis of band intensities normalized against HSC70 and obtained using ImageJ™. Asterisks indicate statistical significance, nsd indicates no significant difference from unpaired two-tailed *t*-tests. **(C)**: siRNA-transfected ECs were seeded onto FN and incubated for 3 h at 37°C and 5% CO_2. Fixed images were taken every 10 min for 15 h at 37°C and 5% CO_2 using an inverted Zeiss Axiovert microscope with one-phase contrast. Random migration speed was quantified using the ImageJ™ plugin mTrackJ in μm/hour. $N = 4$ independent experiments, $n \geq 30$ ECs per experimental condition, $^{****}P < 0.0001$.

To explore the possibility of a regulatory axis between NRP2 and ITGB3 further, we examined cellular migration. Angiogenesis relies on the ability of ECs to respond to angiogenic stimuli by migrating over an extracellular matrix (ECM). We have shown previously that NRP1 plays a role in promoting EC migration over fibronectin (FN) matrices, but only when ITGB3 levels are reduced (Ellison et al., 2015). Independent studies have also described NRP2 silencing to inhibit migration of human microvascular ECs (Favier et al., 2006) and human lymphatic ECs (Caunt et al., 2008). We therefore chose to examine the effects of NRP2 depletion on EC migration over FN in our mLMECs, and to determine whether any effect is dependent upon ITGB3 expression. To achieve this, control and NRP2 siRNA transfected WT and β3HET ECs were plated on FN and random migration speed was measured by time-lapse microscopy over 15 h. As previously reported, we observed β3HET ECs migrate faster over a FN matrix than WT ECs (Ellison et al., 2015). However, unlike NRP1, whilst depletion of NRP2 significantly reduced EC migration speed, it did so independently of ITGB3 expression (**Figure 1C**). We therefore conclude that ITGB3 does not regulate NRP2 function during these angiogenic processes.

Depletion of NRP2 in ECs Disrupts Adhesion to FN Matrices

Whilst the upregulation of NRP2 expression we observe in β3HET ECs suggests a regulatory crosstalk between NRP2 and ITGB3 (**Figure 1A**), NRP2 regulated signaling and migration show no dependence on ITGB3. As NRP2 depletion significantly impaired the ability of ECs to migrate over FN (**Figure 1C**), but not to undergo proliferation (**Supplementary Figure S2A**) we next chose to directly examine the effect of NRP2 depletion on cell adhesion to FN. To do this we compared the relative number of cells adhered to 96-well plates pre-coated with FN for either 15 or 30 min. At both timepoints significantly fewer cells adhered to FN following NRP2 siRNA treatment compared to control siRNA treated ECs (**Figure 2A** and **Supplementary Figure S2B**). Migration is dependent on the ability of cells to adhere to a matrix via the formation of FA complexes that continuously cycle through phases of assembly and disassembly. FAs comprise a module of recruited intracellular proteins, such as paxillin and integrins, that link to the actin cytoskeleton to mediate mechanical changes in the cell (Small et al., 1998; Webb et al., 2002; Valdembri and Serini, 2012; De Pascalis and Etienne-Manneville, 2017). Whilst NRP2 depletion had no effect on total or phosphorylated levels of paxillin in our ECs (**Figure 2B**), we did observe it to negatively impact the rate of focal adhesion (FA) turnover itself. FA assembly and disassembly were monitored in ECs treated with either control or NRP2 siRNAs, transfected with paxillin-GFP, by time-lapse microscopy for 30 min over a FN matrix. Silencing of NRP2 in mLMECs significantly reduced the rate of both FA assembly and disassembly compared to control siRNA treated cells (**Figure 2C**). We also measured FA number and size distribution in ECs using two different NRP2 siRNAs by immunolabelling for endogenous paxillin in cells that had adhered to FN for 90 min, a time that allows for mature FAs to form (Ridley et al., 2003; Schiller et al., 2013; Atkinson et al., 2018). Despite no significant difference in average cell area (**Supplementary Figure S2C**), FAs were significantly fewer in number and smaller in average size in NRP2 siRNA treated cells compared to control siRNA treated ECs (**Figure 2D**, **Supplementary Figure S2D**), suggesting NRP2 depletion inhibits FA maturation. Finally, we considered whether NRP2 promotes EC adhesion and migration on FN by regulating Rac1 activation. Rac1 is a small Rho GTPase that mediates cell motility following integrin engagement, regulating leading edge cytoskeletal dynamics and promoting the formation of FAs (Nobes and Hall, 1995; Price et al., 1998; Suzuki-Inoue et al., 2001; Ridley, 2011). Using a recombinant PBD-domain protein (PAK-1) fused to glutathione-magnetic beads, we captured the relative abundance of active Rac1-GTP in control and NRP2 siRNA treated ECs stimulated for 180 min on FN. Compared to our control siRNA treated ECs, NRP2 depleted ECs exhibited a significantly reduced level of active Rac1 (**Figure 2E**), suggesting that NRP2 promotes EC adhesion and migration on FN by regulating Rac1 activation.

NRP2 Regulates ITGA5 Expression in ECs

Cells adhere to the ECM via heterodimeric integrin receptors, which are recruited to FA complexes during cell migration (Avraamides et al., 2008; Goel et al., 2012) and which activate Rho family GTPases such as Rac1 (Price et al., 1998; Suzuki-Inoue et al., 2001). α5β1 integrin is the principle FN binding integrin in ECs (Valdembri et al., 2009; Valdembri and Serini, 2012), and has been previously described as being upregulated during developmental angiogenesis to promote EC migration and survival (Kim et al., 2002; Goodman and Picard, 2012). Studies have also shown NRP1, through its cytoplasmic SEA motif, to specifically promote α5β1 integrin-mediated EC adhesion to FN matrices in a VEGF independent fashion (Valdembri et al., 2009; Cao et al., 2013). As NRP2 depletion significantly impaired mLMEC migration and adhesion on FN, and given the structural homology shared between NRP1 and NRP2, we considered whether a similar association exists between NRP2 and α5β1 integrin. First, we examined whether NRP2 knockdown regulated the expression of either integrin subunit. Western blot analysis revealed that siRNA-mediated silencing of NRP2 resulted in a significant upregulation of ITGA5 subunit expression in four different EC lines (**Figure 3A**), whilst β1-integrin (ITGB1) expression remained unchanged (data not shown). Whilst endothelial ITGA5 specifically pairs with ITGB1 (Avraamides et al., 2008), ITGB1 can form heterodimers with α subunits 1–9 (with the exception of α7) (Velling et al., 1996; Hynes, 2002), suggesting α5β1-integrin behavior can be studied by examining ITGA5 discretely (e.g., ITGB1 expression profiles are sum measures of its interactions with multiple α subunits present in the cell). Therefore, we chose to subsequently focus our attentions on ITGA5 and its interplay with NRP2.

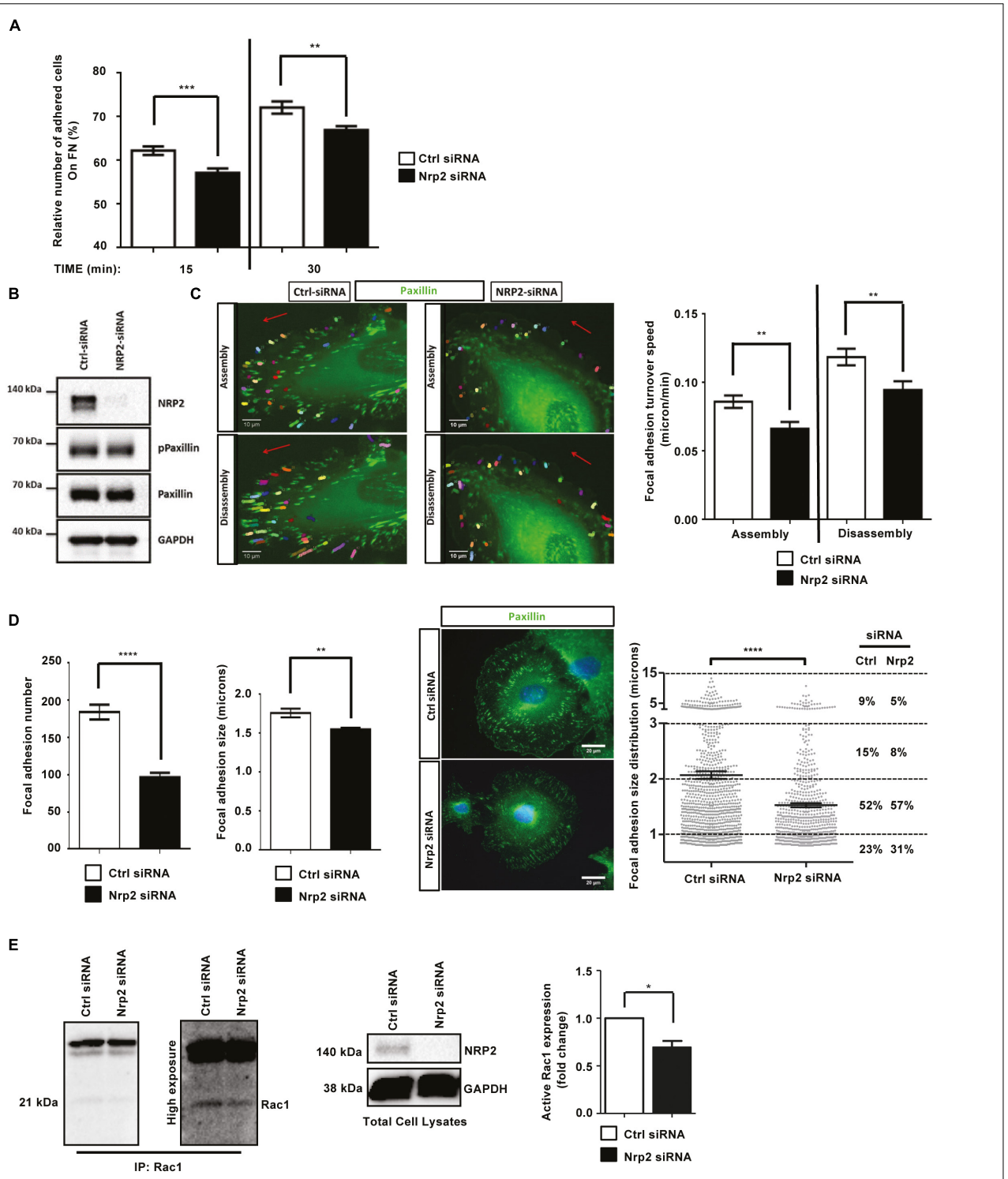

FIGURE 2 | Depletion of NRP2 in ECs disrupts migration and adhesion to FN matrices by affecting Rac1 activation **(A)**: siRNA-transfected ECs were seeded onto FN coated 96-well plates pre-blocked with 5% bovine serum albumin (BSA), and incubated for either 15 or 30 min at 37°C and 5% CO_2. ECs were subsequently fixed in 4% PFA and stained with methylene blue. Absorbance was read at 630 nm. Data was normalized to the relative number of the total cells seeded in a 3-h incubation control plate. $N = 3$ independent experiments, $^{**}P < 0.01$, $^{***}P < 0.001$. Asterisks indicate statistical significance from unpaired two-tailed *t*-tests. **(B)** siRNA-transfected ECs were plated onto FN and incubated for 48 h at 37°C and 5% CO_2. EC lysates were immunoblotted using antibodies to NRP2, phospho-paxillin, paxillin and GAPDH. **(C)** siRNA-transfected ECs were double transfected with a GFP paxillin construct, seeded onto FN and incubated for 48 h at 37°C and 5% CO_2. ECs were fixed in a Ludin chamber and live imaged at 37°C and 5% CO_2 using an inverted Axiovert microscope in which an individual

(Continued)

FIGURE 2 | Continued
cell was captured every one minute for 30 min (left panels). Focal adhesion (FA) assembly and disassembly speeds were analyzed using the ImageJ™ plugin mTrackJ in μm/min. In each respective bar, $n \geq 100$ FAs, $^{**}P < 0.01$ (right panel). **(D)** siRNA-transfected ECs were seeded onto FN and incubated for 90 min at 37°C and 5% CO_2 before being fixed and stained for paxillin. Images were taken using a Zeiss AxioImager M2 microscope at 63x magnification. FA number and size was quantified using ImageJ™ software as previously described by Lambert et al. (2020). A FA size lower detection limit was set at 0.8 microns. The center panel shows representative images for fixed ECs transfected either with control or NRP2 siRNA. Image quantification for FA number and size is shown in the left panel. Quantification performed on mean data from $n \geq 25$ ECs over $N = 3$ independent experiments. % FA size distribution analysis is shown in the right panel on mean data from $n \geq 25$ ECs over $N = 3$ independent experiments. Asterisks indicate statistical significance from an unpaired two-tailed *t*-test. **(E)** siRNA-transfected ECs were seeded onto FN and incubated for 180 min at 37°C and 5% CO_2. EC extracts were immunoprecipitated by incubation with 10 μg Rac1 assay reagent (PAK-1 PBD magnetic beads) for 45 min at 4°C with gentle agitation. Immunoprecipitated complexes were subjected to Western blot analysis using antibodies against Rac1. Left panel: low and high exposure images showing active Rac1 levels in control and NRP2 siRNA transfected lysate. Middle panel: NRP2 depletion was confirmed by Western blot analysis using antibodies against NRP2 and GAPDH. Right panel: densitometric analysis of band intensities normalized against GAPDH and obtained using ImageJ™. Asterisks indicate statistical significance from an unpaired two-tailed *t*-test.

Studies have previously reported NRP1 to complex with ITGA5 in HUVECs (Valdembri et al., 2009) and NRP2 to complex with ITGA5 from co-cultures between HUVECs and renal cell carcinoma (Cao et al., 2013). To investigate whether a direct interaction between NRP2 and ITGA5 exists in mLMECs, lysates were subjected to a series of co-immunoprecipitation studies followed by Western blot analysis. We found both NRP2 and ITGA5 co-immunoprecipitate with each other, indicating a physical interaction between the two receptors (**Figure 3B**). Immuno-staining using a highly specific NRP2 antibody, reported previously not to cross-react with NRP1 (Bae et al., 2008; Goel et al., 2012), also showed a strong co-localization between NRP2 and ITGA5 close to the cell membrane (**Figure 3C**). Given the significant upregulation of ITGA5 subunit expression following NRP2 depletion, and evidence to suggest a physical interaction between NRP2 and ITGA5, we next examined whether NRP2 depletion elicited an effect on ITGA5 localization within our immortalized cells. Following treatment with either control or NRP2 siRNA, ECs were seeded overnight on a FN matrix and subsequently fixed to visualize endogenous ITGA5 expression. Compared to control siRNA treated ECs, NRP2 depleted ECs exhibited significant disruptions in ITGA5 organization: ITGA5 appeared in elongated fibrillar-like structures (**Figure 3D**), reminiscent of what has been described as fibrillar adhesions (Webb et al., 2002). ImageJ™ analysis of these ITGA5 containing structures confirmed a significant increase in the length of ITGA5 fibrils in NRP2 siRNA treated ECs suggestive of a disruption in ITGA5 trafficking (**Supplementary Figure S3A**). We see this NRP2-dependent ITGA5 phenotype when using multiple NRP2 specific siRNAs (**Supplementary Figure S3B**) and in primary ECs (**Supplementary Figures S3C,D**). It is becoming increasingly clear that microtubule-actin highways co-ordinately regulate a range of intracellular trafficking mechanisms, including integrin transport (Goley and Welch, 2006; Kaksonen et al., 2006; Valdembri et al., 2009; Zech et al., 2011; Duleh and Welch, 2012). Co-immunostaining for both phalloidin and ITGA5 revealed that whilst ITGA5 localized to the ends of actin filaments in control treated ECs, at what we assume to be FAs, in NRP2 depleted cells, the elongated ITGA5 fibrils share a strong co-localization along the actin filaments themselves (**Figure 3E**). We believe this to support a mechanism of actin-dependent ITGA5 trafficking, whereby loss of NRP2 impedes the transport of ITGA5 to FAs at the leading edge of the cell.

ITGA5 Trafficking Is Dependent on NRP2 in ECs

Whilst a role for NRP2 in trafficking ITGA5 is novel, NRP1 has been shown previously to promote endocytosis of active α5β1 integrin through a Rab5 pathway (Valdembri et al., 2009). In order to take an unbiased approach to elucidating candidate trafficking proteins NRP2 may associate with to regulate ITGA5 localization in ECs, we used label-free quantitative (LFQ) mass spectrometry. Mass spectrometry was performed on two WT EC lines, transfected either with control or NRP2 siRNA, and immunoprecipitated for NRP2. siRNA-mediated depletion of NRP2 was confirmed for both cell lines. This analysis revealed proteins immunoprecipitating with NRP2 at a significantly increased fold-change compared to proteins analyzed from a NRP2 knockdown cell-lysate. Shown are protein hits detected in both cell lines, including both ITGA5 and ITGB1. A number of endocytic trafficking proteins were also detected as candidate binding partners of NRP2, including clathrin, caveolin-1, lamtor1, scamp1, and annexin-A1 (**Figure 4A**). The full list of identified co-immunoprecipitated proteins is shown in **Supplementary Table S1**.

α5β1 integrin is known to be internalized both by clathrin and caveolae-mediated endocytosis (Shi and Sottile, 2008; Margadant et al., 2011). In order to validate a potential mechanism by which NRP2 regulates ITGA5 internalization via its contact with clathrin and caveolin, we performed coimmunoprecipitation assays to prove a physical interaction. NRP2 coimmunoprecipitated with both clathrin heavy chain-1 and caveolin-1 (**Figure 4B**), supporting the mass spectrometry results. We subsequently conducted cell surface biotinylation assays to examine ITGA5 internalization directly, in ECs treated either with control siRNA or NRP2 siRNA. We observed no change in the rate of ITGA5 internalization in NRP2 depleted ECs (**Figure 4C**), suggesting that NRP2 does not regulate internalization of total ITGA5 levels. We subsequently considered whether NRP2 regulates ITGA5 recycling back to the membrane.

Integrin recycling is mediated by Rab GTPase proteins (Roberts et al., 2001; Paul et al., 2015), specifically, α5β1

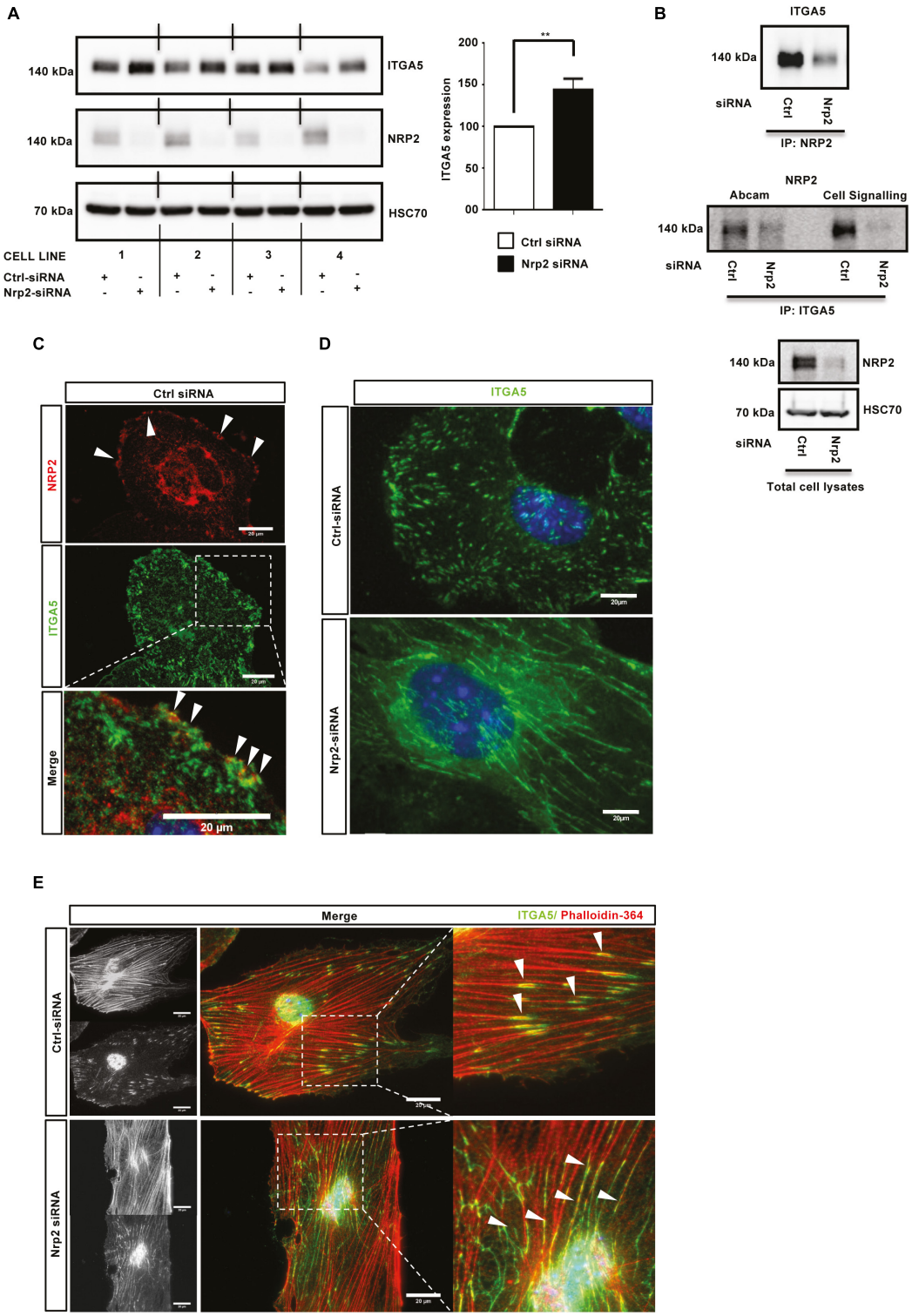

FIGURE 3 | NRP2 regulates ITGA5 expression in ECs. **(A)**: siRNA-transfected ECs from four different clones were seeded onto FN and incubated for 48 h. EC extracts were immunoblotted using antibodies to ITGA5, NRP2, and HSC70. Left panel shows Western blot image, right panel shows densitometric analysis of ITGA5 band intensities normalized against HSC70 and obtained using ImageJ™. $^{**}P < 0.01$. **(B)**: siRNA-transfected ECs were seeded onto FN and incubated for 48 h. Left panel: EC extracts were immunoprecipitated by incubation with protein-G Dynabeads® coupled to a NRP2 antibody. Middle panel: EC extracts were immunoprecipitated by incubation with protein-G Dynabeads® coupled to two different ITGA5 antibodies (as indicated). Immunoprecipitated complexes were subjected to Western blot analysis using antibodies against ITGA5 and NRP2, respectively. Right panel: NRP2 silencing was confirmed by subjecting the total cell

(Continued)

FIGURE 3 | Continued
lysate to Western blot analysis and incubating blots in antibodies against NRP2 and HSC70. **(C)**: Control siRNA-transfected ECs were prepared as described in **Figure 2D** legend. Fixed ECs were incubated in primary antibodies against NRP2 and ITGA5. Images were captured using a Zeiss AxioImager M2 microscope at 63x magnification. Arrows indicate co-localization of NRP2 and ITGA5. **(D)**: siRNA-transfected ECs were prepared as described in **Figure 2D** legend, however, ECs were allowed to adhere overnight prior to fixation. ECs were incubated in primary antibody against ITGA5. **(E)** siRNA-transfected ECs were prepared as described in **(D)**, however, fixed cells were incubated in ITGA5 primary antibody and phalloidin-364. Arrows indicate localization of ITGA5 with actin filaments. Image panels shown in **(C–E)** are representative of $n \geq 10$ cells per condition/treatment.

integrin follows long-loop recycling via a Rab11 dependent mechanism (Laukaitis et al., 2001; Caswell et al., 2007). NRP2 coimmunoprecipitated with Rab11 in both directions (**Figure 4D**). However, NRP2 did not co-immunoprecipitate with NRP1 in our mass spec studies (see **Supplementary Table S1**), suggesting these two structurally related proteins regulate ITGA5 trafficking through distinct pathways. As our mass spectrometry analysis had identified candidate interactions between NRP2 and other trafficking and recycling molecules, such as Rab11Fip5, an adaptor for Rab11 recycling vesicles and previously reported to co-immunoprecipitate with ITGA5, we performed biotin recycling assays. In these assays, the biotin-labeled cell surface proteins were allowed to internalize before stripping off any remaining surface biotin. Cells were then incubated over 20 min to stimulate the recycling process. In contrast to our internalization assays, NRP2 silencing significantly attenuated the rate of total ITGA5 recycling back to the membrane compared to ECs treated with control siRNA (**Figure 4E**). We therefore present a potential mechanism whereby NRP2 promotes mLMEC migration and adhesion to FN by regulating actin dependent ITGA5 recycling back to the cell membrane (**Figure 5**).

DISCUSSION

NRP2 is known to regulate ECM adhesion and migration in various cell lines, including human ECs (Favier et al., 2006), immune cells (Curreli et al., 2007) and cancer cells (Kawakami et al., 2002; Fukahi et al., 2004; Caunt et al., 2008; Dallas et al., 2008; Cao et al., 2013). In the latter, it has been described as a biomarker for poor prognosis because its expression correlates with increased migratory and invasive behavior (Kawakami et al., 2002; Caunt et al., 2008; Dallas et al., 2008; Cao et al., 2013). In many of these examples, NRP2 promotes cell adhesion and migration by exerting influence over VEGF-mediated pro-angiogenic pathways and inducing integrin engagement. ITGA5 and FN are known to be upregulated in ECs during angiogenesis (Kim et al., 2002; Goodman and Picard, 2012), and are key players in formation of neo-vasculature (Brooks et al., 1994; Kim et al., 2000). The data we present here support a model whereby NRP2 promotes EC adhesion and migration on FN by regulating actin-dependent ITGA5 recycling. Importantly, the means by which it does so appears to be mechanistically distinct from that of NRP1, which is known to regulate internalization of active ITGA5 via a rab5-dependent pathway (Valdembri et al., 2009).

We previously demonstrated an ITGB3-dependent role for NRP1 in mediating EC migration and FA turnover on FN. EC migration on FN becomes NRP1 dependent when ITGB3 levels are perturbed (Ellison et al., 2015). Like NRP1, NRP2 expression is upregulated in ITGB3 depleted cells (**Figure 1A**). Given this observation, and the structural and domain homologies between NRP1 and NRP2 (Zachary, 2014), we sought to investigate whether NRP2 shared a similar regulatory interplay with ITGB3. We demonstrated by siRNA knockdown that EC migration depends on NRP2, but this is independent of ITGB3 expression levels (**Figure 1C**).

Like NRP1, NRP2 also regulates a number of integrin-dependent cellular processes on FN. Upon NRP2 knockdown, EC adhesion is reduced (**Figure 2A**), FA dynamics are altered (**Figures 2C,D**), and Rac1 activation is impaired (**Figure 2E**). Rac1 was also identified from our mass spectrometry analysis as a candidate binding partner of NRP2, which supports these findings. Integrins provide the structural link that allows for: (1) adhesion to the ECM; (2) anchorage of actin stress fibers to the membrane; (3) the generation of force that is required for migration (Laukaitis et al., 2001; Le Boeuf et al., 2004; Buskermolen et al., 2018). Both αvβ3- and α5β1-integrins are FN receptors in ECs (Brooks et al., 1994; Kim et al., 2000), but given the lack of any ITGB3 input into the NRP2 processes we were examining, and the upregulation of ITGA5 expression upon NRP2 depletion (**Figure 3A**), we focused our attention on this integrin subunit. Cao et al. (2013) demonstrated NRP2 to interact with ITGA5 in co-cultures between HUVECs and renal cell carcinoma to promote FN-mediated adhesion. To our knowledge, though, we are the first to show evidence of a direct interaction between NRP2 and ITGA5 in microvascular ECs (**Figures 3B,C**). Furthermore, our findings demonstrate that NRP2 modulates ITGA5 function by regulating its subcellular trafficking along the actin cytoskeleton. Importantly, the disrupted ITGA5 phenotype we see following NRP2 depletion in our immortalized ECs is also present in primary ECs. Along with our previous studies demonstrating they express a canonical adhesome (Atkinson et al., 2018), this rebuts the concept that immortalized ECs are an inappropriate model for studying angiogenic processes.

NRP2's role in trafficking ITGA5 in ECs also appears to be distinct from that of NRP1. It has been reported that NRP1 regulates active α5β1 integrin endocytosis via GIPC1 (Valdembri et al., 2009), however, interactions between GIPC and NRP2 were not detected from either mass spectrometry analysis or co-immunoprecipitation studies (data not shown). Although we did not observe any changes in internalization of total ITGA5

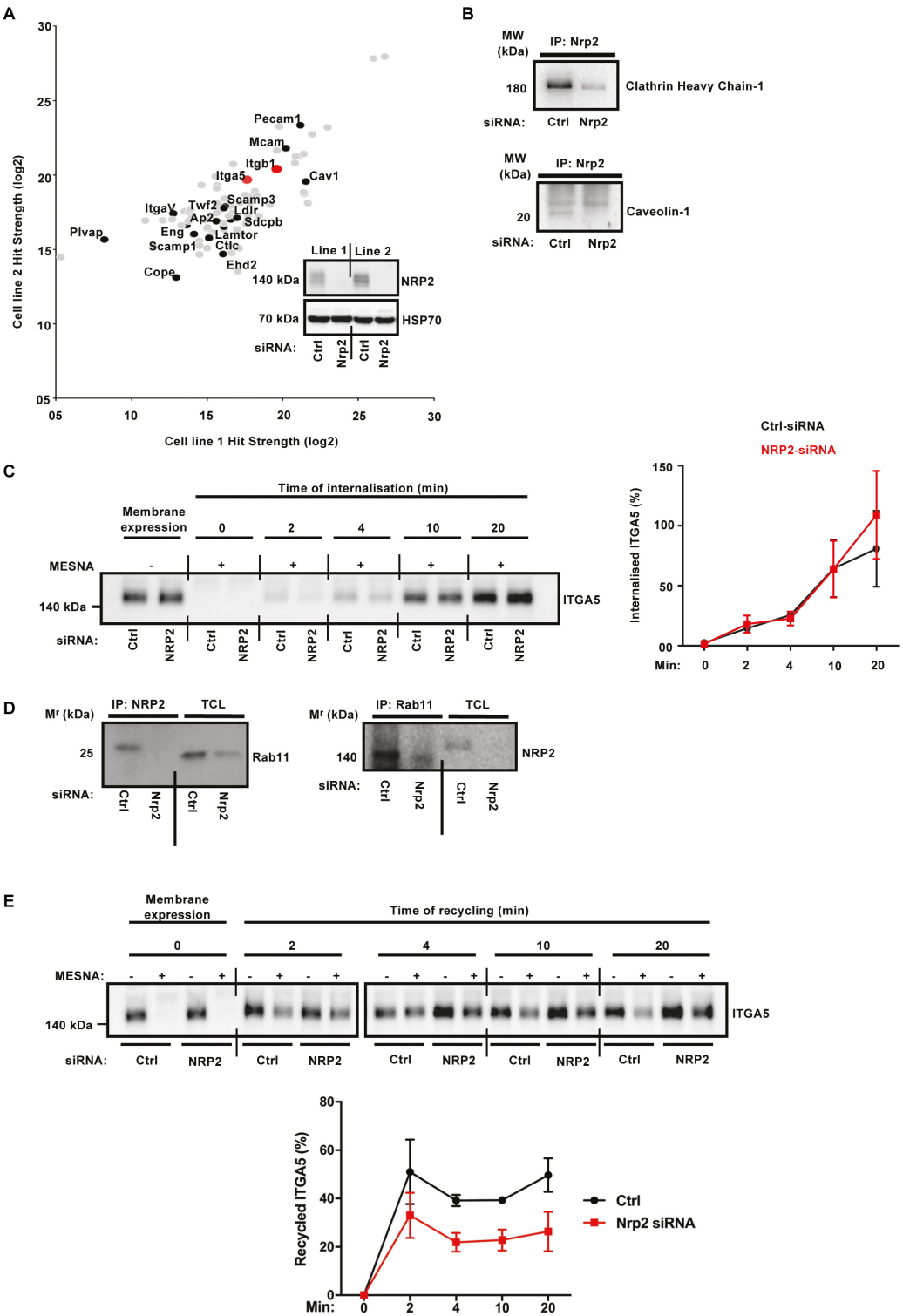

FIGURE 4 | ITGA5 trafficking in ECs is NRP2 dependent. **(A)**: Label-free quantitative mass spectrometry peptide hits identified using MaxQuant software from the Andromeda peptide database. Panel depicts peptide hits detected at a higher fold-change in two control siRNA treated EC lines than those detected from two NRP2 siRNA treated EC lines. NRP2 silencing was confirmed by subjecting EC extracts to Western blot analysis. **(B)**: siRNA-transfected ECs were seeded onto FN and incubated for 48 h. EC extracts were immunoprecipitated by incubation with protein-G Dynabeads® coupled to a NRP2 antibody. Immunoprecipitated complexes were subjected to Western blot analysis using antibodies against clathrin heavy chain-1 (top) and caveolin-1 (bottom). **(C)**: siRNA-transfected ECs were seeded onto

(Continued)

FIGURE 4 | Continued
FN and incubated for 48 h. ECs were subsequently starved in serum-free media, before being placed on ice. EC cell surface proteins were labeled with 0.3 mg/ml biotin. ECs were then incubated for the indicated timepoints at 37°C, 5% CO_2. A sample of ECs were maintained at 4°C as (±Mesna) controls. Following incubation at 37°C, ECs were placed on ice and incubated with 100 mM Mesna. EC lysates were then immunoprecipitated with protein-G Dynabeads® coupled to an anti-biotin antibody. Immunoprecipitated biotin-labeled proteins were separated by SDS-PAGE and subjected to Western bolt analysis. The level of internalized ITGA5 at each time of incubation was normalized to the (-) Mesna control. Left panel shows Western blot image, right panel shows the mean densitometric analysis obtained using ImageJ™. Also shown is confirmation of NRP2 silencing. *N* = 3 independent experiments. **(D)**: Co-immunoprecipitation study as described in **(B)**, immunoprecipitated complexes were subjected to Western blot analysis using anti-Rab11 and anti-NRP2 antibodies, respectively. **(E)**: siRNA-transfected ECs were prepared as described in **(C)**, after biotin surface labeling, ECs were incubated in serum free media for 20 min at 37°C to allow for internalization. A sample of ECs were maintained at 4°C for use as positive/negative controls. The remaining ECs were then placed on ice, and any un-internalized biotin-labeled proteins stripped off using 100 mM Mesna. The internalized protein fraction was allowed to recycle by incubating the ECs for the indicated timepoints at 37°C. ECs were then returned to ice and incubated in 100 mM Mesna. No Mesna treatment dishes at each timepoint were used as comparative controls. All subsequent stages were performed in the same manner as described in **(C)**, the level of the recycled ITGA5 was determined by normalizing the amount of ITGA5 quantified from dishes treated with Mesna to the total ITGA5 on the membranes of the Mesna-untreated cells in the same period of incubation. *N* = 3 independent experiments.

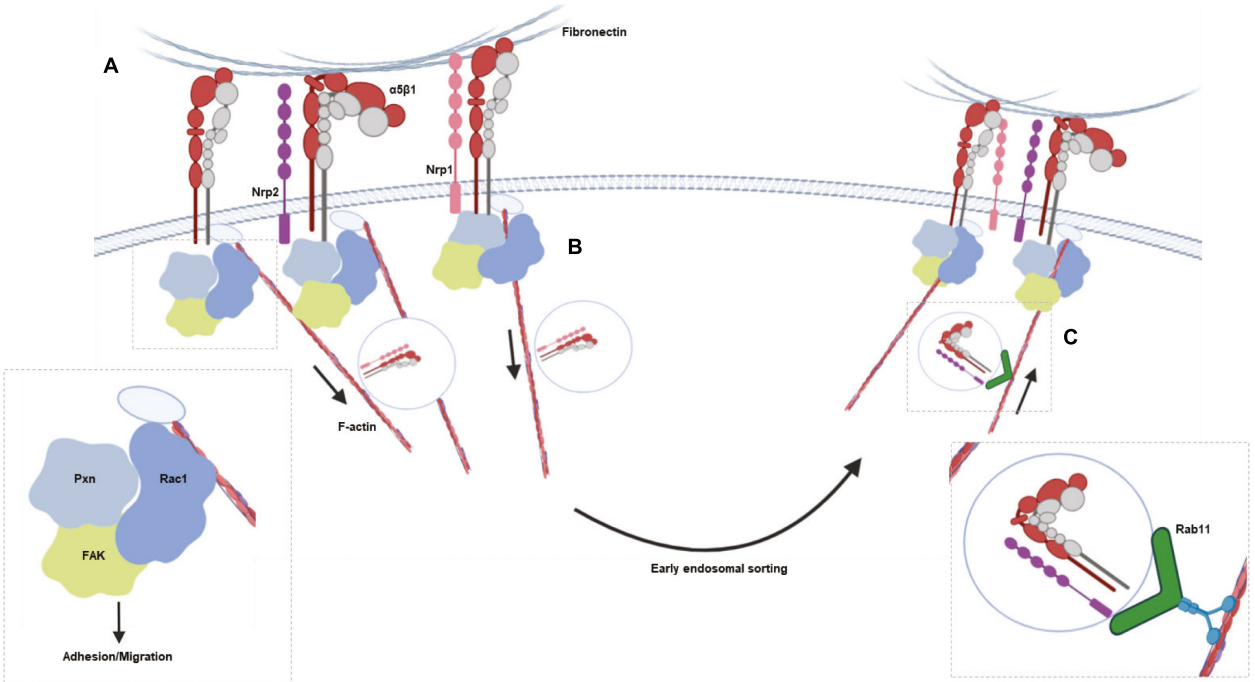

FIGURE 5 | Schematic summarizing the major results. **(A)**, NRP2 and ITGA5 share an interaction at the cell membrane, promoting EC adhesion and migration on FN matrices by regulating Rac1 activation. **(B)**, NRP1 is known to selectively stimulate internalization of active α5β1 integrin from fibrillar adhesions along F-actin microfilaments to early endosomes in a Rab5 dependent manner. **(C)** NRP2 then regulates Rab11 dependent recycling of total ITGA5 back to adhesion sites along the actin cytoskeleton.

upon NRP2 depletion (**Figure 4C**), we were unable to examine trafficking of active α5β1 in our murine cells. In fact, we observed physical interactions between NRP2 and both clathrin and caveolin by immunoprecipitation (**Figure 4B**) suggesting NRP2 at least has the potential to regulate the endocytosis of active α5β1 integrin. Following internalization by clathrin or caveolin-dependent mechanisms, α5β1 integrin has been shown to undergo long-loop recycling back to the membrane within Rab11 positive vesicles (Laukaitis et al., 2001; Caswell et al., 2007). To our knowledge neither NRP1 or NRP2 have been reported to regulate ITGA5 recycling in microvascular ECs. Not only do we show NRP2 depletion slows total ITGA5 recycling (**Figure 4D**), we also show NRP2 co-immunoprecipitates with Rab11 in our ECs (**Figure 4E**).

Finally, the elevated total cellular levels of ITGA5 that occur when NRP2 is knocked-down, particularly in light of no changes at the cell surface (data not shown), suggest other points in the ITGA5 life cycle are governed by NRP2. Given NRP2's interactions with clathrin and caveolin, both known to play a role in endosomal trafficking to lysosomes (Sachse et al., 2002; Shi and Sottile, 2008; Margadant et al., 2011), we speculate a role for the molecule in regulating ITGA5 degradation. We support this hypothesis by showing NRP2 also immunoprecipitates with both Lamtor1 and Scamp1 (**Figure 4A**), proteins previously shown to regulate lysosomal trafficking (Cai et al., 2011; Malek et al., 2012).

In close, we propose a novel mechanism by which NRP2, independently of its role as a coreceptor for VEGF-A, promotes Rac1-mediated EC adhesion and migration to FN matrices by

regulating recycling of ITGA5. Importantly, we provide evidence to suggest that NRP2 acts in a mechanistically distinct manner to NRP1. Finally, whilst we have not yet shown any phenotypic interactions between NRP2 and ITGB3, we cannot rule out a role for ITGB3 in regulating NRP2 trafficking. Like NRP1, NRP2 levels are significantly elevated when ITGB3 expression is reduced (**Figure 1A**). Our findings allude to a complex interplay between FN-binding integrins and neuropilins which regulate EC migration.

MATERIALS AND METHODS

Animal Generation

All experiments were performed in accordance with United Kingdom home office regulations and the European Legal Framework for the Protection of Animals used for Scientific Purposes (European Directive 86/609/EEC), prior to the start of this project. Transgenic mice expressing a knockout for the β3-integrin allele (KO-Itgb3) were generated by substituting a 1.4 kb *Hin*dIII fragment of the β3 gene including exons I and II with a 1.7 kb construct containing a Pgk-neomycin (neo)-resistance cassette (**Supplementary Figure S1G**). The PCR analysis was carried out using the following oligonucleotide primers as previously described by Hodivala-Dilke et al. (1999). Forward primer 1: 5′-CTTAGACACCTGCTACGGGC-3′ Reverse primer 2: 5′-CACGAGACTAGTGAGACGTG-3′.

Cell Isolation, Immortalization and Cell Culture

Primary mouse lung microvascular endothelial cells (mLMECs) were isolated from adult mice bred on a mixed C57BL6/129 background. Primary ECs were twice positively selected for their expression of intracellular adhesion molecule-2 (ICAM-2) by magnetic activated cell sorting (MACS) as previously described by Reynolds and Hodivala-Dilke (Reynolds and Hodivala-Dilke, 2006). ECs were immortalized using polyoma-middle-T-antigen (PyMT) retroviral transfection as previously described by Robinson et al. (2009). Immortalized mLMECs were cultured in IMMLEC media, a 1:1 mix of Ham's F-12:DMEM medium (low glucose) supplemented with 10% FBS, 100 units/mL penicillin/streptomycin (P/S), 2 mM glutamax, 50 μg/mL heparin (Sigma). Immortalized mLMECs were cultured on 0.1% gelatin coated flasks at 37°C in a humidified incubator with 5% CO_2. For experimental analyses, plates, dishes, flasks and coverslips were coated in 10 μg/ml human plasma fibronectin (FN) (Millipore) overnight at 4°C. Vascular endothelial growth factor-A (VEGF-A164: mouse equivalent of VEGF-A165) was made in-house as previously described by Krilleke et al. (2007).

siRNA Transfection

ECs were transfected with non-targeting control siRNA or mouse-specific NRP2 siRNA constructs (Dharmacon), suspended in nucleofection buffer (200 mM Hepes, 137 mM NaCl, 5 mM KCl, 6 mM D-glucose, and 7 mM Na_2HPO_4 in nuclease-free water) using either the Amaxa nucleofector system II (Lonza) under nucleofection program T-005 or the Amaxa 4Dnucleofector system (Lonza) under nucleofection program EO-100 according to manufacturer's instructions. For the majority of our studies we used siGENOME mouse Nrp2 siRNA D-040423-03 (denoted as Nrp2 siRNA on figures). We confirmed key observations with siGENOME mouse Nrp2 siRNA D-040423-04 (denoted as Nrp2 siRNA#4 on figures).

Western Blot Analysis

siRNA transfected ECs were seeded into FN-coated 6-well plates at a seeding density of 5×10^5 cells/well and incubated for 48 h at 37°C in a 5% CO_2 incubator. ECs were lysed in electrophoresis sample buffer (ESB) (Tris–HCL: 65 mM pH 7.4, sucrose: 60 mM, 3% SDS), and homogenized using a Tissue Lyser (Qiagen) with acid-washed glass beads (Sigma). Following protein quantification using the DC BioRad assay, 30 μg of protein from each sample was loaded onto 8% polyacrylamide gels and subjected to SDS-PAGE. Proteins were transferred to a nitrocellulose membrane (Sigma) and incubated in 5% milk powder in PBS 0.1% Tween-20 (0.1% PBST) for 1 h at room temperature followed by an overnight incubation in primary antibody diluted 1:1000 in 5% bovine serum albumin (BSA) in 0.1% PBST at 4°C. Membranes were washed 3× with 0.1% PBST and incubated in an appropriate horseradish peroxidase (HRP)-conjugated secondary antibody (Dako) diluted 1:2000 in 5% milk powder in 0.1% PBST for 2 h at room temperature. Membranes were washed again 3× with 0.1% PBST before being incubated with Pierce ECL Western Blotting Substrate solution (Thermo Scientific). Chemiluminescence was detected on a ChemiDoc™ MP Imaging System darkroom (BioRad). Densitometric readings of band intensities for blots were obtained using ImageJ™. Primary antibodies (all used at 1:1000 dilution and purchased from Cell Signaling Technology, unless noted otherwise) were: anti-NRP2 (clone D39A5), anti-ITGB3 (clone 4702S), anti-HSC70 (clone B-6, Santa Cruz Biotechnology), anti-phospho VEGFR2 (Y1175) (clone 2478), anti-VEGFR2 (clone 2479), anti-NRP1 (clone 3725S), anti-phospho ERK1/2 (clone 9101), anti-ERK1/2 (clone 4695), anti-ITGA5 (clone 4705S), anti-ITGB1 (clone ab179471, Abcam), anti-clathrin heavy chain-1 (clone ab21679, Abcam), anti-caveolin-1 (clone ab18199, Abcam), anti-Rab11 (clone 3539), ERG: Ab92513, Pecam-1 (77699), prox-1 (clone ab11941, Abcam), claudin-5 (clone ab131259, Abcam), VE-cadherin (clone ab205336, Abcam).

Signaling Assays

siRNA-transfected ECs were seeded into FN-coated 6 cm cultures dishes at a density of 5×10^5 cells/well and incubated for 48 h at 37°C and 5% CO_2. ECs were then PBS washed and starved for 3 h in serum free medium (OptiMEM®; Invitrogen). VEGF was then added at a final concentration of 30 ng/ml. After the desired time of VEGF-stimulation, ECs were subjected to lysing, protein quantification and protein expression analysis by Western blot.

Random Migration Assays

siRNA-transfected ECs were seeded into FN coated 24-well plates at a density of 7×10^4 cells/well 24 h post nucleofection, and allowed to adhere for 3 h at 37°C and 5% CO_2. Fixed images

of multiple fields/well were taken every 10 min for 15 h at 37°C and 5% CO_2 using an inverted Zeiss Axiovert microscope with one-phase contrast. Random migration was quantified by manually tracking individual cells using the ImageJ™ plugin mTrackJ. Random migration speed was calculated in μ m/hour.

Colorimetric Adhesion Assays

siRNA-transfected ECs were seeded into 96-well plates at a density of 4×10^4 cells/well 48 h post nucleofection. 96-well plates were pre-coated with FN overnight, then blocked in 5% BSA for 1 h at room temperature. ECs were then incubated at 37°C in a 5% CO_2 incubator for the indicated timepoints, in addition to a 3-h incubation control plate. Following incubation, ECs were washed 3× with PBS + 1 mM $MgCl_2$ + 1 mM $CaCl_2$, fixed in 4% PFA, and stained with methylene blue for 30 min at room temperature. ECs were washed in dH_2O and air-dried, before the dye from stained adhered ECs was extracted by a de-stain solution (50% ethanol, 50% 0.1 M HCL). The absorbance of each well was then read at 630 nm. Data was normalized to the relative number of the total cells seeded in the 3-h incubation plate.

Focal Adhesion Turnover Assays

ECs double transfected with control or NRP2 siRNA and a GFP-tagged paxillin construct (kindly provided by Professor Maddy Parsons, Kings College, London) were seeded onto FN-coated acid-washed, oven sterilized glass coverslips in 24-well plates at a seeding density of 4×10^4 cells/well. 48 h post nucleofection, coverslips were PBS washed, fixed in a Ludin chamber (Life Imaging Services GmbH), and live imaged in OptiMEM® phenol-red free medium supplemented with 2% FBS and P/S at 37°C and 5% CO_2 using an inverted Axiovert (Carl Zeiss Ltd.) microscope in which an individual cell was captured every one minute for 30 min. Focal adhesion (FA) assembly and disassembly speeds were analyzed by manually tracking the number of selected GFP-paxillin-positive focal adhesions using the Image J™ MTrackJ plugin software.

Immunocytochemistry

siRNA-transfected ECs were seeded onto FN-coated acid-washed, oven sterilized glass coverslips in 24-well plates at a seeding density of 2.5×10^4 cells/well, and incubated at 37°C and 5% CO_2. ECs were fixed at indicated timepoints in 4% paraformaldehyde (PFA) for 10 min, washed in PBS, blocked and permeabilized with 10% goat serum, PBS 0.3% triton X-100 for 1 h at room temperature. Cells were incubated in primary antibody diluted 1:100 in PBS overnight at 4°C. Primary antibodies were: anti-paxillin (clone ab32084; Abcam), anti-ITGA5 (clone ab150361; Abcam). Coverslips were PBS washed, and incubated with donkey anti-rabbit Alexa fluor-488 secondary antibody diluted 1:200 in PBS for 2 h at room temperature. F actin staining was performed by incubating cells in phalloidin-564 diluted 1:40 in PBS for 2 h at room temperature during secondary antibody incubation. Coverslips were PBS washed again, before being mounted onto slides with Prolong® Gold containing DAPI (Invitrogen). Images were captured using a Zeiss AxioImager M2 microscope (AxioCam MRm camera) at 63× magnification. FA number and size was quantified using ImageJ™ software as previously described by Lambert et al. (2020). A FA size lower detection limit was set at 0.8 microns. ITGA5 length was measured using the ImageJ™ software plugin simple neurite tracer.

Rac1 Pulldown

siRNA-transfected ECs were seeded onto FN at a density of 2×10^5 cells/dish and incubated for 180 min at 37°C and 5% CO_2. ECs were lysed on ice with MLB (Sigma) (diluted to 1× with sterile water containing 10% glycerol and 1× Halt™ protease inhibitor cocktail (Thermo Scientific). EC lysates were cleared by centrifugation. EC extracts were immunoprecipitated by incubation with 10 μg Rac1 assay reagent (PAK-1 PBD magnetic beads, Sigma) for 45 min at 4°C with gentle agitation. Immunoprecipitated complexes were subjected to Western blot analysis. Nitrocellulose membranes were immunoblotted using 1 μg/mL of anti-Rac1, clone 23A8 (Sigma).

Co-Immunoprecipitation Assays

siRNA-transfected ECs were seeded into FN-coated 10 cm dishes at a density of 2×10^6 cells/dish, and incubated for 48 h at 37°C and 5% CO_2. ECs were then lysed on ice in lysis buffer as previously described by Valdembri et al. (2009) in the presence of 1× Halt protease inhibitor cocktail (Thermo Scientific) and protein quantified using the DC BioRad assay. 100 μg protein from each sample was immunoprecipitated by incubation with protein-G Dynabeads® (Invitrogen) coupled to a rabbit anti-NRP2 antibody (clone 3366, Cell Signaling Technology) on a rotator overnight at 4°C. Immunoprecipitated complexes were then washed 3× with lysis buffer + 1× Halt™ protease inhibitor cocktail, and once in PBS, before being added to and boiled in NuPAGE sample reducing agent and sample buffer (Life Technologies) for Western blot analysis.

Co-localization Assays

siRNA-transfected ECs were prepared the same as for immuno-cytochemistry. Cells were incubated in primary antibody diluted 1:50 in PBS overnight at 4°C. Primary antibodies were: anti-NRP2 (clone sc-13117, Santa Cruz Biotechnology), and anti-ITGA5 (clone ab150361; Abcam). Coverslips were PBS washed, and incubated with both donkey anti-rabbit Alexa fluor-488, and goat anti-mouse Alexa fluor-546 secondary antibodies diluted 1:200 in PBS for 2 h at room temperature. Coverslips were PBS washed again, before being mounted onto slides with Prolong® Gold containing DAPI (Invitrogen). Images were captured using a Zeiss AxioImager M2 microscope (AxioCam MRm camera) at 63× magnification.

Mass Spectrometry Analysis

NRP2 co-immunoprecipitation samples were sent to Fingerprints Proteomics Facility (Dundee University, United Kingdom), which carried out LFQ mass spectrometry and peptide identification using the MaxQuant software based on the Andromeda peptide database as described by Schiller et al. (2011). **Figure 4A** depicts peptide hits detected at a higher

fold-change in two control siRNA treated EC lines than those detected from two NRP2 siRNA treated EC lines.

Internalization and Recycling Assays

Internalization

siRNA-transfected ECs were seeded into FN-coated 10 cm dishes at a density of 2×10^6 cells/dish, and incubated for 48 h at 37°C and 5% CO_2. ECs were then starved in serum-free OptiMEM® for 3 h at 37°C in a 5% CO_2 incubator, before being placed on ice for 5 min, then washed twice with Soerensen buffer (SBS) pH 7.8 (14.7 mM KH_2PO_4, 2 mM Na_2HPO_4, and 120 mM Sorbitol pH 7.8) as previously described by Remacle et al. (2003). EC cell surface proteins were labeled with 0.3 mg/ml biotin (Thermo Scientific) in SBS for 30 min at 4°C. Unreacted biotin was quenched with 100 mM glycine for 10 min at 4°C. ECs were then incubated in pre-warmed serum-free OptiMEM® for the indicated time points at 37°C in a 5% CO_2 incubator. A sample of ECs were maintained at 4°C for use as positive/negative (±Mesna) controls. Following incubation, dishes were immediately placed on ice, washed twice with SBS pH 8.2, and incubated with 100 mM Mesna (Sigma) for 75 min at 4°C (with the exception of Mesna control plates, which were lysed in lysis buffer (25mM Tris–HCl, pH 7.4, 100 mM NaCl, 2mM $MgCl_2$, 1mM Na_3VO_4, 0.5 mM EGTA, 1% Triton X-100, 5% glycerol, and protease inhibitors), and placed on ice). Following Mesna incubation, excess Mesna was quenched with 100mM iodoacetamide (Sigma) for 10 min at 4°C, then ECs were washed twice with SBS pH 8.2 and lysed. Lysates were cleared by centrifugation at 12,000 *g* for 20 min at 4°C. Supernatant proteins were then quantified using the DC BioRad assay, and subsequently immunoprecipitated with Dynabeads coupled to mouse anti-biotin antibody overnight at 4°C. Immunoprecipitated biotin-labeled proteins were separated by SDS-PAGE and subjected to Western bolt analysis. The level of internalized ITGA5 at each time of incubation was normalized to the (− Mesna) control.

Recycling

After surface labeling, ECs were incubated in pre-warmed serum free OptiMEM® for 20 min at 37°C to allow internalization. A sample of ECs were maintained at 4°C for use as positive/negative controls. The remaining dishes were subsequently placed on ice, washed twice with SBS pH 8.2, and any un-internalized biotin-labeled proteins were stripped off using 100 mM Mesna in Tris buffer for 75 min at 4°C. The internalized fraction of proteins was then allowed to recycle to the membrane by incubating the ECs for the indicated time points in serum-free OptiMEM® at 37°C. Following the indicated times of incubation, dishes were placed on ice, washed twice with SBS pH 8.2, and subjected to Mesna incubation for 75 min at 4°C. No Mesna treatment dishes at each timepoint were used as controls. All subsequent stages were performed in the same manner as the internalization assay. The level of the recycled ITGA5 was determined by normalizing the amount of ITGA5 quantified from dishes treated with Mesna, to the total ITGA5 on the membranes of the Mesna-untreated cells in the same period of incubation.

Statistical Analysis

The graphic illustrations and analyses to determine statistical significance were generated using GraphPad Prism 6.0 software and Student's *t*-tests, respectively. Bar charts show mean values and the standard error of the mean (±SEM). Asterisks indicate the statistical significance of *P*-values: $P > 0.05$ = ns (not significant), $^{*}P < 0.05$, $^{**}P < 0.01$, $^{***}P < 0.001$, and $^{****}P < 0.0001$.

DATA AVAILABILITY STATEMENT

The raw data supporting the conclusions of this article will be made available by the authors, without undue reservation, to any qualified researcher.

ETHICS STATEMENT

The animal study was reviewed and approved by University of East Anglia Animal Welfare and Ethical Review.

AUTHOR CONTRIBUTIONS

AA, CB, SA, RJ, and JL performed data acquisition, formal analyses, data visualisation, and participated in review and editing of the manuscript. SR performed investigation conceptualisation, data acquisition, formal analyses, data visualisation, participated in review and editing of the manuscript, acquired resources and funding, and performed supervision of the study.

FUNDING

This work was supported by funding from: the UKRI Biotechnology and Biological Sciences Research Council Norwich Research Park Biosciences Doctoral Training Partnership (Grant numbers BB/M011216/1, BB/J014524/1, BB/M011216/1); BHF (Grant number PG/15/25/31369); The Ministry of Education, Saudi Arabia. Additionally, we thank Norfolk Fundraisers, Mrs Margaret Doggett, and the Colin Wright Fund for their kind support and fundraising over the years. Robinson is also partially funded by the BBSRC Institute Strategic Programme Gut Microbes and Health BB/R012490/1 and its constituent project (BBS/E/F/000PR10355). This manuscript has been released as a pre-print at BioRxiv (Alghamdi et al., 2020).

SUPPLEMENTARY MATERIAL

The Supplementary Material for this article can be found online at: https://www.frontiersin.org/articles/10.3389/fcell.2020.00395/full#supplementary-material

FIGURE S1 | (A): PyMT transfected mLMEC pellets from nine different immortalized EC lines were subjected to DNA extraction and PCR-based genotyping at the ITGB3 locus. Shown is an agarose gel of P1/P3 and P1/P2 primer products from all EC lines. Lines 1–5 show only a P1/P3 product and are therefore wild-type (WT) for the ITGB3 locus, whilst lines 6–9 show both a P1/P3 product, and a P1/P2 product, and are therefore heterozygous (β3HET) for the ITGB3 locus. **(B)**: Western blot analysis of VE-Cadherin and ITGB3 expression in the same clones shown in **(A)**. HSC70 was used as a loading control. Because the antibody used for detection of ITGB3 recognizes a non-specific band at approximately (135kDa), a β3-knockout (NULL) lysate was included as a control (cell line #10). **(C)**: Left panel shows the densitometric analysis of mean ITGB3 band intensities normalized against HSC70 obtained using ImageJ™ [from the Western blot shown in **(B)**]. $^{**}P < 0.01$. **(D)**: The EC identity of three immortalized EC lines was re-confirmed by Western blot analysis, immunoblotting against additional EC markers Pecam-1, Endomucin, ERG and Claudin-5, alongside a GAPDH loading control and a lymphatic marker Prox-1. **(E)**: ECs were transfected either with control siRNA or one of four different NRP2-specific siRNAs (01–04) and incubated for 48 h. EC extracts were then subjected to Western blot analysis using antibodies against NRP2, NRP1 and HSC70. Except where noted (**Supplementary Figure S3**), NRP2 siRNA #03 was used for all subsequent experiments to silence NRP2 expression. **(F)**: siRNA-transfected ECs were incubated for the indicated timepoints before being lysed and subjected to Western blot analysis using antibodies against NRP2 and HSC70. Asterisks indicate statistical significance from unpaired two-tailed *t*-tests. **(G)**: Schematic diagram of the ITGB3 (WT) and (HET) loci, showing where PCR genotyping primers align. P1 and P3 amplify a wild-type product of 446-bp, whilst P1 and P2 amplify a knockout product of 538-bp.

FIGURE S2 | (A): siRNA-transfected ECs were seeded onto FN and incubated for 30 h. ECs were then re-seeded onto FN-coated coverslips, and allowed to adhere for 4 h in serum-free media. Media was then replaced with 10 μM BrdU in complete culture medium, and the cells incubated for 12 h at 37°C. ECs were then fixed with 4% PFA, before hydrolyzing the DNA with 1 M HCL. ECs were permeabilized and blocked with Dako® Protein Block Serum-Free. ECs were then incubated with anti-BrdU at 4°C overnight in a humidified chamber, followed by incubation in secondary antibody. Coverslips were subsequently mounted and the number of cells in S-phase (proliferating cells) was determined by dividing the number of the BrdU-labeled cells by the number of DAPI-labeled cells. $n = 19$ independent fields of view, containing on average 50 cells per field, per condition. **(B)**: Adhesion assay performed as described in **Figure 2A**, however, ECs were transfected with either control or NRP2 siRNA#04. Bars show mean number of adhered cells calculated from absorbance readings from 40 wells per condition, per timepoint, normalized to a 3-h incubation control plate, $N = 1$. **(C)**: Accompanying analysis to **Figure 2D**. The cell area (microns^2) was measured using ImageJ™. Quantification performed on mean data from $n \geq 25$ ECs over $N = 3$ independent experiments, nsd = not significantly different from unpaired two-tailed *t*-test. **(D)**: siRNA-transfected ECs were prepared as described in **Figure 2D** legend, measuring mean FA number, FA size and FA distribution, however, ECs were transfected with either control or NRP2 siRNA#04. Quantification performed on mean data from $n = 15$ ECs. Asterisks indicate statistical significance from an unpaired two-tailed *t*-test.

FIGURE S3 | (A): Accompanying analysis to **Figure 3D**. siRNA-transfected ECs were prepared for immunocytochemistry as described in **Figure 2C**. Fixed ECs were incubated in primary antibodies against ITGA5 overnight at 4°C. ITGA5 length was measured using the ImageJ™ software plugin simple neurite tracer. $n = 490$ cells per condition, $^{****}P$ (0.0001). Asterisks indicate statistical significance from unpaired two-tailed *t*-tests. **(B)**: siRNA-transfected ECs from three different immortalized EC lines were prepared as described in **Figure 3D** legend, however, ECs were transfected with either control (top) or NRP2 siRNA#04 (bottom). Panels show representative images from $N = 3$ independent lines, $n \geq 10$ cells per line. **(C)**: Western blot analysis of cell lysates from both primary EC clones alongside a lysate from a known fibroblast control cell line. EC extracts were immunoblotted using antibodies against known EC markers Endomucin, ERG and Claudin-5, alongside a GAPDH loading control. **(D)**: Primary ECs were transfected with either ctrl or NRP2 siRNA and prepared for immunostaining as described in **Figure 3E**. Panels show representative images from $n = 10$ cells per condition from two independent primary EC lines.

TABLE S1 | NRP2-immunoprecipitating label-free quantitative (LFQ) mass spectrometry list.

REFERENCES

Alghamdi, A. A., Benwell, C., Atkinson, S. J., Lambert, J., and Robinson, S. D. (2020). NRP2 as an emerging angiogenic player; promoting endothelial cell adhesion and migration by regulating recycling of α5 integrin. *BioRxiv [Preprint]* doi: 10.1101/744763

Atkinson, S. J., Gontarczyk, A. M., Alghamdi, A. A., Ellison, T. S., Johnson, R. T., Fowler, W. J., et al. (2018). The beta3-integrin endothelial adhesome regulates microtubule-dependent cell migration. *EMBO Rep.* 19:e44578. doi: 10.15252/embr.201744578

Avraamides, C. J., Garmy-Susini, B., and Varner, J. A. (2008). Integrins in angiogenesis and lymphangiogenesis. *Nat. Rev. Cancer* 8, 604–617. doi: 10.1038/nrc2353

Bachelder, R. E., Crago, A., Chung, J., Wendt, M. A., Shaw, L. M., Robinson, G., et al. (2001). Vascular endothelial growth factor is an autocrine survival factor for neuropilin-expressing breast carcinoma cells. *Cancer Res.* 61, 5736–5740.

Bae, D., Lu, S., Taglienti, C. A., and Mercurio, A. M. (2008). Metabolic stress induces the lysosomal degradation of neuropilin-1 but not neuropilin-2. *J. Biol. Chem.* 283, 28074–28080. doi: 10.1074/jbc.M804203200

Bielenberg, D. R., Hida, Y., Shimizu, A., Kaipainen, A., Kreuter, M., Kim, C. C., et al. (2004). Semaphorin 3F, a chemorepulsant for endothelial cells, induces a poorly vascularized, encapsulated, nonmetastatic tumor phenotype. *J. Clin. Invest.* 114, 1260–1271. doi: 10.1172/jci21378

Bouvree, K., Brunet, I., Del Toro, R., Gordon, E., Prahst, C., Cristofaro, B., et al. (2012). Semaphorin3A, neuropilin-1, and plexinA1 are required for lymphatic valve formation. *Circ. Res.* 111, 437–445. doi: 10.1161/CIRCRESAHA.112.269316

Brooks, P. C., Clark, R. A., and Cheresh, D. A. (1994). Requirement of vascular integrin alpha v beta 3 for angiogenesis. *Science* 264, 569–571. doi: 10.1126/science.7512751

Buskermolen, A. B. C., Kurniawan, N. A., and Bouten, C. V. C. (2018). An automated quantitative analysis of cell, nucleus and focal adhesion morphology. *PLoS One* 13:e0195201. doi: 10.1371/journal.pone.0195201

Cai, Y., Jia, T., Lam, S. K., Ding, Y., Gao, C., San, M. W., et al. (2011). Multiple cytosolic and transmembrane determinants are required for the trafficking of SCAMP1 via an ER-Golgi-TGN-PM pathway. *Plant J.* 65, 882–896. doi: 10.1111/j.1365-313X.2010.04469.x

Cao, Y., Hoeppner, L. H., Bach, S., E, G., Guo, Y., Wang, E., et al. (2013). Neuropilin-2 promotes extravasation and metastasis by interacting with endothelial alpha5 integrin. *Cancer Res.* 73, 4579–4590. doi: 10.1158/0008-5472.CAN-13-0529

Caswell, P. T., Spence, H. J., Parsons, M., White, D. P., Clark, K., Cheng, K. W., et al. (2007). Rab25 associates with alpha5beta1 integrin to promote invasive migration in 3D microenvironments. *Dev. Cell* 13, 496–510. doi: 10.1016/j.devcel.2007.08.012

Caunt, M., Mak, J., Liang, W. C., Stawicki, S., Pan, Q., Tong, R. K., et al. (2008). Blocking neuropilin-2 function inhibits tumor cell metastasis. *Cancer Cell* 13, 331–342. doi: 10.1016/j.ccr.2008.01.029

Curreli, S., Arany, Z., Gerardy-Schahn, R., Mann, D., and Stamatos, N. M. (2007). Polysialylated neuropilin-2 is expressed on the surface of human dendritic cells and modulates dendritic cell-T lymphocyte interactions. *J. Biol. Chem.* 282, 30346–30356. doi: 10.1074/jbc.m702965200

Dallas, N. A., Gray, M. J., Xia, L., Fan, F., Van Buren, G. II, Gaur, P., et al. (2008). Neuropilin-2-mediated tumor growth and angiogenesis in pancreatic adenocarcinoma. *Clin. Cancer Res.* 14, 8052–8060. doi: 10.1158/1078-0432.CCR-08-1520

De Pascalis, C., and Etienne-Manneville, S. (2017). Single and collective cell migration: the mechanics of adhesions. *Mol. Biol. Cell* 28, 1833–1846. doi: 10.1091/mbc.E17-03-0134

Duleh, S. N., and Welch, M. D. (2012). Regulation of integrin trafficking, cell adhesion, and cell migration by WASH and the Arp2/3 complex. *Cytoskeleton* 69, 1047–1058. doi: 10.1002/cm.21069

Ellison, T. S., Atkinson, S. J., Steri, V., Kirkup, B. M., Preedy, M. E., Johnson, R. T., et al. (2015). Suppression of beta3-integrin in mice triggers a neuropilin-1-dependent change in focal adhesion remodelling that can be targeted to block pathological angiogenesis. *Dis. Model. Mech.* 8, 1105–1119. doi: 10.1242/dmm.019927

Fakhari, M., Pullirsch, D., Abraham, D., Paya, K., Hofbauer, R., Holzfeind, P., et al. (2002). Selective upregulation of vascular endothelial growth factor receptors neuropilin-1 and -2 in human neuroblastoma. *Cancer* 94, 258–263. doi: 10.1002/cncr.10177

Favier, B., Alam, A., Barron, P., Bonnin, J., Laboudie, P., Fons, P., et al. (2006). Neuropilin-2 interacts with VEGFR-2 and VEGFR-3 and promotes human endothelial cell survival and migration. *Blood* 108, 1243–1250. doi: 10.1182/blood-2005-11-4447

Fukahi, K., Fukasawa, M., Neufeld, G., Itakura, J., and Korc, M. (2004). Aberrant expression of neuropilin-1 and -2 in human pancreatic cancer cells. *Clin. Cancer Res.* 10, 581–590. doi: 10.1158/1078-0432.ccr-0930-03

Fukasawa, M., Matsushita, A., and Korc, M. (2007). Neuropilin-1 interacts with integrin beta1 and modulates pancreatic cancer cell growth, survival and invasion. *Cancer Biol. Ther.* 6, 1173–1180.

Goel, H. L., Pursell, B., Standley, C., Fogarty, K., and Mercurio, A. M. (2012). Neuropilin-2 regulates alpha6beta1 integrin in the formation of focal adhesions and signaling. *J. Cell Sci.* 125, 497–506. doi: 10.1242/jcs.094433

Goley, E. D., and Welch, M. D. (2006). The ARP2/3 complex: an actin nucleator comes of age. *Nat. Rev. Mol. Cell Biol.* 7, 713–726. doi: 10.1038/nrm2026

Goodman, S. L., and Picard, M. (2012). Integrins as therapeutic targets. *Trends Pharmacol. Sci.* 33, 405–412. doi: 10.1016/j.tips.2012.04.002

Herzog, Y., Kalcheim, C., Kahane, N., Reshef, R., and Neufeld, G. (2001). Differential expression of neuropilin-1 and neuropilin-2 in arteries and veins. *Mech. Dev.* 109, 115–119. doi: 10.1016/s0925-4773(01)00518-4

Hodivala-Dilke, K. M., Mchugh, K. P., Tsakiris, D. A., Rayburn, H., Crowley, D., Ullman-Cullere, M., et al. (1999). Beta3-integrin-deficient mice are a model for Glanzmann thrombasthenia showing placental defects and reduced survival. *J. Clin. Invest.* 103, 229–238. doi: 10.1172/jci5487

Hynes, R. O. (2002). Integrins: bidirectional, allosteric signaling machines. *Cell* 110, 673–687.

Ikuno, T., Masumoto, H., Yamamizu, K., Yoshioka, M., Minakata, K., Ikeda, T., et al. (2017). Efficient and robust differentiation of endothelial cells from human induced pluripotent stem cells via lineage control with VEGF and cyclic AMP. *PLoS One* 12:e0173271. doi: 10.1371/journal.pone.0173271

Jurisic, G., Maby-El Hajjami, H., Karaman, S., Ochsenbein, A. M., Alitalo, A., Siddiqui, S. S., et al. (2012). An unexpected role of semaphorin3a-neuropilin-1 signaling in lymphatic vessel maturation and valve formation. *Circ. Res.* 111, 426–436. doi: 10.1161/CIRCRESAHA.112.269399

Kaksonen, M., Toret, C. P., and Drubin, D. G. (2006). Harnessing actin dynamics for clathrin-mediated endocytosis. *Nat. Rev. Mol. Cell Biol.* 7, 404–414. doi: 10.1038/nrm1940

Kawakami, T., Tokunaga, T., Hatanaka, H., Kijima, H., Yamazaki, H., Abe, Y., et al. (2002). Neuropilin 1 and neuropilin 2 co-expression is significantly correlated with increased vascularity and poor prognosis in nonsmall cell lung carcinoma. *Cancer* 95, 2196–2201. doi: 10.1002/cncr.10936

Kim, S., Bakre, M., Yin, H., and Varner, J. A. (2002). Inhibition of endothelial cell survival and angiogenesis by protein kinase A. *J. Clin. Invest.* 110, 933–941. doi: 10.1172/jci0214268

Kim, S., Bell, K., Mousa, S. A., and Varner, J. A. (2000). Regulation of angiogenesis in vivo by ligation of integrin alpha5beta1 with the central cell-binding domain of fibronectin. *Am. J. Pathol.* 156, 1345–1362. doi: 10.1016/s0002-9440(10)65005-5

Krilleke, D., Deerkenez, A., Schubert, W., Giri, I., Robinson, G. S., Ng, Y. S., et al. (2007). Molecular mapping and functional characterization of the VEGF164 heparin-binding domain. *J. Biol. Chem.* 282, 280450–280456.

Lambert, J., Makin, K., Akbareian, S., Johnson, R. T., Alghamdi, A. A., Robinson, S. D., et al. (2020). ADAMTS-1 and Syndecan-4 intersect in the regulation of cell migration and angiogenesis. *J. Cell Sci.* 133:jcs235762. doi: 10.1242/jcs.235762

Lantuejoul, S., Constantin, B., Drabkin, H., Brambilla, C., Roche, J., and Brambilla, E. (2003). Expression of VEGF, semaphorin SEMA3F, and their common receptors neuropilins NP1 and NP2 in preinvasive bronchial lesions, lung tumours, and cell lines. *J. Pathol.* 200, 336–347. doi: 10.1002/path.1367

Laukaitis, C. M., Webb, D. J., Donais, K., and Horwitz, A. F. (2001). Differential dynamics of alpha 5 integrin, paxillin, and alpha-actinin during formation and disassembly of adhesions in migrating cells. *J. Cell Biol.* 153, 1427–1440. doi: 10.1083/jcb.153.7.1427

Le Boeuf, F., Houle, F., and Huot, J. (2004). Regulation of vascular endothelial growth factor receptor 2-mediated phosphorylation of focal adhesion kinase by heat shock protein 90 and Src kinase activities. *J. Biol. Chem.* 279, 39175–39185. doi: 10.1074/jbc.m405493200

Malek, M., Guillaumot, P., Huber, A. L., Lebeau, J., Petrilli, V., Kfoury, A., et al. (2012). LAMTOR1 depletion induces p53-dependent apoptosis via aberrant lysosomal activation. *Cell Death Dis.* 3:e300. doi: 10.1038/cddis.2012.39

Margadant, C., Monsuur, H. N., Norman, J. C., and Sonnenberg, A. (2011). Mechanisms of integrin activation and trafficking. *Curr. Opin. Cell Biol.* 23, 607–614. doi: 10.1016/j.ceb.2011.08.005

Mucka, P., Levonyak, N., Geretti, E., Zwaans, B. M. M., Li, X., Adini, I., et al. (2016). Inflammation and lymphedema are exacerbated and prolonged by neuropilin 2 deficiency. *Am. J. Pathol.* 186, 2803–2812. doi: 10.1016/j.ajpath.2016.07.022

Nobes, C. D., and Hall, A. (1995). Rho, rac, and cdc42 GTPases regulate the assembly of multimolecular focal complexes associated with actin stress fibers, lamellipodia, and filopodia. *Cell* 81, 53–62. doi: 10.1016/0092-8674(95)90370-4

Paul, N. R., Jacquemet, G., and Caswell, P. T. (2015). Endocytic trafficking of integrins in cell migration. *Curr. Biol.* 25, R1092–R1105. doi: 10.1016/j.cub.2015.09.049

Pellet-Many, C., Frankel, P., Jia, H., and Zachary, I. (2008). Neuropilins: structure, function and role in disease. *Biochem. J.* 411, 211–226. doi: 10.1042/bj20071639

Prahst, C., Heroult, M., Lanahan, A. A., Uziel, N., Kessler, O., Shraga-Heled, N., et al. (2008). Neuropilin-1-VEGFR-2 complexing requires the PDZ-binding domain of neuropilin-1. *J. Biol. Chem.* 283, 25110–25114. doi: 10.1074/jbc.C800137200

Price, L. S., Leng, J., Schwartz, M. A., and Bokoch, G. M. (1998). Activation of Rac and Cdc42 by integrins mediates cell spreading. *Mol. Biol. Cell* 9, 1863–1871. doi: 10.1091/mbc.9.7.1863

Remacle, A., Murphy, G., and Roghi, C. (2003). Membrane type I-matrix metalloproteinase (MT1-MMP) is internalised by two different pathways and is recycled to the cell surface. *J. Cell Sci.* 116, 3905–3916. doi: 10.1242/jcs.00710

Reynolds, L. E., and Hodivala-Dilke, K. M. (2006). Primary mouse endothelial cell culture for assays of angiogenesis. *Methods Mol. Med.* 120, 503–509.

Ridley, A. J. (2011). Life at the leading edge. *Cell* 145, 1012–1022. doi: 10.1016/j.cell.2011.06.010

Ridley, A. J., Schwartz, M. A., Burridge, K., Firtel, R. A., Ginsberg, M. H., Borisy, G., et al. (2003). Cell migration: integrating signals from front to back. *Science* 302, 1704–1709. doi: 10.1126/science.1092053

Roberts, M., Barry, S., Woods, A., Van Der Sluijs, P., and Norman, J. (2001). PDGF-regulated rab4-dependent recycling of alphavbeta3 integrin from early endosomes is necessary for cell adhesion and spreading. *Curr. Biol.* 11, 1392–1402. doi: 10.1016/s0960-9822(01)00442-0

Robinson, S. D., Reynolds, L. E., Kostourou, V., Reynolds, A. R., Da Silva, R. G., Tavora, B., et al. (2009). Alphav beta3 integrin limits the contribution of neuropilin-1 to vascular endothelial growth factor-induced angiogenesis. *J. Biol. Chem.* 284, 33966–33981. doi: 10.1074/jbc.M109.030700

Robinson, S. D., Reynolds, L. E., Wyder, L., Hicklin, D. J., and Hodivala-Dilke, K. M. (2004). Beta3-integrin regulates vascular endothelial growth factor-A-dependent permeability. *Arterioscler. Thromb. Vasc. Biol.* 24, 2108–2114. doi: 10.1161/01.atv.0000143857.27408.de

Sachse, M., Urbe, S., Oorschot, V., Strous, G. J., and Klumperman, J. (2002). Bilayered clathrin coats on endosomal vacuoles are involved in protein sorting toward lysosomes. *Mol. Biol. Cell* 13, 1313–1328. doi: 10.1091/mbc.01-10-0525

Schiller, H. B., Friedel, C. C., Boulegue, C., and Fassler, R. (2011). Quantitative proteomics of the integrin adhesome show a myosin II-dependent recruitment of LIM domain proteins. *EMBO Rep.* 12, 259–266. doi: 10.1038/embor.2011.5

Schiller, H. B., Hermann, M. R., Polleux, J., Vignaud, T., Zanivan, S., Friedel, C. C., et al. (2013). beta1- and alphav-class integrins cooperate to regulate myosin II during rigidity sensing of fibronectin-based microenvironments. *Nat. Cell Biol.* 15, 625–636. doi: 10.1038/ncb2747

Shi, F., and Sottile, J. (2008). Caveolin-1-dependent beta1 integrin endocytosis is a critical regulator of fibronectin turnover. *J. Cell Sci.* 121, 2360–2371. doi: 10.1242/jcs.014977

Sivarapatna, A., Ghaedi, M., Le, A. V., Mendez, J. J., Qyang, Y., and Niklason, L. E. (2015). Arterial specification of endothelial cells derived from human induced pluripotent stem cells in a biomimetic flow bioreactor. *Biomaterials* 53, 621–633. doi: 10.1016/j.biomaterials.2015.02.121

Small, J. V., Rottner, K., Kaverina, I., and Anderson, K. I. (1998). Assembling an actin cytoskeleton for cell attachment and movement. *Biochim. Biophys. Acta* 1404, 271–281. doi: 10.1016/s0167-4889(98)00080-9

Soker, S., Takashima, S., Miao, H. Q., Neufeld, G., and Klagsbrun, M. (1998). Neuropilin-1 is expressed by endothelial and tumor cells as an isoform-specific receptor for vascular endothelial growth factor. *Cell* 92, 735–745. doi: 10.1016/s0092-8674(00)81402-6

Suzuki-Inoue, K., Yatomi, Y., Asazuma, N., Kainoh, M., Tanaka, T., Satoh, K., et al. (2001). Rac, a small guanosine triphosphate-binding protein, and p21-activated kinase are activated during platelet spreading on collagen-coated surfaces: roles of integrin alpha(2)beta(1). *Blood* 98, 3708–3716. doi: 10.1182/blood.v98.13.3708

Tomizawa, Y., Sekido, Y., Kondo, M., Gao, B., Yokota, J., Roche, J., et al. (2001). Inhibition of lung cancer cell growth and induction of apoptosis after reexpression of 3p21.3 candidate tumor suppressor gene SEMA3B. *Proc. Natl. Acad. Sci. U.S.A.* 98, 13954–13959. doi: 10.1073/pnas.231490898

Valdembri, D., Caswell, P. T., Anderson, K. I., Schwarz, J. P., Konig, I., Astanina, E., et al. (2009). Neuropilin-1/GIPC1 signaling regulates alpha5beta1 integrin traffic and function in endothelial cells. *PLoS Biol.* 7:e25. doi: 10.1371/journal.pbio.1000025

Valdembri, D., and Serini, G. (2012). Regulation of adhesion site dynamics by integrin traffic. *Curr. Opin. Cell Biol.* 24, 582–591. doi: 10.1016/j.ceb.2012.08.004

Vales, A., Kondo, R., Aichberger, K. J., Mayerhofer, M., Kainz, B., Sperr, W. R., et al. (2007). Myeloid leukemias express a broad spectrum of VEGF receptors including neuropilin-1 (NRP1) and NRP2. *Leuk. Lymphoma* 48, 1997–2007. doi: 10.1080/10428190701534424

Velling, T., Collo, G., Sorokin, L., Durbeej, M., Zhang, H., and Gullberg, D. (1996). Distinct alpha 7A beta 1 and alpha 7B beta 1 integrin expression patterns during mouse development: alpha 7A is restricted to skeletal muscle but alpha 7B is expressed in striated muscle, vasculature, and nervous system. *Dev. Dyn.* 207, 355–371. doi: 10.1002/(sici)1097-0177(199612)207:4<355::aid-aja1>3.0.co;2-g

Webb, D. J., Parsons, J. T., and Horwitz, A. F. (2002). Adhesion assembly, disassembly and turnover in migrating cells – over and over and over again. *Nat. Cell Biol.* 4, E97–E100.

Yuan, L., Moyon, D., Pardanaud, L., Breant, C., Karkkainen, M. J., Alitalo, K., et al. (2002). Abnormal lymphatic vessel development in neuropilin 2 mutant mice. *Development* 129, 4797–4806.

Zachary, I. (2014). Neuropilins: role in signalling, angiogenesis and disease. *Chem. Immunol. Allergy* 99, 37–70. doi: 10.1159/000354169

Zech, T., Calaminus, S. D., Caswell, P., Spence, H. J., Carnell, M., Insall, R. H., et al. (2011). The Arp2/3 activator WASH regulates alpha5beta1-integrin-mediated invasive migration. *J. Cell Sci.* 124, 3753–3759. doi: 10.1242/jcs.080986

Conflict of Interest: The authors declare that the research was conducted in the absence of any commercial or financial relationships that could be construed as a potential conflict of interest.

frontiers in Physiology

REVIEW
published: 05 June 2020
doi: 10.3389/fphys.2020.00552

Blood Flow Forces in Shaping the Vascular System: A Focus on Endothelial Cell Behavior

Pedro Campinho[1,2,3,4], *Andrej Vilfan*[5,6] *and Julien Vermot*[1,2,3,4,7]*

[1] *Institut de Génétique et de Biologie Moléculaire et Cellulaire, Illkirch, France,* [2] *Centre National de la Recherche Scientifique, UMR 7104, Illkirch, France,* [3] *Institut National de la Santé et de la Recherche Médicale, U964, Illkirch, France,* [4] *Department of Development and Stem Cells, Université de Strasbourg, Illkirch, France,* [5] *Department of Living Matter Physics, Max Planck Institute for Dynamics and Self-Organization, Göttingen, Germany,* [6] *Department of Condensed Matter Physics, J. Stefan Institute, Ljubljana, Slovenia,* [7] *Department of Bioengineering, Imperial College London, London, United Kingdom*

The endothelium is the cell monolayer that lines the interior of the blood vessels separating the vessel lumen where blood circulates, from the surrounding tissues. During embryonic development, endothelial cells (ECs) must ensure that a tight barrier function is maintained whilst dynamically adapting to the growing vascular tree that is being formed and remodeled. Blood circulation generates mechanical forces, such as shear stress and circumferential stretch that are directly acting on the endothelium. ECs actively respond to flow-derived mechanical cues by becoming polarized, migrating and changing neighbors, undergoing shape changes, proliferating or even leaving the tissue and changing identity. It is now accepted that coordinated changes at the single cell level drive fundamental processes governing vascular network morphogenesis such as angiogenic sprouting, network pruning, lumen formation, regulation of vessel caliber and stability or cell fate transitions. Here we summarize the cell biology and mechanics of ECs in response to flow-derived forces, discuss the latest advances made at the single cell level with particular emphasis on *in vivo* studies and highlight potential implications for vascular pathologies.

Keywords: cardiovascular, stretch, low Reynolds number, angiogenesis, *Danio rerio* (zebrafish), live imaging, cilia, mechanotransduction

OPEN ACCESS

Edited by:
Elizabeth Anne Vincent Jones, KU Leuven, Belgium

Reviewed by:
Nicolas Baeyens, Université libre de Bruxelles, Belgium
Claudio Areias Franco, Instituto de Medicina Molecular, Portugal

***Correspondence:**
Julien Vermot
jvermot@ic.ac.uk

Specialty section:
This article was submitted to Vascular Physiology, a section of the journal Frontiers in Physiology

Received: *13 March 2020*
Accepted: *30 April 2020*
Published: *05 June 2020*

Citation:
Campinho P, Vilfan A and Vermot J (2020) Blood Flow Forces in Shaping the Vascular System: A Focus on Endothelial Cell Behavior. Front. Physiol. 11:552. doi: 10.3389/fphys.2020.00552

INTRODUCTION

The endothelium is a squamous cell monolayer that lines the lumen of all blood vessels and keeps the vessel interior sealed from the neighboring environment. Endothelial cells (ECs) are interconnected by cellular junctions that confer selective permeability and have their apical side facing the vessel lumen where fluids, nutrients, gases, cells, hormones, and other factors circulate to reach the entire organism. To ensure distribution to virtually all tissues in the body during embryonic development, ECs assemble into a vast tree-like network of tubes – the vascular system. Network development is achieved in a series of stereotyped steps. First, a primary network that consists mostly of the main axial vessels, the aortic arches, and the umbilical vessels is formed in a process termed vasculogenesis (Downs et al., 1998; Swift and Weinstein, 2009; Potente et al., 2011; Arora and Papaioannou, 2012; Frisdal and Trainor, 2014). In zebrafish, EC precursors – the angioblasts – migrate from both sides of the lateral plate mesoderm to meet at the embryonic midline where they coalesce into a chord like structure that later splits into two axial vessels in

which eventually a lumen opens up to form the main artery and vein before circulation initiates (Swift and Weinstein, 2009; Sato, 2013). In amniotes, the process is slightly different and first two independent lateral dorsal aortae are formed at each side of the notochord that later fuse to give rise to the common dorsal aorta (Strilic et al., 2009; Sato, 2013). The rest of the vasculature (secondary network) arises in the presence of blood flow and is constantly being remodeled to adapt to embryonic growth and to new physiological demands like the irrigation of newly formed organs. This process is called angiogenesis and will be the main focus of this review. New branches arise from pre-existing vessels in a process called sprouting angiogenesis that involves the differentiation of a tip cell leading the way as well as stalk cells that follow, although these roles are not fixed and cells can dynamically swap positions (Geudens and Gerhardt, 2011; Siekmann et al., 2013). Afterward, the newly growing sprouts fuse with one another or with previously existing vessels, thus forming new connections in a process named anastomosis (Betz et al., 2016). Alongside, the newly formed connections become patent, allowing the formation of a lumen where blood can circulate. Finally, the network is optimized by the stabilization of some branches while others regress in what is known as vascular pruning (Betz et al., 2016). Another important type of angiogenesis involved in network remodeling and optimization is the so-called intussusceptive (splitting) angiogenesis in which ECs from opposing vascular walls protrude inwards, toward the vessel lumen, forming transluminal pillars that can ultimately split a pre-existing vessel in two (Makanya et al., 2009).

The majority of growth and remodeling of the vascular network takes place when blood circulation has already initiated and the endothelium is exposed to flow-derived mechanical forces such as shear stress, circumferential stress and axial stress (**Figure 1**). Shear stress is the force parallel to the tissue surface that arises due to shear flow of the viscous fluid and depends on the flow rate, viscosity of the blood, as well as on the geometry of the tube. The other two forces are governed by the intraluminal pressure. Circumferential stress is the force tangential to the vessel wall in the azimuthal direction (around the circumference) and axial stress is the force along the longitudinal (long) axis of the vessel. These three stresses dictate blood vessel mechanics and influence geometrical parameters of vessels, such as the radius, wall thickness, and length (Hoefer et al., 2013). Although the importance of axial stress has long been recognized, its impact on blood vessel morphogenesis is still less well studied (Humphrey et al., 2009). EC behaviors induced by shear stress or circumferential stretch are better studied, particularly during embryonic development, and will be the focus of our review. Besides intravascular flow, we will also mention interstitial (transvascular) flow due to vessel permeability, which generates shear stress that has been shown to influence sprouting angiogenesis and is particularly relevant in the context of tumor vascular biology (Kutys and Chen, 2016).

As a physical stimulus, blood flow can be highly diverse and since ECs are sensitive to many different features of flows it is important to consider the details of the flow profiles in the developing vascular system. As the heart is maturing during the earliest steps of vascular morphogenesis, the flow generated as a result of its immature activity is constantly changing (Boselli et al., 2015). As a consequence, different types of flow can be generated in the same vessel as it matures. Embryonic blood flow falls into the low Reynolds number regime; see in zebrafish (Anton et al., 2013; Goetz et al., 2014), the early embryonic vascular network in mouse (Jones et al., 2004) and chick (Al-Roubaie et al., 2011), where viscous forces dominate and inertia is negligible (Freund et al., 2012). This leads to flow profiles that are not intuitive, from unidirectional to bidirectional flow and pulsatile to disturbed flow, all of them in theory capable of eliciting distinct cellular behaviors (Freund et al., 2012; Boselli et al., 2015) or different transcriptional responses (LaMack and Friedman, 2007; Yee et al., 2008; Feaver et al., 2013). The most extreme flow rates are certainly experienced by the ECs of the heart outflow tract (Duchemin et al., 2019a) as well as endocardial cells, where the flow profiles can be mapped and the shear stress dissected into components (Boselli et al., 2017), all of which may contain mechanical information that is sensed by ECs. It has been proposed that the difference between arterial and venous identity is enhanced by flow (Le Noble et al., 2004) but the complexity is augmented by the cell behaviors involved in the process which will be discussed here. In addition, the mechanics of the vascular system follows basic principles of blood vessel mechanics described in adults. For example, the maturing main trunk artery in the zebrafish embryo deforms at each pulse of heart contraction (Anton et al., 2013; Campinho et al., 2018). Overall, significant advances coming from progresses in live-imaging performed in zebrafish and other species in combination with tailor-made sophisticated image analysis algorithms and mathematical modeling will be discussed here in the perspective of cell behaviors.

Flow-derived mechanical cues (Jones et al., 2006; Freund et al., 2012; Duchemin et al., 2019b) in combination with a tightly regulated genetic and metabolic program (Potente and Makinen, 2017) are well known to be essential for controlling the growth, identity and shaping of the vascular network. Tissue morphogenesis and homeostasis is driven by coordinated changes at the single cell level, such as cell shape changes, rearrangements, proliferation and extrusion or cell fate specification, which are well described for epithelial morphogenesis (Guillot and Lecuit, 2013). Recent studies have shed light on cellular changes triggered by blood flow in the developing vasculature. In this review, we attempt to summarize the latest advances on flow-induced single EC behavior in the early development of the vascular system *in vivo*.

ENDOTHELIAL CELL POLARIZATION AND MIGRATION

Flow induced polarization of cells within the plane of the endothelium is well established and certainly participates to the morphogenetic changes activated by flow forces. Cultured ECs respond to shear stress by becoming elongated and oriented along the axis of flow (Levesque and Nerem, 1985) via re-organization of the cytoskeleton (Wojciak-Stothard and Ridley, 2003; Noria et al., 2004). Shear stress sensing can occur at

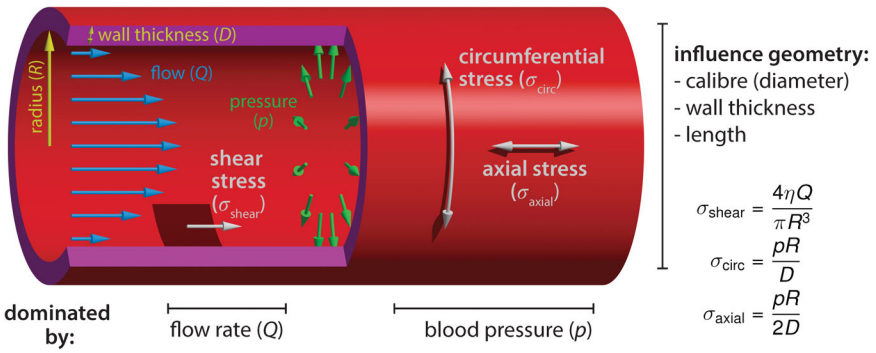

FIGURE 1 | Blood flow-derived forces. Schematic representation of the mechanical forces experienced by endothelial cells due to blood circulation inside the vessels. The blood flow, measured by the volume flow rate Q, causes a shear stress σ_{shear} on the wall. The shear stress depends on the flow rate Q, the blood viscosity η and the vessel radius R. The relationship shown is valid in laminar flow, occurring at low Reynolds numbers. Independently of the flow, the hydrostatic pressure p causes a circumferential (hoop) stress σ_{circ} and an axial stress σ_{axial}. Contrary to shear stress, they increase linearly with the vessel radius. The circumferential stress has twice the magnitude of the axial stress. The equations hold for thin walls ($D \ll R$). Furthermore, we assumed that no external forces are acting on the vessel, such that the pressure forces are fully counterbalanced by the stress in the walls (depending on the mechanical environment, the force-free condition may not always be fulfiled, especially in the axial direction).

junctional complexes, membrane receptors or channels and at the glycocalyx – for review see Duchemin et al. (2019b), Shurer et al. (2019). The glycocalyx is a thin sugar matrix covering the apical side of ECs present at blood flow onset that is required for the formation of a normal vascular network in chicken (Henderson-Toth et al., 2012). Moreover, its selective stimulation results in endothelial nitric oxide production, a potent vascular signaling molecule (Bartosch et al., 2017). Shear stress induced cytoskeletal remodeling works via force transmission at the cellular junctions (Baeyens et al., 2016a; Duchemin et al., 2019b), which simultaneously causes tension to increase at junctional platelet endothelial cell adhesion molecule (PECAM)-1 while decreasing at junctional vascular endothelial (VE)-cadherin. This is in line with observations that even acute loss of blood flow does not lead to clear changes in the tension at the junctional VE-cadherin in the zebrafish dorsal aorta (DA) (Lagendijk et al., 2017). The tension rising across junctional PECAM-1 promotes its association with vimentin that in turn transmits back myosin-generated forces to PECAM-1, thus working as a signal amplification mechanism. Tension building-up across the cytoskeleton appears to be counterbalanced by phosphoinositide (PI) 3-kinase dependent inhibition of actomyosin contractility, which prevents ECs from becoming overstretched and facilitates cellular rearrangements (Angulo-Urarte et al., 2018). On the other hand, ECs exposed to cyclic mechanical strain re-orient perpendicularly to the axis of strain by remodeling their cytoskeleton (Thodeti et al., 2009). Here the force sensing mechanism works via the transient receptor potential channel 4, which results in β1-integrin activation at focal adhesions through PI3-kinase activity. Recently, β1-integrin has also been proposed to function as a sensor of the flow direction (Xanthis et al., 2019) and as a regulator of *klf2a* (Krüppel-like factor 2, *klf2*) expression in zebrafish (Renz et al., 2015). At the tissue scale, the endothelium mechanical state is thus defined by the influence of forces generated both by the mechanical environment (flow, stretch) and the EC contractile activity.

Besides altering their shape and orientation, ECs can also migrate in response to flow forces. A recent *in vitro* study reported EC migration in response to gradients of shear stress created by impinging flow (Ostrowski et al., 2014). However, the migration direction varied depending on the cell density; high confluent cells migrate against the flow direction whereas low-density (isolated) cells migrate with the flow. In addition, cell orientation relative to flow seems to be cell type dependent. Aortic valve ECs elongate perpendicularly to the unidirectional shear stress generated by steady laminar flow (Butcher et al., 2004), contrary to ECs that align with the shear axis (Levesque and Nerem, 1985). Similarly, endocardial cells tend to converge toward the area of high shear and oscillatory flow and do not exactly follow the direction of the net flow during the initial steps of valve development in zebrafish (Boselli et al., 2017). Despite the crucial role for flow-induced cell polarization and migration during development and remodeling of the vascular network, the cellular and molecular mechanisms involved have remained elusive until recently. Besides the macroscopic changes in cell shape and alignment, cell polarization is also reflected by the internal organization of cellular organelles or compartments which is particularly relevant in migrating cells or in establishing tissue polarity (**Figure 2**). Two independent studies used mouse retinas and zebrafish embryos to follow EC polarity *in vivo* by monitoring the position of the Golgi apparatus relative to the cell nucleus (Franco et al., 2016; Kwon et al., 2016). This approach revealed that ECs polarize against the flow direction with the Golgi located in front of the nucleus and that the degree of polarization is positively correlated with the flow and shear stress magnitude (Franco et al., 2016). The response is similar in other developing blood vessels and is reversible depending on the flow forces ECs experience (Kwon et al., 2016). Mechanistically, the Golgi complex localization at the leading edge of migrating ECs requires the Apelin receptor, a G-protein coupled receptor. Nevertheless, EC response to flow differs between arteries and veins, with arterial ECs displaying, in general, a higher degree of

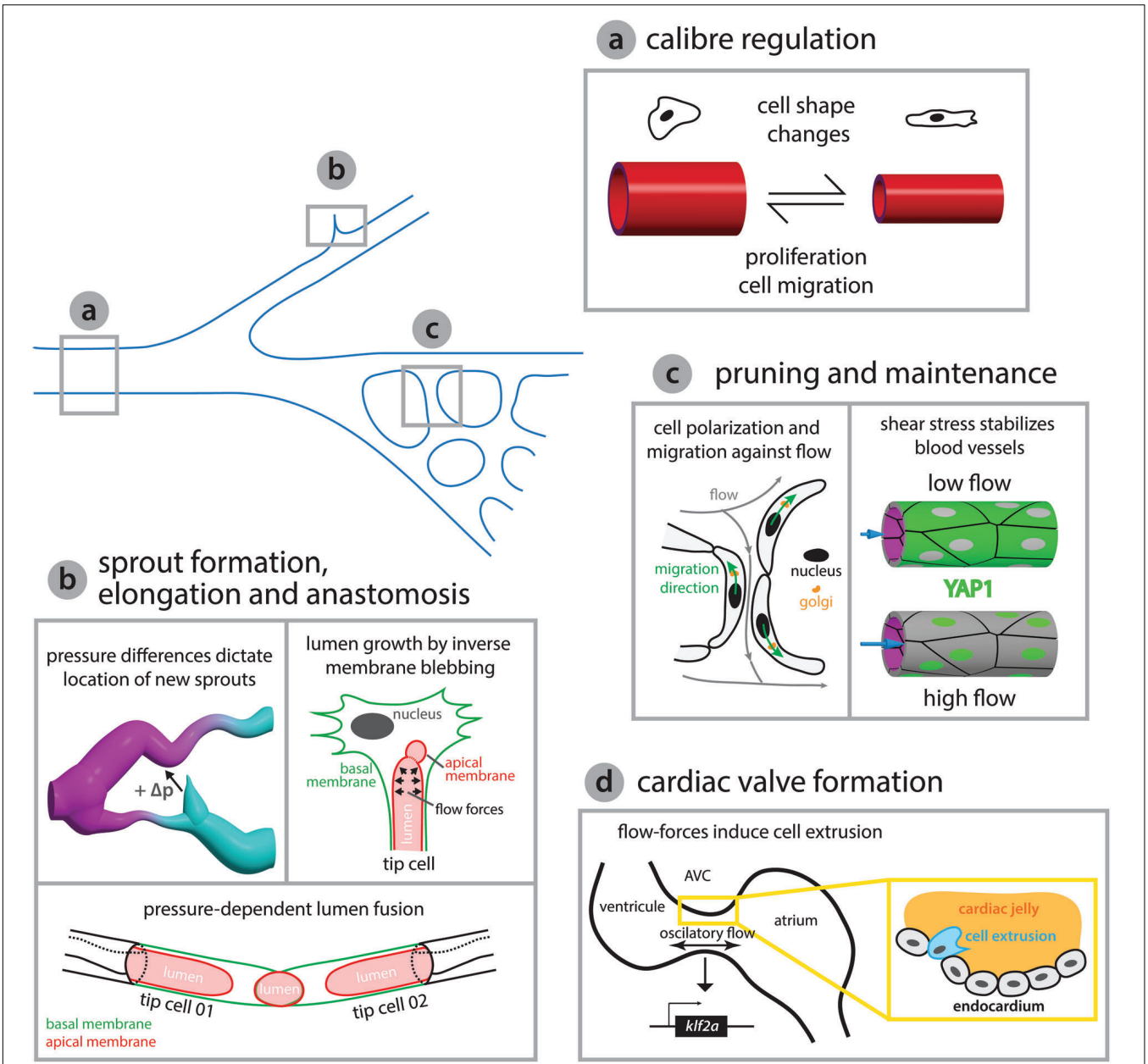

FIGURE 2 | Endothelial cell behaviors triggered by flow-derived mechanical cues during vascular network growth and development. **(a)** Arteries adjust their caliber in response to hemodynamic forces. Arteries can either reduce their diameter via coordinated cell shape changes (Sugden et al., 2017) or increase the diameter by cell proliferation and migration toward enlarging vessels (Udan et al., 2013; Poduri et al., 2017). **(b)** Blood pressure has been shown to play a central role in network growth. The location and growth of newly forming sprouts is set by local differences in blood pressure (high and low pressure, magenta and cyan, respectively, Ghaffari et al., 2015). In addition, intraluminal pressure causes inverse blebbing of the apical membrane that drives lumen growth in new sprouts – drawn after Gebala et al. (2016). Similarly, during vessel anastomosis the apical membranes of two adjacent tip cells are pushed toward each other in a blood pressure-dependent fashion – illustration after Lenard et al. (2013). **(c)** Vascular networks can be remodeled in response to shear stress. Cell polarization and migration against the flow direction can lead to retraction of poorly irrigated vessels – sketched after Franco et al. (2016) – while vessels exposed to vigorous flow are kept by shear stress induced translocation of YAP to the nucleus – depiction after Nakajima et al. (2017). **(d)** Flow-derived mechanical cues can lead to cell extrusion and the formation of new structures such as the atrioventricular canal (AVC) valve or trigger cell fate transitions as seen during hematopoietic stem cell formation (see **Figure 3**). During AVC valve formation oscillatory blood flow triggers expression of the transcription factor *klf2a*, which is thought to promote invasion of the cardiac jelly by endocardial cells thus initiating the formation of the valve leaflets. Diagram after Heckel et al. (2015) and Steed et al. (2016).

polarization (Kwon et al., 2016). In addition, shear stress-induced EC polarization and migration requires Dachshund homolog 1 DACH1 dependent activation of the C-X-C motif chemokine (CXC) ligand 12 and its CXC receptor 4 (Chang et al., 2017). The signaling axis formed by the CXC receptor 4 – ligand 12 is known to be involved in cell migration against blood flow

during artery formation (Xu et al., 2014), which is coupled to sprouting angiogenesis by Notch function and its ligand Delta-like 4 (Pitulescu et al., 2017). The transcription factor DACH1 is strongly expressed in developing arteries exposed to low (variable) flow and down-regulated in mature vessels exposed to high (laminar uniform) blood flow. Thus, DACH1 levels of expression depend on blood flow intensity (Chang et al., 2017). Considering that ECs experience a broad range of mechanical stimuli, including different flow profiles, numerous evidences indicate that their sensitivity is tuned to certain differences in the flow patterns. They may include shear stress magnitude, direction, temporal gradients and frequency content (Orr et al., 2007; Simmers et al., 2007; Feaver et al., 2010, 2013). When simply considering shear, cultivated ECs display preferential response to a range of shear stress which is cell line dependent (Baeyens et al., 2015). Where is this selectivity to certain flow features coming from? This may be partly explained by cellular context. For example, EC response is modulated by Vascular endothelial growth factor receptor (VEGFR) 3 expression levels, which tune the sensitivity of the shear stress sensor PECAM-1/VE-cadherin. Furthermore, non-canonical Wingless-related integration site (Wnt) signaling provides an additional layer of modulation of EC sensitivity to flow (Franco et al., 2015). Genetic knock-out of Wnt5a and Wnt11 produced mouse embryos with ECs that became responsive to lower shear stress levels. Wnt5 and Wnt11 depleted ECs have no alteration in the expression of many flow responsive genes, suggesting that Wnt acts downstream of the flow sensing machinery (Franco et al., 2015). This just highlights one mode of regulation but there are many other ways, including modes where the mechanosensitive apparatus could be directly modulated to tune flow sensing.

SPROUTING ANGIOGENESIS

Blood flow forces have been implicated in the regulation of new angiogenic sprout formation as well as elongation. Nevertheless, the flow-derived forces and the cellular responses at work are only now starting to be understood. Because they allow system simplification and control over several parameters, *in vitro* studies using microfluidic devices have contributed extensively to our understanding of sprouting regulation by blood flow. Interstitial (transvascular) flow generated between two parallel channels lined by ECs, separated by a collagen matrix, revealed that sprouting is enhanced by interstitial flow and always initiates in the channel without shear stress (Song and Munn, 2011). At the cellular level, this behavior certainly depends on a global change in gene expression profile governed by epigenetic changes modulated by active histone deacetylase-1 (HDAC1) (Bazou et al., 2016). These gene expression changes include factors involved in cell migration, such as matrix metalloproteinases (Galie et al., 2014; Bazou et al., 2016). Yet, the role of flow-derived forces might have a more global control of the network growth by dictating the location of sprout initiation in response to spatial patterns of shear stress (Galie et al., 2014). Once again, the response is dependent on the flow profile ECs experience. For example, flow-derived forces can compete to regulate angiogenic sprouting and sometimes have opposite effects on sprouting location (Akbari et al., 2019). Sprout formation is supressed by impinging flow stagnation or by laminar shear stress, at the bifurcation point or downstream of it, respectively, while combined application of transvascular and intraluminar flow promotes angiogenic sprouting (Akbari et al., 2019). Thus, flow forces are integrated both at cellular and tissue levels. As a consequence, growing tissues should be considered as more than the sum of isolated cell responses.

Sprouting angiogenesis constitutes a great model system to study collective cell behaviors elicited in remodeling tissues in response to biological flows *in vivo*. Live-imaging of the quail embryo capillary plexus combined with computational fluid dynamics allows simultaneous characterization of hemodynamics and network remodeling. Here, the key predictor for sprout location is directly associated with pressure differences (**Figure 2**) (Ghaffari et al., 2015). The sprouts always originate from a low pressured vessel and connect to a higher pressured vessel. In addition, sprouts start at local shear stress minima except in confluence regions where two blood streams meet. Importantly, sprouting requires a positive pressure difference between two locations and the sprout elongation rate is proportional to that difference (Ghaffari et al., 2015). These pressure differences are most likely associated with interstitial flows and it will be interesting to assess if they generate meaningful signaling molecule gradients that could explain the activation of sprouting behavior. For example, in the zebrafish branchial arches flow-induced *klf2a* expression activates endothelial-specific expression of the *mir-126* microRNA, which via inhibition of *spred1* is permissive for Vegf-driven sprouting since *spred1* normally inhibits Vegf signaling (Nicoli et al., 2010). Cilia dependent shear stress sensing appears to be involved in venous sprout formation since reduced *pkd2* expression leads to network defects that are similar to those observed in the absence of blood flow (Goetz et al., 2014). Even though numerous breakthroughs in the field have helped to better understand how flow can affect cell behaviors during angiogenic processes, we are only starting to grasp how flow-derived mechanical cues affect EC sprouting. Important future work is expected in understanding the mechanosensing involved in triggering sprouting, its downstream effectors and the cross-regulation with biochemical signals involved in this process.

INTUSSUSCEPTIVE ANGIOGENESIS

Intussusceptive angiogenesis has also been shown to be governed by blood flow forces (Makanya et al., 2009). The correlation between blood flow dynamics and network optimization via intussusceptive angiogenesis was first demonstrated by locally altering the blood flow in the chick chorioallantoic membrane (CAM) and observing an accelerated formation of intussusceptive pillars (Djonov et al., 2002). Flow simulations revealed that formation of new pillars is restricted to regions of low shear stress, thus shaping the developing network (Lee et al., 2010). In addition, intussusception can also be driven by tissue-level forces. This was demonstrated by application of

uniaxial stretch to the CAM, which revealed that pillar density in stretched regions of the CAM was increased relative to non-stretched control regions (Belle et al., 2014). Live-imaging of the zebrafish caudal vein (CV) plexus and hemodynamic simulations confirmed that new pillars arise at shear stress minima and the direction of elongation and pillar fusion follows shear stress patterns (Karthik et al., 2018). In addition, this work emphasized that development of the zebrafish CV plexus is achieved by the concerted action of sprouting and intussusceptive angiogenesis, thus proving to be a valuable model to study the cross-regulation between these two modes of angiogenesis *in vivo* (Karthik et al., 2018). How do ECs decide between sprouting or intussusceptive angiogenesis? Is it one followed by the other, as suggested for the developing zebrafish CV plexus (Karthik et al., 2018)? It is possible that different flow profiles trigger either sprouting or intussusception or simply that the same mechanical stimulus triggers distinct cell behaviors in different environments like the vascular bed, location within the embryo or developmental context, since these could mean that cells express different gene profiles and/or are exposed to different types of biochemical signals.

ANASTOMOSIS AND LUMEN FORMATION/EXPANSION

Vessel fusion can occur between two tip cells of newly forming sprouts (head-to-head anastomosis) or between a tip cell and a perfused blood vessel (head-to-side anastomosis). In both instances, a lumen that runs inside the entire newly established connection is created, in a proximal to distal fashion, thus forming a multicellular tube were blood circulates. This process can occur either in the presence of blood flow by membrane invagination or in the absence of flow through chord hollowing (Betz et al., 2016). Here, we are going to focus on flow-dependent anastomosis and summarize the most recent findings obtained using the zebrafish and mouse models. In lumenized angiogenic sprouts the proximal apical membrane of the tip cell invaginates toward the cell center due to blood pressure inside the lumen of the adjacent stalk cell (**Figure 2**; Herwig et al., 2011). The apical membrane invagination is then extended until it reaches the most distal side of the tip cell where it fuses with the lumen of the connecting blood vessel or sprout. The resulting section of vessel is formed solely by one cell, which is later converted into a multicellular tube by stereotyped cellular rearrangements that involve EC splitting and junction remodeling (Herwig et al., 2011; Lenard et al., 2013).

Lumen formation and growth appear to be driven by a newly described blood pressure-dependent cellular process named inverse membrane blebbing (**Figure 2**), which is analogous to bleb-driven cell locomotion except that the membrane bulges in the opposite direction toward the cell body; hence the name inverse blebbing (Gebala et al., 2016). Blood pressure inside the lumen causes the apical membrane to detach from the actomyosin cortex forming blebs at locations where the membrane-cortex anchoring is weak. Following formation and expansion by continuous blood pressure, blebs can either persist causing the lumen to grow or retract by assembly and contraction of new actomyosin cortex inside the bleb. Selective bleb retraction at the sides of the expanding lumen combined with bleb retention at the tip of the expanding lumen confers directionality to the process (Gebala et al., 2016). Lumen growth via inverse membrane blebbing can occur in angiogenic sprouts that contain one or two tip cells thus leading to unicellular or multicellular lumen formation, respectively (Gebala et al., 2016). Further work will be necessary to understand how the correct location for lumen growth and expansion is sensed and restricted by ECs, so that blebs can be selectively maintained or retracted in order to steer lumen growth in the correct direction. The process appears to be driven by pressure differences, but what are the mechanosensing elements at play and how these stimuli are transduced to the cytoskeleton remains elusive. Likewise, how the transformation of a unicellular tube into a multicellular tube by EC splitting and junction remodeling is regulated at the molecular level to achieve such cellular behaviors in response to blood flow still remains an open question. Is the junction remodeling solely driven by shear stress sensed by junctional PECAM-1/VE-cadherin, which then transmits these signals down to the cytoskeleton, or is pressure also involved? It is possible that ZO1 mechanosensation plays a role as recently observed for epithelial tissues (Schwayer et al., 2019).

VESSEL PRUNING AND STABILIZATION

The formation of vascular networks, plexus in particular, is not always pre-patterned and this leads to the formation of highly branched networks that are convoluted and require optimization. This process is driven by blood flow forces and occurs through selective elimination of poorly irrigated branches (pruning) and, simultaneously, maintenance of vigorously irrigated blood vessels (stabilization). Nevertheless, the cellular behaviors and signaling pathways that are involved in vascular network optimization in response to flow have only recently begun to be understood.

Experimental manipulation of hemodynamics in the developing zebrafish demonstrated that in the brain vasculature pruning occurs by lateral migration of ECs from vessels exposed to low and variable blood flow toward the neighboring vessels with stronger flow that are kept (Chen et al., 2012). Similarly, vessel pruning associated with blood flow changes was also reported in the developing vasculature of the zebrafish eye via EC rearrangements and cell death (Kochhan et al., 2013) as well as in the subintestinal vein plexus where pruning is driven by lateral migration of ECs and involves the formation of unicellular tubes by EC self-fusion (Lenard et al., 2015). In both examples, the sequence of events leading to vessel pruning resembles vessel anastomosis in reverse order. Results obtained in the developing vasculature of the mouse retina and the zebrafish embryo confirm that pruning occurs via migration of ECs away from the network branches with low flow and toward the ones with high flow levels (Franco et al., 2016). This leads to an interesting model explaining how blood flow can participate in network optimization. The model proposes

that shear stress-induced EC polarization directed against the main flow direction serves as an instructive cue defining EC migration direction (**Figure 2**). EC movement is usually directed toward higher levels of shear stress leading to the simultaneous retraction and elimination (pruning) of blood vessels exposed to low blood flow along with the stabilization of vessel connections experiencing higher blood flow (Franco et al., 2016). As a consequence, blood vessel maintenance (stabilization) is working hand-in-hand with vessel pruning during network optimization. This is exemplified in many remodeling vascular systems where flow limits angiogenesis to stabilize the network. For example, blood circulation downregulates the expression of the *cxc* receptor *4a*, a known proangiogenic factor (Packham et al., 2009; Bussmann et al., 2011). By modulating the expression of the *cxc* receptor *4a,* blood flow promotes the maintenance and stabilization of newly established vascular connections in the zebrafish trunk and brain vasculature. Similarly, non-canonical Wnt signaling has been proposed to tune EC response thus preventing premature vessel regression (Franco et al., 2015). Flow can also positively regulate gene expression to control vessel stability by modulating the expression of the sphingosine-1-phosphate receptor 1 (S1P1) and the transcription factor Yes-activated protein (YAP) 1 (Jung et al., 2012; Nakajima et al., 2017). The S1P1 is a G protein-coupled receptor that stabilizes the primary vascular network by inhibiting angiogenic sprouting and enhancing cell-to-cell adhesion (Gaengel et al., 2012). In cultured human ECs, nuclear translocation of YAP is regulated by shear-dependent conformational changes induced to the actin cytoskeleton that in turn affect the binding of angiomotin (AMOT) to YAP (Nakajima et al., 2017). The authors propose that under low flow conditions YAP1 is bound to AMOT and thus kept in the cytoplasm, but when blood flow is high, shear stress increases the number of F-actin bundles in the cytoplasm causing AMOT to associate with F-actin and release YAP to the nucleus (**Figure 2**).

It is worth mentioning that YAP and TAZ also have an important role during sprouting angiogenesis. In the mouse, genetic loss of YAP/TAZ leads to arrested sprouting, while forced expression of TAZ in the nucleus causes increased sprouting. The ECs mechanical environment is slightly different here because the vessels are not perfused, but are subjected to stretch. In response to stretch, YAP/TAZ activity increases and promotes EC proliferation and cell rearrangement by increasing VE-cadherin turnover and the formation of junction associated intermediate lamellipodia (Neto et al., 2018). Interestingly, YAP/TAZ activity is enhanced by lowering levels of Bone morphogenetic protein (BMP) signaling, thus suggesting that ECs integrate mechanical stimuli with biochemical signals in order to regulate junction remodeling and cell rearrangements necessary for tissue homeostasis maintenance (Neto et al., 2018).

The effectors of flow forces during vessel pruning and stabilization are diverse and can have opposite roles in remodeling vascular tissues. The ECs have thus important capacities of mechanical and biochemical signal integration in order to adopt the adequate cellular behavior in each context. If this process is not functioning properly will, most likely lead to pathological response.

VESSEL CALIBER REGULATION

Vascular network remodeling can also be achieved by altering the caliber (diameter) of the existing blood vessels and usually this takes place in response to hemodynamic changes. Work in the developing pharyngeal arch arteries of the chicken embryo combined fluid dynamics simulations with artery occlusion experiments to demonstrate that other factors besides wall shear stress, such as complex shear stress patterns or pressure, are necessary to account for the morphological changes observed (Lindsey et al., 2015). Nevertheless, a developmental atlas of the pharyngeal arch arteries morphology correlated with fluid dynamics maps suggests that shear stress is the main driver of artery growth while pressure is the secondary driver (Lindsey et al., 2018). The situation may be more complicated in the developing vascular network in the mouse yolk sac where two distinct modes of artery caliber expansion are observed in response to changes in blood flow. Fusion of two adjacent vessels in the case of strong flow conditions or by migration of ECs from neighboring capillaries to expand the larger arteries (Udan et al., 2013). The signaling pathways involved also start to be uncovered. It has been proposed that VEGFR3 modulates EC response to shear stress such that above a given threshold vessels enlarge in response to shear stress while below that threshold vessels narrow thus keeping homeostasis (Baeyens et al., 2015). Supporting this view, reduced expression of VEGFR3 in zebrafish embryos and adult mice leads to decreased artery diameter (Baeyens et al., 2015). Blood flow-driven expression of the BMP receptor, activin receptor-like kinase 1 (*Alk1*), appears to limit the caliber of nascent arteries (exposed to vigorous flow) since zebrafish mutant embryos for *alk1* display aberrantly enlarged arteries (Corti et al., 2011). This phenotype is initially due to an increase in the EC number and followed by a decrease in the EC density (cell enlargement), which eventually leads to the formation of flow-dependent arteriovenous malformations (AVMs) (Corti et al., 2011). It was proposed that the abnormal artery dilation in *alk1* mutants was due to cell migration defects (Rochon et al., 2016) as well as loss of expression of the Transforming growth factor-β receptor *endoglin* (eng) and its vasoconstrictive action (Corti et al., 2011). Accordingly, the ECs of the zebrafish DA continue to enlarge causing expansion of the artery caliber in *eng* mutants when normally, at that stage (72 h post-fertilization), it should decrease (Sugden et al., 2017). At the cellular level, EC shape changes explain the DA caliber reduction in response to blood flow as cells elongate after being exposed to flow (**Figure 2**). In *eng* mutants ECs fail to elongate and, moreover, mutant cells transplanted into wild type embryos caused intersegmental vessels to enlarge locally (Sugden et al., 2017). How the flow-derived cues are transduced to *eng* and what is the cellular machinery driving the cell shape changes downstream of *eng* still remains elusive. In mouse retinas, mosaic deletion of *eng* was used in combination with an excision reporter to reveal that AVMs have an arterial origin despite *Eng* mutant cells displaying a venous phenotype (Jin et al., 2017). Besides a direct flow activation, *Eng*-dependent EC response seems to be involved in ligand-mediated signaling, since the response to VEGF signaling was partially affected in *eng* loss of function

(Jin et al., 2017). It is to note that a distinction between EC polarity and migration needs to be done in *Eng* mutants. Knockdown of eng in cultured human ECs does not affect cell alignment with the flow direction (Sugden et al., 2017) while, eng loss disrupts cell polarity evaluated by the relative Golgi and nuclei positions and causes migration defects in mice (Jin et al., 2017). Importantly, it was shown that *Eng* dependent induction of BMP 9/10 signaling is enhanced by flow (Baeyens et al., 2016b). Deletion of *Smad4* leads to an increase of the coronary artery caliber upon blood flow initiation, which is concurrent with activation of Smad1/5/8 (Poduri et al., 2017). The abnormal expansion of the coronary artery observed *in vivo* after depletion of *Smad4* appears to be due to an increase in cell proliferation and cell size (Poduri et al., 2017) resembling what was observed in the nascent arteries of zebrafish *alk1* mutant embryos (Corti et al., 2011). However, the *in vitro* observations suggest that the artery caliber defects could also arise due to cell migration defects against the flow direction (Poduri et al., 2017) as previously observed in the developing vascular network of the mouse yolk sac (Udan et al., 2013) and the zebrafish head (Rochon et al., 2016). Since flow forces are different in these settings, the variability in the cell behaviors may reflect different EC adaptation to the experienced flow regime. A key factor in the cell response to flow and AVMs is certainly Connexin (Cx) 37, which is deferentially regulated by shear stress and Smad1/5 signaling, and is downregulated in AVMs (Peacock et al., 2020). ECs appear to use different behaviors to adapt vessel size in response to flow depending on the developmental context. So far, most of our knowledge about vessel diameter regulation comes from work done on arteries and it is likely that vessel identity affects cell response to flow. It is clear for example that flow participates in reinforcing arterial vs. venous identity (Buschmann et al., 2010; Orsenigo et al., 2012). Yet arterial and venous identity is strongly dictated by genetic factors that are established before flow is observed (Su et al., 2018; Weijts et al., 2018; Geudens et al., 2019). This is certainly a general feature where flow profiles are enhancing and maintaining genetic programs established in early developmental stages.

ENDOTHELIAL TO HEMATOPOIETIC TRANSITION

Hematopoietic stem cell (HSC) emergence has been shown to occur *de novo* via endothelial-to-hematopoietic transition (EHT) from cells in the ventral wall of the DA (**Figure 3A**), so-called hemogenic endothelium, in both mouse and zebrafish embryos (Bertrand et al., 2010; Boisset et al., 2010; Kissa and Herbomel, 2010). During definitive hematopoiesis (Clements and Traver, 2013) emergent HSCs express the transcription factors runt-related transcription factor 1 (*Runx1*) and *cmyb*, which are amongst the earliest markers allowing HSC identification (Burns et al., 2002; Kalev-Zylinska et al., 2002; North et al., 2002). The ventral region of the DA is constantly exposed to blood flow

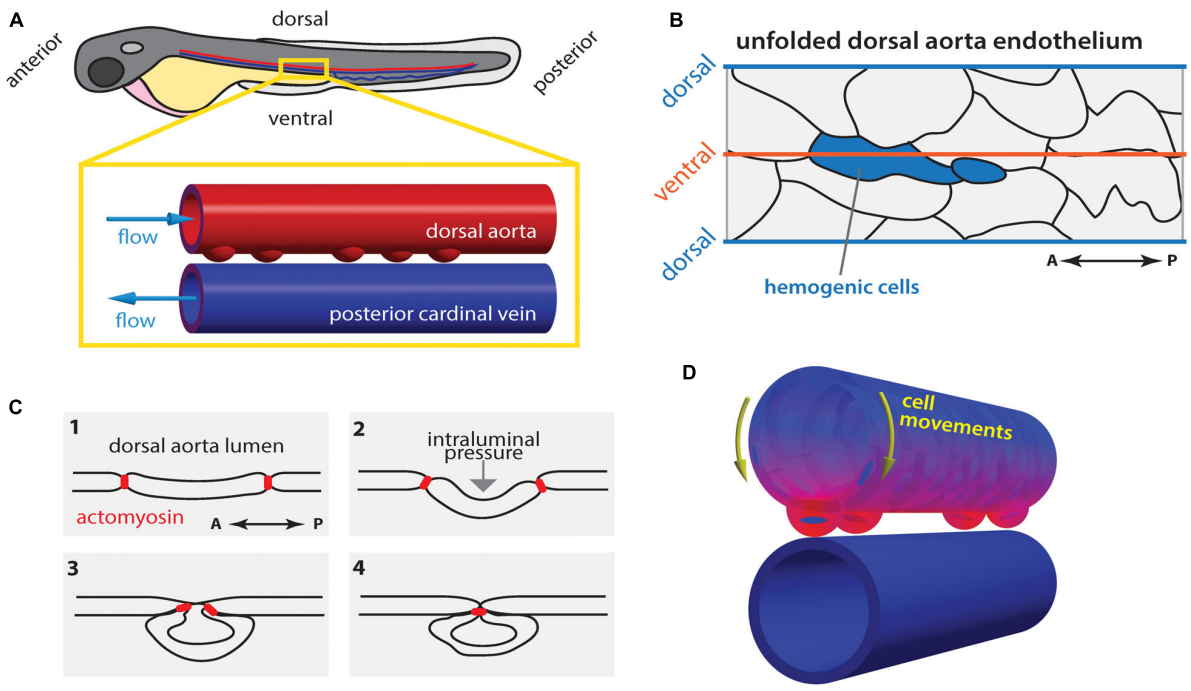

FIGURE 3 | Hematopoietic stem cell emergence is blood flow dependent. **(A)** During definitive hematopoiesis, hematopoietic stem cell progenitors arise at the ventral side of the dorsal aorta (DA) via cell extrusion from the endothelium. **(B)** Potential hemogenic cells (blue) located at the ventral region of the DA are elongated along the anterior-posterior (AP) axis. **(C)** Cells are extruded from the endothelium by contraction of actomyosin that accumulated at the AP poles of the cell. **(D)** Concomitantly, the majority of endothelial cells move toward the ventral side of the DA (yellow arrows). At each heartbeat, the DA wall deforms asymmetrically: the deformation is highest (magenta) in the ventral region and lowest (blue) in the dorsal side. Drawings in **(B,C)** after Lancino et al. (2018).

and, in zebrafish at least, corresponds to an area that is highly deformable in response to pulsatile blood flow (Anton et al., 2013; Campinho et al., 2018). Indeed, work in cultured mouse embryonic stem cells (Adamo et al., 2009) as well as in zebrafish embryos (North et al., 2009; Lam et al., 2010) demonstrated that HSC differentiation is strongly dependent on blood flow-derived mechanical forces. It reflects the requirement for a sequential series of events involving the expression of the transcription factor *klf2a* (Wang et al., 2011) and the activation of nitric oxide synthase (North et al., 2009) in response to flow. Blocking primary cilia formation or function in the zebrafish embryo leads to defects in HSC specification (Liu et al., 2019) which is in agreement with a previously suggested cilia-dependent shear-sensing mechanism (Goetz et al., 2014). In the developing mouse embryo, shear stress acts through prostaglandin (PG) E2-cyclic adenosine monophosphate (cAMP)-protein kinase (PK) A, the cAMP response element-binding (CREB) protein and BMP signaling pathway to regulate HSC emergence via EHT (Diaz et al., 2015; Kim et al., 2015). In zebrafish, binding of adenosine to the A2b adenylyl cyclase-stimulatory receptor on the endothelium leads to up-regulation of the cAMP–PKA–CREB pathway to activate HSC development suggesting that this mechanism is conserved in vertebrates (Jing et al., 2015). In addition, Yap is involved in propagating flow force signals intracellularly and promotes the maintenance of HSC cell identity within the hemogenic endothelium (Lundin et al., 2020).

In zebrafish, the hemogenic cells undergo stereotypic shape changes during EHT leading up to cell extrusion from the endothelium in a process that requires actomyosin contractility and is hindered in the absence of blood flow (**Figures 3B,C**; Lancino et al., 2018). Hemogenic cells are elongated along the vessels length (anterior-posterior axis; **Figure 3B**) and actomyosin becomes enriched at the anterior-posterior poles of the cell, which are brought together by periodic contraction of the actomyosin network (**Figure 3C**; Lancino et al., 2018). Flow-forces possibly push the extruding cell outwards causing it to bulge out and acquire its, previously described (Kissa and Herbomel, 2010), characteristic cup-shaped morphology (**Figure 3C**).

While it is well established that flow-derived shear stress plays a crucial role in EHT and HSC development, it has only recently become clear that other flow-derived forces are involved in the process such as their cyclic component (Lundin et al., 2020) as initially suggested (Adamo et al., 2009). During the peak of EHT there is a generalized movement of ECs toward the ventral DA (extrusion region; yellow arrows **Figure 3D**; Poullet et al., 2019; Campinho et al., 2018), which corresponds to the region of greatest tissue deformation and computed tissue stress caused by pulsatile blood flow (**Figure 3D**; Campinho et al., 2018). Additionally, low blood flow leads to increased EC extrusion. As a consequence, the time spent by hemogenic cells in the ventral DA where they experience the appropriate biomechanical environment (shear and cyclic stretch) decreases when flow forces are too low (Campinho et al., 2018). At the cellular and tissue scale, the contribution of pressure-induced cyclic tissue-stretch to EHT and HSC development is thus to guide ECs to the ventral DA and regulate the extrusion rate. Yet, further experimental proof is necessary particularly if pressure-induced cyclic tissue-stretch is to be disentangled from the role of shear stress. *In vitro* approaches where shear and stretch can be applied in isolation will certainly help to address this issue.

CONCLUSION

How blood flow forces affect vascular morphogenesis is an exciting field of research. Flow effects on cell polarization, shape changes and migration are obviously at the center of blood flows morphogenetic activity. Yet how these cell behaviors are coordinated with the angiogenic genetic programs, developmental pre-patterning and mechanotransduction is far from being understood. The mechanical environment that ECs experience is also highly relevant, since it affects the way cells react to forces (Ruehle et al., 2020). In addition, the contribution of different flow-derived forces (e.g., shear stress and circumferential stretch) to specific EC behaviors involved in vascular morphogenesis still needs to be clarified. These open questions are difficult and will benefit from a number of new tools: optogenetics (Chow and Vermot, 2017; Krueger et al., 2019), functionalized protein binders (Bieli et al., 2016), three dimensional live-imaging and processing (Campinho et al., 2020; Prahst et al., 2020) as well as tissue engineering approaches where forces are trackable and accurately controlled (Duchemin et al., 2019b; Vianello and Lutolf, 2019).

AUTHOR CONTRIBUTIONS

All the authors participated in the design and writing of the manuscript.

FUNDING

PC was supported by FRM (Grant No. FRM SPF20140129238), EMBO (Grant No. ALTF 100-2014) and by the foundation Lefoullon Delalande (2017). ANR Grant No. ANR-SNF 310030E-164245.

REFERENCES

Adamo, L., Naveiras, O., Wenzel, P. L., McKinney-Freeman, S., Mack, P. J., Gracia-Sancho, J., et al. (2009). Biomechanical forces promote embryonic haematopoiesis. *Nature* 459, 1131–1135. doi: 10.1038/nature08073

Akbari, E., Spychalski, G. B., Rangharajan, K. K., Prakash, S., and Song, J. W. (2019). Competing fluid forces control endothelial sprouting in a 3-D microfluidic vessel bifurcation model. *Micromachines (Basel)* 10:E451. doi: 10.3390/mi10070451

Al-Roubaie, S., Jahnsen, E. D., Mohammed, M., Henderson-Toth, C., and Jones, E. A. (2011). Rheology of embryonic avian blood. *Am. J. Physiol. Heart Circ. Physiol.* 301, H2473–H2481. doi: 10.1152/ajpheart.00475.2011

Angulo-Urarte, A., Casado, P., Castillo, S. D., Kobialka, P., Kotini, M. P., Figueiredo, A. M., et al. (2018). Endothelial cell rearrangements during vascular

patterning require PI3-kinase-mediated inhibition of actomyosin contractility. *Nat. Commun.* 9:4826. doi: 10.1038/s41467-018-07172-3

Anton, H., Harlepp, S., Ramspacher, C., Wu, D., Monduc, F., Bhat, S., et al. (2013). Pulse propagation by a capacitive mechanism drives embryonic blood flow. *Development* 140, 4426–4434. doi: 10.1242/dev.096768

Arora, R., and Papaioannou, V. E. (2012). The murine allantois: a model system for the study of blood vessel formation. *Blood* 120, 2562–2572. doi: 10.1182/blood-2012-03-390070

Baeyens, N., Bandyopadhyay, C., Coon, B. G., Yun, S., and Schwartz, M. A. (2016a). Endothelial fluid shear stress sensing in vascular health and disease. *J Clin Invest* 126, 821–828. doi: 10.1172/JCI83083

Baeyens, N., Larrivee, B., Ola, R., Hayward-Piatkowskyi, B., Dubrac, A., Huang, B., et al. (2016b). Defective fluid shear stress mechanotransduction mediates hereditary hemorrhagic telangiectasia. *J. Cell Biol.* 214, 807–816. doi: 10.1083/jcb.201603106

Baeyens, N., Nicoli, S., Coon, B. G., Ross, T. D., Van den Dries, K., Han, J., et al. (2015). Vascular remodeling is governed by a VEGFR3-dependent fluid shear stress set point. *Elife* 4. doi: 10.7554/eLife.04645

Bartosch, A. M. W., Mathews, R., and Tarbell, J. M. (2017). Endothelial glycocalyx-mediated nitric oxide production in response to selective AFM pulling. *Biophys. J.* 113, 101–108. doi: 10.1016/j.bpj.2017.05.033

Bazou, D., Ng, M. R., Song, J. W., Chin, S. M., Maimon, N., and Munn, L. L. (2016). Flow-induced HDAC1 phosphorylation and nuclear export in angiogenic sprouting. *Sci. Rep.* 6:34046. doi: 10.1038/srep34046

Belle, J., Ysasi, A., Bennett, R. D., Filipovic, N., Nejad, M. I., Trumper, D. L., et al. (2014). Stretch-induced intussuceptive and sprouting angiogenesis in the chick chorioallantoic membrane. *Microvasc Res.* 95, 60–67. doi: 10.1016/j.mvr.2014.06.009

Bertrand, J. Y., Chi, N. C., Santoso, B., Teng, S., Stainier, D. Y., and Traver, D. (2010). Haematopoietic stem cells derive directly from aortic endothelium during development. *Nature* 464, 108–111. doi: 10.1038/nature08738

Betz, C., Lenard, A., Belting, H. G., and Affolter, M. (2016). Cell behaviors and dynamics during angiogenesis. *Development* 143, 2249–2260. doi: 10.1242/dev.135616

Bieli, D., Alborelli, I., Harmansa, S., Matsuda, S., Caussinus, E., and Affolter, M. (2016). Development and application of functionalized protein binders in multicellular organisms. *Int. Rev. Cell Mol. Biol.* 325, 181–213. doi: 10.1016/bs.ircmb.2016.02.006

Boisset, J. C., Van Cappellen, W., Andrieu-Soler, C., Galjart, N., Dzierzak, E., and Robin, C. (2010). In vivo imaging of haematopoietic cells emerging from the mouse aortic endothelium. *Nature* 464, 116–120. doi: 10.1038/nature08764

Boselli, F., Freund, J. B., and Vermot, J. (2015). Blood flow mechanics in cardiovascular development. *Cell Mol. Life Sci.* 72, 2545–2559. doi: 10.1007/s00018-015-1885-3

Boselli, F., Steed, E., Freund, J. B., and Vermot, J. (2017). Anisotropic shear stress patterns predict the orientation of convergent tissue movements in the embryonic heart. *Development* 144, 4322–4327. doi: 10.1242/dev.152124

Burns, C. E., DeBlasio, T., Zhou, Y., Zhang, J., Zon, L., and Nimer, S. D. (2002). Isolation and characterization of runxa and runxb, zebrafish members of the runt family of transcriptional regulators. *Exp. Hematol.* 30, 1381–1389. doi: 10.1016/s0301-472x(02)00955-4

Buschmann, I., Pries, A., Styp-Rekowska, B., Hillmeister, P., Loufrani, L., Henrion, D., et al. (2010). Pulsatile shear and Gja5 modulate arterial identity and remodeling events during flow-driven arteriogenesis. *Development* 137, 2187–2196. doi: 10.1242/dev.045351

Bussmann, J., Wolfe, S. A., and Siekmann, A. F. (2011). Arterial-venous network formation during brain vascularization involves hemodynamic regulation of chemokine signaling. *Development* 138, 1717–1726. doi: 10.1242/dev.059881

Butcher, J. T., Penrod, A. M., Garcia, A. J., and Nerem, R. M. (2004). Unique morphology and focal adhesion development of valvular endothelial cells in static and fluid flow environments. *Arterioscler. Thromb. Vasc. Biol.* 24, 1429–1434. doi: 10.1161/01.ATV.0000130462.50769.5a

Campinho, P., Lamperti, P., Boselli, F., and Vermot, J. (2018). Three-dimensional microscopy and image analysis methodology for mapping and quantification of nuclear positions in tissues with approximate cylindrical geometry. *Philos. Trans. R. Soc. Lond. B Biol. Sci.* 373:20170332. doi: 10.1098/rstb.2017.0332

Campinho, P., Lamperti, P., Boselli, F., Vilfan, A., and Vermot, J. (2020). Blood flow limits endothelial cell extrusion in the zebrafish dorsal aorta. *Cell Rep.* 31:107505. doi: 10.1016/j.celrep.2020.03.069

Chang, A. H., Raftrey, B. C., D'Amato, G., Surya, V. N., Poduri, A., Chen, H. I., et al. (2017). DACH1 stimulates shear stress-guided endothelial cell migration and coronary artery growth through the CXCL12-CXCR4 signaling axis. *Genes Dev.* 31, 1308–1324. doi: 10.1101/gad.301549.117

Chen, Q., Jiang, L., Li, C., Hu, D., Bu, J. W., Cai, D., et al. (2012). Haemodynamics-driven developmental pruning of brain vasculature in zebrafish. *PLoS Biol.* 10:e1001374. doi: 10.1371/journal.pbio.1001374

Chow, R. W., and Vermot, J. (2017). The rise of photoresponsive protein technologies applications in vivo: a spotlight on zebrafish developmental and cell biology. *F1000Res* 6. doi: 10.12688/f1000research.10617.1

Clements, W. K., and Traver, D. (2013). Signalling pathways that control vertebrate haematopoietic stem cell specification. *Nat. Rev. Immunol.* 13, 336–348. doi: 10.1038/nri3443

Corti, P., Young, S., Chen, C. Y., Patrick, M. J., Rochon, E. R., Pekkan, K., et al. (2011). Interaction between alk1 and blood flow in the development of arteriovenous malformations. *Development* 138, 1573–1582. doi: 10.1242/dev.060467

Diaz, M. F., Li, N., Lee, H. J., Adamo, L., Evans, S. M., Willey, H. E., et al. (2015). Biomechanical forces promote blood development through prostaglandin E2 and the cAMP-PKA signaling axis. *J. Exp. Med.* 212, 665–680. doi: 10.1084/jem.20142235

Djonov, V. G., Kurz, H., and Burri, P. H. (2002). Optimality in the developing vascular system: branching remodeling by means of intussusception as an efficient adaptation mechanism. *Dev. Dyn.* 224, 391–402. doi: 10.1002/dvdy.10119

Downs, K. M., Gifford, S., Blahnik, M., and Gardner, R. L. (1998). Vascularization in the murine allantois occurs by vasculogenesis without accompanying erythropoiesis. *Development* 125, 4507–4520.

Duchemin, A. L., Vignes, H., and Vermot, J. (2019a). Mechanically activated piezo channels modulate outflow tract valve development through the Yap1 and Klf2-Notch signaling axis. *Elife* 8:e44706. doi: 10.7554/eLife.44706

Duchemin, A. L., Vignes, H., Vermot, J., and Chow, R. (2019b). Mechanotransduction in cardiovascular morphogenesis and tissue engineering. *Curr. Opin. Genet. Dev.* 57, 106–116. doi: 10.1016/j.gde.2019.08.002

Feaver, R. E., Gelfand, B. D., and Blackman, B. R. (2013). Human haemodynamic frequency harmonics regulate the inflammatory phenotype of vascular endothelial cells. *Nat. Commun.* 4:1525. doi: 10.1038/ncomms2530

Feaver, R. E., Gelfand, B. D., Wang, C., Schwartz, M. A., and Blackman, B. R. (2010). Atheroprone hemodynamics regulate fibronectin deposition to create positive feedback that sustains endothelial inflammation. *Circ. Res.* 106, 1703–1711. doi: 10.1161/CIRCRESAHA.109.216283

Franco, C. A., Jones, M. L., Bernabeu, M. O., Geudens, I., Mathivet, T., Rosa, A., et al. (2015). Dynamic endothelial cell rearrangements drive developmental vessel regression. *PLoS Biol.* 13:e1002125. doi: 10.1371/journal.pbio.1002125

Franco, C. A., Jones, M. L., Bernabeu, M. O., Vion, A. C., Barbacena, P., Fan, J., et al. (2016). Non-canonical Wnt signalling modulates the endothelial shear stress flow sensor in vascular remodelling. *Elife* 5:e07727. doi: 10.7554/eLife.07727

Freund, J. B., Goetz, J. G., Hill, K. L., and Vermot, J. (2012). Fluid flows and forces in development: functions, features and biophysical principles. *Development* 139, 1229–1245. doi: 10.1242/dev.073593

Frisdal, A., and Trainor, P. A. (2014). Development and evolution of the pharyngeal apparatus. *Wiley Interdiscip. Rev. Dev. Biol.* 3, 403–418. doi: 10.1002/wdev.147

Gaengel, K., Niaudet, C., Hagikura, K., Lavina, B., Muhl, L., Hofmann, J. J., et al. (2012). The sphingosine-1-phosphate receptor S1PR1 restricts sprouting angiogenesis by regulating the interplay between VE-cadherin and VEGFR2. *Dev. Cell* 23, 587–599. doi: 10.1016/j.devcel.2012.08.005

Galie, P. A., Nguyen, D. H., Choi, C. K., Cohen, D. M., Janmey, P. A., and Chen, C. S. (2014). Fluid shear stress threshold regulates angiogenic sprouting. *Proc. Natl. Acad. Sci. U.S.A.* 111, 7968–7973. doi: 10.1073/pnas.1310842111

Gebala, V., Collins, R., Geudens, I., Phng, L. K., and Gerhardt, H. (2016). Blood flow drives lumen formation by inverse membrane blebbing during angiogenesis in vivo. *Nat. Cell Biol.* 18, 443–450. doi: 10.1038/ncb3320

Geudens, I., Coxam, B., Alt, S., Gebala, V., Vion, A.-C., Meier, K., et al. (2019). Artery-vein specification in the zebrafish trunk is pre-patterned by

heterogeneous Notch activity and balanced by flow-mediated fine-tuning. *Development* 146:dev181024. doi: 10.1242/dev.181024

Geudens, I., and Gerhardt, H. (2011). Coordinating cell behaviour during blood vessel formation. *Development* 138, 4569–4583. doi: 10.1242/dev.062323

Ghaffari, S., Leask, R. L., and Jones, E. A. (2015). Flow dynamics control the location of sprouting and direct elongation during developmental angiogenesis. *Development* 142, 4151–4157. doi: 10.1242/dev.128058

Goetz, J. G., Steed, E., Ferreira, R. R., Roth, S., Ramspacher, C., Boselli, F., et al. (2014). Endothelial cilia mediate low flow sensing during zebrafish vascular development. *Cell Rep.* 6, 799–808. doi: 10.1016/j.celrep.2014.01.032

Guillot, C., and Lecuit, T. (2013). Mechanics of epithelial tissue homeostasis and morphogenesis. *Science* 340, 1185–1189. doi: 10.1126/science.1235249

Heckel, E., Boselli, F., Roth, S., Krudewig, A., Belting, H. G., Charvin, G., et al. (2015). Oscillatory flow modulates mechanosensitive klf2a expression through trpv4 and trpp2 during heart valve development. *Curr. Biol.* 25, 1354–1361. doi: 10.1016/j.cub.2015.03.038

Henderson-Toth, C. E., Jahnsen, E. D., Jamarani, R., Al-Roubaie, S., and Jones, E. A. (2012). The glycocalyx is present as soon as blood flow is initiated and is required for normal vascular development. *Dev. Biol.* 369, 330–339. doi: 10.1016/j.ydbio.2012.07.009

Herwig, L., Blum, Y., Krudewig, A., Ellertsdottir, E., Lenard, A., Belting, H. G., et al. (2011). Distinct cellular mechanisms of blood vessel fusion in the zebrafish embryo. *Curr. Biol.* 21, 1942–1948. doi: 10.1016/j.cub.2011.10.016

Hoefer, I. E., den Adel, B., and Daemen, M. J. (2013). Biomechanical factors as triggers of vascular growth. *Cardiovasc Res.* 99, 276–283. doi: 10.1093/cvr/cvt089

Humphrey, J. D., Eberth, J. F., Dye, W. W., and Gleason, R. L. (2009). Fundamental role of axial stress in compensatory adaptations by arteries. *J. Biomech.* 42, 1–8. doi: 10.1016/j.jbiomech.2008.11.011

Jin, Y., Muhl, L., Burmakin, M., Wang, Y., Duchez, A. C., Betsholtz, C., et al. (2017). Endoglin prevents vascular malformation by regulating flow-induced cell migration and specification through VEGFR2 signalling. *Nat. Cell Biol.* 19, 639–652. doi: 10.1038/ncb3534

Jing, L., Tamplin, O. J., Chen, M. J., Deng, Q., Patterson, S., Kim, P. G., et al. (2015). Adenosine signaling promotes hematopoietic stem and progenitor cell emergence. *J. Exp. Med.* 212, 649–663. doi: 10.1084/jem.20141528

Jones, E. A., Baron, M. H., Fraser, S. E., and Dickinson, M. E. (2004). Measuring hemodynamic changes during mammalian development. *Am. J. Physiol. Heart Circ. Physiol.* 287, H1561–H1569. doi: 10.1152/ajpheart.00081.2004

Jones, E. A., Le Noble, F., and Eichmann, A. (2006). What determines blood vessel structure? Genetic prespecification vs. hemodynamics. *Physiology (Bethesda)* 21, 388–395. doi: 10.1152/physiol.00020.2006

Jung, B., Obinata, H., Galvani, S., Mendelson, K., Ding, B. S., Skoura, A., et al. (2012). Flowregulated endothelial S1P receptor-1 signaling sustains vascular development. *Dev. Cell* 23, 600–610. doi: 10.1016/j.devcel.2012.07.015

Kalev-Zylinska, M. L., Horsfield, J. A., Flores, M. V., Postlethwait, J. H., Vitas, M. R., Baas, A. M., et al. (2002). Runx1 is required for zebrafish blood and vessel development and expression of a human RUNX1-CBF2T1 transgene advances a model for studies of leukemogenesis. *Development* 129, 2015–2030.

Karthik, S., Djukic, T., Kim, J. D., Zuber, B., Makanya, A., Odriozola, A., et al. (2018). Synergistic interaction of sprouting and intussusceptive angiogenesis during zebrafish caudal vein plexus development. *Sci. Rep.* 8:9840. doi: 10.1038/s41598-018-27791-6

Kim, P. G., Nakano, H., Das, P. P., Chen, M. J., Rowe, R. G., Chou, S. S., et al. (2015). Flowinduced protein kinase A-CREB pathway acts via BMP signaling to promote HSC emergence. *J. Exp. Med.* 212, 633–648. doi: 10.1084/jem.20141514

Kissa, K., and Herbomel, P. (2010). Blood stem cells emerge from aortic endothelium by a novel type of cell transition. *Nature* 464, 112–115. doi: 10.1038/nature08761

Kochhan, E., Lenard, A., Ellertsdottir, E., Herwig, L., Affolter, M., Belting, H. G., et al. (2013). Blood flow changes coincide with cellular rearrangements during blood vessel pruning in zebrafish embryos. *PLoS One* 8:e75060. doi: 10.1371/journal.pone.0075060

Krueger, D., Izquierdo, E., Viswanathan, R., Hartmann, J., Pallares, C. C., and De Renzis, S. (2019). Principles and applications of optogenetics in developmental biology. *Development* 146:dev175067. doi: 10.1242/dev.175067

Kutys, M. L., and Chen, C. S. (2016). Forces and mechanotransduction in 3D vascular biology. *Curr. Opin. Cell Biol.* 42, 73–79. doi: 10.1016/j.ceb.2016.04.011

Kwon, H. B., Wang, S., Helker, C. S., Rasouli, S. J., Maischein, H. M., Offermanns, S., et al. (2016). In vivo modulation of endothelial polarization by Apelin receptor signalling. *Nat. Commun.* 7:11805. doi: 10.1038/ncomms11805

Lagendijk, A. K., Gomez, G. A., Baek, S., Hesselson, D., Hughes, W. E., Paterson, S., et al. (2017). Live imaging molecular changes in junctional tension upon VE-cadherin in zebrafish. *Nat. Commun.* 8:1402. doi: 10.1038/s41467-017-01325-6

Lam, E. Y., Hall, C. J., Crosier, P. S., Crosier, K. E., and Flores, M. V. (2010). Live imaging of Runx1 expression in the dorsal aorta tracks the emergence of blood progenitors from endothelial cells. *Blood* 116, 909–914. doi: 10.1182/blood-2010-01-264382

LaMack, J. A., and Friedman, M. H. (2007). Individual and combined effects of shear stress magnitude and spatial gradient on endothelial cell gene expression. *Am. J. Physiol. Heart Circ. Physiol.* 293, H2853–H2859. doi: 10.1152/ajpheart.00244.2007

Lancino, M., Majello, S., Herbert, S., De Chaumont, F., Tinevez, J. Y., Olivo-Marin, J. C., et al. (2018). Anisotropic organization of circumferential actomyosin characterizes hematopoietic stem cells emergence in the zebrafish. *Elife* 7:e37355. doi: 10.7554/eLife.37355

Le Noble, F., Moyon, D., Pardanaud, L., Yuan, L., Djonov, V., Matthijsen, R., et al. (2004). Flow regulates arterial-venous differentiation in the chick embryo yolk sac. *Development* 131, 361–375. doi: 10.1242/dev.00929

Lee, G. S., Filipovic, N., Miele, L. F., Lin, M., Simpson, D. C., Giney, B., et al. (2010). Blood flow shapes intravascular pillar geometry in the chick chorioallantoic membrane. *J. Angiogenes Res.* 2:11. doi: 10.1186/2040-2384-2-11

Lenard, A., Daetwyler, S., Betz, C., Ellertsdottir, E., Belting, H. G., Huisken, J., et al. (2015). Endothelial cell self-fusion during vascular pruning. *PLoS Biol.* 13:e1002126. doi: 10.1371/journal.pbio.1002126

Lenard, A., Ellertsdottir, E., Herwig, L., Krudewig, A., Sauteur, L., Belting, H. G., et al. (2013). In vivo analysis reveals a highly stereotypic morphogenetic pathway of vascular anastomosis. *Dev. Cell* 25, 492–506. doi: 10.1016/j.devcel.2013.05.010

Levesque, M. J., and Nerem, R. M. (1985). The elongation and orientation of cultured endothelial cells in response to shear stress. *J. Biomech. Eng.* 107, 341–347. doi: 10.1115/1.3138567

Lindsey, S. E., Butcher, J. T., and Vignon-Clementel, I. E. (2018). Cohort-based multiscale analysis of hemodynamic-driven growth and remodeling of the embryonic pharyngeal arch arteries. *Development* 145:dev162578. doi: 10.1242/dev.162578

Lindsey, S. E., Menon, P. G., Kowalski, W. J., Shekhar, A., Yalcin, H. C., Nishimura, N., et al. (2015). Growth and hemodynamics after early embryonic aortic arch occlusion. *Biomech. Model Mechanobiol.* 14, 735–751. doi: 10.1007/s10237-014-0633-1

Liu, Z., Tu, H., Kang, Y., Xue, Y., Ma, D., Zhao, C., et al. (2019). Primary cilia regulate hematopoietic stem and progenitor cell specification through Notch signaling in zebrafish. *Nat. Commun.* 10:1839. doi: 10.1038/s41467-019-09403-7

Lundin, V., Sugden, W. W., Theodore, L. N., Sousa, P. M., Han, A., Chou, S., et al. (2020). YAP regulates hematopoietic stem cell formation in response to the biomechanical forces of blood flow. *Dev Cell* 52, 446–460.e5. doi: 10.1016/j.devcel.2020.01.006

Makanya, A. N., Hlushchuk, R., and Djonov, V. G. (2009). Intussusceptive angiogenesis and its role in vascular morphogenesis, patterning, and remodeling. *Angiogenesis* 12, 113–123. doi: 10.1007/s10456-009-9129-5

Nakajima, H., Yamamoto, K., Agarwala, S., Terai, K., Fukui, H., Fukuhara, S., et al. (2017). Flow-dependent endothelial YAP regulation contributes to vessel maintenance. *Dev. Cell* 52:e526. doi: 10.1016/j.devcel.2017.02.019

Neto, F., Klaus-Bergmann, A., Ong, Y. T., Alt, S., Vion, A. C., Szymborska, A., et al. (2018). YAP and TAZ regulate adherens junction dynamics and endothelial cell distribution during vascular development. *Elife* 7:e31037. doi: 10.7554/eLife.31037

Nicoli, S., Standley, C., Walker, P., Hurlstone, A., Fogarty, K. E., and Lawson, N. D. (2010). MicroRNA-mediated integration of haemodynamics and Vegf signalling during angiogenesis. *Nature* 464, 1196–1200. doi: 10.1038/nature08889

Noria, S., Xu, F., McCue, S., Jones, M., Gotlieb, A. I., and Langille, B. L. (2004). Assembly and reorientation of stress fibers drives morphological changes to endothelial cells exposed to shear stress. *Am. J. Pathol.* 164, 1211–1223. doi: 10.1016/S0002-9440(10)63209-9

North, T. E., de Bruijn, M. F., Stacy, T., Talebian, L., Lind, E., Robin, C., et al. (2002). Runx1 expression marks long-term repopulating hematopoietic stem cells in the midgestation mouse embryo. *Immunity* 16, 661–672. doi: 10.1016/s1074-7613(02)00296-0

North, T. E., Goessling, W., Peeters, M., Li, P., Ceol, C., Lord, A. M., et al. (2009). Hematopoietic stem cell development is dependent on blood flow. *Cell* 137, 736–748. doi: 10.1016/j.cell.2009.04.023

Orr, A. W., Stockton, R., Simmers, M. B., Sanders, J. M., Sarembock, I. J., Blackman, B. R., et al. (2007). Matrix-specific p21-activated kinase activation regulates vascular permeability in atherogenesis. *J. Cell Biol.* 176, 719–727. doi: 10.1083/jcb.200609008

Orsenigo, F., Giampietro, C., Ferrari, A., Corada, M., Galaup, A., Sigismund, S., et al. (2012). Phosphorylation of VE-cadherin is modulated by haemodynamic forces and contributes to the regulation of vascular permeability in vivo. *Nat. Commun.* 3:1208. doi: 10.1038/ncomms2199

Ostrowski, M. A., Huang, N. F., Walker, T. W., Verwijlen, T., Poplawski, C., Khoo, A. S., et al. (2014). Microvascular endothelial cells migrate upstream and align against the shear stress field created by impinging flow. *Biophys. J.* 106, 366–374. doi: 10.1016/j.bpj.2013.11.4502

Packham, I. M., Gray, C., Heath, P. R., Hellewell, P. G., Ingham, P. W., Crossman, D. C., et al. (2009). Microarray profiling reveals CXCR4a is downregulated by blood flow in vivo and mediates collateral formation in zebrafish embryos. *Physiol. Genomics* 38, 319–327. doi: 10.1152/physiolgenomics.00049.2009

Peacock, H. M., Tabibian, A., Criem, N., Caolo, V., Hamard, L., Deryckere, A., et al. (2020). Impaired SMAD1/5 Mechanotransduction and Cx37 (Connexin37) expression enable pathological vessel enlargement and shunting. *Arterioscler. Thromb. Vasc. Biol.* 40, e87–e104. doi: 10.1161/ATVBAHA.119.313122

Pitulescu, M. E., Schmidt, I., Giaimo, B. D., Antoine, T., Berkenfeld, F., Ferrante, F., et al. (2017). Dll4 and Notch signalling couples sprouting angiogenesis and artery formation. *Nat. Cell Biol.* 19, 915–927. doi: 10.1038/ncb3555

Poduri, A., Chang, A. H., Raftrey, B., Rhee, S., Van, M., and Red-Horse, K. (2017). Endothelial cells respond to the direction of mechanical stimuli through SMAD signaling to regulate coronary artery size. *Development* 144, 3241–3252. doi: 10.1242/dev.150904

Potente, M., Gerhardt, H., and Carmeliet, P. (2011). Basic and therapeutic aspects of angiogenesis. *Cell* 146, 873–887. doi: 10.1016/j.cell.2011.08.039

Potente, M., and Makinen, T. (2017). Vascular heterogeneity and specialization in development and disease. *Nat. Rev. Mol. Cell Biol.* 18, 477–494. doi: 10.1038/nrm.2017.36

Poullet, N., Golushko, I., Lorman, V., Travnickova, J., Bureau, C., Chalin, D., et al. (2019). Mechanical instabilities of aorta drive blood stem cell production: a live study. *Cell Mol. Life Sci.* doi: 10.1007/s00018-019-03372-2

Prahst, C., Ashrafzadeh, P., Mead, T., Figueiredo, A., Chang, K., Richardson, D., et al. (2020). Mouse retinal cell behaviour in space and time using light sheet fluorescence microscopy. *Elife* 9:e49779. doi: 10.7554/eLife.49779

Renz, M., Otten, C., Faurobert, E., Rudolph, F., Zhu, Y., Boulday, G., et al. (2015). Regulation of beta1 integrin-Klf2-mediated angiogenesis by CCM proteins. *Dev. Cell* 32, 181–190. doi: 10.1016/j.devcel.2014.12.016

Rochon, E. R., Menon, P. G., and Roman, B. L. (2016). Alk1 controls arterial endothelial cell migration in lumenized vessels. *Development* 143, 2593–2602. doi: 10.1242/dev.135392

Ruehle, M. A., Eastburn, E. A., LaBelle, S. A., Krishnan, L., Weiss, J. A., Boerckel, J. D., et al. (2020). Mechanical regulation of microvascular angiogenesis. *bioRxiv* [Preprint]. doi: 10.1101/2020.01.14.906354

Sato, Y. (2013). Dorsal aorta formation: separate origins, lateral-to-medial migration, and remodeling. *Dev. Growth. Differ* 55, 113–129. doi: 10.1111/dgd.12010

Schwayer, C., Shamipour, S., Pranjic-Ferscha, K., Schauer, A., Balda, M., Tada, M., et al. (2019). Mechanosensation of tight junctions depends on ZO-1 phase separation and flow. *Cell* 93:e918. doi: 10.1016/j.cell.2019.10.006

Shurer, C. R., Kuo, J. C., Roberts, L. M., Gandhi, J. G., Colville, M. J., Enoki, T. A., et al. (2019). Physical Principles of Membrane Shape Regulation by the Glycocalyx. *Cell* 177, 1757–1770.e1721. doi: 10.1016/j.cell.2019.04.017

Siekmann, A. F., Affolter, M., and Belting, H. G. (2013). The tip cell concept 10 years after: new players tune in for a common theme. *Exp. Cell Res.* 319, 1255–1263. doi: 10.1016/j.yexcr.2013.01.019

Simmers, M. B., Pryor, A. W., and Blackman, B. R. (2007). Arterial shear stress regulates endothelial cell-directed migration, polarity, and morphology in confluent monolayers. *Am. J. Physiol. Heart Circ. Physiol.* 293, H1937–H1946. doi: 10.1152/ajpheart.00534.2007

Song, J. W., and Munn, L. L. (2011). Fluid forces control endothelial sprouting. *Proc. Natl. Acad. Sci. U.S.A.* 108, 15342–15347. doi: 10.1073/pnas.1105316108

Steed, E., Faggianelli, N., Roth, S., Ramspacher, C., Concordet, J. P., and Vermot, J. (2016). klf2a couples mechanotransduction and zebrafish valve morphogenesis through fibronectin synthesis. *Nat. Commun.* 7:11646. doi: 10.1038/ncomms11646

Strilic, B., Kucera, T., Eglinger, J., Hughes, M. R., McNagny, K. M., Tsukita, S., et al. (2009). The molecular basis of vascular lumen formation in the developing mouse aorta. *Dev. Cell* 17, 505–515. doi: 10.1016/j.devcel.2009.08.011

Su, T., Stanley, G., Sinha, R., D'Amato, G., Das, S., Rhee, S., et al. (2018). Single-cell analysis of early progenitor cells that build coronary arteries. *Nature* 559, 356–362. doi: 10.1038/s41586-018-0288-7

Sugden, W. W., Meissner, R., Aegerter-Wilmsen, T., Tsaryk, R., Leonard, E. V., Bussmann, J., et al. (2017). Endoglin controls blood vessel diameter through endothelial cell shape changes in response to haemodynamic cues. *Nat. Cell Biol.* 19, 653–665. doi: 10.1038/ncb3528

Swift, M. R., and Weinstein, B. M. (2009). Arterial-venous specification during development. *Circ Res.* 104, 576–588. doi: 10.1161/CIRCRESAHA.108.188805

Thodeti, C. K., Matthews, B., Ravi, A., Mammoto, A., Ghosh, K., Bracha, A. L., et al. (2009). TRPV4 channels mediate cyclic strain-induced endothelial cell reorientation through integrin-to-integrin signaling. *Circ. Res.* 104, 1123–1130. doi: 10.1161/CIRCRESAHA.108.192930

Udan, R. S., Vadakkan, T. J., and Dickinson, M. E. (2013). Dynamic responses of endothelial cells to changes in blood flow during vascular remodeling of the mouse yolk sac. *Development* 140, 4041–4050. doi: 10.1242/dev.096255

Vianello, S., and Lutolf, M. P. (2019). Understanding the mechanobiology of early mammalian development through bioengineered models. *Dev Cell* 48, 751–763. doi: 10.1016/j.devcel.2019.02.024

Wang, L., Zhang, P., Wei, Y., Gao, Y., Patient, R., and Liu, F. (2011). A blood flow-dependent klf2a-NO signaling cascade is required for stabilization of hematopoietic stem cell programming in zebrafish embryos. *Blood* 118, 4102–4110. doi: 10.1182/blood-2011-05-353235

Weijts, B., Gutierrez, E., Saikin, S. K., Ablooglu, A. J., Traver, D., Groisman, A., et al. (2018). Blood flow-induced Notch activation and endothelial migration enable vascular remodeling in zebrafish embryos. *Nat. Commun.* 9:5314. doi: 10.1038/s41467-018-07732-7

Wojciak-Stothard, B., and Ridley, A. J. (2003). Shear stress-induced endothelial cell polarization is mediated by Rho and Rac but not Cdc42 or PI 3-kinases. *J. Cell Biol.* 161, 429–439. doi: 10.1083/jcb.200210135

Xanthis, I., Souilhol, C., Serbanovic-Canic, J., Roddie, H., Kalli, A. C., Fragiadaki, M., et al. (2019). beta1 integrin is a sensor of blood flow direction. *J. Cell Sci.* 132, doi: 10.1242/jcs.229542

Xu, C., Hasan, S. S., Schmidt, I., Rocha, S. F., Pitulescu, M. E., Bussmann, J., et al. (2014). Arteries are formed by vein-derived endothelial tip cells. *Nat. Commun.* 5:5758. doi: 10.1038/ncomms6758

Yee, A., Bosworth, K. A., Conway, D. E., Eskin, S. G., and McIntire, L. V. (2008). Gene expression of endothelial cells under pulsatile non-reversing vs. steady shear stress; comparison of nitric oxide production. *Ann. Biomed. Eng.* 36, 571–579. doi: 10.1007/s10439-008-9452-9

Conflict of Interest: The authors declare that the research was conducted in the absence of any commercial or financial relationships that could be construed as a potential conflict of interest.

frontiers in Physiology

REVIEW
published: 18 June 2020
doi: 10.3389/fphys.2020.00684

The Importance of Mechanical Forces for *in vitro* Endothelial Cell Biology

Emma Gordon[1], Lilian Schimmel[1] and Maike Frye[2]**

[1] Division of Cell and Developmental Biology, Institute for Molecular Bioscience, The University of Queensland, Brisbane, QLD, Australia, [2] Institute of Clinical Chemistry and Laboratory Medicine, University Medical Center Hamburg-Eppendorf, Hamburg, Germany

Blood and lymphatic vessels are lined by endothelial cells which constantly interact with their luminal and abluminal extracellular environments. These interactions confer physical forces on the endothelium, such as shear stress, stretch and stiffness, to mediate biological responses. These physical forces are often altered during disease, driving abnormal endothelial cell behavior and pathology. Therefore, it is critical that we understand the mechanisms by which endothelial cells respond to physical forces. Traditionally, endothelial cells in culture are grown in the absence of flow on stiff substrates such as plastic or glass. These cells are not subjected to the physical forces that endothelial cells endure *in vivo*, thus the results of these experiments often do not mimic those observed in the body. The field of vascular biology now realize that an intricate analysis of endothelial signaling mechanisms requires complex *in vitro* systems to mimic *in vivo* conditions. Here, we will review what is known about the mechanical forces that guide endothelial cell behavior and then discuss the advancements in endothelial cell culture models designed to better mimic the *in vivo* vascular microenvironment. A wider application of these technologies will provide more biologically relevant information from cultured cells which will be reproducible to conditions found in the body.

Keywords: blood endothelial cells, lymphatic endothelial cells, mechanotransduction, fluid shear stress, matrix stiffness, ECM - extracellular matrix, *in vitro* model culture system, (lymph-)angiogenesis

OPEN ACCESS

Edited by:
Stephan Huveneers, Amsterdam University Medical Center (UMC), Netherlands

Reviewed by:
Julian Albarran Juarez, Aarhus University, Denmark
Elizabeth Anne Vincent Jones, KU Leuven, Belgium

****Correspondence:***
Emma Gordon
e.gordon@imb.uq.edu.au
Maike Frye
m.frye@uke.de

Specialty section:
This article was submitted to Vascular Physiology, a section of the journal Frontiers in Physiology

Received: *27 February 2020*
Accepted: *26 May 2020*
Published: *18 June 2020*

Citation:
Gordon E, Schimmel L and Frye M (2020) The Importance of Mechanical Forces for in vitro Endothelial Cell Biology. Front. Physiol. 11:684. doi: 10.3389/fphys.2020.00684

INTRODUCTION

Blood and lymphatic vessels are critical components of the vascular system, controlling the transport, delivery and recycling of nutrients and waste to all tissues in the body. The blood vascular system is comprised of a closed circulatory network of arteries, veins and capillaries. Arteries transport oxygenated blood with gases, nutrients, metabolites and immune cells to the organs, while veins return oxygen-poor blood to the heart. In contrast to the blood vascular system, lymphatic vessels are comprised of a blind-end, unidirectional vascular network of lymphatic collecting vessels and capillaries. Due to their specialized button-like cell junctions, lymphatic capillaries are able to take up fluid, macromolecules and immune cells. The lymph is then transported through collecting vessels that are equipped with zipper-like junctions and drained back into the venous circulation (Potente and Makinen, 2017).

As a result of their unique functions, each vessel sub-type is subjected to unique mechanical stresses. They are comprised of specialized subtypes of endothelial cells (ECs) with unique properties and genetic profiles, allowing them to perform their specific function

(Potente and Makinen, 2017). Not only does each vessel have unique ECs, the EC properties also differ across tissue beds. For example, blood vascular ECs are continuously aligned in most tissues, but fenestrated in tissues involved in filtration and secretion (kidney and intestinal mucosa) or discontinuous in sinusoidal vascular beds (liver and bone marrow) [reviewed in detail by Augustin and Koh (2017)]. Lymphatic endothelial cells also display heterogeneity across tissue beds, with specialized Schlemm's canal vessels found in the eye and meningeal lymphatics found in the brain [reviewed in detail by Petrova and Koh (2018)].

In addition to the heterogeneity of ECs, vessels are surrounded by a wide range of support structures with differing mechanical properties. They may be surrounded by supportive mural cells [such as pericytes and smooth muscle cells (SMCs)] and varying components of extracellular matrix, which is comprised of basement membrane (BM) and the interstitial matrix (occupying/filling the interstitial space). Large arteries and veins are characterized by a continuous lining of BM and layers of mural cells, whereas lymphatic collecting vessels only exhibit a thin BM layer and sparse SMC support. Lymphatic capillaries lack mural cell support and are characterized by a discontinuous or absent BM (Potente and Makinen, 2017). These features allow each vessel subtype to maintain its integrity while performing its unique function.

Much of the pioneering work characterizing EC structure and function was performed using cells grown *in vitro*. It is beginning to be appreciated that ECs within their *in vivo* environment differ greatly to those that are cultured in static two-dimensional or three-dimensional (2D/3D) settings. Indeed, the physical forces that ECs are subjected to *in vivo*, such as fluid shear stress, stiffness and stretch, greatly influence how these cells function. Here, we will briefly summarize what is known about the mechanical forces that regulate EC function and further discuss existing and emerging techniques to model these forces *in vitro*. By growing cells in mechanically relevant conditions, we can more accurately predict cellular behavior in physiological environments.

MECHANOTRANSDUCTION OF FLUID SHEAR STRESS

Blood ECs lining the vessel wall are subjected to mechanical forces due to the friction between the ECs and the blood being pumped from the heart, known as fluid shear stress (FSS). The effects of FSS depends on a multitude of factors, such as the magnitude and direction of flow and the speed and strength of pump pulses (Baeyens et al., 2016). Shear stress can be steady laminar (where fluid moves in one direction at a steady magnitude), disturbed laminar (where flow is separated, recirculates and subsequently reattaches) oscillatory (where laminar flow fluid moves in a bidirectional manner) and turbulent (where flow is chaotic and moves in all directions) (Chatzizisis et al., 2007). All FSS may be pulsatile, where magnitude of flow is varied. Both oscillatory and turbulent flow may also be classified as disturbed. These different stresses play a key role in regulating vascular physiology, as alterations to FSS parameters or changes in the EC response can lead to a range of vascular pathologies [reviewed in Baeyens et al. (2016)]. Indeed, disturbed flow is known to have a wide range of effects on ECs, inducing changes in gene expression, cell shape and inflammatory profiles. This can lead to diseases such as atherosclerosis and pulmonary arterial hypertension. For a more detailed view on the effects of disturbed flow in the blood vasculature, please see the recent review by Souilhol et al. (2020).

As arteries transport blood away from the heart, they are subjected to high FSS (10–50 dyn/cm^2) which is highly pulsatile, whereas veins are subjected to a more consistent flow with forces around 10-fold less (Paszkowiak and Dardik, 2003). Unlike blood vessels which are controlled by a central pump, lymphatic capillaries are exposed to interstitial fluid flow, thus are exposed to the lowest FSS, approximately 10-fold less than blood vessels (Dixon et al., 2006). The uptake of interstitial fluid and resulting forces are guided by hydrostatic and osmotic pressure between lymphatic vessels, blood vessels and the interstitial space [known as Starling forces (Swartz and Fleury, 2007; Levick and Michel, 2010)]. Collecting lymphatic vessels have an intrinsic pumping capacity and smooth muscle cell coverage, thus are exposed to greater FSS than capillaries to ensure efficient transport of the lymph back to the venous circulation (Scallan et al., 2016). Here, we will discuss how ECs sense and respond to these different forces to generate and maintain a functional vascular network.

Flow Mediated Mechanosensory Hubs at Junctions

In order for ECs to respond to FSS, they require mechanisms to sense changes in flow conditions. This may be done via cilia, glycocalyx, ion channels, G-proteins or protein kinases (Hahn and Schwartz, 2009; Goetz et al., 2014; Wang et al., 2015; Givens and Tzima, 2016; Chistiakov et al., 2017). Perhaps the most well characterized mechanism of FSS sensing is through cell surface receptor 'mechanosensory hubs' found at cell–cell junctions [otherwise known as adherens junctions (AJs)]. Receptors within these AJ hubs include PECAM-1 (CD31), Vascular endothelial (VE)-cadherin, VEGFR2 and VEGFR3 (Tzima et al., 2005; Conway et al., 2013; Coon et al., 2015). Most central to this hub is PECAM-1, which is a direct sensor of shear stress tension (Tzima et al., 2005). Increased tension on PECAM-1 via steady laminar FSS [12 dyn/cm^2 for 16 hours (h)] triggers association of this cell surface receptor with the vimentin cytoskeleton, which permits transmission of force from myosin to PECAM-1 (Conway et al., 2013). These tensile forces on PECAM-1 trigger the activation of Src family kinases (SFK), which in turn phosphorylate VEGF receptors in a ligand independent manner. Phosphorylated VEGFRs then activate downstream signaling cascades, including the PI(3)K and NFκB pathways (Tzima et al., 2005; Coon et al., 2015). Within this complex, VE-cadherin acts to assemble VEGFRs at the junction through its transmembrane domain, facilitating their activation by SFK (Coon et al., 2015).

While known to be a critical component of AJ mechanosensory hubs and a key controller of vascular integrity and sprouting (Coon et al., 2015; Schimmel and Gordon,

2018), the precise role of VE-cadherin as a sensor of tension in response to shear stress remains undefined. In contrast to PECAM-1, when steady laminar FSS is applied to VE-cadherin (15 dyn/cm^2), tension is reduced within 2 min (Conway et al., 2013). Interestingly, 2 min at 15 dyn/cm^2 is sufficient to induce tension on PECAM-1 (Conway et al., 2013). *In vivo*, VE-cadherin tension in vessels under high levels of FSS (arteries) is lower than that observed in low shear, immature vessels (Lagendijk et al., 2017). However, VE-cadherin can be phosphorylated in response to PECAM-1-SFK on its Tyr658 site (Conway et al., 2017). This results in dissociation of p120-catenin and association with polarity protein LGN, which subsequently activates inflammatory pathways at sites of disturbed flow. Additional research is required to fully elucidate the mechanosensory role of VE-cadherin in response to FSS in physiological settings.

Flow Mediated Mechanosensory Hubs at Cell-Matrix Interfaces

In addition to junctions, mechanosensory hubs are found at sites of cell-matrix adhesion [otherwise known as focal adhesions (FAs)]. FAs are comprised of extracellular matrix (ECM) binding proteins known as integrins, which are coupled to the cytoskeleton through actin binding proteins, including the mechanosensors vinculin and talin (Bays and DeMali, 2017; Goult et al., 2018). FAs are vital components of the EC mechanosensory complex, mediating a wide range of signaling cascades in response to traction forces and FSS (Katsumi et al., 2004; Yurdagul and Orr, 2016). However, while FAs are remodeled in response to FSS and ECs display larger FA under steady laminar flow (17 dyn/cm^2) than those under disturbed flow after 14 h (Ting et al., 2012), whether FA proteins themselves can physically sense changes in tension in response to FSS remains unclear.

Within FAs, integrins play a central role in transducing chemical and physical signals from their surroundings by interacting and binding to their adhesion ligands presented by the BM. For a detailed overview of integrins and their ECM interactions, please see the following reviews (Ross et al., 2013; Hamidi and Ivaska, 2018). Notably, integrin can mediate bi-directional signaling. "Inside-out" signaling activates the ligand binding function of integrins (for example when FSS is sensed and subsequently transduced inside the EC) and "outside-in" signaling mediates cellular responses (for example in response to changes in ECM stiffness) leading to changes in cell spreading, retraction, migration, and proliferation (Hamidi and Ivaska, 2018). Although integrins do physically respond to FSS, albeit at a significantly lower degree compared to their response to traction forces (Katsumi et al., 2004), whether they confer biologically relevant tension changes in response to FSS remains unclear. However, they are activated downstream of PECAM-1 and PI(3)K activity (Collins et al., 2012; Russell-Puleri et al., 2017), revealing they may indeed involved in a FSS mechanosensory complex. The Integrin-actin linker protein talin is a well-established traction force mechanosensor (Kumar et al., 2016, 2018; Goult et al., 2018). Yet similar to integrins, whether it confers physical tension sensing capacity in response to FSS remains unclear. Talin activates integrins by binding to the β-tail (Yurdagul and Orr, 2016) and loss of talin results in impaired integrin activation (Monkley et al., 2000). EC-specific knockout of either integrin-β1 itself or talin (leading to loss of integrin-β1 activation) leads to perturbed VE-cadherin localization and loss of junctional integrity (Yamamoto et al., 2015; Pulous et al., 2019). This reveals that FAs are intimately associated with AJs, potentially through their attachment to the cytoskeleton. However, it may also suggest that integrins and talin may not be FSS tension sensors, but are simply activated downstream of AJ mechanosensory hubs though the physical link with the cytoskeleton or by downstream signaling pathways. More work is required to elucidate the FSS tension sensing capacity of integrins and their associated actin-binding proteins.

Recently, it was reported that guidance receptor PlexinD1 is a mechanosensor, and upon loss of PlexinD1 cells fail to align after 24 h steady laminar FSS (12 dyn/cm^2). This occurs through a PlexinD1-Neuropilin-1 complex with VEGFR2, which acts as a mechanosensor upstream of the PECAM-1 mediated junctional complex and integrin-based focal adhesions (Mehta et al., 2020). If PlexinD1 is held in its ring-like conformation it cannot act as a mechanosensor, suggesting it is not only the expression, but also the structure, of each mechanosensory component which confers its role.

Sensing Flow Dynamics During Vessel Sprouting and Remodeling

As blood and lymphatic vessels sprout, mature and remodel, they become subjected to different FSS. Therefore, EC mechanosensors need to be able to adapt to each vessel's physiological requirements. During formation of the initial blood vascular plexus *in vivo*, angiogenic sprouting is more likely to occur at sites of low FSS (Ghaffari et al., 2015) and vascular fusion is induced by steady laminar low FSS and VE-cadherin phosphorylation (induced at 1.8 dyn/cm^2 but not 10 dyn/cm^2 for 4 h) (Caolo et al., 2018). Later in development during vascular remodeling, in vessels with low FSS (such as capillaries) ECs are less likely to align against the direction of flow than ECs in regions of high FSS (such as arteries) (Franco et al., 2015). This prevents polarity-induced migration into regions of high flow and subsequent vessel regression. ECs deficient in canonical Wnt signaling display increased sensitivity to FSS-induced regression *in vivo* or after being subjected to steady laminar FSS in culture (20 dyn/cm^2 for 4 h) (Franco et al., 2016), suggesting that a FSS 'setpoint' controlling EC polarity and vascular stability is modulated by Wnt. These 'setpoints' define the optimal FSS exposure for normal vascular function, whereby if FSS is above or below the setpoint, vascular abnormalities occur. Interestingly, loss of Wnt signaling leads to reduced sprouting capacity (Korn et al., 2014; Carvalho et al., 2019), yet whether this is guided through altered sensitivity to a low FSS setpoint remains unclear.

In addition to FSS setpoints being defined during EC polarity and remodeling, they must be specified across different vessel sub-types in order for each vessel to exert its biological function. As blood vessels are exposed to higher FSS in the body than lymphatic vessels, blood ECs become misaligned and activate

NFκB at much higher steady laminar FSS levels (25 dyn/cm^2 and over for 16 h) than that of lymphatic ECs (10 dyn/cm^2 and over for 16 h) (Baeyens et al., 2015). This allows blood vessels to be exposed to higher rates of FSS without causing inflammation and disease. This is a reflection of vessel physiology – lymphatics are exposed to significantly lower FSS *in vivo* as their function is to transport interstitial fluid back to venous circulation. The FSS setpoint in blood EC versus lymphatic EC is mediated though expression of VEGFR3, which is enriched in lymphatic ECs compared to blood ECs (Kaipainen et al., 1995). The elevated expression of VEGFR3 in lymphatic EC causes them to respond to FSS at lower levels to that of blood ECs, and reducing VEGFR3 expression in lymphatic ECs increases the FSS setpoint (Baeyens et al., 2015). Conversely, increasing VEGFR3 expression in blood EC decreases the FSS setpoint, causing induction of inflammatory profiles at FSS levels seen in lymphatic EC.

Although FSS is lower in lymphatic compared to blood vessels, there are still physiologically relevant fluctuations in flow that drive genetic and morphological changes in lymphatics. During early development, functional lymphatic drainage can be detected as early as embryonic day (E) 11.5 (Planas-Paz et al., 2012) suggesting that induction of FSS might contribute to the development of the primary lymphatic plexus by inducing lymphatic EC proliferation. Indeed, steady laminar FSS has been shown to induce proliferation via ORAI1 and KLF2/4-mediated upregulation of VEGF-A, VEGF-C, FGFR3 and p57 (2 dyn/cm^2 for 12–24 h) (Choi et al., 2017a) and downregulation of NOTCH1 activity (2 dyn/cm^2 for 12–24 h) (Choi et al., 2017b). Lymphatic valve development is predominantly initiated in areas of disturbed flow, and oscillatory flow (4 dyn/cm^2 for 48 h) has been shown to reproduce a lymphatic valve EC phenotype *in vitro* (Sabine et al., 2012). Oscillatory flow but not steady laminar flow (4 dyn/cm^2 for 48 h) induces expression of the transcription factor GATA2 in valve-forming lymphatic ECs, which in turn upregulates expression of the lymphatic endothelial transcription factors PROX1 and FOXC2 (Kazenwadel et al., 2015), both of which are key regulators of valve formation. In agreement, loss of lymphatic flow in a mouse model of CLEC2-deficiency (in which blood backfills the lymphatic network and thereby blocks lymph flow) results in a phenotype identical to that observed upon loss of FOXC2 (Petrova et al., 2004; Sweet et al., 2015). In the postnatal lymphatic vasculature, FOXC2 is necessary to maintain collecting vessel quiescence and stability in valve areas by linking oscillatory flow responses to cell junction stabilization and cell-cycle arrest (Sabine et al., 2015), revealing flow dynamics as key regulators of the formation and maintenance of a functional lymphatic system.

Changes in Membrane Tension by FSS

Interestingly, FSS can induce changes in membrane curvature, leading to activation of a range of cell surface receptors including calcium and ion channels. The ion channel Piezo1, which is sensitive to changes in membrane tension (Lewis and Grandl, 2015; Cox et al., 2016), is also required for FSS sensing (Ranade et al., 2014; Albarran-Juarez et al., 2018), thereby coupling FSS and membrane stretch. Piezo1 regulates vascular permeability in the lungs by inducing VE-cadherin internalization, and subsequent leakage, in response to increased hydrostatic pressure (Friedrich et al., 2019). Piezo1 is also mechanically activated in lymphatic vessels and is required for lymphatic valve formation (Nonomura et al., 2018) by sensing disturbed flow to induce GATA2 and FOXC2 expression (Choi et al., 2019). Although not as widely studied, ion channels such as TRPV4 have also been implicated in FSS sensing to regulate vascular permeability (Thorneloe et al., 2012). Not only is membrane curvature altered, but membrane fluidity changes upon the onset of shear stress, which may directly induce the difference in tension that opens up channels such as Piezo1. However, these changes occur in biologically inactive lipid membranes, thus may be a basic physical phenomena that can transduce shear stress (Yamamoto and Ando, 2013).

In addition to Piezo1, caveolae (invaginations on the cell membrane) are sensitive to changes in membrane tension and are known to be altered in response to FSS (Shihata et al., 2016). ECs flatten their caveolae in response to increased osmotic pressure to allow for membrane 'stretching,' which may be a survival mechanism by increasing cell surface area (Sinha et al., 2011; Parton and del Pozo, 2013). Interestingly, a recent study found caveolae are abundant in arterial ECs of the central nervous system and are responsible for transmitting signals from the neurovascular unit to adjacent SMC to induce vasodilation (Chow et al., 2020). This was proposed to be through the ability of caveolae to cluster TRPV4 ion channels (Goedicke-Fritz et al., 2015) rather than mediating changes in arterial membrane stretch. Precisely how physical stretch by FSS alters membrane components in ECs remains largely unknown.

MECHANOTRANSDUCTION OF EXTRACELLULAR MATRIX (ECM) STIFFNESS

Extracellular matrix stiffness has been shown to guide the behavior of ECs to form the initial functional vascular network. Embryonic stem cells (ESCs) depend on the mechanical environment of the stem cell niche, as the fate of vascular progenitor cells (VPC) was shown to be dependent on substrate stiffness, with EC lineages favoring softer substrates (10 kPa) and SMC lineages favoring stiffer substrates (plastic, GPa range) (Wong et al., 2019). During early lymphatic development, venous lymphatic EC progenitors laminate from the cardinal vein and encounter very soft surrounding tissue (0.27 kPa) while they migrate dorsally to form primary lymphatic structures (Frye et al., 2018). This value matches those measured in early chicken embryos (0.3 kPa) (Majkut et al., 2013) and adult brain (0.33 kPa) (Georges et al., 2006) but are significantly lower compared to values from most other adult tissues, such as muscle (around 12 kPa) (Engler et al., 2004) or bone (GPa range) (Rho et al., 1993). Upon remodeling and maturation, ECs form the inner layer of blood and lymphatic vessels and are attached to the underlying 2D ECM environment. The composition and mechanical properties of the ECM differ along vascular trees, across tissues and during development and disease states (Di Russo et al., 2017).

The range of venous tissue stiffness in mammals is about 3–50 kPa (Xue et al., 2017; Frye et al., 2018), which is positioned between the stiffness of the epithelium and cartilage. Unlike veins, arteries must be able to withstand higher blood pressure and are surrounded by several layers of smooth muscle cells and connective tissue (Corada et al., 2014). Therefore, arteries are stiffer, ranging from about 50–150 kPa (Kohn et al., 2015). Differences in ECM stiffness experienced by endothelial progenitor cells (EPCs) have been implicated in the regulation of arterial-venous differentiation *in vitro* (Xue et al., 2017). In contrast to EPCs cultured on venous substrate stiffness (7 kPa), EPCs cultured on arterial substrate stiffness (128 kPa) showed an increase in expression of the arterial marker EphrinB2 (Xue et al., 2017).

The stiffness values experienced by the endothelium must be interpreted with caution as substantially different measurement techniques have been employed to generate values [reviewed by Kohn et al. (2015) and Guimarães et al. (2020)]. Macroscale techniques, such as Shear Wave Elastography (SWE) (Maksuti et al., 2016) generally analyze the entire vessel structure as a uniform material, and do not take into account cell-scale differences of the individual vessel components, such as the endothelial or SMC layer or the surrounding ECM. Furthermore, macroscale techniques typically provide values of the stiffest component of a vessel structure. Therefore, these data underscore the importance of analyzing mechanical properties of individual vessel components using microscale techniques, such as Atomic Force Microscopy (AFM) (Alsteens et al., 2017; Frye et al., 2018) and Scanning Ion Conductance Microscopy (SICM) (Schaffer, 2013). It is important to attempt comprehensive measurements of *in vivo* ECM stiffness experienced by ECs to accurately choose the stiffness values for studies on EC-type or organ-specific vasculature.

EC-Induced ECM Deformation

Adherent cells sense ECM stiffness by probing their extracellular environment, resulting in substrate displacements when substrates are compliant. The measurement of compliant ECM substrate deformations (and calculation of deformation-based metrics) via Traction Force Microscopy (TFM) (Califano and Reinhart-King, 2009) or 4D displacement microscopy (Vaeyens et al., 2020) can provide quantitative information on cell-ECM mechanical interactions. For example, by employing 4D displacement microscopy, it has been demonstrated that ECM substrate deformations are spatio-temporally correlated with sprout-morphological dynamics during sprouting angiogenesis (Vaeyens et al., 2020). Interestingly, protrusions from extending sprouts increase their pulling forces, while retracting protrusions reduce pulling.

In vitro ECM substrate deformation analysis can provide insight into how ECs exert forces into their surroundings. However, which ECM components or EC-surrounding cells are responsible to generate the absolute *in vivo* ECM stiffness that counteracts those deformation forces is poorly defined. The BM underlying ECs in most mature vessel types is a very thin layer (30–500 nm) and is comprised of ECM matrix molecules such as elastin, collagen, enactin/nidogen, heparan-sulfate proteoglycans, and laminin (Liliensiek et al., 2009). Interestingly, a study by Sen et al. (2009) showed that cells can "feel" up to several micrometers deep into a compliant substrate. Consistently, induction of EC network formation on compliant substrate (0.4 kPa) was prevented on very thin compliant substrates (<20 μm) as ECs sensed the stiffness of the underlying coverslip (Davidson et al., 2019). These findings suggest that absolute *in vivo* ECM stiffness experienced by ECs might rather be generated by several different EC-surrounding structures, including the BM, the interstitial matrix and, importantly, the adjacent cells.

Mechanosensing of ECM Stiffness

Similar to their FSS mechanotransduction capacity, FAs are fundamental mechanotransducers of ECM-endothelial stiffness. FAs propagate ECM stiffness stimuli to the actin cytoskeleton, resulting in cytoskeletal rearrangements that can lead to an immediate adaptation of cells to their physiological environment, such as alignment (Maniotis et al., 1997) or translocalization of proteins to the nucleus in order to modify the genetic program and thereby cellular behavior [reviewed in detail in Martino et al. (2018)]. Within FAs, the expression of integrins is highly cell type- and substrate-specific, and this integrin diversity can regulate intracellular signaling cascades in response to different mechanical stimuli (Seetharaman and Etienne-Manneville, 2018). In epithelial cells, an increase in matrix stiffness (0.2 kPa vs. GPa range) regulates the expression of β1 integrin and Cav1 to regulate FA assembly and turnover (Yeh et al., 2017). Similarly, ECs matrix stiffening (3 kPa vs. 70 kPa) has been shown to induce β1 integrin activity (Bastounis et al., 2019). Strong changes in expression of β1 integrin were not observed in this study, however, analysis of ECs on softer matrices were not included.

Intracellularly, FAs are dynamically associated with a variety of proteins that can sense and/or transduce force, such as focal adhesion kinase (FAK), vinculin and talin (Martino et al., 2018). FAK is one of the first proteins recruited to FAs in response to extracellular mechanical stimuli. In fibroblasts, autophosphorylation of FAK is required for induction of adhesion and integrin-binding responses (Michael et al., 2009). Furthermore, FAK activity is necessary to regulate directed migration of fibroblasts toward stiffer substrates (Plotnikov et al., 2012) and to induce matrix stiffness-mediated translocation of the mechanotransducer Yes-associated protein (YAP) to the nucleus of hepatic stellate cells (Lachowski et al., 2018). The mechanosensor talin is a 270 kDa protein composed of an N-terminal globular head, a flexible rod domain and C-terminal helices. It binds to the cytoplasmic domain of integrin β-subunits and regulates integrin signaling in a switch-like behavior via the helix bundles of its flexible rod domains (Goult et al., 2018). It has been suggested that individual domains open at different tension levels, exerting positive or negative effects on different protein interactions (Goult et al., 2018). For example, force loading of talin leads to the exposure of cryptic hydrophobic binding sites, which can subsequently bind vinculin (Rahikainen et al., 2017). As increasing force is applied to talin, more bundles are unfolded, revealing additional vinculin binding sites and thus activation of an increasing number of vinculin molecules

(Haining et al., 2016). These FA molecules have been extensively studied as general tension sensors/transducers in non-endothelial cell types (Provenzano et al., 2009; Zhou et al., 2017; Martino et al., 2018). It will be important to study the expression and function of those proteins specifically in the context of matrix stiffness-regulated EC behavior.

After they have been engaged downstream of integrins, FAs propagate mechanical stimuli to the actin cytoskeleton. Culturing ECs on different stiffness matrices leads to a substantial remodeling of the actin cytoskeleton (Jannatbabaei et al., 2019). With increasing matrix stiffness (3 kPa, 12 kPa, and 1.5 MPa), actin cytoskeleton remodeling becomes more organized, with an increasing amount of actin stress fibers. Interestingly, increasing matrix stiffness translates to increased EC stiffness in 2D (1.7 kPa vs. 9 kPa) and 3D (0.125 kPa vs. 0.5 kPa) environments (Byfield et al., 2009; Jannatbabaei et al., 2019). The actin cytoskeleton is connected to VE-cadherin via its intracellularly associated proteins β-catenin and α-catenin (Lampugnani et al., 1995). Tension-induced actin remodeling tightly controls assembly and disassembly of VE-cadherin-based junctions (Oldenburg and de Rooij, 2014). Cytoskeletal pulling at the VE-cadherin complex also recruits the FA tension sensor protein vinculin via α-catenin to reinforce endothelial junctions (Huveneers et al., 2012; Daneshjou et al., 2015).

Besides a direct effect on endothelial junction stability, cytoskeletal mechanotransduction can result in structural modification of membrane-bound or cytoplasmic proteins and their subsequent shuttling to the nucleus. β-catenin is not only a structural protein within the VE-cadherin adhesion complex, but can also shuttle to the nucleus upon cytoskeletal remodeling to act as a transcriptional co-activator. In chondrocytes, β-catenin expression is induced and localized to the nucleus in a β1-integrin/FAK dependent manner in cells seeded on stiff matrices (100 kPa vs. 0.5–1 kPa) (Du et al., 2016). Furthermore, β-catenin was shown to localize to the nucleus in valvular ECs grown on stiff matrices (50 kPa vs. 5 kPa) (Zhong et al., 2018). Another class of nuclear shuttling proteins consists of YAP and WW Domain-Containing Transcription Regulator Protein 1 (WWTR1/TAZ), which are downstream effectors of the Hippo pathway (Zhong et al., 2018). YAP/TAZ are shuttled to the nucleus in lymphatic ECs grown on stiff substrates (25 kPa vs. 0.2 kPa) as evident by the induction of their target genes CTGF and ANKRD1 (Frye et al., 2018). YAP/TAZ function has been extensively studied in the development of the vasculature (Kim et al., 2017; Sakabe et al., 2017; Wang et al., 2017b; Neto et al., 2018; Cho et al., 2019; Sivaraj et al., 2020). Precisely how changes in ECM stiffness experienced by ECs might regulate those processes remains to be elucidated.

ECM Stiffness and Endothelial Proliferation and Migration

During angiogenesis, VEGFR2 activation and internalization induces proliferation of ECs to enable nascent blood vessels and tumor vessels to expand (Simons et al., 2016). In blood and lymphatic ECs, proliferation is decreased on soft 2D substrates and enhanced on stiff 2D substrates. Sub-confluent HUVECs grown on stiffer substrates (10 kPa vs. 1 kPa) increase VEGFR2 internalization, mediated via Rho activity and actin contractility (LaValley et al., 2017). Additionally, expression of Septin9, a negative upstream effector of RhoA, is increased in ECs grown on soft 2D substrates (1.72 kPa vs. 21.5 kPa), attenuates Src/Vav2 phosphorylation and inhibits RhoA-dependent EC proliferation (Yeh et al., 2012). However, in a confluent endothelial monolayer, stiffness-enhanced VEGF signaling is no longer observed (LaValley et al., 2017), suggesting this mechanism is unique to actively proliferating cells and angiogenic processes.

In contrast, maximal VEGFR2 expression and capillary blood vessel formation in an *in vivo* 3D Matrigel implant assay was detected in a relatively soft microenvironment of 0.8 kPa (Mammoto et al., 2009). Similarly, lymphatic ECs leave the stiffer cardinal vein (4 kPa) to migrate through a very soft 3D environment (0.27 kPa) (Frye et al., 2018). The decrease in matrix stiffness experienced by those cells induces an increase in VEGFR3 expression that is necessary to allow efficient migration. As has been suggested by Mammoto et al. (2009), a difference in migratory and sprouting response to matrix stiffness could be explained by differential EC requirements on a 2D ECM versus a 3D ECM environment. This hypothesis is further supported by the finding that sprouting of blood ECs is increased in synthetic 3D hydrogels with lower matrix crosslinking, which is accompanied by a decrease in matrix stiffness (1 kPa vs. 6 kPa) (Trappmann et al., 2017).

Furthermore, it is important to note that *in vitro* studies have been performed using different definitions of a stiff substrate. Comparing the absolute kPa values reveals that 'stiff' ECM values (such as 4 kPa) are used as the 'soft' ECM standards in other studies (Canver et al., 2016). This underscores the necessity to comprehensively measure *in vivo* stiffness of blood and lymphatic vasculature to better define the ranges that can be adapted for *in vitro* studies.

ECM Stiffness and Disease

More than 80% of all cardiovascular deaths in developed countries occurs in the population aged 65 or older, making aging a major risk factor for cardiovascular disease. It is well established that age-induced stiffening of the ECM in the intima alters the function of blood vessels. These alterations of ECM stiffness affect EC health, resulting in inflammation, hypertension and ultimately disease progression in disorders such as atherosclerosis and pulmonary arterial hypertension (PAH) (Zieman et al., 2005; Ley et al., 2007; Wang and Chesler, 2011; Marti et al., 2012; Tan et al., 2014). Indeed, increased vascular ECM stiffness is induced upon aging and/or inflammation, as revealed by rigidity measurements using murine aortas of different ages (Huynh et al., 2011) and murine and human atherosclerotic plaques (Tracqui et al., 2011; Chai et al., 2013). Vascular calcification is often observed in human atherosclerotic plaques and is known to induce EC dysfunction, which is one of the main characteristics of arterial aging (Lee and Oh, 2010). This calcification seems to be irreversible, with a number of studies attempting to inhibit or reverse ECM stiffening being unsuccessful (Little et al., 2005; Hope and Hughes, 2007; Zieman et al., 2007; Willemsen et al.,

2010). Hence, current research has shifted toward investigating the translational effects of ECM stiffness on ECs, to explore the possibilities of reversing the EC response to increased ECM stiffness, instead of directly targeting ECM stiffening.

In the context of cancer biology, it is well appreciated that a solid tumor environment is stiffer than that of healthy tissue (Levental et al., 2009). How tumors overcome the mechanical barrier of a stiffer environment to promote tumor angiogenesis is likely through matrix metalloproteinase (MMP) signaling, which was found to be induced in ECs cultured in stiffer 3D collagen gels (Levental et al., 2009). Endothelial dysregulation results in vascular leakage due to a loss of cell junction integrity. In tumors, this dysregulation has been largely attributed to an increase in pro-angiogenic growth factors. However, tumor ECM stiffness has been shown to also play a central role in promoting a characteristically leakier tumor vasculature (Bordeleau et al., 2017). Sub-confluent ECs on compliant substrates assemble spontaneously into networks reminiscent of an angiogenic process (Califano and Reinhart-King, 2008). Therefore, sub-confluent ECs grown on soft substrates (0.2 kPa) form continuous VE-cadherin-positive junctions, which are highly discontinuous and punctuated compared to those grown on stiff, tumorigenic substrates (10 kPa) (Bordeleau et al., 2017).

Mechanistically, increased matrix stiffness activates FAK, resulting in Src localization to cell–cell junctions and subsequent Src-mediated VE-cadherin phosphorylation (Wang et al., 2019). Interestingly, loss of VE-cadherin function activates intercellular force transduction signals that increase integrin-dependent cell contractility, disrupting both cell–cell and cell-matrix adhesions. Increased substrate stiffness (40 kPa vs. 1.1 kPa) further exacerbates these effects (Andresen Eguiluz et al., 2017). Tumor matrix stiffening not only impacts angiogenesis and tumor vessel leakage, but is also implicated in regulating metastasis. Matrix stiffening from 0.4 kPa to 22 kPa induced matricellular protein CCN1, which in turn upregulates N-cadherin levels on the EC surface to facilitate cancer cell binding to the endothelium and intravasation into the vessel lumen (Reid et al., 2017). These data suggest that identifying and targeting EC behavior in response to altered stiffness in solid tumors could provide novel therapeutic approaches to normalize tumor vasculature.

Endothelial Cellular Stiffness and Leukocyte *Trans*-Endothelial Migration (TEM)

It has become clear that changes in ECM stiffness can directly regulate EC internal stiffness and/or expression of endothelial adhesion molecules, which is correlated with altered leukocyte extravasation (Stroka and Aranda-Espinoza, 2010, 2011; Schimmel et al., 2018; Chen et al., 2019). Whereas differences in ECM stiffness directs EC migration during angiogenesis, in the case of leukocyte *trans*-endothelial migration (TEM), it is the internal EC stiffness that guides the direction of leukocyte migration. The internal stiffness of ECs is regulated by crosslinking of ICAM-1 to the actin cytoskeleton via actin binding proteins (ABPs) α-actinin and cortactin (Schaefer et al., 2014). DLC-1, a Rho GTPase Activating Protein induced by ECM stiffness, is able to stabilize this crosslinking (Schimmel et al., 2018). Loss of DLC-1 in ECs cultured on stiff substrates results in leukocyte transmigration kinetics similar to those observed for ECs cultured on soft substrates, revealing DLC-1 as a critical transmitter of ECM-induced EC stiffness required for TEM. These changes in TEM and EC internal stiffness caused by the ECM are observed in inflammatory diseases, as in areas of increased ECM stiffening (such as atherosclerotic lesions or in the lung microvasculature of PAH patients) increased leukocyte extravasation is observed (Dorfmuller et al., 2003).

Besides the effects of ECM stiffness on leukocyte TEM via changes in EC internal stiffness, it has been shown that ECM stiffness regulates leukocyte and monocyte transmigration via microRNAs. Expression of adhesion molecules ICAM-1 and VCAM-1 on ECs, both essential for leukocyte and monocyte adhesion, is regulated by miR-222 and miR-126, respectively (Harris et al., 2008; Ueda et al., 2009). ECs cultured on high stiffness substrates (20 kPa) showed reduced migration of monocytes, which correlated with higher levels of miR-222 and miR-126 to inhibit endothelial ICAM-1 and VCAM-1 expression compared to soft (8 kPa) and diseased (40 kPa) stiffness values (Chen et al., 2019). This suggest that matrix stiffness exerts a biphasic regulation of endothelial adhesion molecules ICAM-1 and VCAM-1, which promotes EC-monocyte interactions both in healthy (soft) and diseased (stiff) environments.

MECHANOTRANSDUCTION OF ENDOTHELIAL CELL STRETCH

While much focus has been placed on the role of FSS sensing and cell-ECM interactions, the role of cyclic stretch (CS) on endothelial cell function is far less studied. This is despite its intricate link to matrix stiffness, as a stiffer matrix will in principle result in a reduction of cyclic stretch. ECs are constantly exposed to cyclical stretch due to dilation across the vessel wall as a result of blood pumping, respiration in the lungs or uptake of interstitial fluid in lymphatics. This stretch of the EC membrane results in activation of signaling pathways and physiological responses, such as sprouting, permeability and remodeling (Jufri et al., 2015).

Stretch in Blood Endothelial Cells

To date, much of our knowledge on how vascular ECs respond to stretch comes from cultured cells. In blood ECs, normal stretch is 5% elongation and pathological stress is 18% elongation, with acute stretch being 15 min and stretch being chronic 48 h (Birukov et al., 2003). Stretch has been associated with a range of pathways, many of which result in loss of barrier integrity. Even after short term exposure to CS, ECs become significantly more prone to leakage in response to thrombin or VEGF, linked to an increase in Rho GTPase activity and MLC phosphorylation (Birukov et al., 2003; Birukova et al., 2008a). However, changes in barrier integrity are not simply linked to changes in mechanical imbalance, as after cells have been re-plated to non-elastic substrates, they continue to be susceptible to leakage (Birukova et al., 2008b). Interestingly, pre-conditioning of ECs to CS

provides protection against barrier breakdown (Birukova et al., 2008a), which is thought to be a result of induction of Rap1 signaling to promote junctional stability and suppress RhoA signaling (Ke et al., 2019). Interestingly, cyclic stretch can also induce EC proliferation in response to mechanical stimulation, in a process that requires cell–cell contacts. Indeed, stretch induced EC proliferation is lost upon VE-cadherin inhibition or knockdown (Liu et al., 2007; Neto et al., 2018) and dependent on the Hippo pathway downstream effector YAP (Neto et al., 2018).

Cardiovascular diseases such as hypertension and atherosclerosis are associated with CS, as an increase in blood pressure or changes in the ECM environment can affect the amount of stretch (Jufri et al., 2015). Pathological but not physiological CS results in activation of VEGFR2 and SFKs, and subsequent phosphorylation of VE-cadherin and disassembly of junctions (Gawlak et al., 2016; Tian et al., 2016a). Pathological and chronic exposure to CS also induces inflammation by upregulation of ICAM1 and secretion of IL-8 (Tian et al., 2016b). Therefore, increased CS can cause both pathological barrier breakdown and induce inflammation. Pulsatile stretch above 10% in brain ECs induces inflammation through ICAM1 and NO and induces amyloid precursor protein expression, which may explain why the severity of Alzheimer's disease is increased with a higher pulsatility index and pressure (Nation et al., 2013; Gangoda et al., 2018). Interestingly, multi-directional stretch, analogous to the forces exerted on ECs in oscillatory FSS, results in upregulation of inflammatory stimulators such as NF-κB (Pedrigi et al., 2017), Both uniaxial and equiaxial stretch (10%) have been shown to drive induction of smooth muscle genes, an effect which is abrogated upon induction of FSS (uniform at 5 dyn/cm^2 or cyclic between 0 and 5 dyn/cm^2), suggesting stretch alone may induce transdifferentiation of ECs toward SMCs (Shoajei et al., 2014). Thus, multidirectional stretch may be directly linked to cellular processes which drive diseases such as fibrosis and atherosclerosis.

Stretch in Lymphatic Endothelial Cells

Lymphatic vessels are exposed to stretch as a result of their fluid uptake and pumping properties. Capillaries take up interstitial fluid via an extrinsic (passive) mechanism, where the lymph enters the lymphatic capillaries against a hydrostatic pressure gradient (Scallan et al., 2016). It has been elegantly demonstrated that during early lymphatic development, fluid that leaks out of newly formed arteries swells the tissue that surrounds the first primary lymphatic structures and stretches these nascent structures (Planas-Paz et al., 2012). Stretching of the lymphatic ECs leads to activation of VEGFR3 and subsequent proliferation, resulting in enlargement of lymphatic structures so they are able to drain the excessive fluid from the embryonic tissue.

Collecting lymphatic vessels pump lymph via cyclic compression and expansion of lymphatic SMCs that surrounds the lymphatic collecting ECs (lymphatic muscle) (Zawieja, 2009). Increased intraluminal lymph pressure after fluid uptake leads to stretching of the collecting lymphatics and activates an intrinsic (active) lymph pump. The impact of stretch on lymphatic EC behavior exerted by SMC surrounding the collecting vessels has not been extensively addressed. In contrast to blood ECs, normal lymphatic ECs stretch is 4% elongation and pathological stretch is 8% elongation (Wang et al., 2017a), suggesting that similar to FSS, lymphatic ECs have a lower stretch setpoint.

To briefly summarize, blood and lymphatic vessels (and their vessel sub-types such as arteries, veins, capillaries and collectors) all display different sensitivities to mechanical stimuli, such as fluid shear stress, stiffness or stretch. These mechanical forces must be considered when performing *in vitro* experiments in the context of the vascular process to be studied, in order to gain biologically relevant insights into EC physiology.

ADVANCES IN *IN VITRO* MODELING OF VASCULAR FORCES

With an appreciation of the importance of the extracellular environment, the vascular field has begun to develop *in vitro* approaches that more closely mimic *in vivo* environments. Bioengineering approaches have been developed *in vitro* to recapitulate *in vivo* forces, providing more cost effective, biologically relevant experimentation. Here, we will review commonly used cell culture techniques to model forces of fluid shear stress, matrix stiffness and cell stretch, and discuss emerging technologies to combine these mechanical forces.

2D Techniques to Model FSS

There are numerous models which have been used in the vascular biology field to identify defined FSS-mediated EC outputs. Traditionally, these have been performed by seeding cells on a 2D flat and stiff substrate, allowing them to adhere and form a monolayer, then passing fluid over them (**Figure 1**) (Akbari et al., 2017). This can be achieved using a cone and plate system, where flow is generated by rotation of a cone around a central axis which is oriented in a perpendicular manner to the surface of a flat plate. More commonly, however, these experiments are performed using a parallel plate chamber, where fluid is pumped using a peristaltic pump, constant pressure head or syringe pump. These models have been particularly useful when modeling how ECs respond to changes in shear stress force and duration, where straight channels model laminar FSS (**Figure 1B**) and bifurcated channels model gradient shear stress regions (**Figure 1C**). Fluid can be pumped in a steady unidirectional manner or in an oscillatory manner, and in both of these cases it may be pulsatile. Examples of knowledge that has come from these models include when exposed to low levels of steady laminar FSS (10 dyn/cm^2 for 5 h), EC junctions become stabilized (DePaola et al., 2001) and when exposed to disturbed shear stress, ECs acquire an inflammatory phenotype typically associated with atherosclerosis (Hahn and Schwartz, 2009; Chiu and Chien, 2011). Similar experiments have also helped to identify the mechanical contribution to formation of the lymphatic valves. When exposed to oscillatory but not steady state laminar FSS (4 dyn/cm^2 or cultured on a rocking platform for 48 h), lymphatic ECs acquire features of lymphatic valves. In line with these findings, lymphatic valves form at sites of disturbed flow *in vivo* (Sabine et al., 2012, 2015; Kazenwadel et al., 2015; Cha et al., 2016).

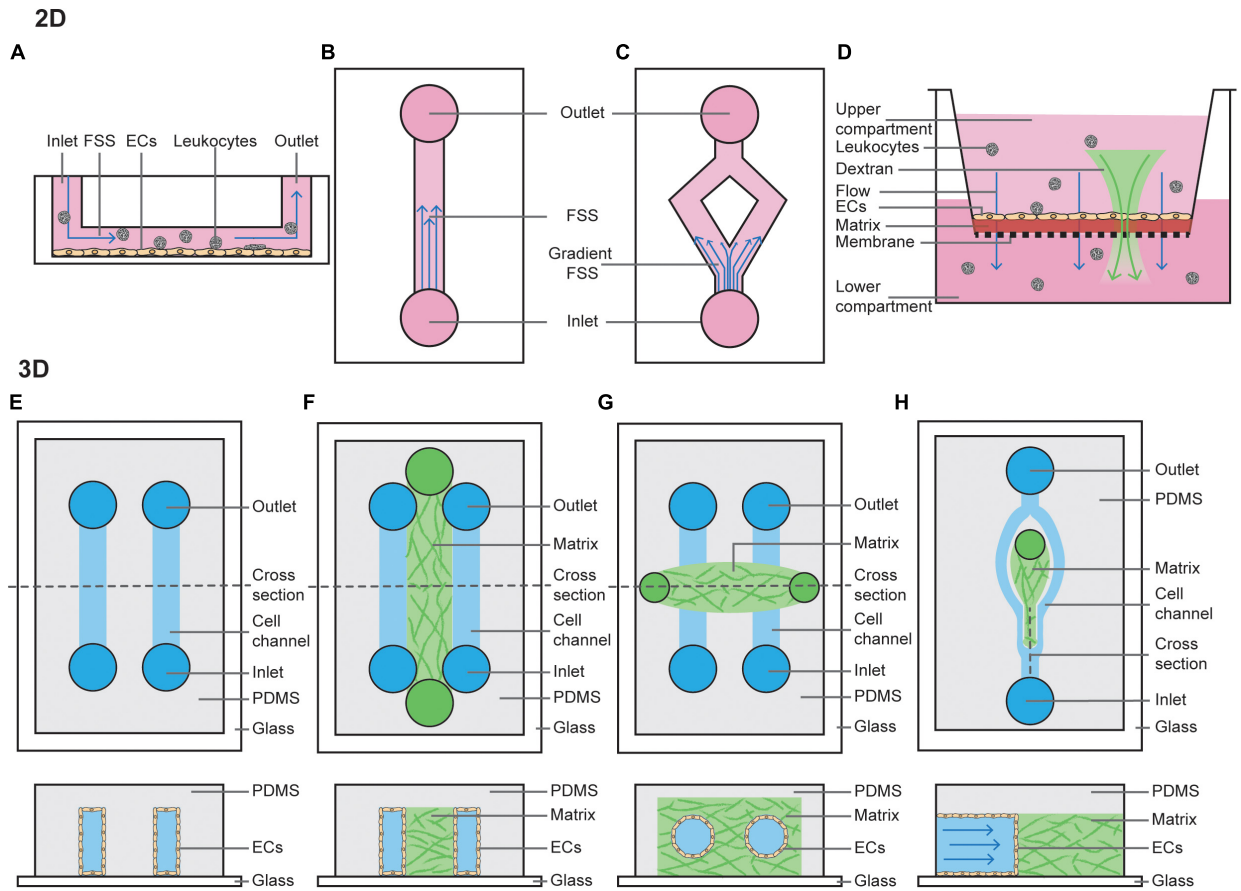

FIGURE 1 | 2D and 3D techniques to model FSS. **(A)** Cross section of a parallel plate flow chamber in which a monolayer of ECs is cultured on the bottom of the channel. Perfusion of media, containing growth factors and/or leukocytes, is added through the inlet and outlets. **(B)** Top view of a parallel plate flow chamber device to mimic steady laminar FSS or oscillatory laminar FSS, when fluid is pumped in a bidirectional manner. **(C)** Top view of a bifurcated channel to model gradient shear stress regions. **(D)** Cross section of a transwell filter system, where ECs are cultured on a thin ECM matrix on top of a porous membrane. The hydrostatic pressure difference between the upper and lower compartment models interstitial flow through the monolayer of ECs. Addition of fluorescent dextran or leukocytes to the upper compartment can be used to study permeability or leukocyte TEM. **(E)** Top view and horizontal cross section of a PDMS-only 3D microchannel in which ECs are grown inside the channels. **(F)** Top view and horizontal cross section of a PDMS-hydrogel hybrid 3D microchannel in which ECs are grown in the outer channels, and then allowed to migrate into the central hydrogel. **(G)** Top view and horizontal cross section of a hydrogel-only 3D microchannel in which ECs are grown fully surrounded by hydrogel. **(H)** Top view and vertical cross section of a PDMS-hydrogel hybrid 3D microchannel incorporating bifurcation.

Models of interstitial flow within lymphatic capillaries have been pioneered by the Swartz lab and are largely performed using Boyden chamber assays (**Figure 1D**) (i.e., transwell filter systems) or radial flow systems (Ng et al., 2004; Helm et al., 2005; Miteva et al., 2010; Swartz and Lund, 2012). Boyden chamber assays are performed by plating cells as a monolayer on a semi-porous ECM, such as collagen or fibrin, and seeded in the upper compartment of a transwell chamber. Then, a fixed hydrostatic pressure difference is maintained between the top and bottom chambers. Alternatively, radial flow chambers consist of ECM with ECs embedded and exposed to flow oriented radially, which is then placed between two glass coverslips and fixed with porous boundaries. Boyden chamber assays are also widely utilized amongst vascular biologists to study vascular permeability and chemotaxis of ECs and leukocytes (Nowak-Sliwinska et al., 2018).

2D FSS assays have been utilized for much of the pioneering work in understanding the mechanisms of how ECs sense flow-mediated mechanotransduction, and continue to provide valuable insights. However, these standard commercial assays are limited in that they do not fully recapitulate vessel physiology, which is significantly more complex. Of relevance to this review, these assays do not incorporate important components that can alter hydrodynamics (Huber et al., 2018) such as mural cells, ECM stiffness, or circular stretch.

3D Techniques to Model FSS

More complex microfluidic systems to model FSS involve growing ECs in 3D microchannels using microfabrication techniques. These can be entirely poly(dimethylsiloxane) (PDMS) derived, PDMS-hydrogel hybrids, or pure hydrogel (Akbari et al., 2017). Similar to 2D FSS models, flow can be controlled using hydrostatic pumps. PDMS-alone devices are typically linear rectangular channels that are optically transparent and permeable to gases, placed with an inlet-channel-outlet flow

system (**Figure 1E**) (Duffy et al., 1998). These channels provide a suitable model to study dynamics of red blood cells or thrombosis (Shevkoplyas et al., 2003; Tsai et al., 2012). However, PDMS does not resemble native tissue environments as it is rigid, impermeable to water and not able to be remodeled by ECs (Stroock and Fischbach, 2010).

PDMS-hydrogel hybrids consist of a channel of hydrogel scaffold (typically collagen or fibrin) lined on both sides by PDMS channels lined with ECs (**Figure 1F**). These ECs then form sprouts and migrate across the hydrogel scaffolds in response to changes in pressure or growth factor gradients (Song and Munn, 2011), forming a perfused capillary plexus with a functional vascular barrier (Moya et al., 2013). ECs lining the PDMS channel can also be co-cultured with mural, stromal and cancer cells, and may be derived from either normal blood, tumor or lymphatic vessels (Kim et al., 2013, 2016). These hybrid models have provided extensive information about how capillaries sprout, revealing that angiogenesis and lymphangiogenesis occur in response to interstitial flow, as sprouts in this model preferentially extend against the direction of flow; i.e., capillaries sprout from vessels with a low pressure gradient toward those with higher pressure (Song and Munn, 2011; Song et al., 2012; Kim et al., 2016). Precisely how FSS applied to the PDMS channel mediates sprouting remains under debate. It has been shown steady laminar FSS (3 dyn/cm^2 for 1–3 days) inhibits VEGF-induced sprouting (Song and Munn, 2011), whereas increasing the magnitude of FSS (to 10 dyn/cm^2 for 24–48 h) can induce angiogenesis (Galie et al., 2014). This suggests a FSS setpoint may regulate the degree of sprouting.

Growing microvessels in pure hydrogels is perhaps the most physiological of all FSS models, as ECs form lumenised vessels surrounded by ECM. In this model, typically a PDMS mold is produced with two media ports at each end and an ECM port in the center (**Figure 1G**). The hydrogel scaffold is allowed to set within this 3D ECM scaffold around a cylindrical needle, before the needle is removed leaving a circular channel within the ECM (Polacheck et al., 2019). Cells (such as EC alone or EC co-culture with pericytes) can then be seeded via the media ports, where they will subsequently adhere and form a cylindrical monolayer (Polacheck et al., 2019). Once ECs have adhered, flow can be applied by a syringe pump or using a laboratory rocker (to produce steady laminar or oscillatory FSS, respectively). As a needle is used to set the channel, it's width can be set to a defined diameter from 15–300 μm (Nguyen et al., 2013; Linville et al., 2016; Polacheck et al., 2017). This is unlike vessels in PDMS-hydrogel hybrids, where form lumens spontaneously. These systems can be used to assess barrier function of the vasculature. Interestingly, in the absence of flow these vessels are leaky but when constant application of low FSS is applied (5 dyn/cm^2 overnight), cell–cell adhesion is induced to prevent leakage of 70-kDa Dextran (Polacheck et al., 2017). If two cylindrical vessels are embedded within the same hydrogel these models can also be used to assess angiogenesis, with newly formed capillaries sprouting across the ECM in response to growth factor gradients between two larger vessels (Nguyen et al., 2013), a process which is dependent on EC-mediated Myosin IIA forces (Yoon et al., 2019).

While hydrogel-embedded microvessels are excellent models to study the effects of FSS on the vasculature, cells are embedded in a linear vessel. Therefore, they do not accurately model the effects of disturbed flow in bifurcating vessels which are found abundantly *in vivo*. Recently, PDMS-hydrogel hybrids have been developed to study the effects of flow at bifurcation points in vessels (**Figure 1H**) (Akbari et al., 2018). Interestingly both angiogenic sprouting and permeability at bifurcation points is reduced after 48 h (where the bifurcation point has stagnation pressure of approximately 38 dyn/cm^2 and branched vessels are exposed to 3 dyn/cm^2) (Akbari et al., 2018, 2019). This suggests bifurcation points stabilize the blood vasculature, as has been demonstrated *in vivo* (Ghaffari et al., 2015).

Models to Study EC Behavior Regulated via Matrix Stiffness and Stretching

Conventional *in vitro* studies have long been performed using plastic or glass matrices to culture ECs. The stiffness of plastic and glass dishes (which is in the GPa range) by far exceeds the physiological stiffness that ECs experience *in vivo* (Wells, 2008; Guimarães et al., 2020). As discussed above, the physiological ECM stiffness experienced by ECs varies from very soft microenvironments during development to stiffer microenvironments in arterial ECs or in aged and diseased tissues. EC behavior in response to more compliant substrates has been assessed more frequently in 2D culture where ECs are seeded on top of those substrates (**Figure 2A**).

Hydrogels, which are water-swollen networks of polymers, have emerged as the most promising choice for cell culture since they mimic salient elements of the ECM, have mechanics similar to those of softer tissues and can support cell adhesion and protein sequestration (Tibbitt and Anseth, 2009). The properties of hydrogels, such as mechanics, swelling, porosity and degradation, are modifiable and can be adjusted to the specific requirements of the desired experiment. For commercially available hydrogels, these properties have been experimentally characterized and can be easily adapted by the user (Caliari and Burdick, 2016). Diverse stiffness hydrogels can be generated from natural materials, such as collagen, fibrin or alginate, and synthetic materials, such as polyacrylamide (PA) or Polyethylene glycol (PEG) (Caliari and Burdick, 2016). In selected settings, the use of natural materials can be advantageous as they exhibit high biocompatibility, allowing for EC interaction via integrin ligation. However, ECM stiffness provided by those natural materials is very soft. For example, the matrix stiffness of collagen hydrogels is very low (<1 kPa) (Mason et al., 2013). Another frequently used natural hydrogel, Matrigel, which is a heterogenic mixture of various ECM proteins, was found to have a stiffness of approximately 0.45 kPa when measured with AFM in an aqueous, temperature controlled environment (Soofi et al., 2009). Furthermore, Matrigel and other natural hydrogel materials do not allow user-defined variability of ECM components.

In contrast, synthetic materials are more inert and usually have to be combined with chemically modified crosslinkers. This allows for integrin ligation to facilitate interaction of ECs with the substrate (Caliari and Burdick, 2016). Synthetic

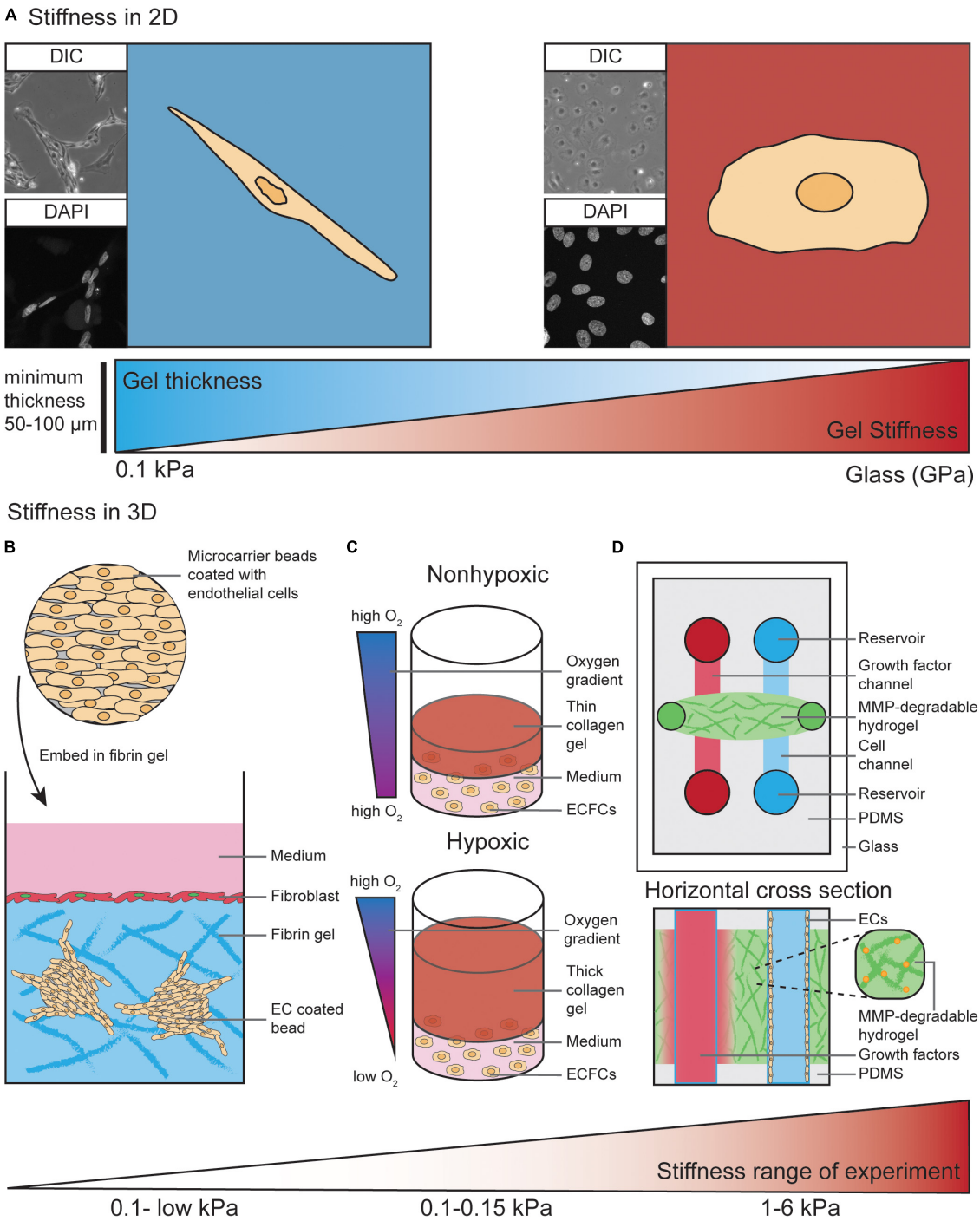

FIGURE 2 | Models to study EC behavior regulated by matrix stiffness. **(A)** ECs cultured on 2D substrates with different stiffness ranging from 0.1 kPa up to GPa (glass) display different morphologies. As an example, on soft substrates human dermal lymphatic endothelial cells (HDLECs, C-12216, PromoCell, Heidelberg, Germany) show a spindle-shaped morphology with a distorted and elongated nucleus and form networks via their cell–cell interactions. On stiff substrates HDLECs flatten out and preferably undergo cell-substrate interactions compared to HDLECs cultured on soft substrates. ECs can "feel" up to several micrometers deep into a compliant substrate, suggesting a minimum hydrogel thickness of 50–100 µm is necessary to analyze ECs on compliant 2D substrates. **(B)** ECs coated on cytodex microcarrier beads are embedded into a fibrin hydrogel to study 3D *in vitro* angiogenic sprouting. Fibroblast are layered on top of the gel to provide necessary factors to promote EC sprouting and lumenisation. The stiffness range of this assay is very low due to the use of natural materials such as fibrin or collagen. **(C)** Encapsulation of endothelial colony-forming cells (ECFCs) in 3D collagen gels with varying thickness provides a temporal hypoxic gradient, where thick gels model hypoxia and thin gels normoxia. Increased matrix stiffness of the 3D collagen gels is performed by crosslinking and results in a stiffness range of 0.1–0.15 kPa. **(D)** Top view and horizontal cross section of PDMS-hydrogel microchannel containing non-swelling MMP-degradable DexMA hydrogel. This allows ECs grown in one channel to migrate toward a growth factor gradient formed by diffusion of growth factors from the other channel. Incorporation of the MMP-degradable peptide crosslinkers into the synthetic hydrogel makes the stiffness variable within a range of 1–6 kPa, compared to non-variable standard hydrogels used in **Figures 1F–H**.

materials, such as PA, can be utilized to generate hydrogels with much wider matrix stiffness ranges, from 0.1 kPa to high kPa values (Tse and Engler, 2010; Denisin and Pruitt, 2016). These characteristics become highly advantageous when matrix stiffness and EC-matrix interactions have to be analyzed separately. For example, PA hydrogels with different matrix stiffness values can be generated with variable collagen I concentrations. This allows for study of the balance between substrate mechanics and matrix chemistry in the process of EC network assembly (Califano and Reinhart-King, 2008).

The impact of ECM stiffness on EC behavior has not been studied extensively in 3D *in vitro* models. Most 3D studies to analyze angiogenic sprouting processes have been performed using natural hydrogel materials, such as collagen type I and fibrin (Juliar et al., 2018). For example, ECs can be coated onto cytodex microcarriers and embedded into a fibrin hydrogel (**Figure 2B**). Here, fibroblasts are layered on top of the gel where they provide necessary soluble factors that promote EC sprouting from the surface of the beads (Nakatsu et al., 2007). These fibroblast derived factors act to minimally stiffen gels (0.03–0.05 kPa) and are required for the lumenisation of sprouting vessels (Newman et al., 2011). In an elegant study by Blatchley et al. (2019), thick 3D collagen gels were demonstrated to provide a temporal hypoxic gradient (**Figure 2C**), allowing for the study of EC behavior in response to changes in both hypoxia and ECM stiffness. These models have simultaneously revealed encapsulation of endothelial colony-forming cells (ECFCs) leads to vasculogenic cluster formation through ROS production in hypoxic (thick) but not normoxic (thin) collagen hydrogels (**Figure 2C**), and that increased matrix stiffness via collagen crosslinking leads to reduced cluster formation (Blatchley et al., 2019).

As described above, natural hydrogels provide a soft microenvironment for ECs in culture, suggesting these 3D *in vitro* models are most suitable to mimic the soft ECM environment that allows ECs to migrate and sprout *in vivo* (Mammoto et al., 2009; Frye et al., 2018). To generate stiffer (>1 kPa) 3D environments to study the impact of higher ECM stiffness on EC behavior, commonly used PA hydrogels are not suitable to encapsulate ECs due to the high toxicity of the hydrogel precursors (Caliari and Burdick, 2016). Therefore, synthetic PEG hydrogels are more widely used to analyze the effects of a stiff ECM in a 3D context (Jonker et al., 2015; Carthew et al., 2018; Whitehead et al., 2018).

In addition to higher matrix stiffness ranges and the ability to independently modulate adhesive ligand presentation, tunable degradation of synthetic hydrogels offers the possibility to alter the microenvironment and stiffness experienced by cells during an experiment. This can be done using ultraviolet light (Kloxin et al., 2009) or by adding engineered, MMP-degradable peptide crosslinkers to the hydrogel solution (Lutolf et al., 2003). Another advantage of using synthetic materials is that the swelling properties of these hydrogels can be modulated. An elegant study by Trappmann et al. (2017) eliminated the swelling properties of a synthetic hydrogel after polymerization, which enabled its integration into microfluidic channels (without channel closure) and subsequent channel colonization with ECs (**Figure 2D**) (Trappmann et al., 2017).

In addition to alterations in stiffness, growing cells on flexible substrates to allow for cyclic stretch has wide implications for EC biology. Most of the studies on stretch are performed using commercial systems, such as the Flexcell Tension Plus system (Flexercell, United States). Here, cells are plated on flexible silicon membranes coated with matrix and grown in standard media before being subjected to stretch. These systems induce cellular elongation in response to stretching and deformation of the elastomere base of the plates, achieved using vacuum pressure which exposes cells to radial, but not uniaxial stretch (Gilbert et al., 1994). High throughput techniques to induce CS in a 96 well place format have been developed using PDMS devices, where cells are exposed to uniaxial stretch. However, these can only reach 10% stretch (Matsui et al., 2018). Advances in models for measuring cyclic stretch are found in lung-on-a-chip models, discussed in further detail in the following section.

INTEGRATIVE AND NOVEL APPROACHES TO MODEL AND VISUALIZE EC FORCES

FRET Biosensors to Visualize Tensile Changes

Förster resonance energy transfer (FRET) reporter constructs have been widely used in the field of cell biology to study protein activity, interactions and conformational changes. FRET biosensors rely on transferring energy from the excited state of the donor fluorescent protein to the unexcited acceptor fluorescent protein, which then emits free photons (Snell et al., 2018). FRET efficiency is sensitive to the distance and orientation of the separation of the two fluorophores which make up the FRET pair, with distance changes as small as 1 nm substantially affecting the amount of energy transfer. Biosensors may consist of an intracellular construct that is sensitive to kinase activity, such as Src and FAK-Lyn (**Figure 3A**) (Wang et al., 2005; Seong et al., 2011) or conformational changes in proteins, such as Src, non-muscle Myosin II and α-catenin (Kim et al., 2015; Markwardt et al., 2018; Koudelkova et al., 2019). Biosensors have also been utilized *in vivo* to measure changes in protein activity, such as Src, AKT, NO, and RhoA (Nobis et al., 2014; Li et al., 2017; Nobis et al., 2017; Conway et al., 2018; Bhuckory et al., 2019).

The vascular biology field has utilized FRET biosensors in EC culture to measure tension across vinculin and talin at FAs (Grashoff et al., 2010; Kumar et al., 2016) and PECAM-1 and VE-cadherin at cell–cell junctions (Conway et al., 2013). These tension sensor constructs consist of a donor fluorophore connected to an acceptor through a nanospring derived from the elastic spider silk protein flagelliform (**Figure 3B**) (Grashoff et al., 2010). Where tension is low or absent, the nanospring is compact and FRET is high, and conversely, application of tension stretches the spring and decreases FRET. These tension sensors are now being utilized *in vivo* in ECs, with a VE-cadherin-tension sensor zebrafish recently described by Lagendijk et al.

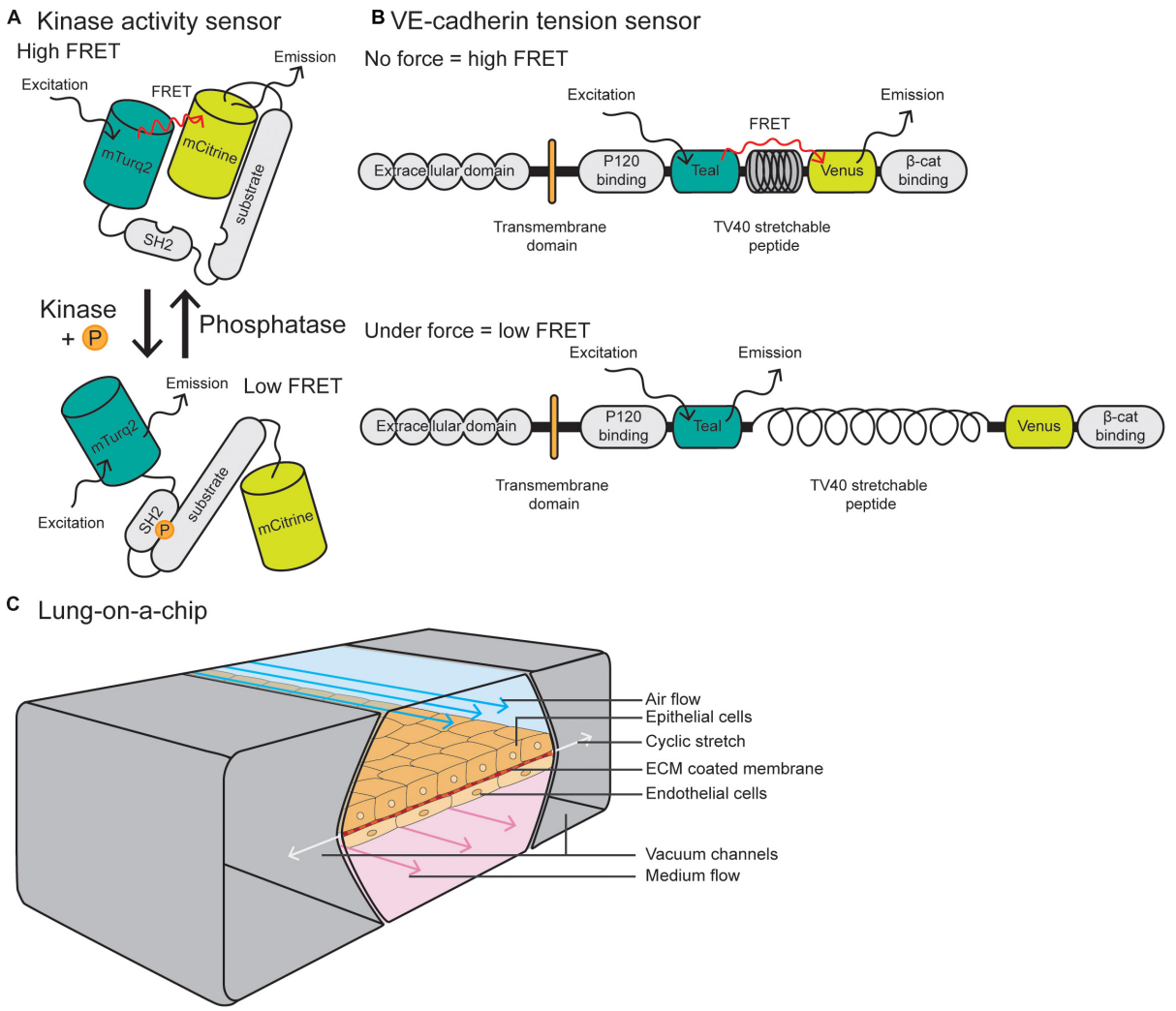

FIGURE 3 | Integrative and novel approaches to study EC forces. **(A)** Schematic of a Src kinase activity FRET biosensor containing mTurqoise2 as donor and mCitrine as acceptor. Upon kinase activation, the substrate becomes phosphorylated and induces intramolecular binding of the SH2 domain, resulting in a conformational change of the molecule and reduction of FRET efficiency. **(B)** The VE-cadherin FRET tension sensor consists of the VE-cadherin protein and the sensor module, containing Teal as donor and Venus as acceptor, connected by the TV40 stretchable peptide. The FRET sensor module was placed in between the p120-catenin and β-catenin binding sites. When there is no force applied on VE-cadherin, there is a high FRET efficiency, while force on the p120-catenin and β-catenin binding sites stretches the TV40 linker and spatially separates the Venus acceptor and Teal donor, resulting in lower FRET efficiency. **(C)** Schematic of a lung-on-a-chip model in which alveolar epithelial cells are plated on the apical side of an ECM-coated porous membrane, and EC are plated on the basal side. The epithelial cells are exposed to air flow and ECs are exposed to fluid flow. Cyclic stretch is applied by a vacuum in the two flanking chambers, resulting in extension and retraction of the epithelial/endothelial cell layer in the center.

(2017). This zebrafish line allows for live, intravital fluorescence lifetime imaging microscopy–fluorescence resonance energy transfer (FLIM- FRET) imaging of tension across junctions. These models and imaging techniques are predicted to be more widely utilized in the vascular biology field to measure changes in tension or subcellular signaling dynamics in tissue culture or *in vivo* models.

Organ-on-a-Chip

Recent scRNA-seq approaches have revealed high levels of EC heterogeneity not only between EC types, but also between organ tissues (He et al., 2018; Vanlandewijck and Betsholtz, 2018; Takeda et al., 2019; Kalucka et al., 2020). To investigate organ-specific vasculature functions, organ-on-a-chip models have been developed to study tumor, gut, liver, pancreas and muscle function. These are also being applied in the field of personalized medicine by incorporating patient samples (van den Berg et al., 2019). These models aim to culture cells in conditions that closely mimic the body, taking into account factors such as tissue geometry and composition, dynamics and flow gradients (Bhatia and Ingber, 2014). Generally, they consist of microfluidic devices integrated with microchip manufacturing methods, which allow for continuously perfused chambers with live cells that have been arranged to simulate tissue- and organ-level physiology.

Due to the fact that the lung vasculature is exposed to multiple mechanical forces, here we will focus on lung-on-a-chip models. Pioneered by the Ingber laboratory, these devices are comprised of alveolar epithelial cells plated on the apical side of an ECM-coated porous membrane, with EC coated on the basal side (Huh et al., 2010; Huh et al., 2013) (**Figure 3C**). Alveolar cells are exposed to air and ECs are exposed to FSS at a range between 1 and 15 dyn/cm^2, similar to forces applied *in vivo*. To model cyclic stretch, suction is applied to two external chambers flanking the cell channel, causing it to extend and retract at a rate and degree to that found in the body (approximately 10% cyclic stretch). This allows for modeling of multiple mechanical forces on the cells, including stretch, ECM components and fluid flow, making them superior to traditional microfluidic devices. Such devices can also can be modified to model other tissues with polarized EC interfaces, such as kidney (EC-podocyte) (Musah et al., 2017), liver (EC-hepatocyte) (Jang et al., 2019), brain (EC-astrocyte) (Herland et al., 2016), and tumor (tumor-epithelium-EC) (Hassell et al., 2017).

Microcirculation-on-a-chip models have been developed to model organizational layers within the vasculature. One such model allows for the co-culture of blood and lymphatic vessels within the same device, separated by a porous polyethylene terephthalate (PET) membrane (Sato et al., 2015). This chip can be utilized to measure vascular permeability and lymphatic absorption. Other devices with an organized composition of ECs and SMCs separated by a porous membrane have been developed to better model the composition of the arterial wall. These allow for a more accurate examination of the interactions and signaling between these cellular components (van Engeland et al., 2018). Finally, models of interconnected, perfused vessels with a high flow arterial input, capillary plexus and low flow venous output have also been developed, to model multiple stages of vascular development including vasculogenesis, angiogenesis to anastomosis (Wang et al., 2016). While advantageous for their complex vascular organization, these chips lack the integration of other organ-specific cells.

In addition to organ-on-a-chip models, the use of organoids for *in vitro* investigation of organ-specific phenotypes is emerging in the fields of biology and drug discovery. A major road block in organoid research is how to incorporate a functional vasculature network. Not only is the field faced with the challenge of EC heterogeneity and matching the vasculature to the type of tissue organoid, organoids *in vitro* remain small and immature due to our inability to grow a perfused, functional vascular network within them. However, when transplanted *in vivo*, organoids can become vascularized due to ECs derived from transplanted iPSCs or the host (Pham et al., 2018; van den Berg et al., 2018). For a detailed review on the challenges in vascularization of organoids, see the review by Daniel and Cleaver (2019).

SUMMARY

The complexity and relevance of mechanical forces to generate and maintain a functional vascular system is well appreciated by vascular biologists. Sophisticated methods have been developed to model and measure forces in 2D cultured monolayers, but are now being adopted into more complex 3D models. The choice of a suitable 2D or 3D model is dependent on the specific endothelial process to be studied. While 3D models may be superior to study FSS within a model of a circular, lumenised vessel, or to model the ECM stiffness microenvironment surrounding sprouting and migrating ECs, stiffness experienced by ECs of a mature vessel network may be more accurately studied in 2D settings. This is due to the fact mature vessels are equipped with a monolayer of ECs which are naturally attached to the underlying ECM in a 2D manner.

Given the transport of fluid exposes ECs to the mechanical forces of FSS and cyclic stretch simultaneously, and the stiffness of the surrounding matrix will affect the degree of cyclic stretch and FSS, techniques to incorporate modeling of all these forces will yield maximal physiological relevance. We believe that further improvements to *in vitro* and *in vivo* force modeling will begin to unravel the precise impact of FSS, stiffness and stretch on the development and function of a heterogeneous vessel network across different tissues.

AUTHOR CONTRIBUTIONS

MF, EG, and LS wrote and edited the manuscript.

FUNDING

MF was supported by the European Union's Horizon 2020 Research and Innovation Programme under the Marie Skłodowska-Curie Grant Agreement No. 840189 and The Werner Otto Stiftung Hamburg (8/95). EG was supported by the Australian Research Council (DE170100167 and DP200100737) and National Health and Medical Research Council (APP1158002). LS was supported by a The University of Queensland ECR grant (UQECR2058733).

ACKNOWLEDGMENTS

We thank Anne Lagendijk for helpful discussions and critical reading of the manuscript. We thank Patricia Essebier for critical reading.

REFERENCES

Akbari, E., Spychalski, G. B., Rangharajan, K. K., Prakash, S., and Song, J. W. (2018). Flow dynamics control endothelial permeability in a microfluidic vessel bifurcation model. *Lab Chip* 18, 1084–1093. doi: 10.1039/c8lc00130h

Akbari, E., Spychalski, G. B., Rangharajan, K. K., Prakash, S., and Song, J. W. (2019). Competing fluid forces control endothelial sprouting in a 3-D microfluidic vessel bifurcation model. *Micromachines (Basel)* 10:451. doi: 10.3390/mi10070451

Akbari, E., Spychalski, G. B., and Song, J. W. (2017). Microfluidic approaches to the study of angiogenesis and the microcirculation. *Microcirculation* 24:e12363. doi: 10.1111/micc.12363

Albarran-Juarez, J., Iring, A., Wang, S., Joseph, S., Grimm, M., Strilic, B., et al. (2018). Piezo1 and Gq/G11 promote endothelial inflammation depending on flow pattern and integrin activation. *J. Exp. Med.* 215, 2655–2672. doi: 10.1084/jem.20180483

Alsteens, D., Gaub, H. E., Newton, R., Pfreundschuh, M., Gerber, C., and Müller, D. J. (2017). Atomic force microscopy-based characterization and design of biointerfaces. *Nat. Rev. Mater.* 2:17008. doi: 10.1038/natrevmats.2017.8

Andresen Eguiluz, R. C., Kaylan, K. B., Underhill, G. H., and Leckband, D. E. (2017). Substrate stiffness and VE-cadherin mechano-transduction coordinate to regulate endothelial monolayer integrity. *Biomaterials* 140, 45–57. doi: 10.1016/j.biomaterials.2017.06.010

Augustin, H. G., and Koh, G. Y. (2017). Organotypic vasculature: from descriptive heterogeneity to functional pathophysiology. *Science* 357:eaal2379. doi: 10.1126/science.aal2379

Baeyens, N., Bandyopadhyay, C., Coon, B. G., Yun, S., and Schwartz, M. A. (2016). Endothelial fluid shear stress sensing in vascular health and disease. *J. Clin. Invest.* 126, 821–828. doi: 10.1172/JCI83083

Baeyens, N., Nicoli, S., Coon, B. G., Ross, T. D., Van den Dries, K., Han, J., et al. (2015). Vascular remodeling is governed by a VEGFR3-dependent fluid shear stress set point. *eLife* 4:e04645. doi: 10.7554/eLife.04645

Bastounis, E. E., Yeh, Y.-T., and Theriot, J. A. (2019). Subendothelial stiffness alters endothelial cell traction force generation while exerting a minimal effect on the transcriptome. *Sci. Rep.* 9:18209. doi: 10.1038/s41598-019-54336-2

Bays, J. L., and DeMali, K. A. (2017). Vinculin in cell-cell and cell-matrix adhesions. *Cell. Mol. Life Sci.* 74, 2999–3009. doi: 10.1007/s00018-017-2511-3

Bhatia, S. N., and Ingber, D. E. (2014). Microfluidic organs-on-chips. *Nat. Biotechnol.* 32, 760–772. doi: 10.1038/nbt.2989

Bhuckory, S., Kays, J. C., and Dennis, A. M. (2019). In vivo biosensing using resonance energy transfer. *Biosensors (Basel)* 9:76. doi: 10.3390/bios9020076

Birukov, K. G., Jacobson, J. R., Flores, A. A., Ye, S. Q., Birukova, A. A., Verin, A. D., et al. (2003). Magnitude-dependent regulation of pulmonary endothelial cell barrier function by cyclic stretch. *Am. J. Physiol. Lung Cell. Mol. Physiol.* 285, L785–L797. doi: 10.1152/ajplung.00336.2002

Birukova, A. A., Moldobaeva, N., Xing, J., and Birukov, K. G. (2008a). Magnitude-dependent effects of cyclic stretch on HGF- and VEGF-induced pulmonary endothelial remodeling and barrier regulation. *Am. J. Physiol. Lung Cell. Mol. Physiol.* 295, L612–L623. doi: 10.1152/ajplung.90236.2008

Birukova, A. A., Rios, A., and Birukov, K. G. (2008b). Long-term cyclic stretch controls pulmonary endothelial permeability at translational and post-translational levels. *Exp. Cell Res.* 314, 3466–3477. doi: 10.1016/j.yexcr.2008.09.003

Blatchley, M. R., Hall, F., Wang, S., Pruitt, H. C., and Gerecht, S. (2019). Hypoxia and matrix viscoelasticity sequentially regulate endothelial progenitor cluster-based vasculogenesis. *Sci. Adv.* 5:eaau7518. doi: 10.1126/sciadv.aau7518

Bordeleau, F., Mason, B. N., Lollis, E. M., Mazzola, M., Zanotelli, M. R., Somasegar, S., et al. (2017). Matrix stiffening promotes a tumor vasculature phenotype. *Proc. Natl. Acad. Sci. U.S.A.* 114, 492–497. doi: 10.1073/pnas.1613855114

Byfield, F. J., Reen, R. K., Shentu, T.-P., Levitan, I., and Gooch, K. J. (2009). Endothelial actin and cell stiffness is modulated by substrate stiffness in 2D and 3D. *J. Biomech.* 42, 1114–1119. doi: 10.1016/j.jbiomech.2009.02.012

Caliari, S. R., and Burdick, J. A. (2016). A practical guide to hydrogels for cell culture. *Nat. Methods* 13, 405–414. doi: 10.1038/nmeth.3839

Califano, J. P., and Reinhart-King, C. A. (2008). A balance of substrate mechanics and matrix chemistry regulates endothelial cell network assembly. *Cell. Mol. Bioeng.* 1:122. doi: 10.1007/s12195-008-0022-x

Califano, J. P., and Reinhart-King, C. A. (2009). The effects of substrate elasticity on endothelial cell network formation and traction force generation. *Conf. Proc. IEEE Eng. Med. Biol. Soc.* 2009, 3343–3345. doi: 10.1109/IEMBS.2009.5333194

Canver, A. C., Ngo, O., Urbano, R. L., and Clyne, A. M. (2016). Endothelial directed collective migration depends on substrate stiffness via localized myosin contractility and cell-matrix interactions. *J. Biomech.* 49, 1369–1380. doi: 10.1016/j.jbiomech.2015.12.037

Caolo, V., Peacock, H. M., Kasaai, B., Swennen, G., Gordon, E., Claesson-Welsh, L., et al. (2018). Shear stress and VE-cadherin: the molecular mechanism of vascular fusion. *Arterioscler Thromb. Vasc. Biol.* 38:ATVBAHA.118.310823. doi: 10.1161/ATVBAHA.118.310823

Carthew, J., Frith, J. E., Forsythe, J. S., and Truong, V. X. (2018). Polyethylene glycol–gelatin hydrogels with tuneable stiffness prepared by horseradish peroxidase-activated tetrazine–norbornene ligation. *J. Mater. Chem. B* 6, 1394–1401. doi: 10.1039/C7TB02764H

Carvalho, J. R., Fortunato, I. C., Fonseca, C. G., Pezzarossa, A., Barbacena, P., Dominguez-Cejudo, M. A., et al. (2019). Non-canonical Wnt signaling regulates junctional mechanocoupling during angiogenic collective cell migration. *eLife* 8:e45853. doi: 10.7554/eLife.45853

Cha, B., Geng, X., Mahamud, M. R., Fu, J., Mukherjee, A., Kim, Y., et al. (2016). Mechanotransduction activates canonical Wnt/beta-catenin signaling to promote lymphatic vascular patterning and the development of lymphatic and lymphovenous valves. *Genes Dev.* 30, 1454–1469. doi: 10.1101/gad.282400.116

Chai, C. K., Akyildiz, A. C., Speelman, L., Gijsen, F. J., Oomens, C. W., van Sambeek, M. R., et al. (2013). Local axial compressive mechanical properties of human carotid atherosclerotic plaques-characterisation by indentation test and inverse finite element analysis. *J. Biomech.* 46, 1759–1766. doi: 10.1016/j.jbiomech.2013.03.017

Chatzizisis, Y. S., Coskun, A. U., Jonas, M., Edelman, E. R., Feldman, C. L., and Stone, P. H. (2007). Role of endothelial shear stress in the natural history of coronary atherosclerosis and vascular remodeling. *Mol. Cell. Vascu. Behav.* 49, 2379–2393. doi: 10.1016/j.jacc.2007.02.059

Chen, W., Tian, B., Liang, J., Yu, S., Zhou, Y., and Li, S. (2019). Matrix stiffness regulates the interactions between endothelial cells and monocytes. *Biomaterials* 221:119362. doi: 10.1016/j.biomaterials.2019.119362

Chistiakov, D. A., Orekhov, A. N., and Bobryshev, Y. V. (2017). Effects of shear stress on endothelial cells: go with the flow. *Acta Physiol. (Oxf)* 219, 382–408. doi: 10.1111/apha.12725

Chiu, J. J., and Chien, S. (2011). Effects of disturbed flow on vascular endothelium: pathophysiological basis and clinical perspectives. *Physiol. Rev.* 91, 327–387. doi: 10.1152/physrev.00047.2009

Cho, H., Kim, J., Ahn, J. H., Hong, Y. K., Makinen, T., Lim, D. S., et al. (2019). YAP and TAZ negatively regulate Prox1 during developmental and pathologic lymphangiogenesis. *Circ. Res.* 124, 225–242. doi: 10.1161/CIRCRESAHA.118.313707

Choi, D., Park, E., Jung, E., Cha, B., Lee, S., Yu, J., et al. (2019). Piezo1 incorporates mechanical force signals into the genetic program that governs lymphatic valve development and maintenance. *JCI Insight* 4:e125068. doi: 10.1172/jci.insight.125068

Choi, D., Park, E., Jung, E., Seong, Y. J., Hong, M., Lee, S., et al. (2017a). ORAI1 activates proliferation of lymphatic endothelial cells in response to laminar flow through kruppel-like factors 2 and 4. *Circ. Res.* 120, 1426–1439. doi: 10.1161/CIRCRESAHA.116.309548

Choi, D., Park, E., Jung, E., Seong, Y. J., Yoo, J., Lee, E., et al. (2017b). Laminar flow downregulates Notch activity to promote lymphatic sprouting. *J. Clin. Invest.* 127, 1225–1240. doi: 10.1172/JCI87442

Chow, B. W., Nuñez, V., Kaplan, L., Granger, A. J., Bistrong, K., Zucker, H. L., et al. (2020). Caveolae in CNS arterioles mediate neurovascular coupling. *Nature* 579, 106–110. doi: 10.1038/s41586-020-2026-1

Collins, C., Guilluy, C., Welch, C., O'Brien, E. T., Hahn, K., Superfine, R., et al. (2012). Localized tensional forces on PECAM-1 elicit a global mechanotransduction response via the integrin-RhoA pathway. *Curr. Biol.* 22, 2087–2094. doi: 10.1016/j.cub.2012.08.051

Conway, D. E., Breckenridge, M. T., Hinde, E., Gratton, E., Chen, C. S., and Schwartz, M. A. (2013). Fluid shear stress on endothelial cells modulates mechanical tension across VE-cadherin and PECAM-1. *Curr. Biol.* 23, 1024–1030. doi: 10.1016/j.cub.2013.04.049

Conway, D. E., Coon, B. G., Budatha, M., Arsenovic, P. T., Orsenigo, F., Wessel, F., et al. (2017). VE-cadherin phosphorylation regulates endothelial fluid shear stress responses through the polarity protein LGN. *Curr. Biol.* 27:2727. doi: 10.1016/j.cub.2017.08.064

Conway, J. R. W., Warren, S. C., Herrmann, D., Murphy, K. J., Cazet, A. S., Vennin, C., et al. (2018). Intravital imaging to monitor therapeutic response in moving hypoxic regions resistant to PI3K pathway targeting in pancreatic cancer. *Cell Rep.* 23, 3312–3326. doi: 10.1016/j.celrep.2018.05.038

Coon, B. G., Baeyens, N., Han, J., Budatha, M., Ross, T. D., Fang, J. S., et al. (2015). Intramembrane binding of VE-cadherin to VEGFR2 and VEGFR3 assembles the endothelial mechanosensory complex. *J. Cell Biol.* 208, 975–986. doi: 10.1083/jcb.201408103

Corada, M., Morini, M. F., and Dejana, E. (2014). Signaling pathways in the specification of arteries and veins. *Arterioscler. Thromb. Vasc. Biol.* 34, 2372–2377. doi: 10.1161/ATVBAHA.114.303218

Cox, C. D., Bae, C., Ziegler, L., Hartley, S., Nikolova-Krstevski, V., Rohde, P. R., et al. (2016). Removal of the mechanoprotective influence of the cytoskeleton reveals PIEZO1 is gated by bilayer tension. *Nat. Commun.* 7:10366. doi: 10.1038/ncomms10366

Daneshjou, N., Sieracki, N., van Nieuw Amerongen, G. P., Conway, D. E., Schwartz, M. A., Komarova, Y. A., et al. (2015). Rac1 functions as a reversible tension modulator to stabilize VE-cadherin trans-interaction. *J. Cell Biol.* 208, 23–32. doi: 10.1083/jcb.201409108

Daniel, E., and Cleaver, O. (2019). Vascularizing organogenesis: lessons from developmental biology and implications for regenerative medicine. *Curr. Top. Dev. Biol.* 132, 177–220. doi: 10.1016/bs.ctdb.2018.12.012

Davidson, C. D., Wang, W. Y., Zaimi, I., Jayco, D. K. P., and Baker, B. M. (2019). Cell force-mediated matrix reorganization underlies multicellular network assembly. *Sci. Rep.* 9:12. doi: 10.1038/s41598-018-37044-1

Denisin, A. K., and Pruitt, B. L. (2016). Tuning the range of polyacrylamide gel stiffness for mechanobiology applications. *ACS Appl. Mater. Interfaces* 8, 21893–21902. doi: 10.1021/acsami.5b09344

DePaola, N., Phelps, J. E., Florez, L., Keese, C. R., Minnear, F. L., Giaever, I., et al. (2001). Electrical impedance of cultured endothelium under fluid flow. *Ann. Biomed. Eng.* 29, 648–656. doi: 10.1114/1.1385811

Di Russo, J., Hannocks, M. J., Luik, A. L., Song, J., Zhang, X., Yousif, L., et al. (2017). Vascular laminins in physiology and pathology. *Matrix Biol.* 5, 140–148. doi: 10.1016/j.matbio.2016.06.008

Dixon, J. B., Greiner, S. T., Gashev, A. A., Cote, G. L., Moore, J. E., and Zawieja, D. C. (2006). Lymph flow, shear stress, and lymphocyte velocity in rat mesenteric prenodal lymphatics. *Microcirculation* 13, 597–610. doi: 10.1080/10739680600893909

Dorfmuller, P., Perros, F., Balabanian, K., and Humbert, M. (2003). Inflammation in pulmonary arterial hypertension. *Eur. Respir. J.* 22, 358–363. doi: 10.1183/09031936.03.00038903

Du, J., Zu, Y., Li, J., Du, S., Xu, Y., Zhang, L., et al. (2016). Extracellular matrix stiffness dictates Wnt expression through integrin pathway. *Sci. Rep.* 6:20395. doi: 10.1038/srep20395

Duffy, D. C., McDonald, J. C., Schueller, O. J., and Whitesides, G. M. (1998). Rapid prototyping of microfluidic systems in poly(dimethylsiloxane). *Anal. Chem.* 70, 4974–4984. doi: 10.1021/ac980656z

Engler, A. J., Griffin, M. A., Sen, S., Bonnemann, C. G., Sweeney, H. L., and Discher, D. E. (2004). Myotubes differentiate optimally on substrates with tissue-like stiffness: pathological implications for soft or stiff microenvironments. *J. Cell Biol.* 166, 877–887. doi: 10.1083/jcb.200405004

Franco, C. A., Jones, M. L., Bernabeu, M. O., Geudens, I., Mathivet, T., Rosa, A., et al. (2015). Dynamic endothelial cell rearrangements drive developmental vessel regression. *PLoS Biol.* 13:e1002125. doi: 10.1371/journal.pbio.1002125

Franco, C. A., Jones, M. L., Bernabeu, M. O., Vion, A. C., Barbacena, P., Fan, J., et al. (2016). Non-canonical Wnt signalling modulates the endothelial shear stress flow sensor in vascular remodelling. *eLife* 5:e07727. doi: 10.7554/eLife.07727

Friedrich, E. E., Hong, Z., Xiong, S., Zhong, M., Di, A., Rehman, J., et al. (2019). Endothelial cell Piezo1 mediates pressure-induced lung vascular hyperpermeability via disruption of adherens junctions. *Proc. Natl. Acad. Sci. U.S.A.* 116, 12980–12985. doi: 10.1073/pnas.1902165116

Frye, M., Taddei, A., Dierkes, C., Martinez-Corral, I., Fielden, M., Ortsater, H., et al. (2018). Matrix stiffness controls lymphatic vessel formation through regulation of a GATA2-dependent transcriptional program. *Nat. Commun.* 9:1511. doi: 10.1038/s41467-018-03959-6

Galie, P. A., Nguyen, D. H., Choi, C. K., Cohen, D. M., Janmey, P. A., and Chen, C. S. (2014). Fluid shear stress threshold regulates angiogenic sprouting. *Proc. Natl. Acad. Sci. U.S.A.* 111, 7968–7973. doi: 10.1073/pnas.1310842111

Gangoda, S. V. S., Avadhanam, B., Jufri, N. F., Sohn, E. H., Butlin, M., Gupta, V., et al. (2018). Pulsatile stretch as a novel modulator of amyloid precursor protein processing and associated inflammatory markers in human cerebral endothelial cells. *Sci. Rep.* 8:1689. doi: 10.1038/s41598-018-20117-6

Gawlak, G., Son, S., Tian, Y., O'Donnell, J. J. III, Birukov, K. G., and Birukova, A. A. (2016). Chronic high-magnitude cyclic stretch stimulates EC inflammatory response via VEGF receptor 2-dependent mechanism. *Am. J. Physiol. Lung Cell. Mol. Physiol.* 310, L1062–L1070. doi: 10.1152/ajplung.00317.2015

Georges, P. C., Miller, W. J., Meaney, D. F., Sawyer, E. S., and Janmey, P. A. (2006). Matrices with compliance comparable to that of brain tissue select neuronal over glial growth in mixed cortical cultures. *Biophys. J.* 90, 3012–3018. doi: 10.1529/biophysj.105.073114

Ghaffari, S., Leask, R. L., and Jones, E. A. (2015). Flow dynamics control the location of sprouting and direct elongation during developmental angiogenesis. *Development* 142, 4151–4157. doi: 10.1242/dev.128058

Gilbert, J. A., Weinhold, P. S., Banes, A. J., Link, G. W., and Jones, G. L. (1994). Strain profiles for circular cell culture plates containing flexible surfaces employed to mechanically deform cells in vitro. *J. Biomech.* 27, 1169–1177. doi: 10.1016/0021-9290(94)90057-4

Givens, C., and Tzima, E. (2016). Endothelial mechanosignaling: does one sensor fit all? *Antioxid. Redox Signal.* 25, 373–388. doi: 10.1089/ars.2015.6493

Goedicke-Fritz, S., Kaistha, A., Kacik, M., Markert, S., Hofmeister, A., Busch, C., et al. (2015). Evidence for functional and dynamic microcompartmentation of Cav-1/TRPV4/K(Ca) in caveolae of endothelial cells. *Eur. J. Cell Biol.* 94, 391–400. doi: 10.1016/j.ejcb.2015.06.002

Goetz, J. G., Steed, E., Ferreira, R. R., Roth, S., Ramspacher, C., Boselli, F., et al. (2014). Endothelial cilia mediate low flow sensing during zebrafish vascular development. *Cell Rep.* 6, 799–808. doi: 10.1016/j.celrep.2014.01.032

Goult, B. T., Yan, J., and Schwartz, M. A. (2018). Talin as a mechanosensitive signaling hub. *J. Cell Biol.* 217, 3776–3784. doi: 10.1083/jcb.201808061

Grashoff, C., Hoffman, B. D., Brenner, M. D., Zhou, R., Parsons, M., Yang, M. T., et al. (2010). Measuring mechanical tension across vinculin reveals regulation of focal adhesion dynamics. *Nature* 466, 263–266. doi: 10.1038/nature09198

Guimarães, C. F., Gasperini, L., Marques, A. P., and Reis, R. L. (2020). The stiffness of living tissues and its implications for tissue engineering. *Nat. Rev. Mater.* 5, 351–370. doi: 10.1038/s41578-019-0169-1

Hahn, C., and Schwartz, M. A. (2009). Mechanotransduction in vascular physiology and atherogenesis. *Nat. Rev. Mol. Cell Biol.* 10, 53–62. doi: 10.1038/nrm2596

Haining, A. W. M., von Essen, M., Attwood, S. J., Hytönen, V. P., and del Río Hernández, A. (2016). All subdomains of the talin rod are mechanically vulnerable and may contribute To cellular mechanosensing. *ACS Nano* 10, 6648–6658. doi: 10.1021/acsnano.6b01658

Hamidi, H., and Ivaska, J. (2018). Every step of the way: integrins in cancer progression and metastasis. *Nat. Rev. Cancer* 18, 533–548. doi: 10.1038/s41568-018-0038-z

Harris, T. A., Yamakuchi, M., Ferlito, M., Mendell, J. T., and Lowenstein, C. J. (2008). MicroRNA-126 regulates endothelial expression of vascular cell adhesion molecule 1. *Proc. Natl. Acad. Sci. U.S.A.* 105, 1516–1521. doi: 10.1073/pnas.0707493105

Hassell, B. A., Goyal, G., Lee, E., Sontheimer-Phelps, A., Levy, O., Chen, C. S., et al. (2017). Human organ chip models recapitulate orthotopic lung cancer growth, therapeutic responses, and tumor dormancy in vitro. *Cell Rep.* 21, 508–516. doi: 10.1016/j.celrep.2017.09.043

He, L., Vanlandewijck, M., Mae, M. A., Andrae, J., Ando, K., Del Gaudio, F., et al. (2018). Single-cell RNA sequencing of mouse brain and lung vascular and vessel-associated cell types. *Sci. Data* 5:180160. doi: 10.1038/sdata.2018.160

Helm, C. L., Fleury, M. E., Zisch, A. H., Boschetti, F., and Swartz, M. A. (2005). Synergy between interstitial flow and VEGF directs capillary morphogenesis in vitro through a gradient amplification mechanism. *Proc. Natl. Acad. Sci. U.S.A.* 102, 15779–15784. doi: 10.1073/pnas.0503681102

Herland, A., van der Meer, A. D., FitzGerald, E. A., Park, T. E., Sleeboom, J. J., and Ingber, D. E. (2016). Distinct contributions of astrocytes and pericytes to neuroinflammation Identified in a 3D human blood-brain barrier on a chip. *PLoS One* 11:e0150360. doi: 10.1371/journal.pone.0150360

Hope, S. A., and Hughes, A. D. (2007). Drug effects on the mechanical properties of large arteries in humans. *Clin. Exp. Pharmacol. Physiol.* 34, 688–693. doi: 10.1111/j.1440-1681.2007.04661.x

Huber, D., Oskooei, A., Casadevall, I. S. X., deMello, A., and Kaigala, G. V. (2018). Hydrodynamics in cell studies. *Chem. Rev.* 118, 2042–2079. doi: 10.1021/acs.chemrev.7b00317

Huh, D., Kim, H. J., Fraser, J. P., Shea, D. E., Khan, M., Bahinski, A., et al. (2013). Microfabrication of human organs-on-chips. *Nat. Protoc.* 8, 2135–2157. doi: 10.1038/nprot.2013.137

Huh, D., Matthews, B. D., Mammoto, A., Montoya-Zavala, M., Hsin, H. Y., and Ingber, D. E. (2010). Reconstituting organ-level lung functions on a chip. *Science* 328, 1662–1668. doi: 10.1126/science.1188302

Huveneers, S., Oldenburg, J., Spanjaard, E., van der Krogt, G., Grigoriev, I., Akhmanova, A., et al. (2012). Vinculin associates with endothelial VE-cadherin junctions to control force-dependent remodeling. *J. Cell Biol.* 196, 641–652. doi: 10.1083/jcb.201108120

Huynh, J., Nishimura, N., Rana, K., Peloquin, J. M., Califano, J. P., Montague, C. R., et al. (2011). Age-related intimal stiffening enhances endothelial permeability and leukocyte transmigration. *Sci. Transl. Med.* 3:112ra122. doi: 10.1126/scitranslmed.3002761

Jang, K. J., Otieno, M. A., Ronxhi, J., Lim, H. K., Ewart, L., Kodella, K. R., et al. (2019). Reproducing human and cross-species drug toxicities using a Liver-Chip. *Sci. Transl. Med.* 11:eaax5516. doi: 10.1126/scitranslmed.aax5516

Jannatbabaei, A., Tafazzoli-Shadpour, M., Seyedjafari, E., and Fatouraee, N. (2019). Cytoskeletal remodeling induced by substrate rigidity regulates rheological behaviors in endothelial cells. *J. Biomed. Mater. Res. Part A* 107, 71–80. doi: 10.1002/jbm.a.36533

Jonker, A. M., Bode, S. A., Kusters, A. H., van Hest, J. C. M., and Löwik, D. W. P. M. (2015). Soft PEG-Hydrogels with independently tunable stiffness and RGDS-content for cell adhesion studies. *Macromol. Biosci.* 15, 1338–1347. doi: 10.1002/mabi.201500110

Jufri, N. F., Mohamedali, A., Avolio, A., and Baker, M. S. (2015). Mechanical stretch: physiological and pathological implications for human vascular endothelial cells. *Vasc. Cell* 7:8. doi: 10.1186/s13221-015-0033-z

Juliar, B. A., Keating, M. T., Kong, Y. P., Botvinick, E. L., and Putnam, A. J. (2018). Sprouting angiogenesis induces significant mechanical heterogeneities and ECM stiffening across length scales in fibrin hydrogels. *Biomaterials* 162, 99–108. doi: 10.1016/j.biomaterials.2018.02.012

Kaipainen, A., Korhonen, J., Mustonen, T., van Hinsbergh, V. W., Fang, G. H., Dumont, D., et al. (1995). Expression of the fms-like tyrosine kinase 4 gene becomes restricted to lymphatic endothelium during development. *Proc. Natl. Acad. Sci. U.S.A.* 92, 3566–3570. doi: 10.1073/pnas.92.8.3566

Kalucka, J., de Rooij, L., Goveia, J., Rohlenova, K., Dumas, S. J., Meta, E., et al. (2020). Single-cell transcriptome atlas of murine endothelial cells. *Cell* 180, 764–779.e20. doi: 10.1016/j.cell.2020.01.015

Katsumi, A., Orr, A. W., Tzima, E., and Schwartz, M. A. (2004). Integrins in mechanotransduction. *J. Biol. Chem.* 279, 12001–12004. doi: 10.1074/jbc.R300038200

Kazenwadel, J., Betterman, K. L., Chong, C. E., Stokes, P. H., Lee, Y. K., Secker, G. A., et al. (2015). GATA2 is required for lymphatic vessel valve development and maintenance. *J. Clin. Invest.* 125, 2979–2994. doi: 10.1172/JCI78888

Ke, Y., Karki, P., Zhang, C., Li, Y., Nguyen, T., and Birukov, K. G. (2019). Mechanosensitive Rap1 activation promotes barrier function of lung vascular endothelium under cyclic stretch. *Mol. Biol. Cell* 30, 959–974. doi: 10.1091/mbc.E18-07-0422

Kim, J., Kim, Y. H., Kim, J., Park, D. Y., Bae, H., Lee, D. H., et al. (2017). YAP/TAZ regulates sprouting angiogenesis and vascular barrier maturation. *J. Clin. Invest.* 127, 3441–3461. doi: 10.1172/JCI93825

Kim, S., Chung, M., and Jeon, N. L. (2016). Three-dimensional biomimetic model to reconstitute sprouting lymphangiogenesis in vitro. *Biomaterials* 78, 115–128. doi: 10.1016/j.biomaterials.2015.11.019

Kim, S., Lee, H., Chung, M., and Jeon, N. L. (2013). Engineering of functional, perfusable 3D microvascular networks on a chip. *Lab Chip* 13, 1489–1500. doi: 10.1039/c3lc41320a

Kim, T. J., Zheng, S., Sun, J., Muhamed, I., Wu, J., Lei, L., et al. (2015). Dynamic visualization of alpha-catenin reveals rapid, reversible conformation switching between tension states. *Curr. Biol.* 25, 218–224. doi: 10.1016/j.cub.2014.11.017

Kloxin, A. M., Kasko, A. M., Salinas, C. N., and Anseth, K. S. (2009). Photodegradable hydrogels for dynamic tuning of physical and chemical properties. *Science* 324, 59–63. doi: 10.1126/science.1169494

Kohn, J. C., Lampi, M. C., and Reinhart-King, C. A. (2015). Age-related vascular stiffening: causes and consequences. *Front. Genet.* 6:112. doi: 10.3389/fgene.2015.00112

Korn, C., Scholz, B., Hu, J., Srivastava, K., Wojtarowicz, J., Arnsperger, T., et al. (2014). Endothelial cell-derived non-canonical Wnt ligands control vascular pruning in angiogenesis. *Development* 141, 1757–1766. doi: 10.1242/dev.104422

Koudelkova, L., Pataki, A. C., Tolde, O., Pavlik, V., Nobis, M., Gemperle, J., et al. (2019). Novel FRET-based Src biosensor reveals mechanisms of Src activation and its dynamics in focal adhesions. *Cell Chem. Biol.* 26, 255–268.e4. doi: 10.1016/j.chembiol.2018.10.024

Kumar, A., Anderson, K. L., Swift, M. F., Hanein, D., Volkmann, N., and Schwartz, M. A. (2018). Local tension on talin in focal adhesions correlates with F-actin alignment at the nanometer scale. *Biophys. J.* 115, 1569–1579. doi: 10.1016/j.bpj.2018.08.045

Kumar, A., Ouyang, M., Van den Dries, K., McGhee, E. J., Tanaka, K., Anderson, M. D., et al. (2016). Talin tension sensor reveals novel features of focal adhesion force transmission and mechanosensitivity. *J. Cell Biol.* 213, 371–383. doi: 10.1083/jcb.201510012

Lachowski, D., Cortes, E., Robinson, B., Rice, A., Rombouts, K., and Del Rio Hernandez, A. E. (2018). FAK controls the mechanical activation of YAP, a transcriptional regulator required for durotaxis. *FASEB J.* 32, 1099–1107. doi: 10.1096/fj.201700721R

Lagendijk, A. K., Gomez, G. A., Baek, S., Hesselson, D., Hughes, W. E., Paterson, S., et al. (2017). Live imaging molecular changes in junctional tension upon VE-cadherin in zebrafish. *Nat. Commun.* 8:1402. doi: 10.1038/s41467-017-01325-6

Lampugnani, M. G., Corada, M., Caveda, L., Breviario, F., Ayalon, O., Geiger, B., et al. (1995). The molecular organization of endothelial cell to cell junctions: differential association of plakoglobin, beta-catenin, and alpha-catenin with vascular endothelial cadherin (VE-cadherin). *J. Cell Biol.* 129, 203–217. doi: 10.1083/jcb.129.1.203

LaValley, D. J., Zanotelli, M. R., Bordeleau, F., Wang, W., Schwager, S. C., and Reinhart-King, C. A. (2017). Matrix stiffness enhances VEGFR-2 internalization, signaling, and proliferation in endothelial cells. *Converg. Sci. Phys. Oncol.* 3:044001. doi: 10.1088/2057-1739/aa9263

Lee, H. Y., and Oh, B. H. (2010). Aging and arterial stiffness. *Circ. J.* 74, 2257–2262. doi: 10.1253/circj.cj-10-0910

Levental, K. R., Yu, H., Kass, L., Lakins, J. N., Egeblad, M., Erler, J. T., et al. (2009). Matrix crosslinking forces tumor progression by enhancing integrin signaling. *Cell* 139, 891–906. doi: 10.1016/j.cell.2009.10.027

Levick, J. R., and Michel, C. C. (2010). Microvascular fluid exchange and the revised Starling principle. *Cardiovasc. Res.* 87, 198–210. doi: 10.1093/cvr/cvq062

Lewis, A. H., and Grandl, J. (2015). Mechanical sensitivity of Piezo1 ion channels can be tuned by cellular membrane tension. *eLife* 4:e12088. doi: 10.7554/eLife.12088

Ley, K., Laudanna, C., Cybulsky, M. I., and Nourshargh, S. (2007). Getting to the site of inflammation: the leukocyte adhesion cascade updated. *Nat. Rev. Immunol.* 7, 678–689. doi: 10.1038/nri2156

Li, H., Zhang, D., Gao, M., Huang, L., Tang, L., Li, Z., et al. (2017). Highly specific C-C bond cleavage induced FRET fluorescence for in vivo biological nitric oxide imaging. *Chem. Sci.* 8, 2199–2203. doi: 10.1039/c6sc04071c

Liliensiek, S. J., Nealey, P., and Murphy, C. J. (2009). Characterization of endothelial basement membrane nanotopography in rhesus macaque as a guide for vessel tissue engineering. *Tissue Eng. Part A* 15, 2643–2651. doi: 10.1089/ten.TEA.2008.0284

Linville, R. M., Boland, N. F., Covarrubias, G., Price, G. M., and Tien, J. (2016). Physical and chemical signals that promote vascularization of capillary-scale channels. *Cell Mol. Bioeng.* 9, 73–84. doi: 10.1007/s12195-016-0429-8

Little, W. C., Zile, M. R., Kitzman, D. W., Hundley, W. G., O'Brien, T. X., and Degroof, R. C. (2005). The effect of alagebrium chloride (ALT-711), a novel glucose cross-link breaker, in the treatment of elderly patients with diastolic heart failure. *J. Card. Fail.* 11, 191–195. doi: 10.1016/j.cardfail.2004.09.010

Liu, W. F., Nelson, C. M., Tan, J. L., and Chen, C. S. (2007). Cadherins, RhoA, and Rac1 are differentially required for stretch-mediated proliferation in endothelial versus smooth muscle cells. *Circ. Res.* 101, e44–e52. doi: 10.1161/CIRCRESAHA.107.158329

Lutolf, M. P., Lauer-Fields, J. L., Schmoekel, H. G., Metters, A. T., Weber, F. E., Fields, G. B., et al. (2003). Synthetic matrix metalloproteinase-sensitive hydrogels for the conduction of tissue regeneration: engineering cell-invasion

characteristics. *Proc. Natl. Acad. Sci. U.S.A.* 100, 5413–5418. doi: 10.1073/pnas.0737381100

Majkut, S., Idema, T., Swift, J., Krieger, C., Liu, A., and Discher, D. E. (2013). Heart-specific stiffening in early embryos parallels matrix and myosin expression to optimize beating. *Curr. Biol.* 23, 2434–2439. doi: 10.1016/j.cub.2013.10.057

Maksuti, E., Widman, E., Larsson, D., Urban, M. W., Larsson, M., and Bjallmark, A. (2016). Arterial stiffness estimation by shear wave elastography: validation in phantoms with mechanical testing. *Ultrasound Med. Biol.* 42, 308–321. doi: 10.1016/j.ultrasmedbio.2015.08.012

Mammoto, A., Connor, K. M., Mammoto, T., Yung, C. W., Huh, D., Aderman, C. M., et al. (2009). A mechanosensitive transcriptional mechanism that controls angiogenesis. *Nature* 457, 1103–1108. doi: 10.1038/nature07765

Maniotis, A. J., Chen, C. S., and Ingber, D. E. (1997). Demonstration of mechanical connections between integrins, cytoskeletal filaments, and nucleoplasm that stabilize nuclear structure. *Proc. Natl. Acad. Sci. U.S.A.* 94, 849–854. doi: 10.1073/pnas.94.3.849

Markwardt, M. L., Snell, N. E., Guo, M., Wu, Y., Christensen, R., Liu, H., et al. (2018). A Genetically encoded biosensor strategy for quantifying non-muscle Myosin II phosphorylation dynamics in living cells and organisms. *Cell Rep.* 24, 1060–1070.e4. doi: 10.1016/j.celrep.2018.06.088

Marti, C. N., Gheorghiade, M., Kalogeropoulos, A. P., Georgiopoulou, V. V., Quyyumi, A. A., and Butler, J. (2012). Endothelial dysfunction, arterial stiffness, and heart failure. *J. Am. Coll. Cardiol.* 60, 1455–1469. doi: 10.1016/j.jacc.2011.11.082

Martino, F., Perestrelo, A. R., Vinarsky, V., Pagliari, S., and Forte, G. (2018). Cellular mechanotransduction: from tension to function. *Front. Physiol.* 9:824. doi: 10.3389/fphys.2018.00824

Mason, B. N., Starchenko, A., Williams, R. M., Bonassar, L. J., and Reinhart-King, C. A. (2013). Tuning three-dimensional collagen matrix stiffness independently of collagen concentration modulates endothelial cell behavior. *Acta Biomater.* 9, 4635–4644. doi: 10.1016/j.actbio.2012.08.007

Matsui, T. S., Wu, H., and Deguchi, S. (2018). Deformable 96-well cell culture plate compatible with high-throughput screening platforms. *PLoS One* 13:e0203448. doi: 10.1371/journal.pone.0203448

Mehta, V., Pang, K. L., Rozbesky, D., Nather, K., Keen, A., Lachowski, D., et al. (2020). The guidance receptor plexin D1 is a mechanosensor in endothelial cells. *Nature* 578, 1–6. doi: 10.1038/s41586-020-1979-4

Michael, K. E., Dumbauld, D. W., Burns, K. L., Hanks, S. K., and Garcia, A. J. (2009). Focal adhesion kinase modulates cell adhesion strengthening via integrin activation. *Mol. Biol. Cell* 20, 2508–2519. doi: 10.1091/mbc.E08-01-0076

Miteva, D. O., Rutkowski, J. M., Dixon, J. B., Kilarski, W., Shields, J. D., and Swartz, M. A. (2010). Transmural flow modulates cell and fluid transport functions of lymphatic endothelium. *Circ. Res.* 106, 920–931. doi: 10.1161/CIRCRESAHA.109.207274

Monkley, S. J., Zhou, X. H., Kinston, S. J., Giblett, S. M., Hemmings, L., Priddle, H., et al. (2000). Disruption of the talin gene arrests mouse development at the gastrulation stage. *Dev. Dyn.* 219, 560–574. doi: 10.1002/1097-0177(2000)9999:9999<::AID-DVDY1079>3.0.CO;2-Y

Moya, M. L., Hsu, Y. H., Lee, A. P., Hughes, C. C., and George, S. C. (2013). In vitro perfused human capillary networks. *Tissue Eng. Part C Methods* 19, 730–737. doi: 10.1089/ten.TEC.2012.0430

Musah, S., Mammoto, A., Ferrante, T. C., Jeanty, S. S. F., Hirano-Kobayashi, M., Mammoto, T., et al. (2017). Mature induced-pluripotent-stem-cell-derived human podocytes reconstitute kidney glomerular-capillary-wall function on a chip. *Nat. Biomed. Eng.* 1:0069. doi: 10.1038/s41551-017-0069

Nakatsu, M. N., Davis, J., and Hughes, C. C. W. (2007). Optimized fibrin gel bead assay for the study of angiogenesis. *J. Vis. Exp.* 3:e186. doi: 10.3791/186

Nation, D. A., Edland, S. D., Bondi, M. W., Salmon, D. P., Delano-Wood, L., Peskind, E. R., et al. (2013). Pulse pressure is associated with Alzheimer biomarkers in cognitively normal older adults. *Neurology* 81, 2024–2027. doi: 10.1212/01.wnl.0000436935.47657.78

Neto, F., Klaus-Bergmann, A., Ong, Y. T., Alt, S., Vion, A. C., Szymborska, A., et al. (2018). YAP and TAZ regulate adherens junction dynamics and endothelial cell distribution during vascular development. *eLife* 7:e31037. doi: 10.7554/eLife.31037

Newman, A. C., Nakatsu, M. N., Chou, W., Gershon, P. D., and Hughes, C. C. (2011). The requirement for fibroblasts in angiogenesis: fibroblast-derived matrix proteins are essential for endothelial cell lumen formation. *Mol. Biol. Cell* 22, 3791–3800. doi: 10.1091/mbc.E11-05-0393

Ng, C. P., Helm, C. L., and Swartz, M. A. (2004). Interstitial flow differentially stimulates blood and lymphatic endothelial cell morphogenesis in vitro. *Microvasc. Res.* 68, 258–264. doi: 10.1016/j.mvr.2004.08.002

Nguyen, D. H., Stapleton, S. C., Yang, M. T., Cha, S. S., Choi, C. K., Galie, P. A., et al. (2013). Biomimetic model to reconstitute angiogenic sprouting morphogenesis in vitro. *Proc. Natl. Acad. Sci. U.S.A.* 110, 6712–6717. doi: 10.1073/pnas.1221526110

Nobis, M., Herrmann, D., Warren, S. C., Kadir, S., Leung, W., Killen, M., et al. (2017). A RhoA-FRET biosensor mouse for intravital imaging in normal tissue homeostasis and disease contexts. *Cell Rep.* 21, 274–288. doi: 10.1016/j.celrep.2017.09.022

Nobis, M., McGhee, E. J., Herrmann, D., Magenau, A., Morton, J. P., Anderson, K. I., et al. (2014). Monitoring the dynamics of Src activity in response to anti-invasive dasatinib treatment at a subcellular level using dual intravital imaging. *Cell Adh. Migr.* 8, 478–486. doi: 10.4161/19336918.2014.970004

Nonomura, K., Lukacs, V., Sweet, D. T., Goddard, L. M., Kanie, A., Whitwam, T., et al. (2018). Mechanically activated ion channel PIEZO1 is required for lymphatic valve formation. *Proc. Natl. Acad. Sci. U.S.A.* 115, 12817–12822. doi: 10.1073/pnas.1817070115

Nowak-Sliwinska, P., Alitalo, K., Allen, E., Anisimov, A., Aplin, A. C., Auerbach, R., et al. (2018). Consensus guidelines for the use and interpretation of angiogenesis assays. *Angiogenesis* 21. doi: 10.1007/s10456-018-9613-x 425-532.

Oldenburg, J., and de Rooij, J. (2014). Mechanical control of the endothelial barrier. *Cell Tissue Res.* 355, 545–555. doi: 10.1007/s00441-013-1792-6

Parton, R. G., and del Pozo, M. A. (2013). Caveolae as plasma membrane sensors, protectors and organizers. *Nat. Rev. Mol. Cell. Biol.* 14, 98–112. doi: 10.1038/nrm3512

Paszkowiak, J. J., and Dardik, A. (2003). Arterial wall shear stress: observations from the bench to the bedside. *Vasc Endovas. Surg.* 37, 47–57. doi: 10.1177/153857440303700107

Pedrigi, R. M., Papadimitriou, K. I., Kondiboyina, A., Sidhu, S., Chau, J., Patel, M. B., et al. (2017). Disturbed cyclical stretch of endothelial cells promotes nuclear expression of the Pro-atherogenic transcription factor NF-kappaB. *Ann. Biomed. Eng.* 45, 898–909. doi: 10.1007/s10439-016-1750-z

Petrova, T. V., Karpanen, T., Norrmen, C., Mellor, R., Tamakoshi, T., Finegold, D., et al. (2004). Defective valves and abnormal mural cell recruitment underlie lymphatic vascular failure in lymphedema distichiasis. *Nat. Med.* 10, 974–981. doi: 10.1038/nm1094

Petrova, T. V., and Koh, G. Y. (2018). Organ-specific lymphatic vasculature: from development to pathophysiology. *J. Exp. Med.* 215, 35–49. doi: 10.1084/jem.20171868

Pham, M. T., Pollock, K. M., Rose, M. D., Cary, W. A., Stewart, H. R., Zhou, P., et al. (2018). Generation of human vascularized brain organoids. *Neuroreport* 29, 588–593. doi: 10.1097/WNR.0000000000001014

Planas-Paz, L., Strilic, B., Goedecke, A., Breier, G., Fassler, R., and Lammert, E. (2012). Mechanoinduction of lymph vessel expansion. *EMBO J.* 31, 788–804. doi: 10.1038/emboj.2011.456

Plotnikov, S. V., Pasapera, A. M., Sabass, B., and Waterman, C. M. (2012). Force fluctuations within focal adhesions mediate ECM-rigidity sensing to guide directed cell migration. *Cell* 151, 1513–1527. doi: 10.1016/j.cell.2012.11.034

Polacheck, W. J., Kutys, M. L., Tefft, J. B., and Chen, C. S. (2019). Microfabricated blood vessels for modeling the vascular transport barrier. *Nat. Protoc.* 14, 1425–1454. doi: 10.1038/s41596-019-0144-8

Polacheck, W. J., Kutys, M. L., Yang, J., Eyckmans, J., Wu, Y., Vasavada, H., et al. (2017). A non-canonical Notch complex regulates adherens junctions and vascular barrier function. *Nature* 552, 258–262. doi: 10.1038/nature24998

Potente, M., and Makinen, T. (2017). Vascular heterogeneity and specialization in development and disease. *Nat. Rev. Mol. Cell. Biol.* 18, 477–494. doi: 10.1038/nrm.2017.36

Provenzano, P. P., Inman, D. R., Eliceiri, K. W., and Keely, P. J. (2009). Matrix density-induced mechanoregulation of breast cell phenotype, signaling and gene expression through a FAK–ERK linkage. *Oncogene* 28, 4326–4343. doi: 10.1038/onc.2009.299

Pulous, F. E., Grimsley-Myers, C. M., Kansal, S., Kowalczyk, A. P., and Petrich, B. G. (2019). Talin-dependent integrin activation regulates VE-Cadherin

localization and endothelial cell barrier function. *Circ. Res.* 124, 891–903. doi: 10.1161/CIRCRESAHA.118.314560

Rahikainen, R., von Essen, M., Schaefer, M., Qi, L., Azizi, L., Kelly, C., et al. (2017). Mechanical stability of talin rod controls cell migration and substrate sensing. *Sci. Rep.* 7:3571. doi: 10.1038/s41598-017-03335-2

Ranade, S. S., Qiu, Z., Woo, S. H., Hur, S. S., Murthy, S. E., Cahalan, S. M., et al. (2014). Piezo1, a mechanically activated ion channel, is required for vascular development in mice. *Proc. Natl. Acad. Sci. U.S.A.* 111, 10347–10352. doi: 10.1073/pnas.1409233111

Reid, S. E., Kay, E. J., Neilson, L. J., Henze, A. T., Serneels, J., McGhee, E. J., et al. (2017). Tumor matrix stiffness promotes metastatic cancer cell interaction with the endothelium. *EMBO J.* 36, 2373–2389. doi: 10.15252/embj.201694912

Rho, J. Y., Ashman, R. B., and Turner, C. H. (1993). Young's modulus of trabecular and cortical bone material: ultrasonic and microtensile measurements. *J. Biomech.* 26, 111–119. doi: 10.1016/0021-9290(93)90042-d

Ross, T. D., Coon, B. G., Yun, S., Baeyens, N., Tanaka, K., Ouyang, M., et al. (2013). Integrins in mechanotransduction. *Curr. Opin. Cell. Biol.* 25, 613–618. doi: 10.1016/j.ceb.2013.05.006

Russell-Puleri, S., Dela Paz, N. G., Adams, D., Chattopadhyay, M., Cancel, L., Ebong, E., et al. (2017). Fluid shear stress induces upregulation of COX-2 and PGI2 release in endothelial cells via a pathway involving PECAM-1, PI3K, FAK, and p38. *Am. J. Physiol. Heart Circ. Physiol.* 312, H485–H500. doi: 10.1152/ajpheart.00035.2016

Sabine, A., Agalarov, Y., Maby-El Hajjami, H., Jaquet, M., Hagerling, R., Pollmann, C., et al. (2012). Mechanotransduction, PROX1, and FOXC2 cooperate to control connexin37 and calcineurin during lymphatic-valve formation. *Dev. Cell* 22, 430–445. doi: 10.1016/j.devcel.2011.12.020

Sabine, A., Bovay, E., Demir, C. S., Kimura, W., Jaquet, M., Agalarov, Y., et al. (2015). FOXC2 and fluid shear stress stabilize postnatal lymphatic vasculature. *J. Clin. Invest.* 125, 3861–3877. doi: 10.1172/JCI80454

Sakabe, M., Fan, J., Odaka, Y., Liu, N., Hassan, A., Duan, X., et al. (2017). YAP/TAZ-CDC42 signaling regulates vascular tip cell migration. *Proc. Natl. Acad. Sci. U.S.A.* 114, 10918–10923. doi: 10.1073/pnas.1704030114

Sato, M., Sasaki, N., Ato, M., Hirakawa, S., Sato, K., and Sato, K. (2015). Microcirculation-on-a-Chip: a microfluidic platform for assaying blood- and lymphatic-vessel permeability. *PLoS One* 10:e0137301. doi: 10.1371/journal.pone.0137301

Scallan, J. P., Zawieja, S. D., Castorena-Gonzalez, J. A., and Davis, M. J. (2016). Lymphatic pumping: mechanics, mechanisms and malfunction. *J. Physiol.* 594, 5749–5768. doi: 10.1113/JP272088

Schaefer, A., Te Riet, J., Ritz, K., Hoogenboezem, M., Anthony, E. C., Mul, F. P., et al. (2014). Actin-binding proteins differentially regulate endothelial cell stiffness, ICAM-1 function and neutrophil transmigration. *J. Cell Sci.* 127(Pt 20), 4470–4482. doi: 10.1242/jcs.154708

Schaffer, T. E. (2013). Nanomechanics of molecules and living cells with scanning ion conductance microscopy. *Anal. Chem.* 85, 6988–6994. doi: 10.1021/ac400686k

Schimmel, L., and Gordon, E. (2018). The precise molecular signals that control endothelial cell-cell adhesion within the vessel wall. *Biochem. Soc. Trans.* 46, 1673–1680. doi: 10.1042/BST20180377

Schimmel, L., van der Stoel, M., Rianna, C., van Stalborch, A. M., de Ligt, A., Hoogenboezem, M., et al. (2018). Stiffness-induced endothelial DLC-1 expression forces leukocyte spreading through stabilization of the ICAM-1 adhesome. *Cell Rep.* 24, 3115–3124. doi: 10.1016/j.celrep.2018.08.045

Seetharaman, S., and Etienne-Manneville, S. (2018). Integrin diversity brings specificity in mechanotransduction. *Biol. Cell* 110, 49–64. doi: 10.1111/boc.201700060

Sen, S., Engler, A. J., and Discher, D. E. (2009). Matrix strains induced by cells: computing how far cells can feel. *Cell Mol. Bioeng.* 2, 39–48. doi: 10.1007/s12195-009-0052-z

Seong, J., Ouyang, M., Kim, T., Sun, J., Wen, P.-C., Lu, S., et al. (2011). Detection of focal adhesion kinase activation at membrane microdomains by fluorescence resonance energy transfer. *Nat. Commun.* 2:406. doi: 10.1038/ncomms1414

Shevkoplyas, S. S., Gifford, S. C., Yoshida, T., and Bitensky, M. W. (2003). Prototype of an in vitro model of the microcirculation. *Microvasc. Res.* 65, 132–136. doi: 10.1016/s0026-2862(02)00034-1

Shihata, W. A., Michell, D. L., Andrews, K. L., and Chin-Dusting, J. P. (2016). Caveolae: a role in endothelial inflammation and mechanotransduction? *Front. Physiol.* 7:628. doi: 10.3389/fphys.2016.00628

Shoajei, S., Tafazzoli-Shahdpour, M., Shokrgozar, M. A., and Haghighipour, N. (2014). Alteration of human umbilical vein endothelial cell gene expression in different biomechanical environments. *Cell. Biol. Int.* 38, 577–581. doi: 10.1002/cbin.10237

Simons, M., Gordon, E., and Claesson-Welsh, L. (2016). Mechanisms and regulation of endothelial VEGF receptor signalling. *Nat. Rev. Mol. Cell. Biol.* 17, 611–625. doi: 10.1038/nrm.2016.87

Sinha, B., Koster, D., Ruez, R., Gonnord, P., Bastiani, M., Abankwa, D., et al. (2011). Cells respond to mechanical stress by rapid disassembly of caveolae. *Cell* 144, 402–413. doi: 10.1016/j.cell.2010.12.031

Sivaraj, K. K., Dharmalingam, B., Mohanakrishnan, V., Jeong, H. W., Kato, K., Schroder, S., et al. (2020). YAP1 and TAZ negatively control bone angiogenesis by limiting hypoxia-inducible factor signaling in endothelial cells. *eLife* 9:e50770. doi: 10.7554/eLife.50770

Snell, N. E., Rao, V. P., Seckinger, K. M., Liang, J., Leser, J., Mancini, A. E., et al. (2018). Homotransfer of FRET reporters for live cell imaging. *Biosensors (Basel)* 8:89. doi: 10.3390/bios8040089

Song, J. W., Daubriac, J., Tse, J. M., Bazou, D., and Munn, L. L. (2012). RhoA mediates flow-induced endothelial sprouting in a 3-D tissue analogue of angiogenesis. *Lab Chip* 12, 5000–5006. doi: 10.1039/c2lc40389g

Song, J. W., and Munn, L. L. (2011). Fluid forces control endothelial sprouting. *Proc. Natl. Acad. Sci. U.S.A.* 108, 15342–15347. doi: 10.1073/pnas.1105316108

Soofi, S. S., Last, J. A., Liliensiek, S. J., Nealey, P. F., and Murphy, C. J. (2009). The elastic modulus of Matrigel as determined by atomic force microscopy. *J. Struct. Biol.* 167, 216–219. doi: 10.1016/j.jsb.2009.05.005

Souilhol, C., Serbanovic-Canic, J., Fragiadaki, M., Chico, T. J., Ridger, V., Roddie, H., et al. (2020). Endothelial responses to shear stress in atherosclerosis: a novel role for developmental genes. *Nat. Rev. Cardiol.* 17, 52–63. doi: 10.1038/s41569-019-0239-5

Stroka, K. M., and Aranda-Espinoza, H. (2010). A biophysical view of the interplay between mechanical forces and signaling pathways during transendothelial cell migration. *FEBS J.* 277, 1145–1158. doi: 10.1111/j.1742-4658.2009.07545.x

Stroka, K. M., and Aranda-Espinoza, H. (2011). Endothelial cell substrate stiffness influences neutrophil transmigration via myosin light chain kinase-dependent cell contraction. *Blood* 118, 1632–1640. doi: 10.1182/blood-2010-11-321125

Stroock, A. D., and Fischbach, C. (2010). Microfluidic culture models of tumor angiogenesis. *Tissue Eng. Part A* 16, 2143–2146. doi: 10.1089/ten.TEA.2009.0689

Swartz, M. A., and Fleury, M. E. (2007). Interstitial flow and its effects in soft tissues. *Annu. Rev. Biomed. Eng.* 9, 229–256. doi: 10.1146/annurev.bioeng.9.060906.151850

Swartz, M. A., and Lund, A. W. (2012). Lymphatic and interstitial flow in the tumour microenvironment: linking mechanobiology with immunity. *Nat. Rev. Cancer* 12, 210–219. doi: 10.1038/nrc3186

Sweet, D. T., Jimenez, J. M., Chang, J., Hess, P. R., Mericko-Ishizuka, P., Fu, J., et al. (2015). Lymph flow regulates collecting lymphatic vessel maturation in vivo. *J. Clin. Invest.* 125, 2995–3007. doi: 10.1172/JCI79386

Takeda, A., Hollmen, M., Dermadi, D., Pan, J., Brulois, K. F., Kaukonen, R., et al. (2019). Single-cell survey of human lymphatics unveils marked endothelial cell heterogeneity and mechanisms of homing for neutrophils. *Immunity* 51, 561–572.e5. doi: 10.1016/j.immuni.2019.06.027

Tan, W., Madhavan, K., Hunter, K. S., Park, D., and Stenmark, K. R. (2014). Vascular stiffening in pulmonary hypertension: cause or consequence? (2013 Grover Conference series). *Pulm. Circ.* 4, 560–580. doi: 10.1086/677370

Thorneloe, K. S., Cheung, M., Bao, W., Alsaid, H., Lenhard, S., Jian, M. Y., et al. (2012). An orally active TRPV4 channel blocker prevents and resolves pulmonary edema induced by heart failure. *Sci. Transl. Med.* 4:159ra148. doi: 10.1126/scitranslmed.3004276

Tian, Y., Gawlak, G., O'Donnell, J. J. III, Birukova, A. A., and Birukov, K. G. (2016a). Activation of vascular endothelial growth factor (VEGF) receptor 2 mediates endothelial permeability caused by cyclic stretch. *J. Biol. Chem.* 291, 10032–10045. doi: 10.1074/jbc.M115.690487

Tian, Y., Gawlak, G., O'Donnell, J. J. III, Mambetsariev, I., and Birukova, A. A. (2016b). Modulation of endothelial inflammation by low and high magnitude cyclic stretch. *PLoS One* 11:e0153387. doi: 10.1371/journal.pone.0153387

Tibbitt, M. W., and Anseth, K. S. (2009). Hydrogels as extracellular matrix mimics for 3D cell culture. *Biotechnol. Bioeng.* 103, 655–663. doi: 10.1002/bit.22361

Ting, L. H., Jahn, J. R., Jung, J. I., Shuman, B. R., Feghhi, S., Han, S. J., et al. (2012). Flow mechanotransduction regulates traction forces, intercellular forces, and adherens junctions. *Am. J. Physiol. Heart Circ. Physiol.* 302, H2220–H2229. doi: 10.1152/ajpheart.00975.2011

Tracqui, P., Broisat, A., Toczek, J., Mesnier, N., Ohayon, J., and Riou, L. (2011). Mapping elasticity moduli of atherosclerotic plaque in situ via atomic force microscopy. *J. Struct. Biol.* 174, 115–123. doi: 10.1016/j.jsb.2011.01.010

Trappmann, B., Baker, B. M., Polacheck, W. J., Choi, C. K., Burdick, J. A., and Chen, C. S. (2017). Matrix degradability controls multicellularity of 3D cell migration. *Nat. Commun.* 8:371. doi: 10.1038/s41467-017-00418-6

Tsai, M., Kita, A., Leach, J., Rounsevell, R., Huang, J. N., Moake, J., et al. (2012). In vitro modeling of the microvascular occlusion and thrombosis that occur in hematologic diseases using microfluidic technology. *J. Clin. Invest.* 122, 408–418. doi: 10.1172/JCI58753

Tse, J. R., and Engler, A. J. (2010). Preparation of hydrogel substrates with tunable mechanical properties. *Curr. Protoc. Cell Biol.* 47, 10.16.1–10.16.16. doi: 10.1002/0471143030.cb1016s47

Tzima, E., Irani-Tehrani, M., Kiosses, W. B., Dejana, E., Schultz, D. A., Engelhardt, B., et al. (2005). A mechanosensory complex that mediates the endothelial cell response to fluid shear stress. *Nature* 437, 426–431. doi: 10.1038/nature03952

Ueda, R., Kohanbash, G., Sasaki, K., Fujita, M., Zhu, X., Kastenhuber, E. R., et al. (2009). Dicer-regulated microRNAs 222 and 339 promote resistance of cancer cells to cytotoxic T-lymphocytes by down-regulation of ICAM-1. *Proc. Natl. Acad. Sci. U.S.A.* 106, 10746–10751. doi: 10.1073/pnas.0811817106

Vaeyens, M. M., Jorge-Penas, A., Barrasa-Fano, J., Steuwe, C., Heck, T., Carmeliet, P., et al. (2020). Matrix deformations around angiogenic sprouts correlate to sprout dynamics and suggest pulling activity. *Angiogenesis* doi: 10.1007/s10456-020-09708-y

van den Berg, A., Mummery, C. L., Passier, R., and van der Meer, A. D. (2019). Personalised organs-on-chips: functional testing for precision medicine. *Lab Chip* 19, 198–205. doi: 10.1039/c8lc00827b

van den Berg, C. W., Ritsma, L., Avramut, M. C., Wiersma, L. E., van den Berg, B. M., Leuning, D. G., et al. (2018). Renal subcapsular transplantation of PSC-derived kidney organoids induces neo-vasculogenesis and significant glomerular and tubular maturation in vivo. *Stem Cell Rep.* 10, 751–765. doi: 10.1016/j.stemcr.2018.01.041

van Engeland, N. C. A., Pollet, A. M. A. O., den Toonder, J. M. J., Bouten, C. V. C., Stassen, O. M. J. A., and Sahlgren, C. M. (2018). A biomimetic microfluidic model to study signalling between endothelial and vascular smooth muscle cells under hemodynamic conditions. *Lab Chip* 18, 1607–1620. doi: 10.1039/C8LC00286J

Vanlandewijck, M., and Betsholtz, C. (2018). Single-cell mRNA sequencing of the mouse brain vasculature. *Methods Mol. Biol.* 1846, 309–324. doi: 10.1007/978-1-4939-8712-2_21

Wang, S., Iring, A., Strilic, B., Albarran Juarez, J., Kaur, H., Troidl, K., et al. (2015). P2Y(2) and Gq/G(1)(1) control blood pressure by mediating endothelial mechanotransduction. *J. Clin. Invest.* 125, 3077–3086. doi: 10.1172/JCI81067

Wang, S., Nie, D., Rubin, J. P., and Kokai, L. (2017a). Lymphatic endothelial cells under mechanical stress: altered expression of inflammatory cytokines and fibrosis. *Lymphat Res. Biol.* 15, 130–135. doi: 10.1089/lrb.2016.0042

Wang, W., Lollis, E. M., Bordeleau, F., and Reinhart-King, C. A. (2019). Matrix stiffness regulates vascular integrity through focal adhesion kinase activity. *FASEB J.* 33, 1199–1208. doi: 10.1096/fj.201800841R

Wang, X., Freire Valls, A., Schermann, G., Shen, Y., Moya, I. M., Castro, L., et al. (2017b). YAP/TAZ orchestrate VEGF signaling during developmental angiogenesis. *Dev. Cell* 42, 462–478.e7. doi: 10.1016/j.devcel.2017.08.002

Wang, X., Phan, D. T. T., Sobrino, A., George, S. C., Hughes, C. C. W., and Lee, A. P. (2016). Engineering anastomosis between living capillary networks and endothelial cell-lined microfluidic channels. *Lab Chip* 16, 282–290. doi: 10.1039/C5LC01050K

Wang, Y., Botvinick, E. L., Zhao, Y., Berns, M. W., Usami, S., Tsien, R. Y., et al. (2005). Visualizing the mechanical activation of Src. *Nature* 434, 1040–1045. doi: 10.1038/nature03469

Wang, Z., and Chesler, N. C. (2011). Pulmonary vascular wall stiffness: an important contributor to the increased right ventricular afterload with pulmonary hypertension. *Pulm. Circ.* 1, 212–223. doi: 10.4103/2045-8932.83453

Wells, R. G. (2008). The role of matrix stiffness in regulating cell behavior. *Hepatology* 47, 1394–1400. doi: 10.1002/hep.22193

Whitehead, A. K., Barnett, H. H., Caldorera-Moore, M. E., and Newman, J. J. (2018). Poly (ethylene glycol) hydrogel elasticity influences human mesenchymal stem cell behavior. *Regener. Biomater.* 5, 167–175. doi: 10.1093/rb/rby008

Willemsen, S., Hartog, J. W., Hummel, Y. M., Posma, J. L., van Wijk, L. M., van Veldhuisen, D. J., et al. (2010). Effects of alagebrium, an advanced glycation end-product breaker, in patients with chronic heart failure: study design and baseline characteristics of the BENEFICIAL trial. *Eur. J. Heart Fail.* 12, 294–300. doi: 10.1093/eurjhf/hfp207

Wong, L., Kumar, A., Gabela-Zuniga, B., Chua, J., Singh, G., Happe, C. L., et al. (2019). Substrate stiffness directs diverging vascular fates. *Acta Biomater.* 96, 321–329. doi: 10.1016/j.actbio.2019.07.030

Xue, C., Zhang, T., Xie, X., Zhang, Q., Zhang, S., Zhu, B., et al. (2017). Substrate stiffness regulates arterial-venous differentiation of endothelial progenitor cells via the Ras/Mek pathway. *Biochim. Biophys. Acta Mol. Cell. Res.* 1864, 1799–1808. doi: 10.1016/j.bbamcr.2017.07.006

Yamamoto, H., Ehling, M., Kato, K., Kanai, K., van Lessen, M., Frye, M., et al. (2015). Integrin beta1 controls VE-cadherin localization and blood vessel stability. *Nat. Commun.* 6:6429. doi: 10.1038/ncomms7429

Yamamoto, K., and Ando, J. (2013). Endothelial cell and model membranes respond to shear stress by rapidly decreasing the order of their lipid phases. *J. Cell Sci.* 126, 1227–1234. doi: 10.1242/jcs.119628

Yeh, Y. C., Ling, J. Y., Chen, W. C., Lin, H. H., and Tang, M. J. (2017). Mechanotransduction of matrix stiffness in regulation of focal adhesion size and number: reciprocal regulation of caveolin-1 and beta1 integrin. *Sci. Rep.* 7:15008. doi: 10.1038/s41598-017-14932-6

Yeh, Y. T., Hur, S. S., Chang, J., Wang, K. C., Chiu, J. J., Li, Y. S., et al. (2012). Matrix stiffness regulates endothelial cell proliferation through septin 9. *PLoS One* 7:e46889. doi: 10.1371/journal.pone.0046889

Yoon, C., Choi, C., Stapleton, S., Mirabella, T., Howes, C., Dong, L., et al. (2019). Myosin IIA-mediated forces regulate multicellular integrity during vascular sprouting. *Mol. Biol. Cell* 30, 1974–1984. doi: 10.1091/mbc.E19-02-0076

Yurdagul, A. Jr., and Orr, A. W. (2016). Blood brothers: hemodynamics and cell-matrix interactions in endothelial function. *Antioxid. Redox Signal.* 25, 415–434. doi: 10.1089/ars.2015.6525

Zawieja, D. C. (2009). Contractile physiology of lymphatics. *Lymphat. Res. Biol.* 7, 87–96. doi: 10.1089/lrb.2009.0007

Zhong, A., Mirzaei, Z., and Simmons, C. A. (2018). The roles of matrix stiffness and ß-catenin signaling in endothelial-to-mesenchymal transition of aortic valve endothelial cells. *Cardiovasc. Eng. Technol.* 9, 158–167. doi: 10.1007/s13239-018-0363-0

Zhou, D. W., Lee, T. T., Weng, S., Fu, J., and Garcia, A. J. (2017). Effects of substrate stiffness and actomyosin contractility on coupling between force transmission and vinculin-paxillin recruitment at single focal adhesions. *Mol. Biol. Cell* 28, 1901–1911. doi: 10.1091/mbc.E17-02-0116

Zieman, S. J., Melenovsky, V., Clattenburg, L., Corretti, M. C., Capriotti, A., Gerstenblith, G., et al. (2007). Advanced glycation endproduct crosslink breaker (alagebrium) improves endothelial function in patients with isolated systolic hypertension. *J. Hypertens.* 25, 577–583. doi: 10.1097/HJH.0b013e328013e7dd

Zieman, S. J., Melenovsky, V., and Kass, D. A. (2005). Mechanisms, pathophysiology, and therapy of arterial stiffness. *Arterioscler. Thromb. Vasc. Biol.* 25, 932–943. doi: 10.1161/01.ATV.0000160548.78317.29

Conflict of Interest: The authors declare that the research was conducted in the absence of any commercial or financial relationships that could be construed as a potential conflict of interest.

The handling editor declared a past co-authorship with one of the authors LS.

frontiers in Physiology

ORIGINAL RESEARCH
published: 09 July 2020
doi: 10.3389/fphys.2020.00763

Suppressed Vascular Leakage and Myocardial Edema Improve Outcome From Myocardial Infarction

Xiujuan Li[1,2], Björn Redfors[3], Miguel Sáinz-Jaspeado[2], Shujing Shi[2†], Pernilla Martinsson[2], Narendra Padhan[2], Margareta Scharin Täng[3], Jan Borén[3], Malin Levin[3] and Lena Claesson-Welsh[2]**

[1] Cyrus Tang Hematology Center, Collaborative Innovation Center of Hematology, State Key Laboratory of Radiation Medicine and Protection, Soochow University, Suzhou, China, [2] Beijer and Science for Life Laboratories, Department of Immunology, Genetics and Pathology, Rudbeck Laboratory, Uppsala University, Uppsala, Sweden, [3] Department of Molecular and Clinical Medicine / Wallenberg Laboratory, Institute of Medicine, The Sahlgrenska Academy at University of Gothenburg and Sahlgrenska University Hospital, Gothenburg, Sweden

OPEN ACCESS

Edited by:
Stephan Huveneers, Amsterdam University Medical Center (UMC), Netherlands

Reviewed by:
Stephane Germain, Institut National de la Santé et de la Recherche Médicale (INSERM), France
Serena Zacchigna, International Centre for Genetic Engineering and Biotechnology, Italy

***Correspondence:**
Xiujuan Li
lixiujuan@suda.edu.cn
Lena Claesson-Welsh
lena.welsh@igp.uu.se

†Present address:
Shujing Shi,
School of Sports and Health, Nanjing Sport Institute, Nanjing, China

Specialty section:
This article was submitted to Vascular Physiology, a section of the journal Frontiers in Physiology

Received: 08 April 2020
Accepted: 11 June 2020
Published: 09 July 2020

Citation:
Li X, Redfors B, Sáinz-Jaspeado M, Shi S, Martinsson P, Padhan N, Scharin Täng M, Borén J, Levin M and Claesson-Welsh L (2020) Suppressed Vascular Leakage and Myocardial Edema Improve Outcome From Myocardial Infarction. Front. Physiol. 11:763. doi: 10.3389/fphys.2020.00763

Aim: The acute phase of myocardial infarction (MI) is accompanied by edema contributing to tissue damage and disease outcome. Here, we aimed to identify the mechanism whereby vascular endothelial growth factor (VEGF)-A induces myocardial edema in the acute phase of MI to eventually promote development of therapeutics to specifically suppress VEGFA-regulated vascular permeability while preserving collateral vessel formation.

Methods and Results: VEGFA regulates vascular permeability and edema by activation of VEGF receptor-2 (VEGFR2), leading to induction of several signaling pathways including the cytoplasmic tyrosine kinase c-Src. The activated c-Src in turn phosphorylates vascular endothelial (VE)-cadherin, leading to dissociation of endothelial adherens junctions. A particular tyrosine at position 949 in mouse VEGFR2 has been shown to be required for activation of c-Src. Wild-type mice and mice with phenylalanine replacing tyrosine (Y) 949 in VEGFR2 (*Vegfr2*$^{Y949F/Y949F}$) were challenged with MI through permanent ligation of the left anterior descending coronary artery. The infarct size was similar in wild-type and mutant mice, but left ventricular wall edema and fibrinogen deposition, indicative of vascular leakage, were reduced in the *Vegfr2*$^{Y949F/Y949F}$ strain. When challenged with large infarcts, the *Vegfr2*$^{Y949F/Y949F}$ mice survived significantly better than the wild-type strain. Moreover, neutrophil infiltration and levels of myeloperoxidase were low in the infarcted *Vegfr2*$^{Y949F/Y949F}$ hearts, correlating with improved survival. *In vivo* tyrosine phosphorylation of VE-cadherin at Y685, implicated in regulation of vascular permeability, was induced by circulating VEGFA in the wild-type but remained at baseline levels in the *Vegfr2*$^{Y949F/Y949F}$ hearts.

Conclusion: Suppression of VEGFA/VEGFR2-regulated vascular permeability leads to diminished edema without affecting vascular density correlating with improved myocardial parameters and survival after MI.

Keywords: VEGF, VE-cadherin, adherens junctions, endothelial, vascular permeability, myocardial infarction

INTRODUCTION

Vascular endothelial growth factor-A (VEGFA) plays a protective role in ischemic heart disease and myocardial infarction (MI) by inducing angiogenesis (Kajdaniuk et al., 2011). However, during the early phase of coronary artery occlusion, VEGFA induced by the acute tissue hypoxia and ensuing inflammation promotes enhanced vascular permeability and extravasation of plasma constituents, causing edema, eventually resulting in tissue damage, and inflammation (Garcia et al., 2019; Hausenloy et al., 2019).

Vascular endothelial growth factor-A together with VEGFB, VEGFC, VEGFD, and placenta growth factor (PlGF) form a family of structurally related growth factors, which bind to three related receptor tyrosine kinases; VEGF receptor-1 (VEGFR1), VEGFR2, and VEGFR3 (Simons et al., 2016). While VEGFR1 is broadly expressed, VEGFR2 and VEGFR3 are mainly although not exclusively expressed on blood vascular and lymphatic endothelial cells (ECs). VEGFA is a potent inducer of vascular permeability; in accordance, it was originally identified as vascular permeability factor (VPF) (Dvorak, 2002). Binding of VEGFA to VEGFR2 leads to activation of the receptor tyrosine kinase and phosphorylation of tyrosine residues (Y) 949, 1052, 1057, 1173, and 1212 (mouse sequence numbering) in the receptor intracellular domain (Matsumoto et al., 2005). Phosphorylated (p) Y949 in VEGFR2 mediates c-Src activation at EC junctions (Sun et al., 2012; Li et al., 2016), and loss of pY949 signaling in $Vegfr2^{Y949F/Y949F}$ mice results in reduced vascular leakage in response to VEGFA administration, in the dermal and tracheal vasculature (Li et al., 2016). Moreover, vascular permeability and edema are lower in $Vegfr2^{Y949F/Y949F}$ mice compared to wild-type, after challenge with GL261 glioma, B16F10 melanoma and RipTag neuroendocrine cancer. The enforced vascular barrier in the $Vegfr2^{Y949F/Y949F}$ mice correlates with decreased metastatic spread from melanoma and neuroendocrine cancer in mice (Li et al., 2016).

Several therapeutic strategies are available to suppress VEGFA biology including neutralizing antibodies Avastin/Lucentis, the recombinant VEGF receptor fragment Aflibercept and a broad range of small molecular weight tyrosine kinase inhibitors. These drugs are used to treat conditions associated with exaggerated formation of dysfunctional, leaky vessels such as diabetic retinopathy and age-related macular degeneration (Avastin/Lucentis, Eylea) (Ferrara and Adamis, 2016) and in treatment of highly vascularized solid tumors such as renal cell carcinoma, hepatocellular carcinoma, colorectal cancer (VEGFR2-targeting kinase inhibitors) (Bhullar et al., 2018). However, complete suppression of VEGFA/VEGFR2 in disease may lead to side effects such as geographical atrophy in retinopathy and exacerbation of the disease in cancer (Ebos et al., 2009; Paez-Ribes et al., 2009). It is therefore important to understand how VEGFA/VEGFR2 contributes to disease and to inhibit only those aspects of the biology that contributes to disease such as induction of vascular permeability, while sparing other aspects such as angiogenesis. This is particularly relevant in myocardial insult where VEGFA biology plays very different roles during different stages of the disease.

Vascular endothelial growth factor-A-induced vascular permeability requires disintegration of homophilic interactions between vascular endothelial (VE)-cadherin molecules in adherens junctions (Dejana et al., 2008), in prevenular capillaries and postcapillary venules (Honkura et al., 2018). In these vascular beds, VE-cadherin is phosphorylated constitutively on Y658 and Y685, through flow-dependent activation of c-Src (Orsenigo et al., 2012). Acute stimulation with VEGFA further increases VE-cadherin phosphorylation (Li et al., 2016). Phosphorylation on Y685 in VE-cadherin correlates with elevated vascular permeability (Orsenigo et al., 2012; Wessel et al., 2014).

Here, we show that genetic suppression of VEGFA-induced vascular permeability in conjunction with MI is accompanied by reduced left ventricular wall edema and improved performance in a range of cardiac parameters. The underlying mechanism involves reduced phosphorylation on Y685 in VE-cadherin due to loss in signaling downstream of Y949 in VEGFR2. These data emphasize the detrimental effect of excess vascular permeability and edema in the acute phase of MI.

MATERIALS AND METHODS

VEGFR2Y949F Mouse Model

A mouse model on the C57BL/6J background with knock-in of phenylalanine (F) to replace the tyrosine (Y) at position 949 of VEGFR2 (designated $Vegfr2^{Y949F/Y949F}$) has been described (Li et al., 2016). Age-matched, (approximately 12 weeks-old) male $Vegfr2^{Y949F/Y949F}$ mutant and wild-type (WT) littermates from Y949F heterozygous breeding were compared.

Ethics Statement

All animal studies were approved by the Uppsala University (approval reference number 5.8.18-06789/2018) and Göteborg University Animal Ethics Committees and conform to the guidelines from Directive 2010/63/EU of the European Parliament on the protection of animals used for scientific purposes. Mice were anesthetized using isoflurane and at the end of experiments, sacrificed by cervical dislocation. Care was taken to avoid unnecessary suffering of the animals during the procedure. No animals were excluded from analysis.

MI Induction

Myocardial infarction was induced in a genotype-blinded manner by left anterior descending (LAD) coronary artery ligation immediately distal to the bifurcation of the left coronary artery (for induction of large infarctions) and at ∼3 mm distal to the bifurcation of the left coronary artery (for induction of smaller infarctions) as described in detail previously (Andersson et al., 2015). To keep the mice sedated and support breathing during the operation, the mice were anesthetized with isoflurane (Forene®, AbbVie Inc., North Chicago, IL, United States), orally incubated and connected to a respirator (SAR-830 small animal ventilator, GENEQ) distributing a mixture of oxygen, air and 2–3% isoflurane.

Induction of MI was immediately verified by characteristic changes in the electrocardiographic pattern and akinesis of the

left ventricular anterior wall. After verification of infarction, the lungs were hyperinflated, positive end-expiratory pressure was applied, and the chest was closed. The mice received Temgesic (3 mg/ml; 0.1 mL administered intraperitoneally (i.p.) to relieve post-operative pain and recovered spontaneously when the isoflurane was turned off. In a survival study, large infarctions were induced by ligation at ∼1 mm below the atrial appendage, and survival rate was analyzed 24 h after infarction.

At 3 days post smaller infarction, infarcted hearts were collected and snap-frozen in dry-ice/isopentane. Heart lysate from the lower half of the heart (about 5 mm) were analyzed using a multiplex human inflammatory protein biomarker panel (Olink Bioscience; see www.olink.com/content/uploads/2015/12/0696-v1.3-Proseek-Multiplex-CVD-I-Validation-Data_final.pdf). where reactivity depended on detected by two antibodies against each marker. An equivalent anti-mouse panel was not available.

Echocardiography

Mice were anesthetized with 1,2% isoflurane (Forene®, AbbVie Inc., North Chicago, IL, United States), and underwent echocardiography examination at baseline and at 24 h after MI induction, using a VEVO 770 system (VisualSonics, Ontario, ON, Canada), as previously described (Drevinge et al., 2016). The animals' chests were shaved and hair removal gel was applied to minimize resistance to ultrasonic beam transmission. The mice were then placed on a heating pad and paws were connected to electrocardiographic (ECG) electrodes. A 45 MHz linear transducer (RMV 704) was used for imaging. An optimal parasternal long axis (LAX) cine loop (i.e., visualization of both the mitral and aortic valves, and maximum distance between the aortic valve and the cardiac apex) of >1000 frames/s was acquired using the ECG-gated kilohertz visualization technique. Parasternal short axis cine-loops were acquired at 1, 3, and 5 mm below the mitral annulus. End-diastolic and end-systolic LV volumes and ejection fraction (EF) were calculated by biplane Simpson's formula using the three parasternal short-axis views and the parasternal long-axis view. M-mode measurements were performed (in the 3 mm level) using the leading-edge method. End-diastole was defined at the onset of the QRS complex, and end-systole was defined as the time of peak inward motion of the interventricular septum. At least three beats were averaged for each measurement. Infarct size was assessed based on wall motion score index (WMSI). WMSI was analyzed by a 24-segments model on the long axis view, three short axis images and 4-chamber views, with the following settings: 0 for normal, 0.5 for reduced wall thickening and excursion in a segment, and 1 for no wall thickening and excursion in a segment. WMSI was calculated as the sum of scores divided by the total number of segments. The stored data was evaluated offline in a genotype-blinded fashion with VevoLab software (VisualSonics).

Antibodies

The following antibodies were used in immunostaining: rat anti-mouse CD31 (BD Biosciences), goat anti-mouse CD45 (BD Pharmingen), goat anti-mouse fibrinogen (Nordic Immunological Laboratories), rat anti-mouse Ly6G (BD Pharmingen). Fluorescently labeled secondary antibodies were derived from donkey (Invitrogen) or goat (Jackson ImmunoResearch). The following antibodies were used in immunoblotting: goat anti-mouse VEGFR2 (R&D), phospho-VEGFR2 (pY1175) (Cell Signaling), goat anti-mouse VE-cadherin (R&D), anti-GAPDH mouse monoclonal antibody (Millipore). Rabbit antibodies against c-Src (32G6), pY418 Src (D49G4), extracellular regulated kinase (Erk)1/2, pT202Y204 Erk1/2 (197G2), Akt, pT308 Akt were all from Cell Signaling. Anti-pY685 VE-cadherin was kindly provided by Dr. Elisabetta Dejana Uppsala University/IFOM Milano (Orsenigo et al., 2012).

Immunostaining

Heart cryo-sections (10 μm) at 5 mm from the apex were collected for immunostaining. The sections were fixed in 4% paraformaldehyde for 10 min, washed with PBS, and blocked/permeabilized with 3% BSA/0.2% Triton X-100 in PBS, followed by incubation with primary antibody at 4°C overnight and with second antibody at room temperature (RT) for 1 h. Nuclei were stained with DAPI for 20 min at RT. Samples were mounted using Fluoromount-G (SouthernBiotech) and images were acquired using a Zeiss LSM700 confocal microscope (10× NA 0.45, 20× NA 0.8 objective). Quantifications were done using ImageJ software.

VEGF Tail-Vein Injection and Immunoblotting

Hearts were collected from mice at 1, 2, 5 min after injection of PBS, or after 1, 2, 5, 10, 15, or 60 min after injection of VEGFA164 (canine, produced in insect cells; kind gift of Dr. Kurt Ballmer-Hofer, 250 μg per kg mouse) in the tail vein, snap-frozen in dry-ice / isopentane, and then stored at −80°C before use. Hearts were lysed in commercial RIPA buffer (ProteinSimple), total lysate was mixed with 2× SDS sample buffer, heated at 70°C for 10 min, loaded on NuPAGE Novex 4–12% Bis-Tris gels (Invitrogen) and processed for immunoblotting.

Blood Component Count

Peripheral leukocyte counts in mice were determined at the governmental agency Statens Veterinärmedicinska Anstalt (Uppsala, Sweden) using "Quantifying Buffy Coat" (QBC-V) (Holst et al., 1994).

RNA Sequencing

RNA was extracted from lungs of 5–8-week old wild-type and $Vegfr2^{Y949F/Y949F}$ mice using the Qiagen RNeasy kit. mRNA purification was performed using Dynabeads mRNA Purification Kit (Ambion, Life Technologies AS, Oslo, Norway). mRNA libraries, three biological replicates per sample, were prepared using the Ion Total RNA-Seq Kit v2 (Life Technologies) using the standard protocol, and sequencing was performed on Ion Proton sequencer (Life Technologies). See Li et al. (2016) for further details on bulk RNAseq. Data were deposited with ArrayExpress, accession E-MTAB-9163.

Statistical Analysis

Data are shown as means ± SEM. Statistical analyses were performed using nonparametric Mann–Whitney test to compare two unpaired groups and Wilcoxon test to

compare two paired groups. Chi-squared test was used for survival assay. p-value < 0.05 was considered statistically significant. All statistical analyses were performed using GraphPad Prism Software.

RESULTS

Outcome After MI in the *Vegfr2*$^{Y949F/Y949F}$ Knock-in Mouse

The VEGFR2 Y949 phosphorylation site been implicated in regulation of the vascular barrier in different organs and in diseases such as cancer and retinopathy (Li et al., 2016; Smith et al., 2020). The potential impact of the pY949 pathway on the coronary circulation and on cardiac function has not been explored. We used mice in which VEGFR2 Y949 is replaced by F949 (*Vegfr2*$^{Y949F/Y949F}$), and where adherens junctions in different vascular beds remain stable when exposed to VEGFA (Li et al., 2016; Smith et al., 2020). Under baseline conditions, *Vegfr2*$^{Y949F/Y949F}$ mice displayed no differences in cardiac function compared with wild-type mice, as evaluated by echocardiography to determine EF, fractional area change (FAC) and cardiac output (CO) (**Figures 1A–C**). Next, mice were challenged by permanent LAD ligation and analyzed

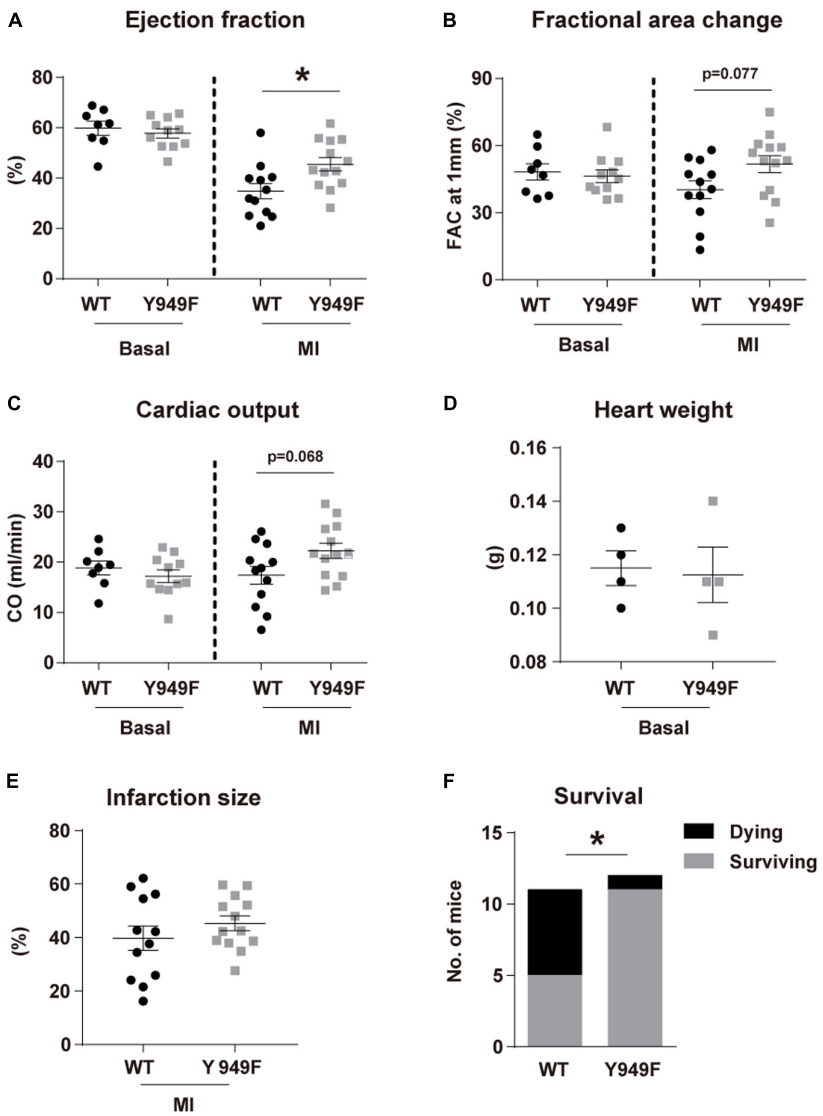

FIGURE 1 | Improved cardiac function following MI in *Vegfr2*$^{Y949F/Y949F}$ mice. **(A–C)** Heart function assessed using echocardiography; **(A)** ejection fraction, **(B)** fractional area change (FAC), **(C)** cardiac output (CO) in *Vegfr2*$^{Y949F/Y949F}$ mice and WT littermates in baseline condition (n = 8–11 mice/strain), and at 24 h following myocardial infarction (n = 12–13 mice/strain, conducted at three different occasions). **(D,E)**. Heart weights before infarction (**D**; n = 4 mice/strain) and induced infarct size at 24 h after ligation **(E)** (n = 12–13 mice/strain) in WT and *Vegfr2*$^{Y949F/Y949F}$ mice. Data in **(A–E)** are shown as mean ± SEM. Statistical significance was determined using Mann–Whitney test, $^*p < 0.05$. **(F)** Survival after large infarct (n = 11–12/strain). Chi-squared test; $^*p < 0.05$. For all panels, n refers to biological replicates.

by echocardiography at 24 h after infarction. As shown in **Figures 1A–C**, the *Vegfr2*$^{Y949F/Y949F}$ strain showed a trend to better performance with regard to FAC and CO, and displayed a significant better outcome in EF, compared to wild-type, after infarction. These data indicate that *Vegfr2*$^{Y949F/Y949F}$ mice have a normal heart function under baseline conditions, and that they are more resilient when exposed to infarction. There was no difference in heart weights before challenge (**Figure 1D**) and the size of the induced infarcts (**Figure 1E**) were not different between strains. In accordance with the improved cardiac performance in mutant mice observed upon induction of smaller infarcts (**Figures 1A–C**), challenge of mice with large infarcts led to significantly better survival for the *Vegfr2*$^{Y949F/Y949F}$ mice (11/12 survived) than for wild-type litter mates (6/11 survived; **Figure 1F**).

Edema and Vascular Leakage Is Reduced in the *Vegfr2*$^{Y949F/Y949F}$ Myocardium

We have shown that VEGFR2 pY949-dependent signaling results in increased vascular permeability in the skin and trachea and that the permeability increase is not seen in the *Vegfr2*$^{Y949F/Y949F}$ (Li et al., 2016). An underlying mechanism contributing to better cardiac function in mice lacking the pY949 signaling pathway could therefore involve improved vascular integrity after MI. In agreement, the left ventricular wall mass was significantly lower 24 h post MI in the *Vegfr2*$^{Y949F/Y949F}$ mice compared to the wild-type (**Figure 2A**), indicating reduced edema compared to wild-type. Fibrinogen is a plasma protein which does not become deposited in tissues unless the vascular barrier is impaired (Davalos et al., 2012; Halder and Milner, 2020). Fibrinogen immunostaining normalized to vascular area was lower in the *Vegfr2*$^{Y949F/Y949F}$ than in the wild-type mouse infarct area (**Figures 2B,C**; quantified in **Figure 2D**), indicating reduced macromolecular leakage, from the mutant vasculature.

In contrast, vascular density or the density of CD45-positive inflammatory cells were similar in the infarct zone between wild-type and mutant hearts (**Figures 3A–C**).

Neutrophil Infiltration Persistently Low in *Vegfr2*$^{Y949F/Y949F}$ MI Tissue

Using a multiplex antibody panel to detect inflammatory markers in infarcted heart lysates, we noted the significantly lower expression of myeloperoxidase (MPO) in *Vegfr2*$^{Y949F/Y949F}$ heart lysates compared to wild-type (**Figure 3D**; see **Table 1** for inflammatory markers detected in the heart lysates). Elevated MPO levels in circulation are associated with inflammation and increased oxidative stress (Ndrepepa, 2019). An important potential source for MPO would be infiltrating neutrophils (Aratani, 2018). Neutrophils were detected in the infarcted areas using immunostaining for Ly6G. Most of the Ly6G-positive cells were also positive for CD45. Wild-type hearts showed large variability of infiltrating neutrophils, while the levels were consistently low in the mutant MI tissue (**Figures 3E,F**). The consistent low degree of infiltration of neutrophils in the Y949F MI tissue was not due to reduced neutrophil numbers in the unchallenged condition (**Table 2**). Indeed, there were no significant differences in the numbers of red blood cells, neutrophils, immune cells or monocytes between wild-type and *Vegfr2*$^{Y949F/Y949F}$ in peripheral blood.

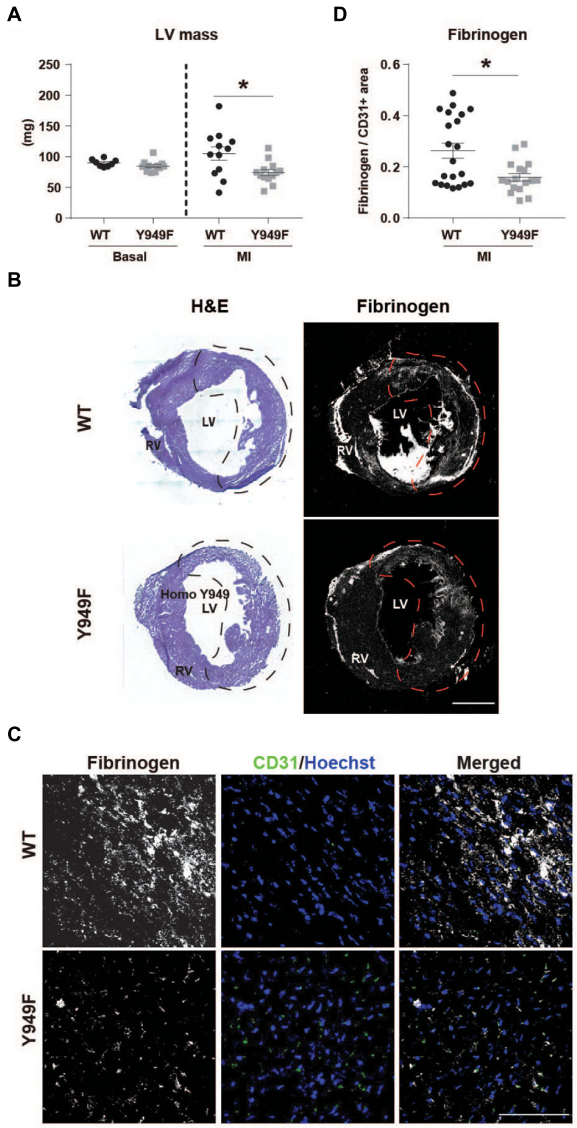

FIGURE 2 | Reduced edema and fibrinogen leakage in *Vegfr2*$^{Y949F/Y949F}$ MI hearts. **(A)** Left ventricular (LV) wall mass (mg) in WT and *Vegfr2*$^{Y949F/Y949F}$ hearts at baseline condition (n = 8–11 mice/strain) and 24 h after MI (n = 12–13 mice/strain). Mann–Whitney test, *$p < 0.05$. **(B)** Hematoxylin/Eosin (H&E) and fibrinogen immunofluorescent staining on total WT (top) or Y949F (bottom) heart sections. Scale bar, 1500 μm. The infarct area detected using echocardiography, is indicated by stippled lines in black or red. **(C)** Fibrinogen (gray) and CD31 (green) immunofluorescent staining of WT and *Vegfr2*$^{Y949F/Y949F}$ hearts at 3 days after MI; sections from the infarcted area. Scale bar, 100 μm. Hoechst (blue) shows nuclei. **(D)** Quantification of fibrinogen area normalized to CD31 area in randomly selected regions in total WT and *Vegfr2*$^{Y949F/Y949F}$ hearts at 3 days after MI (n = 17–21 fields/section from 6 to 7 individual hearts/strain and 2–3 sections/heart). Mann–Whitney test, *$p < 0.05$. For all panels, n refers to biological replicates.

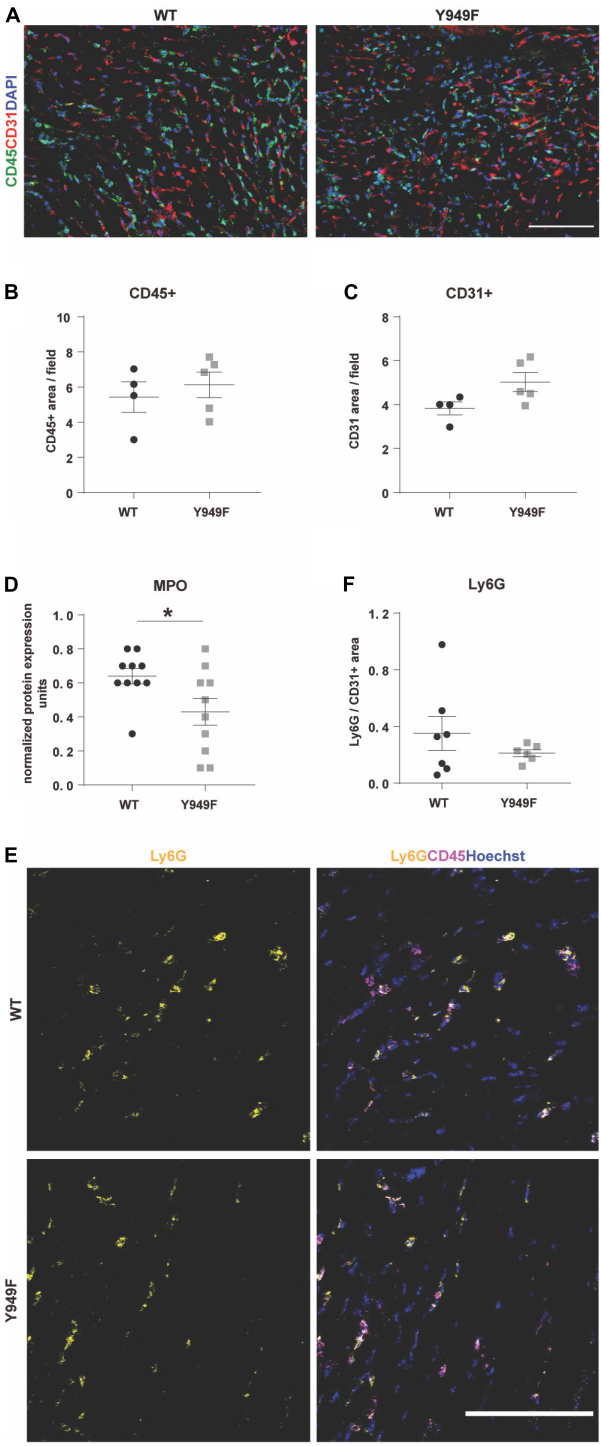

FIGURE 3 | Inflammation, neutrophil infiltration and MPO levels in conjunction with MI. **(A)** Immunostaining for CD45 (green) and CD31 (red) to visualize infiltrating leukocytes and the vasculature, respectively, in the infarcted areas of WT and *Vegfr2*$^{Y949F/Y949F}$ hearts at 3 days post-MI. DAPI (blue) shows nuclei. Scale bar, 100 μm. **(B,C)** Quantification of CD45-positive and CD31-positive area/field (n = 4–5 individual hearts/strain, 5 fields/section, and 3 sections/heart) in the infarcted part of the heart shows no significant differences using Mann–Whitney test. **(D)** Myeloperoxidase (MPO) protein *(Continued)*

FIGURE 3 | Continued
levels in heart lysate measured using a multiplex inflammatory protein biomarker panel (n = 10 individual heart lysates/strain). Mann–Whitney test $^*p < 0.05$. **(E)** Immunostaining for Ly6G (yellow) and CD45 (magenta) in the infarcted area of WT and *Vegfr2*$^{Y949F/Y949F}$ hearts at 3 days after MI. Hoechst (blue) shows nuclei. Scale bar, 100 μm. **(F)** Quantification of Ly6G area normalized to CD31 area in the infarcted part of the heart (n = 6–7 individual hearts/strain, 5 fields/section, and 3 sections/heart) shows no significant differences using Mann–Whitney test. For all panels, n refers to biological replicates.

Moreover, the reduced levels of MPO in infarcted heart lysates was not due to reduced basal expression of MPO. In fact, in the mutant, *Mpo* transcript levels were slightly elevated (0.142 DESeqlog2 increase according to statistical analysis of transcript expression, performed in R) in lung tissue from *Vegfr2*$^{Y949F/Y949F}$ compared to wild-type (Li et al., 2016). Thus, these data show that base line levels of MPO expression and of circulating neutrophils were similar in the mutant and wild-type strains. Therefore, we suggest that the lower MPO levels detected in the mutant heart lysates was due to reduced infiltration of neutrophils as a consequence of the improved vascular barrier in the mutant *Vegfr2*$^{Y949F/Y949F}$ strain and not e.g., to congenital changes in MPO expression or neutrophil numbers.

Reduced VE-Cadherin pY685 Levels in the *Vegfr2*$^{Y949F/Y949F}$ Vasculature

To address the mechanisms underlying the vascular barrier properties in the *Vegfr2*$^{Y949F/Y949F}$ vasculature, VEGFA, or as a control, PBS, was injected in the tail-vein of wild-type and mutant mice, followed by harvesting of hearts after different time periods of circulation. Hearts were lysed and samples processed for immunoblotting. Phosphorylation on Y685 in VE-cadherin correlates with vascular permeability (Orsenigo et al., 2012; Wessel et al., 2014; Smith et al., 2020). Levels of pY685 in VE-cadherin in the heart endothelium increased at 2–5 min after VEGFA injection in the wild-type, whereafter it returned to basal levels. In contrast, VE-cadherin phosphorylation remained unaffected in the *Vegfr2*$^{Y949F/Y949F}$ heart endothelium (**Figures 4A,B**). To ensure that VEGFR2 had been activated, samples were probed also with antibodies against pY1173 VEGFR2; the main phosphorylation sites in VEGFR2. As seen in **Figure 4A**, VEGFR2 became phosphorylated in both wild-type and mutant hearts in response to VEGFA. Moreover, downstream signaling pathways involving activation of c-Src, Akt, and Erk1/2 were examined using phosphor-specific antibodies. As seen in **Figures 4C–F**, pY418 c-Src, pT308 Akt, and pT202/Y204 Erk1/2 were induced to wild-type levels or even elevated levels in the *Vegfr2*$^{Y949F/Y949F}$ endothelium, further demonstrating the capacity of the mutant receptor to respond to VEGFA. The elevated responsiveness of the mutant receptor may indicate the establishment of compensatory mechanisms in the mutant strain.

TABLE 1 | Expression of inflammatory markers estimated from Proseek Multiplex CVDI assay on heart lysates after myocardial infarction.

Marker	Abbreviation	Levels[§] in wild-type hearts[#]	Levels in *VEGFR2*$^{Y949F/Y949F}$ *hearts*	*p*-value*
CD40 ligand	CD40L	2.920 ± 0.07	2.959 ± 0.05	0.601
Galectin-3	Gal-3	2.061 ± 0.09	1.942 ± 0.11	0.280
Myeloperoxidase	MPO	0.641 ± 0.04	0.420 ± 0.08	0.017*
β-nerve growth factor	β-NGF	1.832 ± 0.05	2.103 ± 0.35	0.280
Myoglobin	MB	5.216 ± 0.04	5.137 ± 0.04	0.190
Cathepsin D	CTSD	3.677 ± 0.04	3.617 ± 0.05	0.342
Melusin	ITGB1BP2	5.015 ± 0.11	4.994 ± 0.010	0.911
Dickkopf-related protein 1	Dkk-1	0.378 ± 0.05	0.387 ± 0.05	0.962
Heparin-binding EGF-like growth factor	HB-EGF	2.407 ± 0.04	2.422 ± 0.06	0.740
Fatty acid-binding protein, adipocyte	FABP4	2.268 ± 0.053	2.281 ± 0.08	0.684
Follistatin	FS	1.822 ± 0.070	1.695 ± 0.06	0.248

*[#] n = 10 heart lysates for each strain, i.e., 10 individual mice/strain. [§] Protein levels are shown as mean ± SEM and are given in arbitrary units. * p-values < 0.05 were considered significant; Mann–Whitney test.*

DISCUSSION

CVD, mainly MI, remains a major cause of premature death globally. Metabolic diseases such as obesity and diabetes predispose to CVD and while women and young adults previously were spared, the spread of these metabolic diseases combined with sedentary life style patterns now result in broader sections of the population being affected (Low Wang et al., 2016). Treatment of the acute infarction includes coronary angioplasty and stenting, and bypass surgery. A major challenge to those who survive the acute phase, is to restore and retain myocardial function by minimizing myocardial death due to tissue damage. The coronary circulation is vital to maintain optimal cardiomyocyte function (Hausenloy et al., 2019).

The hypothesis underlying the current study was that alleviation of edema in conjunction with MI would decrease tissue damage and allow improved cardiac function, of vital consequence for the long-term outcome after MI. In accordance, we show that genetic interference with the ability of VEGFA/VEGFR2 to mediate increased vascular permeability, correlated with reduced left ventricular edema in mice and improved survival after MI, while coronary vascular density was unaffected (see **Figure 5** for a schematic outline). The MI-challenged mutant *Vegfr2*$^{Y949F/Y949F}$ mice showed better cardiac function with a significant increase in EF, compared to the wild-type littermates. The principal underlying mechanism involved persistent stability of adherens junctions in the presence of VEGFA, as indicated by the reduced phosphorylation of VE-cadherin on Y685 in *Vegfr2*$^{Y949F/Y949F}$ heart ECs in response to VEGFA.

Phosphorylation of VE-cadherin on Y685, correlates with adherens junction disruption and vascular permeability (Wessel et al., 2014). Orsenigo et al. (2012) showed that flow-dependent phosphorylation of Y685 in VE-cadherin occurs in venules and not in arteries, which is agreement with that VEGFA induces permeability in prevenular capillaries and venules but not in arteries (Honkura et al., 2018). c-Src is implicated as the tyrosine kinase responsible for phosphorylation of VE-cadherin. Thus, genetic inactivation or pharmacological suppression of c-Src activity stabilizes endothelial adherens junctions (Weis et al., 2004). In heart lysates, c-Src activity was induced to the same extent or higher in the *Vegfr2*$^{Y949F/Y949F}$ mutant compared to wild-type in response to VEGFA (**Figure 4**), and therefore, we cannot infer from this study that c-Src is responsible for VE-cadherin phosphorylation in the coronary vasculature. However, constitutive *c-Src* gene inactivation is accompanied by reduced edema and improved long-term outcome after MI (Weis et al., 2004) strongly indicating that c-Src indeed phosphorylates VE-cadherin. A caveat in analysis of c-Src activation is the lack of reagents that specifically detects only activated c-Src and not the related Fyn and Yes, thus, it is possible that reduced levels of c-Src activity in the mutant was compensated for by increased Fyn/Yes activities. Moreover, it is known that barrier regulation involves translocation of c-Src to endothelial junctions which can be studied in tissue culture or in whole-mounted tissues (Sun et al., 2012; Li et al., 2016). As the coronary vasculature does not lend itself to whole-mount procedures, the subcellular localization of pY418 c-Src in the coronary endothelium could not be determined.

A limitation in the VE-cadherin analyses performed here, is the use of total organ lysates rather than e.g., isolated ECs. However, isolation of ECs after *in situ* VEGFA stimulation would

TABLE 2 | Peripheral blood cell counts.

Blood cell types	Wild-type[#]	*VEGFR2*$^{Y949F/Y949F}$	*p*-Value*
Red blood cells (×10^{12}/L)	8.72 ± 0.471[§]	8.85 ± 0.126	0.563
White blood cells (×10^{9}/L)	3.32 ± 0.739	3.95 ± 0.780	0.329
◦ Neutrophils (×10^{9}/L)	0.28 ± 0.040	0.40 ± 0.115	0.102
◦ Lymphocytes (×10^{9}/L)	2.86 ± 0.689	3.26 ± 0.730	0.307
◦ Monocytes (×10^{9}/L)	0.08 ± 0.040	0.12 ± 0.069	0.636

*[#] n = 5–6 for wild-type and mutant strains, respectively. [§] Values are shown as mean ± SEM. *There were no significant differences between groups using Mann–Whitney test.*

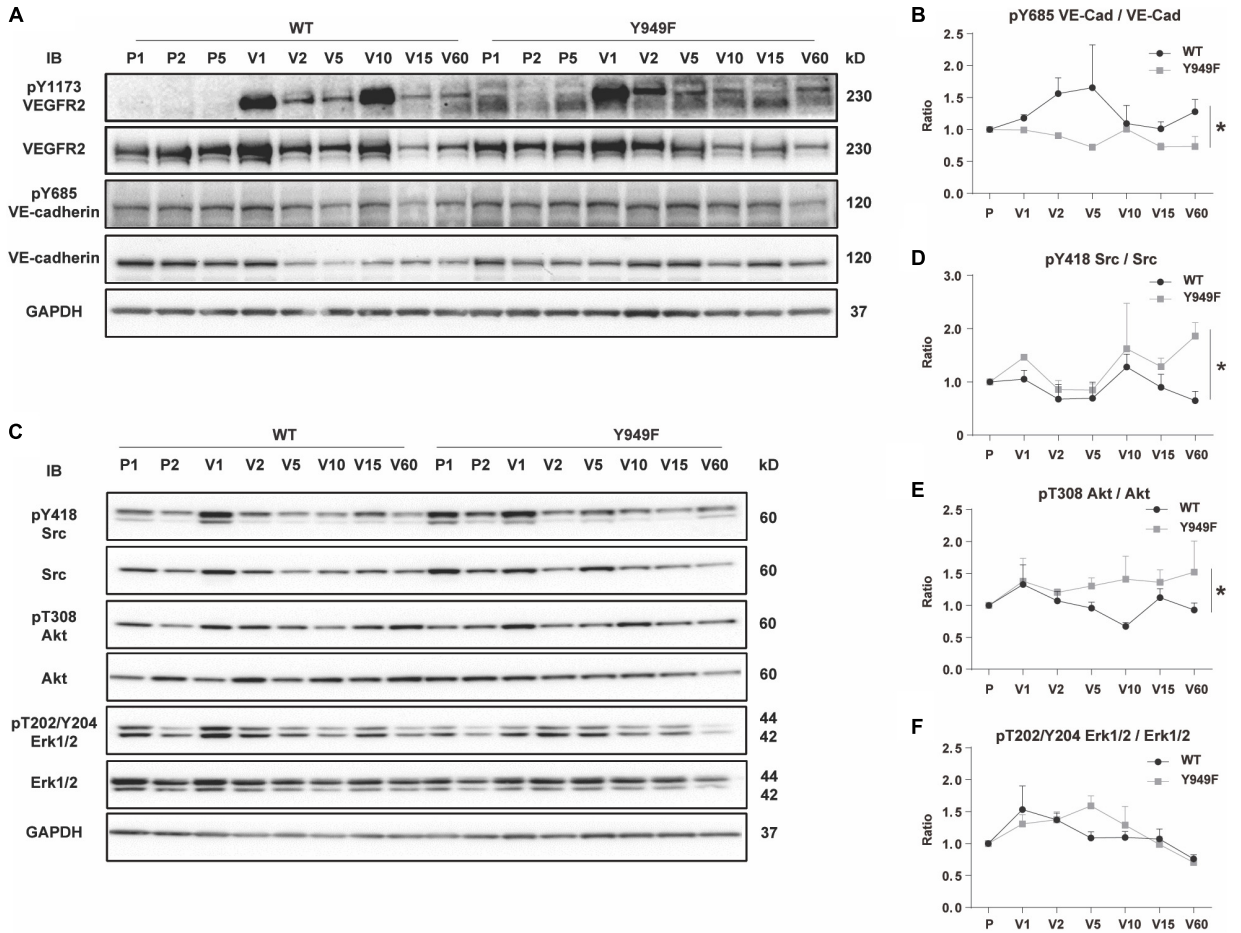

FIGURE 4 | VEGF-induced VE-cadherin pY685 accumulation in hearts. **(A)** Immunoblot for pY1173 VEGFR2 and total VEGFR2, and pY685 VE-cadherin and total VE-cadherin on heart lysates from WT and *Vegfr2*$^{Y949F/Y949F}$ mice. Mice were injected with PBS or VEGFA in the tail-vein, followed by circulation for different time periods; PBS was injected and left to circulate for 1, 2 or 5 min (denoted P1, P2, P5). Alternatively VEGFA was injected and left to circulate for 1, 2, 5 min etc. (denoted V1, V2, V5 etc.). Heart lysates were immunoblotted for 3-phosphate dehydrogenase (GAPDH) as a loading control. **(B)** Quantification of pY685 VE-cadherin normalized to total VE-cadherin in samples shown in **(A)**. **(C)** Immunoblotting for pY418 c-Src and total c-Src, pT308 Akt and total Akt, pT202/Y204 Erk1/2 and total Erk1/2. **(D–F)** Quantification of phosphorylated protein bands normalized to the corresponding total protein. $n = 3$; i.e., three independent replicates of experiments as shown in panel **(A)** with one mouse/time point for each strain and nine mice in total/strain for each experiment. Wilcoxon test, $^*p < 0.05$.

introduce technical issues in maintaining the phosphorylation patterns over the time-consuming isolation procedure. An alternative strategy would be to treat isolated cardiac ECs with VEGFA followed by biochemical analyses. The drawback with this procedure is that the establishment of cells in culture attenuates the organotypic features of the cells. We conclude that, as both VEGFR2 and VE-cadherin are preferentially expressed on ECs and not for example on cardiomyocytes, the analyses performed in this study can be assumed to reflect endothelial-specific regulation of vascular permeability in the heart. Moreover, since the coronary vasculature needs to be studied by sectioning the tissue the degree of stability of the endothelial cell–cell contacts cannot be visualized as for tissues that can be whole-mounted (skin, trachea, mesentery, diaphragm). However, we suggest that based on the reduced LV edema, the reduced fibrinogen/fibrin deposition and the changes in MPO levels and low neutrophil accumulation in the heart, combined with the reduced VE-cadherin phosphorylation on Y685, strongly indicate that the stringency of the vascular barrier is maintained in the mutant tissues including the heart, when exposed to VEGFA. In contrast, exposure to VEGFA leads to barrier breakdown in the wild-type tissues.

The data presented here complement and advance previous studies showing that VEGFA-induced phosphorylation of VE-cadherin is reduced in *Vegfr2*$^{Y949F/Y949F}$ lung ECs, correlating with reduced vascular leakage (Li et al., 2016). We now confirm this pattern in the heart, thus, VEGFA/VEGFR2 regulation of vascular permeability in the coronary vasculature appears to be similar to that in several other organs such as the brain, the pancreas, the heart and the skin. Moreover, as the vascular development, vascular density and morphology for example in the kidney and retina, was unaffected in the *Vegfr2*$^{Y949F/Y949F}$ model (Li et al., 2016), it appears that limiting VEGFA-regulated permeability is dispensable for physiological angiogenesis and

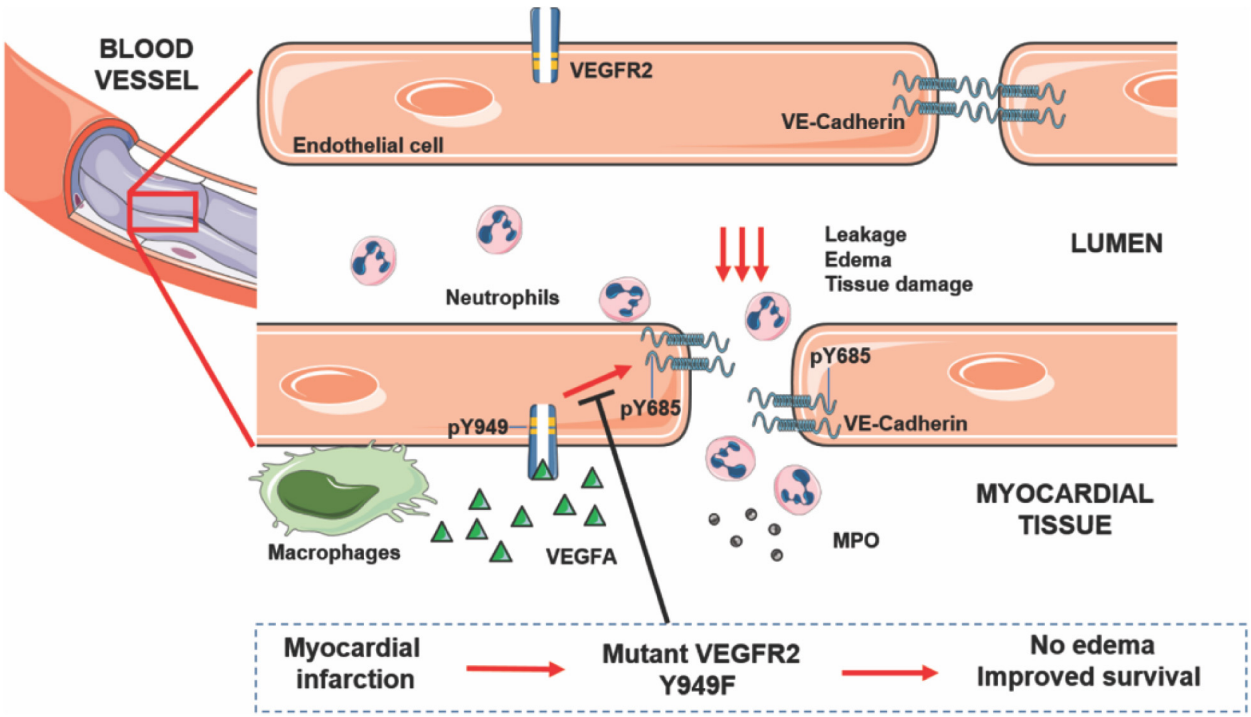

FIGURE 5 | VEGFA/VEGFR2 regulates edema and tissue damage in myocardial infarction. Activation of VEGFR2 on endothelial cells leads to phosphorylation on Y949 and subsequently, phosphorylation of VE-cadherin on Y685, leading to dismantling of adherens junctions and leakage, edema, neutrophil infiltration, MPO release, and tissue damage. Mutation of Y949 in VEGFR2 halts edema and improves survival after myocardial infarction.

inflammation. Of note, infiltration of CD45+ cells was unaffected in the VEGFR2 mutant hearts (cf. **Figure 3**). In agreement, inflammatory cell infiltration in melanoma occurs to the same extent when comparing *Vegfr2*$^{Y949F/Y949F}$ and wild-type mice (Li et al., 2016) and similarly, inflammation accompanying oxygen-induced retinopathy is unaffected by the VEGFR2 mutation (Smith et al., 2020). A fraction of the CD45+ cells infiltration the myocardial tissue after infarction were neutrophils (cf. **Figure 3**), which are highly motile cells. The spread of neutrophil infiltration between individuals was much higher in the wild-type hearts than in the *Vegfr2*$^{Y949F/Y949F}$ hearts, which may be a consequence of the more extensive edema in the wild-type infarcted hearts (cf. **Figure 2**), correlating with the increased demise of wild-type mice (cf. **Figure 1**), compared to the mutants. However, we cannot exclude that the extent of infiltration of subsets of inflammatory cell populations into the infarcted area was affected in the mutant at earlier or later time points after infarction.

We conclude that suppressing vascular permeability in the acute MI phase while preserving other aspects of VEGFR2 functions required e.g., for subsequent formation of collaterals is a highly relevant option for future refined MI treatment.

DATA AVAILABILITY STATEMENT

The RNAseq data was deposited with ArrayExpress: accession E-MTAB-9163. The raw data supporting the conclusions of this article will be made available by the authors, without undue reservation.

ETHICS STATEMENT

The animal study was reviewed and approved by Uppsala University (approval reference number 5.8.18-06789/2018) and Göteborg University Animal Ethics Committees.

AUTHOR CONTRIBUTIONS

XL and LC-W devised the project and the main conceptual ideas, and composed the manuscript. BR, MS, and ML performed the cardiovascular tests. XL, MS-J, SS, NP, and PM performed the biochemical and cell biological assays. XL, MS-J and ML performed the data analyses. All authors commented and approved the text.

FUNDING

This work was supported by Stiftelsen för internationalisering av högre utbildning och forskning (STINT; CH2018-7817), the Swedish Research Council (2015-02375) to LC-W, and (2017-01340) to ML; the Knut and Alice Wallenberg Foundation project grant (KAW 20150030) and a Wallenberg Scholar grant (KAW 2015.0275) to LC-W;

Fondation Leducq Transatlantic Network of Excellence Grant in Neurovascular Disease (17 CVD 03) to LC-W; the Heart and Lung Foundation (20170482) to ML; the National Natural Science Foundation of China (81773081) to XL.

ACKNOWLEDGMENTS

We gratefully acknowledge the expert assistance of Marie Hedlund, Uppsala University.

REFERENCES

Andersson, L., Scharin Tang, M., Lundqvist, A., Lindbom, M., Mardani, I., Fogelstrand, P., et al. (2015). Rip2 modifies VEGF-induced signalling and vascular permeability in myocardial ischaemia. *Cardiovasc. Res.* 107, 478–486. doi: 10.1093/cvr/cvv186

Aratani, Y. (2018). Myeloperoxidase: its role for host defense, inflammation, and neutrophil function. *Arch. Biochem. Biophys.* 640, 47–52. doi: 10.1016/j.abb.2018.01.004

Bhullar, K. S., Lagaron, N. O., McGowan, E. M., Parmar, I., Jha, A., Hubbard, B. P., et al. (2018). Kinase-targeted cancer therapies: progress, challenges and future directions. *Mol. Cancer* 17:48.

Davalos, D., Ryu, J. K., Merlini, M., Baeten, K. M., Le Moan, N., Petersen, M. A., et al. (2012). Fibrinogen-induced perivascular microglial clustering is required for the development of axonal damage in neuroinflammation. *Nat. Commun.* 3:1227.

Dejana, E., Orsenigo, F., and Lampugnani, M. G. (2008). The role of adherens junctions and VE-cadherin in the control of vascular permeability. *J. Cell Sci.* 121(Pt 13), 2115–2122. doi: 10.1242/jcs.017897

Drevinge, C., Dalen, K. T., Mannila, M. N., Tang, M. S., Stahlman, M., Klevstig, M., et al. (2016). Perilipin 5 is protective in the ischemic heart. *Int. J. Cardiol.* 219, 446–454.

Dvorak, H. F. (2002). Vascular permeability factor/vascular endothelial growth factor: a critical cytokine in tumor angiogenesis and a potential target for diagnosis and therapy. *J. Clin. Oncol.* 20, 4368–4380. doi: 10.1200/jco.2002.10.088

Ebos, J. M., Lee, C. R., and Kerbel, R. S. (2009). Tumor and host-mediated pathways of resistance and disease progression in response to antiangiogenic therapy. *Clin. Cancer Res.* 2009, 5020–5025. doi: 10.1158/1078-0432.ccr-09-0095

Ferrara, N., and Adamis, A. P. (2016). Ten years of anti-vascular endothelial growth factor therapy. *Nat. Rev.* 15, 385–403. doi: 10.1038/nrd.2015.17

Garcia, R., Bouleti, C., Sirol, M., Logeart, D., Monnot, C., Ardidie-Robouant, C., et al. (2019). VEGF-A plasma levels are associated with microvascular obstruction in patients with ST-segment elevation myocardial infarction. *Int. J. Cardiol.* 291, 19–24. doi: 10.1016/j.ijcard.2019.02.067

Halder, S. K., and Milner, R. (2020). Chronic mild hypoxia accelerates recovery from preexisting EAE by enhancing vascular integrity and apoptosis of infiltrated monocytes. *Proc. Natl. Acad. Sci. U.S.A.* 117, 11126–11135. doi: 10.1073/pnas.1920935117

Hausenloy, D. J., Chilian, W., Crea, F., Davidson, S. M., Ferdinandy, P., Garcia-Dorado, D., et al. (2019). The coronary circulation in acute myocardial ischaemia/reperfusion injury: a target for cardioprotection. *Cardiovasc. Res.* 115, 1143–1155. doi: 10.1093/cvr/cvy286

Holst, H., Edqvist, L. E., Kindahl, H., and Rylander, R. (1994). Hematological, blood biochemical, and cytological bronchoalveolar lavage studies in prepubertal gilts after endotoxin inhalation and ingestion. *Zentralbl. Veterinarmed. A* 41, 159–166. doi: 10.1111/j.1439-0442.1994.tb00079.x

Honkura, N., Richards, M., Lavina, B., Sainz-Jaspeado, M., Betsholtz, C., and Claesson-Welsh, L. (2018). Intravital imaging-based analysis tools for vessel identification and assessment of concurrent dynamic vascular events. *Nat. Commun.* 9:2746.

Kajdaniuk, D., Marek, B., Borgiel-Marek, H., and Kos-Kudla, B. (2011). Vascular endothelial growth factor (VEGF) - part 1: in physiology and pathophysiology. *Endokrynol. Pol.* 62, 444–455.

Li, X., Padhan, N., Sjostrom, E. O., Roche, F. P., Testini, C., Honkura, N., et al. (2016). VEGFR2 pY949 signalling regulates adherens junction integrity and metastatic spread. *Nat. Commun.* 7:11017.

Low Wang, C. C., Hess, C. N., Hiatt, W. R., and Goldfine, A. B. (2016). Clinical update: cardiovascular disease in diabetes mellitus: atherosclerotic cardiovascular disease and heart failure in type 2 diabetes mellitus - mechanisms, management, and clinical considerations. *Circulation* 133, 2459–2502. doi: 10.1161/circulationaha.116.022194

Matsumoto, T., Bohman, S., Dixelius, J., Berge, T., Dimberg, A., Magnusson, P., et al. (2005). VEGF receptor-2 Y951 signaling and a role for the adapter molecule TSAd in tumor angiogenesis. *EMBO J.* 24, 2342–2353. doi: 10.1038/sj.emboj.7600709

Ndrepepa, G. (2019). Myeloperoxidase - A bridge linking inflammation and oxidative stress with cardiovascular disease. *Clin. Chim. Acta* 493, 36–51. doi: 10.1016/j.cca.2019.02.022

Orsenigo, F., Giampietro, C., Ferrari, A., Corada, M., Galaup, A., Sigismund, S., et al. (2012). Phosphorylation of VE-cadherin is modulated by haemodynamic forces and contributes to the regulation of vascular permeability in vivo. *Nat. Commun.* 3:1208.

Paez-Ribes, M., Allen, E., Hudock, J., Takeda, T., Okuyama, H., Vinals, F., et al. (2009). Antiangiogenic therapy elicits malignant progression of tumors to increased local invasion and distant metastasis. *Cancer Cell* 15, 220–231. doi: 10.1016/j.ccr.2009.01.027

Simons, M., Gordon, E., and Claesson-Welsh, L. (2016). Mechanisms and regulation of endothelial VEGF receptor signalling. *Nat. Rev. Mol. Cell Biol.* 17, 611–625. doi: 10.1038/nrm.2016.87

Smith, R. O., Ninchoji, T., Gordon, E., Andre, H., Dejana, E., Vestweber, D., et al. (2020). Vascular permeability in retinopathy is regulated by VEGFR2 Y949 signaling to VE-cadherin. *eLife* 9:e54056.

Sun, Z., Li, X., Massena, S., Kutschera, S., Padhan, N., Gualandi, L., et al. (2012). VEGFR2 induces c-Src signaling and vascular permeability in vivo via the adaptor protein TSAd. *J. Exp. Med.* 209, 1363–1377. doi: 10.1084/jem.20111343

Weis, S., Shintani, S., Weber, A., Kirchmair, R., Wood, M., Cravens, A., et al. (2004). Src blockade stabilizes a Flk/cadherin complex, reducing edema and tissue injury following myocardial infarction. *J. Clin. Invest.* 113, 885–894. doi: 10.1172/jci200420702

Wessel, F., Winderlich, M., Holm, M., Frye, M., Rivera-Galdos, R., Vockel, M., et al. (2014). Leukocyte extravasation and vascular permeability are each controlled *in vivo* by different tyrosine residues of VE-cadherin. *Nat. Immunol.* 15, 223–230. doi: 10.1038/ni.2824

Conflict of Interest: The authors declare that the research was conducted in the absence of any commercial or financial relationships that could be construed as a potential conflict of interest.

frontiers in Physiology

REVIEW
published: 22 July 2020
doi: 10.3389/fphys.2020.00842

Endothelial Cell Dynamics in Vascular Development: Insights From Live-Imaging in Zebrafish

Kazuhide S. Okuda[1,2] *and Benjamin M. Hogan*[1,2,3]*

[1] Organogenesis and Cancer Program, Peter MacCallum Cancer Centre, Melbourne, VIC, Australia, [2] Sir Peter MacCallum Department of Oncology, University of Melbourne, Melbourne, VIC, Australia, [3] Department of Anatomy and Neuroscience, University of Melbourne, Melbourne, VIC, Australia

The formation of the vertebrate vasculature involves the acquisition of endothelial cell identities, sprouting, migration, remodeling and maturation of functional vessel networks. To understand the cellular and molecular processes that drive vascular development, live-imaging of dynamic cellular events in the zebrafish embryo have proven highly informative. This review focusses on recent advances, new tools and new insights from imaging studies in vascular cell biology using zebrafish as a model system.

Keywords: vasculogenesis, angiogenesis, lymphangiogenesis, anastomosis, endothelial cell, zebrafish

OPEN ACCESS

Edited by:
Elizabeth Anne Vincent Jones, KU Leuven, Belgium

Reviewed by:
Anna Rita Cantelmo, Université Lille Nord de France, France
Jingjing Zhang, Affiliated Hospital of Guangdong Medical University, China

***Correspondence:**
Benjamin M. Hogan
ben.hogan@petermac.org

Specialty section:
This article was submitted to Vascular Physiology, a section of the journal Frontiers in Physiology

Received: *08 April 2020*
Accepted: *23 June 2020*
Published: *22 July 2020*

Citation:
Okuda KS and Hogan BM (2020) Endothelial Cell Dynamics in Vascular Development: Insights From Live-Imaging in Zebrafish. Front. Physiol. 11:842. doi: 10.3389/fphys.2020.00842

INTRODUCTION

Vascular development is an early and essential process in the formation of a viable vertebrate embryo. Blood and lymphatic vascular networks are composed of a complex mix of cell types: for example smooth muscle cells, fibroblasts, pericytes and immune cells are intimately associated and even integrated within mature vessel walls (Rouget, 1873; Horstmann, 1952; Nicosia and Madri, 1987; Fantin et al., 2010; Gordon et al., 2010). The inner lining of the vasculature, made up of endothelial cells (ECs), is the earliest part of the vasculature to develop in the embryo and is instructive in recruiting other lineages and cell types as the vascular system matures. Vascular ECs derive from the mesoderm of the gastrula stage embryo and specifically from the lateral plate mesoderm (LPM) (Sabin, 1920; Coffin and Poole, 1988; Zhong et al., 2001). The process by which early undifferentiated mesoderm is progressively restricted in its fate to form ECs has fascinated developmental biologists for decades.

Early studies of developing ECs relied heavily on genetics and lineage tracing approaches in mice and uncovered a wealth of information about how the vasculature forms (reviewed in detail elsewhere; Eilken and Adams, 2010; Welti et al., 2013). However, more recently researchers have begun to delve into the cellular behaviors that drive EC development and to appreciate the importance of cell dynamics in shaping vascular development in the embryo. One especially useful system for studying spatiotemporal events at a cellular level is the zebrafish, which has become a standard model to investigate how the vasculature develops. The use of zebrafish has demonstrated new gene functions and molecular mechanisms that are highly conserved in mammals, including uncovering mechanisms of disease (Hogan and Schulte-Merker, 2017). This field has benefited from significant technological advances that improve the model's utility for the study of EC biology *in vivo*. New cellular labels have been developed (see **Table 1**), new imaging modalities applied and the increasing use of biosensors to dissect key cell biological processes has opened up exciting new possibilities. In this review, we investigate recent studies that have used dynamic imaging and *in vivo* cell biology to understand EC development in zebrafish. We highlight key

technical achievements and new biology uncovered, we will also give a broad overview of the current toolbox available and we briefly describe potential new future directions.

CELL BEHAVIOR AND REGULATION OF VASCULOGENESIS

Vascular development is typically thought of as occurring in a stepwise manner progressing through vasculogenesis, angiogenesis, lymphangiogenesis, vessel remodeling, and maturation. Vasculogenesis involves the initial formation of the major vessels in the embryonic midline from angioblasts that originate in the LPM (Risau and Flamme, 1995). In zebrafish, this process begins at about 12 h post-fertilization (hpf) and concludes by around 22 hpf with formation of a medial vascular rod (Fouquet et al., 1997; Sumoy et al., 1997). The genetic control of this process has been well defined and is driven by neuronal PAS domain protein 4 like (Npas4l), which is the master regulator of angioblast specification in zebrafish (Reischauer et al., 2016). Npas4l is a transcription factor that regulates expression of early angioblast and endothelial markers *ets1-related protein* (*etv2*), *T-cell acute lymphocytic leukemia 1* (*tal1)* and *fli1 proto-oncogene, ETS transcription factor a (fli1a)*. In addition to genetic analyses, recent studies have used dynamic imaging of cell behavior as angioblasts migrate to the midline to give rise to the dorsal aorta (DA) and the posterior cardinal vein (PCV).

The origin of angioblast cell populations has been a matter of debate: it was unclear if distinct angioblast populations in the LPM are pre-determined as progenitors of the DA and PCV, or if all LPM EC progenitors share the same potential. Using live-imaging of angioblast migration during vasculogenesis with a *Tg(etv2:EGFP)*^{ci1} transgenic line, Kohli and colleagues observed that two distinct medial and lateral angioblast pools migrate to the midline separately and sequentially (Kohli et al., 2013). Using *Tg(etv2:kaede)*^{ci6}, the angioblast populations could be labeled in a spatially and temporally controlled manner with Kaede (a photoconvertible protein; Ando et al., 2002) and dynamically imaged. This revealed that the medial angioblasts, that migrate to the midline first, predominantly give rise to the DA ECs. The lateral angioblasts, arise later and migrate to the midline to give rise to the PCV ECs (Kohli et al., 2013). A similar observation was made by Helker et al. (2013) when *fli1a*-positive angioblasts were live imaged and lineage traced during vasculogenesis. This demonstrated that the dynamic staging of arterial and venous LPM migration is different and suggests a very early difference between DA- and PCV-generating angioblasts that had not been earlier appreciated. Consistent with these data, lineage tracing of early angioblasts using a *Tg(tp1:creert2)*^{ih12}*;Tg(fli1ep:loxP-nblue-loxP;mcherry)*^{um43} transgenic line to label Notch-signaling active ECs, revealed that all Notch active early angioblasts contribute to the DA but not the PCV (Quillien et al., 2014). Similarly, early angioblasts of the arterial system have since been shown to have highly active Erk signaling, suggesting signaling differences in future arterial and venous angioblasts as they depart the LPM (Shin et al., 2016a).

It was long hypothesized that Vascular endothelial growth factor a (Vegfa)/Kdrl (one of two zebrafish VEGFR ohnologs functionally similar to VEGFR2) signaling is essential for angioblast migration (Shalaby et al., 1995; Ferrara et al., 1996). In the zebrafish, notochord-derived Sonic Hedgehog induces *vegfa* expression in the ventral somite, which was proposed to guide angioblast migration toward the midline (Lawson et al., 2002). However, vasculogenesis ensues in both *vegfaa* and *kdrl* mutant zebrafish (Helker et al., 2015; Rossi et al., 2016). In an elegant study that utilized dynamic time-lapse imaging of angioblast migration, Helker and colleagues found that Apelin receptor a (Aplnra), Apelin receptor b (Aplnrb) and a peptide hormone Elabela (Ela) (which binds to Aplnr's in zebrafish; Chng et al., 2013; Pauli et al., 2014) are required for angioblast migration to the midline (Helker et al., 2015). Angioblasts fail in medial migration in the absence of these key signaling components, while still displaying active filopodial extensions. When *ela* was ectopically overexpressed in notochord mutants lacking *ela* expression, angioblasts preferably migrated toward cells overexpressing *ela*, confirming Elabela as a novel regulator of angioblast medial migration (Helker et al., 2015).

Studies of the dynamic process of angioblast migration from the LPM have significantly improved our understanding of vasculogenesis, yet much remains to be understood. Recently, lineage tracing somite cells using the Kaede protein and Cre/loxP technology revealed that a subset of somite cells termed endotome give rise to angioblasts that colonize the DA (Nguyen et al., 2014). How this movement of cells from the early somite generates angioblasts as a developmental spatio-temporal sequence, requires further investigation. Furthermore, studies have shown that Notch active angioblasts can later give rise to both arterial and venous intersegmental vessels (ISVs), following their incorporation into the DA (Quillien et al., 2014) and movement of ECs can occur between the arterial and venous cords following medial migration in both zebrafish and in mice (Herbert et al., 2009; Lindskog et al., 2014). These studies suggest ongoing refinements following vasculogenesis that remain to be fully understood. Interestingly, late forming angioblasts have been shown to contribute to caudal vasculature between 25 and 29 hpf, after vasculogenesis in the trunk is complete (Fukuhara et al., 2014). In the head, a population of late forming angioblasts have also been found to colonize both lymphatic and arterial vessels (Eng et al., 2019). These studies suggest that apart from LPM and endotome, additional sources of angioblasts may exist to support development of some specific late-forming vessels.

CELLULAR AND SIGNALING MECHANISMS IN PRIMARY ANGIOGENESIS

Once the DA and the PCV are formed at around 22 h post-fertilization, ECs sprout from the DA and migrate to form the ISVs, a process termed primary angiogenesis (Isogai et al., 2003). In this section, recent studies that use live imaging to elucidate EC behavior and signaling dynamics during primary angiogenesis are discussed.

TABLE 1 | A toolbox for zebrafish vascular cell biology and selection of recent findings.

Endothelial cell biology applications	Transgenic line name/s	Specific applications for transgenic	Recent biological insights using this strain	References
Cell lineage tracing reporters	*TgBAC(etv2:kaede)*^{ci6}	Lineage tracing of angioblasts	Distinct populations of angioblasts give rise to endothelial cells of either the dorsal aorta or the posterior cardinal vein. Angioblasts that originate near the ventral aorta give rise to facial lymphatic endothelial cells. Posterior cardinal vein angioblasts give rise to endothelial cells of the intestinal vessels.	Kohli et al., 2013; Koenig et al., 2016; Eng et al., 2019
	Tg(msgn1:NLS-Kaede)^{pc8} *Tg(msgn1:Cre-ERT2)*^{pc9}; *Tg(actb2:LOXP-AcGFP1-LOXP-mCherry)*^{pc18}	Lineage tracing of somitic origins of endothelial cells	A subset of somite cells (endotome) give rise to angioblasts.	Nguyen et al., 2014
	Tg(EPV.Tp1-Ocu.Hbb2:CreERT2)^{jh12}; *Tg(fli1:LOXP-Cerulean-Hsa.HIST1H2BJ-LOXP,mCherry)*^{um43}	Lineage tracing Notch-active angioblasts	Notch active angioblasts give rise to dorsal aorta endothelial cells but not posterior cardinal vein endothelial cells.	Wang et al., 2011; Quillien et al., 2014
	Tg(EPV.TP1-Mmu.Hbb:Kaede)^{um15}	Lineage tracing Notch-active endothelial cells	Notch active endothelial cells early in development can give rise to both arterial intersegmental vessel and venous intersegmental vessel endothelial cells. Notch signaling is active specifically in arterial intersegmental vessels even before they anastomose with secondary sprouts to form mature vessels.	Clements et al., 2011; Quillien et al., 2014; Geudens et al., 2019
	Tg(kdrl:NLS-Eos)^{ncv6} *Tg(Kdrl:Dendra2)*^{cq52} *Tg(fli1a:Gal4FF)*^{ubs3}; *Tg(UAS:Kaede)*^{rk8}	Lineage tracing blood vascular endothelial cells	Intersegmental vessel tip cell mitosis results in generation of daughter cells with different size. Later forming angioblasts (25–29 hpf) give rise to endothelial cells in the caudal vessel. Arterial endothelial cells in venous intersegmental vessels migrate dorsally against the flow after secondary sprout anastomosis and are replaced by posterior cardinal vein endothelial cells. Ventral posterior cardinal vein endothelial cells give rise to parachordal lymphatic endothelial cells. Ventral posterior cardinal vein angioblasts give rise to both arterial and venous intestinal vessels.	Hatta et al., 2006; Zygmunt et al., 2011; Fukuhara et al., 2014; Hen et al., 2015; Nicenboim et al., 2015; Costa et al., 2016; Tian et al., 2017; Weijts et al., 2018
	Tg(lyve1b:Kaede)^{nz102}	Lineage trace ventral aorta angioblasts, and venous/lymphatic endothelial cells	Angioblasts that originate near the ventral aorta give rise to the lymphatic endothelial cells of the facial lymphatics and endothelial cells of the hypobranchial artery.	Eng et al., 2019
Notch signaling reporters	*Tg(tp1-MmHbb:EGFP)*^{um14}	Detection of Notch active cells	A subset of angioblasts is Notch active. The tip cell of the venous primordial midbrain channel sprout becomes Notch active prior to fusing with the Notch active arterial system.	Parsons et al., 2009; Quillien et al., 2014; Kaufman et al., 2015; Hasan et al., 2017
	Tg(EPV.Tp1-Mmu.Hbb.d2GFP)^{mw43} *Tg(EPV.TP1-Mmu.Hbb:Venus-Mmu.Odc1)*^{s940}	Dynamic detection of Notch active cells.	Arterial blood flow promotes Notch signaling in arterial intersegmental vessels. Notch signaling in arterial intersegmental vessel prevents it from secondary sprout anastomoses. The tip cell of venous primordial midbrain channel sprout becomes Notch active prior to fusing with the Notch active arterial system.	Clark et al., 2012; Ninov et al., 2012; Hasan et al., 2017; Weijts et al., 2018

(Continued)

TABLE 1 | Continued

Endothelial cell biology applications	Transgenic line name/s	Specific applications for transgenic	Recent biological insights using this strain	References
	TgBAC(dll4:GAL4FF)^{mu106}*;Tg(5xUAS:EGFP)*^{nkuasgfp1a}*; Tg(EPV.TP1-Mmu.Hbb:hist2h2l-mCherry)*^{s939}	Simultaneous visualization of *dll4* transcription and Notch activation	*dll4* expression is initiated at the tip cell of venous primordial midbrain channel sprout before it becomes Notch active.	Ninov et al., 2012; Hasan et al., 2017
Ca^{2+} signaling reporters	*Tg(10.5xUAS:GCaMP5G)*^{uq2} *Tg(UAS:GCaMP7a)*^{zf415} *Tg(UAS:GCaMP7a)*^{sh392} *Tg(UAS:GCaMP3)*^{zf350} *Tg(Tol2 fliEbasP::mCherry V2A GCaMP6m)*^{ric100}	Visualization of Ca^{2+} signaling	Intersegmental vessel tip cells show Ca^{2+} oscillation that is Vegfa/Kdr/Kdrl-signaling dependent. Intersegmental vessel stalk cells also show Ca^{2+} oscillation. Ca^{2+} oscillation patterns correlate with intersegmental vessel endothelial cell migration and proliferation potential. Calcium signaling increases as dorsal aorta endothelial cells mature. Tmem33 is required for tip endothelial cell Ca^{2+} signaling. The degree of flow-mediated endothelial primary cilia deflection correlates with increased calcium signaling in the dorsal aorta.	Warp et al., 2012; Muto et al., 2013; Goetz et al., 2014; Kita et al., 2015; Yokota et al., 2015; Noren et al., 2016; Lagendijk et al., 2017; Savage et al., 2019
Endothelial cell junction cytoskeleton reporter	*Tg(fli1:LIFEACT-EGFP)*^{zf495} *Tg(fli1:LIFEACT-EGFP)*^{mu240} *Tg(fli1:LIFEACT-mClover)*^{sh467} *Tg(UAS:LIFEACT-GFP)*^{mu271} *Tg(4xUAS:Has.UTRN-EGFP)*^{ubs18}	Visualize F-actin polymerization on F-actin-based structures in endothelial cells such as filopodia and endothelial cell junctions	Filopodia are not required for endothelial cell migration but are essential for tip cell anastomosis. Initial contact site of filopodia (junctional spot) and junctional rings on endothelial cells have high F-actin polymerization. F-actin polymerization is required for retraction of blebs during intersegmental vessel lumenization. Dorsal aorta endothelial cells align in the direction of flow as the dorsal aorta matures. Dynamic F-actin polymerization is observed at the Kuglen "neck." Arterial endothelial cells in venous intersegmental vessels migrate dorsally against the flow after secondary sprout anastomosis and is replaced by posterior cardinal vein endothelial cells. The common cardinal vein lumenize via lumen ensheathment. The lumen and flow are maintained when endothelial cells in multicellular tube divide. Endothelial cells form multicellular tubes using junction-based lamellipodia.	Helker et al., 2013; Phng et al., 2013; Sauteur et al., 2014; Aydogan et al., 2015; Gebala et al., 2016; Hamm et al., 2016; Sauteur et al., 2017; Sugden et al., 2017; Paatero et al., 2018; Weijts et al., 2018; Kugler et al., 2019; Savage et al., 2019
	Tg(4XUAS:mClavGR2-Has.UTRN)^{ubs27}	Lineage trace endothelial cell junctions	Endothelial cells form multicellular tubes using junction-based lamellipodia.	Paatero et al., 2018
Endothelial cell junctional protein reporter	*Tg(14XUAS:EGFP-Hsa.TJP1,myl7:EGFP)*^{ubs5} *Tg(5XUAS:cdh5-EGFP)*^{ubs12} *Tg(fli1:pecam1-EGFP)*^{ncv27}	Visualize ZO1, Ve-cadherin, or Pecam1 localization in endothelial cell junctions.	Junctional spots and junctional rings on endothelial cells have high level of ZO1 and Ve-cadherin. The lumen and flow are maintained when endothelial cells in multicellular tube divide. Endothelial cells form multicellular tubes using junction-based lamellipodia. Intersegmental vessels that remain arterial have a multicellular intersegmental vessel base while intersegmental vessels that will become venous intersegmental vessel have a unicellular base.	Herwig et al., 2011; Lenard et al., 2013; Aydogan et al., 2015; Ando et al., 2016; Paatero et al., 2018; Geudens et al., 2019

(Continued)

TABLE 1 | Continued

Endothelial cell biology applications	Transgenic line name/s	Specific applications for transgenic	Recent biological insights using this strain	References
Endothelial cell junctional tension sensor	*Tg(cdh5:cdh5-TFP-TENS-Venus)*^{uq11bh}	Quantification of Ve-cadherin tension in endothelial cell junctions	Dorsal aorta endothelial cell junctional tension decreases as the dorsal aorta mature.	Lagendijk et al., 2017
Endothelial cell membrane reporter	*Tg(kdrl:HsHRAS-mCherry)*^{s916} *Tg(fli1:EGFP-CAAX)*^{md13} *Tg(kdrl:mCherry-CAAX)*^{y171}	Visualize EC membrane and filopodia	Lumenization in the intersegmental vessel is flow-dependent. Cerebral vessels form transient Kuglen structure. Filopodia is not required for endothelial cell migration but is essential for tip cell anastomosis. Initial contact site of filopodia (junctional spot) and junctional rings on endothelial cells have high F-actin polymerization. Lumenization in the intersegmental vessel occur through inverse blebbing. Immature cranial vessels are enriched with primary cilia.	Chi et al., 2008; Fujita et al., 2011; Phng et al., 2013; Gebala et al., 2016; Eisa-Beygi et al., 2018; Kugler et al., 2019
Endothelial cell apical membrane reporter	*Tg(fli1:Has.PLCD1-RFP)*^{md14}	Visualize endothelial cell apical membrane	Lumenization in the intersegmental vessel occur through inverse blebbing.	Gebala et al., 2016
Endothelial cell golgi reporter	*Tg(fli1:Hsa.B4GALT1-mCherry)*^{bns9}	Visualize endothelial cell polarity	Endothelial cells polarize against flow when blood flow is initiated. Arterial endothelial cells in venous intersegmental vessels migrate dorsally against the flow after secondary sprout anastomosis and is replaced by posterior cardinal vein endothelial cells. The difference in endothelial cell polarity between venous intersegmental vessel and arterial intersegmental vessel endothelial cells is pre-determined prior to secondary sprout anastomosis.	Kwon et al., 2016; Weijts et al., 2018; Geudens et al., 2019
Primary cilia reporter	*Tg(actb2:Arl13b-GFP)*^{hsc5}	Visualize primary cilia	Immature cranial vessels are enriched with primary cilia. The degree of flow-mediated endothelial primary cilia deflection correlates with increased calcium signaling in the dorsal aorta.	Borovina et al., 2010; Goetz et al., 2014; Eisa-Beygi et al., 2018
Lymphatic endothelial cell fate reporter	*TgBAC(prox1a:KALTA4,4xUAS-E1B:TagRFP)*^{nim5}	Visualize *prox1a* expression in endothelial cells	*prox1a*-positive endothelial cells in the posterior cardinal vein undergo mitosis giving rise to a daughter endothelial cell which retains *prox1a* expression and sprout out of the posterior cardinal vein, and a daughter endothelial cell that lose *prox1a* expression and remain in the posterior cardinal vein.	Dunworth et al., 2014; Koltowska et al., 2015; Nicenboim et al., 2015
Hyaluronic acid reporter	*Tg(ubb:SEC-Rno.Ncan-EGFP)*^{uq25bh}	Visualize hyaluronic acid localization	Hyaluronic acid turnover in the extracellular matrix is essential for proper Vegfa/Kdr/Kdrl signaling during primary angiogenesis.	De Angelis et al., 2017; Grassini et al., 2018
Cell cycle progression reporter	*Tg(kdrl:mVenus-gmnn)*^{ncv3}	Visualize endothelial cells in the S/G2/M phase	Intersegmental vessel endothelial cells leaving the dorsal aorta are in the S/G2/M phase and undergo division shortly after.	Fukuhara et al., 2014
Endothelial cell nuclear reporter	*Tg(fli1:nEGFP)*^{y7} *Tg(kdrl:nlsmCherry)*^{is4} *Tg(kdrl:nlsEGFP)*^{ubs1}	Visualize EC nucleus	These transgenic lines are widely used to visualize endothelial cell sprouting, migration, division and anastomosis at single cell resolution.	Roman et al., 2002; Blum et al., 2008; Wang et al., 2010

The interplay between Notch and Vegfa/Kdr/Kdrl pathways is essential for proper angiogenic sprouting and the determination of tip/stalk cell identity in sprouting ECs. Vegfa/Kdr/Kdrl signaling induces EC sprouting from the DA, and also stimulates expression of Notch ligand *dll4* in tip cells (Lobov et al., 2007; Jakobsson et al., 2010; Ubezio et al., 2016). This in turn *trans*-activates Notch signaling in trailing stalk cells, which suppresses Vegfa/Kdr/Kdrl signaling (Hellstrom et al., 2007; Leslie et al., 2007; Siekmann and Lawson, 2007; Suchting et al., 2007). This signaling interplay is crucial in angiogenesis but still remains to be understood as a molecular mechanism acting in concert with dynamic cellular behaviors.

One significant insight into tip cell behaviors came from direct imaging of vascular Ca^{2+} during angiogenesis. Yokota and colleagues generated the *Tg(fli1a:Gal4FF)*^{ubs4}*;Tg(UAS:GCaMP7a)*^{zf415} transgenic line, which expresses a Ca^{2+} indicator in ECs (Muto et al., 2013; Yokota et al., 2015). Timelapse imaging revealed that ECs actively budding from the DA display dynamic Ca^{2+} oscillations (**Figure 1**; Yokota et al., 2015). These oscillations were found to be Vegfa/Kdr/Kdrl signaling dependent, indicating that this model serves as a sensor for Vegfa/Kdr/Kdrl signaling. In this context, it was observed that when neighboring ECs prepare to sprout from the DA, both the sprouting and non-sprouting ECs display Ca^{2+} oscillations. Active Ca^{2+} signaling is only maintained by the EC that sprouts, identifying a previously unappreciated dynamic tip cell selection event. In an additional unexpected turn, high speed imaging revealed that stalk cells also showed Ca^{2+} oscillations as they departed the DA following tip cells. Ca^{2+} signaling increased in intensity as the stalk cells migrated away from the DA (**Figure 1**). Patterned Ca^{2+} oscillations also occur in cultured mammalian cells and are dependent on VEGFA levels, correlating with distinct EC migration behaviors and proliferation potential *in vitro* (Noren et al., 2016). Savage and colleagues recently showed that transmembrane protein 33 (Tmem33) is required for Ca^{2+} oscillations in sprouting ISV ECs. Tmem33 functions downstream of the Vegfa/Kdr/Kdrl pathway to regulate Notch signaling and Erk phosphorylation (Savage et al., 2019). The precise function of oscillatory Ca^{2+} signaling in angiogenesis remains unclear, but these observations indicate signaling events that correlate with cell behaviors during angiogenic sprouting, while not fitting a simple model of high signaling in tip- and low signaling in stalk-cells. Better live imaging of dynamic signaling events and integration of observations with existing models of tip-stalk cell cross talk is clearly needed.

Live imaging has been used to probe the role of cell cycle progression in primary angiogenesis and revealed links between cell cycle, cell divisions and angiogenic signaling. Using the *Tg(kdrl:mVenus-gmnn)*^{ncv3} transgenic line, ECs were fluorescently labeled as they progress through S/G2/M phase of the cell cycle (Fukuhara et al., 2014). This revealed that the majority of ECs that sprout are in the S/G2/M phase as they emerge from the DA and then undergo cell division shortly after sprouting, potentially coupling cell cycle state with cell spouting behaviors. Costa and colleagues live imaged this cell-division event using a transgenic marker that labeled EC nuclei and noticed that tip cells undergo a distinctive cell division event which is followed by a seamless reestablishment of tip/stalk cell hierarchy and motility (Costa et al., 2016). Surprisingly, this was not driven by Notch signaling. Dynamic imaging using a photoconvertible *Tg(kdrl:nlsEos)*^{ncv6} transgenic and a GFP-tagged alpha tubulin construct revealed differences in daughter cell size post tip-cell mitosis that were due to asymmetric cytoplasm redistribution (**Figure 1**). This was caused by the mitotic spindle shifting to the proximal pole of the dividing tip cell. Asymmetry in the size of daughter cells was associated with the tip daughter cell displaying higher Erk-signaling activity than the stalk daughter cell (by staged immunofluorescence staining), potentially indicating asymmetric Vegfr activity between daughter cells. This highly quantitative study suggested that asymmetric cell size and asymmetric Vegfr activity, after tip cell division, re-establishes tip/stalk cell hierarchy to maintain coordinated and uninterrupted migration during primary angiogenesis (Costa et al., 2016).

Switches in EC phenotype and signaling occur rapidly and constantly to accommodate changing cell-cell interactions and extracellular cues as angiogenesis progresses (Jakobsson et al., 2010). Recently, computational modeling of the molecular interactions that drive tip cell selection suggested that a positive feedback mechanism should exist to amplify Vegfa/Kdr/Kdrl signaling and to accelerate EC phenotypic switching (Page et al., 2019). Page and colleagues identified genes that were upregulated by Vegfa/Kdr/Kdrl signaling but downregulated by Notch signaling and identified *transmembrane 4 L six family membrane 18* (*tm4sf18*), which is only expressed in ISV ECs when they are sprouting. To ask whether Tm4sf18 is a novel amplifier of Vegfa/Kdr/Kdrl signaling, embryos were treated with a suboptimal dose of Vegfr inhibitor to force the ECs to rely on the proposed positive feedback mechanism. EC dynamics during ISV sprouting in *tm4sf18* mutants were then analyzed. Consistent with Tm4sf18 being an amplifier of Vegfa/Kdr/Kdrl signaling, *tm4sf18* mutants had delayed emergence of both tip and stalk cells from the DA. *tm4sf18* mutants also showed delayed recovery of Vegfa/Kdr/Kdrl/Erk signaling after brief treatment of Vegfr inhibitor (Page et al., 2019). Tm4sf18 seems likely to work in concert with Notch-Vegfr feedback, and also cellular mechanisms such as the asymmetric division of tip cells, to help orchestrate angiogenesis.

While signaling downstream of Vegfr's is crucial to control sprouting, recent studies have probed the fundamental mechanics of cellular control of angiogenesis. Tip cells extend many filopodia which were thought to guide vascular migration and patterning (Gerhardt et al., 2003). To visualize filopodia formation in developing ECs, Phng and colleagues generated the *Tg(fli1:LIFEACT-EGFP)*^{zf495} transgenic line that expresses F-actin-binding peptide LIFEACT tagged with EGFP in ECs (Riedl et al., 2008; Phng et al., 2013). Dynamic live imaging of ISV development enabled real-time visualization of F-actin polymerization in the filopodia, contractile ring, cell cortex, and cell junctions, revealing distinct F-actin turnover rates in different intracellular compartments (Phng et al., 2013). To determine the role of filopodia in EC migration and guidance, Phng and colleagues inhibited EC filopodia formation using a low dose of

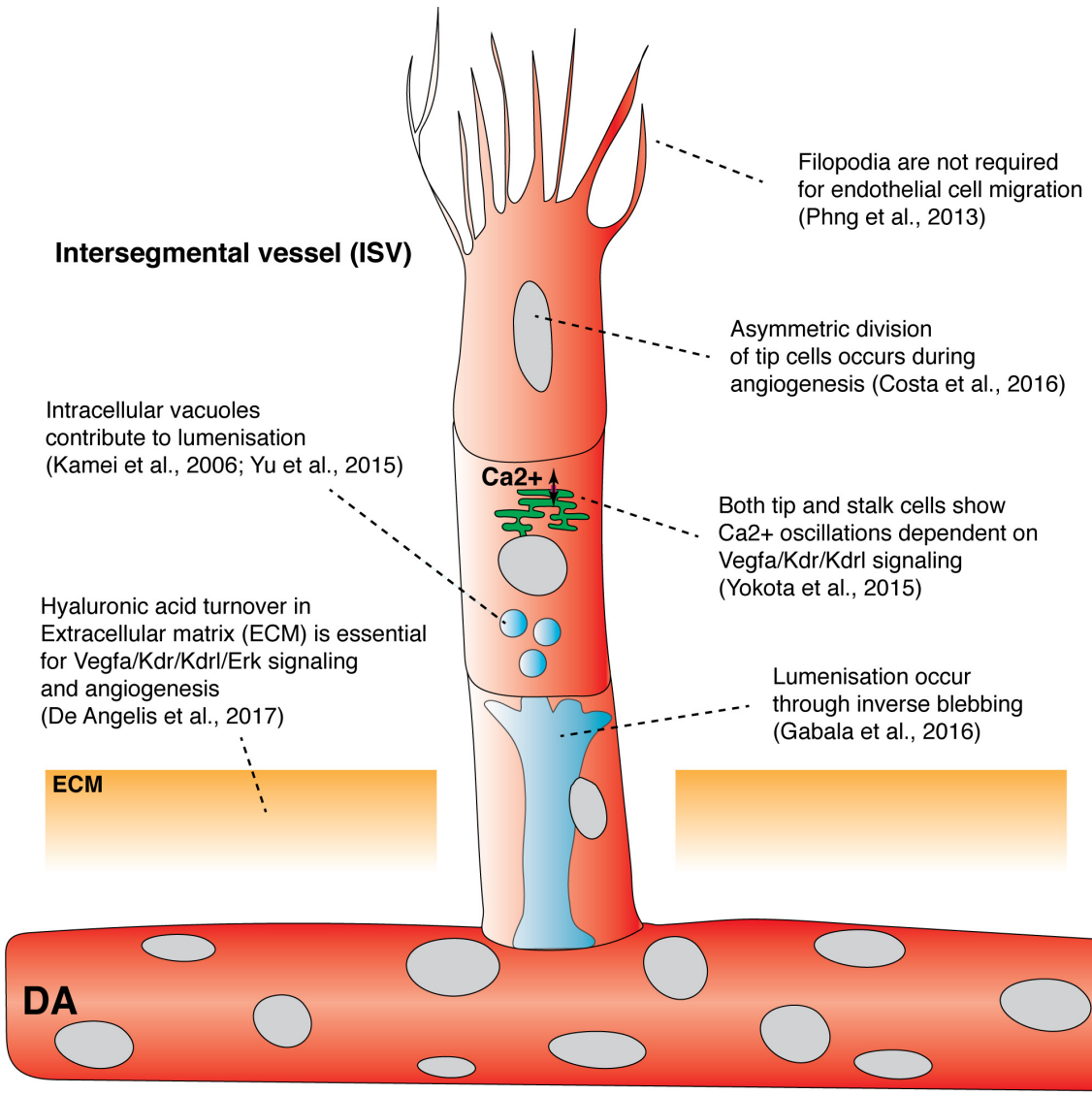

FIGURE 1 | Recent findings from live imaging primary angiogenesis and lumenization in the zebrafish trunk. Recent studies have shown that asymmetric division of intersegmental filopodia have been shown to be dispensable vessel tip cells, hyaluronic acid turnover in extracellular matrix, and Ca^{2+} oscillation in both tip and stalk cells, drive primary angiogenesis. In contrast, filopodia has been shown to be dispensable for endothelial cell migration. Both vacuolar fusion and inverse blebbing have been proposed as mechanisms for lumenization in intersegmental vessels. DA, dorsal aorta; ECM, extracellular matrix; ISV, Intersegmental vessel.

Latrunculin B, a toxin that inhibits actin polymerization (Morton et al., 2000). Surprisingly, ECs lacking filopodia were still able to migrate and form stereotypic patterns of ISVs (**Figure 1**; Phng et al., 2013). Filopodia depleted tip cells were also able to respond to changes in guidance cues in the surrounding tissue. Timelapse imaging revealed that ECs lacking filopodia generated lamellipodia that were sufficient to drive EC migration, albeit at reduced velocity. Although EC filopodia are not required for EC guidance during primary angiogenesis, filopodia are required for tip cell anastomosis as tip cells lacking filopodia failed to form stable connections with neighboring tip cells (discussed in detail below). Taken together, the above imaging studies highlight previously unappreciated mechanisms that control endothelial tip cell behavior, EC-EC communication, signaling and mechanics; essential cell autonomous mechanisms during angiogenesis.

Extracellular factors, extracellular matrix (ECM) and the microenvironment in angiogenesis, have received less attention than EC autonomous mechanisms, with imaging the ECM a particular challenge. Using forward genetic screening, transmembrane protein 2 (Tmem2) was found to be required for both primary angiogenesis and hyaluronic acid (HA) turnover in the ECM (De Angelis et al., 2017). When HA localization was visualized using the HA-binding domain of mouse Neurocan tagged with GFP, *tmem2* mutants displayed ectopic HA accumulation in the ECM around the DA and the PCV consistent

with a failure of HA turnover (De Angelis et al., 2017). The use of this HA biosensor for live imaging has also now been applied to live-image ECM in the heart (Grassini et al., 2018). A product of HA depolymerization, the small oligosaccharide fragment o-HA, was shown to be essential for proper Vegfa/Kdr/Kdrl signaling during primary angiogenesis (**Figure 1**). Importantly, injection of either hyaluronidase or o-HA restored primary angiogenesis in *tmem2* mutants (De Angelis et al., 2017). Consistent with zebrafish epistasis experiments, Tmem2 was recently identified as a long-hypothesized membrane bound Hyaluronidase capable of enzymatic breakdown of long HA but tethered to the cell membrane in mammalian systems (Yamamoto et al., 2017). Thus, *tmem2* mutants demonstrate the importance of correct patterning and function of ECM for angiogenic signaling and vascular development. Developing improved tools to image and study the role of the ECM in angiogenesis is needed.

THE DYNAMICS AND STOCHASTICITY OF SECONDARY ANGIOGENESIS

Once ISVs and the DLAV are formed, a second wave of angiogenesis, termed secondary angiogenesis, commences from the PCV from around 32 hpf (**Figure 2A**; Isogai et al., 2003). Secondary sprouting of ECs from the PCV occurs in a dorsal direction. These sprouts will ultimately give rise to intersegmental veins and the lymphatic vasculature (Isogai et al., 2003; Hogan and Schulte-Merker, 2017). In a remarkably variable process along the trunk of the animal, half of the venous derived sprouts will anastomose with primary ISVs to form venous ISVs (vISVs) that will carry blood. The other half of the secondary sprouts will ultimately not form stable anastomoses but will migrate further dorsally to the horizontal myoseptum and form a parachordal pool of lymphatic endothelial cells (parachordal LECs, PLs), these will go on to form the trunk lymphatic vasculature. The process that decides vISV versus PL identity is not pre-determined by position in the embryo but is stochastic. At any given segmental location in the body plan (except the earliest body segments) a secondary sprout has a 50:50 chance of becoming vISV or PL. The identity of the adjacent vessel as development proceeds is deterministic – the system appears to be patterned as a whole. If a sprout at any position forms a vISV, the probability that the adjacent sprout will now form a PL is vastly increased. ISVs that do not form connections with the PCV remain arterial and are termed arterial ISVs (aISVs) (Isogai et al., 2003; Bussmann et al., 2010).

Recently, Geudens et al. (2019) showed that ISV fates are pre-determined before secondary sprouting and anastomosis. Live imaging EC polarity in arterial and venous ISVs using the *Tg(fli1:Has.B4GALT1-mCherry)*^{bns9} transgenic, which labels endothelial Golgi, revealed that most ECs polarize against flow, resulting in most aISV ECs having a ventral polarity, while most vISV ECs have a dorsal polarity (**Figure 3A**; Kwon et al., 2016; Geudens et al., 2019). Surprisingly, this polarity difference between arterial and venous ISVs is already established *before* secondary sprouts begin to anastomose to ISVs (**Figure 2B**; Geudens et al., 2019). There is a high degree of variation and "noise" in cell behavior during the secondary sprouting process. Some secondary sprouts can anastomose with adjacent ISVs but only transiently, forming a temporary three-way circulation between the ISV, DA, and the PCV before disconnecting to then form PLs (**Figure 2A**). However, ECs that are future aISVs specifically have a multicellular attachment to the DA, but future vISVs have a unicellular attachment to the DA before secondary sprouts begin to anastomose.

Mechanistically, it was found that high Notch activity was only observed in future aISVs even before secondary sprout anastomosis (**Figure 2B**; Weijts et al., 2018; Geudens et al., 2019). Furthermore, when all secondary sprouting was blocked genetically, future vISVs disconnected from the DA as they

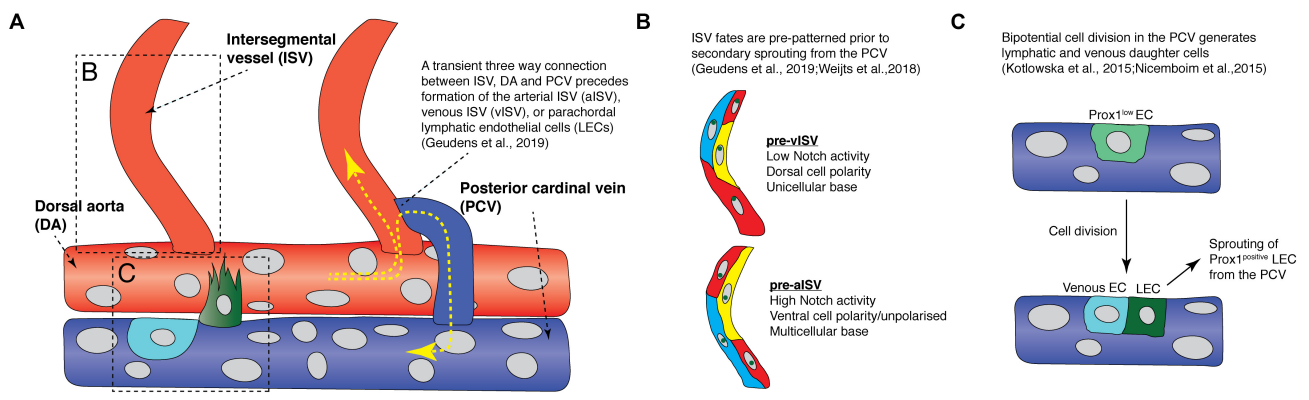

FIGURE 2 | Recent findings from live imaging secondary angiogenesis/lymphatic sprouting in the zebrafish trunk. **(A)** Schematic diagram showing events that occur during secondary angiogenesis and anastomosis in the zebrafish trunk. Yellow arrows indicate direction of blood flow. Red vessels are arteries while blue vessels are veins. Light blue cell is a venous endothelial cell (EC) and the green cell is a fated lymphatic EC. **(B)** Schematic diagram illustrating the difference in Notch activity, cell polarity, and cell arrangements between future arterial intersegmental vessels and venous intersegmental vessels prior to secondary sprout anastomosis. **(C)** Schematic diagram showing how a Prox1-low EC (light green cell) in the posterior cardinal vein undergo bipotential cell division to give rise to a lymphatic EC (green cell) and a venous EC (light blue cell). aISV, arterial intersegmental vessel; DA, dorsal aorta; LEC, lymphatic endothelial cell; ISV, intersegmental vessel; PCV, posterior cardinal vein; vISV, venous intersegmental vessel.

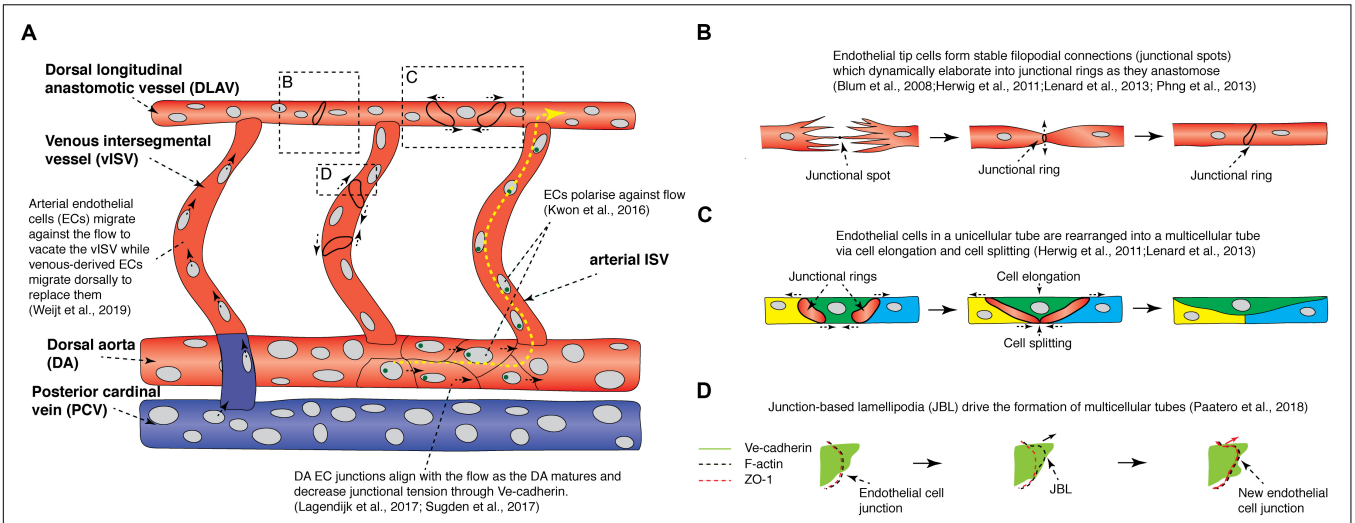

FIGURE 3 | Recent findings from live imaging vessel remodeling and tip cell anastomosis in the zebrafish trunk. **(A)** Schematic diagram showing events that occur during vessel remodeling and tip cell anastomosis in the zebrafish trunk. Yellow arrows indicate direction of blood flow. Red vessels are arteries while blue vessels are veins. Green circles are golgi bodies. **(B)** Schematic diagram illustrating the different steps of tip cell anastomosis. A stable filopodial connection is first established (junctional spot), which elaborates into a junctional ring as the cell-cell junction expands. **(C)** Schematic diagram illustrating how cell elongation and cell splitting occur in the dorsal longitudinal anastomotic vessel to remodel a unicellular tube into a multicellular tube. **(D)** Endothelial cells migrate on top of each other via junctional-based lamellipodia (JBLs) which emanate from the front end of junctional rings. VE-cadherin provides support for F-actin based JBLs to protrude, driving the ZO-1-positive cell junction to migrate forward toward the front end of the JBL via a ratchet-like mechanism. DA, dorsal aorta; DLAV, dorsal longitudinal anastomotic vessel; EC, endothelial cell; JBL, junction-based lamellipodia; PCV, posterior cardinal vein; vISV, venous intersegmental vessel.

would during a normal anastomosis event with a secondary sprout (Geudens et al., 2019). This showed that the state of the initial arterial derived ISVs is pre-determined and will control the ongoing patterning of the mature segmental vasculature. It is unclear if blood flow plays a role in establishing the initial pattern of Notch signaling in the arterial ISVs, with two key studies presenting conflicting data (Weijts et al., 2018; Geudens et al., 2019). How the pattern of aISVs is first determined in the future arteries currently remains unknown. After their formation, as the venous and arterial ISVs mature, all initially DA-derived ECs migrate dorsally against the blood flow and vacate the newly formed vISVs, while venous-derived ECs from the PCV migrate dorsally to replace the arterial ECs over time (**Figure 3A**; Weijts et al., 2018). This unique system by which different vascular lineages are determined in the zebrafish trunk is highly dynamic, involving complex cell rearrangements, EC-EC interactions, stochasticity and noise.

During secondary angiogenesis, the cells of the future lymphatic system are also established. Recent studies have suggested that LEC fate is beginning to be refined even before secondary sprouting. This process has been reviewed in detail elsewhere (Ulvmar and Makinen, 2016; Hogan and Schulte-Merker, 2017) but there are dynamic cellular behaviors that will be revisited here briefly. In vertebrates, the key marker of LEC fate is the transcription factor PROX1 (Wigle and Oliver, 1999; Wigle et al., 2002). In zebrafish, Prox1 (mainly the *prox1a* homolog) is expressed preceding secondary sprouting in a subset of venous ECs, largely along the dorsal wall of the PCV (Koltowska et al., 2015; Nicenboim et al., 2015; Shin et al., 2016b; Baek et al., 2019). Dynamic imaging using the *TgBAC(prox1a:KALTA4,4xUAS-E1B:TagRFP)*^{nim5} transgenic line revealed that a subset of PCV ECs expressing *prox1a* in the PCV display distinctive behaviors preceding sprouting (Koltowska et al., 2015; Nicenboim et al., 2015). Prox1-positive LECs in the PCV undergo division, giving rise to daughter cells with different fates, a dorsally migrating daughter cell that progressively upregulates *prox1a* and a daughter cell that progressively down-regulates *prox1a* expression and remains in the PCV (**Figure 2C**; Koltowska et al., 2015). This is likely a mechanism that allows for maintenance of sufficient numbers of ECs in the PCV despite departure of ECs during secondary angiogenesis. Interestingly, Prox1 protein is expressed by as many as 65% of sprouts that depart the vein, but only 50% of sprouts will go on to form LECs, suggesting plasticity whereby Prox1 expression can be lost in some ECs, a process not currently understood (Koltowska et al., 2015). A number of new molecular regulators have recently been identified that at least in part control how cells along the PCV are selected to express Prox1 (Koltowska et al., 2015; Nicenboim et al., 2015; Gauvrit et al., 2018; Baek et al., 2019). Nevertheless, understanding how stochasticity of progenitor selection, cell fate plasticity and LEC sprouting are interrelated now calls for a dynamic real time assessment, by imaging the processes as they occur.

VASCULAR LUMEN FORMATION, VESSEL REMODELING, AND ANASTOMOSIS

To form a functional vessel that supports blood flow and normal physiological function, angiogenic sprouts must form correct connections with each other, lumenize, and mature.

Multiple mechanisms of vascular lumen formation have been proposed in multiple systems and include cell hollowing, which involves intracellular fusion of vacuoles, or cord hollowing, which is driven by EC rearrangement (reviewed in Charpentier and Conlon, 2014; Betz et al., 2016). The exact cellular mechanism governing vascular lumenization in zebrafish has been the source of much debate. Kamei and colleagues used live imaging to show that intracellular vacuoles sequentially fuse to form a single lumen between multiple cells during primary angiogenesis (**Figure 1**; Kamei et al., 2006). More recently, live imaging of individual ECs expressing membranous eGFP-farnesyl during primary angiogenesis showed that eGFP-farnesyl-positive intracellular vacuoles could fuse to form larger vacuoles present within the cytoplasm of non-lumenized ECs (**Figure 1**; Yu et al., 2015). These studies suggested vacuolar fusion as a major mechanism in lumen formation.

Gabala and colleagues performed dynamic imaging of the EC membrane in the *Tg(fli1:EGFP-CAAX)*^{md13} strain during ISV lumenization. They found that lumen expansion is driven by flow-induced hemodynamic forces that drive formation of highly dynamic apical membrane protrusions into the cell body, a mechanism they termed "inverse blebbing" (**Figure 1**; Gebala et al., 2016). While inverse blebbing at the lateral sides of an expanding lumen rapidly retracts, blebs that are found at the top of the growing lumen persist, allowing directional expansion of the lumen. Bleb retraction is dependent on actomyosin contraction, with live imaging revealing recruitment of F-actin and Myosin-II to blebs during retraction. Inhibition of actomyosin contraction resulted in excessive and uncoordinated blebbing and resulted in a disorganized, collapsed lumen (Gebala et al., 2016). One further mechanism that can contribute to lumen formation in a different context has been termed lumen ensheathment. The common cardinal vein (CCV) develops over the embryonic yolk in a context where blood flow initially occurs in the absence of an EC-lined blood vessel. Dynamic live imaging of EC migration during CCV development revealed that ECs collectively migrate as a sheet over the initially avascular space created by circulating blood. The ECs eventually enclose this luminal space via lumen ensheathment (Helker et al., 2013). Altogether, it appears that several different cellular mechanisms can be used to facilitate lumenization and that these approaches may differ between vessels of various vascular beds.

In the zebrafish trunk, once ISVs are formed and vascular lumenization commences, tip cells anastomose to form the dorsal longitudinal anastomosing vessel (DLAV) (Isogai et al., 2003). The first step of tip cell anastomosis involves the formation of a stable filopodial connection between the two tip cells (**Figure 3B**; Herwig et al., 2011; Phng et al., 2013; Sauteur et al., 2017). Timelapse imaging of the *Tg(fli1a:GAL4FF)*^{ubs3}*;Tg(14XUAS:EGFP-Has.TJP1,myl7:EGFP)*^{ubs5} line, which expresses the EGFP tagged junctional protein Zona Occludens 1 (ZO1), revealed that the initial contact site between filopodia form ZO1-positive junctional spots. These initial contacts dynamically elaborate into junctional rings as the mutual surface area between the tip cells increases (**Figure 3B**; Blum et al., 2008; Herwig et al., 2011). A similar cellular mechanism was observed when vascular anastomosis was live imaged during formation of the cranial vascular palatocerebral artery (Lenard et al., 2013). Apart from ZO1, live imaging revealed that these anastomotic junctional spots and rings have high Ve-cadherin and F-actin levels (Lenard et al., 2013; Phng et al., 2013; Sauteur et al., 2017). The formation of a stable connection between tip cells requires VE-cadherin, as *ve-cadherin* mutants fail to form a mature junctional ring but do initiate filopodial connections (Lenard et al., 2013; Sauteur et al., 2017). This results in the formation of multiple ZO1-positive junctional spots in *ve-cadherin* mutants. The adhesion protein Esama is also required for the formation of filopodial connections with *ve-cadherin* and *esama* double mutants failing to form any junctional spots (Sauteur et al., 2017).

Live imaging has thus revealed how junctional rings are formed and how key molecules regulate this process. Following the formation of junctional rings, junctional remodeling and lumenization commence, which involves either ECs migrating over each other to form elongated junctional rings and a multicellular lumen, or lumen extension through via membrane invagination to form a unicellular lumen (**Figure 3C**; Herwig et al., 2011; Lenard et al., 2013). For a detailed description of this morphogenesis process see Betz et al. (2016). Timelapse imaging of junctional rings during palatocerebral artery (PLA) formation revealed that an initially unicellular lumen is actively remodeled into a multicellular tube by cell splitting, a unique cellular mechanism which encompasses splitting of the EC cytoplasm to allow the adjacent junctional rings to elongate and connect forming a new cell-cell junction between three ECs (**Figure 3C**; Lenard et al., 2013). Cell splitting was also observed when larger, later forming vessels anastomose, and when unicellular tip cells anastomose with multicellular lumenized vessels. Multicellular tubes provide additional advantages to the organism as blood flow is readily maintained during cell division along the tube (Aydogan et al., 2015). In contrast, the lumen is collapsed and flow is temporarily stopped during EC division in unicellular tubes.

As discussed above, a key step in formation of a mature multicellular tube is elongation of initial junctional rings between ECs (Blum et al., 2008; Herwig et al., 2011; Lenard et al., 2013). High-resolution and high-speed imaging of junctional ring dynamics has shown that junctional rings are associated with oscillating lamellipodia-like protrusions, termed junction-based lamellipodia (JBL) (**Figure 3D**; Paatero et al., 2018). JBLs emanate from the front end of elongating junctional rings and orient along the vessel axis. F-actin polymerization is observed on protruding JBLs, while Ve-cadherin localization is diffused, covering both the F-actin-based JBL and the surrounding cell membrane (**Figure 3D**). The ZO1-positive junction is initially localized at the proximal end of the JBL, but at later stages, ZO1-positive junctions gradually move forward toward the front end of the JBL protrusion, forming a new junction (**Figure 3D**). Based on these observations, Paatero and colleagues proposed that during vessel remodeling and junctional maturation, F-actin-based JBLs form new protrusions that provide adhesive support via intra-endothelial cell adhesions, this drives cell migration

along neighboring cells by a ratchet-like mechanism. JBLs also drive DA EC remodeling (described in detail below). F-actin polymerization and Ve-cadherin localization is essential for proper JBL formation and normal JBL oscillation dynamics, ultimately controlling the EC rearrangements that dynamically drive vessel maturation (Sauteur et al., 2014; Paatero et al., 2018).

As embryonic vasculature expands, blood flow patterns are modulated as new vessel connections are made and alternative routes for flow arise (Sugden et al., 2017). In the trunk, maturation and establishment of normal flow patterns in the ISVs from 2 to 3 days post fertilization (dpf) results in lowering of flow velocity and shear stress. The change in flow is accompanied by a reduction in DA and PCV diameter (Lagendijk et al., 2017; Sugden et al., 2017). Live imaging of the architecture of ECs between 2 and 3 dpf has revealed how blood flow modulates DA diameter. DA ECs in 2 dpf embryos have a rounded morphology but DA ECs in 3 dpf larvae are elongated and more aligned with the direction of the flow, resulting in a narrower and more elongated DA (**Figure 3A**; Lagendijk et al., 2017; Sugden et al., 2017). This change in EC morphology was abrogated in the absence of flow (Sugden et al., 2017). Live imaging of *TgBAC(cdh5:cdh5-TFP-TENS-Venous)*^{uq11bh} transgenic vessels, which express a FRET-based Ve-cadherin tension sensor at the junctions, revealed that the Ve-cadherin tension in DA EC junctions decreases progressively during this vessel maturation process (**Figure 3A**; Lagendijk et al., 2017). Calcium signaling modulates DA EC junctional tension and vessel maturation and the Vegfa/Kdr/Kdrl/Erk pathway also modulates Ve-cadherin tension and DA maturation. Strikingly, TGF-beta pathway component Endoglin, which is associated with arteriovenous malformation (Tual-Chalot et al., 2015), was found to be an essential molecular regulator of both these key cellular rearrangements and overall vessel morphogenesis in the DA during this distinctive transition (Sugden et al., 2017). In mice, corneal ECs lacking Endoglin fail to migrate against the direction of flow resulting in arterio-venous malformation, suggesting that the role of Endoglin in vessel morphogenesis is highly conserved between vertebrates (Jin et al., 2017).

While the mechanosensory mechanisms that detect and transduce flow into cellular responses in endothelium remain to be fully understood, recently the primary cilia on ECs have been examined in detail (Hierck et al., 2008; Goetz et al., 2014; Chen et al., 2017; Vion et al., 2018). Live imaging endothelial cilia using transgenic approaches including the *Tg(actb2:Arl13b-GFP)*^{hsc5} transgenic line that expresses ciliary axoneme GTPase ADP ribosylation factor-like GTPase 13B (Arl13b) tagged with GFP revealed that endothelial primary cilia bend in response to flow and local mechanical forces (Caspary et al., 2007; Borovina et al., 2010; Goetz et al., 2014; Eisa-Beygi et al., 2018). Interestingly, loss of cilia in zebrafish mutant models has been reported to lead to intracranial hemorrhage phenotypes (Kallakuri et al., 2015; Eisa-Beygi et al., 2018). In mammals, endothelial cilia dysfunction results in abnormal retinal vessels and increased incidence of intracranial aneurysm (Chapman et al., 1992; Pirson et al., 2002; Rozenfeld et al., 2014; Liu et al., 2018; Vion et al., 2018). Thus, there appears to be evolutionarily conserved functions of cilia in the endothelium between vertebrates. The live-imaging tools developed in zebrafish offer unique opportunities to further explore these functions in-depth.

Overall, the normal morphogenesis and maturation of patent vessels can involve different cellular mechanisms of anastomosis, lumenization, patterned regulation of cell-cell adhesions, remodeling of junctions and key mechanical and signaling regulators. This area of vascular cell biology in particular is benefiting from the unique capacity of the zebrafish model for live imaging cell biology as it happens. Of note, an important step in vascular maturation involves acquisition of mural cell coverage. The use of zebrafish is beginning to shed light on molecular and cellular mechanisms controlling mural cell development in zebrafish, that are conserved in mammals (Jain, 2003; Santoro et al., 2009; Ando et al., 2016, 2019; Stratman et al., 2017). EC-mural cell interactions play many important roles in development and disease and have been reviewed in detail elsewhere (Armulik et al., 2011; Sweeney and Foldes, 2018).

HETEROGENEITY IN CELLULAR MECHANISMS IN ZEBRAFISH VASCULAR DEVELOPMENT

While live imaging of trunk vascular formation in zebrafish has pioneered our understanding of EC dynamics during development, studies in other vascular beds, particularly late forming vessels have been limited. Recent work has uncovered unique cellular and molecular mechanisms required for development of intestinal vessels (Hen et al., 2015; Goi and Childs, 2016; Koenig et al., 2016), coronary vessels (Harrison et al., 2015; Ivins et al., 2015; Gancz et al., 2019; Harrison et al., 2019; Vivien et al., 2019), caudal vessels (Fukuhara et al., 2014; Goetz et al., 2014; Karthik et al., 2018) and the CCV (Helker et al., 2013) among others. Here, we highlight a few recent studies revealing heterogeneity in cellular mechanisms.

In vascular beds in the fin, eyes and the brain, the remarkable observation was made that venous ECs can contribute to arterial vessel formation, highlighting surprising heterogeneity in developmental mechanisms (Bussmann et al., 2011; Fujita et al., 2011; Xu et al., 2014; Kametani et al., 2015; Kaufman et al., 2015; Hasan et al., 2017). During fin regeneration in zebrafish, live-imaging of intubated adult animals revealed that venous tip cells can migrate against the direction of the moving vascular front and integrate into the remodeling artery (Xu et al., 2014; Kametani et al., 2015). Chemokine receptor Cxcr4a is essential for this process as *cxcr4a* mutants lacked arteries in the regenerating fin because venous ECs fail to migrate toward the remodeling artery (Xu et al., 2014). Similarly, in eye development when venous ECs emanating from the primordial midbrain channel (PMBC) were dynamically imaged using Notch activity reporters, stable Notch activation was detected in cells of the venous sprout derived from the PMBC (Kaufman et al., 2015; Hasan et al., 2017). This venous, Notch active sprout from the PMBC fuses to the Notch-active arterial system. *dll4* is first expressed in both tip and stalk cells of the venous sprout before Notch activation commences, and Notch signaling in the tip cell is induced in *trans* by *dll4* in neighboring stalk cells in a mechanism leading to expression of

chemokine receptor *cxcr4a* (Hasan et al., 2017). Similar to the fin, Cxcr4a is essential for proper venous EC migration and artery formation as venous sprouts from the PMBC do not fuse with the arterial system in *cxcr4a* mutants. In mice, CXCR4 is expressed in tip cells in developing retinal vessels, and these cells give rise to retinal arterial ECs (Xu et al., 2014; Pitulescu et al., 2017). However, it remains to be understood in detail the degree to which venous derived tip cells are conserved between zebrafish and mammals. More studies are clearly required to investigate how Notch/Cxcr4a signaling is regulated in different vascular beds to drive blood vessel morphogenesis of both early and late forming vessels.

The cerebral vessels in zebrafish develop under the control of brain specific molecular pathways (reviewed in Hogan and Schulte-Merker, 2017). Imaging of developing cerebral vessels revealed the formation of striking, large, transient, vesicle-like membranous protrusions, termed kugeln, that never detach from the parental ECs (Kugler et al., 2019). Kugeln do not have an EC nucleus and contain little cytoplasm, but dynamic F-actin polymerization is observed at the kugeln neck. Similar to cellular blebs, inhibition of F-actin polymerization using Latrunculin B increases kugeln number, while Myosin II inhibition by Blebbistatin reduces kugeln number (Charras et al., 2008; Kugler et al., 2019). Kugeln formation is modulated by various signaling pathways such as Vegfa/Kdr/Kdrl, Notch, and Wnt signaling, but their formation is not dependent on blood flow (Kugler et al., 2019). While a similar structure has not been reported in mammals, this may be due to its transient nature, making it difficult to identify unless live-imaged. Future studies are needed to investigate the function of this unusual cellular component of vessels and whether they are involved in maintaining brain vascular homeostasis.

The formation of the craniofacial lymphatic vasculature occurs in a very different manner to lymphatics in other tissues and provides compelling evidence for heterogeneity in developmental and cellular processes (Okuda et al., 2012; Astin et al., 2014; Shin et al., 2016b, 2019; Eng et al., 2019; Vogrin et al., 2019). For example, Eng and colleagues lineage traced cells that contribute to facial lymphatics using the photoconvertible Kaede protein. They revealed that facial LECs located laterally originate from veins such as the posterior head sinus (PHS) and the CCV, while facial LECs located ventrally are derived from a population of *etv2*-positive angioblasts first detected close to the ventral aorta [termed the ventral aorta angioblasts (VA-As)] (Okuda et al., 2012; Eng et al., 2019). Dynamic timelapse imaging of the *Tg(etv2:EGFP)*^{ci6} transgenic strain demonstrated that the VA-As migrate as a string of cells and do not connect to a lumenized vessel prior to connecting to the facial lymphatic sprout (Eng et al., 2019). Unlike all other cells that contribute to the early larval lymphatic network, these angioblasts appear to derive from a non-venous source. Further studies are needed to identify the exact cell origin of these non-venous VA-As. Studies in mice have also proposed non-venous origins of cardiac, dermal and mesenteric lymphatic networks (Klotz et al., 2015; Martinez-Corral et al., 2015; Stanczuk et al., 2015; Pichol-Thievend et al., 2018; Maruyama et al., 2019; Stone and Stainier, 2019).

In the later larval brain, live imaging of the meningeal vessels revealed that the cerebral blood vessels are closely associated with mural lymphatic ECs [muLECs, also known as brain lymphatic endothelial cells (BLECs) and fluorescent granular perithelial cells (FGPs)], which express lymphatic markers such as *lyve1b*, *flt4*, *mrc1a,* and *prox1a* (Bower et al., 2017; Van Lessen et al., 2017; Venero Galanternik et al., 2017). These enigmatic cells do not form patent vessels but rather appear to function as local scavenger cells that clear tissue waste. However, muLECs sprout out from the choroidal vascular plexus at approximately 54 hpf in a process clearly akin to lymphangiogenesis and in a Vegfc/Ccbe1/Flt4 signaling-dependent manner (Bower et al., 2017; Van Lessen et al., 2017; Venero Galanternik et al., 2017). Therefore, a classical angiogenic process appears to give rise to a non-vascular lineage. The mechanisms involved in muLEC formation, why muLECs express lymphatic markers, are driven by lymphatic cues, but do not form lymphatic vessels, remain unclear. One recent study has highlighted a role for muLECs in cerebrovascular regeneration upon injury of local blood vessels (Chen et al., 2019), perhaps suggesting roles for this lineage in tissue repair and regeneration.

Overall, the above examples of venous derived tip cells contributing to arteries, novel vascular structures, unique contributions to developing vasculature and vessels giving rise to potentially non-vascular cells, all serve as examples of the plasticity and heterogeneity of the vasculature. Of particular note, these studies all relied upon the utility of the zebrafish model for live-cell imaging and dynamic *in vivo* cell biology.

CONCLUDING REMARKS

In recent years, a combination of developmental genetics and live cell imaging using the zebrafish as a model system, have uncovered highly conserved molecular mechanisms in vascular development and led to a deeper understanding of the EC phenotype. Deciphering molecular mechanisms in blood and lymphatic vessels during development and pathogenesis has increasingly pushed the boundaries of genetic and genomic studies. This is partly motivated by new techniques and opportunities, such as single cell RNA-seq and CRISPR-based gene editing. While new genetic approaches will allow us to resolve the transcriptional changes associated with single cells and to manipulate any gene in the genome, it will become increasingly important to understand how genetic changes influence the cellular phenotype. Understanding phenotype in physiologically intact *in vivo* systems is essential. With the unique attributes of the zebrafish for cellular imaging, continued advancements in microscopy and the expanding numbers of transgenic tools available, we can expect that future efforts will lead to unprecedented resolution of the cellular and molecular mechanisms controlling dynamic EC development and maturation. Live imaging of EC behaviors, analysis of cellular heterogeneity, organ-specific vessel formation and function is expected to continue

to uncover novel mechanisms in the future. Moreover, the development of disease models for a range of vascular pathologies coupled with application of the approaches discussed in this review, offer exciting prospects to understand disease biology and generate new therapeutic avenues.

AUTHOR CONTRIBUTIONS

KO wrote the manuscript and designed the figures. BH reviewed and edited the text and figures. Both authors contributed to the article and approved the submitted version.

FUNDING

BH was supported by the National Health and Medical Research Council (NHMRC Australia) senior research fellowship 1155221.

ACKNOWLEDGMENTS

We acknowledge that we have not been able to cite all of the excellent literature and published studies in zebrafish vascular cell and developmental biology in this review and are sorry that this was not possible.

REFERENCES

Ando, K., Fukuhara, S., Izumi, N., Nakajima, H., Fukui, H., Kelsh, R. N., et al. (2016). Clarification of mural cell coverage of vascular endothelial cells by live imaging of zebrafish. *Development* 143, 1328–1339. doi: 10.1242/dev.132654

Ando, K., Wang, W., Peng, D., Chiba, A., Lagendijk, A. K., Barske, L., et al. (2019). Peri-arterial specification of vascular mural cells from naive mesenchyme requires Notch signaling. *Development* 146:dev165589. doi: 10.1242/dev.165589

Ando, R., Hama, H., Yamamoto-Hino, M., Mizuno, H., and Miyawaki, A. (2002). An optical marker based on the UV-induced green-to-red photoconversion of a fluorescent protein. *Proc. Natl. Acad. Sci. U.S.A.* 99, 12651–12656. doi: 10.1073/pnas.202320599

Armulik, A., Genove, G., and Betsholtz, C. (2011). Pericytes: developmental, physiological, and pathological perspectives, problems, and promises. *Dev. Cell* 21, 193–215. doi: 10.1016/j.devcel.2011.07.001

Astin, J. W., Haggerty, M. J., Okuda, K. S., Le Guen, L., Misa, J. P., Tromp, A., et al. (2014). Vegfd can compensate for loss of Vegfc in zebrafish facial lymphatic sprouting. *Development* 141, 2680–2690. doi: 10.1242/dev.106591

Aydogan, V., Lenard, A., Denes, A. S., Sauteur, L., Belting, H. G., and Affolter, M. (2015). Endothelial cell division in angiogenic sprouts of differing cellular architecture. *Biol. Open* 4, 1259–1269. doi: 10.1242/bio.012740

Baek, S., Oh, T. G., Secker, G., Sutton, D. L., Okuda, K. S., Paterson, S., et al. (2019). The alternative splicing regulator nova2 constrains vascular Erk signaling to limit specification of the lymphatic lineage. *Dev. Cell* 49, 279–292.e5. doi: 10.1016/j.devcel.2019.03.017

Betz, C., Lenard, A., Belting, H. G., and Affolter, M. (2016). Cell behaviors and dynamics during angiogenesis. *Development* 143, 2249–2260. doi: 10.1242/dev.135616

Blum, Y., Belting, H. G., Ellertsdottir, E., Herwig, L., Luders, F., and Affolter, M. (2008). Complex cell rearrangements during intersegmental vessel sprouting and vessel fusion in the zebrafish embryo. *Dev. Biol.* 316, 312–322. doi: 10.1016/j.ydbio.2008.01.038

Borovina, A., Superina, S., Voskas, D., and Ciruna, B. (2010). Vangl2 directs the posterior tilting and asymmetric localization of motile primary cilia. *Nat. Cell Biol.* 12, 407–412. doi: 10.1038/ncb2042

Bower, N. I., Koltowska, K., Pichol-Thievend, C., Virshup, I., Paterson, S., Lagendijk, A. K., et al. (2017). Mural lymphatic endothelial cells regulate meningeal angiogenesis in the zebrafish. *Nat. Neurosci.* 20, 774–783. doi: 10.1038/nn.4558

Bussmann, J., Bos, F. L., Urasaki, A., Kawakami, K., Duckers, H. J., and Schulte-Merker, S. (2010). Arteries provide essential guidance cues for lymphatic endothelial cells in the zebrafish trunk. *Development* 137, 2653–2657. doi: 10.1242/dev.048207

Bussmann, J., Wolfe, S. A., and Siekmann, A. F. (2011). Arterial-venous network formation during brain vascularization involves hemodynamic regulation of chemokine signaling. *Development* 138, 1717–1726. doi: 10.1242/dev.059881

Caspary, T., Larkins, C. E., and Anderson, K. V. (2007). The graded response to Sonic Hedgehog depends on cilia architecture. *Dev. Cell* 12, 767–778. doi: 10.1016/j.devcel.2007.03.004

Chapman, A. B., Rubinstein, D., Hughes, R., Stears, J. C., Earnest, M. P., Johnson, A. M., et al. (1992). Intracranial aneurysms in autosomal dominant polycystic kidney disease. *N. Engl. J. Med.* 327, 916–920.

Charpentier, M. S., and Conlon, F. L. (2014). Cellular and molecular mechanisms underlying blood vessel lumen formation. *Bioessays* 36, 251–259. doi: 10.1002/bies.201300133

Charras, G. T., Coughlin, M., Mitchison, T. J., and Mahadevan, L. (2008). Life and times of a cellular bleb. *Biophys. J.* 94, 1836–1853. doi: 10.1529/biophysj.107.113605

Chen, J., He, J., Ni, R., Yang, Q., Zhang, Y., and Luo, L. (2019). Cerebrovascular injuries induce lymphatic invasion into brain parenchyma to guide vascular regeneration in zebrafish. *Dev. Cell* 49, 697–710.e5. doi: 10.1016/j.devcel.2019.03.022

Chen, X., Gays, D., Milia, C., and Santoro, M. M. (2017). Cilia control vascular mural cell recruitment in vertebrates. *Cell Rep.* 18, 1033–1047. doi: 10.1016/j.celrep.2016.12.044

Chi, N. C., Shaw, R. M., De Val, S., Kang, G., Jan, L. Y., Black, B. L., et al. (2008). Foxn4 directly regulates tbx2b expression and atrioventricular canal formation. *Genes Dev.* 22, 734–739. doi: 10.1101/gad.1629408

Chng, S. C., Ho, L., Tian, J., and Reversade, B. (2013). ELABELA: a hormone essential for heart development signals via the apelin receptor. *Dev. Cell* 27, 672–680. doi: 10.1016/j.devcel.2013.11.002

Clark, B. S., Cui, S., Miesfeld, J. B., Klezovitch, O., Vasioukhin, V., and Link, B. A. (2012). Loss of Llgl1 in retinal neuroepithelia reveals links between apical domain size, Notch activity and neurogenesis. *Development* 139, 1599–1610. doi: 10.1242/dev.078097

Clements, W. K., Kim, A. D., Ong, K. G., Moore, J. C., Lawson, N. D., and Traver, D. (2011). A somitic Wnt16/Notch pathway specifies haematopoietic stem cells. *Nature* 474, 220–224. doi: 10.1038/nature10107

Coffin, J. D., and Poole, T. J. (1988). Embryonic vascular development: immunohistochemical identification of the origin and subsequent morphogenesis of the major vessel primordia in quail embryos. *Development* 102, 735–748.

Costa, G., Harrington, K. I., Lovegrove, H. E., Page, D. J., Chakravartula, S., Bentley, K., et al. (2016). Asymmetric division coordinates collective cell migration in angiogenesis. *Nat. Cell Biol.* 18, 1292–1301. doi: 10.1038/ncb3443

De Angelis, J. E., Lagendijk, A. K., Chen, H., Tromp, A., Bower, N. I., Tunny, K. A., et al. (2017). Tmem2 regulates embryonic Vegf signaling by controlling hyaluronic acid turnover. *Dev. Cell* 40, 123–136. doi: 10.1016/j.devcel.2016.12.017

Dunworth, W. P., Cardona-Costa, J., Bozkulak, E. C., Kim, J. D., Meadows, S., Fischer, J. C., et al. (2014). Bone morphogenetic protein 2 signaling negatively modulates lymphatic development in vertebrate embryos. *Circ. Res.* 114, 56–66. doi: 10.1161/circresaha.114.302452

Eilken, H. M., and Adams, R. H. (2010). Dynamics of endothelial cell behavior in sprouting angiogenesis. *Curr. Opin. Cell Biol.* 22, 617–625. doi: 10.1016/j.ceb.2010.08.010

Eisa-Beygi, S., Benslimane, F. M., El-Rass, S., Prabhudesai, S., Abdelrasoul, M. K. A., Simpson, P. M., et al. (2018). Characterization of endothelial cilia distribution during cerebral-vascular development in zebrafish (*Danio rerio*). *Arterioscl. Thromb. Vasc. Biol.* 38, 2806–2818. doi: 10.1161/atvbaha.118.311231

Eng, T. C., Chen, W., Okuda, K. S., Misa, J. P., Padberg, Y., Crosier, K. E., et al. (2019). Zebrafish facial lymphatics develop through sequential addition of venous and non-venous progenitors. *EMBO Rep.* 20:e47079.

Fantin, A., Vieira, J. M., Gestri, G., Denti, L., Schwarz, Q., Prykhozhij, S., et al. (2010). Tissue macrophages act as cellular chaperones for vascular anastomosis downstream of VEGF-mediated endothelial tip cell induction. *Blood* 116, 829–840. doi: 10.1182/blood-2009-12-257832

Ferrara, N., Carver-Moore, K., Chen, H., Dowd, M., Lu, L., O'shea, K. S., et al. (1996). Heterozygous embryonic lethality induced by targeted inactivation of the VEGF gene. *Nature* 380, 439–442. doi: 10.1038/380439a0

Fouquet, B., Weinstein, B. M., Serluca, F. C., and Fishman, M. C. (1997). Vessel patterning in the embryo of the zebrafish: guidance by notochord. *Dev. Biol.* 183, 37–48. doi: 10.1006/dbio.1996.8495

Fujita, M., Cha, Y. R., Pham, V. N., Sakurai, A., Roman, B. L., Gutkind, J. S., et al. (2011). Assembly and patterning of the vascular network of the vertebrate hindbrain. *Development* 138, 1705–1715. doi: 10.1242/dev.058776

Fukuhara, S., Zhang, J., Yuge, S., Ando, K., Wakayama, Y., Sakaue-Sawano, A., et al. (2014). Visualizing the cell-cycle progression of endothelial cells in zebrafish. *Dev. Biol.* 393, 10–23. doi: 10.1016/j.ydbio.2014.06.015

Gancz, D., Raftrey, B. C., Perlmoter, G., Marin-Juez, R., Semo, J., Matsuoka, R. L., et al. (2019). Distinct origins and molecular mechanisms contribute to lymphatic formation during cardiac growth and regeneration. *eLife* 8:e44153.

Gauvrit, S., Villasenor, A., Strilic, B., Kitchen, P., Collins, M. M., Marin-Juez, R., et al. (2018). HHEX is a transcriptional regulator of the VEGFC/FLT4/PROX1 signaling axis during vascular development. *Nat. Commun.* 9:2704.

Gebala, V., Collins, R., Geudens, I., Phng, L. K., and Gerhardt, H. (2016). Blood flow drives lumen formation by inverse membrane blebbing during angiogenesis in vivo. *Nat. Cell Biol.* 18, 443–450. doi: 10.1038/ncb3320

Gerhardt, H., Golding, M., Fruttiger, M., Ruhrberg, C., Lundkvist, A., Abramsson, A., et al. (2003). VEGF guides angiogenic sprouting utilizing endothelial tip cell filopodia. *J. Cell Biol.* 161, 1163–1177. doi: 10.1083/jcb.200302047

Geudens, I., Coxam, B., Alt, S., Gebala, V., Vion, A. C., Meier, K., et al. (2019). Artery-vein specification in the zebrafish trunk is pre-patterned by heterogeneous Notch activity and balanced by flow-mediated fine-tuning. *Development* 146:dev181024. doi: 10.1242/dev.181024

Goetz, J. G., Steed, E., Ferreira, R. R., Roth, S., Ramspacher, C., Boselli, F., et al. (2014). Endothelial cilia mediate low flow sensing during zebrafish vascular development. *Cell Rep.* 6, 799–808. doi: 10.1016/j.celrep.2014.01.032

Goi, M., and Childs, S. J. (2016). Patterning mechanisms of the sub-intestinal venous plexus in zebrafish. *Dev. Biol.* 409, 114–128. doi: 10.1016/j.ydbio.2015.10.017

Gordon, E. J., Rao, S., Pollard, J. W., Nutt, S. L., Lang, R. A., and Harvey, N. L. (2010). Macrophages define dermal lymphatic vessel calibre during development by regulating lymphatic endothelial cell proliferation. *Development* 137, 3899–3910. doi: 10.1242/dev.050021

Grassini, D. R., Lagendijk, A. K., De Angelis, J. E., Da Silva, J., Jeanes, A., Zettler, N., et al. (2018). Nppa and Nppb act redundantly during zebrafish cardiac development to confine AVC marker expression and reduce cardiac jelly volume. *Development* 145:dev160739. doi: 10.1242/dev.160739

Hamm, M. J., Kirchmaier, B. C., and Herzog, W. (2016). Sema3d controls collective endothelial cell migration by distinct mechanisms via Nrp1 and PlxnD1. *J. Cell Biol.* 215, 415–430. doi: 10.1083/jcb.201603100

Harrison, M. R., Bussmann, J., Huang, Y., Zhao, L., Osorio, A., Burns, C. G., et al. (2015). Chemokine-guided angiogenesis directs coronary vasculature formation in zebrafish. *Dev. Cell* 33, 442–454. doi: 10.1016/j.devcel.2015.04.001

Harrison, M. R., Feng, X., Mo, G., Aguayo, A., Villafuerte, J., Yoshida, T., et al. (2019). Late developing cardiac lymphatic vasculature supports adult zebrafish heart function and regeneration. *eLife* 8:e42762.

Hasan, S. S., Tsaryk, R., Lange, M., Wisniewski, L., Moore, J. C., Lawson, N. D., et al. (2017). Endothelial Notch signalling limits angiogenesis via control of artery formation. *Nat. Cell Biol.* 19, 928–940. doi: 10.1038/ncb3574

Hatta, K., Tsujii, H., and Omura, T. (2006). Cell tracking using a photoconvertible fluorescent protein. *Nat. Protoc.* 1, 960–967. doi: 10.1038/nprot.2006.96

Helker, C. S., Schuermann, A., Karpanen, T., Zeuschner, D., Belting, H. G., Affolter, M., et al. (2013). The zebrafish common cardinal veins develop by a novel mechanism: lumen ensheathment. *Development* 140, 2776–2786. doi: 10.1242/dev.091876

Helker, C. S., Schuermann, A., Pollmann, C., Chng, S. C., Kiefer, F., Reversade, B., et al. (2015). The hormonal peptide Elabela guides angioblasts to the midline during vasculogenesis. *eLife* 4:e06726.

Hellstrom, M., Phng, L. K., Hofmann, J. J., Wallgard, E., Coultas, L., Lindblom, P., et al. (2007). Dll4 signalling through Notch1 regulates formation of tip cells during angiogenesis. *Nature* 445, 776–780. doi: 10.1038/nature05571

Hen, G., Nicenboim, J., Mayseless, O., Asaf, L., Shin, M., Busolin, G., et al. (2015). Venous-derived angioblasts generate organ-specific vessels during zebrafish embryonic development. *Development* 142, 4266–4278. doi: 10.1242/dev.129247

Herbert, S. P., Huisken, J., Kim, T. N., Feldman, M. E., Houseman, B. T., Wang, R. A., et al. (2009). Arterial-venous segregation by selective cell sprouting: an alternative mode of blood vessel formation. *Science* 326, 294–298. doi: 10.1126/science.1178577

Herwig, L., Blum, Y., Krudewig, A., Ellertsdottir, E., Lenard, A., Belting, H. G., et al. (2011). Distinct cellular mechanisms of blood vessel fusion in the zebrafish embryo. *Curr. Biol.* 21, 1942–1948. doi: 10.1016/j.cub.2011.10.016

Hierck, B. P., Van Der Heiden, K., Alkemade, F. E., Van De Pas, S., Van Thienen, J. V., Groenendijk, B. C., et al. (2008). Primary cilia sensitize endothelial cells for fluid shear stress. *Dev. Dyn.* 237, 725–735. doi: 10.1002/dvdy.21472

Hogan, B. M., and Schulte-Merker, S. (2017). How to plumb a pisces: understanding vascular development and disease using zebrafish embryos. *Dev. Cell* 42, 567–583. doi: 10.1016/j.devcel.2017.08.015

Horstmann, E. (1952). Uber die funktionelle Struktur der mesenterialen Lymphgefasse. *Morphol. Jahrbuch* 91, 483–510.

Isogai, S., Lawson, N. D., Torrealday, S., Horiguchi, M., and Weinstein, B. M. (2003). Angiogenic network formation in the developing vertebrate trunk. *Development* 130, 5281–5290. doi: 10.1242/dev.00733

Ivins, S., Chappell, J., Vernay, B., Suntharalingham, J., Martineau, A., Mohun, T. J., et al. (2015). The CXCL12/CXCR4 axis plays a critical role in coronary artery development. *Dev. Cell* 33, 455–468. doi: 10.1016/j.devcel.2015.03.026

Jain, R. K. (2003). Molecular regulation of vessel maturation. *Nat. Med.* 9, 685–693. doi: 10.1038/nm0603-685

Jakobsson, L., Franco, C. A., Bentley, K., Collins, R. T., Ponsioen, B., Aspalter, I. M., et al. (2010). Endothelial cells dynamically compete for the tip cell position during angiogenic sprouting. *Nat. Cell Biol.* 12, 943–953. doi: 10.1038/ncb2103

Jin, Y., Muhl, L., Burmakin, M., Wang, Y., Duchez, A. C., Betsholtz, C., et al. (2017). Endoglin prevents vascular malformation by regulating flow-induced cell migration and specification through VEGFR2 signalling. *Nat. Cell Biol.* 19, 639–652. doi: 10.1038/ncb3534

Kallakuri, S., Yu, J. A., Li, J., Li, Y., Weinstein, B. M., Nicoli, S., et al. (2015). Endothelial cilia are essential for developmental vascular integrity in zebrafish. *J. Am. Soc. Nephrol.* 26, 864–875. doi: 10.1681/asn.2013121314

Kamei, M., Saunders, W. B., Bayless, K. J., Dye, L., Davis, G. E., and Weinstein, B. M. (2006). Endothelial tubes assemble from intracellular vacuoles in vivo. *Nature* 442, 453–456. doi: 10.1038/nature04923

Kametani, Y., Chi, N. C., Stainier, D. Y., and Takada, S. (2015). Notch signaling regulates venous arterialization during zebrafish fin regeneration. *Genes Cells* 20, 427–438. doi: 10.1111/gtc.12234

Karthik, S., Djukic, T., Kim, J. D., Zuber, B., Makanya, A., Odriozola, A., et al. (2018). Synergistic interaction of sprouting and intussusceptive angiogenesis during zebrafish caudal vein plexus development. *Sci. Rep.* 8:9840.

Kaufman, R., Weiss, O., Sebbagh, M., Ravid, R., Gibbs-Bar, L., Yaniv, K., et al. (2015). Development and origins of zebrafish ocular vasculature. *BMC Dev. Biol.* 15:18. doi: 10.1186/s12861-015-0066-9

Kita, E. M., Scott, E. K., and Goodhill, G. J. (2015). The influence of activity on axon pathfinding in the optic tectum. *Dev. Neurobiol.* 75, 608–620. doi: 10.1002/dneu.22262

Klotz, L., Norman, S., Vieira, J. M., Masters, M., Rohling, M., Dube, K. N., et al. (2015). Cardiac lymphatics are heterogeneous in origin and respond to injury. *Nature* 522, 62–67. doi: 10.1038/nature14483

Koenig, A. L., Baltrunaite, K., Bower, N. I., Rossi, A., Stainier, D. Y., Hogan, B. M., et al. (2016). Vegfa signaling promotes zebrafish intestinal vasculature development through endothelial cell migration from the posterior cardinal vein. *Dev. Biol.* 411, 115–127. doi: 10.1016/j.ydbio.2016.01.002

Kohli, V., Schumacher, J. A., Desai, S. P., Rehn, K., and Sumanas, S. (2013). Arterial and venous progenitors of the major axial vessels originate at distinct locations. *Dev. Cell* 25, 196–206. doi: 10.1016/j.devcel.2013.03.017

Koltowska, K., Lagendijk, A. K., Pichol-Thievend, C., Fischer, J. C., Francois, M., Ober, E. A., et al. (2015). Vegfc regulates bipotential precursor division and prox1 expression to promote lymphatic identity in zebrafish. *Cell Rep.* 13, 1828–1841. doi: 10.1016/j.celrep.2015.10.055

Kugler, E. C., Van Lessen, M., Daetwyler, S., Chhabria, K., Savage, A. M., Silva, V., et al. (2019). Cerebrovascular endothelial cells form transient Notch-dependent cystic structures in zebrafish. *EMBO Rep.* 20:e47047.

Kwon, H. B., Wang, S., Helker, C. S., Rasouli, S. J., Maischein, H. M., Offermanns, S., et al. (2016). In vivo modulation of endothelial polarization by Apelin receptor signalling. *Nat. Commun.* 7:11805.

Lagendijk, A. K., Gomez, G. A., Baek, S., Hesselson, D., Hughes, W. E., Paterson, S., et al. (2017). Live imaging molecular changes in junctional tension upon VE-cadherin in zebrafish. *Nat. Commun.* 8:1402.

Lawson, N. D., Vogel, A. M., and Weinstein, B. M. (2002). sonic hedgehog and vascular endothelial growth factor act upstream of the Notch pathway during arterial endothelial differentiation. *Dev. Cell* 3, 127–136. doi: 10.1016/s1534-5807(02)00198-3

Lenard, A., Ellertsdottir, E., Herwig, L., Krudewig, A., Sauteur, L., Belting, H. G., et al. (2013). In vivo analysis reveals a highly stereotypic morphogenetic pathway of vascular anastomosis. *Dev. Cell* 25, 492–506. doi: 10.1016/j.devcel.2013.05.010

Leslie, J. D., Ariza-Mcnaughton, L., Bermange, A. L., Mcadow, R., Johnson, S. L., and Lewis, J. (2007). Endothelial signalling by the Notch ligand Delta-like 4 restricts angiogenesis. *Development* 134, 839–844. doi: 10.1242/dev.003244

Lindskog, H., Kim, Y. H., Jelin, E. B., Kong, Y., Guevara-Gallardo, S., Kim, T. N., et al. (2014). Molecular identification of venous progenitors in the dorsal aorta reveals an aortic origin for the cardinal vein in mammals. *Development* 141, 1120–1128. doi: 10.1242/dev.101808

Liu, M., Zhao, J., Zhou, Q., Peng, Y., Zhou, Y., and Jiang, Y. (2018). Primary cilia deficiency induces intracranial aneurysm. *Shock* 49, 604–611. doi: 10.1097/shk.0000000000000961

Lobov, I. B., Renard, R. A., Papadopoulos, N., Gale, N. W., Thurston, G., Yancopoulos, G. D., et al. (2007). Delta-like ligand 4 (Dll4) is induced by VEGF as a negative regulator of angiogenic sprouting. *Proc. Natl. Acad. Sci. U.S.A.* 104, 3219–3224. doi: 10.1073/pnas.0611206104

Martinez-Corral, I., Ulvmar, M. H., Stanczuk, L., Tatin, F., Kizhatil, K., John, S. W., et al. (2015). Nonvenous origin of dermal lymphatic vasculature. *Circ. Res.* 116, 1649–1654. doi: 10.1161/circresaha.116.306170

Maruyama, K., Miyagawa-Tomita, S., Mizukami, K., Matsuzaki, F., and Kurihara, H. (2019). Isl1-expressing non-venous cell lineage contributes to cardiac lymphatic vessel development. *Dev. Biol.* 452, 134–143. doi: 10.1016/j.ydbio.2019.05.002

Morton, W. M., Ayscough, K. R., and Mclaughlin, P. J. (2000). Latrunculin alters the actin-monomer subunit interface to prevent polymerization. *Nat. Cell Biol.* 2, 376–378. doi: 10.1038/35014075

Muto, A., Ohkura, M., Abe, G., Nakai, J., and Kawakami, K. (2013). Real-time visualization of neuronal activity during perception. *Curr. Biol.* 23, 307–311. doi: 10.1016/j.cub.2012.12.040

Nguyen, P. D., Hollway, G. E., Sonntag, C., Miles, L. B., Hall, T. E., Berger, S., et al. (2014). Haematopoietic stem cell induction by somite-derived endothelial cells controlled by meox1. *Nature* 512, 314–318. doi: 10.1038/nature13678

Nicenboim, J., Malkinson, G., Lupo, T., Asaf, L., Sela, Y., Mayseless, O., et al. (2015). Lymphatic vessels arise from specialized angioblasts within a venous niche. *Nature* 522, 56–61. doi: 10.1038/nature14425

Nicosia, R. F., and Madri, J. A. (1987). The microvascular extracellular matrix. Developmental changes during angiogenesis in the aortic ring-plasma clot model. *Am. J. Pathol.* 128, 78–90.

Ninov, N., Borius, M., and Stainier, D. Y. (2012). Different levels of Notch signaling regulate quiescence, renewal and differentiation in pancreatic endocrine progenitors. *Development* 139, 1557–1567. doi: 10.1242/dev.076000

Noren, D. P., Chou, W. H., Lee, S. H., Qutub, A. A., Warmflash, A., Wagner, D. S., et al. (2016). Endothelial cells decode VEGF-mediated Ca2+ signaling patterns to produce distinct functional responses. *Sci. Signal.* 9:ra20. doi: 10.1126/scisignal.aad3188

Okuda, K. S., Astin, J. W., Misa, J. P., Flores, M. V., Crosier, K. E., and Crosier, P. S. (2012). lyve1 expression reveals novel lymphatic vessels and new mechanisms for lymphatic vessel development in zebrafish. *Development* 139, 2381–2391. doi: 10.1242/dev.077701

Paatero, I., Sauteur, L., Lee, M., Lagendijk, A. K., Heutschi, D., Wiesner, C., et al. (2018). Junction-based lamellipodia drive endothelial cell rearrangements in vivo via a VE-cadherin-F-actin based oscillatory cell-cell interaction. *Nat. Commun.* 9:3545.

Page, D. J., Thuret, R., Venkatraman, L., Takahashi, T., Bentley, K., and Herbert, S. P. (2019). Positive feedback defines the timing, magnitude, and robustness of angiogenesis. *Cell Rep.* 27, 3139–3151.e5. doi: 10.1016/j.celrep.2019.05.052

Parsons, M. J., Pisharath, H., Yusuff, S., Moore, J. C., Siekmann, A. F., Lawson, N., et al. (2009). Notch-responsive cells initiate the secondary transition in larval zebrafish pancreas. *Mech. Dev.* 126, 898–912. doi: 10.1016/j.mod.2009.07.002

Pauli, A., Norris, M. L., Valen, E., Chew, G. L., Gagnon, J. A., Zimmerman, S., et al. (2014). Toddler: an embryonic signal that promotes cell movement via Apelin receptors. *Science* 343:1248636. doi: 10.1126/science.1248636

Phng, L. K., Stanchi, F., and Gerhardt, H. (2013). Filopodia are dispensable for endothelial tip cell guidance. *Development* 140, 4031–4040. doi: 10.1242/dev.097352

Pichol-Thievend, C., Betterman, K. L., Liu, X., Ma, W., Skoczylas, R., Lesieur, E., et al. (2018). A blood capillary plexus-derived population of progenitor cells contributes to genesis of the dermal lymphatic vasculature during embryonic development. *Development* 145:dev160184. doi: 10.1242/dev.160184

Pirson, Y., Chauveau, D., and Torres, V. (2002). Management of cerebral aneurysms in autosomal dominant polycystic kidney disease. *J. Am. Soc. Nephrol.* 13, 269–276.

Pitulescu, M. E., Schmidt, I., Giaimo, B. D., Antoine, T., Berkenfeld, F., Ferrante, F., et al. (2017). Dll4 and Notch signalling couples sprouting angiogenesis and artery formation. *Nat. Cell Biol.* 19, 915–927. doi: 10.1038/ncb3555

Quillien, A., Moore, J. C., Shin, M., Siekmann, A. F., Smith, T., Pan, L., et al. (2014). Distinct Notch signaling outputs pattern the developing arterial system. *Development* 141, 1544–1552. doi: 10.1242/dev.099986

Reischauer, S., Stone, O. A., Villasenor, A., Chi, N., Jin, S. W., Martin, M., et al. (2016). Cloche is a bHLH-PAS transcription factor that drives haemato-vascular specification. *Nature* 535, 294–298. doi: 10.1038/nature18614

Riedl, J., Crevenna, A. H., Kessenbrock, K., Yu, J. H., Neukirchen, D., Bista, M., et al. (2008). Lifeact: a versatile marker to visualize F-actin. *Nat. Methods* 5, 605–607. doi: 10.1038/nmeth.1220

Risau, W., and Flamme, I. (1995). Vasculogenesis. *Annu. Rev. Cell Dev. Biol.* 11, 73–91.

Roman, B. L., Pham, V. N., Lawson, N. D., Kulik, M., Childs, S., Lekven, A. C., et al. (2002). Disruption of acvrl1 increases endothelial cell number in zebrafish cranial vessels. *Development* 129, 3009–3019.

Rossi, A., Gauvrit, S., Marass, M., Pan, L., Moens, C. B., and Stainier, D. Y. R. (2016). Regulation of Vegf signaling by natural and synthetic ligands. *Blood* 128, 2359–2366. doi: 10.1182/blood-2016-04-711192

Rouget, C. (1873). Memoire sur le developpement, la structure et les proprietes physiologiques des capillaires sanguins. *Arch. Physiol. Norm. Pathol.* 5, 603–633.

Rozenfeld, M. N., Ansari, S. A., Shaibani, A., Russell, E. J., Mohan, P., and Hurley, M. C. (2014). Should patients with autosomal dominant polycystic kidney disease be screened for cerebral aneurysms? *AJNR Am. J. Neuroradiol.* 35, 3–9. doi: 10.3174/ajnr.a3437

Sabin, F. (1920). Studies on the origin of the blood vessels and of red blood corpuscles as seen in the living blastoderm of chick during the second day of incubation. *Contrib. Embryol. Carnegie Inst. Washinton* 9, 214–262.

Santoro, M. M., Pesce, G., and Stainier, D. Y. (2009). Characterization of vascular mural cells during zebrafish development. *Mech. Dev.* 126, 638–649.

Sauteur, L., Affolter, M., and Belting, H. G. (2017). Distinct and redundant functions of Esama and VE-cadherin during vascular morphogenesis. *Development* 144, 1554–1565. doi: 10.1242/dev.140038

Sauteur, L., Krudewig, A., Herwig, L., Ehrenfeuchter, N., Lenard, A., Affolter, M., et al. (2014). Cdh5/VE-cadherin promotes endothelial cell interface elongation via cortical actin polymerization during angiogenic sprouting. *Cell Rep.* 9, 504–513. doi: 10.1016/j.celrep.2014.09.024

Savage, A. M., Kurusamy, S., Chen, Y., Jiang, Z., Chhabria, K., Macdonald, R. B., et al. (2019). tmem33 is essential for VEGF-mediated endothelial calcium oscillations and angiogenesis. *Nat. Commun.* 10:732.

Shalaby, F., Rossant, J., Yamaguchi, T. P., Gertsenstein, M., Wu, X. F., Breitman, M. L., et al. (1995). Failure of blood-island formation and vasculogenesis in Flk-1-deficient mice. *Nature* 376, 62–66. doi: 10.1038/376062a0

Shin, M., Beane, T. J., Quillien, A., Male, I., Zhu, L. J., and Lawson, N. D. (2016a). Vegfa signals through ERK to promote angiogenesis, but not artery differentiation. *Development* 143, 3796–3805. doi: 10.1242/dev.137919

Shin, M., Male, I., Beane, T. J., Villefranc, J. A., Kok, F. O., Zhu, L. J., et al. (2016b). Vegfc acts through ERK to induce sprouting and differentiation of trunk lymphatic progenitors. *Development* 143, 3785–3795. doi: 10.1242/dev.137901

Shin, M., Nozaki, T., Idrizi, F., Isogai, S., Ogasawara, K., Ishida, K., et al. (2019). Valves are a conserved feature of the zebrafish lymphatic system. *Dev. Cell* 51, 374–386.e5. doi: 10.1016/j.devcel.2019.08.019

Siekmann, A. F., and Lawson, N. D. (2007). Notch signalling limits angiogenic cell behaviour in developing zebrafish arteries. *Nature* 445, 781–784. doi: 10.1038/nature05577

Stanczuk, L., Martinez-Corral, I., Ulvmar, M. H., Zhang, Y., Lavina, B., Fruttiger, M., et al. (2015). cKit lineage hemogenic endothelium-derived cells contribute to mesenteric lymphatic vessels. *Cell Rep.* 10, 1708–1721. doi: 10.1016/j.celrep.2015.02.026

Stone, O. A., and Stainier, D. Y. R. (2019). Paraxial mesoderm is the major source of lymphatic endothelium. *Dev. Cell* 50, 247–255.e3. doi: 10.1016/j.devcel.2019.04.034

Stratman, A. N., Pezoa, S. A., Farrelly, O. M., Castranova, D., Dye, L. E. III, Butler, M. G., et al. (2017). Interactions between mural cells and endothelial cells stabilize the developing zebrafish dorsal aorta. *Development* 144, 115–127. doi: 10.1242/dev.143131

Suchting, S., Freitas, C., Le Noble, F., Benedito, R., Breant, C., Duarte, A., et al. (2007). The Notch ligand Delta-like 4 negatively regulates endothelial tip cell formation and vessel branching. *Proc. Natl. Acad. Sci. U.S.A.* 104, 3225–3230. doi: 10.1073/pnas.0611177104

Sugden, W. W., Meissner, R., Aegerter-Wilmsen, T., Tsaryk, R., Leonard, E. V., Bussmann, J., et al. (2017). Endoglin controls blood vessel diameter through endothelial cell shape changes in response to haemodynamic cues. *Nat. Cell Biol.* 19, 653–665. doi: 10.1038/ncb3528

Sumoy, L., Keasey, J. B., Dittman, T. D., and Kimelman, D. (1997). A role for notochord in axial vascular development revealed by analysis of phenotype and the expression of VEGR-2 in zebrafish flh and ntl mutant embryos. *Mech. Dev.* 63, 15–27. doi: 10.1016/s0925-4773(97)00671-0

Sweeney, M., and Foldes, G. (2018). It takes two: endothelial-perivascular cell cross-talk in vascular development and disease. *Front. Cardiovasc. Med.* 5:154. doi: 10.3389/fcvm.2018.00154

Tian, Y., Xu, J., Feng, S., He, S., Zhao, S., Zhu, L., et al. (2017). The first wave of T lymphopoiesis in zebrafish arises from aorta endothelium independent of hematopoietic stem cells. *J. Exp. Med.* 214, 3347–3360. doi: 10.1084/jem.20170488

Tual-Chalot, S., Oh, S. P., and Arthur, H. M. (2015). Mouse models of hereditary hemorrhagic telangiectasia: recent advances and future challenges. *Front. Genet.* 6:25. doi: 10.3389/fgene.2015.00025

Ubezio, B., Blanco, R. A., Geudens, I., Stanchi, F., Mathivet, T., Jones, M. L., et al. (2016). Synchronization of endothelial Dll4-Notch dynamics switch blood vessels from branching to expansion. *eLife* 5:e12167.

Ulvmar, M. H., and Makinen, T. (2016). Heterogeneity in the lymphatic vascular system and its origin. *Cardiovasc. Res.* 111, 310–321. doi: 10.1093/cvr/cvw175

Van Lessen, M., Shibata-Germanos, S., Van Impel, A., Hawkins, T. A., Rihel, J., and Schulte-Merker, S. (2017). Intracellular uptake of macromolecules by brain lymphatic endothelial cells during zebrafish embryonic development. *eLife* 6:e25932.

Venero Galanternik, M., Castranova, D., Gore, A. V., Blewett, N. H., Jung, H. M., Stratman, A. N., et al. (2017). A novel perivascular cell population in the zebrafish brain. *eLife* 6:e24369.

Vion, A. C., Alt, S., Klaus-Bergmann, A., Szymborska, A., Zheng, T., Perovic, T., et al. (2018). Primary cilia sensitize endothelial cells to BMP and prevent excessive vascular regression. *J. Cell Biol.* 217, 1651–1665. doi: 10.1083/jcb.201706151

Vivien, C. J., Pichol-Thievend, C., Sim, C. B., Smith, J. B., Bower, N. I., Hogan, B. M., et al. (2019). Vegfc/d-dependent regulation of the lymphatic vasculature during cardiac regeneration is influenced by injury context. *NPJ Regen. Med.* 4:18.

Vogrin, A. J., Bower, N. I., Gunzburg, M. J., Roufail, S., Okuda, K. S., Paterson, S., et al. (2019). Evolutionary differences in the Vegf/Vegfr code reveal organotypic roles for the endothelial cell receptor Kdr in developmental lymphangiogenesis. *Cell Rep.* 28, 2023–2036.e4. doi: 10.1016/j.celrep.2019.07.055

Wang, Y., Kaiser, M. S., Larson, J. D., Nasevicius, A., Clark, K. J., Wadman, S. A., et al. (2010). Moesin1 and Ve-cadherin are required in endothelial cells during in vivo tubulogenesis. *Development* 137, 3119–3128. doi: 10.1242/dev.048785

Wang, Y., Rovira, M., Yusuff, S., and Parsons, M. J. (2011). Genetic inducible fate mapping in larval zebrafish reveals origins of adult insulin-producing beta-cells. *Development* 138, 609–617. doi: 10.1242/dev.059097

Warp, E., Agarwal, G., Wyart, C., Friedmann, D., Oldfield, C. S., Conner, A., et al. (2012). Emergence of patterned activity in the developing zebrafish spinal cord. *Curr. Biol.* 22, 93–102. doi: 10.1016/j.cub.2011.12.002

Weijts, B., Gutierrez, E., Saikin, S. K., Ablooglu, A. J., Traver, D., Groisman, A., et al. (2018). Blood flow-induced Notch activation and endothelial migration enable vascular remodeling in zebrafish embryos. *Nat. Commun.* 9:5314.

Welti, J., Loges, S., Dimmeler, S., and Carmeliet, P. (2013). Recent molecular discoveries in angiogenesis and antiangiogenic therapies in cancer. *J. Clin. Invest.* 123, 3190–3200. doi: 10.1172/jci70212

Wigle, J. T., Harvey, N., Detmar, M., Lagutina, I., Grosveld, G., Gunn, M. D., et al. (2002). An essential role for Prox1 in the induction of the lymphatic endothelial cell phenotype. *EMBO J.* 21, 1505–1513. doi: 10.1093/emboj/21.7.1505

Wigle, J. T., and Oliver, G. (1999). Prox1 function is required for the development of the murine lymphatic system. *Cell* 98, 769–778. doi: 10.1016/s0092-8674(00)81511-1

Xu, C., Hasan, S. S., Schmidt, I., Rocha, S. F., Pitulescu, M. E., Bussmann, J., et al. (2014). Arteries are formed by vein-derived endothelial tip cells. *Nat. Commun.* 5:5758.

Yamamoto, H., Tobisawa, Y., Inubushi, T., Irie, F., Ohyama, C., and Yamaguchi, Y. (2017). A mammalian homolog of the zebrafish transmembrane protein 2 (TMEM2) is the long-sought-after cell-surface hyaluronidase. *J. Biol. Chem.* 292, 7304–7313. doi: 10.1074/jbc.m116.770149

Yokota, Y., Nakajima, H., Wakayama, Y., Muto, A., Kawakami, K., Fukuhara, S., et al. (2015). Endothelial Ca 2+ oscillations reflect VEGFR signaling-regulated angiogenic capacity in vivo. *eLife* 4:e08817.

Yu, J. A., Castranova, D., Pham, V. N., and Weinstein, B. M. (2015). Single-cell analysis of endothelial morphogenesis in vivo. *Development* 142, 2951–2961. doi: 10.1242/dev.123174

Zhong, T. P., Childs, S., Leu, J. P., and Fishman, M. C. (2001). Gridlock signalling pathway fashions the first embryonic artery. *Nature* 414, 216–220. doi: 10.1038/35102599

Zygmunt, T., Gay, C. M., Blondelle, J., Singh, M. K., Flaherty, K. M., Means, P. C., et al. (2011). Semaphorin-PlexinD1 signaling limits angiogenic potential via the VEGF decoy receptor sFlt1. *Dev. Cell* 21, 301–314. doi: 10.1016/j.devcel.2011.06.033

Conflict of Interest: The authors declare that the research was conducted in the absence of any commercial or financial relationships that could be construed as a potential conflict of interest.

frontiers in Cell and Developmental Biology

ORIGINAL RESEARCH
published: 31 July 2020
doi: 10.3389/fcell.2020.00708

Coronin 1B Controls Endothelial Actin Dynamics at Cell–Cell Junctions and Is Required for Endothelial Network Assembly

Ann-Cathrin Werner[1,2†], Ludwig T. Weckbach[1,2,3†], Melanie Salvermoser[1,2], Bettina Pitter[1,2], Jiahui Cao[4], Daniela Maier-Begandt[1,2], Ignasi Forné[5], Hans-Joachim Schnittler[4], Barbara Walzog[1,2] and Eloi Montanez[1,2,6]**

[1] Institute of Cardiovascular Physiology and Pathophysiology, Biomedical Center, LMU Munich, Munich, Germany, [2] Walter Brendel Center of Experimental Medicine, University Hospital, LMU Munich, Munich, Germany, [3] Medizinische Klinik I, Klinikum Großhadern, Munich, Germany, [4] Institute of Anatomy and Vascular Biology, Westfälische Wilhelms-Universität Münster, Münster, Germany, [5] Protein Analysis Unit, Biomedical Center, LMU Munich, Munich, Germany, [6] Department of Physiological Sciences, Faculty of Medicine and Health Sciences, University of Barcelona and IDIBELL, Barcelona, Spain

OPEN ACCESS

Edited by:
Jaap Diederik Van Buul,
University of Amsterdam, Netherlands

Reviewed by:
Stephan Huveneers,
Amsterdam University Medical Center (UMC), Netherlands
Orest William Blaschuk,
McGill University, Canada

***Correspondence:**
Barbara Walzog
walzog@lrz.uni-muenchen.de
Eloi Montanez
emontanez@ub.edu

[†] These authors have contributed equally to this work

Specialty section:
This article was submitted to Cell Adhesion and Migration, a section of the journal Frontiers in Cell and Developmental Biology

Received: 02 June 2020
Accepted: 13 July 2020
Published: 31 July 2020

Citation:
Werner A-C, Weckbach LT, Salvermoser M, Pitter B, Cao J, Maier-Begandt D, Forné I, Schnittler H-J, Walzog B and Montanez E (2020) Coronin 1B Controls Endothelial Actin Dynamics at Cell–Cell Junctions and Is Required for Endothelial Network Assembly. Front. Cell Dev. Biol. 8:708. doi: 10.3389/fcell.2020.00708

Development and homeostasis of blood vessels critically depend on the regulation of endothelial cell–cell junctions. VE-cadherin (VEcad)-based cell–cell junctions are connected to the actin cytoskeleton and regulated by actin-binding proteins. Coronin 1B (Coro1B) is an actin binding protein that controls actin networks at classical lamellipodia. The role of Coro1B in endothelial cells (ECs) is not fully understood and investigated in this study. Here, we demonstrate that Coro1B is a novel component and regulator of cell–cell junctions in ECs. Immunofluorescence studies show that Coro1B colocalizes with VEcad at cell–cell junctions in monolayers of ECs. Live-cell imaging reveals that Coro1B is recruited to, and operated at actin-driven membrane protrusions at cell–cell junctions. Coro1B is recruited to cell–cell junctions via a mechanism that requires the relaxation of the actomyosin cytoskeleton. By analyzing the Coro1B interactome, we identify integrin-linked kinase (ILK) as new Coro1B-associated protein. Coro1B colocalizes with α-parvin, an interactor of ILK, at the leading edge of lamellipodia protrusions. Functional experiments reveal that depletion of Coro1B causes defects in the actin cytoskeleton and cell–cell junctions. Finally, in matrigel tube network assays, depletion of Coro1B results in reduced network complexity, tube number and tube length. Together, our findings point toward a critical role for Coro1B in the dynamic remodeling of endothelial cell–cell junctions and the assembly of endothelial networks.

Keywords: endothelial cells, cell–cell junction, actin, tube formation, coronin 1B

INTRODUCTION

The formation of new blood vessels through angiogenesis involves endothelial cell (EC) adhesion, migration and proliferation and is critical for embryo development and tissue regeneration (Potente et al., 2011). Angiogenesis relies on the dynamic rearrangement of VE-cadherin (VEcad)-mediated cell–cell junctions (Giannotta et al., 2013; Cao and Schnittler, 2019). Endothelial cell–cell junctions are also crucial for vessel permeability, vessel stability and vascular integrity

(Dejana et al., 2009). Consequently, perturbations in cell–cell junction organization and function result in developmental defects and vascular pathologies including chronic inflammation, edema and atherosclerosis (Weis et al., 2004; Dejana et al., 2009). In addition to VEcad, ECs also express N-cadherin (Ncad) (Lampugnani et al., 1992), which has a dispersed distribution along cell membranes (Navarro et al., 1998; Kruse et al., 2019). Both cadherins contribute to establishing the endothelial barrier, but Ncad plays a key role in recruiting pericytes during angiogenesis (Gerhardt et al., 2000; Luo and Radice, 2005; Tillet et al., 2005). Although many aspects of blood vessel formation and homeostasis depend on cell–cell junctions, the molecular mechanisms that regulate their dynamic rearrangement are not fully understood.

The VEcad-catenin complex, which constitute the molecular basis of the adherens junctions, is connected to the actin cytoskeleton and its function is regulated by signal transduction, cytoskeletal contraction, and actin-driven plasma membrane protrusions (Dejana and Vestweber, 2013; Giannotta et al., 2013; Cao et al., 2017; Paatero et al., 2018; Cao and Schnittler, 2019). Endothelial adherens junctions are highly dynamic and therefore require constant VEcad rearrangement (Bentley et al., 2014). Junction-associated intermitted lamellipodia (JAIL) are small actin-driven protrusions at cell–cell junctions controlled by the actin related protein 2/3 (Arp2/3)-complex that contribute to the regulation of cell–cell junctions (Abu et al., 2014). JAIL driving VEcad dynamics within the cell–cell junction is critical for monolayer integrity, cell migration and angiogenesis (Abu et al., 2014; Fraccaroli et al., 2015; Cao et al., 2017). JAIL develop from branched actin filament and protrude across a small area of the apical membrane of the adjacent cell. In the overlapping area, VEcad plaques emerge due to trans-interactions between VEcad molecules (Abu et al., 2014). JAIL formation is terminated by the dissociation of the Arp2/3 complex from actin filaments. Actin disassembly leads to translocation of clustered VEcad molecules from the VEcad plaque to the junction resulting in the formation of a new VEcad adhesion site. JAIL formation depends on the relative concentration of VEcad at the cell–cell junction, however, the molecular mechanisms regulating JAIL during vessel development are not completely understood.

Actin-binding proteins regulate actin cytoskeleton dynamics thereby controlling the remodeling of endothelial cell–cell junctions, cell migration and vessel integrity (Pollard et al., 2000; Edwards et al., 2014). Several actin-binding proteins including EPLIN and α-parvin (α-pv) colocalize with and control JAIL formation (Fraccaroli et al., 2015; Taha et al., 2019). Parvins are a family of adaptor proteins that localize to focal complexes and focal adhesions, and facilitate the interaction of integrins with the actin cytoskeleton (Olski et al., 2001; Legate et al., 2006). Coronins are a family of actin-binding proteins that regulate actin polymerization via binding to and inhibiting the Arp2/3 complex (Cai et al., 2008; Chan et al., 2011; Howell et al., 2015). Type I coronins, such as coronin 1B (Coro1B), localize to the leading edge of migrating cells where they regulate actin dynamics in the lamellipodia via both Arp2/3 complex and cofilin-mediated pathways (Mishima and Nishida, 1999; Chan et al., 2011). Coro1B also fine-tunes ROCK-signaling pathway to regulate myosin activity (Rana and Worthylake, 2012; Priya et al., 2016). As such, type I coronins regulate actin-dependent processes including cell migration (Foger et al., 2006; Cai et al., 2007; Samarin et al., 2010; Howell et al., 2015). In epithelial cells, Coro1B controls actin cytoskeleton reorganization and cell–cell junction stability through RhoA signaling (Michael et al., 2016; Priya et al., 2016). Coro1B is expressed in ECs suggesting that it might regulate actin dynamics of blood vessels (Usatyuk et al., 2013; Kim et al., 2016), however, its role in ECs is not fully understood. In the current study we identify Coro1B as a new regulator of JAIL formation, cell–cell junction and the assembly of endothelial network *in vitro*.

MATERIALS AND METHODS

Cell Culture

Mouse embryonic ECs were isolated as previously described (Fraccaroli et al., 2015) and cultured in EC growth medium (Promocell). Human umbilical vein endothelial cells (HUVECs) (Pelobiotech) were cultured in EC medium (Promocell). Human dermal microvascular endothelial cells (HMECs) (American Type Culture Collection) were cultured in Dulbecco's Modified Eagle Medium (Thermo Fisher Scientific) supplemented with 10% EC growth medium (Promocell), 10% fetal calf serum (FCS) and 1% Penicillin/Streptomycin.

Antibodies and Reagents

The following antibodies and reagents were used for the analyses: the rabbit antibody against Coronin 1B (Sigma-Aldrich); mouse antibody against CD144 (VE-cadherin) (eBioscience), rabbit antibody against integrin-linked kinase (ILK) (Cell Signaling Technology) and rabbit antibody against α-parvin (Cell Signaling Technology). For secondary detection, species-specific Alexa Fluor-coupled secondary antibodies (Invitrogen) were used. Filamentous actin (F-actin) was visualized with Phalloidin Alexa-633 (Invitrogen). HUVEC cells were treated with thrombin (Sigma-Aldrich) and Y-27632 (Merck Millipore).

Immunostaining

For immunostaining, cells were seeded on glass coverslips coated with 0.15% gelatin. In indicated experiments, cells were treated with 0.2 U/ml thrombin or 10 μM Y-27632 for 10 min. Cells were fixed in 4% paraformaldehyde for 10 min, permeabilized with 0.1% Triton X-100 for 30 min and incubated with blocking solution (1% bovine serum albumin, 0.1% Triton X-100 in PBS) for 1 h at room temperature. Cells were exposed to primary antibodies overnight at 4°C. After washing three times with 0.1% Triton X-100 in PBS for 15 min, secondary antibodies were applied for 1 h at RT. After washing three times with PBS for 15 min, cells were embedded in Fluoromount (Southern Biotech) and analyzed with a Leica SP8X WLL upright confocal microscope (Leica).

Cloning, Gene Transduction, Transfection, and Live-Cell Imaging

To generate the Coro1B-GFP fusion protein, the Coro1B_pMK-RQ plasmid (Invitrogen) was amplified with the primers 5′-GCATAAGCTTATGTCCTTCCG-3′ and 5′-GTGAAAGGAAGGCCCATGA-3′ and the coding region for Coro1B was cloned into the vector pEGFP-N1 (Clontech) with using *Sac*II and *Hin*dIII and T4-Ligase (New England Biolabs). Recombinant lentiviral vectors carrying Lifeact-mCherry and VEcad-mCherry were kindly provided by Hans Schnittler. HUVECs were transduced with Lifeact-mCherry or VEcad-mCherry by incubation with viral particles resuspended in EC growth medium containing 3% poly-vinyl-pyrrolidone for 1 h. Afterward cells were transfected with Coro1B-GFP by using the MATra-A reagent (Promocell) and a magnet plate (Promocell) according to manufacturer's protocol. Cells were further cultured and after 48–72 h time-lapse recording with 63× objective at a spinning-disk confocal microscope (Carl Zeiss) at 37°C and 5% CO_2 was performed. The coding region for Coro1B-GFP was amplified with the primers 5′-TCG GCGCGCCACGCGTATGTCCTTCCGCAAAGTGG-3′ and 5′-AATGTTAACGACCGTTTACTTTACTTGTACAGCTCGTCC AT-3′ and by using *Mlu*I and *Age*I restriction sites with In-Fusion® HD Cloning Kit (Clontech) cloned into the lentiviral vector pLV-CMV-MCS-IRES-PURO-SIN. The coding region of GFP was amplified with the primers 5′-TCGGCGCGCCACGCGTATGGTGAGCAAGGGCGAGGAGC-3′ and 5′-CGGCATGGACGAGCTGTACAAGTAAACCGGTCG TTAACATT-3′ and subcloned into pLV-CMV-MCS-IRES-PURO-SIN using *Mlu*I and *Age*I restriction sites with In-Fusion® HD Cloning Kit (Clontech). Lentivirus encoding for Coro1B-GFP or GFP as control and a puromycin resistance was produced by transfection of human embryonic kidney 293T cells with the generated pLV-CMV-Coro1B-EGFP-IRES-PURO-SIN vector or pLV-CMV-EGFP-IRES-PURO-SIN vector, respectively, the envelope vector pCMV-VSV-G (Addgene) and the packaging vector pCMV-ΔR8.91 (Addgene) using Lipofectamin 2000 (Thermo Fisher Scientific) according to the manufacturer's protocol. Supernatant was collected after 48 h and filtered using 0.45 μm filters. HMECs were transduced by incubating with viral particles resuspended in Dulbecco's Modified Eagle Medium containing 10% EC growth medium, 10% FCS and 1% Penicillin/Streptomycin for 24 h. To generate cell lines stably expressing Coro1B-GFP and GFP, respectively, 72 h post transduction 10 μg/mL puromycin was added to the culture medium.

Co-immunoprecipitation and Western Blot

Stably Coro1B-GFP or GFP expressing HMECs were lysed with lysis buffer containing 25 mM trizma hydrochloride, 150 mM sodium chloride, 0.5 mM ethylenediaminetetraacetic acid, 1% Triton-X 100, 1% sodium deoxycholate, 1mM dithiothreitol, 1 mM diisopropylfluorphosphat, 10 mM sodium fluoride and 250 μM sodium orthovanadate and protease inhibitor mix B (Sigma-Aldrich) on a spinning wheel for 30 min at 4°C. Protein GFP-Trap beads (Chromotek) (Rothbauer et al., 2008) were equilibrated with PBS/lysis buffer. Protein lysate was sonicated, centrifuged for 10 min at 13.000 rpm and 2500 μg protein lysate supernatant was added to beads and incubated for 2 h at 4°C. After washing with PBS/lysis buffer GFP-Trap beads were resuspended in 2× Lämmli sample buffer and boiled 10 min at 95°C. Western blot was performed using primary antibodies against Coro1B (Sigma-Aldrich) and Integrin linked kinase-1 (ILK1) (Cell Signaling Technology) and secondary IRDye 600 and 800 CW infra-red anti-mouse and anti-rabbit antibodies (LI-COR Biotechnology). Immune reactive bands were detected using the LICOR Infra-red reading system according to the manufacturer's protocol.

On-Bead Digestion and Mass Spectrometry

GFP-Trap beads (Chromotek) were incubated with protein lysate supernatants prepared as described above and processed with the iST Sample Preparation Kit (Preomics) according to the manufacturer's protocol.

For LC-MS/MS purposes, desalted peptides were injected in an Ultimate 3000 RSLCnano system (Thermo Fisher Scientific) and separated using a 15-cm analytical column (75 μm ID home-packed with ReproSil-Pur C18-AQ 2.4 μm from Dr. Maisch) with a 50-min gradient from 5 to 60% acetonitrile in 0.1% formic acid. The effluent from the HPLC was directly electrosprayed into a Q_Exactive HF (Thermo Fisher Scientific) operated in data dependent mode to automatically switch between full scan MS and MS/MS acquisition. Survey full scan MS spectra (from m/z 375–1600) were acquired with resolution R = 60,000 at m/z 400 (AGC target of 3 × 106). The 10 most intense peptide ions with charge states between 2 and 5 were sequentially isolated to a target value of 1×10^5, and fragmented at 27% normalized collision energy. Typical mass spectrometric conditions were: spray voltage, 1.5 kV; no sheath and auxiliary gas flow; heated capillary temperature, 250°C; ion selection threshold, 33.000 counts. MaxQuant 1.5.2.8 was used to identify proteins and quantify by iBAQ with the following parameters: Database, UP000005640_Hsapiens_170526; MS tol, 10 ppm; MS/MS tol, 10 ppm; Peptide FDR, 0.1; Protein FDR, 0.01 Min. peptide Length, five; Variable modifications, Oxidation (M); Fixed modifications, Carbamidomethyl (C); Peptides for protein quantitation, razor and unique; Min. peptides, 1; Min. ratio count, 2. Identified proteins were considered as interaction partners if their MaxQuant iBAQ values were greater than log2 two-fold enrichment and p-value 0.05 when compared to the control. Mass spectrometry data are available via ProteomeXchange with identifier PXD018947.

Small Interfering RNA Transfection

HUVECs were transfected with small interfering RNA (siRNA) duplex against Coro1B (Sigma-Aldrich, SASI_Hs01_00084499 [siCoro1B #1] and SASI_Hs01_00084500 [siCoro1B #2]) and a scrambled control (Sigma-Aldrich, SIC001) using the MATra-si reagent (Promocell) and a magnet plate (Promocell) according to manufacturer's protocol. Experiments were performed 72 h

after transfection. All experiments were conducted with the two independent siRNA against Coro1B.

Tube Formation in Matrigel

Matrigel basement membrane matrix (Corning) was plated on coverslips and incubated for 30 min at 37°C to allow polymerization. After treatment with siControl, siCoro1B #1 and siCoro1B #2 for 72 h, 85.000 HUVECs per mL were seeded on top of the matrigel matrix. Light microscopy images were taken with a 5× objective at an inverted laboratory microscope Leica DM IL LED. The total tube length and the number of master segments were analyzed with the ImageJ plugin angiogenesis analyzer.

Statistics

Statistical analysis was performed using GraphPad Prism 6 (La Jolla, CA, United States). For pairwise comparison, the Student *t*-test, and for multiple comparisons, one-way ANOVA with the Dunnett's method was applied. $P < 0.05$ were considered significant. Data are presented as the mean ± SD of at least three independent experiments.

RESULTS

Coro1B Localizes to Cell–Cell Junctions in ECs

Coro1B regulates actin cytoskeleton organization at classical lamellipodia during cell spreading and migration (Mishima and Nishida, 1999; Chan et al., 2011). To study the role of Coro1B in actin cytoskeleton remodeling in ECs we first performed immunostaining of mouse and human primary ECs using specific antibodies against Coro1B and VEcad. As expected, the analysis showed that Coro1B localizes at the leading edge of classical lamellipodia in single cells as well as in subconfluent cell monolayers (**Figures 1A,B**). Interestingly, the analysis also revealed that a subset of Coro1B protein localizes close to cell–cell junctions where it partially colocalizes with VEcad (**Figures 1A,B**). In contrast to VEcad, Coro1B showed a discontinuous distribution pattern at cell–cell junctions (**Figures 1A,B**). This suggested that Coro1B is involved in actin cytoskeleton remodeling at cell–cell junctions. To investigate if Coro1B associates with F-actin at cell–cell junctions, we performed immunostaining on subconfluent HUVEC monolayers for Coro1B, VEcad and F-actin. The analysis showed that Coro1B is present at the leading edge of JAIL where it colocalizes with F-actin (**Figure 1C**). Immunofluorescent stainings in HMEC corroborate these findings (**Supplementary Figure S1** in the Data Supplement). Together, these results demonstrated that Coro1B is present at cell–cell junctions of ECs where it localizes at leading edges of JAIL.

Coro1B Is Dynamically Recruited to JAIL

To assess Coro1B recruitment in relation to JAIL formation, we performed live imaging of HUVECs using lentiviral expression of Coro1B-GFP and Lifeact-mCherry. Imaging of subconfluent monolayers of these cells with spinning disk confocal microscopy revealed the highly dynamic occurrence of classical lamellipodia protrusions and JAIL at cell–cell junctions (**Figure 2A**; Video I in the Data Supplement). Coro1B was consistently recruited to the leading edge of classical lamellipodia protrusions and JAIL where it colocalizes with F-actin during the whole process of JAIL dynamics (**Figure 2A**). These findings suggest the involvement of Coro1B in the actin remodeling processes associated to JAIL formation. JAIL drive the dynamic rearrangement of VEcad at cell junctions, while maintaining monolayer integrity (Abu et al., 2014). Therefore, localization and dynamics of Coro1B and VEcad were evaluated in subconfluent monolayers of Coro1B-GFP and VEcad-mCherry expressing HUVECs (**Figure 2B**; Video II in the Data Supplement). The analysis showed that Coro1B protrusions appeared at the cell–cell junction in spots with a local reduction of VEcad expression (**Figure 2B**, 25 s). The Coro1B protrusion was followed by the formation of a VEcad plaque, which is the result of JAIL that overlap adjacent cells and lead directly to VEcad transactions in this area (**Figure 2B**, 50 s). Subsequently, the Coro1B protrusion regressed and VEcad showed a linear continuous distribution along the plasma membrane (**Figure 2B**, 100 s). JAIL formation was accompanied by the movement of the cell–cell junction (**Supplementary Figure S2** in the Data Supplement).

Localization of Coro1B at Cell–Cell Junctions Is Actin-Dependent

To understand how Coro1B is recruited to cell junctions, we investigated the formation of JAIL by manipulating actin cytoskeleton contraction. First, we used the endothelial permeability factor thrombin that induces actomyosin contraction and cell–cell junction disruption by activating RhoA (Wojciak-Stothard and Ridley, 2002). Treatment of subconfluent monolayers of HUVECs with thrombin for 10 min resulted in increased levels of radial actin bundles and discontinuous VEcad staining (**Figure 3A**). Additionally, quantification analysis revealed a strong significant reduction in JAIL number per cell–cell junction length in thrombin treated cells compared to control cells (**Figure 3A**). Interestingly, staining of Coro1B at the cell–cell junction was markedly reduced after thrombin stimulation (**Figure 3A**). In contrast, inhibition of actin cytoskeleton tension by using the Rho-kinase inhibitor Y-27632 resulted in continuous VEcad staining, increased levels of VEcad-associated cortical actin, a significant increase of the number of JAIL per cell junction field and a decidedly increased localization of Coro1B at cell–cell junctions (**Figures 3A,B**). Together, these data suggest that reduction of actomyosin contraction induces JAIL formation and Coro1B recruitment at cell–cell junctions.

Coro1B Interacts With ILK and Colocalizes With α-pv in ECs

To gain insights into the molecular mechanism of Coro1B recruitment to JAIL, we screened for interacting partners of Coro1B in ECs. To this end, we conducted immunoprecipitation experiments with HMECs expressing Coro1B-GFP or GFP alone followed by mass spectrometry analysis. Among the proteins

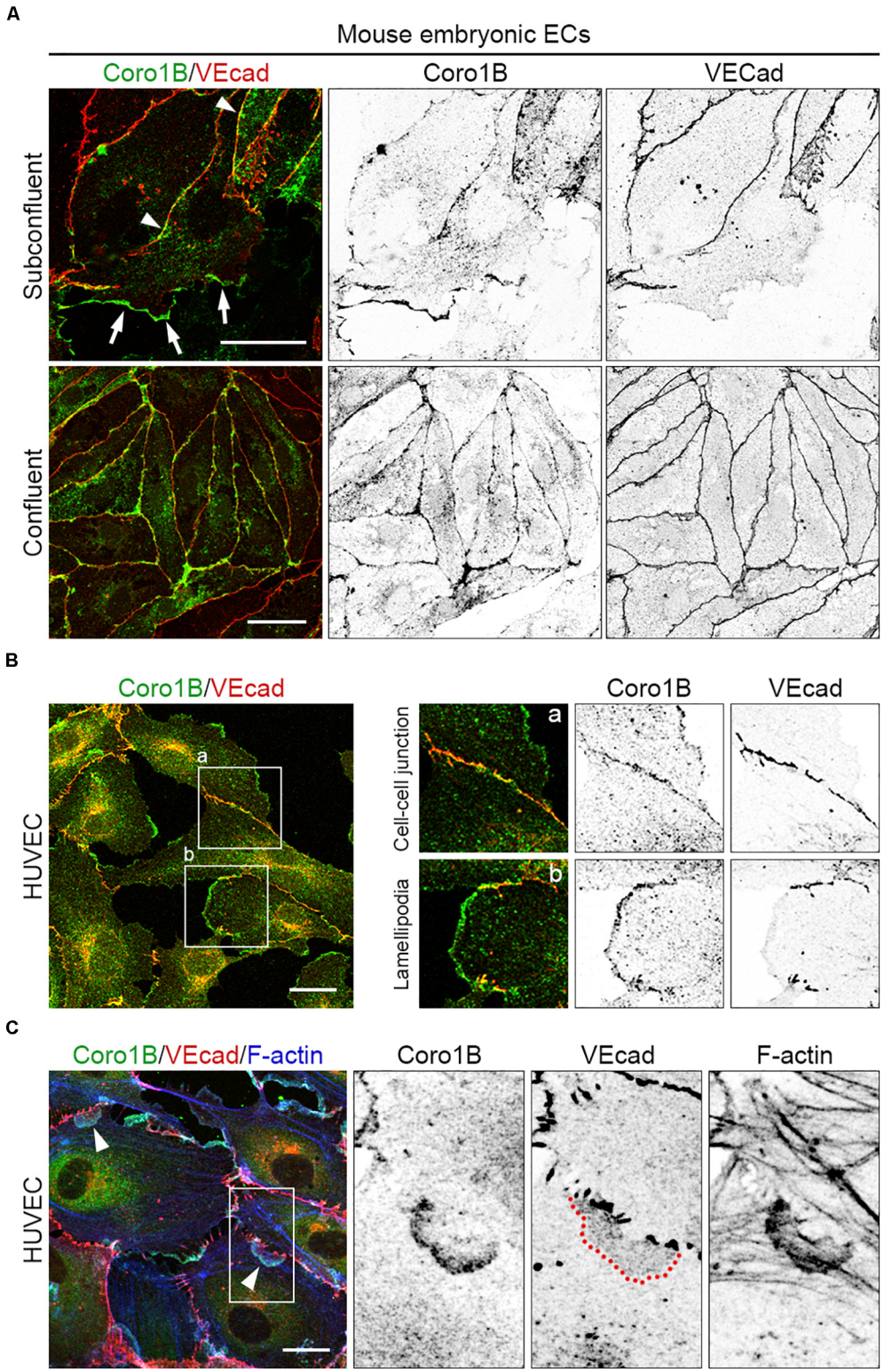

FIGURE 1 | Coro1B localizes to endothelial cell–cell junctions. **(A)** Mouse embryonic ECs immunostained for Coro1B (green) and VEcad (red) under subconfluent and confluent conditions. Arrows point to localization of Coro1B at classical lamellipodia, arrowheads indicate Coro1B at cell–cell junctions. **(B)** HUVECs labeled with Coro1B (green) and VEcad (red). Localization of Coro1B at cell–cell junctions (a, zoom-in right, upper panel) and at classical lamellipodia (b, zoom-in right, lower panel). **(C)** Localization of Coro1B (green), VEcad (red) and F-actin (blue) in subconfluent HUVEC monolayers. Arrowheads point to localization of Coro1B and F-actin at the leading edge of JAIL. Red line indicates VEcad plaque appearance. Scale bars = 25 μm.

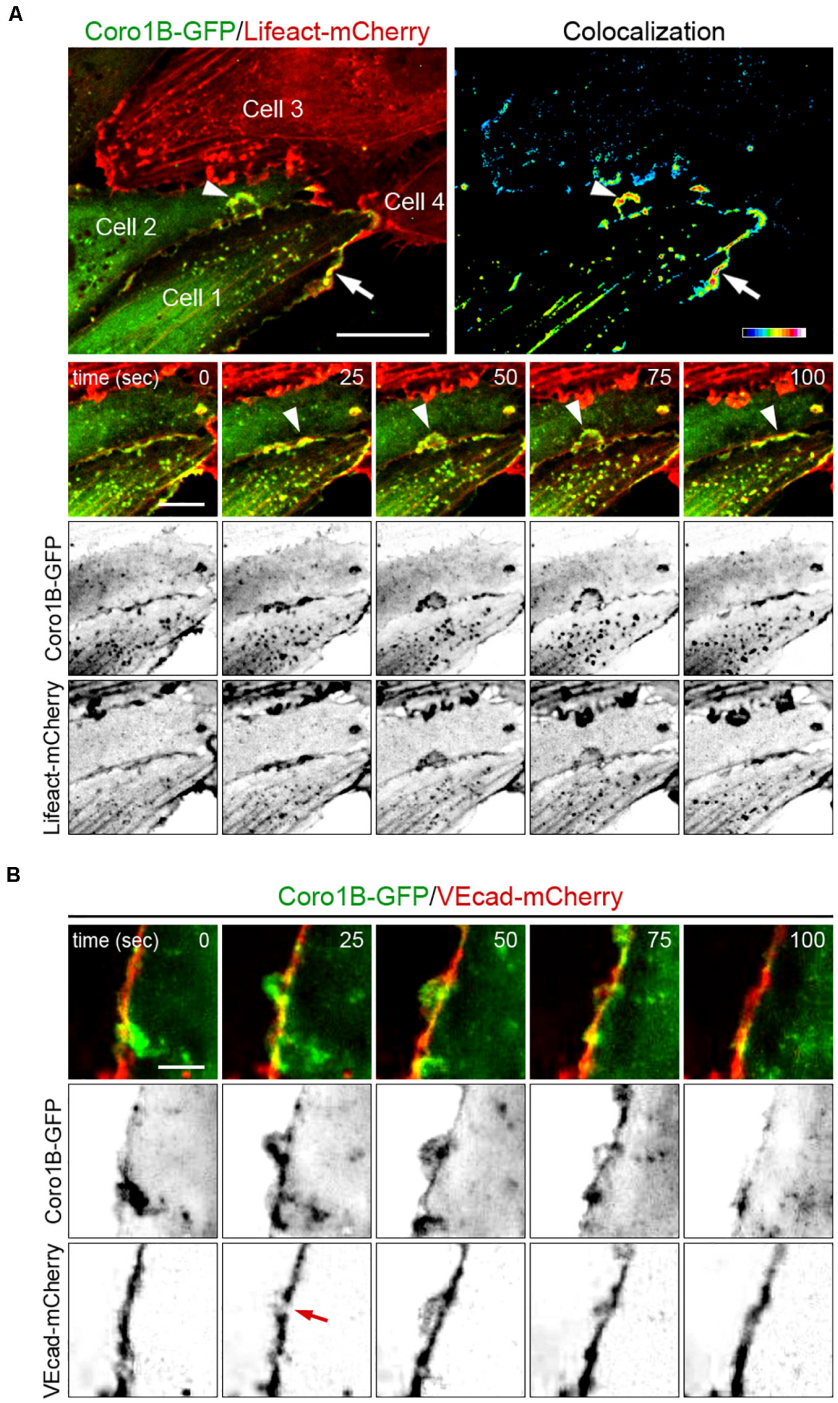

FIGURE 2 | Dynamics of Coro1B, F-actin and VEcad at cell–cell junctions. Still images from time-lapse recording of HUVECs expressing **(A)** Lifeact-mCherry (red) and Coro1B-GFP (green), and **(B)** VEcad-mCherry (red) and Coro1B-GFP (green). **(A)** Localization of Coro1B-GFP and Lifeact-mCherry at the leading edge of lamellipodia (arrow) and JAIL (arrowheads) at indicated time points. Upper panel, right: Colocalization of Coro1B-GFP and Lifeact-mCherry is displayed in a heat map. Scale bar = 10 μm, color scale. Scale bar = 5 μm. **(B)** Localization of Coro1B-GFP (green) and VEcad-mCherry (red) in double transfected HUVECs during JAIL formation in still images at indicated time points. Red arrow points to local reduction of VEcad. Scale bar = 5 μm.

that were precipitated with Coro1B we identified known Coro1B binding partners such as subunits of the Arp2/3 complex and cofilin as well as the novel interactor ILK (**Figure 4A** and **Supplementary Table S1** in the Data Supplement) (Howell et al., 2015). Given that ILK has also been identified as a key regulator of EC function and blood vessel homeostasis,

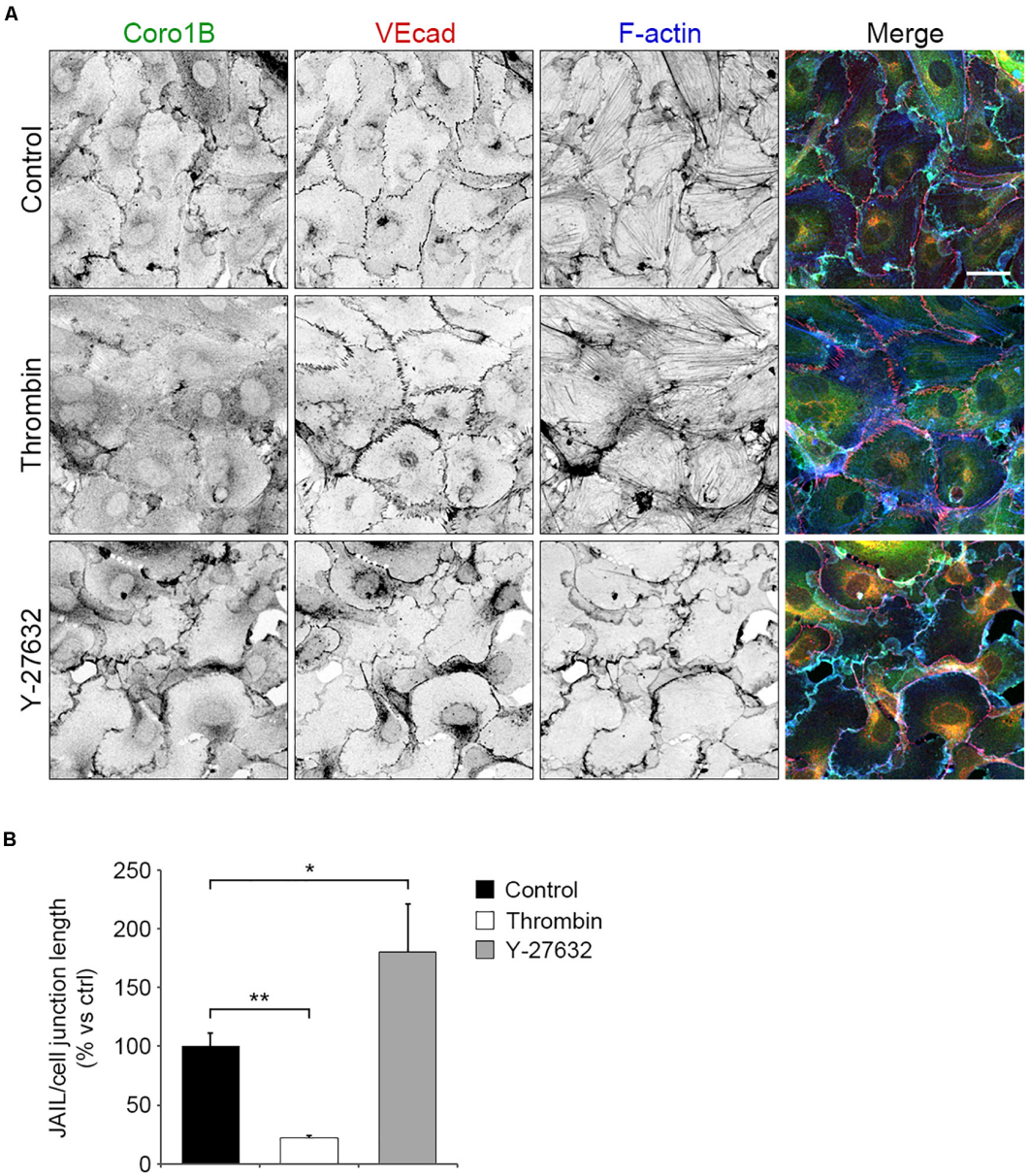

FIGURE 3 | Coro1B localization at cell–cell junctions is regulated by actomyosin contraction. **(A)** HUVECs untreated (control) and treated with thrombin (0.2 U/ml) or Y-27632 (10 μM) and immunostained for Coro1B (green), VEcad (red) and F-actin (blue). Scale bar = 25 μm. **(B)** Quantitative analysis of JAIL number per cell–cell junction length in control and treated cells. Data represent mean ± SD. $^{*}P < 0.05$, $^{**}P < 0.01$. $n = 3$.

we further characterized the Coro1B-ILK interaction (Friedrich et al., 2004; Park et al., 2019). Consistently with the proteomic data, endogenous ILK was co-immunoprecipitated with Coro1B-GFP (**Figure 4B**). ILK forms a ternary complex (the IPP complex) with the adaptor proteins PINCH and α-pv, which stabilize each other and link the integrin-mediated cell-matrix adhesions to the actin cytoskeleton (Legate et al., 2006). As endothelial α-pv localizes at JAIL and is required for proper JAIL formation (Fraccaroli et al., 2015), we performed α-pv immunostaining in Coro1B-GFP expressing HMEC and HUVECs. The analysis showed that Coro1B colocalizes with α-pv at the leading edge of classical lamellipodia and JAIL (**Figures 4C,D**). These results support the hypothesis that JAIL formation involves Coro1B.

Coro1B Controls Actin Cytoskeleton Organization and JAIL Formation

To decipher the functional relevance of Coro1B for JAIL formation in ECs, we depleted Coro1B expression through siRNAs. Two of the siRNA tested induced efficient significant knockdown of Coro1B protein levels in HUVECs (**Figures 5A,B**). To study the role of Coro1B on the actin cytoskeleton and

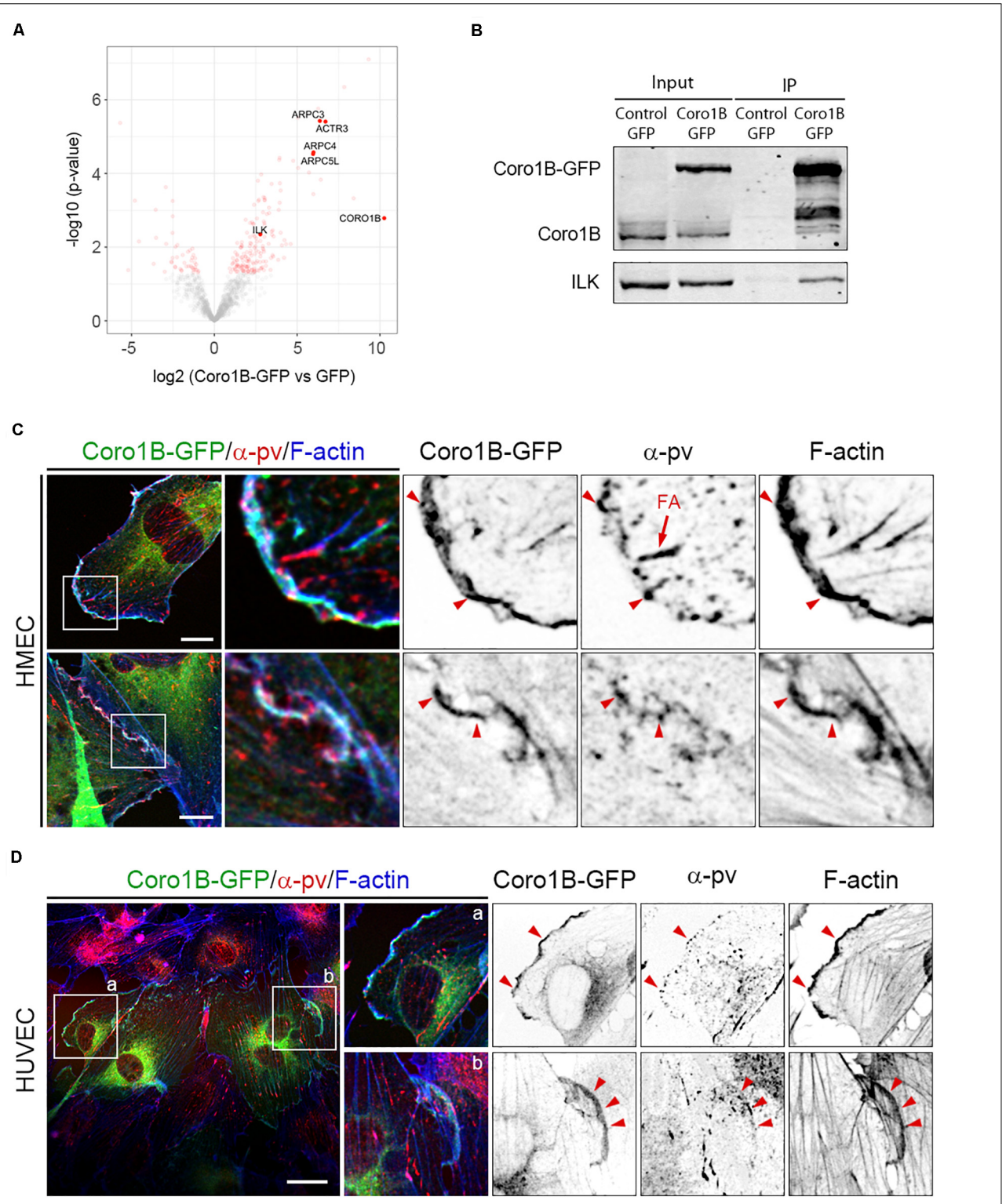

FIGURE 4 | ILK is a new Coro1B-interacting protein. **(A)** Volcano plot showing the log2 fold enrichment of the proteins identified by label-free mass spectrometry in immunoprecipitates from Coro1B-GFP HMECs compared to the GFP control HMECs and the *p*-value (–log10) of the adjusted *t*-test comparing the abundance of these proteins in both immunoprecipitates. Proteins with a log2 fold enrichment above 2.0 and a *p*-value below 0.05 were considered significant ($n = 4$, see **Supplementary Table S1**). **(B)** Coro1B-GFP immunoprecipitation of ILK in Coro1B-GFP expressing HMECs. GFP expressing HMECs were used as a control. Whole-cell lysates are shown as the input. Coro1B-GFP expressing **(C)** HMECs and **(D)** HUVECs transfected with Coro1B-GFP (green) and stained for α-pv (red) and F-actin (blue). Arrowheads point to Coro1B-GFP,α-pv and F-actin colocalization. FA (arrow): focal adhesions. Scale bar = 25 μm.

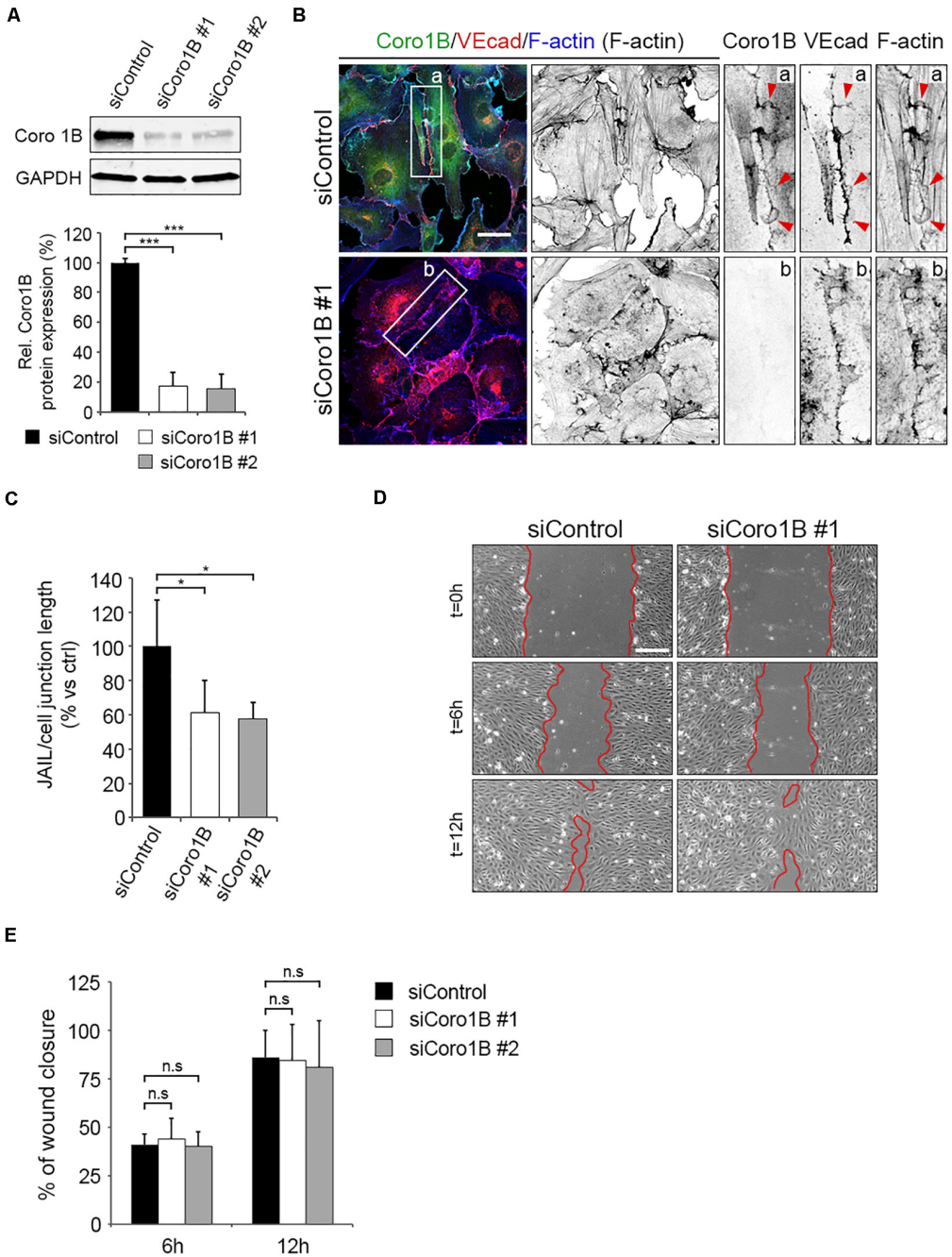

FIGURE 5 | Depletion of Coro1B in ECs alters the organization of the actin cytoskeleton and the formation of JAIL. **(A)** Representative western blot analysis of Coro1B and GAPDH (loading control) in total lysates of control and Coro1B-depleted HUVECs. Graph shows three independent experiments. Values represent mean ± SD. ***$P < 0.001$. Data are from three independent experiments. **(B)** Control and Coro1B-depleted HUVEC immunostained for Coro1B (green), VEcad (red) and F-actin (blue). Zoom-in indicate presence (a) or absence (b) of Coro1B at cell–cell junctions. Arrowheads point to JAIL. Scale bar = 25 μm. **(C)** Quantitative analysis of JAIL number per cell–cell junction length in control and Coro1B-depleted HUVECs. Values are normalized to control. Data represent mean ± SD. *$P < 0.05$, $n = 4$. **(D)** Representative phase-contrast images of control and Coro1B-depleted HUVECs in a scratch-wound assay ($t = 0$, $t = 6$, and $t = 12$ h after scratch). Red lines highlight the unclosed wound area. Scale bar = 200 μm. **(E)** Graph showing the mean ± SD percentage of wound closure of control and Coro1B-depleted HUVECs at two time points during scratch-wound assay. Data are from three independent experiments. ns; not significant.

JAIL formation, we immunostained subconfluent monolayers of control and Coro1B-depleted HUVECs for Coro1B, VEcad and F-actin. Coro1B knockdown resulted in reduced stress fibers, discontinuous cortical actin, and disorganized VEcad compared to control cells (**Figure 5B**). Quantification analysis showed a significant decrease in number of JAIL per cell–cell junction

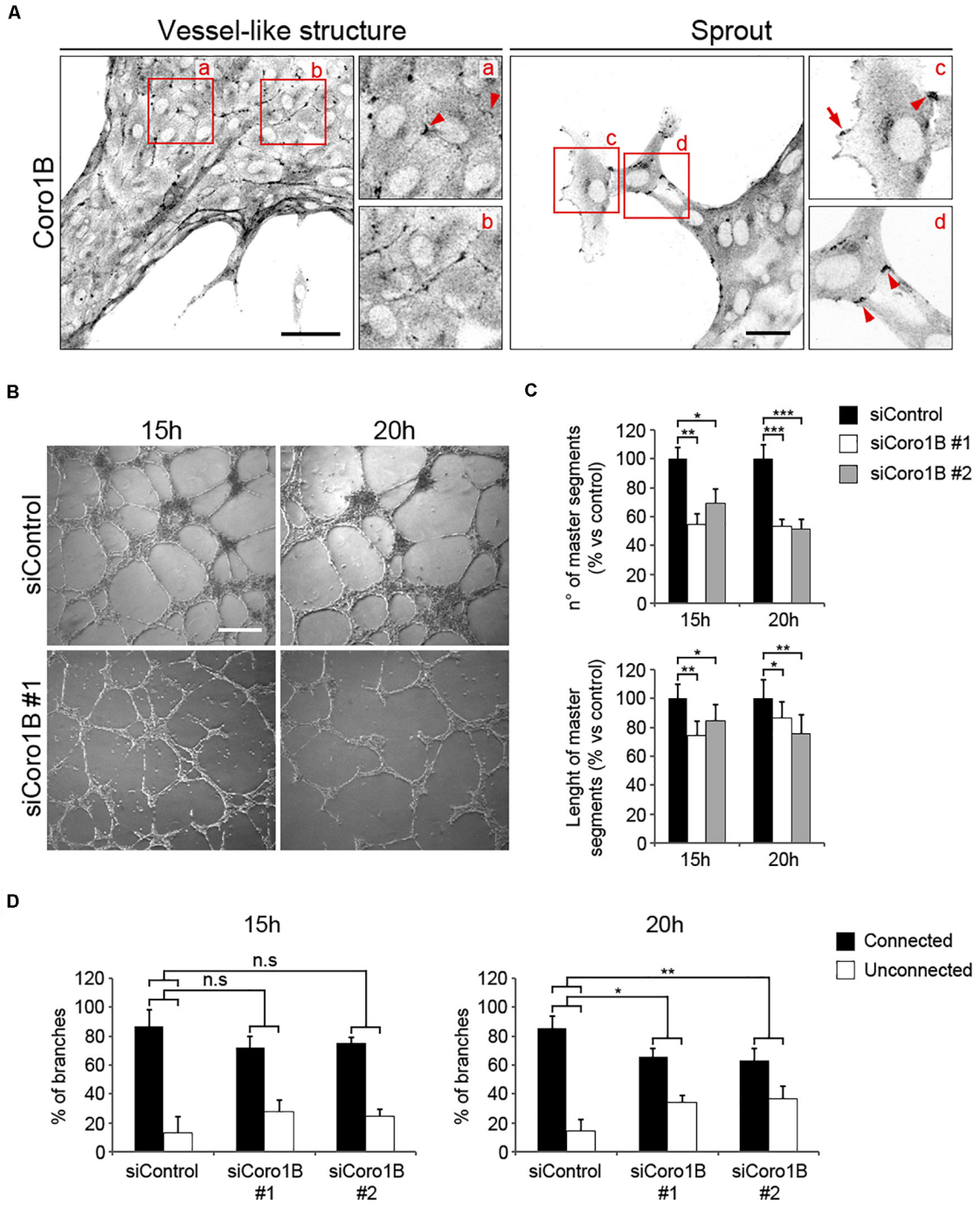

FIGURE 6 | Coro1B is required for proper endothelial network assembly in matrigel. **(A)** HUVECs cultured on matrigel for 20 h and immunostained for Coro1B. Scale bar = 50 μm (left) and 25 μm (right). Arrowheads point to Coro1B localization at JAIL-like structures and arrow indicates Coro1B localization at classical lamellipodium. **(B)** Representative phase-contrast images of tube networks of control and Coro1B-depleted HUVECs at indicated time points after seeding. Scale bar = 200 μm. Quantitative analysis of **(C)** the number and length of master segments and **(D)** connected and unconnected tube networks of control and Coro1B-depleted HUVECs. Values are normalized to control. Data represent mean ± SD of three independent experiments. $^{*}P < 0.05$, $^{**}P < 0.01$, $^{***}P < 0.001$. ns; not significant.

length in Coro1B-depleted cells when compared to control cells (**Figure 5C**). We next examined whether endothelial Coro1B is involved in collective cell migration. To do this, we performed scratch wound assays and found no differences in cell migration between control and Coro1B-depleted cells (**Figures 5D,E**). Together, these results indicated that Coro1B controls actin

cytoskeleton rearrangement and JAIL formation in ECs but it is dispensable for collective EC migration.

Coro1B Is Critical for Endothelial Network Assembly *in vitro*

It has been recently shown that JAIL are essential for blood vessel formation and vascular homeostasis (Cao et al., 2017). To establish whether Coro1B plays a role in vessel formation, control and Coro1B-depleted HUVECs were cultured on matrigel coats and tube formation was assessed as previously described (Montanez et al., 2002). First, we performed immunostaining of control vessel-like structures with Coro1B. The analysis showed that Coro1B localizes at putative JAIL at cell junctions (**Figure 6A**, Box a,b). In vessel sprouts Coro1B was localized at classical lamellipodia (**Figure 6A**, Box c) and cell–cell junctions (**Figure 6A**, Box c,d). To address the functional role of Coro1B for EC tube formation, we performed the matrigel assay using HUVECs after treatment with siRNA against Coro1B or control siRNA and subsequently analyzed tube formation. The analysis showed that depletion of Coro1B significantly reduced the number of master segments as well as the length of master segments compared to control conditions (**Figures 6B,C**). Furthermore, the percentage of connected branches was significantly diminished in Coro1B-depleted cells (**Figure 6D**). These results indicate that Coro1B is critically required for proper *in vitro* tube network formation.

DISCUSSION

In this study we identified the actin-binding protein Coro1B as a novel component and regulator of endothelial cell–cell junctions. Our data show that Coro1B is recruited to, and operates at, actin-driven protrusions at cell–cell junctions called JAIL. The recruitment of Coro1B to cell–cell junctions and the formation of JAIL are regulated by actin cytoskeleton remodeling and contraction. Using mass spectrometry, we identified ILK as a new Coro1B-interacting protein in ECs. Finally, depletion of Coro1B in ECs leads to defects in actin cytoskeleton organization, reduced number of JAIL, altered cell–cell junction morphology and impaired endothelial network assembly.

The actin cytoskeleton enables many dynamic cellular activities, including lamellipodia protrusion, cell migration and cell–cell junction formation and maintenance (Edwards et al., 2014). To do this, the actin filaments undergo continuous cycles of polymerization and depolymerization regulated by actin-binding proteins including the Arp2/3 complex, cofilin and coronins, and are often induced in response to extracellular signals. The actin polymerizing proteins of the Arp2/3 complex regulate migration of EC and integrity of endothelial cell–cell junctions, thereby being essential for angiogenesis (De Smet et al., 2009; Garcia-Ponce et al., 2015; Phng et al., 2015). Recently it has been shown that JAIL, actin-driven and Arp2/3 complex-controlled plasma membrane protrusions that develop at cell–cell junction sites with decreased or lost VEcad, regulate the local dynamics and patterning of VEcad, thereby controlling junctional integrity and monolayer formation *in vitro* and sprouting angiogenesis *in vivo* (Fraccaroli et al., 2015; Cao et al., 2017). Our results showed that in addition to classical lamellipodia, Coro1B is found at cell–cell junctions and at the leading edge of JAIL in ECs, suggesting that Coro1B regulates actin cytoskeleton dynamics at cell–cell junctions. Cytoskeleton manipulation experiments showed that the mechanisms underlying Coro1B recruitment to cell–cell junctions involve actin cytoskeleton tension. While thrombin-stimulated actomyosin contraction reduces Coro1B localization at the cell–cell junction and JAIL formation, inhibition of actomyosin contraction with the Rho-kinase inhibitor Y-27632 increases Coro1B localization at the cell–cell junctions and JAIL formation. These findings suggest a functional interaction between Coro1B, the actin cytoskeleton and JAIL, which is in agreement with previous reports (Cao et al., 2017). Quantification analysis of JAIL in control and Coro1B-depleted ECs clearly show that once Coro1B is functionally perturbed, the frequency of JAIL is reduced. This reduction in JAIL formation is associated with disorganized actin cytoskeleton and discontinuous distribution of VEcad at cell–cell junctions. In migrating fibroblasts, Coro1B induced the dissociation of the Arp2/3 complex from actin filaments, which is critical for classical lamellipodia formation, thereby promoting the disassembly of the actin network in lamellipodia (Cai et al., 2008). By the same mechanism, Coro1B could regulate JAIL formation at cell–cell junctions in ECs. In epithelial cells, Coro1B was shown to regulate actin cytoskeleton reorganization and cell–cell junction stability through RhoA signaling (Michael et al., 2016; Priya et al., 2016). Together with our experiments, this data point to an essential role of Coro1B in regulating endothelial and epithelial cell–cell junctions.

To understand how Coro1B localizes to cell–cell junctions and JAIL, we performed pulldown experiments followed by mass spectrometry analysis. The finding of well-known Coro1B binding proteins such as several subunits of the Arp2/3 complex among the top hits in our interactome screen validates our results. Although our immunostaining studies show partial colocalization of Coro1B and the VEcad-catenin complex at cell–cell junctions, we did not find VEcad or α- or β-catenin in our interactome suggesting no direct binding between Coro1B and the VEcad-catenin complex. Our analysis identified ILK as a new Coro1B-interacting protein. ILK is known to bind to α-pv and PINCH to form the IPP-complex, which critically controls integrin signaling at focal complexes and focal adhesions (Legate et al., 2006; Wickstrom et al., 2010). ILK is essential for vessel development and vessel homeostasis (Friedrich et al., 2004; Tan et al., 2004; Park et al., 2019). Moreover, ILK regulates cell–cell junctions in epithelial cells (Vespa et al., 2005). In addition to its localization to integrin-mediated adhesions, α-pv is recruited to JAIL in ECs, where it regulates actin rearrangement and VEcad organization (Fraccaroli et al., 2015). As such, α-pv controls sprouting angiogenesis and blood vessel stability (Fraccaroli et al., 2015). Our immunostaining studies show that Coro1B is not present in the focal adhesions and suggest that Coro1B-ILK interaction takes place in the focal complexes at the leading edge of classical lamellipodia. The analysis also demonstrates a colocalization of Coro1B and α-pv at JAIL, suggesting that they cooperate at JAIL to control F-actin remodeling.

Our functional analysis data shows that Coro1B is not essential for collective migration of ECs. However, JAIL-mediated cell–cell junction remodeling is critical for sprouting angiogenesis and blood vessel network formation in mice (Cao et al., 2017). To decipher whether Coro1B is needed for vessel network assembling, we conducted tube network formation assays on matrigel, a matrix rich in ECM components such as laminin and collagen-IV. The depletion of Coro1B reduces the number of tubes, their length and the complexity of the network. Moreover, the number of unconnected tubes increases over time in Coro1B-depleted cells compared to control cells, suggesting that Coro1B is needed for tube stability. Taken together, our findings suggest that Coro1B is required for endothelial cell–cell junction remodeling and blood vessel network formation/maintenance. New experiments are now needed to determine the role of Coro1B on sprouting angiogenesis, endothelial barrier and blood vessel permeability *in vivo*.

DATA AVAILABILITY STATEMENT

All datasets presented in this study are included in the article/**Supplementary Material**.

AUTHOR CONTRIBUTIONS

H-JS, BW, and EM designed the experiments. A-CW, LW, MS, BP, JC, and DM-B performed the experiments. IF, H-JS, BW, and EM interpreted the results. A-CW, LW, and EM wrote the manuscript. All authors contributed to the article and approved the submitted version.

FUNDING

This work was supported by grants from the Deutsche Forschungsgemeinschaft (MO2561/1-2 [EM], SFB 914/A02 [DM-B and BW], Z03 [BW] and B10 [LW], and SPP 1782 [H-JS]).

ACKNOWLEDGMENTS

The authors thank Brigitte Bergner for excellent technical assistance. The authors are grateful to Dr. Steffen Dietzel and Dr. Andreas Thomae (Core Facility Bioimaging, Biomedical Center, LMU, Munich, Germany) for their support with the confocal laser-scanning microscopy. The authors thank Dr. Tobias Straub (Core Facility Bioinformatics, Biomedical Center, LMU, Munich, Germany) for his support with the statistical analysis.

SUPPLEMENTARY MATERIAL

The Supplementary Material for this article can be found online at: https://www.frontiersin.org/articles/10.3389/fcell.2020.00708/full#supplementary-material

REFERENCES

Abu, T. A., Taha, M., Seebach, J., and Schnittler, H. J. (2014). ARP2/3-mediated junction-associated lamellipodia control VE-cadherin-based cell junction dynamics and maintain monolayer integrity. *Mol. Biol. Cell* 25, 245–256. doi: 10.1091/mbc.E13-07-0404

Bentley, K., Franco, C. A., Philippides, A., Blanco, R., Dierkes, M., Gebala, V., et al. (2014). The role of differential VE-cadherin dynamics in cell rearrangement during angiogenesis. *Nat. Cell Biol.* 16, 309–321. doi: 10.1038/ncb2926

Cai, L., Makhov, A. M., Schafer, D. A., and Bear, J. E. (2008). Coronin 1B antagonizes cortactin and remodels Arp2/3-containing actin branches in lamellipodia. *Cell* 134, 828–842. doi: 10.1016/j.cell.2008.06.054

Cai, L., Marshall, T. W., Uetrecht, A. C., Schafer, D. A., and Bear, J. E. (2007). Coronin 1B coordinates Arp2/3 complex and cofilin activities at the leading edge. *Cell* 128, 915–929. doi: 10.1016/j.cell.2007.01.031

Cao, J., Ehling, M., Marz, S., Seebach, J., Tarbashevich, K., Sixta, T., et al. (2017). Polarized actin and VE-cadherin dynamics regulate junctional remodelling and cell migration during sprouting angiogenesis. *Nat. Commun.* 8:2210. doi: 10.1038/s41467-017-02373-8

Cao, J., and Schnittler, H. (2019). Putting VE-cadherin into JAIL for junction remodeling. *J. Cell Sci.* 132:893. doi: 10.1242/jcs.222893

Chan, K. T., Creed, S. J., and Bear, J. E. (2011). Unraveling the enigma: progress towards understanding the coronin family of actin regulators. *Trends Cell Biol.* 21, 481–488. doi: 10.1016/j.tcb.2011.04.004

De Smet, F., Segura, I., De Bock, K., Hohensinner, P. J., and Carmeliet, P. (2009). Mechanisms of vessel branching: filopodia on endothelial tip cells lead the way. *Arterioscler. Thromb. Vasc. Biol.* 29, 639–649. doi: 10.1161/atvbaha.109.185165

Dejana, E., Tournier-Lasserve, E., and Weinstein, B. M. (2009). The control of vascular integrity by endothelial cell junctions: molecular basis and pathological implications. *Dev. Cell* 16, 209–221. doi: 10.1016/j.devcel.2009.01.004

Dejana, E., and Vestweber, D. (2013). The role of VE-cadherin in vascular morphogenesis and permeability control. *Prog. Mol. Biol. Transl. Sci.* 116, 119–144. doi: 10.1016/b978-0-12-394311-8.00006-6

Edwards, M., Zwolak, A., Schafer, D. A., Sept, D., Dominguez, R., and Cooper, J. A. (2014). Capping protein regulators fine-tune actin assembly dynamics. *Nat. Rev. Mol. Cell Biol.* 15, 677–689. doi: 10.1038/nrm3869

Foger, N., Rangell, L., Danilenko, D. M., and Chan, A. C. (2006). Requirement for coronin 1 in T lymphocyte trafficking and cellular homeostasis. *Science* 313, 839–842. doi: 10.1126/science.1130563

Fraccaroli, A., Pitter, B., Taha, A. A., Seebach, J., Huveneers, S., Kirsch, J., et al. (2015). Endothelial alpha-parvin controls integrity of developing vasculature and is required for maintenance of cell-cell junctions. *Circulat. Res.* 117, 29–40. doi: 10.1161/CIRCRESAHA.117.305818

Friedrich, E. B., Liu, E., Sinha, S., Cook, S., Milstone, D. S., MacRae, C. A., et al. (2004). Integrin-linked kinase regulates endothelial cell survival and vascular development. *Mol. Cell Biol.* 24, 8134–8144. doi: 10.1128/mcb.24.18.8134-8144.2004

Garcia-Ponce, A., Citalan-Madrid, A. F., Velazquez-Avila, M., Vargas-Robles, H., and Schnoor, M. (2015). The role of actin-binding proteins in the control of endothelial barrier integrity. *Thromb. Haemost.* 113, 20–36. doi: 10.1160/th14-04-0298

Gerhardt, H., Wolburg, H., and Redies, C. (2000). N-cadherin mediates pericytic-endothelial interaction during brain angiogenesis in the chicken. *Dev. Dyn.* 218, 472–479. doi: 10.1002/1097-0177(200007)218:3<472::Aid-dvdy1008<3.0.Co;2-\#

Giannotta, M., Trani, M., and Dejana, E. (2013). VE-cadherin and endothelial adherens junctions: active guardians of vascular integrity. *Dev. Cell* 26, 441–454. doi: 10.1016/j.devcel.2013.08.020

Howell, M., Brickner, H., Delorme-Walker, V. D., Choi, J., Saffin, J. M., Miller, D., et al. (2015). WISp39 binds phosphorylated Coronin 1B to regulate Arp2/3 localization and Cofilin-dependent motility. *J. Cell Biol.* 208, 961–974. doi: 10.1083/jcb.201410095

Kim, G. Y., Park, J. H., Kim, H., Lim, H. J., and Park, H. Y. (2016). Coronin 1B serine 2 phosphorylation by p38alpha is critical for vascular endothelial growth factor-induced migration of human umbilical vein endothelial cells. *Cell Signal* 28, 1817–1825. doi: 10.1016/j.cellsig.2016.08.009

Kruse, K., Lee, Q. S., Sun, Y., Klomp, J., Yang, X., Huang, F., et al. (2019). N-cadherin signaling via Trio assembles adherens junctions to restrict endothelial permeability. *J. Cell Biol.* 218, 299–316. doi: 10.1083/jcb.201802076

Lampugnani, M. G., Resnati, M., Raiteri, M., Pigott, R., Pisacane, A., Houen, G., et al. (1992). A novel endothelial-specific membrane protein is a marker of cell-cell contacts. *J. Cell Biol.* 118, 1511–1522. doi: 10.1083/jcb.118.6.1511

Legate, K. R., Montanez, E., Kudlacek, O., and Fassler, R. (2006). ILK, PINCH and parvin: the tIPP of integrin signalling. *Nat. Rev. Mol. Cell Biol.* 7, 20–31. doi: 10.1038/nrm1789

Luo, Y., and Radice, G. L. (2005). N-cadherin acts upstream of VE-cadherin in controlling vascular morphogenesis. *J. Cell Biol.* 169, 29–34. doi: 10.1083/jcb.200411127

Michael, M., Meiring, J. C. M., Acharya, B. R., Matthews, D. R., Verma, S., Han, S. P., et al. (2016). Coronin 1B reorganizes the architecture of F-actin networks for contractility at steady-state and apoptotic adherens junctions. *Dev. Cell* 37, 58–71. doi: 10.1016/j.devcel.2016.03.008

Mishima, M., and Nishida, E. (1999). Coronin localizes to leading edges and is involved in cell spreading and lamellipodium extension in vertebrate cells. *J. Cell Sci.* 112(Pt 17), 2833–2842.

Montanez, E., Casaroli-Marano, R. P., Vilaro, S., and Pagan, R. (2002). Comparative study of tube assembly in three-dimensional collagen matrix and on Matrigel coats. *Angiogenesis* 5, 167–172. doi: 10.1023/a:1023837821062

Navarro, P., Ruco, L., and Dejana, E. (1998). Differential localization of VE- and N-cadherins in human endothelial cells: VE-cadherin competes with N-cadherin for junctional localization. *J. Cell Biol.* 140, 1475–1484. doi: 10.1083/jcb.140.6.1475

Olski, T. M., Noegel, A. A., and Korenbaum, E. (2001). Parvin, a 42 kDa focal adhesion protein, related to the alpha-actinin superfamily. *J. Cell Sci.* 114(Pt 3), 525–538.

Paatero, I., Sauteur, L., Lee, M., Lagendijk, A. K., Heutschi, D., Wiesner, C., et al. (2018). Junction-based lamellipodia drive endothelial cell rearrangements in vivo via a VE-cadherin-F-actin based oscillatory cell-cell interaction. *Nat. Commun.* 9:3545. doi: 10.1038/s41467-018-05851-9

Park, H., Yamamoto, H., Mohn, L., Ambuhl, L., Kanai, K., Schmidt, I., et al. (2019). Integrin-linked kinase controls retinal angiogenesis and is linked to Wnt signaling and exudative vitreoretinopathy. *Nat. Commun.* 10:5243. doi: 10.1038/s41467-019-13220-3

Phng, L. K., Gebala, V., Bentley, K., Philippides, A., Wacker, A., Mathivet, T., et al. (2015). Formin-mediated actin polymerization at endothelial junctions is required for vessel lumen formation and stabilization. *Dev. Cell* 32, 123–132. doi: 10.1016/j.devcel.2014.11.017

Pollard, T. D., Blanchoin, L., and Mullins, R. D. (2000). Molecular mechanisms controlling actin filament dynamics in nonmuscle cells. *Annu. Rev. Biophys. Biomol. Struct.* 29, 545–576. doi: 10.1146/annurev.biophys.29.1.545

Potente, M., Gerhardt, H., and Carmeliet, P. (2011). Basic and therapeutic aspects of angiogenesis. *Cell* 146, 873–887. doi: 10.1016/j.cell.2011.08.039

Priya, R., Wee, K., Budnar, S., Gomez, G. A., Yap, A. S., and Michael, M. (2016). Coronin 1B supports RhoA signaling at cell-cell junctions through Myosin II. *Cell Cycle* 15, 3033–3041. doi: 10.1080/15384101.2016.1234549

Rana, M. K., and Worthylake, R. A. (2012). Novel mechanism for negatively regulating Rho-kinase (ROCK) signaling through Coronin1B protein in neuregulin 1 (NRG-1)-induced tumor cell motility. *J. Biol. Chem.* 287, 21836–21845. doi: 10.1074/jbc.M112.346114

Rothbauer, U., Zolghadr, K., Muyldermans, S., Schepers, A., Cardoso, M. C., and Leonhardt, H. (2008). A versatile nanotrap for biochemical and functional studies with fluorescent fusion proteins. *Mol. Cell Proteomics* 7, 282–289. doi: 10.1074/mcp.M700342-MCP200

Samarin, S. N., Koch, S., Ivanov, A. I., Parkos, C. A., and Nusrat, A. (2010). Coronin 1C negatively regulates cell-matrix adhesion and motility of intestinal epithelial cells. *Biochem. Biophys. Res. Commun.* 391, 394–400. doi: 10.1016/j.bbrc.2009.11.069

Taha, M., Aldirawi, M., Marz, S., Seebach, J., Odenthal-Schnittler, M., Bondareva, O., et al. (2019). EPLIN-alpha and -beta isoforms modulate endothelial cell dynamics through a spatiotemporally differentiated interaction with actin. *Cell Rep* 29, 1010–1026.e1016. doi: 10.1016/j.celrep.2019.09.043

Tan, C., Cruet-Hennequart, S., Troussard, A., Fazli, L., Costello, P., Sutton, K., et al. (2004). Regulation of tumor angiogenesis by integrin-linked kinase (ILK). *Cancer Cell* 5, 79–90.

Tillet, E., Vittet, D., Féraud, O., Moore, R., Kemler, R., and Huber, P. (2005). N-cadherin deficiency impairs pericyte recruitment, and not endothelial differentiation or sprouting, in embryonic stem cell-derived angiogenesis. *Exp. Cell Res.* 310, 392–400. doi: 10.1016/j.yexcr.2005.08.021

Usatyuk, P. V., Burns, M., Mohan, V., Pendyala, S., He, D., Ebenezer, D. L., et al. (2013). Coronin 1B regulates S1P-induced human lung endothelial cell chemotaxis: role of PLD2, protein kinase C and Rac1 signal transduction. *PLoS One* 8:e63007. doi: 10.1371/journal.pone.0063007

Vespa, A., D'Souza, S. J., and Dagnino, L. (2005). A novel role for integrin-linked kinase in epithelial sheet morphogenesis. *Mol. Biol. Cell* 16, 4084–4095. doi: 10.1091/mbc.e05-02-0087

Weis, S., Shintani, S., Weber, A., Kirchmair, R., Wood, M., Cravens, A., et al. (2004). Src blockade stabilizes a Flk/cadherin complex, reducing edema and tissue injury following myocardial infarction. *J. Clin. Invest.* 113, 885–894. doi: 10.1172/jci20702

Wickstrom, S. A., Lange, A., Montanez, E., and Fassler, R. (2010). The ILK/PINCH/parvin complex: the kinase is dead, long live the pseudokinase! *Embo J.* 29, 281–291. doi: 10.1038/emboj.2009.376

Wojciak-Stothard, B., and Ridley, A. J. (2002). Rho GTPases and the regulation of endothelial permeability. *Vasc. Pharm.* 39, 187–199. doi: 10.1016/s1537-1891(03)00008-9

Conflict of Interest: The authors declare that the research was conducted in the absence of any commercial or financial relationships that could be construed as a potential conflict of interest.

frontiers in Physiology

ORIGINAL RESEARCH
published: 16 September 2020
doi: 10.3389/fphys.2020.00951

Angiotensin-Converting Enzyme Gene D/I Polymorphism in Relation to Endothelial Function and Endothelial-Released Factors in Chinese Women

Yuanyuan Lv[1†], Wenying Zhao[2†], Laikang Yu[3], Ji-Guo Yu[4] and Li Zhao[5*]*

[1] China Institute of Sport and Health Science, Beijing Sport University, Beijing, China, [2] Children's Hospital of Shanxi, Taiyuan, China, [3] Department of Strength and Conditioning Training, Beijing Sport University, Beijing, China, [4] Department of Community Medicine and Rehabilitation, Section of Sports Medicine, Umeå University, Umeå, Sweden, [5] Department of Exercise Physiology, Beijing Sport University, Beijing, China

OPEN ACCESS

Edited by:
Jaap Diederik Van Buul, University of Amsterdam, Netherlands

Reviewed by:
Bradley T. Andresen, Western University of Health Sciences, United States
Jesus A. Olivares-Reyes, Instituto Politécnico Nacional de México (CINVESTAV), Mexico

***Correspondence:**
Ji-Guo Yu
jiguo.yu@umu.se
Li Zhao
zhaolispring@126.com

[†] These authors have contributed equally to this work

Specialty section:
This article was submitted to Vascular Physiology, a section of the journal Frontiers in Physiology

Received: *05 May 2020*
Accepted: *14 July 2020*
Published: *16 September 2020*

Citation:
Lv Y, Zhao W, Yu L, Yu J-G and Zhao L (2020) Angiotensin-Converting Enzyme Gene D/I Polymorphism in Relation to Endothelial Function and Endothelial-Released Factors in Chinese Women. Front. Physiol. 11:951. doi: 10.3389/fphys.2020.00951

Many studies have investigated the relationship between angiotensin-converting enzyme (*ACE*) D/I polymorphism and cardiovascular disease or endothelial dysfunction; however, hardly any of these studies has taken aging or menopause into consideration. Furthermore, despite that many studies have examined the regulatory effects of endothelial-released factors (ERFs) on endothelial function, no study has evaluated the relationship between ERFs and endothelial function with respect to *ACE* D/I polymorphism and menopause status. To answer these questions, 391 healthy Chinese women over a wide range of ages (22–75 years) were enrolled and divided into pre-menopause group and post-menopause group. After *ACE* D/I genotype being identified, the women were then classified into either DI/II or DD genotype. Flow-mediated dilatation (FMD) of brachial endothelium and plasma levels of ERFs: nitric oxide (NO), endothelin-1 (ET-1), and angiotensin II (Ang II) were measured. The results showed that frequencies of *ACE* D/I genotypes were in accordance with the Hardy-Weinberg equilibrium, and the frequency of I allele was higher than D allele. In pre-menopause group, FMD was significantly higher in women of DI/II than DD ($P = 0.032$), and age-dependent in both genotypes (DD, $P = 0.0472$; DI/II, $P < 0.0001$). In post-menopause group, FMD was similar between women of DI/II and DD, and age-dependent only in women of DI/II ($P < 0.0001$). In pre-menopause group, Ang II level was significantly higher in women of DD than DI/II ($P = 0.029$), and FMD was significantly correlated with all ERFs in women of DD (NO, $P = 0.032$; ET-1, $P = 0.017$; Ang II, $P = 0.002$), but only with Ang II in women of DI/II ($P = 0.026$). In post-menopause group, no significant difference was observed in any ERF between women of DI/II and DD, and FMD was only significantly correlated with ET-1 in women of DD ($P = 0.010$). In summary, FMD in women of DI/II was superior to DD in pre-menopause and more age-dependent than DD in post-menopause, and FMD was closely associated with ERFs. In conclusion, Chinese women of DI/II seem to have lower risk than DD in pre-menopause, but similar risk as DD in post-menopause in developing cardiovascular disease.

Keywords: *ACE* D/I gene polymorphism, Chinese women, endothelial function, endothelial-released factors, aging, menopause

INTRODUCTION

Endothelium-dependent vasodilation impairment is believed to be the initial factor in the pathogenesis of atherosclerosis, according to the "endothelial damage response theory" (Gimbrone and García-Cardeña, 2016; Ungvari et al., 2018b), and reduction in endothelial function presents a strong correlation with aging, especially after the age of 45 years (Shi et al., 2014; Sepúlveda et al., 2017; Jia et al., 2019) when menopausal transition generally occurs. Thus, endothelial dysfunction represents one of the earliest signs of developing cardiovascular and cerebrovascular diseases, such as atherosclerosis, coronary heart disease, hypertension (Rossman et al., 2018; Ungvari et al., 2018b). Flow-mediated dilation (FMD) of the brachial artery is currently a widely used parameter in evaluating vasodilation (Aeschlimann et al., 2004; Thijssen et al., 2011) and in clinical studies to independently predict the risk of cardiovascular diseases (Takase et al., 1998; Corretti et al., 2002; Inaba et al., 2010; Green et al., 2011; Donato et al., 2018; Nemoto et al., 2019).

Angiotensin-converting enzyme (*ACE*) is a single-chain polypeptide acid glycoprotein and was first discovered in the vascular endothelium, where it is often in a membrane-bound form (Kim et al., 2001). *ACE* is a key enzyme of renin-angiotensin system, which together with kallikrein-kinin system is important in maintaining physiological functions of the heart, blood vessels, and kidneys through the regulation of blood pressure, blood flow, homeostasis, and the vasomotor system (Bader, 2010; Masuyer et al., 2012). In the 16th intron of the *ACE* gene, there is a 287 bp Alu repeat insertion/deletion, and when the *ACE* allele contains this fragment, it is called "I" (insertion type). If not, it is called "D" (deletion type); thus, *ACE* has three different genotypes: type II, DI, and DD (Kim et al., 2001).

Angiotensin-converting enzyme gene D/I polymorphism has been shown to present significant linkage disequilibrium, and DD genotype has the highest *ACE* activity, DI genotype of moderate, and II genotype of the lowest (Cambien et al., 1988; Rigat et al., 1990). Thus, high number of D allele indicates high *ACE* activity and vice versa (Masuyer et al., 2012). Although *ACE* activity varies greatly among individuals, it remains generally constant in different tissues/organs of the same individual as it is hardly affected by external factors (Shafiee et al., 2010). Recent studies have revealed some differences in distribution of *ACE* D/I gene polymorphism between different ethnic groups and even within the same ethnic group (Alhenc-Gelas et al., 1991; Cambien and Evans, 1995).

Angiotensin-converting enzyme gene D/I polymorphism has been shown to be associated with various cardiovascular diseases (Sayed-Tabatabaei et al., 2006). In a previous study, the frequency of *ACE* D allele in myocardial infarction subjects has been shown to be significantly higher than in healthy control subjects (Cambien et al., 1992). The authors suggested that the *ACE* D allele was an independent risk factor for myocardial infarction in European. The *ACE* DD genotype has also been reported to be highly correlated with the incidence of hypertension (Kato et al., 2011) and cerebrovascular disease/stroke (Kalita et al., 2011). In addition, *ACE* gene polymorphism has been shown to be closely associated with endothelial dysfunction (Tanriverdi et al., 2007). In a study of post-menopausal women, endothelial function was observed to be significantly lower in *ACE* DD than in *ACE* II (Méthot et al., 2006). Similarly, in another study of male patients with chronic obstructive pulmonary disease, a significantly lower incidence of endothelial dysfunction (FMD < 10%) was observed in patients of *ACE* DI/II than in *ACE* DD (Kuzubova et al., 2013). It is well-known that endothelial function is age-dependent (Ungvari et al., 2018a), and estrogen has a strong protective effect on endothelial function, which decreases significantly after menopause (Taddei et al., 1996). However, to our knowledge no study to date has investigated the relationship between *ACE* polymorphism and endothelial function in women following aging, particularly across the age of menopause.

Physiologically, the vascular endothelium can produce and release a variety of vasoactive substances, such as nitric oxide (NO), angiotensin II (Ang II), endothelin-1 (ET-1) (Donato et al., 2018; Stanhewicz et al., 2018). These substances can cause vasodilation or contraction of vascular smooth muscles, thus regulating vascular tone (Godo et al., 2016; Somani et al., 2019). NO is the most important factor in the vascular endothelial vasodilation system and plays a fundamental role in regulating vascular resistance and tissue perfusion. ET-1 is the strongest vasoconstrictor produced by the vascular endothelium (D'Orléans-Juste et al., 2008) and plays an important role in vascular dysfunction during aging. Ang II can increase total peripheral resistance and lead to high blood pressure, thus playing a major role in the occurrence of cardiovascular disease (Al-Hazzani et al., 2014). Overall, NO, ET-1, and Ang II are closely related and interact with each other to regulate the normal function of vascular endothelium (Godo et al., 2016; Somani et al., 2019).

Despite the fact that many studies have examined the regulatory effects of endothelial-released factors (ERFs) on endothelial function, no study has ever examined the differences of these factors in affecting endothelial function in relation to *ACE* gene D/I polymorphism, especially in women across the life stage of menopause. To answer these questions, the present study examined the distribution of *ACE* gene D/I genotypes in a large group of Chinese women including both pre-menopause stage and post-menopause stage. Endothelial-dependent vasodilation function and ERFs were examined. We aimed to reveal the relationship between the *ACE* gene D/I genotype, endothelial function, and plasma levels of ERFs following aging in pre- and post-menopausal women. We hope the results will help us to know more about the potential risk in developing cardiovascular disease in Chinese women of different *ACE* gene D/I genotypes at different menopause stages.

MATERIALS AND METHODS

Subjects

A total of 391 healthy women of Han nationality (22–75 years) from the local region (Beijing, China) were recruited for this cross-sectional study. Questionnaires with questions about health status, medicines intake, menstrual status, and use of hormonal contraceptives were distributed to all participants. Women with

diabetes, cardiovascular diseases, or other metabolic diseases, or taking medicines for blood pressure control or blood lipid regulation were excluded. We used the World Health Organization's definition of menopause, i.e., the cessation of menstruation being longer than 12 months. On basis of menopause status of each individual, the subjects were divided into two groups: pre-menopause group (n = 155) and post-menopause group (n = 236).

Ethics Statement

The protocol used in this study was approved by the Ethics Committee of Beijing Sport University (2019014H). The study was in accordance with the recommendations of the Declaration of Helsinki. All participants were informed about the study and written informed consent was obtained from all the participants.

ACE Gene D/I Polymorphism Identification and Classification

Detailed description of the procedure of *ACE* gene D/I genotype identification has been described previously (Comey et al., 1994; Sun et al., 2018; He et al., 2019). DNA samples were extracted from buccal mucosal cells by cotton swabs. *ACE* gene D/I polymorphism was determined using polymerase chain reaction (PCR). DNA samples were extracted using 5% chelex-100 (165 μl) and proteinase K (3 μl, 20 mg/μl) and amplified using the forward primer of 5'-CTG GAG ACC ACT CCC ATC CTT TCT-3' and the reverse primer 5'-GAT GTG GCC ATC ACA TTC GTC AGA T-3' (Lian et al., 2012). The PCR reaction system (15 μl) consisted of ddH_2O (10.8 μl), dNTP (1.2 μl), 10 × buffer (1.5 μl), TAKARA HS Taq polymerase (0.1 μl), each primer (0.2 μl), and template (1.0 μl). The DNA was amplified by 35 cycles using PCR Thermal (iCycler, Bio-Rad, United States). Every cycle was started with pre-denaturation at 94°C for 5 min, followed by 30 s of denaturation at 94, 55, and 72°C. The amplification was ended with a final elongation of 10 min at 72°C and kept at 15°C. To identify the *ACE* D/I genotype, 2 μl PCR amplicon was electrophoresed using a 2.5% agarose gel with the presence of a 190 bp fragment for D allele and a 470 bp fragment for I allele.

Measurement of Brachial Endothelium-Dependent Vasodilation – FMD

Details of the procedures of FMD measurement have been described previously (Celermajer et al., 1992, 1994; Yeboah et al., 2009; Larsen et al., 2016). Briefly, the subjects rested supine for at least 10 min, and the forearm was pressurized below the elbow joint at 280–300 mmHg for 5 min with an inflatable tourniquet and then suddenly deflated. Two-dimensional images of the brachial artery were obtained at baseline (D_0) and between 45 to 60 s after cuff release (D_1) with a 7.5 to 13 MHz high frequency linear array probe (GE Vivid 7, United States; D'Andrea et al., 2007). An electrocardiogram was recorded synchronously using an electrocardiograph (Custo med cardio 100, Germany). All measurements were performed at the end of the diastole to reduce the effect of possible vascular compliance. The R-wave of the ECG was used as the standard of the end-diastole. FMD was calculated using the formula: FMD = $(D_1-D_0)/D_0 \times 100\%$. Conventionally, FMD could be categorized into three different levels, FMD > 10%, 7% ≤ FMD ≤ 10%, FMD < 7%, representing normal, mildly abnormal, and moderately- to severely abnormal vascular endothelial function, respectively (Neunteufl et al., 1997; Berzigotti et al., 2013; Basyigit et al., 2015).

Measurements of ERFs

Blood samples were collected from each subject from the antecubital vein in the morning after overnight fasting. For Ang II analysis, blood sample of 5 ml was collected in Vacutainer tube containing ethylene diamine tetraacetic acid (EDTA) for anticoagulation, and then three different types of enzyme inhibitors (EDTANa, 0.3 M, 250 μl; 8-hydroxyquinoline, 0.34 M, 50 μl; dimercaptopropanol, 0.32 M, 25 μl) were added into the tube. Another blood sample of 3 ml was collected for analysis of ET-1 and NO. NO was measured using the nitric acid reductase method (Fabricio et al., 2017). Ang II (Huang et al., 2004b) and ET-1 (Al-Fakhri et al., 2003) were measured using radioimmunoassay. The analysis kits for ET-1 and NO were provided by the Nanjing Jincheng Institute of Biological Engineering (Nanjing, China), and the kit for Ang II was provided by the North Institute of Biotechnology (Beijing, China). The analysis procedures have been described in previous study (Ramzy et al., 2006a,b; González-González et al., 2018). NO, Ang II and ET-1 were analyzed at the cardiovascular laboratory, Beijing Sport University, following standardized procedures.

Statistical Analysis

All statistical analyses were performed using SPSS (version 20.0, International Business Machines Corporation, United States). Continuous variables were shown as mean ± standard deviation, and enumeration data were shown as rates. Chi-Square (χ^2) tests were used in Hardy-Weinberg equilibrium calculations of the *ACE* D/I allele frequencies of the subjects and in comparisons of the proportions of women at different FMD levels between groups (When the sample size was less than five, Yates' correction was applied). Comparisons of continuous variables between the pre-menopause group and the post-menopause group or between the *ACE* DI/II and the *ACE* DD genotypes were performed using independent-samples t-test. Multivariate analysis of variance was used to evaluate the determinants of *ACE* gene D/I polymorphism, age, and menopause status on FMD. Multivariate regression analysis was used to evaluate the determinants of ERFs on FMD. A two-tailed P-value of less than 0.05 was considered statistically significant.

RESULTS

Anthropometric Data and *ACE* Genotype Classification

Based on their menopause stages, the women were classified into either the pre-menopause group or the post-menopause group

(**Table 1**). The frequencies of women of both D allele and I allele were calculated for each group, and a χ^2 test showed that the distributions were in accordance with the Hardy-Weinberg equilibrium. General anthropometry and blood pressure are shown in **Table 2**. Comparisons of the data between women of *ACE* DI/II and *ACE* DD within each group showed that in pre-menopause group, the average age of women with *ACE* DI/II was significantly higher than that of *ACE* DD ($P = 0.000$), and both systolic blood pressure (SBP) and diastolic blood pressure (DBP) were significantly lower in women of DI/II than in women of *ACE* DD ($P = 0.009$ and $P = 0.015$, respectively). Comparisons of the data between pre-menopause group and post-menopause group of the same *ACE* genotype revealed that women of *ACE* DI/II had significantly higher of both SBP and DBP in post-menopause group than in pre-menopause group ($P = 0.012$ and $P = 0.006$, respectively).

Results and Comparisons of FMD Measurements

The results of FMD are shown in **Table 3**. Comparisons in mean values of FMD between women of *ACE* DD and *ACE* DI/II within pre-menopause group and post-menopause group showed significant difference only in pre-menopause group, where FMD mean value was significantly lower in women of *ACE* DD than *ACE* DI/II ($P = 0.032$). Comparisons in mean values of FMD in women of the same *ACE* genotype between pre-menopause group and post-menopause group revealed significant difference only in women of *ACE* DI/II, which presented significantly higher FMD mean value in pre-menopause group than in post-menopause group ($P = 0.000$).

Frequencies of women of both *ACE* genotypes in both groups at different FMD levels (FMD $< 7\%$; $7\% \leq$ FMD $\leq 10\%$; FMD $> 10\%$) are shown in **Table 3**. In pre-menopause group, the highest proportions of women for both *ACE* genotypes were at normal FMD level (FMD $> 10\%$; DD, 43.8% and DI/II, 54.7%), and the proportion of women at moderately- to severely abnormal FMD level (FMD $< 7\%$) was significantly higher in *ACE* DD than in *ACE* DI/II ($P = 0.008$). In post-menopause group, the highest proportion of women of *ACE* DD (60%) was at mildly abnormal FMD level ($7\% <$ FMD $< 10\%$), whereas the highest proportion of women of *ACE* DI/II (43.2%) was at moderately- to severely abnormal FMD level (FMD $< 7\%$).

Comparisons of proportions of women of the same *ACE* genotype at different FMD levels between pre-menopause group and post-menopause group showed that at normal FMD level (FMD $> 10\%$), the proportions of women for both *ACE* genotypes in post-menopause group were significantly lower than that of respective *ACE* genotype in pre-menopause group (DD, $P = 0.009$ and DI/II, $P = 0.000$; **Table 3**). By contrast, women at mildly abnormal FMD level ($7\% \leq$ FMD $\leq 10\%$), no significant difference was observed in women of either *ACE* DD or *ACE* DI/II between pre-menopause group and post-menopause group (DD, $P = 0.063$ and DI/II, $P = 0.295$). At moderately- to severely abnormal FMD level (FMD $< 7\%$), significant difference was observed only in women of *ACE* DI/II, who presented significantly higher proportion in post-menopause group than in pre-menopause group ($P = 0.000$).

TABLE 1 | Distribution of *ACE* gene polymorphism of pre- and post-menopause groups and the Hardy-Weinberg equilibrium.

Groups	Proportions of phenotype			Proportions of D/I allele		χ^2 (*p*)
	DD	DI	II	D	I	
Pre-menopause (*n* = 155)	10.32% (*n* = 16)	47.74% (*n* = 74)	41.94% (*n* = 65)	34.19% (*n* = 106)	65.81% (*n* = 204)	0.259 (0.879)
Post-menopause (*n* = 236)	12.71% (*n* = 30)	46.19% (*n* = 109)	41.10% (*n* = 97)	35.81% (*n* = 169)	64.19% (*n* = 303)	0.003 (0.999)
Pre vs. post χ^2 (*p*)	0.514 (0.473)	0.091 (0.763)	0.027 (0.870)	0.115 (0.735)	0.115 (0.735)	

A chi-square (χ^2) test was used for genotype distribution. DD, homozygous deletion; DI, DI heterozygote; II, homozygous insertion; D/I, deletion/insertion; χ^2, chi-square statistic. Pre vs. Post, comparison of pre- and post-menopausal women.

TABLE 2 | Comparisons of anthropometric parameters between angiotensin-converting enzyme insertion/deletion subgroups of the pre- and post-menopause groups (M ± SD).

Characteristics	Pre-menopause (*n* = 155)			Post-menopause (*n* = 236)			Pre vs. post (DD)	Pre vs. post (DI/II)
	DD (*n* = 16)	DI/II (*n* = 139)	*P*	DD (*n* = 30)	DI/II (*n* = 206)	*P*	*P*	*P*
Age (y)	42.88 ± 1.93	46.42 ± 3.61	0.000[a]	60.77 ± 6.61	61.88 ± 6.15	0.360		
Height (cm)	160.81 ± 7.12	157.94 ± 6.18	0.053	158.02 ± 5.66	157.03 ± 6.06	0.390	0.293	0.801
Weight (Kg)	61.97 ± 7.98	61.67 ± 7.13	0.765	61.09 ± 7.50	59.74 ± 7.78	0.373	0.658	0.216
SBP (mm Hg)	132.09 ± 9.85	118.95 ± 9.02	0.009[a]	131.10 ± 10.91	129.68 ± 9.85	0.899	0.117	0.012[d]
DBP (mm Hg)	76.05 ± 7.86	68.37 ± 6.15	0.015[b]	77.43 ± 8.51	75.69 ± 9.38	0.436	0.300	0.006[c]

Independent-samples t-tests were used to compare continuous variables between pre- and post-menopause groups, and between ACE DI/II and ACE DD genotypes. SBP, systolic blood pressure; DBP, diastolic blood pressure; DD, homozygous deletion; DI/II, I allele carriers. Pre vs. Post (DD), comparison of pre- and post-menopausal women in DD group; Pre vs. Post (DI/II), comparison of pre- and post-menopausal women in I allele carriers. [a]Significantly different between DD and II/ID groups, $P < 0.01$. [b]Significantly different between DD and II/ID groups, $P < 0.05$. [c]Significantly different between pre- and post-menopause groups, $P < 0.01$. [d]Significantly different between pre- and post-menopause groups, $P < 0.05$.

TABLE 3 | Results and comparisons of FMD measurements.

FMD (%)	Pre-menopause (*n* = 155)			Post-menopause (*n* = 236)			Pre vs. Post (DD)	Pre vs. Post (DI/II)
	DD (*n* = 16)	DI/II (*n* = 139)	*P*	DD (*n* = 30)	DI/II (*n* = 206)	*P*	*P*	*P*
M ± SD	8.89 ± 2.56	10.20 ± 2.27	0.032[b]	8.62 ± 1.62	8.43 ± 2.91	0.365	0.172	0.000[c]
>10	43.8% (7)	54.7% (76)	0.407	6.7% (2)	21.4% (44)	0.099	0.009[c]	0.000[c]
≤10, ≥7	31.3% (5)	41.0% (57)	0.451	60.0% (18)	35.4% (73)	0.010[b]	0.063	0.295
<7	25% (4)	4.3% (6)	0.008[a]	33.3% (10)	43.2% (89)	0.306	0.804	0.000[c]

Independent-samples t-tests were used to compare FMD mean values between pre- and post-menopause groups and between ACE DI/II and ACE DD genotypes. Chi-Square ($\chi 2$) tests were used to compare the proportions of women at different FMD levels between pre- and post-menopause groups, and between ACE DI/II and ACE DD genotypes (When sample size was less than five, Yates' correction was applied). FMD, flow-mediated dilatation. FMD > 10% is normal; 7% ≤ FMD ≤ 10% is mild abnormality; FMD < 7% is moderate to severe abnormality. Pre vs. Post (DD), comparison of pre- and post-menopausal women in DD group; Pre vs. Post (DI/II), comparison of pre- and post-menopausal women in I allele carriers. [a]Significantly different between DD and DI/II groups, P < 0.01. [b]Significantly different between DD and DI/II groups, P < 0.05. [c]Significantly different between pre-and post-menopausal women, P < 0.01.

Multivariate Analysis of Variance of FMD With Independent Variables of *ACE* Genotype, Age, and Menopause Status

Results of multivariate analyses of variance are shown in **Table 4**. Among the three independent variables, only age and menopause status were significantly correlated with FMD ($P = 0.006$ and $P = 0.012$, respectively). In addition, interactions of *ACE* genotype with both age and menopause status presented significant correlations with FMD ($P = 0.012$ and $P = 0.015$, respectively).

TABLE 4 | Multivariate analysis of variance of FMD with independent variables of *ACE* genotype, age, and menopause status.

Variable	F-statistic	*P* value
Age	5.354	0.006
ACE genotype	3.093	0.081
Age**ACE* genotype	6.070	0.012
Menopause status	4.962	0.026
Menopause status **ACE* genotype	8.077	0.015

*Multivariate analysis of variance was used to evaluate the effects of ACE gene D/I polymorphism, age, and menopause status on FMD. ACE, angiotensin-converting enzyme; Age*ACE genotype, interaction of Age and ACE genotype; Menopause status *ACE genotype, interaction of menopause status and ACE genotype.*

Correlation Analysis Between FMD and Age in Women of the Pre-menopause Group and the Post-menopause Group

Results of correlation analyses between FMD and age for women of *ACE* DI/II and *ACE* DD in pre-menopause group and post-menopause group are shown in **Figure 1**. In pre-menopause group, FMD was low, yet, significantly and negatively correlated with age for women of both *ACE* genotypes; (DD, $r = -0.4845$, $P = 0.0472$; DI/II, $r = -0.3424$, $P < 0.0001$). In post-menopause group, FMD was also low and negatively correlated with age for women of both *ACE* genotypes (DD: $r = -0.3291$; DI/II: $r = -0.4451$), but significant correlation was only observed in women of DI/II ($P < 0.0001$).

ERFs Levels and Comparisons

In pre-menopause group, among the three ERFs, only Ang II level presented significant difference between women of *ACE* DI/II and *ACE* DD, i.e., significantly higher in women of *ACE* DD than in *ACE* DI/II ($P = 0.029$; **Table 5**). In post-menopause group, none of the three ERFs presented significant difference between women of *ACE* DI/II and *ACE* DD. Further comparisons of ERFs levels in women of the same *ACE* genotype between pre- and post-menopause groups revealed no significant difference in any factor in women of *ACE* DD, whereas in women of *ACE* DI/II, only ET-1 level presented significant difference, i.e., significantly

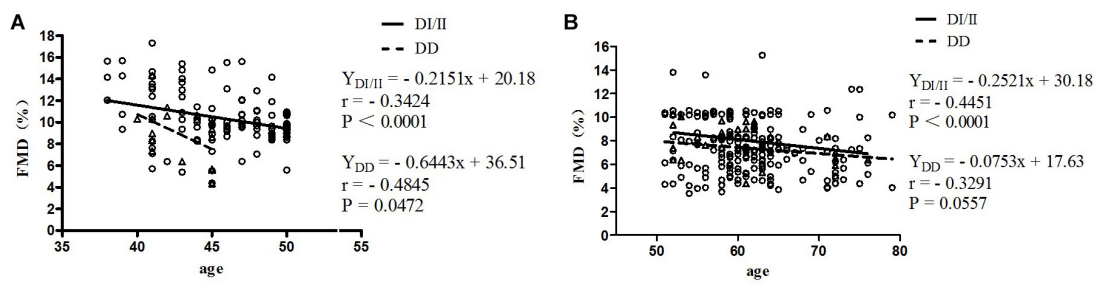

FIGURE 1 | Correlation analysis between FMD and age in women of the pre-menopause group **(A)** and the post-menopause group **(B)**. FMD, flow-mediated dilatation; DD, homozygous deletion; DI/II, I allele carriers. The subjects were classified as belonging to pre- or post-menopause groups according to their menopause status. Age as the abscissa and FMD as the ordinate, two-dimensional FMD plot of women with different *ACE* genotypes in different menopause stages were made; linear regression was performed for FMD and age. **(A)** Pre-menopause group; **(B)** Post-menopause group.

TABLE 5 | ERFs levels and comparisons (M ± SD).

Genotype	Pre-menopause (*n* = 155)			Post-menopause (*n* = 236)			Pre vs. Post (DD)	Pre vs. Post (DI/II)
	DD (*n* = 16)	DI/II (*n* = 139)	*P*	DD (*n* = 30)	DI/II (*n* = 206)	*P*	*P*	*P*
NO (μmol/l)	61.23 ± 9.78	66.19 ± 10.04	0.087	64.29 ± 8.40	64.32 ± 8.21	0.986	0.272	0.107
ET-1 (ng/l)	70.12 ± 6.00	66.00 ± 7.84	0.337	74.52 ± 9.85	70.46 ± 10.21	0.202	0.379	0.014[b]
Ang II (pg/ml)	135.51 ± 14.29	122.07 ± 12.89	0.029[a]	126.89 ± 18.35	124.00 ± 17.99	0.540	0.202	0.463

Independent-samples t-tests were used to compare continuous variables between pre- and post-menopause groups, and between ACE DI/II and ACE DD genotypes. DD, homozygous deletion; DI/II, I allele carriers. NO, nitric oxide; ET-1, endothelin-1; Ang II, angiotensin II. Pre vs. Post (DD), comparison of pre- and post-menopausal women in DD group; Pre vs. Post (DI/II), comparison of pre- and post-menopausal women in I allele carriers. [a]Significantly different between DD and DI/II groups, P < 0.05. [b]Significantly different between pre- and post-menopause groups, P < 0.05.

higher in post-menopause group than in pre-menopause group ($P = 0.014$).

Multivariate Regression Analysis Between FMD and ERFs

We used FMD as a dependent variable, and ERFs as independent variables for multivariate regression analyses, the results are shown in **Table 6**. In pre-menopause group, Ang II had significant correlation with FMD in women of both *ACE* genotypes (DD, $P = 0.002$; DI/II, $P = 0.026$), whereas NO and ET-1 had significant correlations with FMD only in women of *ACE* DD ($P = 0.032$ and $P = 0.017$, respectively). In post-menopause group, only ET-1 presented significant correlation with FMD in women of *ACE* DD ($P = 0.010$).

DISCUSSION

ACE D/I Polymorphism in Relation to FMD, Aging, and Menopause Status

The study revealed that *ACE* D/I allele frequencies in Chinese women of Han nationality were in accordance with the Hardy-Weinberg equilibrium (see **Table 1**). The frequency of *ACE* I allele was higher than that of *ACE* D allele, similar to previous studies on the same ethnic population (Gao et al., 2014; Cai et al., 2019). However, this was different from other nations in the world, where the frequency of *ACE* D allele was in general higher than that of *ACE* I allele (Moran et al., 2005; Daniela et al., 2008; Dankova et al., 2009). Nevertheless, it has been long recognized that the frequencies of *ACE* D/I allele were ethnic and regional (Wiwanitkit, 2004; Saab et al., 2007).

TABLE 6 | Multivariate regression analysis between FMD and ERFs.

Variable	Pre-menopause		Post-menopause	
	DD (*P*-value)	DI/II (*P*-value)	DD (*P*-value)	DI/II (*P*-value)
NO	0.032	0.301	0.614	0.442
ET-1	0.017	0.439	0.010	0.308
Ang II	0.002	0.026	0.759	0.647

Multivariate regression analysis was used to evaluate the effects of ERFs on FMD. DD, homozygous deletion; DI/II, I allele carriers. NO, nitric oxide; ET-1, endothelin-1; Ang II, angiotensin II.

Comparisons of FMD mean values between different *ACE* genotypes within pre-menopause group and post-menopause group revealed that in pre-menopause group, FMD mean value was significantly higher in women of *ACE* DI/II than in *ACE* DD, but in post-menopause group, no significant difference was observed (see **Table 3**). In addition, comparisons of FMD mean values in women of the same *ACE* genotype between pre-menopause group and post-menopause group revealed that FMD in women of *ACE* DI/II was significantly higher in pre-menopause group than in post-menopause group, but FMD in women of *ACE* DD did not present significant difference. The results indicate clearly that in pre-menopause group, women of *ACE* DI/II had better endothelial function of FMD than those of *ACE* DD, but that advantage disappeared in post-menopause stage. In support of this, in the pre-menopause group, women of *ACE* DI/II had significantly lower values of both systolic- and diastolic blood pressure than those of *ACE* DD, whereas in the post-menopause group, women of the two *ACE* genotypes did not present significant difference in either systolic- or diastolic blood pressure (see **Table 2**). The conclusion was also supported by the comparisons at different FMD levels (see **Table 3**). In pre-menopause group, percentage of women at moderately- to severely abnormal FMD level (FMD < 7%) was significantly lower in women of *ACE* DI/II than in women of *ACE* DD, whereas in post-menopause group, no significant difference was observed. Interestingly, in pre-menopause group, women of *ACE* DI/II were on average older than that of *ACE* DD (see **Table 2**), strengthening further our conclusion that women of *ACE* DI/II had advantage in FMD over women of *ACE* DD.

Previous studies have shown that *ACE* DD had close association with a high incidence of cardiovascular disease or endothelial dysfunction (Alvarez et al., 2001; Brand and van der Schouw, 2010; Kuzubova et al., 2013; Al-Hazzani et al., 2014; Amara et al., 2018). In the present study, only the result of pre-menopause group was consistent with previous studies, i.e., women of *ACE* DD had lower FMD than women of *ACE* DI/II, and in post-menopause group, women of the two *ACE* genotypes did not present significant difference in FMD. Interestingly, in another study on post-menopausal women, endothelial function was significantly lower in *ACE* DD than in *ACE* II (Méthot et al., 2006). It has been shown that different ethnic groups may vary in age of menopause (Santoro and Chervenak, 2004), whereas menopause is closely associated with different hormones and

factors such as ERFs (Kang et al., 2011), exerting different regulatory effects on FMD. Thus, it would be interesting to compare the difference in endothelial function in relation to menopause status, aging, and *ACE* D/I genotype between different ethnic groups.

Previous studies have shown a high correlation between FMD, menopause status, and aging (Ungvari et al., 2018b). In support of this, the present study observed that in post-menopause group, percentages of women of both *ACE* genotypes at normal FMD level (FMD > 10%) were significantly lower than those of respective *ACE* genotypes in pre-menopause group (see **Table 3**). In fact, when all of the women were taken as one group, no significant correlation between FMD and *ACE* genotype was observed (see **Table 4**). However, interactions of *ACE* genotype with both age and menopause status presented significant correlations with FMD (see **Table 4**). As age and menopause are intertwined, it is no surprise that if age shows a statistical association, then menopause will too. To break down the intertwining, we performed further correlation analyses between FMD and age for women of both *ACE* genotypes in both pre- and post-menopause groups. The results revealed that in pre-menopause group, FMD was significantly correlated with age in women of both *ACE* genotypes, but in post-menopause group, significant correlation between FMD and age was only observed in women of *ACE* DI/II (see **Figure 1**). A simple comparison of the slopes of the regressions in women of the same *ACE* D/I genotype between pre- and post-menopause groups revealed that the slopes in women of *ACE* DI/II were similar (pre-menopause group: −0.2151 vs. post-menopause groups: −0.2521), indicating that FMD in women of *ACE* DI/II declined at similar speed following aging in pre- and post-menopause stages. However, the slopes for women of *ACE* DD were much deeper in pre-menopause group (−0.6443) than in post-menopause group (−0.0753), suggesting that FMD in women of *ACE* DD declined much faster following aging in pre-menopause stage than in post-menopause stage. To our knowledge, this is the first study to date to investigate the relationship between FMD and aging in women of different menopause stages and different *ACE* D/I genotypes. Our results strongly suggest the importance of menopause status in affecting FMD following aging in women of different *ACE* D/I genotypes.

Flow-mediated dilatation has been shown to be significantly lower in post-menopausal women than in pre-menopausal women (Moreau et al., 2012, 2013; Santos-Parker et al., 2017). The reduction in vascular function in the transition to menopause has been suggested to be due to decline of gonadal hormones (Moreau, 2018), especially estrogen (Witkowski and Serviente, 2018). However, the hypothesis could not fully explain our observations, because in post-menopause group, significantly lower FMD mean value was observed only in women of *ACE* DI/II, not in women of *ACE* DD, in comparison to respective *ACE* genotypes in pre-menopause group. Taken together, FMD is related not only to menopause status, but also to *ACE* genotype. Interestingly, it has also been reported that the largest decline in FMD occurred between the pre-menopausal and perimenopausal (transitional) stages, not in the post-menopausal stage (Moreau, 2018).

ACE D/I Polymorphism in Relation With FMD, ERFs, Age, and Menopause Status

The present study revealed that in pre-menopause group, plasma levels of NO and ET-1 were similar in women of *ACE* DD and *ACE* DI/II, but Ang II level was significantly higher in women of *ACE* DD than in women of *ACE* DI/II (see **Table 5**). Higher Ang II level has previously been observed in patients (both men and women with chronic heart failure) of *ACE* DD than *ACE* DI/II (Huang et al., 2004a,b). Recent studies have shown that Ang II promoted the onset and progression of vascular senescence, which was associated with vascular functional and structural changes, contributing to age-related vascular diseases (Min et al., 2009). Thus, the significantly higher Ang II level in women of *ACE* DD than in *ACE* DI/II is in support of the observation that FMD was prior in women of *ACE* DI/II to *ACE* DD in pre-menopausal group.

Further correlation analyses between FMD and ERFs revealed that in pre-menopause group, FMD in women of *ACE* DD was significantly affected by all the three ERFs, whereas FMD in women of *ACE* DI/II was only significantly affected by Ang II (see **Table 6**). Therefore, women of *ACE* DD had two extra ERFs: NO and ET-1 exerting significant effects on FMD. NO is the most important factor in the vasodilation system and plays an important role in age-related vascular dysfunction (Thijssen et al., 2016). ET-1 is the strongest vasoconstrictor, and an important regulator of vascular dysfunction during aging (Trindade et al., 2017). ET-1 has been known to act as a natural counterpart of vasodilator NO and contribute to vasocontraction through ETA and ETB receptors on smooth muscle. In contrast, activation of ETB receptors on endothelial cells results in transient Ca^{2+} and stimulation of endothelial nitric oxide synthase (eNOS), leading to vasodilation (Halcox et al., 2007; Tykocki et al., 2009). Physical factors such as shear stress, Ang II, and cytokines enhance secretion of ET-1, whereas NO, cyclic GMP, and prostacyclin reduce the release of ET-1 (Marasciulo et al., 2006; Houde et al., 2016). Under physiological conditions, the effects of ET-1 are precisely regulated through inhibitors or stimulators of ET-1. Furthermore, reduced function of ETB receptors or overactivated ETA receptors can eliminate the protective effect of NO on the vascular system (Bourque et al., 2011; Ohkita et al., 2012). Age-related impairment in vascular function has been proposed to be due to an imbalance between decrease in NO and increase in ET-1 (Godo et al., 2016; Stanhewicz et al., 2018). It is well-know that NO, ET-1 and Ang II are closely related and interact with each other to regulate the normal function of vascular endothelium (Godo et al., 2016: Somani et al., 2019). We speculate that the two extra ERFs: NO and ET-1 exerted negative effects on FMD, leading to the lower level of FMD in women of *ACE* DD in comparison to women of *ACE* DI/II in pre-menopause group. It is worth noticing that plasma ET-1 concentration is normally at nanogram level. Given that ET-1 has a molecular weight of 2491.9 g/mol, the statistically significant difference in ET-1 level in women of *ACE* DI/II between pre- and post-menopause groups (see **Table 5**) seems biologically meaningless. Thus, interpretation of the present data of plasma levels of ERFs in relation to FMD needs to be cautious.

The study revealed that in post-menopause group, none of the ERFs presented significant differences between women of *ACE* DD and *ACE* DI/II (see **Table 5**). Comparisons of ERFs levels in women of the same *ACE* genotype between pre- and post-menopause groups revealed that only ET-1 level in women of *ACE* DI/II was significantly higher in post-menopause group than in pre-menopause group (see **Table 5**). Estrogen has been reported to reduce aging rate of the vascular endothelium induced by Ang II (Imanishi et al., 2005), and to inhibit the release of ET-1 and reduce the response of blood vessels to Ang II (Lekontseva et al., 2010; Gohar et al., 2016). We speculate that women of *ACE* DI/II might be more sensitive to estrogen than DD, and estrogen reduction from pre-menopause to post-menopause led to reduced inhibition of estrogen on ET-1, resulting in the increased ET-1 level in post-menopausal women of *ACE* DI/II. ET-1 has been known to be an important regulator of vascular dysfunction during aging (Trindade et al., 2017). Its significant increase in post-menopausal women of *ACE* DI/II may be associated with the FMD reduction in women of *ACE* DI/II from pre-menopause stage to post-menopausal stage. The study revealed also that among all the ERFs, only ET-1 had significant correlation with FMD in post-menopausal women of *ACE* DD (see **Table 6**), which was believed to be associated with the significant reduction in percentage of *ACE* DD women at normal FMD level from pre-menopause to post-menopause (see **Table 3**).

CONCLUSION

The present study observed that in the pre-menopause group, women of DI/II had higher FMD level than women of DD, and in the post-menopause group, FMD in women of DI/II was more age-dependent than in women of DD. The variations in FMD between women of different *ACE* genotypes were closely associated with plasma levels of ERFs, which varied with *ACE* D/I polymorphism and menopause status. In conclusion, women of *ACE* DI/II in pre-menopausal stage seem to have lower risk in developing cardiovascular disease than women of *ACE* DD, and in post-menopausal stage, the risk was similar in women of the two different *ACE* genotypes.

DATA AVAILABILITY STATEMENT

The raw data supporting the conclusions of this article will be made available by the authors, without undue reservation.

ETHICS STATEMENT

The studies involving human participants were reviewed and approved by the Ethics Committee of Beijing Sport University (2019014H). The patients/participants provided their written informed consent to participate in this study.

AUTHOR CONTRIBUTIONS

LZ and J-GY designed the research study and analyzed the data. YL, WZ, and LY carried out the experiments. YL, J-GY, and WZ analyzed the results and performed statistical analysis in collaboration with LY. YL wrote the manuscript with help from J-GY and LZ. LZ and J-GY had primary responsibility for the final content. All authors read and approved the final manuscript.

FUNDING

This study was funded by the National Natural Science Foundation of China (31571229) and Chinese Universities Scientific Fund (2019PT007).

ACKNOWLEDGMENTS

We thank the participants, staffs, and other investigators for their valuable contributions to this study.

REFERENCES

Aeschlimann, S. E., Mitchell, C. K., and Korcarz, C. E. (2004). Ultrasound brachial artery reactivity testing: technical considerations. *J. Am. Soc. Echocardiogr.* 17, 697–699. doi: 10.1016/j.echo.2004.03.017

Al-Fakhri, N., Linhart, R. E., Philipp, M., Heidt, M., Hehrlein, F. W., Gardemann, A., et al. (2003). Endothelin-1 and vasopressin plasma levels are not associated with the insertion/deletion polymorphism of the human angiotensin I-converting enzyme gene in patients with coronary artery disease. *J. Hum. Hypertens.* 17, 133–138. doi: 10.1038/sj.jhh.1001519

Al-Hazzani, A., Daoud, M. S., Ataya, F. S., Fouad, D. and Al-Jafari, A. A. (2014). Renin-angiotensin system gene polymorphisms among Saudi patients with coronary artery disease. *J Biol Res.* 21, 1–9. doi: 10.1186/2241-5793-21-8

Alhenc-Gelas, F., Richard, J., Courbon, D., Warnet, J. M., and Corvol, P. (1991). Distribution of plasma angiotensin I-converting enzyme levels in healthy men: relationship to environmental and hormonal parameters. *J. Lab. Clin. Med.* 117, 33–39.

Alvarez, R., González, P., Batalla, A., Reguero, J. R., Iglesias-Cubero, G., Hevia, S., et al. (2001). Association between the NOS3 (-786 T/C) and the ACE (I/D) DNA genotypes and early coronary artery disease. *Nitric. Oxide* 5, 343–348. doi: 10.1006/niox.2001.0351

Amara, A., Mrad, M., Sayeh, A., Lahideb, D., Layouni, S., Haggui, A., et al. (2018). The Effect of ACE I/D Polymorphisms Alone and With Concomitant Risk Factors on Coronary Artery Disease. *Clin. Appl. Thromb. Hemost* 24, 157–163. doi: 10.1177/1076029616679505

Bader, M. (2010). Tissue renin-angiotensin-aldosterone systems: targets for pharmacological therapy. *Annu. Rev. Pharmacol. Toxicol.* 50, 439–465. doi: 10.1146/annurev.pharmtox.010909.105610

Basyigit, S., Ozkan, S., Uzman, M., Ertugrul, D. T., Kefeli, A., Aktas, B., et al. (2015). Should screening for colorectal neoplasm be recommended in patients at high risk for coronary heart disease: a cross-sectional study. *Medicine* 94:e793. doi: 10.1097/MD.0000000000000793

Berzigotti, A., Erice, E., Gilabert, R., Reverter, E., Abraldes, J. G., García-Pagan, J. C., et al. (2013). Cardiovascular risk factors and systemic endothelial function

in patients with cirrhosis. *Am. J. Gastroenterol.* 108, 75–82. doi: 10.1038/ajg.2012.362

Bourque, S. L., Davidge, S. T., and Adams, M. A. (2011). The interaction between endothelin-1 and nitric oxide in the vasculature: new perspectives. *Am. J. Physiol. Regul. Integr. Comp. Physiol.* 300, R1288–R1295. doi: 10.1152/ajpregu.00397.2010

Brand, J. S., and van der Schouw, Y. T. (2010). Testosterone, SHBG and cardiovascular health in postmenopausal women. *Int. J. Impot. Res.* 22, 91–104. doi: 10.1038/ijir.2009.64

Cai, Y., Li, X., Sun, Z., Lu, Y., Zhao, H., Hanson, J., et al. (2019). SPOT-Fold: fragment-free protein structure prediction guided by predicted backbone structure and contact map. *J. Comput. Chem.* 8, 745–750. doi: 10.1002/jcc.26132

Cambien, F., Alhenc-Gelas, F., Herbeth, B., Andre, J. L., Rakotovao, R., Gonzales, M. F., et al. (1988). Familial resemblance of plasma angiotensin-converting enzyme level: the Nancy Study. *Am. J. Hum. Genet.* 43, 774–780.

Cambien, F., and Evans, A. (1995). Angiotensin I converting enzyme gene polymorphism and coronary heart disease. *Eur. Heart J.* 16(Suppl. K), 13–22. doi: 10.1093/eurheartj/16.suppl_k.13

Cambien, F., Poirier, O., Lecerf, L., Evans, A., Cambou, J. P., Arveiler, D., et al. (1992). Deletion polymorphism in the gene for angiotensin-converting enzyme is a potent risk factor for myocardial infarction. *Nature* 359, 641–644. doi: 10.1038/359641a0

Celermajer, D. S., Sorensen, K. E., Bull, C., Robinson, J., and Deanfield, J. E. (1994). Endothelium-dependent dilation in the systemic arteries of asymptomatic subjects relates to coronary risk factors and their interaction. *J. Am. Coll. Cardiol.* 24, 1468–1474. doi: 10.1016/0735-1097(94)90141-4

Celermajer, D. S., Sorensen, K. E., Gooch, V. M., Spiegel halter, D. J., Miller, O. I, Sullivan, I. D., et al. (1992). Non-invasive detection of endothelial dysfunction in children and adults at risk of atherosclerosis. *Lancet* 340, 1111–1115. doi: 10.1016/0140-6736(92)93147-f

Comey, C. T., Koons, B. W., Presley, K. W., Smerick, J. B., Sobieralski, C., Stanley, D., et al. (1994). DNA Extraction Strategies for Amplified Fragment Length Polymorphism Analysis. *J. Forensic Sci.* 39, 1254–1269.

Corretti, M. C., Anderson, T. J., Benjamin, E. J., Celermajer, D., Charbonneau, F., Creager, M. A., et al. (2002). Guidelines for the ultrasound assessment of endothelial-dependent flow-mediated vasodilation of the brachial artery: a report of the International Brachial Artery Reactivity Task Force. *J. Am. Coll. Cardiol.* 39, 257–265. doi: 10.1016/s0735-1097(01)01746-6

D'Andrea, A., Stisi, S., Caso, P., Uccio, F. S. D., Bellissimo, S., Salerno, G., et al. (2007). Associations between left ventricular myocardial involvement and endothelial dysfunction in systemic sclerosis: noninvasive assessment in asymptomatic patients. *Echocardiography* 24, 587–597. doi: 10.1111/j.1540-8175.2007.00436.x

Daniela, S., Alica, L., Zuzana, B., Marta, C., Patrícia, K., and Pavel, B. (2008). Relationships between blood pressure, polymorphism angiotensin-converting enzyme (ACE), body composition and biochemical characteristics in elder slovaks. *Anthropol. Anz.* 66, 199–209. doi: 10.1127/aa/66/2008/199

Dankova, Z., Sivakova, D., Luptakova, L., and Blazicek, P. (2009). Association of ACE (I/D) polymorphism with metabolic syndrome and hypertension in two ethnic groups in Slovakia. *Anthropol. Anz.* 67, 305–316. doi: 10.1127/0003-5548/2009/0035

Donato, A. J., Machin, D. R., and Lesniewski, L. A. (2018). Mechanisms of Dysfunction in the Aging Vasculature and Role in Age-Related Disease. *Circ. Res.* 123, 825–848. doi: 10.1161/circresaha.118.312563

D'Orléans-Juste, P., Houde, M., Rae, G. A., Bkaily, G., Carrier, E., and Simard, E. (2008). Endothelin-1 (1-31): from chymase-dependent synthesis to cardiovascular pathologies. *Vascul Pharmacol.* 49, 51–62. doi: 10.1016/j.vph.2008.06.007

Fabricio, V., Oishi, J. C., Biffe, B. G., Ruffoni, L. D. G., Silva, K. A. D., Nonaka, K. O., et al. (2017). Resveratrol Treatment Normalizes the Endothelial Function and Blood Pressure in Ovariectomized Rats. *Arq. Bras. Cardiol.* 108, 116–121. doi: 10.5935/abc.20170012

Gao, S., McMillan, R. P., Jacas, J., Zhu, Q., Li, X., Kumar, G. K., et al. (2014). Regulation of substrate oxidation preferences in muscle by the peptide hormone adropin. *Diabetes Metab. Res. Rev.* 63, 3242–3252. doi: 10.2337/db14-0388

Gimbrone, M. A., and García-Cardeña, G. (2016). Endothelial Cell Dysfunction and the Pathobiology of Atherosclerosis. *Circ. Res.* 118, 620–636. doi: 10.1161/circresaha.115.306301

Godo, S., Sawada, A., Saito, H., Ikeda, S., Enkhjargal, B., Suzuki, K., et al. (2016). Disruption of physiological balance between nitric oxide and endothelium-dependent hyperpolarization impairs cardiovascular homeostasis in mice. *Arterioscler. Thromb. Vasc. Biol.* 1, 97–107. doi: 10.1161/ATVBAHA.115.306499

Gohar, E. Y., Giachini, F. R., Pollock, D. M., and Tostes, R. C. (2016). Role of the endothelin system in sexual dimorphism in cardiovascular and renal diseases. *Life Sci.* 159, 20–29. doi: 10.1016/j.lfs.2016.02.093

González-González, A., González, A., Alonso-González, C., Menéndez-Menéndez, J., Martínez-Campa, C., and Cos, S. (2018). Complementary actions of melatonin on angiogenic factors, the angiopoietin/Tie2 axis and VEGF, in co-cultures of human endothelial and breast cancer cells. *Oncol. Rep.* 39, 433–441. doi: 10.3892/or.2017.6070

Green, D. J., Jones, H., Thijssen, D., Cable, N. T., and Atkinson, G. (2011). Flow-mediated dilation and cardiovascular event prediction: does nitric oxide matter? *Hypertension* 57, 363–369. doi: 10.1161/HYPERTENSIONAHA.110.167015

Halcox, J. P., Nour, K. R., Zalos, G., and Quyyumi, A. A. (2007). Endogenous endothelin in human coronary vascular function: differential contribution of endothelin receptor types A and B. *Hypertension* 49, 1134–1141. doi: 10.1161/HYPERTENSIONAHA.106.083303

He, L., Zhang, X., Lv, Y., Gu, B., and Zhao, L. (2019). Effects of 8 weeks of moderate-intensity resistance training on muscle changes in postmenopausal women with different angiotensin-converting enzyme insertion/deletion polymorphisms of interest. *Menopause* 26, 899–905. doi: 10.1097/GME.0000000000001364

Houde, M., Desbiens, L., and D'Orléans-Juste, P. (2016). Endothelin-1: biosynthesis signaling and vasoreactivity. *Adv. Pharmacol.* 77, 143–175. doi: 10.1016/bs.apha.2016.05.002

Huang, W., Sun, M., and Zhou, H. (2004a). Effect of Angiotensin Converting Enzyme Gene Polymorphism on Plasma Angiotensin? Level and Heart Failure. *J. Central South Univ.* 29, 198–200.

Huang, W., Xie, C., Zhou, H., Yang, T., and Sun, M. (2004b). Association of the angiotensin-converting enzyme gene polymorphism with chronic heart failure in Chinese Han patients. *Eur. J. Heart Fail.* 6, 23–27. doi: 10.1016/j.ejheart.2003.09.004

Imanishi, T., Han, T., and Nishio, I. (2005). Estrogen reduces angiotensin II-induced acceleration of senescence in endothelial progenitor cells. *Hypertens. Res.* 28, 263–271. doi: 10.1291/hypres.28.263

Inaba, Y., Chen, J. A., and Bergmann, S. R. (2010). Prediction of future cardiovascular outcomes by flow-mediated vasodilatation of brachial artery: a meta-analysis. *Int. J. Cardiovasc. Imaging* 26, 631–640. doi: 10.1007/s10554-010-9616-1

Jia, G., Aroor, A. R., Jia, C., and Sowers, J. R. (2019). Endothelial cell senescence in aging-related vascular dysfunction. *Biochim. Biophys. Acta* 1865, 1802–1809. doi: 10.1016/j.bbadis.2018.08.008

Kalita, J., Somarajan, B. I., Kumar, B., Mittal, B., and Misra, U. K. (2011). A study of ACE and ADD1 polymorphism in ischemic and hemorrhagic stroke. *Clin. Chim. Acta* 412, 642–646. doi: 10.1016/j.cca.2010.12.022

Kang, L. S., Chen, B., Reyes, R. A., Leblanc, A. J., Teng, B., Mustafa, S. J., et al. (2011). Aging and estrogen alter endothelial reactivity to reactive oxygen species in coronary arterioles. *Am. J. Physiol. Heart Circ. Physiol.* 300, H2105–H2115. doi: 10.1152/ajpheart.00349.2010

Kato, N., Tatara, Y., Ohishi, M., Takeya, Y., Onishi, M., Maekawa, Y., et al. (2011). Angiotensin-converting enzyme single nucleotide polymorphism is a genetic risk factor for cardiovascular disease: a cohort study of hypertensive patients. *Hypertens. Res.* 34, 728–734. doi: 10.1038/hr.2011.28

Kim, C. H., Yun, S. K., Byun, D. W., Yoo, M. H., and Lee, K. U. (2001). Codon 54 polymorphism of the fatty acid binding protein 2 gene is associated with increased fat oxidation and hyperinsulinemia, but not with intestinal fatty acid absorption in Korean men*. *Metabolism* 50, 473–476. doi: 10.1053/meta.2001.21022

Kuzubova, N. A., Chukhlovin, A. B., Morozova, E. B., Totolian, A. A., and Titova, O. N. (2013). Common intronic D variant of ACE gene is associated with

endothelial dysfunction in COPD. *Respir. Med.* 107, 1217–1221. doi: 10.1016/j.rmed.2012.12.025

Larsen, J. S., Skaug, E. A., Wisløff, U., Ellingsen, Ø, Stovner, L. J., Linde, M., et al. (2016). Migraine and endothelial function: the HUNT3 Study. *Cephalalgia* 36, 1341–1349. doi: 10.1177/0333102416631961

Lekontseva, O., Chakrabart, S., and Davidge, S. T. (2010). Endothelin in the female vasculature: a role in aging? *Am. J. Physiol. Regul. Integr. Comp. Physiol.* 298, R509–R516.

Lian, L. H., Lau, T. P., Ching, A. S., and Chua, K. H. (2012). Angiotensin-converting enzyme gene I/D dimorphism does not play a major role in the susceptibility of Malaysian systemic lupus erythematosus patients. *Genet. Mol. Res.* 11, 863–871. doi: 10.4238/2012.April.10.2

Marasciulo, F. L., Montagnani, M., and Potenza, M. A. (2006). Endothelin-1: the yin and yang on vascular function. *Curr. Med. Chem.* 13, 1655–1665. doi: 10.2174/092986706777441968

Masuyer, G., Schwager, S. L. U., Sturrock, E. D., Isaac, R. E., and Acharya, K. R. (2012). Molecular recognition and regulation of human angiotensin-I converting enzyme (ACE) activity by natural inhibitory peptides. *Sci. Rep.* 2:717. doi: 10.1038/srep00717

Méthot, J., Hamelin, B. A., Arsenault, M., Bogaty, P., Plante, S., and Poirier, P. (2006). The ACE-DD genotype is associated with endothelial dysfunction in postmenopausal women. *Menopause* 13, 959–966. doi: 10.1097/01.gme.0000243576.09065.93

Min, L. J., Mogi, M., Iwai, M., and Horiuchi, M. (2009). Signaling mechanisms of angiotensin II in regulating vascular senescence. *Ageing Res. Rev.* 8, 113–121. doi: 10.1016/j.arr.2008.12.002

Moran, C. N., Vassilopoulos, C., Tsiokanos, A., Jamurtas, A. Z., Bailey, M. E. S., Wilson, R. H., et al. (2005). Effects of interaction between angiotensin I-converting enzyme polymorphisms and lifestyle on adiposity in adolescent Greeks. *Obes. Res.* 13, 1499–1504. doi: 10.1038/oby.2005.181

Moreau, K. L. (2018). Intersection between gonadal function and vascular aging in women. *J. Appl. Physiol.* 125, 1881–1887. doi: 10.1152/japplphysiol.00117.2018

Moreau, K. L., Deane, K. D., Meditz, A. L., and Kohrt, W. M. (2013). Tumor necrosis factor-α inhibition improves endothelial function and decreases arterial stiffness in estrogen-deficient postmenopausal women. *Atherosclerosis* 230, 390–396. doi: 10.1016/j.atherosclerosis.2013.07.057

Moreau, K. L., Meditz, A., Deane, K. D., and Kohrt, W. M. (2012). Tetrahydrobiopterin improves endothelial function and decreases arterial stiffness in estrogen-deficient postmenopausal women. *Am. J. Physiol. Heart Circ. Physiol.* 302, H1211–H1218. doi: 10.1152/ajpheart.01065.2011

Nemoto, T., Minami, Y., Yamaoka-Tojo, M., Sato, T., Muramatsu, Y., Kakizaki, R., et al. (2019). Impaired Flow-Mediated Dilation and Severity and Vulnerability of Culprit Plaque in Patients with Coronary Artery Disease. *Int. Heart J.* 60, 539–545. doi: 10.1536/ihj.18-531

Neunteufl, T., Katzenschlager, R., Hassan, A., Klaar, U., Schwarzacher, S., Glogar, D., et al. (1997). Systemic endothelial dysfunction is related to the extent and severity of coronary artery disease. *Atherosclerosis* 129, 111–118. doi: 10.1016/s0021-9150(96)06018-2

Ohkita, M., Tawa, M., Kitada, K., and Matsumura, Y. (2012). Pathophysiological roles of endothelin receptors in cardiovascular diseases. *J. Pharmacol. Sci.* 119, 302–313. doi: 10.1254/jphs.12r01cr

Ramzy, D., Rao, V., Tumiati, L. C., Xu, N., Miriuka, S., Delgado, D., et al. (2006a). Role of endothelin-1 and nitric oxide bioavailability in transplant-related vascular injury: comparative effects of rapamycin and cyclosporine. *Circulation* 114, I214–I219.

Ramzy, D., Rao, V., Tumiati, L. C., Xu, N., Sheshgiri, R., Miriuka, S., et al. (2006b). Elevated endothelin-1 levels impair nitric oxide homeostasis through a PKC-dependent pathway. *Circulation* 114, I319–I326. doi: 10.1161/CIRCULATIONAHA.105.001503

Rigat, B., Hubert, C., Alhenc-Gelas, F., Cambien, F., Corvol, P., and Soubrier, F. (1990). An insertion/deletion polymorphism in the angiotensin I-converting enzyme gene accounting for half the variance of serum enzyme levels. *J. Clin. Invest.* 86, 1343–1346. doi: 10.1172/JCI114844

Rossman, M. J., LaRocca, T. J., Martens, C. R., and Seals, D. R. (2018). Healthy lifestyle-based approaches for successful vascular aging. *J. Appl. Physiol.* 125, 1888–1900. doi: 10.1152/japplphysiol.00521.2018

Saab, Y. B., Gard, P. R., and Overall, A. D. (2007). The geographic distribution of the ACE II genotype: a novel finding. *Genet. Res.* 89, 259–267. doi: 10.1017/S0016672307009019

Santoro, N., and Chervenak, J. L. (2004). The menopause transitions. *Endocrinol. Metab. Clin. North. Am.* 33, 627–636. doi: 10.1016/j.ecl.2004.07.002

Santos-Parker, J. R., Strahler, T. R., Vorwald, V. M., Pierce, G. L., and Seals, D. R. (2017). Habitual aerobic exercise does not protect against micro- or macrovascular endothelial dysfunction in healthy estrogen-deficient postmenopausal women. *J. Appl. Physiol.* 122, 11–19. doi: 10.1152/japplphysiol.00732.2016

Sayed-Tabatabaei, F. A., Oostra, B. A., Isaacs, A., van Duijn, C. M., and Witteman, J. C. M. (2006). ACE polymorphisms. *Circ. Res.* 98, 1123–1133.

Sepúlveda, C., Palomo, I., and Fuentes, E. (2017). Mechanisms of endothelial dysfunction during aging: predisposition to thrombosis. *Mech. Ageing Dev.* 164, 91–99. doi: 10.1016/j.mad.2017.04.011

Shafiee, S. M., Firoozrai, M., Salimi, S., Zand, H., Hesabi, B., and Mohebbi, A. (2010). Angiotensin converting enzyme DD genotype not associated with increased risk of coronary artery disease in the Iranian population. *Pathophysiology* 17, 163–167. doi: 10.1016/j.pathophys.2009.10.001

Shi, Y., Savarese, G., Perrone-Filardi, P., Lüscher, T. F., and Camici, G. G. (2014). Enhanced age-dependent cerebrovascular dysfunction is mediated by adaptor protein p66Shc. *Int. J. Cardiol.* 175, 446–450. doi: 10.1016/j.ijcard.2014.06.025

Somani, Y. B., Pawelczyk, J. A., De Souza, M. J., Kris-Etherton, P. M., and Proctor, D. N. (2019). Aging women and their endothelium: probing the relative role of estrogen on vasodilator function. *Am. J. Physiol. Heart Circ. Physiol.* 317, H395–H404. doi: 10.1152/ajpheart.00430.2018

Stanhewicz, A. E., Wenner, M. M., and Stachenfeld, N. S. (2018). Sex differences in endothelial function important to vascular health and overall cardiovascular disease risk across the lifespan. *Am. J. Physiol. Heart Circ. Physiol.* 315, H1569–H1588. doi: 10.1152/ajpheart.00396.2018

Sun, F., He, N., Zhang, K., Wu, N., Zhao, J., and Qiu, C. (2018). Association of ACE gene A2350G and I/D polymorphisms with essential hypertension in the northernmost province of China. *Clin. Exp. Hypertens.* 40, 32–38. doi: 10.1080/10641963

Taddei, S., Virdis, A., Ghiadoni, L., Mattei, P., Sudano, I., Bernini, G., et al. (1996). Menopause is associated with endothelial dysfunction in women. *Hypertension* 28, 576–582. doi: 10.1161/01.hyp.28.4.576

Takase, B., Uehata, A., Akima, T., Nagai, T., Nishioka, T., Hamabe, A., et al. (1998). Endothelium-dependent flow-mediated vasodilation in coronary and brachial arteries in suspected coronary artery disease. *Am. J. Cardiol.* 82, A7–A8. doi: 10.1016/s0002-9149(98)00702-4

Tanriverdi, H., Evrengul, H., Mergen, H., Acar, C., Seleci, D., Kuru, O., et al. (2007). Early sign of atherosclerosis in slow coronary flow and relationship with angiotensin-converting enzyme I/D polymorphism. *Heart Vessels* 22, 1–8. doi: 10.1007/s00380-006-0925-1

Thijssen, D. H., Carter, S. E., and Green, D. J. (2016). Arterial structure and function in vascular ageing: are you as old as your arteries? *J. Physiol.* 594, 2275–2284. doi: 10.1113/JP270597

Thijssen, D. H. J., Black, M. A., Pyke, K. E., Padilla, J., Atkinson, G., Harris, R. A., et al. (2011). Assessment of flow-mediated dilation in humans: a methodological and physiological guideline. *Am. J. Physiol. Heart Circ. Physiol.* 300, H2–H12. doi: 10.1152/ajpheart.00471.2010

Trindade, M., Oigman, W., and Fritsch Neves, M. (2017). Potential Role of Endothelin in Early Vascular Aging. *Curr. Hypertens. Rev.* 13, 33–40. doi: 10.2174/1573402113666170414165735

Tykocki, N. R., Gariepy, C. E., and Watts, S. W. (2009). Endothelin ET(B) receptors in arteries and veins: multiple actions in the vein. *J. Pharmacol. Exp. Ther.* 329, 875–881. doi: 10.1124/jpet.108.145953

Ungvari, Z., Tarantini, S., Donato, A. J., Galvan, V., and Csiszar, A. (2018a). Mechanisms of vascular aging. *Circ. Res.* 123, 849–867. doi: 10.1161/CIRCRESAHA.118.311378

Ungvari, Z., Tarantini, S., Kiss, T., Wren, J. D., Giles, C. B., Griffin, C. T., et al. (2018b). Endothelial dysfunction and angiogenesis impairment in the ageing vasculature. *Nat. Rev. Cardiol.* 15, 555–565. doi: 10.1038/s41569-018-0030-z

Witkowski, S., and Serviente, C. (2018). Endothelial dysfunction and menopause: are exercise an effective countermeasure? *Climacteric* 21, 267–275. doi: 10.1080/13697137.2018.1441822

Wiwanitkit, V. (2004). Angiotensin-converting enzyme gene polymorphism: I and D alleles from some different countries. *Clin. Appl. Thromb. Hemost* 10, 179–182. doi: 10.1177/107602960401000209

Yeboah, J., Folsom, A. R., Burke, G. L., Johnson, C., Polak, J. F., Post, W., et al. (2009). Predictive value of brachial flow-mediated dilation for incident cardiovascular events in a population-based study: the multi-ethnic study of atherosclerosis. *Circulation* 120, 502–509. doi: 10.1161/CIRCULATIONAHA.109.864801

Conflict of Interest: The authors declare that the research was conducted in the absence of any commercial or financial relationships that could be construed as a potential conflict of interest.

frontiers in Physiology

REVIEW
published: 24 September 2020
doi: 10.3389/fphys.2020.577584

Cellular Origins of the Lymphatic Endothelium: Implications for Cancer Lymphangiogenesis

*Laura Gutierrez-Miranda and Karina Yaniv**

Department of Biological Regulation, Weizmann Institute of Science, Rehovot, Israel

The lymphatic system plays important roles in physiological and pathological conditions. During cancer progression in particular, lymphangiogenesis can exert both positive and negative effects. While the formation of tumor associated lymphatic vessels correlates with metastatic dissemination, increased severity and poor patient prognosis, the presence of functional lymphatics is regarded as beneficial for anti-tumor immunity and cancer immunotherapy delivery. Therefore, a profound understanding of the cellular origins of tumor lymphatics and the molecular mechanisms controlling their formation is required in order to improve current strategies to control malignant spread. Data accumulated over the last decades have led to a controversy regarding the cellular sources of tumor-associated lymphatic vessels and the putative contribution of non-endothelial cells to this process. Although it is widely accepted that lymphatic endothelial cells (LECs) arise mainly from pre-existing lymphatic vessels, additional contribution from bone marrow-derived cells, myeloid precursors and terminally differentiated macrophages, has also been claimed. Here, we review recent findings describing new origins of LECs during embryonic development and discuss their relevance to cancer lymphangiogenesis.

Keywords: lymphatic, origin, lymphangiogenesis, tumor, development

OPEN ACCESS

Edited by:
Mariona Graupera, Institut d'Investigacio Biomedica de Bellvitge (IDIBELL), Spain

Reviewed by:
Natasha Harvey, University of South Australia, Australia
Sophia Ran, Southern Illinois University School of Medicine, United States

****Correspondence:***
Karina Yaniv
karina.yaniv@weizmann.ac.il

Specialty section:
This article was submitted to Vascular Physiology, a section of the journal Frontiers in Physiology

Received: *29 June 2020*
Accepted: *25 August 2020*
Published: *24 September 2020*

Citation:
Gutierrez-Miranda L and Yaniv K (2020) Cellular Origins of the Lymphatic Endothelium: Implications for Cancer Lymphangiogenesis. Front. Physiol. 11:577584. doi: 10.3389/fphys.2020.577584

STRUCTURE AND FUNCTIONS OF THE LYMPHATIC SYSTEM

The lymphatic system is composed of an extended network of vessels and secondary lymphoid organs [e.g., lymph nodes, Peyer Patches, spleen and mucosa-associated lymphoid tissue (MALT)], distributed throughout the entire organism. Lymphatic vessels are arranged in a tree-shaped hierarchy. Each vessel type – capillaries, pre-collecting and collecting lymphatics –, displays specific structural and functional features (Ulvmar and Mäkinen, 2016; Petrova and Koh, 2020). The lymphatic capillaries are blind-ended tubes formed by one single lining of lymphatic endothelial cells (LECs) that exhibit discontinuous button-like junctions to facilitate fluid entry into the vessel (Leak and Burke, 1966; Baluk et al., 2007). In contrast, collecting lymphatics are complex vessels with continuous intracellular zipper-like junctions, basement membrane and a contractile smooth muscle layer that help pump the lymph through the lymph node back to the bloodstream (Baluk et al., 2007; Muthuchamy and Zawieja, 2008). In addition, they contain bi-leaflet valves that prevent lymph backflow, and assure unidirectional transport (Kampmeier, 1928; Smith, 1949). Besides uptaking fluids and plasma solutes from the interstitium and returning them back to the venous circulation, lymphatics also actively regulate immune trafficking of antigens and antigen-presenting

cells toward the lymph nodes (Alitalo and Carmeliet, 2002), and absorb lipids in the gut through the intestinal lacteals (Tso and Balint, 1986; Huang et al., 2015).

Absence or malfunction of lymphatic vessels leads to the onset of many pathologies, including lymphedema, an incurable disease characterized by a disabling swelling of the extremities, accompanied by recurrent life-threatening infections (Alitalo and Carmeliet, 2002; Brouillard et al., 2014; Yuan et al., 2019; Azhar et al., 2020). In addition, since lymphatics proliferate under inflammatory conditions (Pullinger and Florey, 1937) and are responsible for immune cell clearance and resolution of inflammation; dysfunctional lymphatics are associated with chronic inflammatory and autoimmune diseases like psoriasis (Kunstfeld et al., 2004) and rheumatoid arthritis (reviewed in Schwartz et al., 2019).

During cancer progression lymphatic vessels can play dual roles (reviewed in Oliver et al., 2020; Petrova and Koh, 2020; Vaahtomeri and Alitalo, 2020). On the one hand, they promote tumor metastasis by providing malignant cells with an escape conduit for dissemination toward the lymph nodes and distal metastatic niches. Accordingly, the presence of lymphatic metastasis is correlated with poor patient prognosis and survival (Pasquali et al., 2013; Stacker et al., 2014; Wilczak et al., 2018). On the other side, the presence of functional lymphatics boosts anti-tumoral immune response and facilitates the delivery of chemotherapy agents enhancing their effect (Lund et al., 2016; Fankhauser et al., 2017; Song et al., 2020). Hence, a profound characterization of the mechanisms underlying lymphatic formation is required in order to improve current strategies for controlling tumor progression, by preventing or encouraging lymphatic vessel growth.

EMBRYONIC DEVELOPMENT OF LYMPHATIC VESSELS

It is a widely held view that during embryogenesis the first LECs derive from venous structures (Sabin, 1902; Wigle and Oliver, 1999; Yaniv et al., 2006; Srinivasan et al., 2007). Specifically, at E9.5 of mouse development, a subpopulation of cells within the cardinal veins acquires lymphatic identity (You et al., 2005; François et al., 2008; Srinivasan et al., 2010) by inducing the expression of prospero homeobox protein 1 (PROX1) the main driver of lymphatic commitment and differentiation (Wigle and Oliver, 1999; Wigle, 2002; Srinivasan and Oliver, 2011). Between E9.5 until E14.5, PROX1 positive cells upregulate the expression of additional lymphatic-specific markers like the membrane receptors vascular endothelial growth factor 3 (VEGFR3) (Kaipainen et al., 1995), Lymphatic vessel endothelial hyaluronan receptor 1 (LYVE1) (Banerji et al., 1999), and podoplanin (PDPN) (Breiteneder-Geleff et al., 1999). Then, following secretion and processing of vascular endothelial growth factor C (VEGFC), VEGFR3+ responsive LECs sprout out of the veins and migrate toward the signal source to assemble the primitive lymphatic structures, the lymph sacs (Wigle and Oliver, 1999; Wigle, 2002). Subsequent sprouting and remodeling of the lymph sacs help assemble a mature lymphatic plexus.

A similar process was found to take place in aquatic animals. In zebrafish, a cluster of angioblasts in the floor of the posterior cardinal vein (PCV) was shown to give rise to lymphatic progenitors in the developing embryo (Nicenboim et al., 2015). The cells committed to the lymphatic fate, migrate to the dorsal part of the PCV and bud toward the midline of the embryo to form the primordial parachordal cells (also known as parachordal lymphangioblasts or PLs), the building blocks of the lymphatic system (Küchler et al., 2006; Yaniv et al., 2006). Another study revealed the existence of bipotent Prox1+ precursor cells in the PCV that generate lymphatics through asymmetric cell division (Koltowska et al., 2015) (**Figure 1A**). Although the process of lymphatic formation is highly conserved among vertebrates, certain divergences between the mammalian and zebrafish systems have also been described (Tao et al., 2011; van Impel et al., 2014; Semo et al., 2016).

Once differentiated, LECs respond to two major stimuli: VEGF-C (Joukov et al., 1996) and VEGF-D (Achen et al., 1998), both of them VEGFR3 ligands. VEGF-C controls both proliferation and migration of LEC (Joukov et al., 1996; Jeltsch, 1997). The VEGF-C/VEGFR3 axis is very active during early lymphangiogenesis in mouse embryonic development (Kukk et al., 1996; Veikkola et al., 2001) and dysregulation of either of these factors results in lymphatic malformations (Dumont, 1998; Karkkainen et al., 2000, 2004). Although VEGF-C does not control LEC specification *per se,* its function is indispensable for the sprouting of primordial lymphatics from the cardinal vein in mice and zebrafish (Karkkainen et al., 2004; Shin et al., 2016). Accordingly, *Vegfc*$^{-/-}$ mouse embryos lack primordial lymphatic structures, develop edema and die prematurely. In addition, loss of *Vegfc* expression or absence of VEGF-C in mice results in the development of defective lymphatics and lymphedema (Mäkinen et al., 2001; Karkkainen et al., 2004). In similar fashion, zebrafish *vegfc* mutants are devoid of lymphatic vessels (Villefranc et al., 2013; Le Guen et al., 2014) and heterozygous *vegfc*$^{+/-}$ animals fail to establish proper lymphatic vessels in various organs, including the heart (Gancz et al., 2019b). Both VEGF-C and VEGF-D are produced and secreted as pre-propeptides and they require to undergo a proteolytic cleavage in order to acquire their mature and active form (Joukov et al., 1997; Stacker et al., 1999). VEGF-C processing requires the formation of the VEGFC-CCBE1-ADAMTS3 multicomplex (Jeltsch et al., 2014) and loss of any of this components leads to lymphatic defects. Collagen and calcium binding EGF domains 1 (CCBE1) is a secreted regulator of VEGF-C activation necessary for proper lymphatic vessel formation in mammals (Bos et al., 2011; Hägerling et al., 2013; Roukens et al., 2015) and zebrafish (Hogan et al., 2009; Le Guen et al., 2014). In addition, *CCBE1* mutations were identified in patients with several lymphatic vessel malformations (Alders et al., 2009; Connell et al., 2010). A disintegrin and metalloproteinase with thrombospondin motifs 3 (ADAMTS3) is a VEGF-C protease, whose total deletion (i.e., *Adamts3*$^{-/-}$ mice) mirrored the phenotypes observed in *Ccbe1* and *Vegfc* null embryos (Bui et al., 2016).

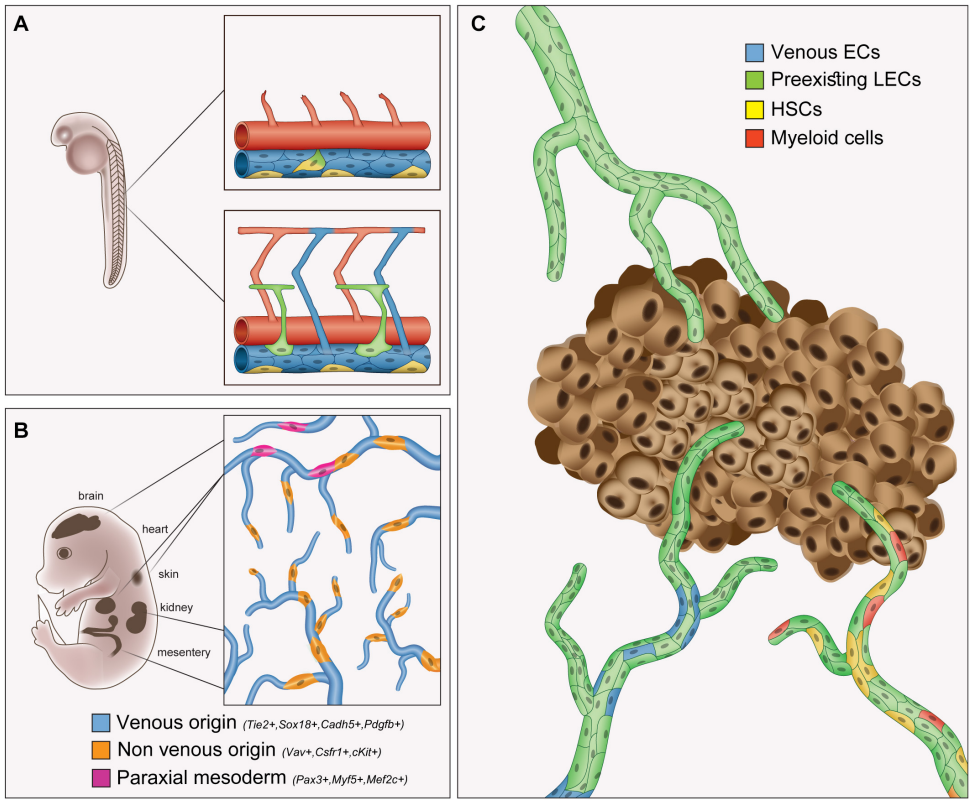

FIGURE 1 | Overview of the origins of lymphatic endothelial cells in embryonic development and cancer. Schematic illustrations depicting the origins of cells contributing to the formation of **(A)** early lymphatics in the zebrafish trunk, **(B)** organ-specific lymphatics in the mouse embryo and **(C)** tumor-associated lymphatics. **(A)** A cluster of angioblasts (yellow) located in the ventral side of the PCV are the source of the parachordal cells (green), the primordial lymphatic progenitors in the embryonic zebrafish trunk. Arteries are depicted in red and veins in blue. **(B)** Lineage-tracing experiments in mice revealed mixed origin of organ-specific lymphatic networks. Venous (blue), paraxial mesoderm (pink) and additional non-venous (orange) origins give rise to organ-specific LECs (detailed in **Table1**). **(C)** Distinct cell populations contribute to tumor lymphatics. Tumor LECs form primarily via sprouting lymphangiogenesis from pre-exiting lymphatics (green). In addition, BMDCs, including hematopoietic stem cells (HSCs), and cells of the myeloid lineage have also been identified as non-endothelial sources of tumor LECs.

Likewise, loss of the Vegfc-processing components *adamts3* and *adamts14* in zebrafish also mimicked the *vegfc* mutant phenotype exhibiting absent trunk, facial and meningeal lining lymphatics (Wang et al., 2020).

VEGFR3 is initially expressed in all embryonic ECs but later on becomes restricted to the LECs (Kaipainen et al., 1995) and fenestrated endothelial cells (Partanen et al., 2000). *Vegfr3* null mutant mice die at midgestation due to delayed vascular development and cardiovascular defects (Dumont, 1998). Likewise, zebrafish *flt4* mutants lack early lymphatic vessels (Kok et al., 2015) as well as adult cardiac lymphatics (Gancz et al., 2019b).

Notably, during the past two decades specific mutations on *VEGFC* (Gordon et al., 2013; Balboa-Beltran et al., 2014; Fastré et al., 2018; Nadarajah et al., 2018), *VEGFR3* (Ferrell, 1998; Irrthum et al., 2000; Karkkainen et al., 2000; Evans, 2003; Brice, 2005; Daniel-Spiegel et al., 2005; Mizuno et al., 2005; Butler et al., 2007; Ghalamkarpour et al., 2006, 2009; Dai et al., 2018) and additional lymphangiogenesis-related genes, have been found to be strongly associated to the onset of primary lymphedema (reviewed in Oliver et al., 2020).

THE ORIGINS OF LYMPHATICS ENDOTHELIAL CELLS

The earliest description of the lymphatic system dates back to Hippocrates, but it was not until the early 1600, where observations of nodes and ducts carrying milky liquid were reported by Gasparo Aselli. During the 20th century, the origin of these vessels was discussed by two conflicting theories. In 1902, the anatomist Florence Sabin suggested, based on her studies of lymphatic development in pig embryos, that the first lymphatic ducts originated from veins (Sabin, 1902). Contrary to this idea, the anatomists George S. Huntington and Charles F. W. McClure postulated that the jugular lymph sacs develop from a cluster of mesenchymal cells in cat embryos (Huntington and McClure, 1910). During the last century, several studies supporting one view or the other were published, underscoring the active debate surrounding the field. While few reports analyzing lymphatic development in turtle (van der Jagt, 1932), chick and quail (Schneider et al., 1999; Wilting et al., 2006) and *Xenopus* (Ny et al., 2005) postulated a dual origin for lymphatic vessels (i.e., with contribution of both the mesenchymal and the venous

compartments) (reviewed in Semo et al., 2016); the model claiming a sole venous origin for the lymphatic endothelium became predominant (Lewis, 1905; Wigle and Oliver, 1999; Wigle, 2002; Yaniv et al., 2006; Srinivasan et al., 2007).

Most recently, however, several studies have revived this debate by revealing new unexpected origins for LECs both during early development and in certain organs (reviewed in Semo et al., 2016; Ulvmar and Mäkinen, 2016; Petrova and Koh, 2018; Gancz et al., 2019a). Accordingly, while the majority of organ-specific lymphatics appears to form through sprouting lymphangiogenesis from neighbor lymphatic vessels, the presence of LECs lineage-traced to different origins was detected. Importantly, the nature of the specific progenitors from which LECs can stem varies in different organs, suggesting that the origin of these LEC populations might be contingent to the specific tissue environments and driven by organ-specific signals (**Figure 1B**). The cellular origins of distinct lymphatic populations identified so far are summarized in **Table1**.

One of the first such examples was the superficial dermal lymphatic network, for which two different LEC origins were reported (Martinez-Corral et al., 2015; Pichol-Thievend et al., 2018). Martinez-Corral et al. (2015) claimed that skin lymphatics in the cervical and thoracic regions of the mouse embryo, form via transdifferentiation of *Tie2*-expressing venous structures and subsequent sprouting from the jugular lymph sacs. In contrast, lymphatics in the lumbar and dorsal midline areas, arise from *Tie2*-negative and *Vav*-negative progenitors, suggesting a non-endothelial and non-hematopoietic origin (Martinez-Corral et al., 2015). Later on, Pichol-Thievend et al. (2018) provided evidence for a novel endothelial progenitor subpopulation located within the capillary bed that gives rise to murine dermal lymphatics in the cervico-thoracic region. According to this study, PROX1+ progenitors in the local vascular plexus bud off the capillaries as single LECs or as small clusters, in a *Ccbe1*-dependent manner. Subsequently, these LECs proliferate and expand, prior to merging into the preexisting dermal lymphatic vasculature (Pichol-Thievend et al., 2018).

The development of mesenteric lymphatics was also shown to involve mixed cell contribution (Mahadevan et al., 2014; Stanczuk et al., 2015). While the mesenteric lymph sacs derive from veins at the mesenteric root, the mesenteric vessels were found to originate from *Pdgfb*+ *cKit*+ hemogenic endothelium, independently of the definitive hematopoietic lineage *Vav*- (Stanczuk et al., 2015).

A similar dual origin – venous and non-venous – of lymphatic progenitors was found also in zebrafish. In this animal, the facial lymphatic network develops in a sequential manner through initial sprouting from the common cardinal vein (CCV) and primary head sinus (PHS), which are of venous origin, followed by an additional non-venous population of lymphangioblasts that connects to this main sprout (Okuda et al., 2012; Eng et al., 2019). In addition, a pool of specialized angioblasts was identified in the floor of the PCV that gives rise to LECs (Nicenboim et al., 2015) as well as to arterial and venous ECs (Hen et al., 2015). These angioblasts were shown to be molecularly distinct from surrounding venous cells, displaying enriched expression of angioblast and arterial markers, and to arise directly from a restricted population in the lateral plate mesoderm.

During the past years, an increasing number of lineage-tracing based studies has determined also the heterogeneous ontology of cardiac lymphatics. In mouse embryos, venous derived lymphatics were shown to give rise to the vessels paralleling the coronaries, while non-venous, *Tie2*-negative yolk sac derived progenitors (Klotz et al., 2015) contribute to the formation of PROX1+ LECs in the developing heart. Recently, three independent studies (Gancz et al., 2019b; Harrison et al., 2019; Vivien et al., 2019) described the development of cardiac lymphatics in zebrafish as well as their role during cardiac regeneration. Interestingly, in addition to conventional lymphatic vessels spanning the cardiac ventricle, Gancz et al. (2019b) reported the presence of isolated *prox1+, lyve1b+, mrc1+ and flt4+* LEC clusters in the zebrafish heart that developed initially into single capillaries, and later on connected to the existing lymphatic plexus. Moreover, a similar PROX1+ population of isolated LEC clusters was detected in the hearts of E14.5 mouse embryos (Gancz et al., 2019b), suggesting that the mechanisms underlying cardiac lymphatic formation are conserved across vertebrates (Gancz et al., 2019b). The second heart field (SHF), a multipotent cell population that contributes to several cardiac structures (Buckingham, 2016; Meilhac and Buckingham, 2018), has also been proposed as an additional non-venous source of cardiac LECs (Maruyama et al., 2019; Lioux et al., 2020). Specifically, *Isl1*+ pharyngeal mesoderm-derived progenitors were shown to contribute to the formation of lymphatics in the outflow tract and in the ventral ventricles of mouse embryos (Maruyama et al., 2019). Further clonal studies and lineage tracing experiments showed that *Islet1*+ and *Mef2c*+ SHF precursors contributed to the formation of cardiac ventral lymphatics but not supported the formation of the dorsal lymphatics. Furthermore, they confirmed that a specific subset of *Isl1*+ sub-mesothelial cells give rise to PROX1+/LYVE1+ vascular structures that comprise around 50% of ventral LECs (Lioux et al., 2020).

The kidney provides another example of how different LEC populations assemble to generate an organ-specific lymphatic plexus. Mouse and human kidneys were reported to bear one "traditional" network of lymphatic capillaries that forms from a ring-like anastomosis in the renal hilum, and a separate population of PROX1+/LYVE1+ isolated LEC clusters similar to those described in the heart (Gancz et al., 2019b), suggesting that both lymphangiogenesis and lymphvasculogenesis play a role in renal lymphatic development (Jafree et al., 2019). Although the isolated LECs were assumed to stem from non-endothelial structures, based on their low PECAM and endomucin expression, the identity of the specific progenitors was not determined by lineage-tracing experiments.

Lymph node LECs were suggested to derive from *Nestin*+ precursors. Fate mapping of these cells in mouse embryos revealed that they contribute to the formation of both CD31+ endothelial cells, and CD31- mesenchymal stromal niches in the lymph nodes. During postnatal development though, *Nestin* expression becomes predominant in the endothelial compartment including the capillaries, high endothelial venules

TABLE 1 | Cellular origins of LECs during embryonic development.

Lymphatics	Species	Venous source	Non-venous source
Jugular sacs	Pig embryo	Sabin (1902)	
Jugular sacs	Cat embryo		Mesenchymal cells (Huntington and McClure, 1910)
Jugular sacs	Mouse embryo	*Tie2*+ (Wigle and Oliver, 1999; Wigle, 2002; Srinivasan et al., 2007)	
Parachordal cells	Zebrafish embryo	*fli1a*+ PCV (Yaniv et al., 2006)	*flt1_9a*+ angioblasts (Nicenboim et al., 2015)
Facial lymphatics	Zebrafish embryo	*lyve1b*+ CCV and PHS (Okuda et al., 2012; Eng et al., 2019)	VA-L (Eng et al., 2019)
Dermal lymphatics	Mouse embryo	*Tie2*+ cervical/thoracic region (Martinez-Corral et al., 2015) *Sox18+/Cadh5+/Tie2*+ cervical/thoracic region (Pichol-Thievend et al., 2018)	*Tie2-/Vav-* dorsal/midline/lumbar region (Martinez-Corral et al., 2015) *Pax3*+ thoracic/lumbar/sacral region (Stone and Stainier, 2019) *Myf5*+ Ear skin (Stone and Stainier, 2019) *Mef2c*+ cervical/thoracic region (Stone and Stainier, 2019)
Cardiac lymphatics	Mouse embryo	*Tie2*+ (Klotz et al., 2015)	*Vav1+/Pdgfb+/Csfr1*+ (Klotz et al., 2015) *Apln-* and *Apj-* (Gancz et al., 2019b) *Isl1*+ (Maruyama et al., 2019; Lioux et al., 2020) *Pax3*+ (Stone and Stainier, 2019)
	Zebrafish	*lyve1b+/prox1a+/mrc1a+/flt4*+ (Gancz et al., 2019b)	Isolated LECs: Undetermined (Gancz et al., 2019b)
Mesenteric lymphatics	Mouse embryo	*Pdgfb*+ (Stanczuk et al., 2015)	*cKit+/Vav1-* (Stanczuk et al., 2015)
Lymph nodes LECs	Mouse embryo		*Nestin*+ (Koning et al., 2016)
Renal lymphatics	Mouse embryo	*Tie2*+ ascending vasa recta: (Kenig-Kozlovsky et al., 2018)	Isolated LECS: Undetermined (Jafree et al., 2019)
Brain	Mouse embryo	Undetermined Aspelund et al. (2015), Louveau et al. (2015)	Undetermined Aspelund et al. (2015), Louveau et al. (2015) *Myf5*+ (Stone and Stainier, 2019)
	Zebrafish	*mrc1a*+ meningeal lymphatics (Castranova et al., 2020) *mrc1a*+ mural LECs (muLECs) */flt4+/prox1a+/lyve1b*+ (Bower et al., 2017; Galanternik et al., 2017; van Lessen et al., 2017)	
Schlemm's canal	Mouse embryo	*Kdr*+ lumbar vasculature (Kizhatil et al., 2014)	

and LECs (Koning et al., 2016). Nevertheless, given that Nestin expression is detected in a wide variety of cells, such as neural stem cells (Mignone et al., 2004) and stem cells from the mesenchymal lineage (Méndez-Ferrer et al., 2010) including endothelial cells (reviewed in Bernal and Arranz, 2018), additional experiments will be required in order to verify the exact origins of lymph node LECs.

Although the earliest observations of meningeal lymphatics date from investigations of Paolo Mascagni in the 18th century, they were mostly neglected (reviewed in Da Mesquita et al., 2018a). Lately, however, two elegant studies have described the presence of a lymphatic network in the mammalian meninges, challenging the old dogma that considered the brain as an immune-privileged organ (Aspelund et al., 2015; Louveau et al., 2015). Louveau et al. (2015) described the presence of meningeal lymphatic vessels aligned with the dural sinuses. These peri-sinusal lymphatics expressed the classical LEC markers such as LYVE1, PDPN, and PROX1. Importantly, a similar LYVE1+, PDPN+, and CD68- structure was also identified in the human dura. These meningeal lymphatic vessels extend from the eye and olfactory bulb toward the sinuses, exiting the skull along vein, arteries and cranial nerves (Aspelund et al., 2015). During the past few years several studies have demonstrated the role of meningeal lymphatics in maintaining brain homeostasis, by clearing fluids, macromolecules and immune cells from the cerebrospinal and interstitial fluids, into the cervical nodes (Ma et al., 2017; Da Mesquita et al., 2018b; Louveau et al., 2018; Ahn et al., 2019). The discovery that this drainage function appears to decrease in aged mice, has prompted research into the putative role of lymphatics in neurodegenerative disorders (Ma et al., 2017; Da Mesquita et al., 2018b; Ahn et al., 2019; Wang et al., 2019; Zou et al., 2019). Hence, regulating the meningeal lymphatics function should be further studied as a therapeutic approach to delay the initiation or development of several neurological pathologies.

Interestingly, a population of isolated, non-lumenized LECs, expressing all the LEC hallmarks was recently identified in the zebrafish brain (Bower et al., 2017; Galanternik et al., 2017; van Lessen et al., 2017). Anatomically, these perivascular LECs were shown to sprout from the choroidal vascular plexus and to cover most of the adult brain (Galanternik et al., 2017; van Lessen et al., 2017). Similar to perivascular macrophages, Mato cells (Mato et al., 1984) or brain perivascular fluorescent granular perithelial cells (FGPs), this population of perivascular mural LECs (muLECs) display high endocytic and phagocytic capabilities (Bower et al., 2017; Galanternik et al., 2017; van Lessen et al., 2017). In addition, it has been proposed that these muLECs might promote or support vessel formation by secreting angiogenic and lymphagiogenic growth factors during embryonic development (Bower et al., 2017) and vascular regeneration (Chen et al., 2019). As reported by Chen et al. (2019), muLECs

could penetrate into the brain parenchyma upon cerebrovascular damage in order to resolve edema and guide the formation of new vessels into the injured tissue. Aside from muLECs, which are detected throughout the brain, proper meningeal lymphatics were also detected in *larvae* and adult zebrafish. *Mrc1*+ meningeal vessels were shown to originate via sprouting of the facial lymphatics and were suggested to play a role in immune cell trafficking (Castranova et al., 2020).

The eye was as well thought to lack lymphatic vessels, until it was discovered that the Schlemm's canal – the vessel that regulates intraocular pressure via drainage of the aqueous humor from the eye chamber –, develops as a hybrid blood and lymphatic structure, through "canalogenesis." This process initiates with the sprouting of ECs from the limbal vascular plexus and the radial vessels, into the corneal intermediate zone, and continues with the clustering of tip cells from the aforementioned blood vessels in the limbus, and assembly of a primordial chain of cells. The developing structure further extends and matures to form a lumenized vessel with distinct properties in its external and internal walls (Kizhatil et al., 2014). Although the Schlemm's canal derives from blood ECs and expresses most of the common blood EC markers, it is considered an hybrid vessel, as the cells in the inner wall express *Prox1* and VEGFR3 although at lower levels than regular lymphatics (Kizhatil et al., 2014; Truong et al., 2014). Another specialized hybrid structure can be found in the ascending vasa recta in the kidney medulla, a structure devoid of *bona fide* lymphatics. The ascending vasa recta (AVS) is a fenestrated vessel that exhibits both lymphatic and blood venous features and is essential for proper fluid drainage. Lineage tracing experiments revealed that ASV as most of the renal microvasculature derived from *Tie2*-expressing cells (Kenig-Kozlovsky et al., 2018).

Besides organ-specific lymphatics, recent lineage-tracing experiments in mice using the dermomyotome *Pax3* and *Myf5* and the SHF *Mef2c* specific drivers revealed that lymphatic progenitors can be traced back to the paraxial mesoderm, suggesting a common origin shared between LECs and the skeletal muscle lineage (Stone and Stainier, 2019). Analysis of *Pax3*-Cre+ cells showed that PROX1-expressing LEC precursors were present in the dorso- lateral wall of the mouse CV, and subsequently in the jugular lymph sacs. Additionally, *Pax3*+ cells gave rise to lymphatics in the skin, the liver and the cardiopulmonary system. In similar fashion, *Myf5*+ muscle progenitors were shown to contribute to the formation of meningeal and lymphatic capillaries in the ear skin, and *Mef2c*+ cells were found in the jugular lymph sacs, heart and skin lymphatics (Stone and Stainier, 2019).

As a whole, work in the recent years has begun to shed light on the heterogeneous origins of organ-specific lymphatics. Yet, it is important to keep in mind that while lineage tracing approaches have been instrumental for identifying novel progenitor populations and establishing lineage relationships within cell progeny/populations (Das and Yaniv, 2020), this technique harbors also intrinsic technical limitations. Unspecific or leaky drivers might erroneously label undesired populations, whereas the absence of specific labeling in certain cells can derive from an inefficient driver, all of these leading to potential misinterpretation of the results (reviewed in Semo et al., 2016). These limitations become especially relevant when coming to analyze the potential contribution of venous/endothelial vs. non-endothelial cells to the formation of tumor-associated lymphatic vessels.

FORMATION OF CANCER-ASSOCIATED LYMPHATICS

As part of the tumor microenvironment, the endothelial cells maintain a coordinated crosstalk with the tumor cells. As the diffusion of oxygen within the tissue decreases (Thomlinson and Gray, 1955; Goldacre and Sylvén, 1962); the tumor cells secrete growth factors that induce the formation of new vessels, allowing them to obtain the nutrients and oxygen required for their survival (Lugano et al., 2020). Since the initial observations of the tumor vasculature in the early 1900s, it was quite clear that the tumor-associated vasculature forms a heterogeneous network (Borst, 1902; Goldmann, 1908; De Palma et al., 2017). Tumor ECs exhibit significant morphological and functional differences when compared to their normal counterparts (Croix, 2000). In addition, they harbor cytogenetic alterations (Hida et al., 2004) and high cell turnover (Hobson and Denekamp, 1984). Nowadays it is widely accepted that the tumor vasculature is organized in a non-hierarchical manner and consists of leaky vessels (Hashizume et al., 2000; Morikawa et al., 2002) with irregular patterning and flow (Jain, 1988).

Once the solid tumor becomes vascularized, there is a rapid switch from a dormant to a malignant state that promotes further growth and tissue dissemination (Lugano et al., 2020). In addition to blood ECs, lymphatic vessels are also present in the tumor microenvironment, and are considered to play an active role in primary tumor progression, metastatic spread and immunomodulation (Stacker et al., 2014; Garnier et al., 2019; Oliver et al., 2020; Petrova and Koh, 2020; Vaahtomeri and Alitalo, 2020). On the one hand, tumor-associated lymphatics uptake the interstitial fluid containing cells and macromolecules of tumor mass origin, and drain them to the sentinel lymph node. The lymphatic vessels thus act as a circulation conduit for the tumor cells to escape the primary site and facilitate cell dissemination to distal organs. Accordingly, lymphatic tumor coverage correlate with poor patient prognosis (Dadras et al., 2003; Pasquali et al., 2013; Stacker et al., 2014; Wilczak et al., 2018). On the other hand, lymphatic vessels carry the antigens and antigen-presenting cells from the periphery to the lymph nodes to initiate the anti-tumor immunity and activate T cell response. LECs were shown to recruit dendritic cells via CCL21-CCR7 signaling, that migrate to present specific tumor antigens to the T cells in the lymph nodes. Therefore, dysfunctional lymphatics hamper a proper immune activation and response (Garnier et al., 2019).

The tumor and tumor microenvironment cells secrete a plethora of lymphangiogenic growth factors that promote lymphatic vessel formation (Vaahtomeri et al., 2017). Among them, the secretion of VEGF-C and VEGF-D stimulate the formation, proliferation and sprouting of LECs

(Joukov et al., 1996; Jeltsch, 1997; Veikkola et al., 2001; Hirakawa et al., 2007) attracting them into the peri- and intra-tumoral areas. The newly formed lymphatics are detected within the tumor mass and in its periphery in close contact with the tumor stroma. While, intratumoral lymphatics are for the most part not functional due to pressure collapse (Leu et al., 2000; Padera, 2002), the peritumoral ones are functional, but appear inflamed and dilated (Leu et al., 2000; Skobe et al., 2001a; Isaka et al., 2004). The formation of lymphatic vessels is not restricted to the primary tumor since the sentinel draining lymph node also forms new lymphatic vessels in preparation of the metastatic niche (Hirakawa et al., 2005, 2007; Stacker et al., 2014).

The active VEGF-C/VEGF-D/VEGFR3 signaling leads to increased lymphatic vessel permeability and intratumoral pressure, thereby augmenting the outflow toward the lymph node and facilitating the intravasation of cancer cells. It is though that the increased drainage activity of the interstitial fluid toward the lymphatic vasculature and lymph nodes significantly contributes to the lymphatic metastatic spread. Indeed, VEGF-C, VEGF-D and VEGFR3 levels are correlated with an increased incidence of lymph node and distal metastasis (Skobe et al., 2001a,b; Stacker et al., 2001; He et al., 2005; Hoshida et al., 2006; Hirakawa et al., 2007; Su et al., 2006, 2007; Karnezis et al., 2012).

THE CELLULAR ORIGINS OF CANCER LYMPHATICS

In contrast to the wealth of information describing the formation of tumor-associated blood vessels, relatively little is known about the process of tumor-induced lymphangiogenesis. Especially, the cellular origins of newly formed lymphatic vessels have been a matter of active debate during the past decade. While early reports suggested that tumor lymphatic vessels derive solely from pre-existing lymphatics (He et al., 2004), other investigations proposed alternative origins for tumor-LECs (Religa et al., 2005; Zumsteg et al., 2009). One of the first studies addressing this question made use of GFP-tagged bone marrow (BM) cell transplantation into mice bearing Lewis lung carcinoma (LLC) or B16 melanoma subcutaneous tumors. Assessment of the newly formed lymphatics surrounding the tumors revealed that although GFP+ cells were found in close proximity to the vessels, no double GFP+ (BM-derived cells, BMDCs) and LYVE1+ LECs were detected, suggesting that peritumoral lymphatics arise primarily from pre-existing vessels, with very little, if any, BDMC contribution (He et al., 2004). In contrast, the BM-derived GFP+ cells were markedly detected in the vicinity of new lymphatic vessels after tumor implantation, suggesting a potential role in neo-lymphangiogenesis through paracrine effects on existing lymphatic vessels. In addition, He et al. (2005) demonstrated that implantation of human LNM35 lung cancer cells expressing high levels of VEGF-C, robustly induced lymphatic sprouting from LYVE1+ vessels in an ear model, further supporting a lymphatic vessel origin for newly formed lymphatic capillaries.

In contrast to these results, other studies have shown integration of certain types of BMDCs into lymphatic vessels during pathological conditions, including tumor-induced lymphangiogenesis (reviewed by Park et al., 2011; Ran and Volk-Draper, 2020). Religa et al. (2005) for instance, showed that circulating BDMCs generate lymphatic vessels *in vivo* in GFP+ BM transplanted mice. In this study, GFP+;LYVE1+ cells were found in the cornea and in the enveloping lymphatics of T241 tumors, suggesting that circulating BM progenitors can indeed be incorporated into new lymphatic vessels (Religa et al., 2005). These progenitor cells were described to incorporate into LECs from many tissues and remain for rather long periods of time, although it was shown that they only comprise a minimum portion of the vasculature in both normal and tumor-associated vasculature (Jiang et al., 2008).

Similarly, a small cluster (∼8%) of cultured BM-derived mononucleated cells that upregulated PDPN expression, was shown to incorporate into lymphatic vessels of the cornea, skin, ear wounds and tumors, following B16-F1 melanoma injection. In addition, this population of PDPN+ lymphatic endothelial progenitors, was significantly enlarged in the bone marrow and peripheral blood of mice harboring tumors, suggesting that these cells could be activated and mobilized during tumorigenesis (Lee et al., 2010).

While these and other early studies (Maruyama et al., 2005; Jiang et al., 2008; Attout et al., 2009; Yamashita et al., 2009; Hall et al., 2012; Ran and Montgomery, 2012) supported the putative contribution of hematopoietic stem cells (HSCs) to neo-lymphangiogenesis in pathological settings; it is important to bear in mind that the expression of PROX1 in the integrated cells was not analyzed, and that the LEC phenotype was confirmed based only on the expression of markers such as PDPN, LYVE1, and VEGFR3, which are expressed by both LECs and hematopoietic cells including monocytes and macrophages.

Additional reports, focusing specifically on the contribution of BMDCs of the myeloid lineage to tumor lymphangiogenesis, examined also PROX1 expression (Zumsteg et al., 2009; Volk-Draper et al., 2017, 2019). Zumsteg et al. (2009) made use of BM transfer in combination with genetic lineage tracing, to investigate the integration of myeloid cells into tumor lymphatic vessels, in both the genetic Rip1Tag2 model of pancreatic cancer, and TRAMP-C1 prostate cancer transplanted animals. Analysis of the presence of GFP+ BMDCs in the vasculature of these two mouse models revealed a minor contribution of BMDCs to the tumor lymphatic network. Interestingly, only ∼3% of the GFP+ cells co-expressed the macrophage marker F4/80 along with PROX1, LYVE1 and PDPN, suggesting the possible differentiation of macrophages toward a LEC fate. However, since not all of the integrated BMDCs expressed F4/80, this suggested mechanism remained inconclusive. The cell transplantation results were further supported by lineage tracing experiments using the CD11b reporter mice. In this case, labeled cells were found to integrate into lymphatic vessels of subcutaneously transplanted TRAMP-C1 tumors, and to co-express LYVE1 and PROX1 (Zumsteg et al., 2009).

Recently, it has been proposed that the myeloid-to-lymphatic transition could be regulated via the Toll-Like Receptor 4 (TLR4). Treatment of primary CD14+ human monocytes and CD11b+ mouse myeloid cells, with the TLR4-ligands LPS, HMGB1 and nab-PXL, triggered the upregulation of *VEGFR3*, *LYVE1* and

PDPN transcripts, shifting the cells to a LEC-like phenotype. Furthermore, *in vitro* TLR4- reprogrammed myeloid lymphatic endothelial cell progenitors (M-LECPs), generated functional cells that integrated into LYVE1+ tumor lymphatics in murine breast cancer models (Volk-Draper et al., 2017). A follow-up study suggested that the tumors might boost the release of myeloid precursors, since CD14+ monocytes expressing LEC specific markers were abundant, albeit being nearly absent in healthy donors. In addition, M-LECPs expressing high levels of *LYVE1, PDPN, PROX1* and *VEGFR3* were uniquely detected in the lymph vessels of breast cancer tissue and their density correlated with the development of lymphatic metastasis in breast cancer patients (Volk-Draper et al., 2019).

Contrasting results regarding the contribution of the myeloid lineage to tumor lymphatics were obtained using a *LysM:Cre* lineage tracing approach (Gordon et al., 2010). According to this study, while lineage-labeled cells integrated within tumor-related lymphatic vessels following subcutaneous implantation of either LLC or EL4 lymphoma cells, they did not express PROX1, thus arguing against a possible mechanism of differentiation of macrophages to LECs. The discrepancy between the various studies could stem from the use of different promoters driving Cre activation. Alternatively, it is possible that distinct cytokine profiles of the tumor models utilize, induce recruitment and/or differentiation of specific myeloid subpopulations into LECs.

Inflammation also takes place during tumor growth and progression. In this regard, formation of lymphatics vessels from BMDCs has also been described in inflammation models (Maruyama et al., 2005; Kerjaschki et al., 2006; Lee et al., 2010; Hos and Cursiefen, 2014). Maruyama et al. (2005) for instance, identified double positive CD11b+/LYVE1+ and CD11b+/PROX1+ cell patches in the lymphatic neo-vasculature, 3 days after corneal transplantation. These results suggested that CD11b+ macrophages, most likely originating in the bone marrow, were the source of LECs in the inflamed mouse cornea. Moreover, the formation of LECs was suppressed upon systemic depletion of macrophages by clodronate liposomes treatment, further supporting these results (Maruyama et al., 2005). Similar findings were obtained in a study analyzing human gender-mismatched transplanted kidneys. There, the rejected kidneys incorporated host-derived macrophages that differentiated into LECs, further supporting the idea that specific lymphatic endothelial precursor cells, most probably of the macrophage lineage, intervene in the formation of new lymphatics (Kerjaschki et al., 2006).

Overall, the mechanisms regulating the formation of tumor-associated lymphatics and, in particular, the putative contribution from non-endothelial and bone marrow-derived cells, still remain controversial (**Figure 1C**). Especially, the observed differences in the precursor type, their ability to be mobilized and incorporated into lymphatic vessels and whether a defined LEC fate is ultimately acquired, varies significantly among the different studies. It is important to bear in mind that there are many variables in the tumor models, starting from the tumor type, their aggressiveness and localization and their metastatic potential. Moreover, there are differences within the mouse models utilized, including genetic background, preconditions, treatments, etc. Since different cell types have been described to give rise to organ-specific lymphatic vessels during embryonic development, it would be interesting to investigate for instance, whether BMDCs are differentially activated in tumors of different organs.

Another question that remains open is the potential mechanism by which circulating cells integrate into lymphatic vessels. The contribution of HSCs and myeloid cells to tumor lymphangiogenesis was typically inspected several weeks after bone marrow transplantation or adoptive transfer of particular populations, thus precluding the understanding of cell differentiation and recruitment events that may occur at early stages of the process. Consequently, it remains to be determined whether the naïve stem-like cells or myeloid cells, which were shown to contribute to lymphatic vessels (Jiang et al., 2008; Zumsteg et al., 2009; Lee et al., 2010), integrate directly into the growing lymphatics and acquire an LEC phenotype only at later stages, or contribute to lymphangiogenesis as fully differentiated LECs, through a process of lymph-vasculogenesis. Finally, an alternative scenario for lymphatic vessel formation is that clusters of vascular progenitors that are spread along the tumor tissue differentiate *in situ* into LECs and contribute to lymphatic vessel growth without prior integration into the blood vasculature, as has been shown during the formation of mesenteric lymphatic vessels in developing mouse embryos (Stanczuk et al., 2015). While there is yet no evidence supporting this model, it is possible that such events are restricted to early stages of tumor lymphangiogenesis that are rather overlooked in studies on non-EC contribution to lymphatic vessels. Intravital imaging of mice carrying both blood and lymphatic EC reporters at high spatiotemporal resolution may reveal the sequence of events and cellular transitions leading to the formation of the tumor-associated lymphatic network.

Finally, the functional relevance of non-endothelial cell contribution to tumor lymphangiogenesis, and its role on tumor progression and metastatic spread remains unclear. Lee et al. (2010) could show that implantation of bone marrow derived PDPN+ cells in the periphery of melanoma tumors in mice led to an increase in the density of VEGFR3+ vessels in the peritumoral tissues. Similarly, bone marrow derived GFP+/CD11+/PDPN+ cells injected into mice bearing EMT6 orthotopic breast carcinomas, augmented as well lymphatic vessel density (Volk-Draper et al., 2017). In a different study, Volk-Draper et al. (2019) showed that *in vitro* TLR4-mediated differentiated M-LECP inoculated in different breast cancer mice models were able to increase LYVE1+ lymphatic density, thereby resulting in a substantial increment in lymphatic metastasis. Moreover, other studies have reported the effect of blocking of myeloid cells in tumor lymphatic vasculature. Inhibition of bone marrow myeloid cell recruitment abolished M-LECPs integration into the lymphatic vessels and reduced tumor lymphatic vessel density (Volk-Draper et al., 2019). Systemic depletion of macrophages in an orthotopic urinary bladder cancer (OUBC) model also caused a decrease in tumor LYVE1+ lymphatic vessel density (Yang et al., 2011).

To conclude, a growing body of literature has examined the potential contribution of different cell types to cancer-associated lymphatics. Nevertheless, several important questions remain

unanswered. For instance, the specific functions that lymphatics play at different stages of tumor progression and the molecular changes LECs may undergo between the pre-metastatic and metastatic states, as well as during therapy require further investigation. Understanding the molecular differences in LECs would undoubtedly help to design novel drugs to selectively block or activate different lymphatic subsets. Finally, further studies will need to be performed to establish the use of lymphatics density or specific lymphatic markers as prognostic markers for segregation of patients for several tumors.

THERAPIES TARGETING THE LYMPHATIC VASCULATURE: IMPLICATIONS FOR CANCER TREATMENT

The potential benefits of anti-lymphangiogenic therapies for cancer treatment have been demonstrated in several pre-clinical cancer models, where blocking of VEGF-C and VEGF-D led to dramatic reduction in lymphatic vessel growth and metastasis formation (reviewed in Zheng et al., 2014). Moreover, several clinical studies targeting tyrosine kinase receptors including VEGFR1-3, FGFR, Tie2, C-MET and PDGFR-beta, that block both angiogenesis and lymphangiogenesis, reported increased survival of tumor bearing mice and human patients following treatment (reviewed in Duong et al., 2012; Dieterich and Detmar, 2016; Yamakawa et al., 2018).

During the past two decades several attempts have been made to block the VEGF-C/VEGFR3 axis at different levels of the signaling cascade. One way is designed to inhibit the VEGF-C/VEGFR3 axis by trapping the available VEGFR3 ligands- VEGF-C and VEGF-D-, before their interaction with the receptor. Several studies have pursued this option by generating soluble forms of VEGFR3 that can act as decoy receptors. For instance, tumor cells expressing soluble VEGFR3-Ig reduced tumor lymphatic formation and lymph node metastasis in mice (He et al., 2002) and rats (Krishnan et al., 2003). Moreover, soluble VEGFR3Ig suppressed both tumor size and tumor-associated lymphatic vessels in VEGF-C expressing tumors (Karpanen et al., 2001) and intravascular administration of soluble AdVEGFR3 IgG in mouse xenotransplants, inhibited also the formation of lymph node macrometastasis (He et al., 2005).

Another way to impede ligand-receptor interactions takes advantage of specific blocking antibodies. One such example is a monoclonal antibody neutralizing VEGF-D, which efficiently blocked lymph node metastasis in mice (Achen et al., 2000; Stacker et al., 2001). Similarly, systemic treatment with anti-VEGF3 antibodies specifically inhibited lymphangiogenesis and reduced lymphatic metastasis (Shimizu et al., 2004; Roberts et al., 2006). Ligand–receptor interactions were also blocked by VEGFR3 monoclonal antibodies (Persaud, 2004). This approach was shown to affect tumor growth and tumor angiogenesis (Kubo et al., 2000; Laakkonen et al., 2007; Tammela et al., 2008) and reduce intratumoral lymphatic formation (Laakkonen et al., 2007) in mouse xenograft models. In contrast, monotherapy using a humanized monoclonal anti-VEGFR3 (LY3022856) in phase 1 clinical trials, revealed no significant anti-tumor effect (Saif et al., 2016).

Finally, the VEGFR3 axis can be neutralized by preventing its downstream signaling. Tyrosine kinase inhibitors (TKIs) have been widely developed as downstream signaling blockers (reviewed by Tan et al., 2018; Qin et al., 2019). These small chemicals are extensively used for clinical and experimental purposes albeit being promiscuous since they block a variety of other kinases. Some of the current FDA-approved multi-kinase inhibitors are: Sorafenib (Ranieri et al., 2012), Sunitinib (Le Tourneau et al., 2007), Pazopanib (Harris et al., 2008), Axitinib, Regorafenib, Cabozantinib, Nintedanib, and Lenvatinib (Qin et al., 2019). Strikingly, the use of Sunitinib induced *Vegfc* expression and promoted lymphangiogenesis *in vivo*. Moreover, renal cell carcinoma patients treated with Sunitinib developed more lymph node metastasis in comparison with patients treated with other therapies (Dufies et al., 2017). Thus, TKIs specifically aimed at preventing lymphatic signaling are yet to be designed. Recently, SAR131675 – a novel VEGFR3-specific TKI – has shown promising results in the modulation of tumor and metastasis growth, by decreasing lymphatic vessel formation and macrophage infiltration *in vivo* in murine tumor and inflammation models (Alam et al., 2012; Hwang et al., 2019). To date, however, no VEGFR3-specific inhibitors have shown potential benefits for human use.

One question that remains open is whether manipulation of VEGF-C/VEGF-D targets only sprouting from pre-existing lymphatics, or affects also non-endothelial cells. The mechanisms underlying lymphatic differentiation from BMDCs and/or alternative progenitors, if any, are still poorly defined and may prove substantially different from that of ECs. Further characterization of the molecular pathways leading to lymphatic specification and integration of non-ECs into lymphatic vessels may provide alternative targets for the inhibition of tumor-induced lymphangiogenesis.

In addition to blocking the VEGF-C/VEGFR3 axis, the identified roles of the WNT and BMP pathways in LEC specification, may provide novel therapeutic opportunities. Notably, *Wnt5a* expression in gastric cancer was found to highly correlate with lymph node metastasis (Kurayoshi et al., 2006). While the proposed mechanism involved direct effects of WNT5A on tumor cell migration (Liu et al., 2013), it is possible that WNT5A acts also as a pro-lymphangiogenic factor in this setting, thereby increasing the incidence of lymph node metastasis. In similar fashion, COUP-TFII has also been associated with increased malignancy, lymph node metastasis, and poor prognosis. High levels of COUP-TFII expression were reported to correlate with aggressive behavior in patients with breast, pancreatic, and colon cancer (Qin et al., 2014), underscoring the potential benefits of blocking this nuclear receptor for cancer treatment. An alternative strategy for targeting lymphangiogenesis could be the use of agonists of BMP signaling, which is known to block this process in the developing embryo (Levet et al., 2013; Yoshimatsu et al., 2013; Dunworth et al., 2014; Jun-Dae and Jongmin, 2014; Cha et al., 2016). Recently, DNA decoys targeting the SOX-HMG family of

transcription factors were shown to inhibit Sox18 activity and to block SOX18 interaction with *PROX1* DNA (Klaus et al., 2016), thereby presenting a unique alternative to target an otherwise undruggable protein.

The above-described treatments are mostly designed to disrupt the tumor-associated lymphatic vasculature in order to block tumor dissemination. Instead, new approaches focus on the idea of making lymphatic vessels more functional, with the ultimate goal of improving the anti-tumoral immune response, as well as immunotherapy delivery (Lund et al., 2016; Fankhauser et al., 2017; Song et al., 2020). In their study, Lund et al. (2016) showed that B16F10 melanoma tumors implanted in mice devoid of skin lymphatics, displayed reduced immune cell infiltration and inflammatory cytokines, suggesting that regional lymphatics are necessary for proper antitumoral and inflammatory response. *Chy* mice with defective lymphangiogenesis also mirrored the reduced immune cell recruitment phenotype in breast tumors. Interestingly, the expression of the lymphatic markers *LYVE1* and *PDPN* correlated as well with the immune response in a cohort of human metastatic cutaneous melanoma samples (Lund et al., 2016). In similar fashion, Fankhauser et al. (2017) showed that inhibition of lymphangiogenesis in a mouse melanoma model inhibited T cell recruitment and blocked the subsequent immune response. Moreover, they could confirm that *VEGFC* levels correlate with immunotherapy response in human patients (Fankhauser et al., 2017). Finally, both lymphatic vessel density and VEGF-C levels correlated also with the infiltration of CD8+ T cells in human primary melanoma and lymph node metastasis (Bordry et al., 2018).

The "re-discovery" of meningeal lymphatics, opens up new therapeutic opportunities for the treatment of rather inaccessible brain tumors. Recently, a new study has described that lymphatic-mediated immune functions in the brain were instrumental to enable a proper immune response against glioblastoma. Ectopic expression of VEGF-C agents increased CD8+ T cell drainage to the cervical lymph nodes, improving immune cell infiltration into the tumor mass. Furthermore, VEGF-C expression in combination with immunotherapy promoted tumor cell elimination and increased survival (Song et al., 2020). Finally, since immune cell infiltration density in tumors can serve as a predictive marker (Mlecnik et al., 2016), it would be interesting to investigate the correlation between tumor lymphatic formation and the potential success of immunotherapy. Altogether, these new lines of investigation present the lymphatics not as passive routes for metastatic cells toward the lymph nodes but rather as active players in the generation of anti-tumoral response.

FUTURE PROSPECTS AND CONCLUSION

The origin of lymphatic vessels in development and cancer has been a subject of intense debate. The proposed contribution of different endothelial and non-endothelial cells to pathological lymphangiogenesis indicates the great complexity underlying the initial stages of lymphatic vessel formation in tumors. Understanding the molecular mechanisms that induce LEC specification in different cell populations contributing to tumor-related lymphatic vessels, as well as those that propel growth and remodeling of pre-existing vessels, will most likely improve our ability to abrogate tumor lymphangiogenesis and promote the treatment of patients with metastatic disease.

AUTHOR CONTRIBUTIONS

KY and LG-M wrote, reviewed, and edited the manuscript. Both authors contributed to the article and approved the submitted version.

FUNDING

This work was supported in part by European Research Council (818858) to KY, Binational Science Foundation (2015289) to KY, Minerva Foundation (712610) to KY, the H&M Kimmel Institute for Stem Cell Research, and the Estate of Emile Mimran (SABRA program). KY is the incumbent of the Enid Barden and Aaron J. Jade Professorial Chair.

ACKNOWLEDGMENTS

We are grateful to all members of the Yaniv laboratory for many fruitful discussions and the Graphic design team at the Weizmann Institute of Science. We sincerely apologize to those of our colleagues whose important work could not be cited due to space limitations.

REFERENCES

Achen, M. G., Jeltsch, M., Kukk, E., Makinen, T., Vitali, A., Wilks, A. F., et al. (1998). Vascular endothelial growth factor D (VEGF-D) is a ligand for the tyrosine kinases VEGF receptor 2 (Flk1) and VEGF receptor 3 (Flt4). *Proc. Natl. Acad. Sci. U.S.A.* 95, 548–553. doi: 10.1073/pnas.95.2.548

Achen, M. G., Roufail, S., Domagala, T., Catimel, B., Nice, E. C., Geleick, D. M., et al. (2000). Monoclonal antibodies to vascular endothelial growth factor-D block its interactions with both VEGF receptor-2 and VEGF receptor-3. *Eur. J. Biochem.* 267, 2505–2515. doi: 10.1046/j.1432-1327.2000.01257.x

Ahn, J. H., Cho, H., Kim, J.-H., Kim, S. H., Ham, J.-S., Park, I., et al. (2019). Meningeal lymphatic vessels at the skull base drain cerebrospinal fluid. *Nature* 572, 62–66. doi: 10.1038/s41586-019-1419-5

Alam, A., Blanc, I., Gueguen-Dorbes, G., Duclos, O., Bonnin, J., Barron, P., et al. (2012). SAR131675, a Potent and Selective VEGFR-3-TK inhibitor with antilymphangiogenic, antitumoral, and antimetastatic activities. *Mol. Cancer Ther.* 11, 1637–1649. doi: 10.1158/1535-7163.MCT-11-0866-T

Alders, M., Hogan, B. M., Gjini, E., Salehi, F., Al-Gazali, L., Hennekam, E. A., et al. (2009). Mutations in CCBE1 cause generalized lymph vessel dysplasia in humans. *Nat. Genet.* 41, 1272–1274. doi: 10.1038/ng.484

Alitalo, K., and Carmeliet, P. (2002). Molecular mechanisms of lymphangiogenesis in health and disease. *Cancer Cell* 1, 219–227. doi: 10.1016/S1535-6108(02)00051-X

Aspelund, A., Antila, S., Proulx, S. T., Karlsen, T. V., Karaman, S., Detmar, M., et al. (2015). A dural lymphatic vascular system that drains brain interstitial fluid and macromolecules. *J. Exp. Med.* 212, 991–999. doi: 10.1084/jem.20142290

Attout, T., Hoerauf, A., Dénécé, G., Debrah, A. Y., Marfo-Debrekyei, Y., Boussinesq, M., et al. (2009). Lymphatic vascularisation and involvement of Lyve-1+ macrophages in the human onchocerca nodule. *PLoS One* 4:e8234. doi: 10.1371/journal.pone.0008234

Azhar, S. H., Lim, H. Y., Tan, B.-K., and Angeli, V. (2020). The unresolved pathophysiology of lymphedema. *Front. Physiol.* 11:137. doi: 10.3389/fphys.2020.00137

Balboa-Beltran, E., Fernández-Seara, M. J., Pérez-Muñuzuri, A., Lago, R., García-Magán, C., Couce, M. L., et al. (2014). A novel stop mutation in the vascular endothelial growth factor-C gene (VEGFC) results in Milroy-like disease. *J. Med. Genet.* 51, 475–478. doi: 10.1136/jmedgenet-2013-102020

Baluk, P., Fuxe, J., Hashizume, H., Romano, T., Lashnits, E., Butz, S., et al. (2007). Functionally specialized junctions between endothelial cells of lymphatic vessels. *J. Exp. Med.* 204, 2349–2362. doi: 10.1084/jem.20062596

Banerji, S., Ni, J., Wang, S.-X., Clasper, S., Su, J., Tammi, R., et al. (1999). LYVE-1, a new homologue of the CD44 glycoprotein, is a lymph-specific receptor for hyaluronan. *J. Cell Biol.* 144, 789–801. doi: 10.1083/jcb.144.4.789

Bernal, A., and Arranz, L. (2018). Nestin-expressing progenitor cells: function, identity and therapeutic implications. *Cell. Mol. Life Sci.* 75, 2177–2195. doi: 10.1007/s00018-018-2794-z

Bordry, N., Broggi, M. A. S., de Jonge, K., Schaeuble, K., Gannon, P. O., Foukas, P. G., et al. (2018). Lymphatic vessel density is associated with CD8 + T cell infiltration and immunosuppressive factors in human melanoma. *OncoImmunology* 7:e1462878. doi: 10.1080/2162402X.2018.1462878

Borst, M. (1902). *Die Lehre von den Geschwülsten mit einem Mikroskopischen Atlas. Erster Band [On tumors, with a microsopic atlas. Volume One]*. Wiesbaden: Harvard University.

Bos, F. L., Caunt, M., Peterson-Maduro, J., Planas-Paz, L., Kowalski, J., Karpanen, T., et al. (2011). CCBE1 is essential for mammalian lymphatic vascular development and enhances the lymphangiogenic effect of vascular endothelial growth Factor-C in vivo. *Circ. Res.* 109, 486–491. doi: 10.1161/CIRCRESAHA.111.250738

Bower, N. I., Koltowska, K., Pichol-Thievend, C., Virshup, I., Paterson, S., Lagendijk, A. K., et al. (2017). Mural lymphatic endothelial cells regulate meningeal angiogenesis in the zebrafish. *Nat. Neurosci.* 20, 774–783. doi: 10.1038/nn.4558

Breiteneder-Geleff, S., Soleiman, A., Kowalski, H., Horvat, R., Amann, G., Kriehuber, E., et al. (1999). Angiosarcomas express mixed endothelial phenotypes of blood and lymphatic capillaries. *Am. J. Pathol.* 154, 385–394. doi: 10.1016/S0002-9440(10)65285-6

Brice, G. (2005). Milroy disease and the VEGFR-3 mutation phenotype. *J. Med. Genet.* 42, 98–102. doi: 10.1136/jmg.2004.024802

Brouillard, P., Boon, L., and Vikkula, M. (2014). Genetics of lymphatic anomalies. *J. Clin. Invest.* 124, 898–904. doi: 10.1172/JCI71614

Buckingham, M. (2016). "First and second heart field," in *Congenital Heart Diseases: The Broken Heart*, eds S. Rickert-Sperling, R. G. Kelly, and D. J. Driscoll (Vienna: Springer), 25–40. doi: 10.1007/978-3-7091-1883-2_3

Bui, H. M., Enis, D., Robciuc, M. R., Nurmi, H. J., Cohen, J., Chen, M., et al. (2016). Proteolytic activation defines distinct lymphangiogenic mechanisms for VEGFC and VEGFD. *J. Clin. Invest.* 126, 2167–2180. doi: 10.1172/JCI83967

Butler, M. G., Dagenais, S. L., Rockson, S. G., and Glover, T. W. (2007). A novelVEGFR3 mutation causes Milroy disease. *Am. J. Med. Genet. A* 143A, 1212–1217. doi: 10.1002/ajmg.a.31703

Castranova, D., Samasa, B., Galanternik, M. V., Jung, H. M., Pham, V. N., and Weinstein, B. M. (2020). Live imaging of intracranial lymphatics in the Zebrafish (preprint). *Dev. Biol.* doi: 10.1101/2020.05.13.094581

Cha, B., Geng, X., Mahamud, R., Fu, J., Mukherjee, A., Kim, Y., et al. (2016). Mechanotransduction activates canonical Wnt/β-catenin signaling to promote lymphatic vascular patterning and the development of lymphatic and lymphovenous valves. *Genes Dev.* 30, 1454–1469. doi: 10.1101/gad.282400.116

Chen, J., He, J., Ni, R., Yang, Q., Zhang, Y., and Luo, L. (2019). Cerebrovascular injuries induce lymphatic invasion into brain parenchyma to guide vascular regeneration in Zebrafish. *Dev. Cell* 49, 697.e5–710.e5. doi: 10.1016/j.devcel.2019.03.022

Connell, F., Ostergaard, P., Brice, G., Homfray, T., Roberts, L., Bunyan, D. J., et al. (2010). Linkage and sequence analysis indicate that CCBE1 is mutated in recessively inherited generalised lymphatic dysplasia. *Hum. Genet.* 127, 231–241. doi: 10.1007/s00439-009-0766-y

Croix, B., and St. (2000). Genes expressed in human tumor endothelium. *Science* 289, 1197–1202. doi: 10.1126/science.289.5482.1197

Da Mesquita, S., Fu, Z., and Kipnis, J. (2018a). The meningeal lymphatic system: a new player in neurophysiology. *Neuron* 100, 375–388. doi: 10.1016/j.neuron.2018.09.022

Da Mesquita, S., Louveau, A., Vaccari, A., Smirnov, I., Cornelison, R. C., Kingsmore, K. M., et al. (2018b). Functional aspects of meningeal lymphatics in ageing and Alzheimer's disease. *Nature* 560, 185–191. doi: 10.1038/s41586-018-0368-8

Dadras, S. S., Paul, T., Bertoncini, J., Brown, L. F., Muzikansky, A., Jackson, D. G., et al. (2003). Tumor lymphangiogenesis. *Am. J. Pathol.* 162, 1951–1960. doi: 10.1016/S0002-9440(10)64328-3

Dai, T., Li, B., He, B., Yan, L., Gu, L., Liu, X., et al. (2018). A novel mutation in the conserved sequence of vascular endothelial growth factor receptor 3 leads to primary lymphoedema. *J. Int. Med. Res.* 46, 3162–3171. doi: 10.1177/0300060518773264

Daniel-Spiegel, E., Ghalamkarpour, A., Spiegel, R., Weiner, E., Vikkula, M., Shalev, E., et al. (2005). Hydrops fetalis: an unusual prenatal presentation of hereditary congenital lymphedema. *Prenat. Diagn.* 25, 1015–1018. doi: 10.1002/pd.1237

Das, R. N., and Yaniv, K. (2020). Discovering new progenitor cell populations through lineage tracing and in vivo imaging. *Cold Spring Harb. Perspect. Biol.* a035618. doi: 10.1101/cshperspect.a035618

De Palma, M., Biziato, D., and Petrova, T. V. (2017). Microenvironmental regulation of tumour angiogenesis. *Nat. Rev. Cancer* 17, 457–474. doi: 10.1038/nrc.2017.51

Dieterich, L. C., and Detmar, M. (2016). Tumor lymphangiogenesis and new drug development. *Adv. Drug Deliv. Rev.* 99, 148–160. doi: 10.1016/j.addr.2015.12.011

Dufies, M., Giuliano, S., Ambrosetti, D., Claren, A., Ndiaye, P. D., Mastri, M., et al. (2017). Sunitinib stimulates expression of VEGFC by tumor cells and promotes lymphangiogenesis in clear cell renal cell carcinomas. *Cancer Res.* 77, 1212–1226. doi: 10.1158/0008-5472.CAN-16-3088

Dumont, D. J. (1998). Cardiovascular failure in mouse embryos deficient in VEGF Receptor-3. *Science* 282, 946–949. doi: 10.1126/science.282.5390.946

Dunworth, W. P., Cardona-Costa, J., Bozkulak, E. C., Kim, J.-D., Meadows, S., Fischer, J. C., et al. (2014). Bone morphogenetic Protein 2 signaling negatively modulates lymphatic development in vertebrate embryos. *Circ. Res.* 114, 56–66. doi: 10.1161/CIRCRESAHA.114.302452

Duong, T., Koopman, P., and Francois, M. (2012). Tumor lymphangiogenesis as a potential therapeutic target. *J. Oncol.* 2012, 1–23. doi: 10.1155/2012/204946

Eng, T. C., Chen, W., Okuda, K. S., Misa, J. P., Padberg, Y., Crosier, K. E., et al. (2019). Zebrafish facial lymphatics develop through sequential addition of venous and non-venous progenitors. *EMBO Rep.* 20:e47079. doi: 10.15252/embr.201847079

Evans, A. L. (2003). Identification of eight novel VEGFR-3 mutations in families with primary congenital lymphoedema. *J. Med. Genet.* 40, 697–703. doi: 10.1136/jmg.40.9.697

Fankhauser, M., Broggi, M. A. S., Potin, L., Bordry, N., Jeanbart, L., Lund, A. W., et al. (2017). Tumor lymphangiogenesis promotes T cell infiltration and potentiates immunotherapy in melanoma. *Sci. Transl. Med.* 9:eaal4712. doi: 10.1126/scitranslmed.aal4712

Fastré, E., Lanteigne, L.-E., Helaers, R., Giacalone, G., Revencu, N., Dionyssiou, D., et al. (2018). Splice-site mutations in VEGFC cause loss of function and Nonne-Milroy-like primary lymphedema. *Clin. Genet.* 94, 179–181. doi: 10.1111/cge.13204

Ferrell, R. (1998). Hereditary lymphedema: evidence for linkage and genetic heterogeneity. *Hum. Mol. Genet.* 7, 2073–2078. doi: 10.1093/hmg/7.13.2073

François, M., Caprini, A., Hosking, B., Orsenigo, F., Wilhelm, D., Browne, C., et al. (2008). Sox18 induces development of the lymphatic vasculature in mice. *Nature* 456, 643–647. doi: 10.1038/nature07391

Galanternik, M. V., Castranova, D., Gore, A. V., Blewett, N. H., Jung, H. M., Stratman, A. N., et al. (2017). A novel perivascular cell population in the zebrafish brain. *eLife* 6:e24369. doi: 10.7554/eLife.24369

Gancz, D., Perlmoter, G., and Yaniv, K. (2019a). Formation and growth of cardiac lymphatics during embryonic development, heart regeneration, and disease. *Cold Spring Harb. Perspect. Biol.* 12:a037176. doi: 10.1101/cshperspect.a037176

Gancz, D., Raftrey, B. C., Perlmoter, G., Marín-Juez, R., Semo, J., Matsuoka, R. L., et al. (2019b). Distinct origins and molecular mechanisms contribute to

lymphatic formation during cardiac growth and regeneration. *eLife* 8:e44153. doi: 10.7554/eLife.44153

Garnier, L., Gkountidi, A.-O., and Hugues, S. (2019). Tumor-associated lymphatic vessel features and immunomodulatory functions. *Front. Immunol.* 10:720. doi: 10.3389/fimmu.2019.00720

Ghalamkarpour, A., Holnthoner, W., Saharinen, P., Boon, L. M., Mulliken, J. B., Alitalo, K., et al. (2009). Recessive primary congenital lymphoedema caused by a VEGFR3 mutation. *J. Med. Genet.* 46, 399–404. doi: 10.1136/jmg.2008.064469

Ghalamkarpour, A., Morlot, S., Raas-Rothschild, A., Utkus, A., Mulliken, J., Boon, L., et al. (2006). Hereditary lymphedema type I associated with VEGFR3 mutation: the first de novo case and atypical presentations. *Clin. Genet.* 70, 330–335. doi: 10.1111/j.1399-0004.2006.00687.x

Goldacre, R. J., and Sylvén, B. (1962). On the access of blood-borne dyes to various tumour regions. *Br. J. Cancer* 16, 306–322. doi: 10.1038/bjc.1962.36

Goldmann, E. (1908). The growth of malignant disease in man and the lower animals, with special reference to the vascular system. *Proc. R. Soc. Med.* 1, 1–13. doi: 10.1177/003591570800101201

Gordon, E. J., Rao, S., Pollard, J. W., Nutt, S. L., Lang, R. A., and Harvey, N. L. (2010). Macrophages define dermal lymphatic vessel calibre during development by regulating lymphatic endothelial cell proliferation. *Development* 137, 3899–3910. doi: 10.1242/dev.050021

Gordon, K., Schulte, D., Brice, G., Simpson, M. A., Roukens, M. G., van Impel, A., et al. (2013). Mutation in vascular endothelial growth Factor-C, a ligand for vascular endothelial growth factor receptor-3, is associated with autosomal dominant milroy-like primary lymphedema. *Circ. Res.* 112, 956–960. doi: 10.1161/CIRCRESAHA.113.300350

Hägerling, R., Pollmann, C., Andreas, M., Schmidt, C., Nurmi, H., Adams, R. H., et al. (2013). A novel multistep mechanism for initial lymphangiogenesis in mouse embryos based on ultramicroscopy. *Embo J.* 32, 629–644. doi: 10.1038/emboj.2012.340

Hall, K. L., Volk-Draper, L. D., Flister, M. J., and Ran, S. (2012). New model of macrophage acquisition of the lymphatic endothelial phenotype. *PLoS One* 7:e31794. doi: 10.1371/journal.pone.0031794

Harris, P. A., Boloor, A., Cheung, M., Kumar, R., Crosby, R. M., Davis-Ward, R. G., et al. (2008). Discovery of 5-[[4-[(2,3-Dimethyl-2 H -indazol-6-yl)methylamino]-2-pyrimidinyl]amino]-2-methyl-benzenesulfonamide (Pazopanib), a novel and potent vascular endothelial growth factor receptor inhibitor †. *J. Med. Chem.* 51, 4632–4640. doi: 10.1021/jm800566m

Harrison, M. R., Feng, X., Mo, G., Aguayo, A., Villafuerte, J., Yoshida, T., et al. (2019). Late developing cardiac lymphatic vasculature supports adult zebrafish heart function and regeneration. *eLife* 8:e42762. doi: 10.7554/eLife.42762

Hashizume, H., Baluk, P., Morikawa, S., McLean, J. W., Thurston, G., Roberge, S., et al. (2000). Openings between defective endothelial cells explain tumor vessel leakiness. *Am. J. Pathol.* 156, 1363–1380. doi: 10.1016/S0002-9440(10)65006-7

He, Y., Kozaki, K.-I., Karpanen, T., Koshikawa, K., Yla-Herttuala, S., Takahashi, T., et al. (2002). Suppression of tumor lymphangiogenesis and lymph node metastasis by blocking vascular endothelial growth factor receptor 3 signaling. *JNCI J. Natl. Cancer Inst.* 94, 819–825. doi: 10.1093/jnci/94.11.819

He, Y., Rajantie, I., Ilmonen, M., Makinen, T., Karkkainen, M. J., Haiko, P., et al. (2004). Preexisting lymphatic endothelium but not endothelial progenitor cells are essential for tumor lymphangiogenesis and lymphatic metastasis. *Cancer Res.* 64, 3737–3740. doi: 10.1158/0008-5472.CAN-04-0088

He, Y., Rajantie, I., Pajusola, K., Jeltsch, M., Holopainen, T., Yla-Herttuala, S., et al. (2005). Vascular endothelial cell growth factor receptor 3–mediated activation of lymphatic endothelium is crucial for tumor cell entry and spread via lymphatic vessels. *Cancer Res.* 65, 4739–4746. doi: 10.1158/0008-5472.CAN-04-4576

Hen, G., Nicenboim, J., Mayseless, O., Asaf, L., Shin, M., Busolin, G., et al. (2015). Venous-derived angioblasts generate organ-specific vessels during zebrafish embryonic development. *Development* 142, 4266–4278. doi: 10.1242/dev.129247

Hida, K., Hida, Y., Amin, D. N., Flint, A. F., Panigrahy, D., Morton, C. C., et al. (2004). Tumor-associated endothelial cells with cytogenetic abnormalities. *Cancer Res.* 64, 8249–8255. doi: 10.1158/0008-5472.CAN-04-1567

Hirakawa, S., Brown, L. F., Kodama, S., Paavonen, K., Alitalo, K., and Detmar, M. (2007). VEGF-C–induced lymphangiogenesis in sentinel lymph nodes promotes tumor metastasis to distant sites. *Blood* 109, 1010–1017. doi: 10.1182/blood-2006-05-021758

Hirakawa, S., Kodama, S., Kunstfeld, R., Kajiya, K., Brown, L. F., and Detmar, M. (2005). VEGF-A induces tumor and sentinel lymph node lymphangiogenesis and promotes lymphatic metastasis. *J. Exp. Med.* 201, 1089–1099. doi: 10.1084/jem.20041896

Hobson, B., and Denekamp, J. (1984). Endothelial proliferation in tumours and normal tissues: continuous labelling studies. *Br. J. Cancer* 49, 405–413. doi: 10.1038/bjc.1984.66

Hogan, B. M., Bos, F. L., Bussmann, J., Witte, M., Chi, N. C., Duckers, H. J., et al. (2009). ccbe1 is required for embryonic lymphangiogenesis and venous sprouting. *Nat. Genet.* 41, 396–398. doi: 10.1038/ng.321

Hos, D., and Cursiefen, C. (2014). "Lymphatic vessels in the development of tissue and organ rejection," in *Developmental Aspects of the Lymphatic Vascular System, Advances in Anatomy, Embryology and Cell Biology*, eds F. Kiefer and S. Schulte-Merker (Vienna: Springer), 119–141. doi: 10.1007/978-3-7091-1646-3_10

Hoshida, T., Isaka, N., Hagendoorn, J., di Tomaso, E., Chen, Y.-L., Pytowski, B., et al. (2006). Imaging steps of lymphatic metastasis reveals that vascular endothelial growth Factor-C increases metastasis by increasing delivery of cancer cells to lymph nodes: therapeutic implications. *Cancer Res.* 66, 8065–8075. doi: 10.1158/0008-5472.CAN-06-1392

Huang, L.-H., Elvington, A., and Randolph, G. J. (2015). The role of the lymphatic system in cholesterol transport. *Front. Pharmacol.* 6:182. doi: 10.3389/fphar.2015.00182

Huntington, G. S., and McClure, C. F. W. (1910). The anatomy and development of the jugular lymph sacs in the domestic cat (*Felis domestica*). *Am. J. Anat.* 10, 177–312. doi: 10.1002/aja.1000100108

Hwang, S. D., Song, J. H., Kim, Y., Lim, J. H., Kim, M. Y., Kim, E. N., et al. (2019). Inhibition of lymphatic proliferation by the selective VEGFR-3 inhibitor SAR131675 ameliorates diabetic nephropathy in db/db mice. *Cell Death Dis.* 10:219. doi: 10.1038/s41419-019-1436-1

Irrthum, A., Karkkainen, M. J., Devriendt, K., Alitalo, K., and Vikkula, M. (2000). Congenital hereditary lymphedema caused by a mutation that inactivates VEGFR3 tyrosine kinase. *Am. J. Hum. Genet.* 67, 295–301. doi: 10.1086/303019

Isaka, N., Padera, T. P., Hagendoorn, J., Fukumura, D., and Jain, R. K. (2004). Peritumor lymphatics induced by vascular endothelial growth Factor-C exhibit abnormal function. *Cancer Res.* 64, 4400–4404. doi: 10.1158/0008-5472.CAN-04-0752

Jafree, D. J., Moulding, D., Kolatsi-Joannou, M., Perretta Tejedor, N., Price, K. L., Milmoe, N. J., et al. (2019). Spatiotemporal dynamics and heterogeneity of renal lymphatics in mammalian development and cystic kidney disease. *eLife* 8:e48183. doi: 10.7554/eLife.48183

Jain, R. K. (1988). Determinants of tumor blood flow: a review. *Cancer Res.* 48, 2641–2658.

Jeltsch, M. (1997). Hyperplasia of lymphatic vessels in VEGF-C transgenic mice. *Science* 276, 1423–1425. doi: 10.1126/science.276.5317.1423

Jeltsch, M., Jha, S. K., Tvorogov, D., Anisimov, A., Leppänen, V.-M., Holopainen, T., et al. (2014). CCBE1 enhances lymphangiogenesis via A disintegrin and metalloprotease with thrombospondin motifs-3–mediated vascular endothelial growth Factor-C activation. *Circulation* 129, 1962–1971. doi: 10.1161/CIRCULATIONAHA.113.002779

Jiang, S., Bailey, A. S., Goldman, D. C., Swain, J. R., Wong, M. H., Streeter, P. R., et al. (2008). Hematopoietic stem cells contribute to lymphatic endothelium. *PLoS One* 3:e3812. doi: 10.1371/journal.pone.0003812

Joukov, V., Pajusola, K., Kaipainen, A., Chilov, D., Lahtinen, I., Kukk, E., et al. (1996). A novel vascular endothelial growth factor, VEGF-C, is a ligand for the Flt4 (VEGFR-3) and KDR (VEGFR-2) receptor tyrosine kinases. *Embo J.* 15, 290–298. doi: 10.1002/j.1460-2075.1996.tb00359.x

Joukov, V., Sorsa, T., Kumar, V., Jeltsch, M., Claesson-Welsh, L., Cao, Y., et al. (1997). Proteolytic processing regulates receptor specificity and activity of VEGF-C. *Embo J.* 16, 3898–3911. doi: 10.1093/emboj/16.13.3898

Jun-Dae, K., and Jongmin, K. (2014). Alk3/Alk3b and Smad5 mediate BMP signaling during lymphatic development in Zebrafish. *Mol. Cells* 37, 270–274. doi: 10.14348/MOLCELLS.2014.0005

Kaipainen, A., Korhonen, J., Mustonen, T., van Hinsbergh, V. W., Fang, G. H., Dumont, D., et al. (1995). Expression of the fms-like tyrosine kinase 4 gene becomes restricted to lymphatic endothelium during development. *Proc. Natl. Acad. Sci. U.S.A.* 92, 3566–3570. doi: 10.1073/pnas.92.8.3566

Kampmeier, O. F. (1928). The genetic history of the valves in the lymphatic system of man. *Am. J. Anat.* 40, 413–457. doi: 10.1002/aja.1000400302

Karkkainen, M. J., Ferrell, R. E., Lawrence, E. C., Kimak, M. A., Levinson, K. L., McTigue, M. A., et al. (2000). Missense mutations interfere with VEGFR-3 signalling in primary lymphoedema. *Nat. Genet.* 25, 153–159. doi: 10.1038/75997

Karkkainen, M. J., Haiko, P., Sainio, K., Partanen, J., Taipale, J., Petrova, T. V., et al. (2004). Vascular endothelial growth factor C is required for sprouting of the first lymphatic vessels from embryonic veins. *Nat. Immunol.* 5, 74–80. doi: 10.1038/ni1013

Karnezis, T., Shayan, R., Caesar, C., Roufail, S., Harris, N. C., Ardipradja, K., et al. (2012). VEGF-D promotes tumor metastasis by regulating prostaglandins produced by the collecting lymphatic endothelium. *Cancer Cell* 21, 181–195. doi: 10.1016/j.ccr.2011.12.026

Karpanen, T., Egeblad, M., Karkkainen, M. J., Kubo, H., Ylä-Herttuala, S., Jäättelä, M., et al. (2001). Vascular endothelial growth factor C promotes tumor lymphangiogenesis and intralymphatic tumor growth. *Cancer Res.* 61, 1786–1790.

Kenig-Kozlovsky, Y., Scott, R. P., Onay, T., Carota, I. A., Thomson, B. R., Gil, H. J., et al. (2018). Ascending vasa recta are angiopoietin/Tie2-dependent lymphatic-like vessels. *J. Am. Soc. Nephrol.* 29, 1097–1107. doi: 10.1681/ASN.2017090962

Kerjaschki, D., Huttary, N., Raab, I., Regele, H., Bojarski-Nagy, K., Bartel, G., et al. (2006). Lymphatic endothelial progenitor cells contribute to de novo lymphangiogenesis in human renal transplants. *Nat. Med.* 12, 230–234. doi: 10.1038/nm1340

Kizhatil, K., Ryan, M., Marchant, J. K., Henrich, S., and John, S. W. M. (2014). Schlemm's canal is a unique vessel with a combination of blood vascular and lymphatic phenotypes that forms by a novel developmental process. *PLoS Biol.* 12:e1001912. doi: 10.1371/journal.pbio.1001912

Klaus, M., Prokoph, N., Girbig, M., Wang, X., Huang, Y.-H., Srivastava, Y., et al. (2016). Structure and decoy-mediated inhibition of the SOX18/Prox1-DNA interaction. *Nucleic Acids Res.* 44, 3922–3935. doi: 10.1093/nar/gkw130

Klotz, L., Norman, S., Vieira, J. M., Masters, M., Rohling, M., Dubé, K. N., et al. (2015). Cardiac lymphatics are heterogeneous in origin and respond to injury. *Nature* 522, 62–67. doi: 10.1038/nature14483

Kok, F. O., Shin, M., Ni, C.-W., Gupta, A., Grosse, A. S., van Impel, A., et al. (2015). Reverse genetic screening reveals poor correlation between morpholino-induced and mutant phenotypes in Zebrafish. *Dev. Cell* 32, 97–108. doi: 10.1016/j.devcel.2014.11.018

Koltowska, K., Lagendijk, A. K., Pichol-Thievend, C., Fischer, J. C., Francois, M., Ober, E. A., et al. (2015). Vegfc regulates bipotential precursor division and prox1 expression to promote lymphatic identity in Zebrafish. *Cell Rep.* 13, 1828–1841. doi: 10.1016/j.celrep.2015.10.055

Koning, J. J., Konijn, T., Lakeman, K. A., O'Toole, T., Kenswil, K. J. G., Raaijmakers, M. H. G. P., et al. (2016). Nestin-expressing precursors give rise to both endothelial as well as nonendothelial lymph node stromal cells. *J. Immunol.* 197, 2686–2694. doi: 10.4049/jimmunol.1501162

Krishnan, J., Kirkin, V., Steffen, A., Hegen, M., Weih, D., Tomarev, S., et al. (2003). Differential in vivo and in vitro expression of vascular endothelial growth factor (VEGF)-C and VEGF-D in tumors and its relationship to lymphatic metastasis in immunocompetent rats. *Cancer Res.* 63, 713–722.

Kubo, H., Fujiwara, T., Jussila, L., Hashi, H., Ogawa, M., Shimizu, K., et al. (2000). Involvement of vascular endothelial growth factor receptor-3 in maintenance of integrity of endothelial cell lining during tumor angiogenesis. *Blood* 96, 546–553. doi: 10.1182/blood.v96.2.546.014k12_546_553

Küchler, A. M., Gjini, E., Peterson-Maduro, J., Cancilla, B., Wolburg, H., and Schulte-Merker, S. (2006). Development of the Zebrafish lymphatic system requires Vegfc signaling. *Curr. Biol.* 16, 1244–1248. doi: 10.1016/j.cub.2006.05.026

Kukk, E., Lymboussaki, A., Taira, S., Kaipainen, A., Jeltsch, M., Joukov, V., et al. (1996). VEGF-C receptor binding and pattern of expression with VEGFR-3 suggests a role in lymphatic vascular development. *Dev. Camb. Engl.* 122, 3829–3837.

Kunstfeld, R., Hirakawa, S., Hong, Y.-K., Schacht, V., Lange-Asschenfeldt, B., Velasco, P., et al. (2004). Induction of cutaneous delayed-type hypersensitivity reactions in VEGF-A transgenic mice results in chronic skin inflammation associated with persistent lymphatic hyperplasia. *Blood* 104, 1048–1057. doi: 10.1182/blood-2003-08-2964

Kurayoshi, M., Oue, N., Yamamoto, H., Kishida, M., Inoue, A., Asahara, T., et al. (2006). Expression of Wnt-5a is correlated with aggressiveness of gastric cancer by stimulating cell migration and invasion. *Cancer Res.* 66, 10439–10448. doi: 10.1158/0008-5472.CAN-06-2359

Laakkonen, P., Waltari, M., Holopainen, T., Takahashi, T., Pytowski, B., Steiner, P., et al. (2007). Vascular endothelial growth factor receptor 3 is involved in tumor angiogenesis and growth. *Cancer Res.* 67, 593–599. doi: 10.1158/0008-5472.CAN-06-3567

Le Guen, L., Karpanen, T., Schulte, D., Harris, N. C., Koltowska, K., Roukens, G., et al. (2014). Ccbe1 regulates Vegfc-mediated induction of Vegfr3 signaling during embryonic lymphangiogenesis. *Development* 141, 1239–1249. doi: 10.1242/dev.100495

Le Tourneau, C., Raymond, E., and Faivre, S. (2007). Sunitinib: a novel tyrosine kinase inhibitor. A brief review of its therapeutic potential in the treatment of renal carcinoma and gastrointestinal stromal tumors (GIST). *Ther. Clin. Risk Manag.* 3, 341–348. doi: 10.2147/tcrm.2007.3.2.341

Leak, L. V., and Burke, J. F. (1966). Fine structure of the lymphatic capillary and the adjoining connective tissue area. *Am. J. Anat.* 118, 785–809. doi: 10.1002/aja.1001180308

Lee, J. Y., Park, C., Cho, Y. P., Lee, E., Kim, H., Kim, P., et al. (2010). Podoplanin-expressing cells derived from bone marrow play a crucial role in postnatal lymphatic neovascularization. *Circulation* 122, 1413–1425. doi: 10.1161/CIRCULATIONAHA.110.941468

Leu, A. J., Berk, D. A., Lymboussaki, A., Alitalo, K., and Jain, R. K. (2000). Absence of functional lymphatics within a murine sarcoma: a molecular and functional evaluation. *Cancer Res.* 60, 4324–4327.

Levet, S., Ciais, D., Merdzhanova, G., Mallet, C., Zimmers, T. A., Lee, S.-J., et al. (2013). Bone morphogenetic protein 9 (BMP9) controls lymphatic vessel maturation and valve formation. *Blood* 122, 598–607. doi: 10.1182/blood-2012-12-472142

Lewis, F. T. (1905). The development of the lymphatic system in rabbits. *Am. J. Anat.* 5, 95–111. doi: 10.1002/aja.1000050107

Lioux, G., Liu, X., Temiño, S., Oxendine, M., Ayala, E., Ortega, S., et al. (2020). A second heart field-derived vasculogenic niche contributes to cardiac lymphatics. *Dev. Cell* 52, 350.e6–363.e6. doi: 10.1016/j.devcel.2019.12.006

Liu, J., Zhang, Y., Xu, R., Du, J., Hu, Z., Yang, L., et al. (2013). PI3K/Akt-dependent phosphorylation of GSK3β and activation of RhoA regulate Wnt5a-induced gastric cancer cell migration. *Cell. Signal.* 25, 447–456. doi: 10.1016/j.cellsig.2012.10.012

Louveau, A., Herz, J., Alme, M. N., Salvador, A. F., Dong, M. Q., Viar, K. E., et al. (2018). CNS lymphatic drainage and neuroinflammation are regulated by meningeal lymphatic vasculature. *Nat. Neurosci.* 21, 1380–1391. doi: 10.1038/s41593-018-0227-9

Louveau, A., Smirnov, I., Keyes, T. J., Eccles, J. D., Rouhani, S. J., Peske, J. D., et al. (2015). Structural and functional features of central nervous system lymphatic vessels. *Nature* 523, 337–341. doi: 10.1038/nature14432

Lugano, R., Ramachandran, M., and Dimberg, A. (2020). Tumor angiogenesis: causes, consequences, challenges and opportunities. *Cell. Mol. Life Sci.* 77, 1745–1770. doi: 10.1007/s00018-019-03351-7

Lund, A. W., Wagner, M., Fankhauser, M., Steinskog, E. S., Broggi, M. A., Spranger, S., et al. (2016). Lymphatic vessels regulate immune microenvironments in human and murine melanoma. *J. Clin. Invest.* 126, 3389–3402. doi: 10.1172/JCI79434

Ma, Q., Ineichen, B. V., Detmar, M., and Proulx, S. T. (2017). Outflow of cerebrospinal fluid is predominantly through lymphatic vessels and is reduced in aged mice. *Nat. Commun.* 8:1434. doi: 10.1038/s41467-017-01484-6

Mahadevan, A., Welsh, I. C., Sivakumar, A., Gludish, D. W., Shilvock, A. R., Noden, D. M., et al. (2014). The left-right Pitx2 pathway drives organ-specific arterial and lymphatic development in the intestine. *Dev. Cell* 31, 690–706. doi: 10.1016/j.devcel.2014.11.002

Mäkinen, T., Jussila, L., Veikkola, T., Karpanen, T., Kettunen, M. I., Pulkkanen, K. J., et al. (2001). Inhibition of lymphangiogenesis with resulting lymphedema in transgenic mice expressing soluble VEGF receptor-3. *Nat. Med.* 7, 199–205. doi: 10.1038/84651

Martinez-Corral, I., Ulvmar, M. H., Stanczuk, L., Tatin, F., Kizhatil, K., John, S. W. M., et al. (2015). Nonvenous origin of dermal lymphatic vasculature. *Circ. Res.* 116, 1649–1654. doi: 10.1161/CIRCRESAHA.116.306170

Maruyama, K., Ii, M., Cursiefen, C., Jackson, D. G., Keino, H., Tomita, M., et al. (2005). Inflammation-induced lymphangiogenesis in the cornea arises from CD11b-positive macrophages. *J. Clin. Invest.* 115, 2363–2372. doi: 10.1172/JCI23874

Maruyama, K., Miyagawa-Tomita, S., Mizukami, K., Matsuzaki, F., and Kurihara, H. (2019). Isl1-expressing non-venous cell lineage contributes to cardiac lymphatic vessel development. *Dev. Biol.* 452, 134–143. doi: 10.1016/j.ydbio.2019.05.002

Mato, M., Ookawara, S., Sugamata, M., and Aikawa, E. (1984). Evidence for the possible function of the fluorescent granular perithelial cells in brain as scavengers of high-molecular-weight waste products. *Experientia* 40, 399–402. doi: 10.1007/BF01952574

Meilhac, S. M., and Buckingham, M. E. (2018). The deployment of cell lineages that form the mammalian heart. *Nat. Rev. Cardiol.* 15, 705–724. doi: 10.1038/s41569-018-0086-9

Méndez-Ferrer, S., Michurina, T. V., Ferraro, F., Mazloom, A. R., MacArthur, B. D., Lira, S. A., et al. (2010). Mesenchymal and haematopoietic stem cells form a unique bone marrow niche. *Nature* 466, 829–834. doi: 10.1038/nature09262

Mignone, J. L., Kukekov, V., Chiang, A.-S., Steindler, D., and Enikolopov, G. (2004). Neural stem and progenitor cells in nestin-GFP transgenic mice. *J. Comp. Neurol.* 469, 311–324. doi: 10.1002/cne.10964

Mizuno, S., Yamada, Y., Yamada, K., Nomura, N., and Wakamatsu, N. (2005). Clinical variability in a Japanese hereditary lymphedema type I family with an FLT4 mutation. *Congenit. Anom.* 45, 59–61. doi: 10.1111/j.1741-4520.2005.00064.x

Mlecnik, B., Bindea, G., Angell, H. K., Maby, P., Angelova, M., Tougeron, D., et al. (2016). Integrative analyses of colorectal cancer show immunoscore is a stronger predictor of patient survival than microsatellite instability. *Immunity* 44, 698–711. doi: 10.1016/j.immuni.2016.02.025

Morikawa, S., Baluk, P., Kaidoh, T., Haskell, A., Jain, R. K., and McDonald, D. M. (2002). Abnormalities in pericytes on blood vessels and endothelial sprouts in tumors. *Am. J. Pathol.* 160, 985–1000. doi: 10.1016/S0002-9440(10)64920-6

Muthuchamy, M., and Zawieja, D. (2008). Molecular regulation of lymphatic contractility. *Ann. N. Y. Acad. Sci.* 1131, 89–99. doi: 10.1196/annals.1413.008

Nadarajah, N., Schulte, D., McConnell, V., Martin-Almedina, S., Karapouliou, C., Mortimer, P., et al. (2018). A novel splice-site mutation in VEGFC is associated with congenital primary lymphoedema of gordon. *Int. J. Mol. Sci.* 19:2259. doi: 10.3390/ijms19082259

Nicenboim, J., Malkinson, G., Lupo, T., Asaf, L., Sela, Y., Mayseless, O., et al. (2015). Lymphatic vessels arise from specialized angioblasts within a venous niche. *Nature* 522, 56–61. doi: 10.1038/nature14425

Ny, A., Koch, M., Schneider, M., Neven, E., Tong, R. T., Maity, S., et al. (2005). A genetic *Xenopus laevis* tadpole model to study lymphangiogenesis. *Nat. Med.* 11, 998–1004. doi: 10.1038/nm1285

Okuda, K. S., Astin, J. W., Misa, J. P., Flores, M. V., Crosier, K. E., and Crosier, P. S. (2012). lyve1 expression reveals novel lymphatic vessels and new mechanisms for lymphatic vessel development in zebrafish. *Development* 139, 2381–2391. doi: 10.1242/dev.077701

Oliver, G., Kipnis, J., Randolph, G. J., and Harvey, N. L. (2020). The lymphatic vasculature in the 21st century: novel functional roles in homeostasis and disease. *Cell* 182, 270–296. doi: 10.1016/j.cell.2020.06.039

Padera, T. P. (2002). Lymphatic metastasis in the absence of functional intratumor lymphatics. *Science* 296, 1883–1886. doi: 10.1126/science.1071420

Park, C., Lee, J. Y., and Yoon, Y. (2011). Role of bone marrow-derived lymphatic endothelial progenitor cells for lymphatic neovascularization. *Trends Cardiovasc. Med.* 21, 135–140. doi: 10.1016/j.tcm.2012.04.002

Partanen, T. A., Arola, J., Saaristo, A., Jussila, L., Ora, A., Miettinen, M., et al. (2000). VEGF-C and VEGF-D expression in neuroendocrine cells and their receptor, VEGFR-3, in fenestrated blood vessels in human tissues. *FASEB J.* 14, 2087–2096. doi: 10.1096/fj.99-1049com

Pasquali, S., van der Ploeg, A. P. T., Mocellin, S., Stretch, J. R., Thompson, J. F., and Scolyer, R. A. (2013). Lymphatic biomarkers in primary melanomas as predictors of regional lymph node metastasis and patient outcomes. *Pigment Cell Melanoma Res.* 26, 326–337. doi: 10.1111/pcmr.12064

Persaud, K. (2004). Involvement of the VEGF receptor 3 in tubular morphogenesis demonstrated with a human anti-human VEGFR-3 monoclonal antibody that antagonizes receptor activation by VEGF-C. *J. Cell Sci.* 117, 2745–2756. doi: 10.1242/jcs.01138

Petrova, T. V., and Koh, G. Y. (2018). Organ-specific lymphatic vasculature: from development to pathophysiology. *J. Exp. Med.* 215, 35–49. doi: 10.1084/jem.20171868

Petrova, T. V., and Koh, G. Y. (2020). Biological functions of lymphatic vessels. *Science* 369:eaax4063. doi: 10.1126/science.aax4063

Pichol-Thievend, C., Betterman, K. L., Liu, X., Ma, W., Skoczylas, R., Lesieur, E., et al. (2018). A blood capillary plexus-derived population of progenitor cells contributes to genesis of the dermal lymphatic vasculature during embryonic development. *Development* 145:dev160184. doi: 10.1242/dev.160184

Pullinger, B. D., and Florey, H. W. (1937). Proliferation of lymphatics in inflammation. *J. Pathol. Bacteriol.* 45, 157–170. doi: 10.1002/path.1700450115

Qin, J., Tsai, S. Y., and Tsai, M.-J. (2014). The critical roles of COUP-TFII in tumor progression and metastasis. *Cell Biosci.* 4:58. doi: 10.1186/2045-3701-4-58

Qin, S., Li, A., Yi, M., Yu, S., Zhang, M., and Wu, K. (2019). Recent advances on anti-angiogenesis receptor tyrosine kinase inhibitors in cancer therapy. *J. Hematol. Oncol.* 12:27. doi: 10.1186/s13045-019-0718-5

Ran, S., and Montgomery, K. E. (2012). Macrophage-mediated lymphangiogenesis: the emerging role of macrophages as lymphatic endothelial progenitors. *Cancers* 4, 618–657. doi: 10.3390/cancers4030618

Ran, S., and Volk-Draper, L. (2020). "Lymphatic endothelial cell progenitors in the tumor microenvironment," in *Tumor Microenvironment, Advances in Experimental Medicine and Biology*, ed. A. Birbrair (Cham: Springer International Publishing), 87–105. doi: 10.1007/978-3-030-37184-5_7

Ranieri, G., Gadaleta-Caldarola, G., Goffredo, V., Patruno, R., Mangia, A., Rizzo, A., et al. (2012). Sorafenib (BAY 43-9006) in hepatocellular carcinoma patients: from discovery to clinical development. *Curr. Med. Chem.* 19, 938–944. doi: 10.2174/092986712799320736

Religa, P., Cao, R., Bjorndahl, M., Zhou, Z., Zhu, Z., and Cao, Y. (2005). Presence of bone marrow–derived circulating progenitor endothelial cells in the newly formed lymphatic vessels. *Blood* 106, 4184–4190. doi: 10.1182/blood-2005-01-0226

Roberts, N., Kloos, B., Cassella, M., Podgrabinska, S., Persaud, K., Wu, Y., et al. (2006). Inhibition of VEGFR-3 activation with the antagonistic antibody more potently suppresses lymph node and distant metastases than inactivation of VEGFR-2. *Cancer Res.* 66, 2650–2657. doi: 10.1158/0008-5472.CAN-05-1843

Roukens, M. G., Peterson-Maduro, J., Padberg, Y., Jeltsch, M., Leppänen, V.-M., Bos, F. L., et al. (2015). Functional dissection of the CCBE1 protein: a crucial requirement for the collagen repeat domain. *Circ. Res.* 116, 1660–1669. doi: 10.1161/CIRCRESAHA.116.304949

Sabin, F. R. (1902). On the origin of the lymphatic system from the veins and the development of the lymph hearts and thoracic duct in the pig. *Am. J. Anat.* 1, 367–389. doi: 10.1002/aja.1000010310

Saif, M. W., Knost, J. A., Chiorean, E. G., Kambhampati, S. R. P., Yu, D., Pytowski, B., et al. (2016). Phase 1 study of the anti-vascular endothelial growth factor receptor 3 monoclonal antibody LY3022856/IMC-3C5 in patients with advanced and refractory solid tumors and advanced colorectal cancer. *Cancer Chemother. Pharmacol.* 78, 815–824. doi: 10.1007/s00280-016-3134-3

Schneider, M., Othman-Hassan, K., Christ, B., and Wilting, J. (1999). Lymphangioblasts in the avian wing bud. . *Dev. Dyn. Off. Publ. Am. Assoc. Anat.* 216, 311–319. doi: 10.1002/(SICI)1097-0177(199912)216:4/5<311::AID-DVDY1>3.0.CO;2-M

Schwartz, N., Chalasani, M. L. S., Li, T. M., Feng, Z., Shipman, W. D., and Lu, T. T. (2019). Lymphatic function in autoimmune diseases. *Front. Immunol.* 10:519. doi: 10.3389/fimmu.2019.00519

Semo, J., Nicenboim, J., and Yaniv, K. (2016). Development of the lymphatic system: new questions and paradigms. *Development* 143, 924–935. doi: 10.1242/dev.132431

Shimizu, K., Kubo, H., Yamaguchi, K., Kawashima, K., Ueda, Y., Matsuo, K., et al. (2004). Suppression of VEGFR-3 signaling inhibits lymph node metastasis in gastric cancer. *Cancer Sci.* 95, 328–333. doi: 10.1111/j.1349-7006.2004.tb03211.x

Shin, M., Male, I., Beane, T. J., Villefranc, J. A., Kok, F. O., Zhu, L. J., et al. (2016). Vegfc acts through ERK to induce sprouting and differentiation of trunk lymphatic progenitors. *Development* 143, 3785–3795. doi: 10.1242/dev.137901

Skobe, M., Hamberg, L. M., Hawighorst, T., Schirner, M., Wolf, G. L., Alitalo, K., et al. (2001a). Concurrent induction of lymphangiogenesis, angiogenesis, and macrophage recruitment by vascular endothelial growth Factor-C in Melanoma. *Am. J. Pathol.* 159, 893–903. doi: 10.1016/S0002-9440(10)61765-8

Skobe, M., Hawighorst, T., Jackson, D. G., Prevo, R., Janes, L., Velasco, P., et al. (2001b). Induction of tumor lymphangiogenesis by VEGF-C promotes breast cancer metastasis. *Nat. Med.* 7, 192–198. doi: 10.1038/84643

Smith, R. O. (1949). Lymphatic contractility. *J. Exp. Med.* 90, 497–509. doi: 10.1084/jem.90.5.497

Song, E., Mao, T., Dong, H., Boisserand, L. S. B., Antila, S., Bosenberg, M., et al. (2020). VEGF-C-driven lymphatic drainage enables immunosurveillance of brain tumours. *Nature* 577, 689–694. doi: 10.1038/s41586-019-1912-x

Srinivasan, R. S., Dillard, M. E., Lagutin, O. V., Lin, F.-J., Tsai, S., Tsai, M.-J., et al. (2007). Lineage tracing demonstrates the venous origin of the mammalian lymphatic vasculature. *Genes Amp. Dev.* 21, 2422–2432. doi: 10.1101/gad.1588407

Srinivasan, R. S., Geng, X., Yang, Y., Wang, Y., Mukatira, S., Studer, M., et al. (2010). The nuclear hormone receptor Coup-TFII is required for the initiation and early maintenance of Prox1 expression in lymphatic endothelial cells. *Genes Dev.* 24, 696–707. doi: 10.1101/gad.1859310

Srinivasan, R. S., and Oliver, G. (2011). Prox1 dosage controls the number of lymphatic endothelial cell progenitors and the formation of the lymphovenous valves. *Genes Dev.* 25, 2187–2197. doi: 10.1101/gad.16974811

Stacker, S. A., Caesar, C., Baldwin, M. E., Thornton, G. E., Williams, R. A., Prevo, R., et al. (2001). VEGF-D promotes the metastatic spread of tumor cells via the lymphatics. *Nat. Med.* 7, 186–191. doi: 10.1038/84635

Stacker, S. A., Stenvers, K., Caesar, C., Vitali, A., Domagala, T., Nice, E., et al. (1999). Biosynthesis of vascular endothelial growth Factor-D involves proteolytic processing which generates non-covalent homodimers. *J. Biol. Chem.* 274, 32127–32136. doi: 10.1074/jbc.274.45.32127

Stacker, S. A., Williams, S. P., Karnezis, T., Shayan, R., Fox, S. B., and Achen, M. G. (2014). Lymphangiogenesis and lymphatic vessel remodelling in cancer. *Nat. Rev. Cancer* 14, 159–172. doi: 10.1038/nrc3677

Stanczuk, L., Martinez-Corral, I., Ulvmar, M. H., Zhang, Y., Laviña, B., Fruttiger, M., et al. (2015). cKit lineage hemogenic endothelium-derived cells contribute to mesenteric lymphatic vessels. *Cell Rep.* 10, 1708–1721. doi: 10.1016/j.celrep.2015.02.026

Stone, O. A., and Stainier, D. Y. R. (2019). Paraxial mesoderm is the major source of lymphatic endothelium. *Dev. Cell* 50, 247.e3–255.e3. doi: 10.1016/j.devcel.2019.04.034

Su, J.-L., Yang, P.-C., Shih, J.-Y., Yang, C.-Y., Wei, L.-H., Hsieh, C.-Y., et al. (2006). The VEGF-C/Flt-4 axis promotes invasion and metastasis of cancer cells. *Cancer Cell* 9, 209–223. doi: 10.1016/j.ccr.2006.02.018

Su, J.-L., Yen, C.-J., Chen, P.-S., Chuang, S.-E., Hong, C.-C., Kuo, I.-H., et al. (2007). The role of the VEGF-C/VEGFR-3 axis in cancer progression. *Br. J. Cancer* 96, 541–545. doi: 10.1038/sj.bjc.6603487

Tammela, T., Zarkada, G., Wallgard, E., Murtomäki, A., Suchting, S., Wirzenius, M., et al. (2008). Blocking VEGFR-3 suppresses angiogenic sprouting and vascular network formation. *Nature* 454, 656–660. doi: 10.1038/nature07083

Tan, H.-Y., Wang, N., Lam, W., Guo, W., Feng, Y., and Cheng, Y.-C. (2018). Targeting tumour microenvironment by tyrosine kinase inhibitor. *Mol. Cancer* 17:43. doi: 10.1186/s12943-018-0800-6

Tao, S., Witte, M., Bryson-Richardson, R. J., Currie, P. D., Hogan, B. M., and Schulte-Merker, S. (2011). Zebrafish prox1b mutants develop a lymphatic vasculature, and prox1b does not specifically mark lymphatic endothelial cells. *PLoS One* 6:e28934. doi: 10.1371/journal.pone.0028934

Thomlinson, R. H., and Gray, L. H. (1955). The histological structure of some human lung cancers and the possible implications for radiotherapy. *Br. J. Cancer* 9, 539–549. doi: 10.1038/bjc.1955.55

Truong, T. N., Li, H., Hong, Y.-K., and Chen, L. (2014). Novel characterization and live imaging of schlemm's canal expressing Prox-1. *PLoS One* 9:e98245. doi: 10.1371/journal.pone.0098245

Tso, P., and Balint, J. A. (1986). Formation and transport of chylomicrons by enterocytes to the lymphatics. *Am. J. Physiol. Gastrointest. Liver Physiol.* 250, G715–G726. doi: 10.1152/ajpgi.1986.250.6.G715

Ulvmar, M. H., and Mäkinen, T. (2016). Heterogeneity in the lymphatic vascular system and its origin. *Cardiovasc. Res.* 111, 310–321. doi: 10.1093/cvr/cvw175

Vaahtomeri, K., and Alitalo, K. (2020). Lymphatic vessels in tumor dissemination vs. immunotherapy. *Cancer Res.* 80, 3463–3465. doi: 10.1158/0008-5472.CAN-20-0156

Vaahtomeri, K., Karaman, S., Mäkinen, T., and Alitalo, K. (2017). Lymphangiogenesis guidance by paracrine and pericellular factors. *Genes Dev.* 31, 1615–1634. doi: 10.1101/gad.303776.117

van der Jagt, E. R. (1932). Memoirs: the origin and development of the anterior lymph-sacs in the Sea-Turtle (*Thalassochelys caretta*). *Q. J. Microsc. Sci. s2*-s75, 151–163.

van Impel, A., Zhao, Z., Hermkens, D. M. A., Roukens, M. G., Fischer, J. C., Peterson-Maduro, J., et al. (2014). Divergence of zebrafish and mouse lymphatic cell fate specification pathways. *Development* 141, 1228–1238. doi: 10.1242/dev.105031

van Lessen, M., Shibata-Germanos, S., van Impel, A., Hawkins, T. A., Rihel, J., and Schulte-Merker, S. (2017). Intracellular uptake of macromolecules by brain lymphatic endothelial cells during zebrafish embryonic development. *eLife* 6:e25932. doi: 10.7554/eLife.25932

Veikkola, T., Jussila, L., Makinen, T., Karpanen, T., Jeltsch, M., Petrova, T. V., et al. (2001). Signalling via vascular endothelial growth factor receptor-3 is sufficient for lymphangiogenesis in transgenic mice. *EMBO J.* 20, 1223–1231. doi: 10.1093/emboj/20.6.1223

Villefranc, J. A., Nicoli, S., Bentley, K., Jeltsch, M., Zarkada, G., Moore, J. C., et al. (2013). A truncation allele in vascular endothelial growth factor c reveals distinct modes of signaling during lymphatic and vascular development. *Development* 140, 1497–1506. doi: 10.1242/dev.084152

Vivien, C. J., Pichol-Thievend, C., Sim, C. B., Smith, J. B., Bower, N. I., Hogan, B. M., et al. (2019). Vegfc/d-dependent regulation of the lymphatic vasculature during cardiac regeneration is influenced by injury context. *NPJ Regen. Med.* 4:18. doi: 10.1038/s41536-019-0079-2

Volk-Draper, L., Patel, R., Bhattarai, N., Yang, J., Wilber, A., DeNardo, D., et al. (2019). Myeloid-derived lymphatic endothelial cell progenitors significantly contribute to lymphatic metastasis in clinical breast cancer. *Am. J. Pathol.* 189, 2269–2292. doi: 10.1016/j.ajpath.2019.07.006

Volk-Draper, L. D., Hall, K. L., Wilber, A. C., and Ran, S. (2017). Lymphatic endothelial progenitors originate from plastic myeloid cells activated by toll-like receptor-4. *PLoS One* 12:e0179257. doi: 10.1371/journal.pone.0179257

Wang, G., Muhl, L., Padberg, Y., Dupont, L., Peterson-Maduro, J., Stehling, M., et al. (2020). Specific fibroblast subpopulations and neuronal structures provide local sources of Vegfc-processing components during zebrafish lymphangiogenesis. *Nat. Commun.* 11:2724. doi: 10.1038/s41467-020-16552-7

Wang, L., Zhang, Y., Zhao, Y., Marshall, C., Wu, T., and Xiao, M. (2019). Deep cervical lymph node ligation aggravates AD-like pathology of APP/PS1 mice. *Brain Pathol.* 29, 176–192. doi: 10.1111/bpa.12656

Wigle, J. T. (2002). An essential role for Prox1 in the induction of the lymphatic endothelial cell phenotype. *Embo J.* 21, 1505–1513. doi: 10.1093/emboj/21.7.1505

Wigle, J. T., and Oliver, G. (1999). Prox1 function is required for the development of the murine lymphatic system. *Cell* 98, 769–778. doi: 10.1016/S0092-8674(00)81511-1

Wilczak, W., Wittmer, C., Clauditz, T., Minner, S., Steurer, S., Büscheck, F., et al. (2018). Marked prognostic impact of minimal lymphatic tumor spread in prostate cancer. *Eur. Urol.* 74, 376–386. doi: 10.1016/j.eururo.2018.05.034

Wilting, J., Aref, Y., Huang, R., Tomarev, S. I., Schweigerer, L., Christ, B., et al. (2006). Dual origin of avian lymphatics. *Dev. Biol.* 292, 165–173. doi: 10.1016/j.ydbio.2005.12.043

Yamakawa, M., Doh, S. J., Santosa, S. M., Montana, M., Qin, E. C., Kong, H., et al. (2018). Potential lymphangiogenesis therapies: learning from current antiangiogenesis therapies-A review. *Med. Res. Rev.* 38, 1769–1798. doi: 10.1002/med.21496

Yamashita, M., Iwama, N., Date, F., Shibata, N., Miki, H., Yamauchi, K., et al. (2009). Macrophages participate in lymphangiogenesis in idiopathic diffuse alveolar damage through CCL19-CCR7 signal. *Hum. Pathol.* 40, 1553–1563. doi: 10.1016/j.humpath.2009.03.021

Yang, H., Kim, C., Kim, M.-J., Schwendener, R. A., Alitalo, K., Heston, W., et al. (2011). Soluble vascular endothelial growth factor receptor-3 suppresses lymphangiogenesis and lymphatic metastasis in bladder cancer. *Mol. Cancer* 10:36. doi: 10.1186/1476-4598-10-36

Yaniv, K., Isogai, S., Castranova, D., Dye, L., Hitomi, J., and Weinstein, B. M. (2006). Live imaging of lymphatic development in the zebrafish. *Nat. Med.* 12, 711–716. doi: 10.1038/nm1427

Yoshimatsu, Y., Lee, Y. G., Akatsu, Y., Taguchi, L., Suzuki, H. I., Cunha, S. I., et al. (2013). Bone morphogenetic protein-9 inhibits lymphatic vessel formation via activin receptor-like kinase 1 during development and cancer progression. *Proc. Natl. Acad. Sci. U.S.A.* 110, 18940–18945. doi: 10.1073/pnas.1310479110

You, L.-R., Lin, F.-J., Lee, C. T., DeMayo, F. J., Tsai, M.-J., and Tsai, S. Y. (2005). Suppression of Notch signalling by the COUP-TFII transcription factor regulates vein identity. *Nature* 435, 98–104. doi: 10.1038/nature03511

Yuan, Y., Arcucci, V., Levy, S. M., and Achen, M. G. (2019). Modulation of immunity by lymphatic dysfunction in lymphedema. *Front. Immunol.* 10:76. doi: 10.3389/fimmu.2019.00076

Zheng, W., Aspelund, A., and Alitalo, K. (2014). Lymphangiogenic factors, mechanisms, and applications. *J. Clin. Invest.* 124, 878–887. doi: 10.1172/JCI71603

Zou, W., Pu, T., Feng, W., Lu, M., Zheng, Y., Du, R., et al. (2019). Blocking meningeal lymphatic drainage aggravates Parkinson's disease-like pathology in mice overexpressing mutated α-synuclein. *Transl. Neurodegener.* 8:7. doi: 10.1186/s40035-019-0147-y

Zumsteg, A., Baeriswyl, V., Imaizumi, N., Schwendener, R., Rüegg, C., and Christofori, G. (2009). Myeloid cells contribute to tumor lymphangiogenesis. *PLoS One* 4:e7067. doi: 10.1371/journal.pone.0007067

Conflict of Interest: The authors declare that the research was conducted in the absence of any commercial or financial relationships that could be construed as a potential conflict of interest.

frontiers in Physiology

REVIEW
published: 24 September 2020
doi: 10.3389/fphys.2020.01084

Genetic Tools to Study Cardiovascular Biology

*Irene Garcia-Gonzalez, Severin Mühleder, Macarena Fernández-Chacón and Rui Benedito**

Molecular Genetics of Angiogenesis Group, Centro Nacional de Investigaciones Cardiovasculares (CNIC), Madrid, Spain

Progress in biomedical science is tightly associated with the improvement of methods and genetic tools to manipulate and analyze gene function in mice, the most widely used model organism in biomedical research. The joint effort of numerous individual laboratories and consortiums has contributed to the creation of a large genetic resource that enables scientists to image cells, probe signaling pathways activities, or modify a gene function in any desired cell type or time point, à la carte. However, as these tools significantly increase in number and become more sophisticated, it is more difficult to keep track of each tool's possibilities and understand their advantages and disadvantages. Knowing the best currently available genetic technology to answer a particular biological question is key to reach a higher standard in biomedical research. In this review, we list and discuss the main advantages and disadvantages of available mammalian genetic technology to analyze cardiovascular cell biology at higher cellular and molecular resolution. We start with the most simple and classical genetic approaches and end with the most advanced technology available to fluorescently label cells, conditionally target their genes, image their clonal expansion, and decode their lineages.

Keywords: genetic tools, mosaics, cardiovascular, imaging, barcoding, transgenics, Cre, clonal analysis

OPEN ACCESS

Edited by:
Stephan Huveneers, Amsterdam University Medical Center (UMC), Netherlands

Reviewed by:
Bin Zhou, Chinese Academy of Sciences, China
Lena Claesson-Welsh, Uppsala University, Sweden

****Correspondence:***
Rui Benedito
rui.benedito@cnic.es

Specialty section:
This article was submitted to Vascular Physiology, a section of the journal Frontiers in Physiology

Received: *25 June 2020*
Accepted: *06 August 2020*
Published: *24 September 2020*

Citation:
Garcia-Gonzalez I, Mühleder S, Fernández-Chacón M and Benedito R (2020) Genetic Tools to Study Cardiovascular Biology. Front. Physiol. 11:1084. doi: 10.3389/fphys.2020.01084

REPORTER AND Cre MOUSE LINES TO ANALYZE AND GENETICALLY TARGET THE CARDIOVASCULAR SYSTEM

For many years, scientists relied on immunostainings to visualize the different cells composing the cardiovascular system. Nowadays, there are antibodies to specifically label most of the cardiovascular cell types. This technique allows the histological examination of an organ or tissue architecture, and the scoring of tissue malformations arising from genetic mutations. However, histological and immunostaining techniques are incompatible with live imaging and often do not allow the isolation of specific cell types. Given that most tissues are formed by tightly-associated cells, these techniques also do not allow the visualization of single cells within the tissue and the study of their morphology or dynamics.

In order to live image and analyze cells at higher morphological and molecular resolution, scientists engineered new mouse models containing genes coding for fluorescent proteins (FP) or recombinases downstream of cell type-specific genes or promoters (**Figure 1**). There are many apparently redundant mouse lines available, using for example the commonly used *Tie2* and *Cdh5* promoters, but each transgenic line has its particularities given the type and location

A

Small plasmid transgenes

PROS
Easier to engineer.
High expression of reporter due to multi-copy integration.

CONS
Lacks most of the regulatory elements of the original gene. (Unreliable reporting in some cases).
Sensitive to genomic position and epigenetic variegation.

PAC and BAC transgenes

PROS
Contains most of the gene's essential regulatory elements.
Less sensitive to genomic position and epigenetic variegation effects.
High expression of reporter due to multi-copy integration.
Does not disrupt original gene function.

CONS
Requires assembly of large vectors.
Expression may be less reliable than direct knock-in reporters.
Some unpredictable expression patterns can arise over generations.

Knock-in alleles

PROS
Most reliable gene expression patterns with all regulatory elements.
Easy to achieve nowadays with Cas9 HDR technology.

CONS
Hemizygous loss of gene function (haploinsufficiency)
Single-copy expression sometimes not sufficient and weaker than BACs/PACs/Small-transgene multicopy expression.

B

Cell-type-specific reporter alleles

Name	Cell / Tissue	Genetics	Reference
Cdh5-mTnG	PAN ECs	PAC transgene	(Jeong et al., 2017)
Tie2-GFP	PAN ECs	Small Transgene	(Motoike et al., 2000)
Pdgfrb-EGFP	Pericytes	BAC transgene	(GENSAT) Project
Prox1-GFP	Lymphatic ECs	BAC transgene	(GENSAT) Project
Prox1-mOrange	Lymphatic ECs	BAC transgene	(Hägerling et al., 2011)
Wt1-GFP-Cre	Proepicardium	Knock-In	(Zhou et al., 2008)

C

Cell-type-specific Cre alleles

Name	Cell / Tissue	Genetics	Reference
Cdh5-CreERT2	PAN ECs	PAC transgene	(Wang et al, 2010)
Tie2-Cre	PAN ECs	BAC transgene	(Kisanuki et al., 2001)
Esm1-CreERT2	Tip ECs	BAC Transgene	(Rocha et al., 2014)
Apln-CreERT2	Angiogenic ECs	BAC transgene	(Tian et al., 2013)
Bmx-CreERT2	Arterial ECs	BAC transgene	(Ehling et al., 2013)
Pdgfrb-CreERT2	Fibroblast and pericytes	BAC transgene	(Chen et al., 2016)
Myh11-CreERT2	SMCs	BAC Transgene	(Wirth et al., 2008)
Prox1-CreERT2	Lymphatic ECs	BAC transgene	(Bazigou et al., 2011)
Vegfr3-CreERT2	Lymphatic and Angiogenic ECs	Knock-In	(Martinez-Corral et al., 2016)
Myhc-Cre and Myhc-CreERT2	Cardiomyocytes	Small Transgene	(Wang et al., 2005)
Wt1-CreERT2	Epicardium Coronary vessels	Knock-In	(Pu et al., 2018)
Nfatc1-Cre / Nfatc1-IRES-CreERT2	Endocardium	Knock-In	(Wu et al., 2012) / (Zhang et al., 2016)

FIGURE 1 | Pros and Cons of transgenic and knock-in lines used in the cardiovascular biology field. **(A)** Summary of advantages and disadvantages of different types of transgenic and knock-in alleles. **(B)** List of commonly used fluorescent reporter mouse lines in the cardiovascular biology field. **(C)** List of commonly used *Cre/CreERT2* mouse lines.

of the transgene. The first generation of mouse lines frequently contained multicopy insertion of small plasmid transgenes in the genome, which often lacked all the elements required to drive robust and specific expression of the FPs or recombinases in all desired cells. They were also sensitive to transgene and genomic position-related epigenetic variegation (Garrick et al., 1998; McBurney et al., 2002). These were followed by second generation mouse lines using larger transgenes such as bacteriophage P1-derived Artificial Chromosomes (PACs, up to 120 Kb) and Bacterial Artificial Chromosomes (BACs, up to 250 Kb) that can carry significantly larger DNA sequences containing most if not all of a gene essential promoter/enhancer elements. These larger transgenes were also significantly less sensitive to genomic position and epigenetic variegation effects (Giraldo and Montoliu, 2001; Adamson et al., 2011). Regardless of their size, transgenes expression is less reliable when compared with direct knock-ins of a reporter or recombinase gene in the native locus of the cell type-specific gene. There are many reports showing that unlike knock-ins, transgene expression can change throughout generations and result in highly unpredictable expression patterns (Koetsier et al., 1996; Mutskov and Felsenfeld, 2004). Knock-ins in the native locus usually guarantee stability and robustness in gene expression patterns. However, knock-in of a reporter within a gene was historically much more difficult to achieve, since it required assembly of large targeting vectors, their genome targeting in totipotent mouse embryonic stem (ES) cells and germline transmission to generate a genetically modified allele to the progeny (Westphal and Leder, 1997). However, with the advent of CRISPR/Cas9 technology, it is now possible to integrate by Cas9-induced DNA break and homology directed repair (HDR), small genetic cassettes downstream of virtually any mouse gene promoter. This is done by standard injection in mouse eggs of Cas9, a guide RNA and a donor DNA molecule containing homologous sequences flanking a DNA insert of interest (Yang et al., 2013; Platt et al., 2014; Chu et al., 2016; Scott and Gruzdev, 2019). This greatly eases the generation of gene or cell type-specific transgenic lines. Despite its current easiness, inserting a reporter or recombinase gene in-frame with the gene endogenous ATG has also disadvantages, such as the hemizygous loss of gene function. There are many reports showing a significant impact on cell biology of a 50% loss in gene expression, such as the haploinsufficiency of genes like *Vegfa*, *Dll4*, and *Kdr* (Carmeliet et al., 1996; Gale et al., 2004; Oladipupo et al., 2018). An alternative is to insert in the 3'-untranslated region (UTR) of a gene (Basak et al., 2018) an internal ribosome entry site (IRES) or a viral 2A peptide containing cassette (Trichas et al., 2008; Alvarez et al., 2015; Basak et al., 2018), in order to better preserve the targeted gene function. But as with everything, there are also cons of using these less disrupting strategies. Reporter genes when introduced downstream of IRES elements are less translated than the upstream genes (Al-Allaf et al., 2019),

which may significantly decrease reporter expression and its detectability. In the case of the 2A peptide approach, care and pre-validation is required in order to avoid decreasing the function of the upstream protein, by the C-terminally fused 11 aa belonging to the 2A peptide. In addition, the 2A peptide decreases overall translation rates due to the required pause and ribosomal skipping step associated with the translation of the 2A-peptide-containing protein (Trichas et al., 2008; Sharma et al., 2012). Another important disadvantage of a gene knock-in is that it always results in single-copy expression, whereas a BAC or plasmid transgenic allele, particularly the best ones, usually contains multiple copies of the same transgene, which often results in higher reporter/Cre expression levels (Sörensen et al., 2009; Ubezio et al., 2016). A good example of this is the comparison between the BAC *Esm1-CreERT2* line (Rocha et al., 2014) that is highly expressed and induces the recombination of standard *Cre*-reporters in most retina endothelial tip cells, and the gene targeted *Esm1-H2B-Cerulean-2A-CreERT2* line (Pontes-Quero et al., 2019), which is significantly less expressed and recombines only few tip cells during retina vascular development.

Taken all these considerations in mind, the best strategy to follow in order to generate a good gene-reporter or gene-recombinase reporter line is dependent on the gene itself, its predicted loss-of-function phenotype, relative expression, and the availability of in house BAC transgenic or CRISPR/Cas9 technology. Use of small plasmid transgenesis or mouse ES cells gene targeting are clearly outdated technologies that on average result in either less robust results, or unnecessary delays and costs, respectively.

In **Figure 1**, we indicate some of the most important, validated and used mouse lines by the cardiovascular research community. There are many more available, but they are either less used or have significant disadvantages such as the nature of the transgene or reporter genes included. With the advent and ease of performing CRISPR knock-ins the trend is for more and better knock-in lines to appear, but as mentioned above, they have significant disadvantages in relation to BAC transgenic lines. What is so far a largely unappreciated and unused technology is the direct CRISPR/Cas9 targeting and modification in mouse eggs of existing and validated BAC transgenic lines, to create new alleles driving the stronger expression of the latest generation and improved versions of fluorescent reporters or recombinases.

To label a given cell of interest, one can use a cell-specific-gene reporter mouse line that allows the direct labeling of cells expressing a given gene (**Figure 1B**) or an indirect labeling strategy combining a specific-gene *Cre* line (**Figure 1C**) with an ubiquitous and Cre-inducible reporter (**Figure 2A**). The first strategy has the advantage of allowing the direct labeling of cells expressing a given gene and hence it reports also the dynamics of the selected gene expression. However, it has the disadvantage of the selected gene-promoter elements not driving sufficiently high levels of the reporter, or the gene may be downregulated and no longer labels the intended cells once a given biological process is completed. An example is the expression of the tip-cell enriched gene *Esm1* (**Figure 2B**) or the angiogenesis restricted gene *Apln*. These genes are not expressed in more mature and quiescent vessels. The strategy involving a combination of an allele driving the expression of the recombinase and a reporter allele has the advantage of allowing the permanent labeling of cells with a constitutively expressed fluorescent reporter, usually driven by the very strong and ubiquituous *CAG/ROSA26* promoters. This usually results in much higher levels of FP expression, which facilitates its detection and increases the cellular resolution in sections or large volumes of tissue. With this strategy, all the progeny of the initially labeled or recombined cells will be labeled, which may lead to lack of specificity in the labeling (**Figure 2C**). One example is the frequent use of the *Tie2-Cre* or *Cdh5-Cre* expressing lines to label endothelial cells. Since embryonic endothelial cells can differentiate to hematopoietic progenitor cells (Ottersbach, 2019) this results in the labeling of the entire hematopoietic compartment as well, which may complicate the imaging of endothelial cells, particularly in inflammation settings, and also confound the interpretation of a given genetic lineage tracing experiment (Alva et al., 2006). In addition, gene-specific *Cre* lines may be weakly expressed in many other cell types, and trigger the recombination of the reporter allele and labeling of cells that are not usually considered to express the gene of interest, a phenomenon usually named as Cre leakiness and a frequent source of lineage-tracing artifacts and misinterpretations. Therefore, standard *Cre* lines should not be used for lineage tracing experiments. Instead, *CreERT2* lines should be used, since they provide temporal control over a genetic modification and are less capable of inducing non-intended recombination of a floxed allele in cells weakly expressing a *CreERT2* transgene. *CreERT2* lines also enable single-cell clonal analysis at low doses of tamoxifen (**Figures 2D,E**).

USING RECOMBINASE TECHNOLOGY TO STUDY CARDIOVASCULAR GENE FUNCTION: MIND YOUR Cre, FLOXED GENE, AND REPORTER ALLELES

The discovery of recombinases that are able to recognize unique palindromic DNA sequences not present in the mammalian genome, and that promote their recombination (deletion/inversion), paved the way to recombinase-based conditional genetic gain and loss-of-function technology (Branda and Dymecki, 2004; Birling et al., 2009). So far the most potent recombinase at 37°C and in mammalian cells is Cre (Anastassiadis et al., 2009), that is able to recognize 34 bp DNA sequences named as *LoxP*. This prompted the generation of thousands of mouse lines containing genes flanked by *LoxP* sites (floxed), and transgenes driving expression of Cre/CreERT2 in specific cell types (Murray et al., 2012). The Cre/*lox* technology requires the combination in the same mouse of one allele driving the expression of Cre or CreERT2 in a particular cell/tissue/organ and floxed alleles. This then enables a given floxed allele to be deleted or activated conditionally to the expression of Cre

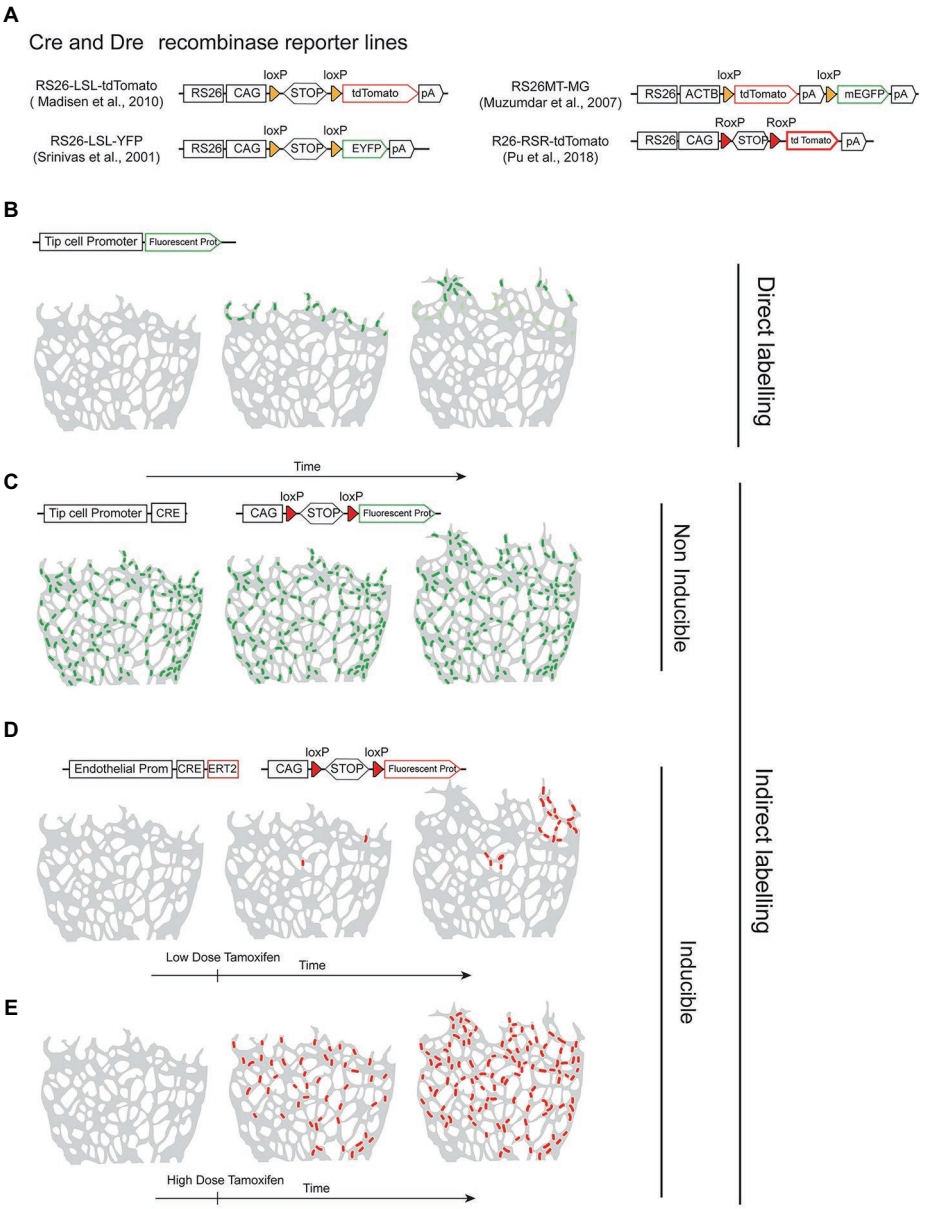

FIGURE 2 | Recombinase reporter lines and their outcomes. **(A)** Schematic overview of distinct recombinase-inducible and Rosa26-locus targeted fluorescent reporters. **(B)** Example of direct labelling achieved by using an allele containing a vascular tip-cell-specific promoter driving expression of a fluorescent protein in the retina angiogenesis model. Only tip cells express the promoter and the reporter protein. **(C)** Example of a non-inducible and indirect labelling strategy using a tip-cell-specific *Cre* line in combination with a fluorescent reporter line. Cre is expressed in tip-cells and all their progeny during tissue development and therefore the fluorescent reporter is expressed in many endothelial cells, not only tip cells. **(D,E)** Example of indirect labelling using an inducible *CreERT2* line expressed in all endothelial cells, in combination with a reporter line. Cre is only activated after tamoxifen administration and recombination/cell labelling occurs at a controlled time-point. Number of recombination events and cellular labelling can be modulated by the dose of tamoxifen.

or its activation by tamoxifen (CreERT2). The final outcome of the technology is the ability to control genetic modifications in space and time.

Recombinase technology can be used not only to label and fatemap cells or tissues of interest (**Figure 2**) but also to perform inducible or conditional genetic deletions. The ability to delete a given known floxed gene at any given time and in any cell/tissue has revolutionized biomedical science and particularly the study of cardiovascular development. It is well-established that gene function varies over time and the cell where it is expressed. It is also known that organs across our body communicate or cross-talk with each other. Therefore, the information arising from the analysis of embryos or animals with a germline deletion of a given gene is often incomplete and its tissue-specific or primary function may be difficult to assess or understand. The global knockout (KO) of genes relevant

for cardiovascular development or basic cellular functions, such as cell proliferation or differentiation are also frequently embryonically lethal, impairing the study of a gene function in subsequent biological processes or in adult organisms. Although it is still common practice in biomedical science, germline gene deletion or in a tissue-specific manner from early embryonic development should be avoided if the purpose is to understand its function in postnatal or adult cancer/heart biology. This is particularly relevant in studies conducted to assess if targeting a given gene/pathway is relevant for the progression of an adult organism disease. Gene function in the adult organism or disease can only be safely assessed by genetically targeting the adult tissue after the onset of the disease, something too often ignored by the biomedical community.

Despite the significant advantages of using conditional genetics, it is often significantly more difficult to achieve the desired conditional genetic modification. In the case of a germline KO mouse line, once it is established, no further gene loss-of-function validation is required. However, in conditional genetics, each and every single experiment needs its proper controls of gene deletion and numerous studies have demonstrated the need for caution in the use of conditional genetic technology. The main problem is that it is often not possible to control all aspects of a conditional genetic experiment. There are three main issues or caveats associated with recombinase-based conditional genetics. The first is related with the transgenes used to drive expression of Cre/CreERT2. There are very often significant and unpredictable position-effect variegation of transgenes due to random epigenetic silencing, which is so far impossible to predict or control. This can lead to variability in Cre/CreERT2 expression within cells of a tissue, littermates, or across generations of mouse breedings (Garrick et al., 1998; Long and Rossi, 2009), turning conditional genetics unpredictable and often unreliable and costly. Even assuming an invariable and high expression of the *Cre/CreERT2* allele in your cells/tissue/organ of interest, the second issue with *Cre/Lox* technology is that *Cre* recombination depends on the location of the *LoxP* sites in the genome and the genetic distance and DNA sequence separating them. Therefore, for every floxed allele one should expect a different recombination efficiency, even when using the same *Cre* or *CreERT2*-expressing allele. An example of how this can affect interpretation of results is a combination of studies in the cardiovascular biology field showing that previously reported cardiac fate mapping studies were misguided by relatively low recombination efficiencies of the reporters used. *Isl1-cre* and *Nkx2-5-Cre* lines were previously used to label and follow distinct cardiac progenitors, using a *CMV β-actin-nlacZ* and a *RS26-β-galactosidase* reporter, respectively. Since in these first studies cells recombined with *Isl1-Cre* line were found to contribute mainly to the second heart field (SHF: right ventricle, outflow tract and atria; Cai et al., 2003), and cells recombined with *Nkx2-5-Cre* were found to give rise mainly to cardiomyocytes (Moses et al., 2001) the authors of these two studies concluded that these cells arise from distinct progenitors. However, in a more recent study, in which the authors used the same Cre lines, but instead used the *Gata4-flap* reporter, significantly more cells were recombined and *Isl1* expressing progenitors were found to contribute not only to the SHF but also to the first heart field (FHF: left ventricle). Similarly, Nkx2-5 progenitors were found to give rise, apart from cardiomyocytes, to endothelium and smooth muscle cells (Ma et al., 2008). In addition to this variability in sensitivity to Cre of distinct reporter alleles located in different loci, recent studies have compared and found significantly different recombination efficiencies of several distinct floxed reporter alleles located in the same *Rosa26* locus (Vooijs et al., 2001; Pontes-Quero et al., 2017). These differences are clearly not only related with the genetic distance between the *LoxP* sites or their position in the genome, but also the nature of the DNA sequences surrounding the *LoxP* sites. This brings us to the third and often overlooked caveat of conditional genetics, which is the reliance on independent fluorescent reporters of recombination to validate the conditional technique and analyze cells having the intended specific genetic deletion. These recombinase reporters are usually alleles targeted to the ubiquitous mouse *Rosa26* locus (Soriano, 1999; Srinivas et al., 2001) and are activated or expressed only after the cell expresses Cre or has induced CreERT2 activity (**Figure 2A**). However, since there is no genetic linkage between the reporter allele and any other floxed alleles in the cell, the correlation between the recombination of a reporter allele and another floxed allele is often very low. Indeed a recent study showed that some commonly used *Rosa26* reporter alleles overreport genetic deletions, whereas others underreport (Fernández-Chacón et al., 2019). In our hands, the commonly used *R26-LSL-YFP* allele (Srinivas et al., 2001), and particularly the *R26-LSL-tdTomato* reporter allele (Madisen et al., 2010), are extremely sensitive to Cre/CreERT2 activity, unlike the majority of other tested floxed genes (Fernández-Chacón et al., 2019). Therefore, when using CreERT2, having a tissue full of cells expressing a recombinase reporter, does not guarantee that your gene is deleted.

For all conditional genetic experiments, it is therefore critical to have reliable methods to confirm that a given gene (not the reporter) is properly recombined/deleted, and only in the desired cell type. However, the large majority of studies employing conditional genetics rely on the use of fast PCR-based or Western blot-based methods to confirm genetic deletions in whole tissues or groups of isolated cells. These methods are insufficient because they only indicate the average gene-deletion efficiency, and cannot quantify the heterogeneity in genetic deletion efficiency among different cells of different tissues, which can lead to misinterpretations of a given conditional mutant phenotype. Also these methods are performed with cells or tissues that were lysed for DNA/Protein extraction, and therefore the tissues/cells analyzed for efficiency of genetic deletion are not the same as the ones used for microscopy/phenotypic analysis. The gold standard and safest method for confirming inducible and specific gene deletion is to co-immunostain for the encoded protein and another tissue or cell marker in the same tissue. However, for most proteins there are no high-quality antibodies able to distinguish between the morphology of cells with and without protein expression in the tissue. Another issue is that gene transcription and

protein stability oscillate in a cell, and thus a cell with no detectable expression of a given gene or protein at a given moment may still be wildtype for the coding gene.

The caveats of conditional genetics mentioned above are significantly more apparent and pronounced when using tamoxifen inducible-*CreERT2* lines, or weaker recombinases such as Dre and Flp. In these experiments, the level of recombinase/Cre activity is significantly lower, and often it is not sufficient to delete two copies of a floxed gene, even though it may be sufficient to recombine and activate a single and sensitive recombinase-reporter allele located in the accessible *Rosa26* locus (Compare **Figure 3A** with **Figure 3B**). This is even more relevant when incomplete genetic induction schemes are used, such as when the induction of low frequency genetic mosaics is desired in order to track single-cell-derived clones or lineages (**Figure 2D**). In this case, most cells expressing the recombinase will not be recombined, and therefore the assumption that the few cells showing recombination of a given reporter allele, have also recombined the intended floxed gene, is even more incorrect.

To overcome the above-mentioned problems associated with conditional genetic deletions, we recently generated a new inducible dual reporter-Cre mouse allele (**Figure 3C**), named as iSuRe-Cre (Fernández-Chacón et al., 2019). This allele enables the significant increase of Cre activity in reporter-expressing cells, providing certainty that these cells have completely recombined all floxed alleles, regardless of their sequence and location in the genome (**Figure 3D**). This tool greatly decreases the occurrence of false positives, i.e., cells expressing a fluorescent reporter and not having other gene/s fully deleted. The tool is particularly relevant for epistasis studies, in which multiple genetic deletions are needed in the same cell or tissue.

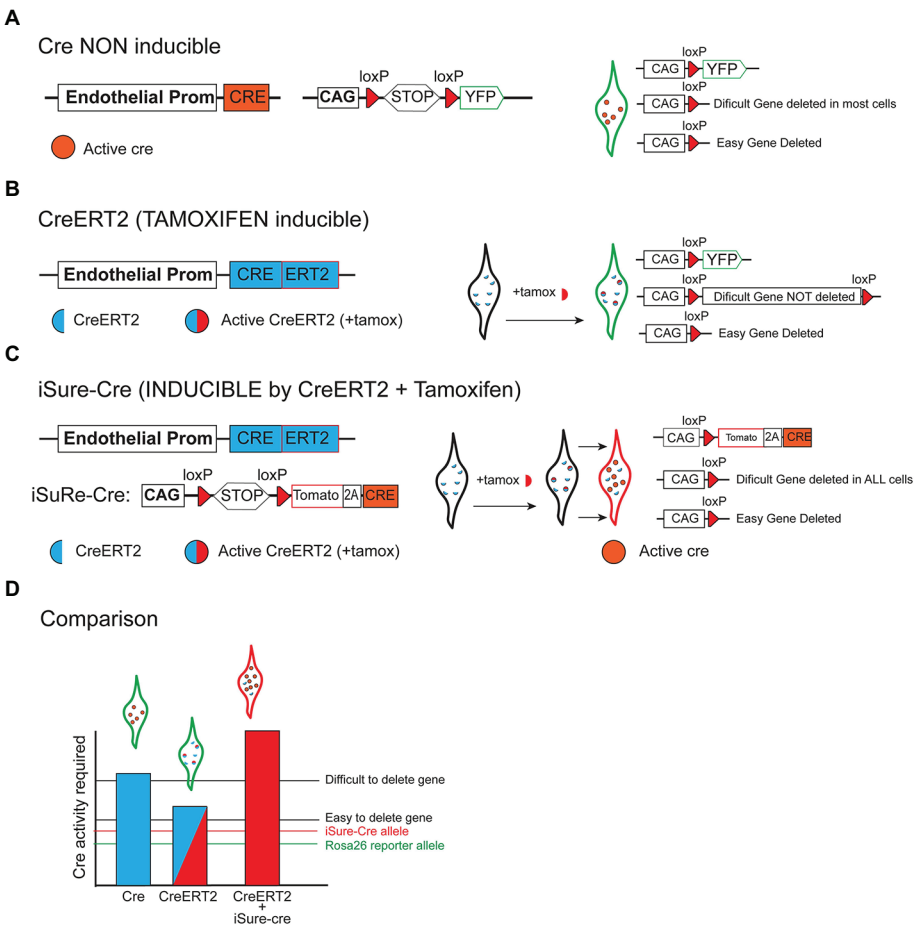

FIGURE 3 | Different strategies to delete floxed genes. **(A)** Scheme showing that when a constitutively active Cre allele (non inducible) is combined with a reporter allele, most cells expressing the reporter recombine/delete both easy and difficult floxed genes. **(B)** When tamoxifen-inducible CreERT2 alleles are used, many cells expressing the Cre-reporter allele may not delete other genes that are more difficult to delete since these require a higher or sustained level of recombinase activity. **(C)** The iSure-Cre allele is inducible by CreERT2, and enables a higher Cre activity in reporter-expressing cells. The use of this strategy guarantees full deletion of floxed genes in reporter-expressing cells. **(D)** Illustrative chart comparing the genetic strategies mentioned above. The bars represent the Cre activity achieved with most Cre/CreERT2 lines and the iSuRe-Cre allele. Different floxed genes require a different level of Cre activity to be deleted (an easy and difficult to delete gene is represented). Only the iSuRe-Cre allele can ensure the deletion of most genes in reporter-expressing cells.

With the iSuRe-Cre allele, because reporter-expressing cells express also Cre and not only the reporter, efficient genetic deletions can also be achieved in a mosaic fashion. In this way, we can have single cells reliably reporting gene deletion within a wildtype tissue, even if the initial Cre/CreERT2-dependent recombination induction was very low. This tool also enables direct conditional genetics and live imaging experiments, since reporter-expressing cells are certainly mutant. In the past, this was always challenging and involved independent and very time-consuming experimental controls, because it is not possible to validate genetic deletions in live cells, given the need to fix or isolate them before performing the necessary genetic deletion validation experiments. In summary, this genetic tool increases the ease, efficiency, and reliability of conditional genetic experiments.

An alternative method presented recently to increase Cre activity after tamoxifen induction of CreERT uses an inducible self-cleaved CreER (sCreER), in which the ER element is flanked by *LoxP* sites. In the non-induced state, Cre-LoxP-ER-LoxP is expressed but inactive, and after tamoxifen the ER portion is deleted in the induced cells, and Cre is free to mobilize to the nucleus and recombine other flanked genes (Tian et al., 2020). This strategy boosts Cre expression and activity in initially CreER recombined cells; however, the sCreER lines generated so far are tissue-specific and also do not contain an internal reporter linked with Cre expression, in order to ensure that cells expressing an independent Cre reporter have full gene deletion.

USING INTERSECTION GENETICS FOR HIGHER GENETIC RESOLUTION

So far, we have mentioned the most common techniques and approaches used to label specific tissues and cell types in order to distinguish or isolate them for downstream analysis, or perform tissue-specific genetic modifications. However, sometimes a single gene promoter is not sufficient to drive the expression of a reporter or Cre to a specific tissue, or fraction of a tissue, of interest. Intersection genetics in mice was made possible after the discovery of other recombinases such as Flp and Dre (Anastassiadis et al., 2009). Intersection genetics relies on the sequential or simultaneous intersection in time or space of two different recombinase systems, so that one is conditional or dependent on the other (Rodríguez et al., 2000; Anastassiadis et al., 2009). This leads to cascades of recombination and the differential labeling or targeting of specific cell populations (Dymecki et al., 2010; Plummer et al., 2015).

Several Dre and Cre mouse lines and dual reporters were generated to perform dual labeling and intersection genetics in the cardiovascular system (**Figure 4A**). In one study, the Bin Zhou laboratory used dual-recombinase-activated lineage tracing with interleaved reporter (DeaLT-IR) to significantly enhance the precision and reduce unintended Cre-LoxP lineage tracing (**Figure 4B**). Using DeaLT-IR they could distinguish cardiomyocytes (Tnni3+/tomato+) from non-cardiomyocytes Kit+ cells (Tnni3−/ZsGreen+) to clearly show that Kit+ non-cardiomyocytes do not give rise to cardiomyocytes in the injured heart and that there is no contribution of Sox9+ biliary epithelial cells to hepatocytes in the liver after injury, two findings against previous dogma arising from the use of simpler or lower resolution genetic approaches (He et al., 2017).

The same laboratory also used similar intersection genetics to solve a recurrent problem in the vascular research field, which is that most endothelial-specific genetic modifications target the entire endothelium of all organs, and not specific organ vascular beds, which may lead to early lethality or distort the interpretation of a gene function in a particular vascular bed. In a very elegant study, Pu and colleagues generated a set of genetic tools that allow the specific targeting of heart or brain endothelium, and not of other organs vessels (Pu et al., 2018). The alleles generated allow the expression of active Cre, and therefore genetic deletions, specifically in Tie2+/Wt1+ coronary ECs or Tie2+/Mfsd2a+ brain ECs and not other organ vascular beds (**Figure 4C**). Using this approach they could delete the most important VEGF receptor (Vegfr2) in each endothelial compartment and understand its organ-specific endothelial function circumventing early lethality and phenotypes derived from deletion in other organs. Thanks to this tool they discovered that Vegfr2 is essential for the integrity of the blood brain barrier (BBB) and for angiogenesis in the central nervous system.

In another study, they used similar mutually exclusive dual recombinase systems (**Figure 4D**) to investigate if all non-cardiomyocyte cells, can originate cardiomyocytes at distinct stages of development and adult tissues, a long-standing question in the field. Using this genetic technology they found that non-cardiomyocytes can only differentiate to cardiomyocytes before E11.5, not at later stages or during neonatal heart regeneration (Li et al., 2018).

MULTISPECTRAL FLUORESCENT MOSAICS FOR HIGH RESOLUTION SINGLE-CELL OR CLONAL ANALYSIS

The above-mentioned lines are sufficient to distinguish cell types and decipher gene function at the tissue or organ level. However, higher genetic and cellular resolution is often required to understand single-cell biology, particularly when live cell imaging is not possible. Tissues are formed by the association of highly heterogeneous cells, each having different proliferation, differentiation or migration properties. Standard conditional genetics is convenient to analyze the average phenotype of wildtype or mutant cell populations within a tissue, but not to discern single-cell biology.

For long, scientists have tried to track and follow single cells from the initial stages of embryonic development to their final stages of differentiation. *Drosophila melanogaster* or *Caenorhabditis elegans* development was initially mapped by visual tracking of non-fluorescent cells, where the researchers had to record the development of the early embryos over time (Sulston and Horvitz, 1977; Underwood et al., 1980; Sulston et al., 1983). With the advent of transgenics expressing FPs,

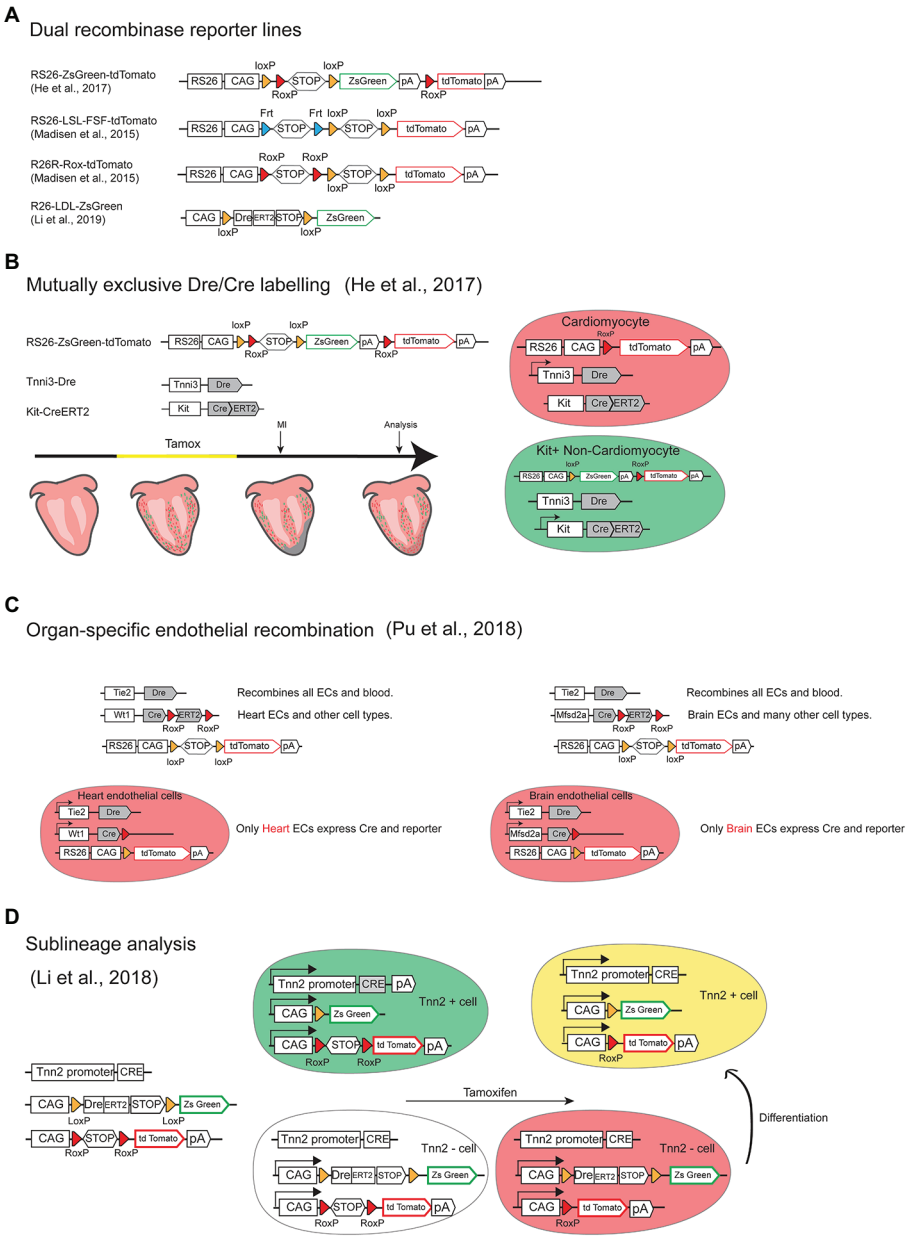

FIGURE 4 | Intersection genetics by combining Cre and Dre mouse lines. **(A)** Schemes of the alleles of dual (Cre/Dre or Cre/Flp) reporter lines available for intersection genetics. **(B)** Scheme of the alleles and strategy used to achieve mutually exclusive Cre and Dre recombination and labeling of cardiomyocyte (Tnni3+/tomato+) and non-cardiomyocyteckit+ cells (Tnni3-/ZsGreen+) to enhance precision of lineage tracing after administration of tamoxifen and myocardial infarction (MI). **(C)** Scheme of the alleles and strategy used to achieve organ-specific (heart or brain) endothelial recombination. **(D)** Scheme of the alleles and strategy used to perform sublineage and fate-mapping analysis of Tnn2+ and Tnn2- cells differentiation to cardiomyocytes.

live imaging of tissues, or individually labeled cells became possible, particularly in lower vertebrate organisms, such as zebrafish (Pan et al., 2013). In the mouse, however, it is still not possible to live image most cell types and tissues, particularly for long periods of time. The discovery of inducible site-specific recombinases (i.e., CreERT2, FlpOERT2, or DreERT2) was therefore an important breakthrough to study single-cell biology since they enabled the pulse and chase of recombinase reporter-expressing cells, or single-cell fate mapping experiments (Legue and Joyner, 2010). This allowed the precise induction of permanent genetic modifications only in a few cells within a tissue (with a low dose of inducer/tamoxifen), and since these are inherited by all the daughter cells, it is possible to perform restrospective clonal analysis to its ancestor (**Figure 2D**). This technique allows the quantification of how a given single progenitor cell proliferates, differentiates or migrates over time

in the tissue. However, depending on the experimental window and dynamics of the tissue, in order for this simple pulse-and-chase restrospective clonal analysis method to be accurate, only very few cells in a tissue or embryo can be induced or recombined, otherwise there is a loss of single-cell or clonal resolution (Compare **Figure 2D** vs. **Figure 2E**). Since with this technique only very few cells, or clones of cells, can be pulsed and reliably followed over time, this method has a very high cost given the large amount of embryos/animals and time needed to generate and analyze enough single-cell-derived clones of cells. This methodological bottleneck, associated with the development of new FPs and multispectral confocal microscopy, created the need to engineer new DNA constructs and mouse lines that allow the induction and detection of numerous clones of differentially labeled cells in the same tissue.

The first mouse line to be developed in order to effectively achieve differentially labeling of multiple cell clones was named as *Brainbow*, and it enabled combinatorial multispectral mosaics in the brain of mice, given the use of the *Thy1* promoter (expressed in brain cells). This method was based on the existence of mutually exclusive Lox sites (*LoxP*, *LoxN*, and *Lox 2272*) that after CreERT2 induction, can be recombined in only one of three possible ways, resulting in the expression of only one of three possible FPs (RFP, YFP, CFP) in each cell (Livet et al., 2007). Since the *Brainbow* transgenic alleles contained the tandem integration of 8–16 copies of a single three-Loxed/FPs construct, they enabled the induction and distinction of up to 90 different combinations of FPs/clones in the same tissue. Given the numerous possibilities and diversity of the stochastic recombination event, this method allowed the safe labeling and distinction of multiple single-cells and their progenies in the brain.

However, the most widely used multispectral mouse line is not the *Brainbow*, but the *Confetti* (Snippert et al., 2010). In contrast to the *Brainbow* mice, the *Confetti* mouse carries a single brainbow construct (*Brainbow 2.1*) downstream of the strong and ubiquitously expressed CAG promoter and is inserted in the safe and ubiquitously expressed *Rosa26* locus, and therefore can be induced in any cell type. This mouse allows the labeling of individual cells with only one of four different FPs (nGFP, mEYFP, tDimer2, and mCerulean; **Figures 5A,A'**). This is a clear disadvantage when compared with the *Brainbow* combinatorial and multicopy alleles that allow significantly more diverse labeling. However, it provides for greater clarity in clone labeling and identification, since the separation of the different relative intensities and nuances of the three channels in *Brainbow* mice can often be challenging, particularly for beginners in microscopy imaging or image analysis.

There are now many derivations of the ubiquituous *Confetti* line and the main differences among them are the targeting or not to the *Rosa26* locus, the relative position of the cassettes, FPs of choice and compatibility or not with standard Cre (**Figures 5B,B',C,C'**).

An alternative to the use of the *Confetti* or *Rosa26* Rainbow mice, is the use of the new *Dual ifgMosaic* mice (Pontes-Quero et al., 2017), with which it is possible to induce in any cell type, up to 15 (instead of four) different clones of cells, six expressing a single FP and nine expressing two FPs, one localized in the nuclei or chromatin (H2B tag) and the other in the membrane (**Figures 5D,D'**). The *Dual ifgMosaic* mouse lines also have the advantage of allowing distinction of the 15 clones of cells not only by direct live imaging of the spectrally distinct FPs, but also by immunostaining, since the different FPs used (MbYFP, MbTomato, HA-MbTfp1, His-H2B-Cherry, H2B-GFP-V5, and HA-H2B-Cerulean) contain distinct tags (HA, V5, or His) that enable distinction of the 15 clones of color-codes by only three antibody signals (Anti-GFP-488, Anti-Dsred-546, or Anti-HA-647). The *Confetti* and *Brainbow* mice rely on the multispectral detection of YFP/GFP/Cerulean, that are not distinguishable by antibody staining and do not allow the simultaneous distinction of the nuclei (for cell unit count) and membrane/filopodia (for cell shape). This is particularly important to quantify the number of cells in clones of epithelial cells (such as endothelial cells) that usually are tightly adherent to each other and are therefore non-distinguishable if labeled with only one cytoplasmic or membrane FP (**Figures 5A'–D'**). Another advantage of *Dual ifgMosaic* mice is the compatibility with Cre (not only CreERT2) expressing mouse lines. In these mice, each recombination event is based on permanent genetic deletions, which are induced when *LoxP* sites are positioned in the same orientation, whereas with *Confetti* the recombination event is based on a reversible genetic inversion that occurs when the LoxP sites are positioned in an opposite orientation (Nagy, 2000; Compare **Figure 5A** with **Figure 5D**). Moreover, in multi-copy tandem transgenic lines like *Brainbow* or the *Rainbow2* (**Figure 5C**), constitutive Cre expression leads to the deletion of the entire multicopy transgene and the full loss of clonal diversity, rendering them incompatible with standard Cre lines or the new iSuRe-Cre line (Fernández-Chacón et al., 2019).

RELIABLE FUNCTIONAL GENETIC MOSAIC SYSTEMS

Functional genetic mosaics are very useful to understand the cell-autonomous role of a given gene. Most studies taking conclusions about a given gene cell-autonomous role, obtain it using standard conditional tissue genetics, and not single-cell genetics. When a gene has a severe impact on cardiovascular development or function, it is difficult to really analyze and understand its cell-autonomous role, given that the surrounding embryonic tissues or organs also do not develop or function well, which feedbacks and induces changes in the biology of the cardiovascular system. These inter-tissue cross-talks and feedbacks prevent the understanding of the real cell-autonomous gene function. An example of this is the consequence of deleting the gene *Dll4* in vascular cells during embryonic development. It leads to early embryonic death and significantly less vascular development, even though the gene is a suppressor of angiogenesis (Duarte et al., 2004; Suchting et al., 2007; Pontes-Quero et al., 2019). Inducible functional genetic mosaics on the other hand, allow us to study the cell-autonomous gene or pathway function for longer periods of time, without the confounding effects

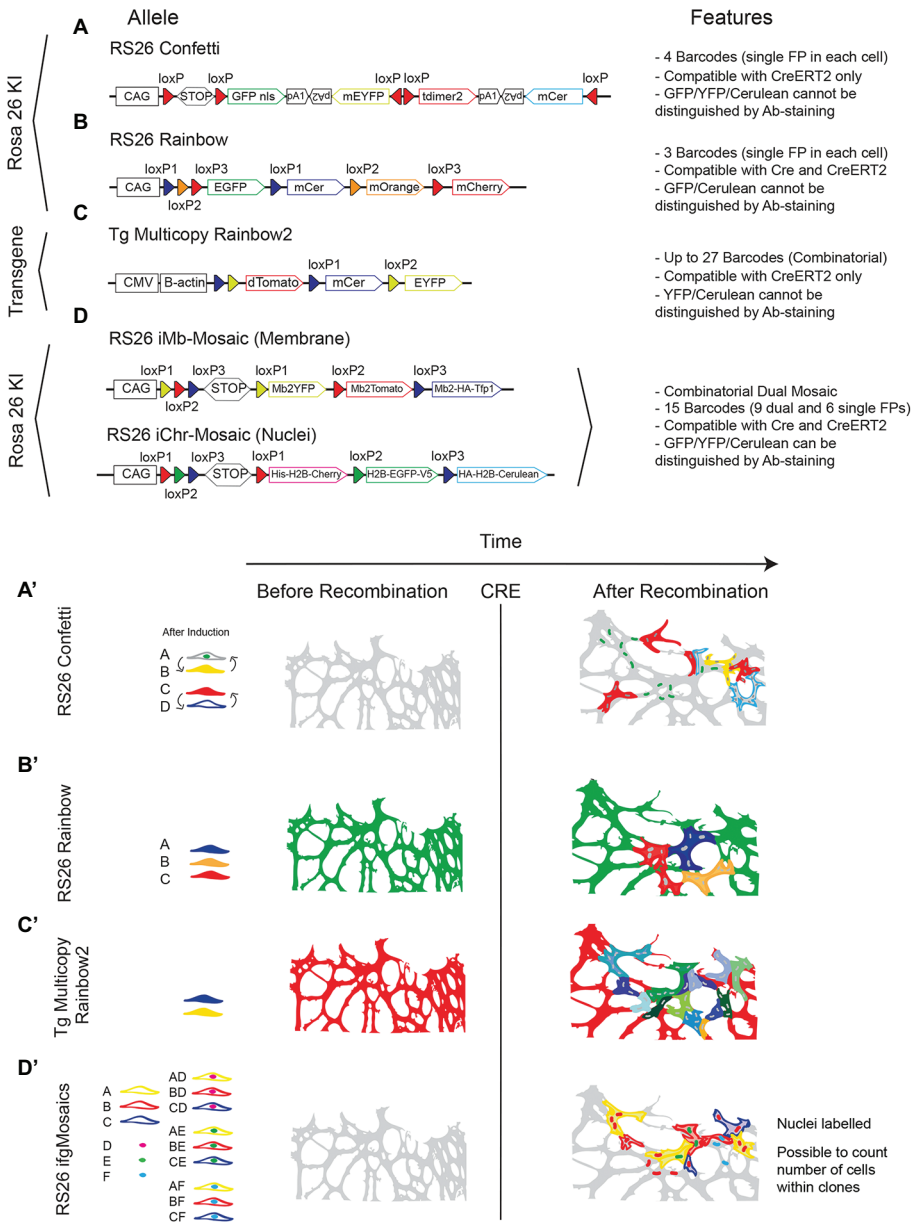

FIGURE 5 | Multispectral fluorescent mosaic alleles. **(A-D)** Schemes of the alleles and main features of available mouse lines to induce stochastic fluorescent genetic mosaics in all cell types. **(A'-D')** Illustration showing the comparison of the endothelial cell labelling achieved before and after Cre activity. Note the difference in colors/channels and cellular/clonal resolution.

from the changing surrounding environment, given that non-mutant (generally named as wildtype) and mutant cells are located in the same tissue microenvironment.

We have mentioned above the caveats of using independent reporters of Cre activity, to induce the mosaic labeling of the desired mutant cells, given the low correlation between recombination of a reporter allele and another floxed gene of interest, particularly with *CreERT2* alleles and tamoxifen. We also showed how the new *iSuRe-Cre* allele (Fernández-Chacón et al., 2019) can be used to ensure genetic deletions in reporter-expressing cells. However, like for any other standard reporter allele, the *iSuRe-Cre* allele does not prevent the occurrence of false negatives, since cells not expressing or recombining the reporter allele may recombine other floxed alleles/genes that are more sensitive to Cre/CreERT2 activity. Therefore, none of these reporter alleles should be used to induce and analyze genetic mosaics of non-mutant and mutant cells, because they do not allow the labeling of the non-mutant cells, and most (with the exception of the *iSuRe-Cre* allele) do not even reliably report mutant cells.

For reliable functional genetic mosaics, there must exist a complete (or almost complete) correlation between expression of a given marker/reporter and the genetic status of the cell, so that there is certainty that the cell in question carries the desired genetic modification, without having to worry about false positives or false negatives. The first system showing that it is possible to genetically link a cell reporter expression with the reliable and accurate labeling of mutant and wildtype cells in a mouse tissue was the mosaic analysis with double markers (MADM) system developed by the Liqun Luo laboratory (Zong et al., 2005; Zong, 2014). The MADM approach (**Figure 6A**) is based on the same principle of *Drosophila* mitotic genetic mosaics.

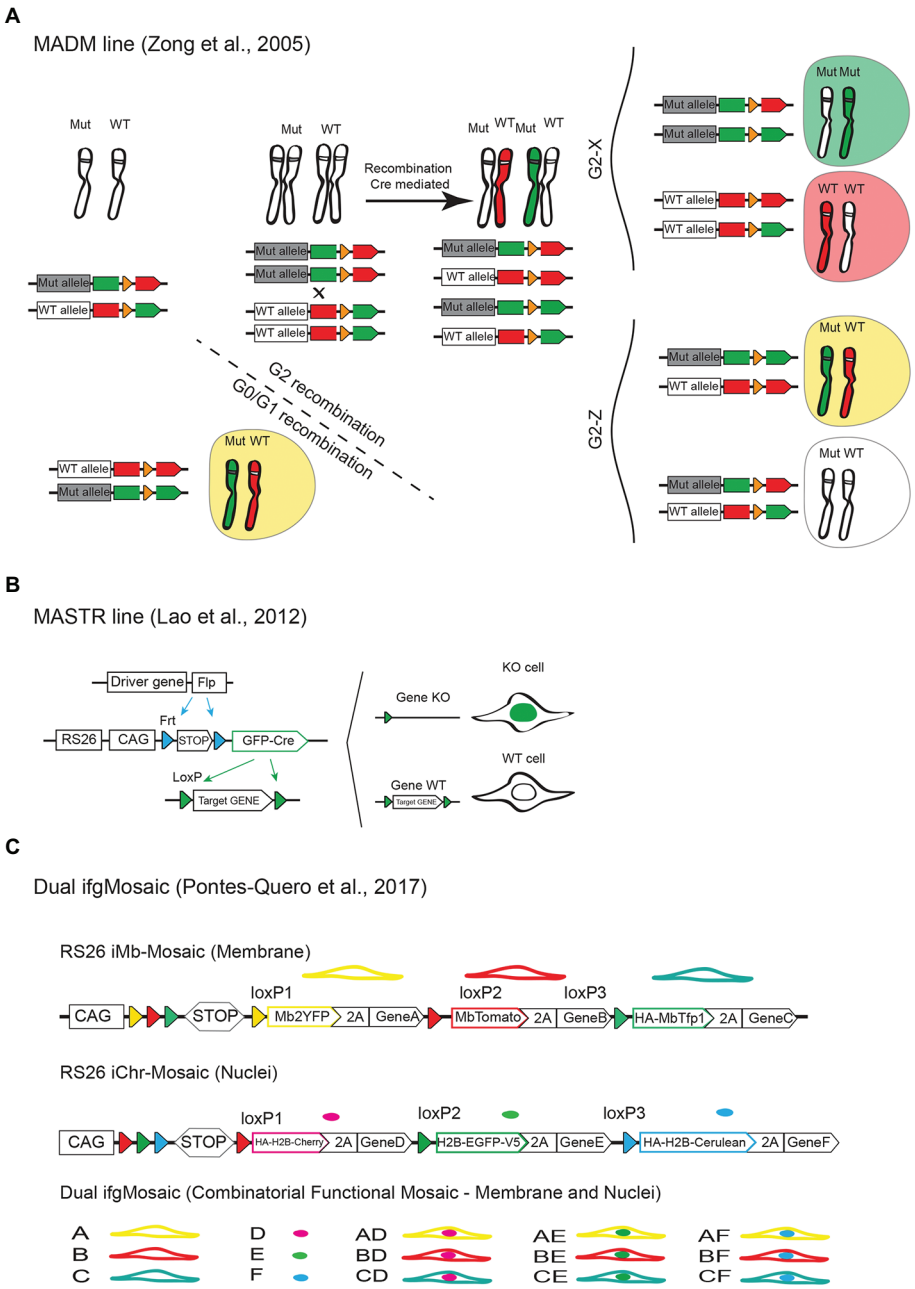

FIGURE 6 | Mouse alleles for functional genetic mosaics. **(A)** The MADM approach is dependent on rare interchromosomal and Cre-dependent recombination events between wildtype and mutant/KO alleles linked to the expression of different fluorescent proteins. This results in the labeling of wildtype (Wt) and mutant (Mut, homozygous or heterozygous) cells with different fluorescent proteins/colors. **(B)** Scheme of the MASTR mouse line and how it allows the Flp-recombinase dependent labelling of the nuclei of cells expressing GFP-Cre and therefore having a given floxed gene deleted (KO). Note that with this approach wildtype cells are not labelled. **(C)** Dual ifgMosaic alleles enable multispectral and combinatorial gene expression for accurate mosaic/clonal functional genetics.

It relies on interchromosomal recombination events between a mutant allele and wildtype allele, which are linked to reporter proteins, to generate differentially labeled control and mutant cells. This system is very useful to study the cell-autonomous effect of a given mutation since the induced labels for wildtype and mutant cells arise from the same progenitor cells and will have the same genetic background and biological context. This technology was used to study the cell-autonomous role of p27 in endothelial cells and its function in cell competition. Interestingly the authors found that in global $p27^{KO}$ animals, $p27^{KO}$ cells proliferate only 0.6 fold more than wildtype cells, whereas when using MADM mosaic animals, and the $p27^{KO}$ cells are surrounded by wildtype cells, they proliferate up to six times more (Defoe et al., 2020). This and other studies using genetic mosaics (Claveria et al., 2013) show how important are these functional mosaic methods to understand cell biology. They may not be relevant to understand the consequences of germline mutations or pharmacological treatments in disease, but they are very important to understand the origin and development of mosaic, or somatic mutations that are at the origin of most cancers and vascular malformations (Fernandez et al., 2016). Despite its great utility, the MADM approach has several drawbacks. The first is related with the very rare frequency of the Cre-dependent interchromosomal recombination events. Even when using constitutive Cre-expressing mouse lines, only very few clones of labeled mutant and wildtype cells are generated in the entire embryo. For this reason, there is no control over the timing of the recombination events and very few clones are obtained for statistical analysis. In addition, the requirement for genetic linkage between the engineered MADM elements and another gene mutation, limits its broad utility, as two *MADM* alleles have to be engineered for each mouse chromosome, and achieve meiotic recombination with a desired gene mutation (Zong, 2014). In order to significantly increase the number of genes that can be targeted mosaicly with this approach, the MADM construct has been targeted to all remaining mouse chromosomes, and this technology has now a coverage of more than 96% of the mouse genome (Contreras et al., 2020), even though there is still the need to interbreed a different *MADM* allele for every mouse gene/chromosome you want to study.

Another simpler approach is the mosaic mutant analysis with spatial and temporal control of recombination (MASTR) method (Lao et al., 2012), developed by the Alexandra Joyner laboratory. The *MASTR* allele (**Figure 6B**) is inducible by the Flp (or FlpE or FlpO) recombinase and subsequently results in the expression of the Cre-GFP fusion protein, which labels the nuclei of the Flp expressing cells. In this case, given that all GFP+ cells express Cre, the correlation between the expression of a reporter and a given floxed gene deletion is very high, even if the initial Flp or FlpOERT2 genetic pulse was very weak. In contrast to the MADM approach, with MASTR there is temporal control of recombination, and the allele is also compatible with any existent floxed allele. One of the disadvantages of the MASTR method, in comparison with the iSuRe-Cre method mentioned above, is the dependence on the very few available (and not tissue-specific) *FlpERT2* mouse lines, which are far less inducible than existent *CreERT2* lines. This results in the induction of very few clones of mutant cells in the tissue (Lao et al., 2012). A disadvantage of this method, in relation to the MADM method, is the absence of wildtype cells labeling, which prevents direct comparisons of mutant and wildtype cell phenotypes over a pulse-and-chase experiment. The exclusive nuclei labeling of the mutant cells expressing the *MASTR* allele also prevents the visualization of the cell shape, even though this allele can be combined with another cytoplasmic or membrane FP expressing Cre-reporter allele (**Figure 2A**). An important caveat noticed by the authors, is that the MASTR allele is leaky in the male germline, presumably due to skipping or alternative splicing of the transcription stop cassette. This results in the expression of GFP-Cre (even if very low) in the absence of Flp recombinase, which further complicates the experimental breedings and raise additional issues and the need of experimental controls to determine the genetic status of MASTR-reporter negative cells. With the MADM and MASTR approaches all mutant or wildtype cells will be labeled with a single FP, which prevents the distinction of different clones of wildtype or mutant cells if they occupy the same location. Therefore with both systems, the single-cell expansion or clonal analysis must rely on the assumption that the recombination events are very rare, and that there are no hot spots of recombination. Hot spots of recombination can occur when the expression of transgenic *Cre* or *Flp/FlpERT2* alleles occurs at very high levels in a small subset of cells, or when tamoxifen gets trapped or enriched in some tissue locations, which can significantly confound the assignment of single-cell-derived clones.

To overcome some of the caveats mentioned above, we recently developed an alternative genetic system, named as *Dual ifgMosaic*, to induce functional and multispectral combinatorial genetic mosaics (Pontes-Quero et al., 2017). This system is based on the Brainbow genetic mosaic system (Livet et al., 2007) mentioned above, and enables the complete correlation between the expression of a given FP and the genetic status of a cell. The functional Dual ifgMosaic lines are similar to the iChr-Mosaic and iMb-Mosaic lines described in **Figures 5D,D'**, but in this case some of the genetic elements contain downstream of the fluorescent proteins the viral 2A peptide and specific genes that either increase or decrease the function of a given signaling pathway in a cell-autonomous manner. In this way, the different fluorescent cells can be unambiguously identified as wildtype (express FP only) or mutant (co-express at equimolar levels FP and gene of interest). The Dual ifgMosaic technology also uses an open-source DNA engineering strategy that greatly simplifies the assembly of new functional genetic mosaic constructs. It allows the induction of one functional chromatin mosaic; expressing up to three different combinations of chromatin/nuclei localized FPs and genes and one functional membrane mosaic; expressing up to three different combinations of membrane localized FPs and genes (**Figure 6C**). By intercrossing mice expressing one functional mosaic allele, with other mice expressing a control (to increase clonal resolution) or functional mosaic allele, is possible to induce up to 15 different clones of cells in the

same tissue, of the same animal, each of the clones expressing a given FP and gene, or combination of two genes and FPs. We have used the Dual ifgMosaic method to induce single and combinatorial Notch and VEGF signaling loss and gain-of-function genetic mosaics, which allowed us to obtain a deeper understanding of the short and long-term cell-autonomous roles of these pathways in vascular biology and how they functionally intersect at the single-cell level (Pontes-Quero et al., 2017, 2019). Given that ifgMosaic alleles rely on the easier to achieve, and Cre/CreERT2 dependent, intrachromosomal recombination events, they can be pulsed in any tissue at high rates. The multispectral and combinatorial dual (membrane and nucleus) cell labeling strategy, further facilitates the identification of single-cell-derived wildtype and mutant clones in the same tissue, and also enable the direct imaging of the wildtype and mutant cell's chromatin and membrane. Like all technologies mentioned above, the ifgMosaic technology also has its caveats. The most important is that with the ifgMosaic system, a given genetic pathway loss-of-function is only partial and can only be achieved by expressing a protein having a dominant negative effect, such as a direct negative regulator of a pathway (i.e., *Oaz1* to suppress *Odc1* activity), a transcription factor that lost its activator domain (i.e., *DN-Maml1* to decrease NICD/*Maml1/Rbpj* complex signaling) or a receptor that lost its tyrosine kinase domain (i.e., *Vegfr2*$^{TK-}$, to decrease VEGFR2 signaling). This requires *a priori* knowledge about a pathway's biology or protein function. In addition, the overexpression of a protein having a dominant negative effect can lead to unpredictable biological consequences that differ from the endogenous pathway or gene function. In contrast to full genetic deletions or endogenous gene loss-of-function achieved with the *MADM* and *MASTR* alleles, with the *ifgMosaic* alleles a pathway or gene function is only partially suppressed, which sometimes can be more informative of a potential pharmacological compound effect, since pharmacological compounds also often do not completely ablate a given gene/protein/pathway function. With the advancement of CRISPR/Cas9 genetics and methods, is now possible to swap the genes in existent *ifgMosaic* alleles and mouse lines, by other genes of interest, which will greatly facilitate the generation of new *ifgMosaic* alleles.

In summary, even though reliable methods to induce and analyze functional genetic mosaics have been developed, all of them have their specific caveats and improvements in these technologies are needed to increase their ease of use, applicability, and reliability.

HIGHER RESOLUTION LINEAGE BARCODING WITH Cre OR Cas9

The microscopy-based methods to follow clones or lineages of cells *in vivo* and *in situ* have their limitations. The first is the relatively low-throughput of microscopy-based imaging methods and analysis. The second is the relatively low number of FPs available, and their combinations, in order to distinguish the different clones of cells *in situ*. With the advancement of CRISPR/Cas9 genetics and DNA/RNA sequencing technologies, it is now possible to encode and decode cell lineages with much higher complexity and throughput by using bioinformatic methods. Most of the methods developed so far only allow *ex situ* lineage analysis, while a few enable *in situ* lineage barcode reading.

The first methods developed to generate single-cell or lineage DNA barcodes consisted in electroporating or infecting cells with a very complex mix of plasmids or viruses with known diverse sequences, so that only some of the many available DNA sequences would integrate in a given cell and generate a clone of cells sharing a given specific combination of sequences or barcode. This was possible after the development of high-scale DNA synthesis methods that enable the generation of a wide range of different sequences. When a group of transfected/infected cells has the same and unique genomic DNA barcode, they are related with a single lineage (Schepers et al., 2008). However, for most *in vivo* single-cell lineage studies the barcoding method needs to be more complex, controllable in time and not dependent on the exogenous delivery of genetic material.

One of the first systems developed to generate inducible barcodes within the genome of mouse cells was inspired by some of the recombinase-based combinatorial mosaic strategies described before. The *R26-Polylox* mouse line (Pei et al., 2017) enables Cre-recombinase-driven DNA barcoding by providing a 2.1 kb DNA cassette containing 10 *LoxP* sites in forward and reverse orientations. This results in highly diverse and stochastic recombination events (**Figure 7A**). Given the large size of the DNA cassette, targeted sequencing of a pre-amplified PCR product derived from single cell DNA must be employed. In practical terms the authors were able to detect only 849 different barcodes (from 1.866.868 theoretically possible) in up to 52% of sequenced cells (Pei et al., 2017). This is because the excision DNA deletion events are intrinsically favored over DNA inversion/flipping events. With *R26-Polylox*, Cre expression needs to be time restricted in order to avoid the collapse of the Polylox DNA cassette which results in a significant reduction in barcoding diversity (Peikon et al., 2014). Another caveat of this technology is that the sequencing of the relatively long barcode (up to 2.1 kb) requires long-read sequencing given the unpredictability of the incomplete recombination event, which is more expensive and has a lower throughput.

With the advancements in the CRIPR-Cas9 genome editing technology, several laboratories moved to inducible sgRNA/Cas9 genome editing systems in order to generate unique DNA barcodes in a cell's genome by exploring the ease of targeting any DNA sequence with sgRNA/Cas9 and the randomness and diversity of the NHEJ repairing event. In contrast to the Polylox technology, the Cas9-based systems have the capacity to generate more barcoding diversity and enable cumulative barcoding, which is essential to understand how lineages of cells branch or develop over time (**Figures 7B,C**). All Cas9-based technologies generate variability due to random NHEJ repair mutations (deletions or insertions) that Cas9 induces after targeting and cutting a DNA sequence.

The first group of Cas9-based barcoding technologies is represented by ScarTrace (Alemany et al., 2018), Gestalt (Raj et al., 2018), and MEMOIR (Frieda et al., 2017). They all contain many repeats of a single target sequence that will

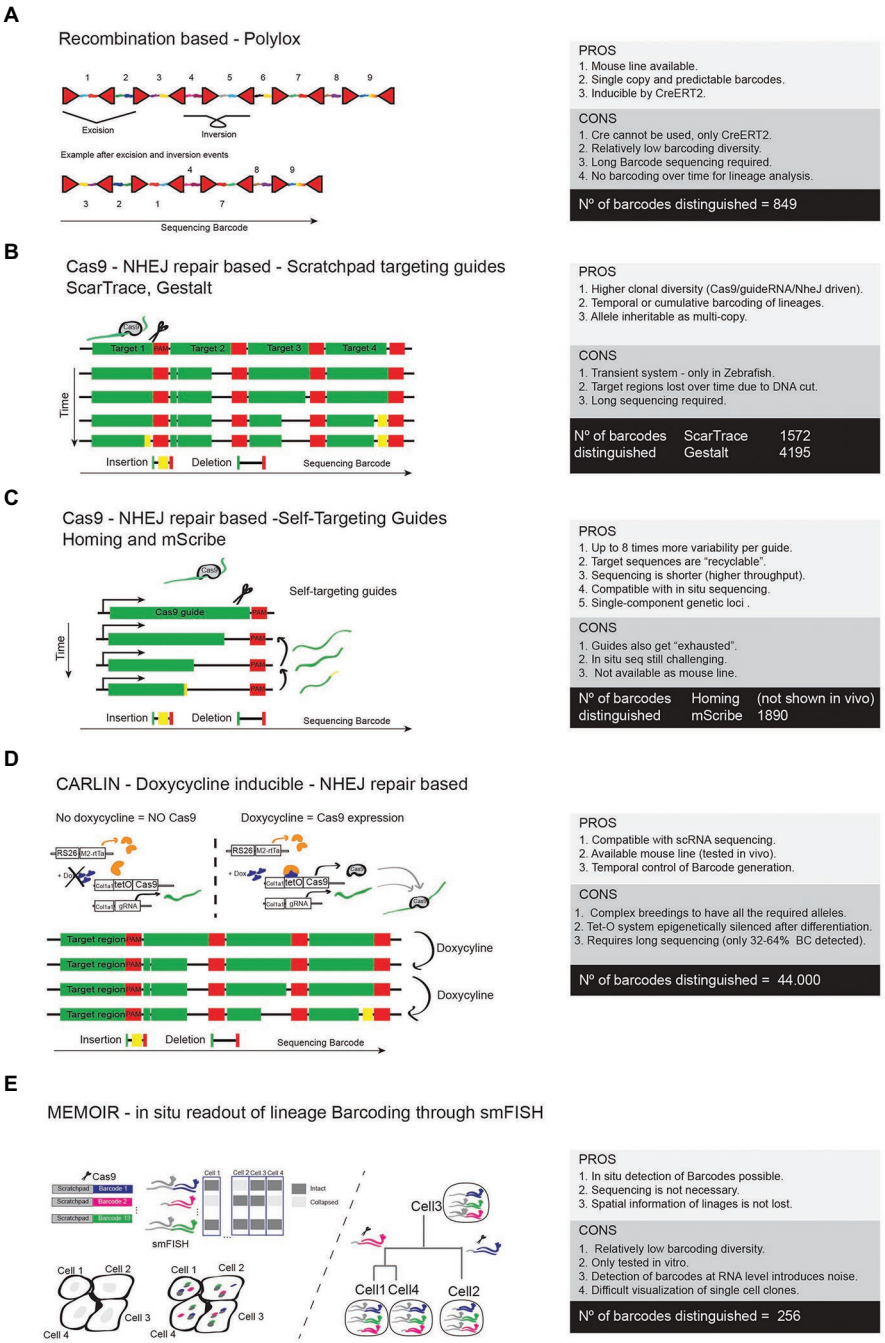

FIGURE 7 | High resolution lineage barcoding with Cre or Cas9. **(A)** Scheme of the allele and main features of the Polylox barcoding method. **(B)** Scheme representing the Cas9/NHEJ-based barcoding methods that rely on guides targeting a pre-designed genomic scratchpad to generate evolving gene editing events and barcoding diversity. **(C)** Methods using self-targeting guides to generate barcoding diversity. **(D)** The CARLIN mouse line is based on the method shown in **B**, but is inducible by doxycycline, allowing temporal control of the genetic barcoding. **(E)** The MEMOIR barcoding approach uses a guide RNA-targeted scratchpad linked to different genetic barcodes. Different cells will accumulate a different combination of edited (collapsed) barcodes that are detectable by smFISH and microscopy.

be recognized and mutated by Cas9 when guided by the corresponding target RNA guide. Their barcode generation relies on the different NHEJ repair events that will occur in each targeted sequence over time (**Figure 7B**). These variable gene editing events can later be detected by targeted single cell RNAseq or DNAseq. With these methods, the barcoding diversity is limited to the number of repeats of the target sequence, because once one of these sequences is mutated it

cannot be recognized and mutated again. In addition, when multiple sequences are targeted simultaneously by Cas9, the target array can be deleted, which results in a reduction of barcoding diversity. Nonetheless, the detected barcoding diversity was in the range from 1,572 to 4,195. ScarTrace and Gestalt were only successfully used in Zebrafish and they rely on direct delivery/injection of Cas9 and target sequences, which is not easy to translate into mouse models.

The second group of Cas9-based barcoding technologies tries to tackle the problem of reduction of available target sequences over time, and is represented here by Homing-CRISPR (Kalhor et al., 2017) and mSCRIBE (Perli et al., 2016). The basic differentiation principle of this technology is that the RNA guide is coded by the target sequence itself (**Figure 7C**). This means that mutation after mutation a different RNA guide is produced and changes in the barcode are accumulated one after the other, which allows for about eight times more variability per guide than the previous technologies. For this reason, this approach does not require a long array of target sequences and therefore a single-component genomic locus can be generated. The shorter sequencing required also turns the technology more cost-effective. However, even though the target sites last longer with Homing-CRISPR and mSCRIBE, the guides and target sequences tend to evolve too fast and after several cycles of mutations they also get "exhausted," limiting the diversity generated by each coding element. Indeed, the detected barcode diversity is in the range of the previous technologies (**Figure 7C**).

Recently a mouse line, named as CARLIN (Bowling et al., 2020), was generated using constructs similar to the GESTALT approach. This mouse enables for the first time simultaneous readout of lineage histories and scRNAseq-based gene expression analysis in mice. The CARLIN mouse requires the combination of three independent alleles targeted to the Col1a1 or *Rosa26* locus (**Figure 7D**). One allele drives the Tet inducible expression of Cas9, the other Dox inducible *rtTA*, and a third construct expresses the Cas9 RNA guide and the targetable scratchpad to generate barcodes. CARLIN barcoding diversity is in the range of 44.000. However, CARLIN is based on the Tet-O system, which is known to be silenced epigenetically once cells differentiate (Godecke et al., 2017). In adult tissues, 7 days of continuous induction with Dox, reached editing ratios close to 0% in brain, heart, and muscle and 31–88% in other organs. In addition, the *CARLIN* Cas9 target array allele undergoes stochastic and unpredictable sgRNA Cas9 editing events that require special bioinformatic analysis. Due to the need for targeted amplification of the long CARLIN array, it could only be detected in 32–64% of single cell transcriptomes. An additional caveat of the CARLIN mouse is its reliance on the combination of three alleles, which need to be combined with at least three more alleles (two floxed alleles and one Cre allele) to induce barcoding of mutant cells, something that may take a long time to achieve.

With most of the barcoding technologies above, the cell *in situ* spatial information is lost, since cells need to be separated from the tissue and sequenced in order to detect the barcode. To solve this problem, some laboratories started to couple methods of cellular barcoding with methods of multiplexed and sequential single-molecule fluorescent *in situ* hybridization (seqFISH or smFISH). One example is the MEMOIR technology (Frieda et al., 2017). MEMOIR uses the same barcoding principle to the first groups of tools presented above (GESTALT and SCARTRACE). MEMOIR barcode is formed by the link between barcode sequences and repeated target sequences (scratchpads) that are sequentially mutated/collapsed by Cas9 activation. In this way, the *in situ* identification is based on the presence (if not collapsed/mutated) or absence (if collapsed/mutated) of the associated scratchpad in a binary way (**Figure 7E**). Identification of these changes relies on seqFISH, where one probe binds and recognizes one barcode and another probe binds to the scratchpad linked to that barcode. If the scratchpad associated to that barcode has collapsed the cell will only have the signal coming from the barcode associated to the FISH probe, but not to the scratchpad probe (**Figure 7E**). Since each cell has up to 13 expressed barcode-scratchpad tandems integrated as multicopy, the final read-out will define the number and location of intact scratchpads, which at the end serves to generate barcoding diversity in each cell. Simplifying, if one cell has intact scratchpads associated with barcodes 1, 3, 5, and 13, we can associate that cell with other cells having the same pattern. We can also detect lineages by the progressive loss of scratchpads. This allows the readout of cell lineages *in situ*, which give us spatial and temporal information of cell linage evolution. However, this technique also has some caveats. In MEMOIR, the seqFISH technology was demonstrated in mouse ES cells cultured *in vitro*, but will be far more difficult to implement this *in vivo* given the number of cells and size of tissues. seqFISH is also very costly and time consuming, and few labs can afford to do it in a routine manner. The seqFISH signals are tiny dots within the cells and do not label the entire cell like a fluorescent reporter, which turns difficult the visualization of single-cell clones in tissues. RNA expression is also known to fluctuate immensely from cell to cell, which introduces noise and false negatives in the clonal analysis. On top of this, this approach has been proven to be able to detect only up to 256 different barcodes, which may not be enough to follow-up complete cell linages *in vivo*. The power and throughput of seqFISH barcoding readout and analysis *in vivo* remains low, when compared to *ex situ* single cell sequencing (Frieda et al., 2017), but new developments in 3D seqFISH and microscopy images processing may improve its capacity and throughput (Wang et al., 2018a; Eng et al., 2019; Xia et al., 2019).

The methods presented above are more a proof-of-concept, than already established and easy-to-use technologies. They are all relatively recent, and need improvements, but they were all published in high profile journals given their enormous potential to allow the reconstruction of lineage relationships of individual cells *in situ* and *ex situ*. There are still several things to optimize in these barcoding technologies, particularly for their efficient use in mouse models and conditional genetic approaches. It is essential to have temporal and spatial control

of barcoding, not just of its start, but also of its progression over time. It is also important to increase the diversity of barcoding and reduce its unpredictability in order to facilitate the downstream bioinformatic analysis. The lineage or single-cell barcoding also needs to be combined with reliable conditional gene loss-of-function methods and both need to be detectable by *in situ* or *ex situ* microscopy and sequencing technologies.

REPORTERS OF CARDIOVASCULAR CELL DYNAMICS AND SIGNALING ACTIVITY

The use of cellular or signaling activity reporters has been very important to visualize the regulation of genes or pathways during tissue development, homeostasis and in disease. One of the most important cellular processes is the cell cycle progression. Being able to track and follow the cell-cycle status in individual cells can be very useful to understand the role of genes in the regulation of the cell-cycle. *Fucci*, is the name of the first method and mouse line to be produced in order to track the different stages of the cell-cycle (Sakaue-Sawano et al., 2008). This method consisted in inducing the strong and continuous expression of two different tagged FPs that are subjected to post-translational regulation depending on the cell-cycle stage. One of the proteins contains the *hCdt1* (*human Chromatin Licensing And DNA Replication Factor 1*) domain and is fused with the fluorescent mCherry, that accumulates in the G0 or G1 phases of the cycle, and is actively degraded in the other stages. The other reporter contains the *hGem (human Geminin)* domain fused with the fluorescent Venus, which accumulates only in the S/G2/M phases of the cycle (Sakaue-Sawano et al., 2008; Mort et al., 2014). By quantifying the relative levels of the two proteins is possible to determine cell-cycle stages and transitions. The first *Fucci* mouse line consisted in the use of two separate transgenes (randomly integrated) driving expression of the two proteins (**Figure 8A**; Sakaue-Sawano et al., 2008), which is not ideal and is sensitive to epigenetic variegation. The second *Fucci* mouse line has a single construct knocked-in the *Rosa26* locus and uses the viral 2A peptide which allows equimolar expression of the two proteins, providing a more reliable readout of the cell-cycle (**Figure 8B**; Mort et al., 2014). Moreover, this *Fucci2a* line is inducible by Cre, which permits tissue specific labeling. In the cardiovascular field, the FUCCI technology has been used to understand the regulation of cell-cycle during vascular network formation (Yasuda et al., 2016); or to study cardiomyocyte cell cycle progression or arrest in the context of myocardial infarction and early postnatal development (Alvarez et al., 2019); or hemogenic endothelium and hematopoietic development (Zape et al., 2017). The line is also available in its zebrafish endothelial-specific version (Fukuhara et al., 2014). A more recent method (FUCCI4) uses four orthogonal fluorescent indicators that together resolve all cell-cycle phases, to provide even more cell-cycle resolution (Bajar et al., 2016). However, a mouse line carrying FUCCI4 still does not exist.

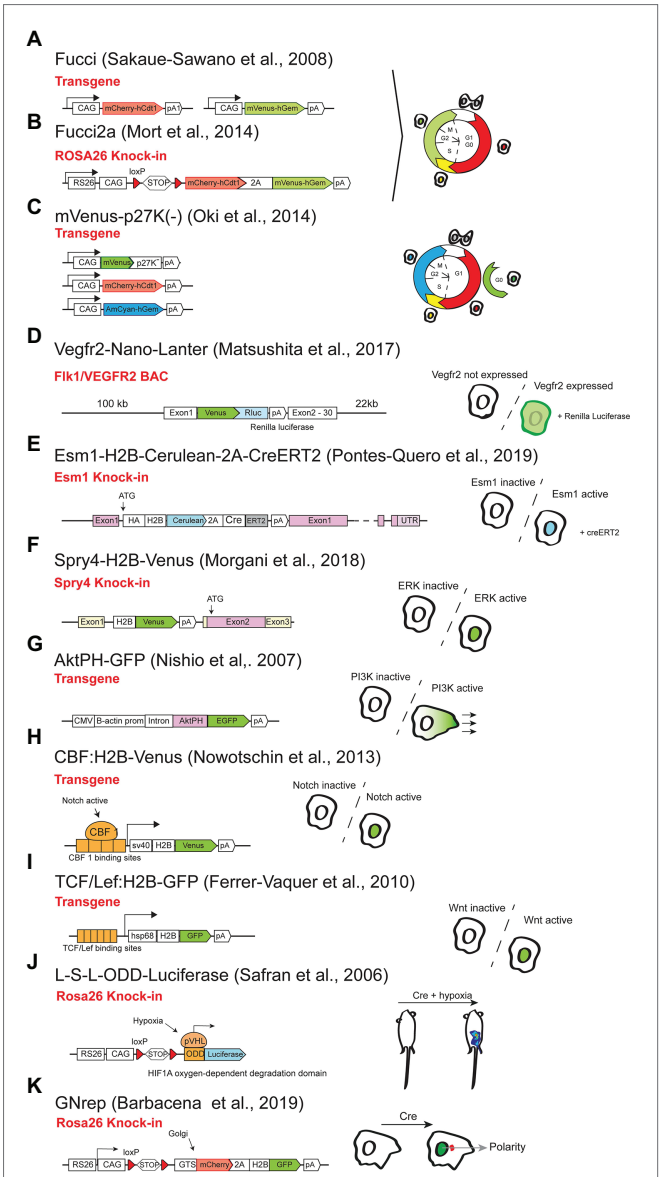

FIGURE 8 | Reporters of cardiovascular cell dynamics and signalling. Representation of the different reporter alleles on the left. On the right is possible to see the type of cell labelling achieved according to the stage of the cell-cycle or cell signalling/polarity activity.

The above mentioned lines can also be used to isolate cells at different stages of the cell-cycle. The main caveats of the FUCCI technology is the lack of distinction between cells in G0 (Ki67−) and G1 (Ki67+) phases of the cell-cycle and the lack of fluorescence in cells after the M-phase or initial G1 phase of the cycle. A solution to this may be the expression of p27-tagged fusion proteins that seem to label G0 cells (**Figure 8C**; Oki et al., 2014). However, this does not seem yet a universal solution. Additionally, it would be ideal to combine all these different cell-cycle markers in an all-in-one genetic tool or mouse line.

The other subset of mouse lines is useful as reporters of activity of signaling pathways important for the biology of

cardiovascular cells. This is the case for reporters of activity for the VEGF, Notch, Wnt, ERK, and PI3K signaling pathways. In the case of the VEGF pathway, there are several mouse lines that report the expression of the VEGF receptors or ligands *Vegfr2-GFP* (Ishitobi et al., 2010), *Vegfr3-YFP* (Calvo et al., 2011), *Vegfr2-nano-LANTER* (**Figure 8D**; Matsushita et al., 2017), but very few reporting VEGF signaling activation. One of the lines that can be used for this purpose is the *Gt(Esm1)*$^{tm1(HA\text{-}H2B\text{-}Cerulean\text{-}2A\text{-}iCreERT2)}$ line, expressing H2B-Cerulean in cells with expression of *Esm1* (**Figure 8E**), a gene that is upregulated only in ECs with very high VEGF signaling, such as retina endothelial tip cells (Rocha et al., 2014; Pontes-Quero et al., 2019). It would be very useful to develop another VEGF signaling reporter, more sensitive to lower or oscillatory levels of VEGF signaling.

Given the strong regulation of ERK signaling by VEGF, and the central importance of this signaling cascade for cell biology, mouse lines reporting its activity can be very useful. In *C. elegans* and Zebrafish a biosensor was successfully used (de la Cova et al., 2017; Mayr et al., 2018) and accurately reports ERK signaling activity. A knock-in of the mouse gene *Spry4*, which is a very sensitive and specific target of ERK activity (**Figure 8F**; Morgani et al., 2018) can also be used, however the high stability of H2B-Venus may be an issue for reporting ERK signaling dynamics. These reporter-expressing approaches are particularly suitable for live imaging experiments or to increase the sensitivity of ERK signaling detection, given that an anti-P-ERK antibody (D13.14.4E – cell signal) already enables the detection of cells with high ERK activation in fixed tissues.

Like the ERK pathway, the PI3K pathway also has a major function in vascular biology, and the *AktPH-GFP* transgenic allele expresses a probe for PtdIns(3,4,5)P_3, which can be used to monitor the activity of this pathway (**Figure 8G**; Nishio et al., 2007), even though it has not been widely used.

For Notch signaling, there are several mouse reporter lines, but none accurately reports the endogenous Notch signaling activity in cardiovascular cells. The *CBF:H2B-Venus* line (Nowotschin et al., 2013) displays high and bright nuclei Venus signal in a subset of tissues with *Rbpj/Notch* activity (**Figure 8H**), such as blood vessels (Mack et al., 2017; Salguero-Jiménez et al., 2018; Diéguez-Hurtado et al., 2019), but intense fluorescent signals are still present for several days after deletion of *Rbpj* or after blocking Notch signaling with DAPT or anti-Dll4 (unpublished data). The *TNR* line (Duncan et al., 2005) has also shown to report Notch activity in some vascular cells (Hellstrom et al., 2007), but its transgene expression pattern is highly variable and does not reflect the endogenous Notch activity in most cardiovascular cells. Several BAC or knock-in reporter lines for the Notch target genes *Hes1/Hes5/Hey1* were generated (Heintz, 2004), with stable or unstable FPs, but they also have the problem of under or over-reporting Notch activity (Imayoshi et al., 2013). Elegant Hes expression reporters using super-unstable luciferase reporters have been successfully used to image oscillations in Notch activity, however, *Hes1/5* genes, unlike *Hey1/2*, are not strong targets of Notch signaling in endothelial cells. In addition the *Hes/Hey* genes are not only regulated by Notch, but also BMP signaling (Itoh et al., 2004). So far the best method to detect Notch receptor activation in vascular cells, is to stain for the active N1ICD protein with the antibody Val1744 (Cell signaling), even though the signal is very weak and often needs tyramide-based signal amplification for adequate detection.

Another relevant pathway in the cardiovascular field is the Wnt pathway. This signaling pathway is an important regulator of cell proliferation, differentiation, and cardiovascular tissue patterning (Foulquier et al., 2018). The *TCF/Lef:H2B-GFP* mouse allele contains six copies of the TCF/Lef Wnt signaling responsive element together with a minimal promoter and a fluorescent reporter, which enables the visualization and isolation of cells with high Wnt activity (**Figure 8I**; Ferrer-Vaquer et al., 2010; Wang et al., 2018b).

Hypoxia and oxygen sensors or reporters are also very useful genetic tools to understand cardiovascular biology and the *ODD-Luc* mouse (Safran et al., 2006), uses the Oxygen-Dependent Degradation Domain (ODD) of the *Hif1a* gene in order to express luciferase protein (**Figure 8J**). A Cas9 editing or conversion of this luciferase into a FP could increase its utility.

Another process that is commonly analyzed in most cardiovascular studies is cell migration. This cellular behavior is not only necessary for development, but it also plays an important role in disease, regeneration, and tissue homeostasis. One of the main features that define cell migration is cell polarity, and being able to *in vivo* label cellular orientation is necessary to predict its migratory direction. The new *GNrep* mouse line (Barbacena et al., 2019) is able to do this by double labeling the nuclei and the Golgi complexes of the cells, which provides a read-out of the cellular migratory axis. Since this line is inducible by Cre, it enables tissue-specific cell polarity labeling and analysis (**Figure 8K**).

A problem that might arise with the use of fluorescent reporter lines, especially the highly expressed ones, is toxicity. Some fluorescent proteins like GFP have been extensively tested in mice, and are known to be generally safe. However, some red fluorescent proteins have been shown to be toxic in mice. For example, there is no mouse line expressing the native dsRed protein due to toxicity. In fact, the oligomerization to a tetramere and its long maturation time have been proposed as an explanation to its toxicity *in vivo* (Shaner et al., 2005). To solve this problem, new red fluorescent proteins derived from dsRed, like Cherry and tdTomato, have been generated and there are today numerous mouse lines expressing these fluorescent proteins constitutively without any reported abnormal phenotype (Muzumdar et al., 2007). Independently of the native protein being more or less toxic, location of the protein within the cell and levels of expression are also very important factors to consider and control in genetic experiments using new reporter lines. Therefore, *in vitro* toxicity reported in transient overexpression assays, in which each cell is transfected with numerous copies of a plasmid, cannot be used to predict toxicity of unicopy expression of fluorescent reporters in mouse lines *in vivo* (Detrait et al., 2002). In addition, expression of tagged fluorescent and non-fluorescent proteins may also interfere with the endogenous reported protein function (Hammond et al., 2010).

Nonetheless, despite the need for adequate controls, reporter lines are valuable tools to better understand the dynamics of cardiovascular related processes and signaling pathways.

CONCLUSION AND OUTLOOK

The study of vascular biology has progressed immensely with the development of new genetic tools and mouse models. From the first endothelial/pericyte/SMC-specific transgenic lines expressing a single FP or Cre, to the use of dual recombinase genetics, multispectral combinatorial labeling, cellular barcoding or scRNAseq to deconstruct single-cell transcriptomes and lineages. The field has now access to an immense diversity of alleles and methodologies. However, animal experiments are costly, and few laboratories can afford to maintain a large stock of animals and mouse lines or alleles. It is therefore essential to make informed decisions on which genetic technology works better and is key to answer a given biological question.

Looking forward it will be very important not only to develop new technologies but also optimize existing technologies. Most of the technologies mentioned in this review have inherent caveats that limit their simplicity of use or direct broad application. Many of these caveats could be overcome with significantly more investment. It is nonetheless frustrating the lack of general funding and investment to refine existing technology or to develop new genetic tools. Most of the new alleles and technologies are being developed by individual laboratories as side-projects, not as grant-funded projects, since it is far easier to get funding to work on cancer or cardiovascular biology and its impact in disease than to "just" establish a new genetic tool or method, even if it may have a much broader impact on the way a field studies and understands cancer or cardiovascular biology. A clear example of this imbalance in disease versus basic/technology-oriented funding is the limited funding devoted over time to the seminal research that allowed the iPSC or CRISPR/Cas9-based technologies to be established and significantly boost biomedical research.

With the new wave of single-cell technologies and CRISPR/Cas9-based cellular barcoding and gene targeting methods, we can now target genomic sequences, record gene editing events, and decode cellular histories and single-cell lineages with unprecedented throughput and resolution *ex situ*. The development of FISH and other multiplexed *in situ* sequencing technologies are also significantly expanding our capacity to detect stochastic cellular barcodes *in situ*. The combination of these technologies will certainly push the limits of what is possible to do with mouse genetics and the type of biological questions that can be answered. They may also allow us one day to deconstruct the entire normal or mutant tissue development or disease dynamics by analyzing only its endpoint. This will require the coordinated efforts of several laboratories with different skills in mouse *in vivo* gene-targeting/editing, microscopy, FISH, scRNAseq, and bioinformatic analysis. The continuous development and refinement of genetic methods of broad interest will certainly set the foundation to increase the efficiency and output of biomedical research.

AUTHOR CONTRIBUTIONS

MF-C and SM did literature search and wrote some sections. IG-G and RB wrote most of the manuscript and assembled the figures. All authors contributed to the article and approved the submitted version.

FUNDING

RB is supported by the European Research Council (ERC-2014-StG-638028), the Centro Nacional de Investigaciones Cardiovasculares (CNIC), and the Ministerio de Ciencia y Innovación (MCIN: SAF2017-89299-P). The CNIC is supported by MCIN, the Pro CNIC Foundation and is a Severo Ochoa Center of Excellence (SEV-2015-0505). IG-G and MF-C were supported by PhD fellowships from Fundación La Caixa (CX-SO-16-1 and CX_E-2015-01, respectively). SM was funded by the Austrian Science Fund (FWF) project J4358.

REFERENCES

Adamson, A. D., Jackson, D., and Davis, J. R. E. (2011). Novel approaches to *in vitro* transgenesis. *J. Endocrinol.* 208, 193–206. doi: 10.1677/JOE-10-0417

Al-Allaf, F. A., Abduljaleel, Z., Athar, M., Taher, M. M., Khan, W., Mehmet, H., et al. (2019). Modifying inter-cistronic sequence significantly enhances IRES dependent second gene expression in bicistronic vector: construction of optimised cassette for gene therapy of familial hypercholesterolemia. *Noncoding RNA Res.* 4, 1–14. doi: 10.1016/j.ncrna.2018.11.005

Alemany, A., Florescu, M., Baron, C. S., Peterson-Maduro, J., and Oudenaarden, A. V. (2018). Whole-organism clone tracing using single-cell sequencing. *Nature* 556, 108–112. doi: 10.1038/nature25969

Alva, J. A., Zovein, A. C., Monvoisin, A., Murphy, T., Salazar, A., Harvey, N. L., et al. (2006). VE-cadherin-Cre-recombinase transgenic mouse: a tool for lineage analysis and gene deletion in endothelial cells. *Dev. Dyn.* 235, 759–767. doi: 10.1002/dvdy.20643

Alvarez, S., Díaz, M., Flach, J., Rodriguez-Acebes, S., López-Contreras, A. J., Martínez, D., et al. (2015). Replication stress caused by low MCM expression limits fetal erythropoiesis and hematopoietic stem cell functionality. *Nat. Commun.* 6:8548. doi: 10.1038/ncomms9548

Alvarez, R., Wang, B. J., Quijada, P. J., Avitabile, D., Ho, T., Shaitrit, M., et al. (2019). Cardiomyocyte cell cycle dynamics and proliferation revealed through cardiac-specific transgenesis of fluorescent ubiquitinated cell cycle indicator (FUCCI). *J. Mol. Cell. Cardiol.* 127, 154–164. doi: 10.1016/j.yjmcc.2018.12.007

Anastassiadis, K., Fu, J., Patsch, C., Hu, S., Weidlich, S., Duerschke, K., et al. (2009). Dre recombinase, like Cre, is a highly efficient site-specific recombinase in *E. coli*, mammalian cells and mice. *Dis. Model. Mech.* 2, 508–515. doi: 10.1242/dmm.003087

Bajar, B. T., Lam, A. J., Badiee, R. K., Oh, Y. H., Chu, J., Zhou, X. X., et al. (2016). Fluorescent indicators for simultaneous reporting of all four cell cycle phases. *Nat. Methods* 13, 993–996. doi: 10.1038/nmeth.4045

Barbacena, P., Ouarne, M., Haigh, J. J., Vasconcelos, F. F., Pezzarossa, A., and Franco, C. A. (2019). GNrep mouse: a reporter mouse for front-rear cell polarity. *Genesis* 57:e23299. doi: 10.1002/dvg.23299

Basak, O., Krieger, T. G., Muraro, M. J., Wiebrands, K., Stange, D. E., Frias-Aldeguer, J., et al. (2018). Troy+ brain stem cells cycle through quiescence

and regulate their number by sensing niche occupancy. *Proc. Natl. Acad. Sci. U. S. A.* 115, E610–E619. doi: 10.1073/pnas.1715911114

Bazigou, E., Lyons, O. T. A., Smith, A., Venn, G. E., Cope, C., Brown, N. A., et al. (2011). Genes regulating lymphangiogenesis control venous valve formation and maintenance in mice. *J. Clin. Invest.* 121, 2984–2992. doi: 10.1172/JCI58050

Birling, M. -C., Gofflot, F., and Warot, X. (2009). Site-specific recombinases for manipulation of the mouse genome. *Methods Mol. Biol.* 561, 245–263. doi: 10.1007/978-1-60327-019-9_16

Bowling, S., Sritharan, D., Osorio, F. G., Nguyen, M., Cheung, P., Rodriguez-Fraticelli, A., et al. (2020). An engineered CRISPR-Cas9 mouse line for simultaneous readout of lineage histories and gene expression profiles in single cells. *Cell* 181, 1693–1694. doi: 10.1016/j.cell.2020.06.018

Branda, C. S., and Dymecki, S. M. (2004). Talking about a revolution: the impact of site-specific recombinases on genetic analyses in mice. *Dev. Cell* 6, 7–28. doi: 10.1016/S1534-5807(03)00399-X

Cai, C. L., Liang, X., Shi, Y., Chu, P. H., Pfaff, S. L., Chen, J., et al. (2003). Isl1 identifies a cardiac progenitor population that proliferates prior to differentiation and contributes a majority of cells to the heart. *Dev. Cell* 5, 877–889. doi: 10.1016/S1534-5807(03)00363-0

Calvo, C. -F., Fontaine, R. H., Soueid, J., Tammela, T., Makinen, T., Alfaro-Cervello, C., et al. (2011). Vascular endothelial growth factor receptor 3 directly regulates murine neurogenesis. *Genes Dev.* 25, 831–844. doi: 10.1101/gad.615311

Carmeliet, P., Ferreira, V., Breier, G., Pollefeyt, S., Kieckens, L., Gertsenstein, M., et al. (1996). Abnormal blood vessel development and lethality in embryos lacking a single VEGF allele. *Nature* 380, 435–439. doi: 10.1038/380435a0

Chen, Q., Zhang, H., Liu, Y., Adams, S., Eilken, H., Stehling, M., et al. (2016). Endothelial cells are progenitors of cardiac pericytes and vascular smooth muscle cells. *Nat. Commun.* 7:12422. doi: 10.1038/ncomms12422

Chu, V. T., Weber, T., Graf, R., Sommermann, T., Petsch, K., Sack, U., et al. (2016). Efficient generation of Rosa26 knock-in mice using CRISPR/Cas9 in C57BL/6 zygotes. *BMC Biotechnol.* 16:4. doi: 10.1186/s12896-016-0234-4

Claveria, C., Giovinazzo, G., Sierra, R., and Torres, M. (2013). Myc-driven endogenous cell competition in the early mammalian embryo. *Nature* 500, 39–44. doi: 10.1038/nature12389

Contreras, X., Davaatseren, A., Amberg, N., Hansen, A. H., Sonntag, J., Andersen, L., et al. (2020). A genome-wide library of MADM mice for single-cell genetic mosaic analysis. bioRxiv [Preprint]. doi: 10.1101/2020.06.05.136192

de la Cova, C., Townley, R., Regot, S., and Greenwald, I. (2017). A real-time biosensor for ERK activity reveals signaling dynamics during *C. elegans* cell fate specification. *Dev. Cell* 42, 542.e4–553.e4. doi: 10.1016/j.devcel.2017.07.014

Defoe, D. M., Rao, H., Harris, D. J., Moore, P. D., Brocher, J., and Harrison, T. A. (2020). A non-canonical role for p27Kip1 in restricting proliferation of corneal endothelial cells during development. *PLoS One* 15:e0226725. doi: 10.1371/journal.pone.0226725

Detrait, E. R., Bowers, W. J., Halterman, M. W., Giuliano, R. E., Bennice, L., Federoff, H. J., et al. (2002). Reporter gene transfer induces apoptosis in primary cortical neurons. *Mol. Ther.* 5, 723–730. doi: 10.1006/mthe.2002.0609

Diéguez-Hurtado, R., Kato, K., Giaimo, B. D., Nieminen-Kelhä, M., Arf, H., Ferrante, F., et al. (2019). Loss of the transcription factor RBPJ induces disease-promoting properties in brain pericytes. *Nat. Commun.* 10:2817. doi: 10.1038/s41467-019-10643-w

Duarte, A., Hirashima, M., Benedito, R., Trindade, A., Diniz, P., Bekman, E., et al. (2004). Dosage-sensitive requirement for mouse Dll4 in artery development. *Genes Dev.* 18, 2474–2478. doi: 10.1101/gad.1239004

Duncan, A. W., Rattis, F. M., DiMascio, L. N., Congdon, K. L., Pazianos, G., Zhao, C., et al. (2005). Integration of notch and Wnt signaling in hematopoietic stem cell maintenance. *Nat. Immunol.* 6, 314–322. doi: 10.1038/ni1164

Dymecki, S. M., Ray, R. S., and Kim, J. C. (2010). Chapter eleven - mapping cell fate and function using recombinase-based intersectional strategies. *Methods Enzymol.* 477, 183–213. doi: 10.1016/S0076-6879(10)77011-7

Ehling, M., Adams, S., Benedito, R., and Adams, R. H. (2013). Notch controls retinal blood vessel maturation and quiescence. *Development* 140, 3051–3061. doi: 10.1242/dev.093351

Eng, C. L., Lawson, M., Zhu, Q., Dries, R., Koulena, N., Takei, Y., et al. (2019). Transcriptome-scale super-resolved imaging in tissues by RNA seqFISH. *Nature* 568, 235–239. doi: 10.1038/s41586-019-1049-y

Fernandez, L. C., Torres, M., and Real, F. X. (2016). Somatic mosaicism: on the road to cancer. *Nat. Rev. Cancer* 16, 43–55. doi: 10.1038/nrc.2015.1

Fernández-Chacón, M., Casquero-García, V., Luo, W., Lunella, F. F., Rocha, S. F., Olmo-Cabrera, S. D., et al. (2019). iSuRe-Cre is a genetic tool to reliably induce and report Cre-dependent genetic modifications. *Nat. Commun.* 10:2262. doi: 10.1038/s41467-019-10239-4

Ferrer-Vaquer, A., Piliszek, A., Tian, G., Aho, R. J., Dufort, D., and Hadjantonakis, A. -K. (2010). A sensitive and bright single-cell resolution live imaging reporter of Wnt/ß-catenin signaling in the mouse. *BMC Dev. Biol.* 10:121. doi: 10.1186/1471-213X-10-121

Foulquier, S., Daskalopoulos, E. P., Lluri, G., Hermans, K. C. M., Deb, A., and Blankesteijn, W. M. (2018). WNT signaling in cardiac and vascular disease. *Pharmacol. Rev.* 70, 68–141. doi: 10.1124/pr.117.013896

Frieda, K. L., Linton, J. M., Hormoz, S., Choi, J., Chow, K. -H. K., Singer, Z. S., et al. (2017). Synthetic recording and in situ readout of lineage information in single cells. *Nature* 541, 107–111. doi: 10.1038/nature20777

Fukuhara, S., Zhang, J., Yuge, S., Ando, K., Wakayama, Y., Sakaue-Sawano, A., et al. (2014). Visualizing the cell-cycle progression of endothelial cells in zebrafish. *Dev. Biol.* 393, 10–23. doi: 10.1016/j.ydbio.2014.06.015

Gale, N. W., Dominguez, M. G., Noguera, I., Pan, L., Hughes, V., Valenzuela, D. M., et al. (2004). Haploinsufficiency of delta-like 4 ligand results in embryonic lethality due to major defects in arterial and vascular development. *Proc. Natl. Acad. Sci. U. S. A.* 101, 15949–15954. doi: 10.1073/pnas.0407290101

Garrick, D., Fiering, S., Martin, D. I., and Whitelaw, E. (1998). Repeat-induced gene silencing in mammals. *Nat. Genet.* 18, 56–59. doi: 10.1038/ng0198-56

Giraldo, P., and Montoliu, L. (2001). Size matters: use of YACs, BACs and PACs in transgenic animals. *Transgenic Res.* 10, 83–103. doi: 10.1023/a:1008918913249

Godecke, N., Zha, L., Spencer, S., Behme, S., Riemer, P., Rehli, M., et al. (2017). Controlled re-activation of epigenetically silenced Tet promoter-driven transgene expression by targeted demethylation. *Nucleic Acids Res.* 45:e147. doi: 10.1093/nar/gkx601

Hägerling, R., Pollmann, C., Kremer, L., Andresen, V., and Kiefer, F. (2011). Intravital two-photon microscopy of lymphatic vessel development and function using a transgenic *Prox1* promoter-directed mOrange2 reporter mouse. *Biochem. Soc. Trans.* 39, 1674–1681. doi: 10.1042/BST20110722

Hammond, J. W., Blasius, T. L., Soppina, V., Cai, D., and Verhey, K. J. (2010). Autoinhibition of the kinesin-2 motor KIF17 via dual intramolecular mechanisms. *J. Cell Biol.* 189, 1013–1025. doi: 10.1083/jcb.201001057

He, L., Li, Y., Li, Y., Pu, W., Huang, X., Tian, X., et al. (2017). Enhancing the precision of genetic lineage tracing using dual recombinases. *Nat. Med.* 23, 1488–1498. doi: 10.1038/nm.4437

Heintz, N. (2004). Gene expression nervous system atlas (GENSAT). *Nat. Neurosci.* 7:483. doi: 10.1038/nn0504-483

Hellstrom, M., Phng, L. K., Hofmann, J. J., Wallgard, E., Coultas, L., Lindblom, P., et al. (2007). Dll4 signalling through Notch1 regulates formation of tip cells during angiogenesis. *Nature* 445, 776–780. doi: 10.1038/nature05571

Imayoshi, I., Shimojo, H., Sakamoto, M., Ohtsuka, T., and Kageyama, R. (2013). Genetic visualization of notch signaling in mammalian neurogenesis. *Cell. Mol. Life Sci.* 70, 2045–2057. doi: 10.1007/s00018-012-1151-x

Ishitobi, H., Matsumoto, K., Azami, T., Itoh, F., Itoh, S., Takahashi, S., et al. (2010). Flk1-GFP BAC Tg mice: an animal model for the study of blood vessel development. *Exp. Anim.* 59, 615–622. doi: 10.1538/expanim.59.615

Itoh, F., Itoh, S., Goumans, M. J., Valdimarsdottir, G., Iso, T., Dotto, G. P., et al. (2004). Synergy and antagonism between notch and BMP receptor signaling pathways in endothelial cells. *EMBO J.* 23, 541–551. doi: 10.1038/sj.emboj.7600065

Jeong, H. W., Hernandez-Rodriguez, B., Kim, J., Kim, K. P., Enriquez-Gasca, R., Yoon, J., et al. (2017). Transcriptional regulation of endothelial cell behavior during sprouting angiogenesis. *Nat. Commun.* 8:726. doi: 10.1038/s41467-017-00738-7

Kalhor, R., Mali, P., and Church, G. M. (2017). Rapidly evolving homing CRISPR barcodes. *Nat. Methods* 14, 195–200. doi: 10.1038/nmeth.4108

Kisanuki, Y. Y., Hammer, R. E., Miyazaki, J., Williams, S. C., Richardson, J. A., and Yanagisawa, M. (2001). Tie2-Cre transgenic mice: a new model for endothelial cell-lineage analysis *in vivo*. *Dev. Biol.* 230, 230–242. doi: 10.1006/dbio.2000.0106

Koetsier, P. A., Mangel, L., Schmitz, B., and Doerfler, W. (1996). Stability of transgene methylation patterns in mice: position effects, strain specificity and cellular mosaicism. *Transgenic Res.* 5, 235–244. doi: 10.1007/BF01972877

Lao, Z., Raju, G. P., Bai, C. B., and Joyner, A. L. (2012). MASTR: a technique for mosaic mutant analysis with spatial and temporal control of recombination using conditional floxed alleles in mice. *Cell Rep.* 2, 386–396. doi: 10.1016/j.celrep.2012.07.004

Legue, E., and Joyner, A. L. (2010). Genetic fate mapping using site-specific recombinases. *Methods Enzymol.* 477, 153–181. doi: 10.1016/S0076-6879(10)77010-5

Li, Y., He, L., Huang, X., Bhaloo Shirin, I., Zhao, H., Zhang, S., et al. (2018). Genetic lineage tracing of nonmyocyte population by dual recombinases. *Circulation* 138, 793–805. doi: 10.1161/CIRCULATIONAHA.118.034250

Li, Y., Lv, Z., He, L., Huang, X., Zhang, S., Zhao, H., et al. (2019). Genetic Tracing Identifies Early Segregation of the Cardiomyocyte and Nonmyocyte Lineages. *Circ. Res.* 125, 343–355. doi: 10.1161/CIRCRESAHA.119.315280

Livet, J., Weissman, T. A., Kang, H., Draft, R. W., Lu, J., Bennis, R. A., et al. (2007). Transgenic strategies for combinatorial expression of fluorescent proteins in the nervous system. *Nature* 450, 56–62. doi: 10.1038/nature06293

Long, M. A., and Rossi, F. M. V. (2009). Silencing inhibits Cre-mediated recombination of the Z/AP and Z/EG reporters in adult cells. *PLoS One* 4:e5435. doi: 10.1371/journal.pone.0005435

Ma, Q., Zhou, B., and Pu, W. T. (2008). Reassessment of Isl1 and Nkx2-5 cardiac fate maps using a Gata4-based reporter of Cre activity. *Dev. Biol.* 323, 98–104. doi: 10.1016/j.ydbio.2008.08.013

Mack, J. J., Mosqueiro, T. S., Archer, B. J., Jones, W. M., Sunshine, H., Faas, G. C., et al. (2017). NOTCH1 is a mechanosensor in adult arteries. *Nat. Commun.* 8:1620. doi: 10.1038/s41467-017-01741-8

Madisen, L., Zwingman, T. A., Sunkin, S. M., Oh, S. W., Zariwala, H. A., Gu, H., et al. (2010). A robust and high-throughput Cre reporting and characterization system for the whole mouse brain. *Nat. Neurosci.* 13, 133–140. doi: 10.1038/nn.2467

Martinez-Corral, I., Stanczuk, L., Frye, M., Ulvmar, M. H., Dieguez-Hurtado, R., Olmeda, D., et al. (2016). *Vegfr3-CreER*^{T2} mouse, a new genetic tool for targeting the lymphatic system. *Angiogenesis* 19, 433–445. doi: 10.1007/s10456-016-9505-x

Matsushita, J., Inagaki, S., Nishie, T., Sakasai, T., Tanaka, J., Watanabe, C., et al. (2017). Fluorescence and bioluminescence imaging of angiogenesis in Flk1-Nano-lantern transgenic mice. *Sci. Rep.* 7:46597. doi: 10.1038/srep46597

Mayr, V., Sturtzel, C., Stadler, M., Grissenberger, S., and Distel, M. (2018). Fast dynamic *in vivo* monitoring of Erk activity at single cell resolution in DREKA zebrafish. *Front. Cell Dev. Biol.* 6:111. doi: 10.3389/fcell.2018.00111

McBurney, M. W., Mai, T., Yang, X., and Jardine, K. (2002). Evidence for repeat-induced gene silencing in cultured mammalian cells: inactivation of tandem repeats of transfected genes. *Exp. Cell Res.* 274, 1–8. doi: 10.1006/excr.2001.5443

Morgani, S. M., Saiz, N., Garg, V., Raina, D., Simon, C. S., Kang, M., et al. (2018). A Sprouty4 reporter to monitor FGF/ERK signaling activity in ESCs and mice. *Dev. Biol.* 441, 104–126. doi: 10.1016/j.ydbio.2018.06.017

Mort, R. L., Ford, M. J., Sakaue-Sawano, A., Lindstrom, N. O., Casadio, A., Douglas, A. T., et al. (2014). Fucci2a: a bicistronic cell cycle reporter that allows Cre mediated tissue specific expression in mice. *Cell Cycle* 13, 2681–2696. doi: 10.4161/15384101.2015.945381

Moses, K. A., DeMayo, F., Braun, R. M., Reecy, J. L., and Schwartz, R. J. (2001). Embryonic expression of an Nkx2-5/Cre gene using ROSA26 reporter mice. *Genesis* 31, 176–180. doi: 10.1002/gene.10022

Motoike, T., Loughna, S., Perens, E., Roman, B. L., Liao, W., Chau, T. C., et al. (2000). Universal GFP reporter for the study of vascular development. *Genesis* 28, 75–81. doi: 10.1002/1526-968x(200010)28:2<75::aid-gene50>3.0.co;2-s

Murray, S. A., Eppig, J. T., Smedley, D., Simpson, E. M., and Rosenthal, N. (2012). Beyond knockouts: cre resources for conditional mutagenesis. *Mamm. Genome* 23, 587–599. doi: 10.1007/s00335-012-9430-2

Mutskov, V., and Felsenfeld, G. (2004). Silencing of transgene transcription precedes methylation of promoter DNA and histone H3 lysine 9. *EMBO J.* 23, 138–149. doi: 10.1038/sj.emboj.7600013

Muzumdar, M. D., Tasic, B., Miyamichi, K., Li, L., and Luo, L. (2007). A global double-fluorescent Cre reporter mouse. *Genesis* 45, 593–605. doi: 10.1002/dvg.20335

Nagy, A. (2000). Cre recombinase: the universal reagent for genome tailoring. *Genesis* 26, 99–109. doi: 10.1002/(SICI)1526-968X(200002)26:2<99::AID-GENE1>3.0.CO;2-B

Nishio, M., Watanabe, K., Sasaki, J., Taya, C., Takasuga, S., Iizuka, R., et al. (2007). Control of cell polarity and motility by the PtdIns(3,4,5)P_3 phosphatase SHIP1. *Nat. Cell Biol.* 9, 36–44. doi: 10.1038/ncb1515

Nowotschin, S., Xenopoulos, P., Schrode, N., and Hadjantonakis, A. -K. (2013). A bright single-cell resolution live imaging reporter of notch signaling in the mouse. *BMC Dev. Biol.* 13:15. doi: 10.1186/1471-213X-13-15

Oki, T., Nishimura, K., Kitaura, J., Togami, K., Maehara, A., Izawa, K., et al. (2014). A novel cell-cycle-indicator, mVenus-p27K$^-$, identifies quiescent cells and visualizes G0-G1 transition. *Sci. Rep.* 4:4012. doi: 10.1038/srep04012

Oladipupo, S. S., Kabir, A. U., Smith, C., Choi, K., and Ornitz, D. M. (2018). Impaired tumor growth and angiogenesis in mice heterozygous for Vegfr2 (Flk1). *Sci. Rep.* 8:14724. doi: 10.1038/s41598-018-33037-2

Ottersbach, K. (2019). Endothelial-to-haematopoietic transition: an update on the process of making blood. *Biochem. Soc. Trans.* 47, 591–601. doi: 10.1042/BST20180320

Pan, Y. A., Freundlich, T., Weissman, T. A., Schoppik, D., Wang, X. C., Zimmerman, S., et al. (2013). Zebrabow: multispectral cell labeling for cell tracing and lineage analysis in zebrafish. *Development* 140, 2835–2846. doi: 10.1242/dev.094631

Pei, W., Feyerabend, T. B., Rössler, J., Wang, X., Postrach, D., Busch, K., et al. (2017). Polylox barcoding reveals haematopoietic stem cell fates realized *in vivo*. *Nature* 548, 456–460. doi: 10.1038/nature23653

Peikon, I. D., Gizatullina, D. I., and Zador, A. M. (2014). *In vivo* generation of DNA sequence diversity for cellular barcoding. *Nucleic Acids Res.* 42:e127. doi: 10.1093/nar/gku604

Perli, S. D., Cui, C. H., and Lu, T. K. (2016). Continuous genetic recording with self-targeting CRISPR-Cas in human cells. *Science* 353:aag0511. doi: 10.1126/science.aag0511

Platt, R. J., Chen, S., Zhou, Y., Yim, M. J., Swiech, L., Kempton, H. R., et al. (2014). CRISPR-Cas9 Knockin mice for genome editing and Cancer modeling. *Cell* 159, 440–455. doi: 10.1016/j.cell.2014.09.014

Plummer, N. W., Evsyukova, I. Y., Robertson, S. D., Marchena, J. D., Tucker, C. J., and Jensen, P. (2015). Expanding the power of recombinase-based labeling to uncover cellular diversity. *Development* 142, 4385–4393. doi: 10.1242/dev.129981

Pontes-Quero, S., Fernández-Chacón, M., Luo, W., Lunella, F. F., Casquero-Garcia, V., Garcia-Gonzalez, I., et al. (2019). High mitogenic stimulation arrests angiogenesis. *Nat. Commun.* 10:2016. doi: 10.1038/s41467-019-09875-7

Pontes-Quero, S., Heredia, L., Casquero-García, V., Fernández-Chacón, M., Luo, W., Hermoso, A., et al. (2017). Dual ifgMosaic: a versatile method for multispectral and combinatorial mosaic gene-function analysis. *Cell* 170, 800.e18–814.e18. doi: 10.1016/j.cell.2017.07.031

Pu, W., He, L., Han, X., Tian, X., Li, Y., Zhang, H., et al. (2018). Genetic targeting of organ-specific blood vessels. *Circ. Res.* 123, 86–99. doi: 10.1161/CIRCRESAHA.118.312981

Raj, B., Wagner, D. E., McKenna, A., Pandey, S., Klein, A. M., Shendure, J., et al. (2018). Simultaneous single-cell profiling of lineages and cell types in the vertebrate brain. *Nat. Biotechnol.* 36, 442–450. doi: 10.1038/nbt.4103

Rocha, S. F., Schiller, M., Jing, D., Li, H., Butz, S., Vestweber, D., et al. (2014). Esm1 modulates endothelial tip cell behavior and vascular permeability by enhancing VEGF bioavailability. *Circ. Res.* 115, 581–590. doi: 10.1161/CIRCRESAHA.115.304718

Rodríguez, C. I., Buchholz, F., Galloway, J., Sequerra, R., Kasper, J., Ayala, R., et al. (2000). High-efficiency deleter mice show that FLPe is an alternative to Cre-loxP. *Nat. Genet.* 25, 139–140. doi: 10.1038/75973

Safran, M., Kim, W. Y., O'Connell, F., Flippin, L., Günzler, V., Horner, J. W., et al. (2006). Mouse model for noninvasive imaging of HIF prolyl hydroxylase activity: assessment of an oral agent that stimulates erythropoietin production. *Proc. Natl. Acad. Sci. U. S. A.* 103, 105–110. doi: 10.1073/pnas.0509459103

Sakaue-Sawano, A., Kurokawa, H., Morimura, T., Hanyu, A., Hama, H., Osawa, H., et al. (2008). Visualizing spatiotemporal dynamics of multicellular cell-cycle progression. *Cell* 132, 487–498. doi: 10.1016/j.cell.2007.12.033

Salguero-Jiménez, A., Grego-Bessa, J., D'Amato, G., Jiménez-Borreguero, L. J., and de la Pompa, J. L. (2018). Myocardial Notch1-Rbpj deletion does not affect NOTCH signaling, heart development or function. *PLoS One* 13:e0203100. doi: 10.1371/journal.pone.0203100

Schepers, K., Swart, E., van Heijst, J. W. J., Gerlach, C., Castrucci, M., Sie, D., et al. (2008). Dissecting T cell lineage relationships by cellular barcoding. *J. Exp. Med.* 205, 2309–2318. doi: 10.1084/jem.20072462

Scott, G. J., and Gruzdev, A. (2019). Genome editing in mouse embryos with CRISPR/Cas9. *Methods Mol. Biol.* 1960, 23–40. doi: 10.1007/978-1-4939-9167-9_2

Shaner, N. C., Steinbach, P. A., and Tsien, R. Y. (2005). A guide to choosing fluorescent proteins. *Nat. Methods* 2, 905–909. doi: 10.1038/nmeth819

Sharma, P., Yan, F., Doronina, V. A., Escuin-Ordinas, H., Ryan, M. D., and Brown, J. D. (2012). 2A peptides provide distinct solutions to driving stop-carry on translational recoding. *Nucleic Acids Res.* 40, 3143–3151. doi: 10.1093/nar/gkr1176

Snippert, H. J., van der Flier, L. G., Sato, T., van Es, J. H., van den Born, M., Kroon-Veenboer, C., et al. (2010). Intestinal crypt homeostasis results from neutral competition between symmetrically dividing Lgr5 stem cells. *Cell* 143, 134–144. doi: 10.1016/j.cell.2010.09.016

Sörensen, I., Adams, R. H., and Gossler, A. (2009). DLL1-mediated notch activation regulates endothelial identity in mouse fetal arteries. *Blood* 113, 5680–5688. doi: 10.1182/blood-2008-08-174508

Soriano, P. (1999). Generalized lacZ expression with the ROSA26 Cre reporter strain. *Nat. Genet.* 21, 70–71. doi: 10.1038/5007

Srinivas, S., Watanabe, T., Lin, C. S., William, C. M., Tanabe, Y., Jessell, T. M., et al. (2001). Cre reporter strains produced by targeted insertion of EYFP and ECFP into the ROSA26 locus. *BMC Dev. Biol.* 1:4. doi: 10.1186/1471-213X-1-4

Suchting, S., Freitas, C., le Noble, F., Benedito, R., Breant, C., Duarte, A., et al. (2007). The notch ligand delta-like 4 negatively regulates endothelial tip cell formation and vessel branching. *Proc. Natl. Acad. Sci. U. S. A.* 104, 3225–3230. doi: 10.1073/pnas.0611177104

Sulston, J. E., and Horvitz, H. R. (1977). Post-embryonic cell lineages of the nematode, *Caenorhabditis elegans*. *Dev. Biol.* 56, 110–156. doi: 10.1016/0012-1606(77)90158-0

Sulston, J. E., Schierenberg, E., White, J. G., and Thomson, J. N. (1983). The embryonic cell lineage of the nematode *Caenorhabditis elegans*. *Dev. Biol.* 100, 64–119. doi: 10.1016/0012-1606(83)90201-4

Tian, X., He, L., Liu, K., Pu, W., Zhao, H., Li, Y., et al. (2020). Generation of a self-cleaved inducible Cre recombinase for efficient temporal genetic manipulation. *EMBO J.* 39:e102675. doi: 10.15252/embj.2019102675

Tian, X., Hu, T., Zhang, H., He, L., Huang, X., Liu, Q., et al. (2013). Subepicardial endothelial cells invade the embryonic ventricle wall to form coronary arteries. *Cell Res.* 23, 1075–1090. doi: 10.1038/cr.2013.83

Trichas, G., Begbie, J., and Srinivas, S. (2008). Use of the viral 2A peptide for bicistronic expression in transgenic mice. *BMC Biol.* 6:40. doi: 10.1186/1741-7007-6-40

Ubezio, B., Blanco, R. A., Geudens, I., Stanchi, F., Mathivet, T., Jones, M. L., et al. (2016). Synchronization of endothelial Dll4-notch dynamics switch blood vessels from branching to expansion. *eLife* 5:e12167. doi: 10.7554/eLife.12167

Underwood, E. M., Turner, F. R., and Mahowald, A. P. (1980). Analysis of cell movements and fate mapping during early embryogenesis in *Drosophila melanogaster*. *Dev. Biol.* 74, 286–301. doi: 10.1016/0012-1606(80)90431-5

Vooijs, M., Jonkers, J., and Berns, A. (2001). A highly efficient ligand-regulated Cre recombinase mouse line shows that LoxP recombination is position dependent. *EMBO Rep.* 2, 292–297. doi: 10.1093/embo-reports/kve064

Wang, J., Xu, N., Feng, X., Hou, N., Zhang, J., Cheng, X., et al. (2005). Targeted disruption of *Smad4* in cardiomyocytes results in cardiac hypertrophy and heart failure. *Circ. Res.* 97, 821–828. doi: 10.1161/01.RES.0000185833.42544.06

Wang, X., Allen, W. E., Wright, M. A., Sylwestrak, E. L., Samusik, N., Vesuna, S., et al. (2018a). Three-dimensional intact-tissue sequencing of single-cell transcriptional states. *Science* 361:eaat5691. doi: 10.1126/science.aat5691

Wang, Y., Nakayama, M., Pitulescu, M. E., Schmidt, T. S., Bochenek, M. L., Sakakibara, A., et al. (2010). Ephrin-B2 controls VEGF-induced angiogenesis and lymphangiogenesis. *Nature* 465, 483–486. doi: 10.1038/nature09002

Wang, Y., Lu, P., Wu, B., Morrow, B. E., and Zhou, B. (2018b). NOTCH maintains developmental cardiac gene network through WNT5A. *J. Mol. Cell. Cardiol.* 125, 98–105. doi: 10.1016/j.yjmcc.2018.10.014

Westphal, C. H., and Leder, P. (1997). Transposon-generated 'knock-out' and 'knock-in' gene-targeting constructs for use in mice. *Curr. Biol.* 7, 530–533. doi: 10.1016/S0960-9822(06)00224-7

Wirth, A., Benyo, Z., Lukasova, M., Leutgeb, B., Wettschureck, N., Gorbey, S., et al. (2008). G_{12}-G_{13}-LARG-mediated signaling in vascular smooth muscle is required for salt-induced hypertension. *Nat. Med.* 14, 64–68. doi: 10.1038/nm1666

Wu, B., Zhang, Z., Lui, W., Chen, X., Wang, Y., Chamberlain, A. A., et al. (2012). Endocardial cells form the coronary arteries by angiogenesis through myocardial-endocardial VEGF signaling. *Cell* 151, 1083–1096. doi: 10.1016/j.cell.2012.10.023

Xia, C., Fan, J., Emanuel, G., Hao, J., and Zhuang, X. (2019). Spatial transcriptome profiling by MERFISH reveals subcellular RNA compartmentalization and cell cycle-dependent gene expression. *Proc. Natl. Acad. Sci. U. S. A.* 116, 19490–19499. doi: 10.1073/pnas.1912459116

Yang, H., Wang, H., Shivalila, C. S., Cheng, A. W., Shi, L., and Jaenisch, R. (2013). One-step generation of mice carrying reporter and conditional alleles by CRISPR/Cas-mediated genome engineering. *Cell* 154, 1370–1379. doi: 10.1016/j.cell.2013.08.022

Yasuda, N., Sekine, H., Bise, R., Okano, T., and Shimizu, T. (2016). Tracing behavior of endothelial cells promotes vascular network formation. *Microvasc. Res.* 105, 125–131. doi: 10.1016/j.mvr.2015.12.005

Zape, J. P., Lizama, C. O., Cautivo, K. M., and Zovein, A. C. (2017). Cell cycle dynamics and complement expression distinguishes mature haematopoietic subsets arising from hemogenic endothelium. *Cell Cycle* 16, 1835–1847. doi: 10.1080/15384101.2017.1361569

Zhang, H., Pu, W., Tian, X., Huang, X., He, L., Liu, Q., et al. (2016). Genetic lineage tracing identifies endocardial origin of liver vasculature. *Nat. Genet.* 48, 537–543. doi: 10.1038/ng.3536

Zhou, B., Ma, Q., Rajagopal, S., Wu, S. M., Domian, I., Rivera-Feliciano, J., et al. (2008). Epicardial progenitors contribute to the cardiomyocyte lineage in the developing heart. *Nature* 454, 109–113. doi: 10.1038/nature07060

Zong, H. (2014). "Generation and applications of MADM-based mouse genetic mosaic system" in *Mouse genetics: Methods and protocols*. eds. S. R. Singh and V. Coppola (New York, NY: Springer), 187–201.

Zong, H., Espinosa, J. S., Su, H. H., Muzumdar, M. D., and Luo, L. (2005). Mosaic analysis with double markers in mice. *Cell* 121, 479–492. doi: 10.1016/j.cell.2005.02.012

Conflict of Interest: The authors declare that the research was conducted in the absence of any commercial or financial relationships that could be construed as a potential conflict of interest.

Advantages of publishing in Frontiers

OPEN ACCESS
Articles are free to read for greatest visibility and readership

FAST PUBLICATION
Around 90 days from submission to decision

HIGH QUALITY PEER-REVIEW
Rigorous, collaborative, and constructive peer-review

TRANSPARENT PEER-REVIEW
Editors and reviewers acknowledged by name on published articles

Frontiers
Avenue du Tribunal-Fédéral 34
1005 Lausanne | Switzerland

Visit us: www.frontiersin.org
Contact us: info@frontiersin.org | +41 21 510 17 00

REPRODUCIBILITY OF RESEARCH
Support open data and methods to enhance research reproducibility

DIGITAL PUBLISHING
Articles designed for optimal readership across devices

FOLLOW US
@frontiersin

IMPACT METRICS
Advanced article metrics track visibility across digital media

EXTENSIVE PROMOTION
Marketing and promotion of impactful research

LOOP RESEARCH NETWORK
Our network increases your article's readership